Behaviour of RC beams strengthened with CFRP laminates at elevated temperatures

by

Diana Petkova

Kingston University London

A thesis submitted in partial fulfilment of the requirements of the Faculty of Engineering at Kingston University for the Degree of Doctor of Philosophy

October 2010

PAGINATION AS IN ORIGINAL

В памет на майка ми

In memory of my mother

Acknowledgements

This work would not be possible without the kind help of a remarkable group of people.

First I would like to thank my supervisors Dr.Homayoun Hadavinia, Prof. Jennifer Wen, Dr. Kamran Etebar for their help and support. My deepest gratitude to my Director of studies Dr. Ted Donchev whose guidance, patience and encouragement have always been and will be deeply appreciated.

I would like to thank Martin Theobald for his excellent work on the first testing device, to Howard Catling for his help in the concrete lab and especially Peter Wells for his patience and wonderful work on the second testing device. Thank you to Chris Somerfield for making the days in the lab more enjoyable. Special thanks to Colin Bradsell for the long hours doing testing, for his generous help and advice.

I would like to thank Prof Mukesh Limbachiya and Dr. David Wertheim for their help and support. Thank you to my colleagues for their patience and understanding, to the other PhD students for their help and encouragement and to my students for willing to spend long hours in the lab.

Thank you to Barry Ephgrave and Weber for their generous support and contributions.

Finally I have to thank my family and friends for their support and patience.

Abstract

Strengthening of existing structures has become an important aspect of civil engineering. Various methods exist and have been developed in the last few decades one of which has become increasingly popular- strengthening using fibre reinforced polymers. Their excellent mechanical properties and resistance to different environmental conditions make them a viable alternative to the traditional materials like concrete and steel. In this study the effect of elevated temperatures on the behaviour of FRP strengthened reinforced concrete beams is investigated.

The behaviour of reinforced concrete beams strengthened with FRP laminates has been investigated by different researchers in the last two decades. Ultimate load, failure modes and improved techniques for strengthening have been the main areas of interest. As a result of the extensive research several classifications and design guidelines have been proposed to ensure better performance and prevent premature failures of the systems. One important aspect of the strengthening is the susceptibility of polymers to significant and rapid reduction of their strength when exposed to elevated temperatures and fire. Little research has been done up-to-date on the residual properties of FRP strengthened systems after heating and cooling.

Three experiments have been conducted for the purpose of this study. The bond strength of CFRP strengthened systems is first investigated for temperature range of 20°C to 300°C. The behaviour of small-scale strengthened beams during the heating process is presented next. The third experiment is then designed to determine the residual flexural capacity of the heated and cooled minibeams. The results are presented and compared indicating residual strength of the systems to 30% compared to their performance at room temperature.

Table of Contents

PAGE NUMBERING AS ORIGINAL

List of figures

List of tables

Nomenclature

A coefficient of curve fitting

A cross-sectional area

b width of concrete

b_2 width of FRP plate

B coefficients of curve fitting

[B] a matrix which relates the strain to nodal displacement

[D] a matrix which relates stress to strain

E elastic modulus of the FRP plate or concrete

E_p elastic modulus of CFRP plate

E_u energy of the system at failure

E_y energy of the system at first steel yield

F force vector

G_a shear modulus of the adhesive

G_f interfacial fracture energy

I second moment of area

[J] a Jacobian matrix

K the stiffness matrix of the system

[k] the stiffness matrix

L length of the element

L_e effective bond width

n a parameter governing the softening branch of the interface law

s distance between cracks

$\bar{s}$ the peak slip

s_p FRP–concrete shear slip

s, t, z' isoparametric coordinates of the nodes

t thickness of the plate or the concrete

t_a thickness of the adhesive

t_p thickness of CFRP plate

Tc temperature of concrete

u vector of the unknowns

x distance from the end of the CFRP

y_1, y_2 the respective distances from the bottom and top of the respective adherends to their centroids.

α effective shear area multiplier

δ relative displacement between the two adherends

Δ deflection of the beam at midspan

μ reinforcement ratio

σ_p axial stress in the concrete

$\bar{\tau}$ peak shear stress.

τ_f local bond strength

τ_p FRP–concrete shear stress

Chapter 1
Introduction

Chapter 1

1.1 Background

In the last two decades fibre reinforced polymers (FRP) have become a popular new material in civil engineering used for strengthening of existing structures. In their various forms and shapes they can be used to improve the structural performance of masonry, reinforced concrete, steel and timber structures. They have excellent mechanical properties such as high strength and low weight, they are corrosion resistant and easy to install. Thus their application and behaviour of strengthened systems have become a popular topic for research in the last few decades resulting in the development of several design guidelines and reports.

Various experimental studies have been carried out to determine and improve the performance of externally strengthened structural elements. These include strengthening of existing reinforced concrete (RC) and steel beams in shear and flexure, FRP confinement of RC columns, strengthening of masonry, environmental durability and fatigue. Although the range of application of the external FRP plates and sheets has increased the strengthened systems have been established to perform poorly when exposed directly to flames and high temperatures. The problem is complex, as the strengthened system consists of three different types of materials- FRP, adhesive and concrete, each of them with its own specific behaviour when subjected to high temperatures and fire. Nevertheless, little information is available in the literature about the effect of elevated temperatures on the behaviour of the strengthened system.

The topic of this research project is the effect of elevated temperatures on the behaviour of carbon fibre reinforced polymer (CFRP) strengthened reinforced concrete (RC) beams. Three main types of experiments were carried out to investigate the residual strength of the specimens. Their behaviour during the heating process and after the samples were heated and cooled was investigated. A total of 63 concrete prisms were cast, strengthened, heated and tested. The heating range covered temperatures from 20°C to 300°C.

The experimental results show that CFRP strengthened beams could retain to 30% of their room temperature strength before the composite action is lost or the system fails at temperatures exceeding the decomposition of the constituent materials.

1.2 Research objectives and experimental programme

The main aim of this study is to investigate experimentally the effect of elevated temperatures up to 300°C on the structural performance of CFRP strengthened beams. Two main types of samples are tested for the study. CFRP-to-concrete bonded joints are designed to investigate the effective stress transfer between FRP and concrete with increase of the temperature. Small-scale beams are designed to study the overall performance of flexurally strengthened RC beams. To achieve the aim of this work the main objectives are identified as follows:

- Review of the existing test methods and experimental work on the bond strength of FRP-to-concrete bonded joints. Design of a single shear testing device to determine the shear strength of the samples after heating and cooling.
- Investigation of the residual bond strength of CFRP-to-concrete bonded joints in the temperature range of 20°C to 300°C. Examine the failure pattern of the tested samples and physical changes of the materials.
- Design of an experimental set-up and carry out an experimental study to investigate the behaviour of small-scale CFRP strengthened beams during heating.
- Review of the possible failure modes of flexurally strengthened RC beams. Investigation of the deflection behaviour of small-scale CFRP strengthened RC beams after heating and cooling under four point bending.
- Investigate the failure modes of the tested small-scale CFRP strengthened RC beams and examine the crack propagation during the loading. Compare the effect of heating on the physical appearance of the materials and loss of composite action.

Comparison of the results and analysis is presented. Numerical models have also been developed and discussed.

1.3 Methodology and outline of the thesis

In order to achieve the research objectives the experimental work is organised and presented in 8 chapters including the introduction and conclusion chapters. Figure 1.1 given below presents a flowchart of the reviewed literature topics, experimental results and analysis.

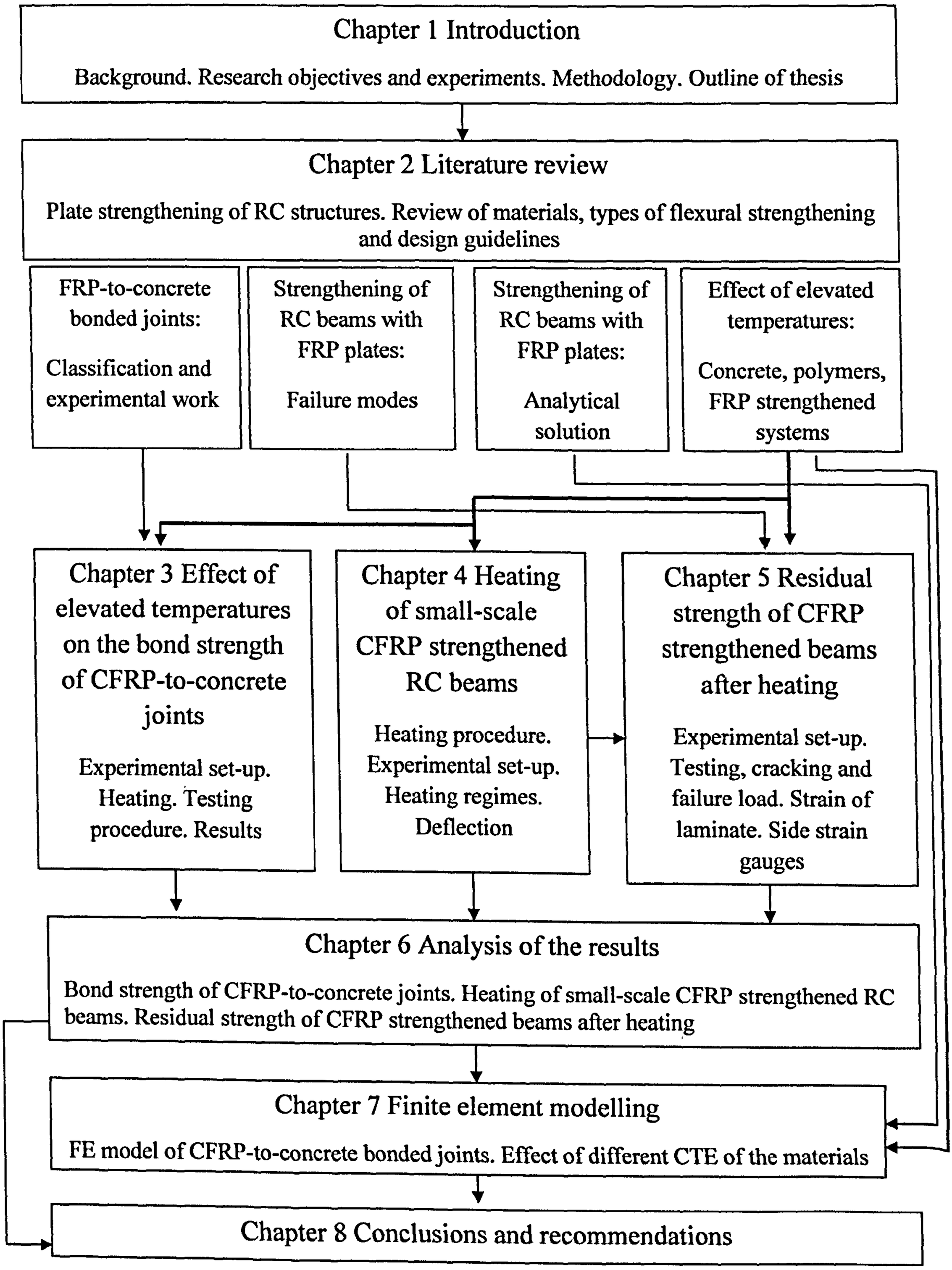

Figure I-1 Organisation of the thesis

Chapter 1

In chapter 2 review of the research progress on FRP strengthened beams is presented. Failure modes, analytical methods and fracture mechanics approaches are described. The effect of elevated temperatures and fire on the mechanical properties of concrete and polymers are then discussed. Experimental studies on FRP strengthened structural members exposed to fire and elevated temperatures are also presented.

The results from the first experiment are described in chapter 3. The experimental set-up, heating procedure and samples are presented first. The deformations, crack propagation and failure mode are then described for every group.

Chapter 4 shows the findings on the deformability of heated and loaded CFRP strengthened minibeams during exposure to elevated temperatures. The same samples are cooled and tested in 4 point bending in chapter 5. Failure modes, crack propagation and local deformations of each sample are described.

In chapter 6 comparison and analysis of the results from the experimental programme are presented. Chapter 7 summarizes two numerical studies on the effect of elevated temperatures on the residual bond strength of CFRP strengthened systems and the effect of different coefficients of thermal expansion (CTE).

Chapter 8 then presents the conclusions and the recommendations for future work. References and appendices are included at the end of the thesis.

Chapter 2
Literature review

2.1 Plate strengthening of RC structures

The deterioration of structures and the need for strengthening have become a challenge for the construction industry in the last few decades. In its lifetime a structure could be subjected to different environmental conditions, it would be designed for live loads determined by the traffic volume or for by use of building at the time of the design and may suffer extreme dynamic loads such as seismic, impact or blast loading. The solutions for a damaged or structurally deficient element are to demolish, repair or strengthen. The strengthening technique under consideration in this project is by using externally bonded FRP plates. The main structural elements which are investigated are simply supported reinforced concrete beams with attached laminates to the tension side and they are referred to as strengthened systems in the text.

Steel plates became the first popular type of plates for strengthening due to their availability, practical application and well known material properties. The effect of steel plates on the behaviour of the strengthened system was then studied and the technique was found to improve the load-bearing capacity and deformation of the RC beams. The experimental results and ultimate loads revealed a tendency for brittle plate separation from the beam initiating from the end of the plate and causing the so called concrete cover rip-off. This particular failure mode was explained by the concentration of normal and shear stressed at the end of the plate due to the stiffness incompatibility of the plate and beam (Hollaway and Leeming, 2000). The use of steel plate allowed introducing bolts at the end of the plates to improve their anchorage to the RC beam. However, their contribution to the performance of the strengthened system was only found to improve the ductility of the system but to have insignificant effect on the ultimate load.

Overall, the steel plate technique is considered to be an effective and economic method for strengthening (Hollaway and Leeming, 2000). Due to its inherent susceptibility to the environmental conditions, however, this method has several disadvantages and possible weaknesses of the system such as corrosion or reduced strength due to exposure to high temperatures. The steel plates require additional support during installation and also increase

the dead load of the structure and therefore affect the load-bearing capacity of the strengthened system.

Most of the disadvantages of the steel plated RC beams are overcome by introducing a new type of material for rehabilitation and repair of structures. The fibre reinforced polymers (FRP) are products developed initially by the aerospace and automotive industries and adapted in the recent years as a strengthening material for the needs and requirements of the construction industry. Compared to steel the FRP materials have higher ultimate strength, lower weight and excellent resistance to chemical attack. Their installation does not require additional support during curing and are available in very long lengths.

However, the main disadvantage of FRP is the effect of high temperatures and fire on the performance of unprotected strengthened structures due to their low decomposition temperature. Impact loading has also been viewed as a potential weakness of FRP externally strengthened elements, i.e. bridge columns where the impact from a vehicle could cause damage to the strengthening system.

2.1.1 Materials and manufacture

A FRP strengthening system consists of two main elements: FRP material and adhesive which bonds the composite to the structural member. Through a bonding action the transfer of stresses between the structural element and the strengthening material is possible and the increase of strength is achieved. In this section an overview of the typical materials used for strengthening purposes is presented.

The FRP composite comprises two materials: fibres and polymer matrix. The strength and stiffness of the composite are determined mainly by the properties of the fibres. The role of the matrix is to transfer stresses between the fibres, to protect the fibres from the environment and limit the effect of moisture, chemicals and oxidation (Hollaway and Leeming, 2000). The fibres used for strengthening are 3 types:

- Carbon, manufactured by controlled pyrolysis and crystallization of an organic precursor (Cadei et al, 2004): rayon, polyacrylonitrile (PAN) and pitch precursors. The fibres produced from PAN precursors exhibit higher strength than rayon and pitch;
- Glass, silica based glass compound manufactured by direct melt process;
- Aramid, produced by an extrusion and spinning process.

The matrix of the composite is usually organic, the four most commonly used are:

- Epoxies, two-part systems with a wide range of properties;
- Polyester, used mostly in preformed composite components;
- Phenolic resins, with good fire-resisting properties;
- Polyurethane, most susceptible to effects during curing.

The tables given below identify the mechanical properties of the materials (Cadei et al, 2004).

	Carbon fibres	Glass fibres	Aramid fibres	Epoxy	Polyester	Phenolic	Poly-urethane
Elastic modulus (GPa)	230-240	70-85	125-130	2.6-3.8	3.1-4.6	3-4	0.5
Tensile Strength (MPa)	4300-4900	2460-2580	3200-3600	60-85	50-75	60-80	15-25
Strain to failure (%)	1.9-2.1	3.5	2.4	1.5-8	1-2.5	1-1.8	10
Density (kg/m^3)	1800	2600	1390-1470	1110-1200	1110-1250	1000-1250	1150-1200
Coefficient of thermal expansion (10^{-6}/°C)	-0.38	4.9	2.1	30-70	30-70	80	40

Table II-1 Mechanical properties of the constituents of FRP materials

	MBT Feb	Weber SBD	Sika
Flexural modulus (GPa)	-	9.8	12.8
Tensile strength (MPa)	32	19	30
Lap shear strength (MPa)	17	18	
Coefficient of thermal expansion (10^{-6}/°C)	-	-	33
Density (kg/m^3)	1800	1535	1800

Table II-2 Mechanical properties of popular structural adhesives

2.1.2 Flexural strengthening of RC beams

Hollaway and Leeming (2000) reviewed the results from experimental investigations on the FRP strengthening of RC beams conducted by different researchers over a period of 20 years. Results from full and small-scale experiments were presented with minimum and maximum increase of 18% to 230% of the ultimate load for the different cases. The overall performance of the strengthened systems was found to be governed by factors such as internal reinforcement, directionality of the FRP sheets, thickness of the FRP plate, width- thickness ratio of the plate and shear span- depth ratio of the RC beam. The effect of strengthening with FRP plate was reported to increase both the strength and stiffness of the RC elements but also caused reduction of the ductility of the strengthened beam. Thus, the load-bearing capacity of the system would improve but the failure mode would often be brittle causing sudden peeling of the laminate due to a shear crack in the concrete or "horizontal shearing of the concrete in the tensile zone" (Hollaway and Leeming, 2000).

The effect of varying degrees of strengthening of RC beams was investigated by Ramana et al. (2000). RC beams with dimensions 100x100x1000mm were strengthened with CFRP composites with 3 different widths of 10, 20 and 40mm. The experimental results confirmed increase of the stiffness with increase of the width of the laminate. The beams were tested under a four point static loading and they all failed by "typical peeling of the laminate due to flexural- shear crack".

Camata et al (2007) presented results from experimental and numerical study of RC post-strengthened slabs and beams. The samples were strengthened with CFRP strips and loaded to failure at a constant rate in four-point bending configuration. The results showed an increase of the ultimate load of 72% and 35% for the slabs and beams respectively. The strengthened samples failed in a brittle manner due to midspan debonding of the laminate. The slabs failure was triggered by the high interfacial stresses between the adhesive and the concrete induced by the flexural crack and by the localized bending caused by the shear cracks. A thin layer of concrete detached from the slab as an indication of the horizontal crack near the adhesive/concrete interface. The beams failed similarly to the slabs.

The significant number of beams which failed due to cracks in the concrete or peeling of the laminate at the end of the plate led to investigations of the possible solutions for the premature

failure of the beams. Cadei et al (2004) proposed several options to reduce the concentration of stresses at the end of the plate:

- Spew fillet of the adhesive;
- Tapered end of the FRP plate;
- Increase of the width of the laminate at the end;
- Applying mechanical restraint such as bolted clamps or additional FRP wrap.

Although these methods have been proposed for strengthening of metallic structures the mechanical restraint was found to be applicable for RC beams as well. However, direct drilling of holes through the laminate could cause additional cracking of the laminate and therefore should be avoided.

Two types of plate end anchorage systems: bolts and clamping force were used by Garden and Hollaway (1998) in order to investigate the influence of plate end anchorage. The RC beams strengthened with CFRP plates were tested in two configurations: four-point bending and as cantilevers. The bolted plate and anchorage system comprised a steel anchorage block of 40mm length, with the same width as the laminate. It was bonded to the laminate by the same adhesive and by bolts. Three types of failure were observed depending on the shear span-depth ratio:

- cover separation: removal of the full thickness of concrete cover throughout one of the shear spans-which starts by a plate end shear crack at the laminate end;
- partial cover separation: initiated by the vertical step at the base of a shear crack approximately half way along the failed shear span;
- triangular separation: initiated by the displacement of the plate due to the rotation of a triangular piece of concrete near one of the loading positions.

Rabinovitch & Frostig (2003) investigated the effect of different shear and longitudinal reinforcement ratio of RC beams with 2.5m length and strengthened with CFRP strips loaded in four-point bending. The edge configuration of the adhesive was also investigated. The effect of the formation of a 'spew-fillet' and the use of additional vertical CFRP straps wrapping were found to increase the maximum load to up to 20%. The results from the experiments showed increase of the flexural strength and stiffness but reduced deformability

and brittle failure modes. The comparison with rehabilitated beams revealed ultimate loads close to the strengthened ones but they would not exhibit a renewed cracking. The reduced shear reinforcement was found to have influence on the failure mode which would lead to the development of diagonal shear crack and would cause unstable failure.

Al-Amery and Al-Mahaidi (2006) investigated CFRP straps for additional strengthening of RC beams. As well as improving the shear resistance of the strengthened system the straps prevented the debonding failure. The use of CFRP straps reduced the slip between the CFRP sheets and the concrete, improved the composite action of the beam and increased the flexural strength by 95%. Interesting result of the additional anchorage was a ductile flexural failure.

Thomsen et al (2004) studied the effect of the laminate length, width and the effect of different load on FRP plate strengthened beams. As established in similar studies with increased length of the laminate an increase of the ultimate load was reported. A change of failure mode was also observed: from plate end to the midspan of the plate and beam. However the authors commented that beyond a certain length the ultimate load would not increase.

Pham and Al-Mahaidi (2004) discussed results from experimental work with 16 RC beams strengthened with CFRP sheets. The beams were tested under four point loading with span of 2300mm and shear span of 700mm. Several parameters were tested: the bond length, the area of the reinforcement, the concrete cover, number of plies and the amount of the shear reinforcement. The authors concluded that the midspan and end debonding modes were result of the high shear stress in concrete and the efficiency of the FRP increases with higher ratio of the FRP bond to concrete depth in shear span.

A total of 42 beam specimens were used in the peeling and spalling resistance study carried out by Wu et al (2005). The effect of different FRP materials, adhesives, surface treatment and concrete strength were investigated. Three types of debonding failure were identified from experiments: within surface concrete layer, in FRP composites- adhesive interface and concrete- adhesive interface. The results from tests with different adhesives showed that fast hardening epoxy decreased the ultimate peeling load and that failure patterns would change from debonding in the concrete layer to debonding in the interface between concrete and adhesive. Lower peeling load was also observed for surfaces which had not been treated. It

was concluded that the peel load was proportional to the FPP sheet stiffness and the interfacial fracture energy.

Three different ways of strengthening were studied by Brena & Macri (2004) to evaluate the effect of the laminates configuration. The experimental programme consisted of 18 small-scale RC beams strengthened in flexure with CFRP composites. The beams were 914mm long with a cross section of 102x102mm and with 2 types of internal reinforcement. The strain results from the different configurations were compared, the stress in the composites was calculated and the shear stress between the laminates and the concrete surface was analysed. The external strengthening was applied in 3 ways: attached on the bottom face; attached to on the sides and partial wrapping with 25mm on the sides. The beams strengthened with one layer of CFRP failed due to debonding of the laminate; the others failed in a combination of debonding and concrete cover separation.

Maalej and Bian (2001) reported increase of ultimate load of 22-46% from experiments conducted with five simply supported beams with variable thickness tested under four point loading system. The beams were strengthened with CFRP sheets with the same width as the beam with variation of the layers of the sheets. The two observed failure modes were CFRP rupture and concrete cover ripping. The increase of the thickness of the CFRP resulted in decreasing efficiency of the strengthening system and an increase of the concentration of stresses at the end of the CFRP. The research suggested that the failure of the beam was a function of the deformation rather than the applied load.

RC beams strengthened with CFRP sheets were tested by Li et al (2006) with variation of the length of and thickness of the FRP of 0.6, 1.2, 1.6m. The beams were subjected to four point bending with a 3kN loading step. The type and layers of the strengthening were found to have a significant influence on the crack patterns and the maximum load of the beams. Depending on the anchorage of the CFRP the observed modes of failure were concrete crushing and shear in the beam.

Wenwei and Guo (2006) also investigated the effect of strengthening on preloaded beams. Seven beams with dimensions 150mmx250mmx2700mm were preloaded to a specified load, strengthened with CFRP laminates (150mm width) and then tested under four point bending.

The results from the tests showed increase of the load-carrying capacity for the strengthened beams and 3 failure modes. Rupture of CFRP and horizontal cracking in the tension zone and shear failure were observed to be the typical modes of failure for the strengthened beams.

2.1.3 Design guidelines for FRP strengthening

2.1.3.1 Ductility

Thomsen et al (2004) adopted two approaches to determine the ductility of strengthened beams: displacement based and energy based where the energy ductility was defined as the ratio between the energy of the system at failure *Eu* and the energy of the system at first steel yield *Ey*. The beams strengthened in flexure with CFRP and GFRP plates of different axial stiffness showed that the more flexible plates tend to have lower interface shear stresses at the plate end and thus needed a shorter anchorage length. The latter would also exhibit more ductile behaviour than the CFRP plate.

Buyukozturk et al (2002) suggested that the three point bending tests would be appropriate for debonding induced by flexural cracks, whilst in four point bending tests the debonding could propagate into the shear span from the flexural cracks close to the load points. The fundamental difference between debonding due to shear failure would be the ductility behaviour. The experiments consisted of RC precracked beams in shear and/or flexure with/without anchoring of the flexural reinforcement and the beams were tested under four point bending until failure. To predict the failure loads of the beams facture mechanics approach was used.

Maalej and Leong (2005) also compared the ductility of RC beams strengthened with CFRP sheets adopting the two ductility criteria: by deflection and by energy and found the results of the two methods to be the same. The authors tested 17 RC under-reinforced beams in three-point bending and found increase of the average strength capacity compared to the control beams. For strengthening ratio of 0.106% an increase of 27-29% was reported, for strengthening ratio of 0.212% an increase of 45% was found. The strengthened beams failed

through flexural crack-induced interfacial debonding. The experimental results were compared to Smith and Teng's model (2002).

Oehlers et al (2003) categorised the different failure modes of plated RC beams. Intermediate crack debonding mechanism was found difficult to predict as it controlled the strength and the ductility of the plated beam. It was also found from the experimental work that strengthening with plates on the sides of the beams could be a better option in some cases as it could improve the strength and ductility of the system. Recently, Oehlers (2006) and Oehlers et al (2009) investigated the problem of the rotational capacity of FRP-plated members. The zero hinge length concept was first explained to illustrate the complexity of ductility of RC elements and a conceptual model was described of the contributing rotational components and the limits to the rotation of plated beams.

Matthys and Taerwe (2006) compared four design guidelines for the ductility of FRP strengthened RC members:

- Fib Bulletin 14 "Design and use of externally bonded fibre reinforced polymer reinforcement (FRP EBR) for reinforced concrete structures";
- ACI 440.2R-02 "Guide for the design and construction of externally bonded FRP systems for strengthening of concrete structures";
- CSA S806-02 "Design and construction of building components with fibre-reinforced polymers";
- JSCE Concrete Engineering Series 41"Recommendations for upgrading of concrete structures with use of continuous fibre sheets".

It was concluded that the ductility of flexural members would be lower than unstrengthened ones and it would decrease with the increase of FRP used. Minimum deformability requirements were found in Fib Bulletin 14 and ACI 440.2R-02 based on the design limit of the strain in the FRP. However, strength safety factor for the acting design load would be the governing criterion. The different failure modes would also implicitly consider the ductility of the system. Ductility enhancement by FRP wrapping could be achieved for confined concrete.

2.1.3.2 Crack width and spacing

Avril et al (2005) investigated numerically the effect of plates on cracked externally strengthened RC beams where the crack opening, the slip of the rebars and the bonding between the composite and concrete surface were taken into account.

Ceroni and Pecce (2007) discussed the cracking behaviour of RC beams strengthened with FRP. The bond behaviour between concrete and laminate and between steel and concrete were compared. The crack width and distance in Eurocode 2 were discussed and a modification for the FRP plate was proposed. ACI 318-95 and fib Bulletin 14 were also presented. A model was proposed which was found to be in good agreement with the experimental results.

Four RC beams were strengthened with 50mm wide, 1.4mm thick CFRP laminate with variation of the length and tested under UDL by Aprile and Feo (2007). The deformation of the laminate was measured with a significant number of strain gauges. The type of observed failure was concrete cover rip-off for all the beams, which was characterized as a detachment of a "tooth" followed by debonding of the whole plate. The crack pattern was evaluated based on three formulations: fib Bulletin 14, CEB Bulleting 234 model and Beeby's approach, where the last two models were found to be best fit with the experimental results.

Ceroni and Pecce (2009) studied crack width and spacing according to EC2-92, EC2-04, ACI 318-95 and fib Bulletin 14. In EC2 the contribution of FRP was taken into account by the reinforcement ratio μ. The experimental values obtained for RC beams and tension members were compared with the design values for external load corresponding to 400MPa stress in the steel. The crack spacing according to EC2 and fib Bulletin was discussed and it was found to be overestimated by the first and underestimated by the second.

Simplified models for a single and multiple cracks for FRP delamination were proposed by Casas and Pascual (2007). Two experiments were carried out to verify the models: small specimens and large scale beams. It was concluded that flexible systems had better structural strength, the rigid laminates were found to be more prone to failure by debonding than flexible sheets. A parameter s/Le (distance between cracks and effective bond width) was used to

indicate the influence of stiffness and the cracking: if the value would be greater than 4 the analysis could be for single crack model.

2.2 FRP-to- concrete bonded joints

2.2.1 Classification of the test methods

There are several typical set-ups when the bond strength of FRP and steel plate strengthened samples are studied experimentally. The position of support for the concrete sample and number of shear surfaces are the governing factors for the failure of the samples. The following classification summarized by Chen et al (2001) of bond strength tests are considered in this study:

- Far-end supported double-shear test;
- Near-end supported double-shear test;
- Far-end supported single-shear test;
- Near-end supported single-shear test;
- Beam test;
- Modified beam test.

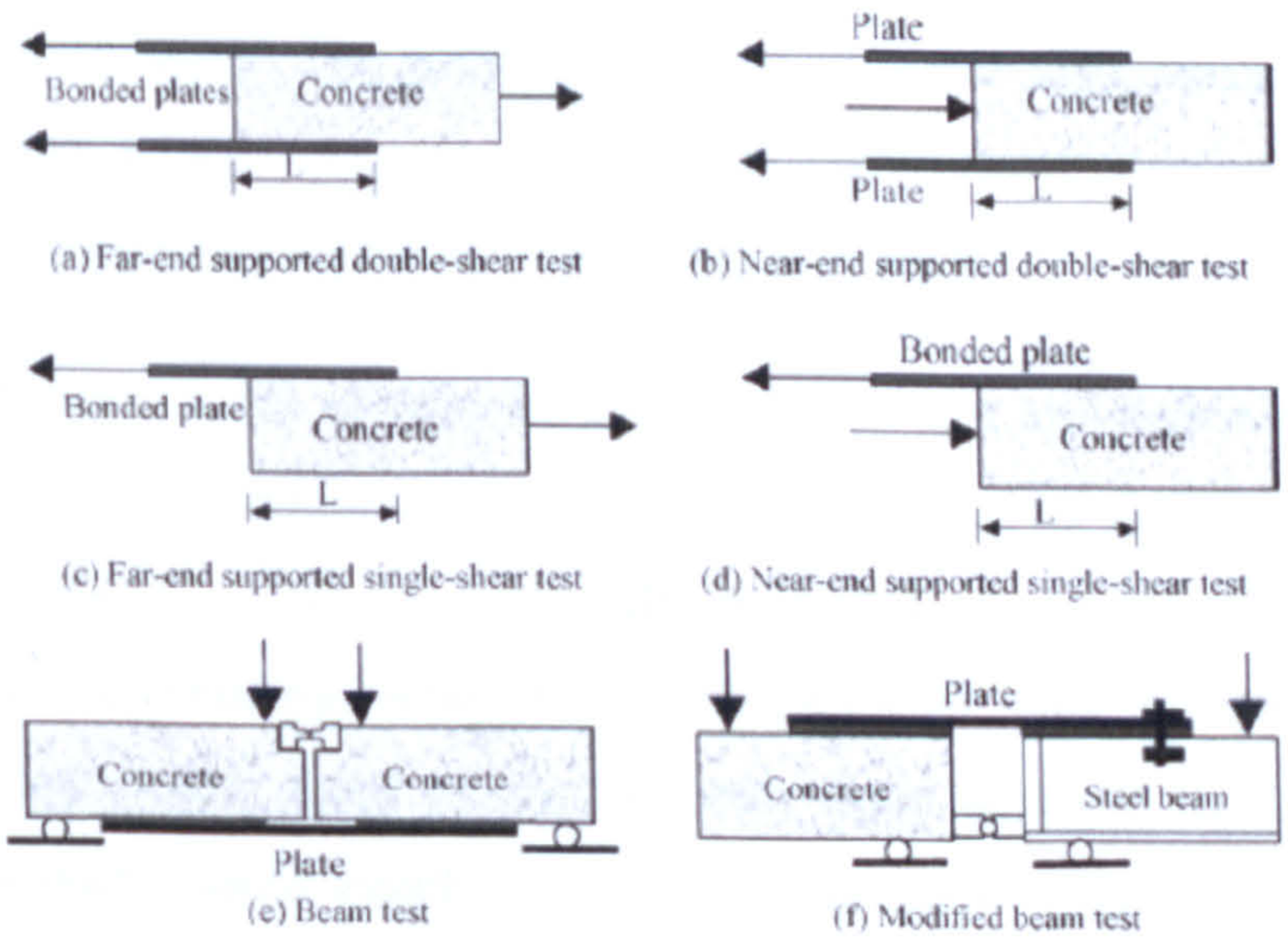

Figure II-1 Bond strength experimental set-up (Chen et al 2001)

The set-up developed for experiments type I in this study was based on the near-end supported single- shear test from the proposed bond strength tests (figure II-1d). To minimize the possible bending stresses at the end of plate the set-up was later modified.

2.2.2 Experimental work and numerical methods

Yao et al (2005) presented the experimental results from a near end supported single shear pull test. Seventy-two specimens strengthened with CFRP and GFRP were tested. The variables of the study included the bond length, the support height, the various FRP-to-concrete width ratios and the offset of the load (relative vertical displacement). The majority of the samples failed by debonding in concrete, small number failed due to concrete failure. One of the conclusions drawn from the experimental study was that samples with FRP-to-concrete width ratios close to 0 and 1 failed due to crack in the concrete.

The observed failure modes were described: debonding in concrete, failure in the adhesive-concrete layer and the concrete prism failure. The concrete prism failure initiated with a crack at the far end of the strip and then immediately to the end of the support. The load-displacement curves were also plotted, the displacement being measured at the end of the grip only, therefore reflecting only the global response. The curves from the specimens which failed by the adhesive-concrete interface showed a plateau before the failure which in turn increased with the bond length. The height of the free edge was also considered and the bond strengths with greater height were found to have lower bond strength which could be attributed to the concentration of stresses near the support edge.

Lu et al (2006) presented a FE method of the direct pull test simulation of crack model in which a non-coaxial rotating angle crack model was employed so that debonding failures of FRP-to-concrete interfaces could be accurately predicted. A model was proposed where debonding could be simulated by modelling the bonded joint without interface elements and where the debonding would occur in the concrete layer adjacent to the adhesive layer. Adopting such approach would avoid defining an interfacial bond-slip model which could only be verified by experimental data. The different methods of modeling of crack of concrete multi-directional fixed angle crack model, non-coaxial and coaxial rotating angle crack model (RACM) and orthogonal fixed angle crack model were described and compared in terms of

shear softening of the material. The latter method would be available in commercial FE programmes and was considered the simplest approach although it could lead to the so called shear stress locking problem. It was suggested that refinement of the mesh although this could require more computation time and effort.

Ferracuti et al (2006) proposed an improved model for the bond-slip law of the interface of bonded joints. In the proposed model of the FRP-concrete delamination problem the plate and concrete were considered to be subjected to axial deformation only, the bending stiffness of the FRP plate was found negligible compared to concrete. The transverse displacement between the plate and the concrete was not taken into account and therefore the peeling stresses due to the small bending stiffness of the plate compared to concrete were ignored.

In the model the slip was taken as the average displacement of the cross section of the concrete therefore the interface law would have to take into account the shearing deformation of the adhesive and the contributing layer of the concrete taken as 25 - 30mm. The interface law would then have to be highly non-linear and accurately expressed as the fracture energy of the interface would be determined by the area under the curve. The following equation based on Popovics-like law was adopted:

$$\tau_p = \bar{\tau}\frac{s_p}{\bar{s}}\frac{n}{(n-1)+(s_p/\bar{s})^n}$$

Equation II-1 Bond-slip law proposed by Ferracuti et al (2006)

where $(\bar{\tau}, \bar{s})$ were the peak shear stress and slip and n was a parameter governing the softening branch.

Mazzotti et al. (2008) carried out experimental work with eight RC samples where different bonded lengths (50, 100, 200 and 400mm) and widths (50 and 80mm) were tested. The samples were numerically modelled with non-linear interface law between the concrete and laminate proposed by Ferracuti (2006). Due to the geometry of the adopted set-up the authors observed a triangular piece of concrete breaking off early in the test when the CFRP plate was bonded close to the front side of the prism. To compensate the high tensile stresses a specified

distance was left between the front side and the adhesive. It was concluded that the effect of the width of the laminate would have significant influence on the interfacial shear stress law.

The following year Mazzotti et al (2009) proposed an experimental set-up designed to allow stable debonding process, where the back end of the concrete and laminate were fixed. The set-up allowed the collection of data for the softening branch of the shear stress-slip law and the data from the experiments were used to calculate the maximum transferred force and the fracture energy of the interface law. The non-linear shear stress-slip interface laws were also been calibrated with the results from the experiments.

The effect of two surface treatments was also reported by Mazzotti et al (2009): sand blasting and grinding and the experimental results revealed increase of the ultimate load of 15-20% when sand blasting was used compared to grinding.

Cho et al (2006) investigated the two types of joints between concrete and FRP to secure composite action of FRP-concrete composite deck. The coarse sand coated and epoxy coated samples were tested in pure shear. The authors investigate the bonded joint called coated joint. The coarse sand coated joints were treated through 3 processes: basic, intermediate and final coating. From the two types of coating the epoxy bonded adhesive joints showed slightly larger strains at failure and the coarse sand coating could increase the bond strength of the bonded joint by 12% when compared to epoxy coating.

2.3 Strengthening of RC beams with FRP plates

2.3.1 Failure modes- classifications

Research on FRP strengthening of RC beams has led to a significant number of various experimental samples, test set-ups, strengthening configuration and techniques. In order to develop relevant analytical solutions for these findings several classifications of the failure modes have been proposed. One example of such classification was one used by Thomsen et al (2004). The failure types of RC beams strengthened with FRP were divided into beams

exhibiting composite action up to failure and beams exhibiting loss of composite action at failure.

Smith and Teng (2002) presented a comprehensive classification of the different failure modes of RC beams strengthened with FRP plates. For the purpose of this study the following categorization was followed. The observed failure modes were described as:

(a) flexural failure by FRP rupture;

(b) flexural failure by crushing of compressive concrete;

(c) shear failure;

(d) concrete cover separation;

(e) plate end interfacial debonding;

(f) intermediate crack induced interfacial debonding.

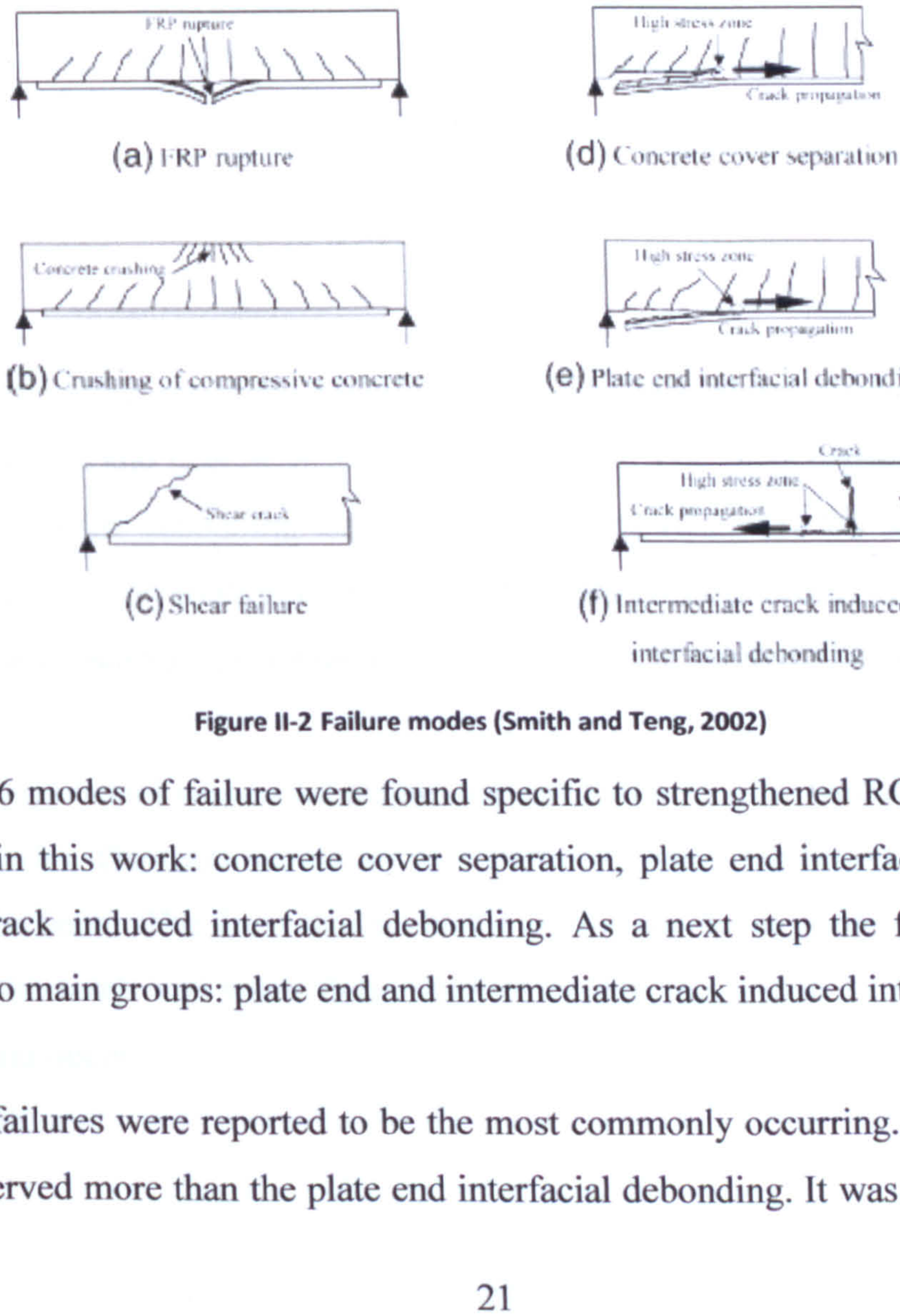

Figure II-2 Failure modes (Smith and Teng, 2002)

Three of these 6 modes of failure were found specific to strengthened RC beams and would be considered in this work: concrete cover separation, plate end interfacial debonding and intermediate crack induced interfacial debonding. As a next step the failure modes were classified in two main groups: plate end and intermediate crack induced interfacial debonding.

The plate end failures were reported to be the most commonly occurring. The concrete cover mode was observed more than the plate end interfacial debonding. It was noted that the same

mode of failure had been referred to elsewhere as "end-of- plate failure through concrete", "concrete rip-off failure", "debond at rebar layer", "concrete cover delamination", and "local shear failure". Alternatively, high concentration of normal and shear stresses at the end of the plate would lead to the initiation of the plate end interfacial debonding. Since the two modes were caused by the same factor, the existing debonding strength models did not differentiate between the two.

Concrete cover separation mode was described to initiate with the formation of a crack in the concrete near the plate end due to high concentration of interfacial shear and normal stresses. Once the crack developed and reached the reinforcement of the beam the crack would propagate horizontally at the level of the reinforcement thus causing the concrete cover to detach.

The plate end interfacial debonding would develop from the plate end along the interface of the FRP and concrete. The debonded laminate would often detach few millimeters of the concrete as well but for the sake of simplicity the failure was considered purely interfacial problem. The contribution of the adhesive layer would often be ignored when referring to the failure modes.

The existing debonding strength models were discussed: shear capacity based models, concrete tooth models and interfacial stress based models. The shear capacity models had been developed based on the debonding failure strength being related to the shear strength of the concrete with partial or no contribution of the steel shear reinforcement. The shear force acting at the plate end was taken as the debonding strength (with or without the moment).

The concrete tooth model was based on the concept that a "tooth" would be formed between two adjacent cracks. The tooth would act as a cantilever under the action of the shear stresses at the base of the beam. The shear stresses at the base of the beam would cause tensile stresses at the root of the tooth and when those stresses exceed the tensile strength of the concrete debonding would occur.

Interfacial stress based models used interfacial stresses and a concrete failure criterion. Model I used Mohr- Coulomb criterion, model II was derived for concrete cover separation based on ACI code.

Smith and Teng (2002) compared the different models and several conclusions were drawn for pultruded plates and wet lay-up method:

- Concrete cover separation occurred more than the plate end interfacial debonding.
- The models based on the shear capacity would yield better results.
- A simplified model based on the shear force was proposed by the authors.

Oehlers et al (2003) proposed a similar classification of the failure modes (see Figure II-3) with the exception of the so called critical diagonal crack (CDC). This particular case was defined for debonding induced by the relative displacement due to the action of the diagonal crack.

Summary of debonding mechanisms

Debonding types	Primary cause	Debonding crack propagation
IC: Intermediate crack	Axial strains in a plate bridging a crack induced by flexure cr flexure/shear	Debonding cracks initiate at the intercept of the plate with a flexural, flexural/shear or diagonal crack. Generally propagates towards the plate end.
CDC: Critical diagonal crack	Rigid body shear displacement across a critical diagonal crack	Debonding cracks initiate at the intercept of the plate with the critical diagonal crack. Propagates towards the plate end.
PE: plate end	Curvature in the beam adjacent to plate end	Debonding cracks initiate at the plate end. Propagates inwards.

Figure II-3 Debonding mechanism according to Oehlers et al (2003)

The plate end debonding mechanism was described to be governed by longitudinal force and moment in the laminate induced by the curvature of the beam, the transfer of the stresses to the beam would cause debonding of the laminate. The critical diagonal crack was also analysed and different solutions were proposed for the negative and positive section of the moment diagram of the beams.

Oehlers (2006) later compared the failure mechanisms in the existing codes and described the generic debonding mechanisms in terms of axial, flexural and shear deformations (see Figure

II-4). Pham and Al-Mahaidi (2004) reviewed the available models for failure mechanisms and maximum loads for beams strengthened with FRP. The main failure modes were described and comparison between ACI 440 and fib Bulletin 14 was presented. The beam theory was able to predict the full composite action of beams strengthened with FRP in which failure occurred with FRP rupture or concrete crushing. Limits for the FRP stress for midspan debonding and interfacial stresses for end debonding failure were proposed although the design would be conservative.

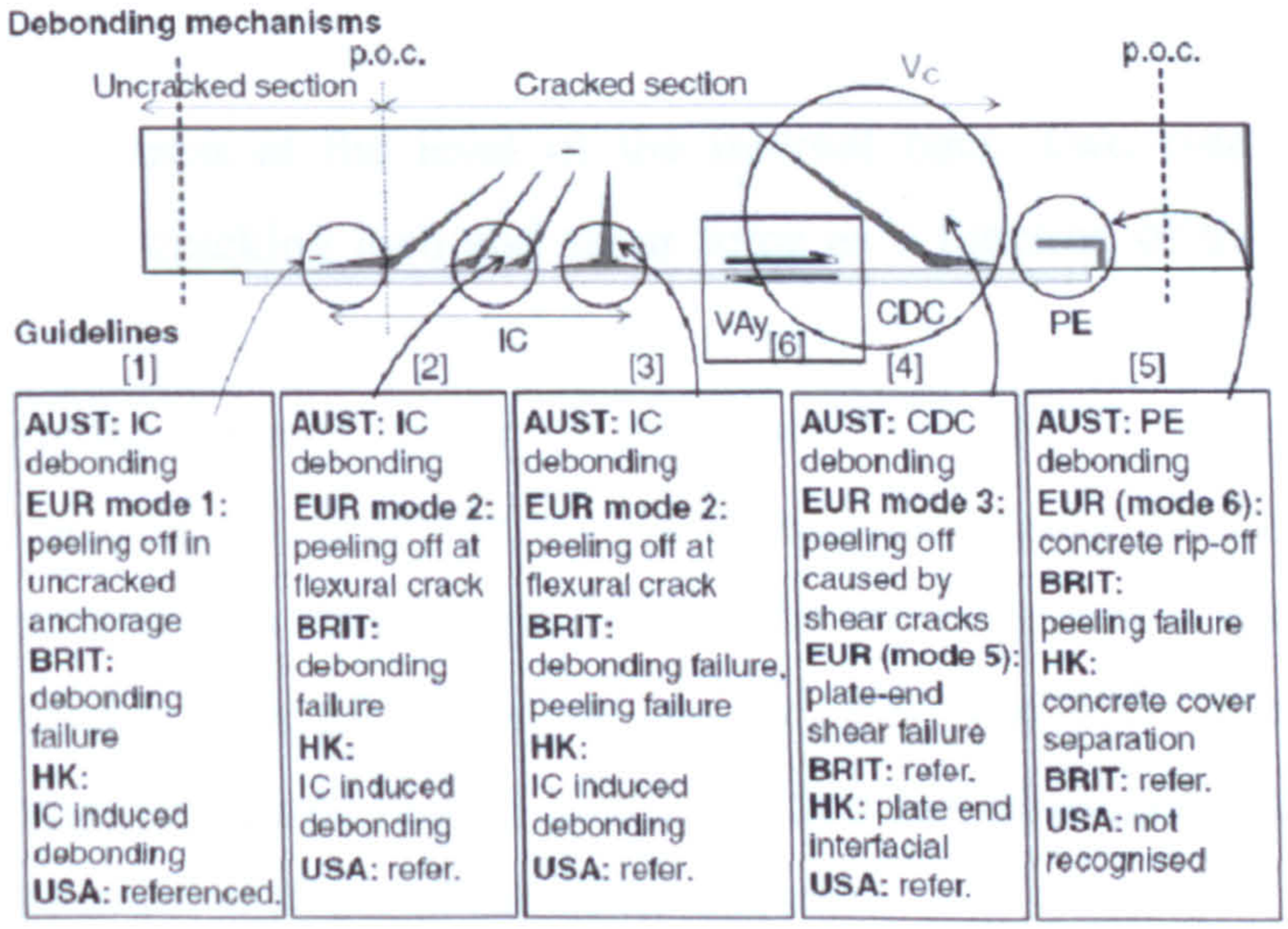

Figure II-4 Debonding mechanisms after Oehlers (2006)

2.3.2 Analytical solutions

2.3.2.1 Plate end debonding solutions

Hassanen and Raoof (2001) proposed a procedure for hand calculations to predict the failure loads of plated RC beams. The concrete cover separation mode was investigated as the common mode of failure for the strengthened beams. The authors considered interfacial failure a rare case, result of bad workmanship.

The theory on the failure of the strengthened system was based on the characteristics of a tooth formed between adjacent stabilized cracks in the concrete cover. A semi-empirical model was developed to estimate the magnitude of tensile (axial) stresses in the plate; the concrete tooth

could be treated as a cantilever bending under the tangential (shear) stresses, the failure occurred when the critical tensile stresses reached the tensile strength of concrete. Simplified models were proposed for the prediction of the depth of the neutral axis and then the plate peeling moment. To calculate the plate peeling moment two stress distributions for concrete were considered: parabolic and uniform. The results based on the peeling moment were found to be more accurate than those based on ultimate load for the two types of stress distribution.

Shear at the end of laminates and concrete cover delamination were considered as the main failure modes in the work of Ahmed et al (2001). They proposed a mathematical model based on a model for shear stress at the level of the internal bars. Two cracking criteria were proposed: flexural shear cracking load and shear force as a function of the flexural cracking moment at a section a_c. An analogous model was proposed by Jansze for beams strengthened by steel plates, where the unplated length was analogous to critical shear crack a_c. A fictitious shear span a_L was proposed to compute the shear resistance using Model Code 1990. The proposed model was based on shear stress in the adhesive layer which had two parts: shear stress due to the variation of bending moment and the stress due to the introduction of forces in the anchoring zones. Compared to steel plates, the first part of the shear stress was found to be smaller due to the lower stiffness of the CFRP laminate.

Maalej & Bian (2001) investigated the interfacial shear stress of CFRP sheets strengthened RC beams. Using the strain readings the shear stress was found by:

$$\tau(x) = t_p E_p d\varepsilon / dx$$

Equation II-2 Calculation of shear stress proposed by Maalej & Bian (2001)

and curve fitting function of the data and by relating the shear stress to the rata of change of strain:

$$\varepsilon(x, \Delta) = A(1 - e^{-Bx})$$

Equation II-3 Curve fitting function proposed by Maalej & Bian (2001)

where x is the distance from the end of the CFRP and Δ is the deflection of the beam at midspan, A and B were coefficients found from the experimental data. The results were compared with previous solutions where the internal shear stress distribution was expressed as a function of the properties of the materials, the specimen size and geometry and the applied load. The latter solution was found to be in close agreement with the test results.

Smith & Teng (2001) proposed a new model to calculate interfacial stresses in plated beams. The model was based on the deformation compatibility of the RC beam, adhesive and strengthening plate with the following assumptions: linear elastic behaviour for the 3 materials, deformations of the two adherends were assumed to be due to bending moments, axial and shear forces, while the stress in the adhesive was assumed to be the constant across its thickness.

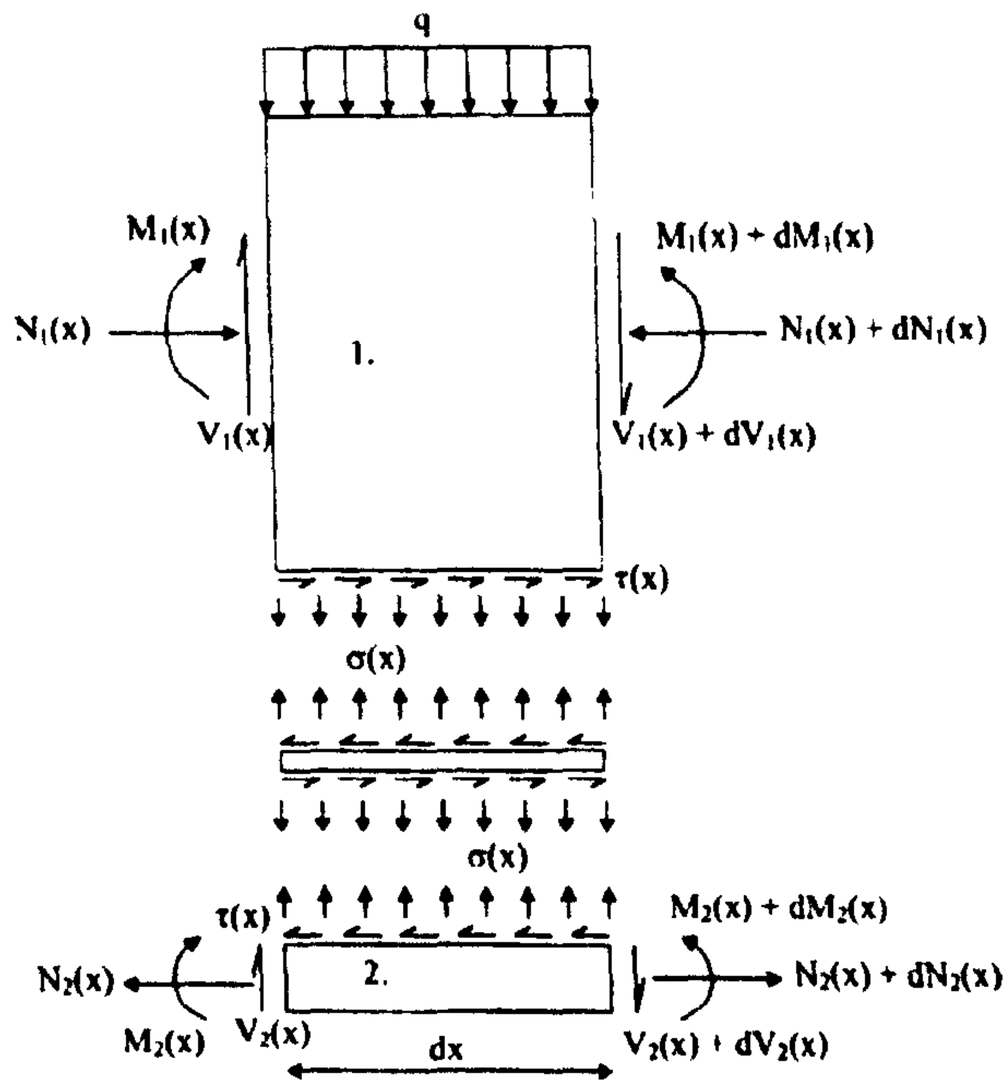

Fig. 2. Differential segment of a soffit-plated beam.

Figure II-5 Differential segment , Smith and Teng (2001)

The authors proposed the following governing equations for shear and normal stresses:

$$\frac{\mathrm{d}^2\tau(x)}{\mathrm{d}x^2} - \frac{G_a b_2}{t_a}\left(\frac{(y_1+y_2)(y_1+y_2+t_a)}{E_1I_1+E_2I_2} + \frac{1}{E_1A_1} + \frac{1}{E_2A_2}\right)\tau(x)$$

$$= -\frac{G_a}{t_a}\left(\frac{y_1+y_2}{E_1I_1+E_2I_2}\right)V_T(x) - \frac{G_a y_1 \mathrm{d}q}{t_a G_1 \alpha A_1 \mathrm{d}x} - \frac{G_a b_2}{\alpha t_a}\left(\frac{y_1}{G_1A_1} - \frac{y_2}{G_2A_2}\right)\frac{\mathrm{d}\sigma(x)}{\mathrm{d}x}$$

Equation II-4 Governing equations for shear stresses, Smith and Teng (2001)

$$\frac{d^4\sigma(x)}{dx^4}-\frac{E_a b_2}{\alpha t_a}\left(\frac{1}{G_1A_1}+\frac{1}{G_2A_2}\right)\frac{d^2\sigma(x)}{dx^2}+\frac{E_a b_2}{t_a}\left(\frac{1}{G_1E_1}+\frac{1}{G_2E_2}\right)\sigma(x)=$$

$$=-\frac{E_a b_2}{t_a}\left(\frac{y_1}{E_1I_1}+\frac{y_2}{E_2I_2}\right)\frac{d\tau(x)}{dx}-\frac{E_a}{t_a}\frac{1}{E_1I_1}q+\frac{E_a}{t_a}\frac{1}{G_1\alpha A_1}\frac{d^2q}{dx^2}$$

Equation II-5 Governing equations for normal stresses, Smith and Teng (2001)

where G_a is the shear modulus of the adhesive, t_a is the thickness of the adhesive, E is the elastic modulus, b_2 is the width of the plate , A is the cross-sectional area , I is the second moment of area , α is the effective shear area multiplier , y_1, y_2 are the respective distances from the bottom and top of the respective adherends to their centroids. The solution for uniformly distributed load, a single point load and two point load were also given.

The solution of governing equations for the normal and shear stresses was found difficult to be developed and as a simplification the shear deformation of the adherends had to be ignored. The presented analytical model by Smith and Teng (2001) was found to be an accurate and widely applicable method for interfacial shear and normal stresses in RC plated beams. In the recent years few modifications have been proposed concerning the shear deformation of the adherends.

Pesic´& Pilakoutas (2003) adopted the analytical model proposed by Smith and Teng (2001) for a plated RC beams subjected to two point loads for the stress concentration at the plate end. At the critical section the principal stress was calculated based on the bi-axial state of tension of the concrete due to a combination of bending stresses, shear and peeling stresses from the transfer of the force from the laminate to the concrete. A linear elastic finite element analysis was performed and the results from the analytical and FE solution were compared with existing data on plate end debonding experiments. The authors found a large scatter of the results and concluded that the flexural and shear cracks would have a significant influence on the results.

Leung (2006) investigated the effect of cracking on stresses near the plate end. The initiation of cracking at the plate end was caused by high concentration of local stresses. As the beams

were over-reinforced with stirrups the shear cracking was not assumed to be the direct cause of the failure. It was found that with increase of load the interfacial stress near the plate end would be reduced, which could be explained by the formation of a crack. A crack at the plate end would cause unloading of longitudinal tension in the concrete and the transfer to the concrete would become much more gradual. The experimental results suggested that once cracking would occur the elastic analysis for the shear stress distribution would no longer be applicable. A numerical model was also performed without and with a discrete crack to study the effect on the shear and normal stresses.

Tounsi (2006) proposed a method for the calculation of the interfacial stresses in a concrete beam based on Smith and Teng's solution. The proposed solution included the shear deformation of the adherends assuming linear shear distribution through the thickness of the adherends. Tounsi and Benyoucef (2007) proposed a solution with variable orientation of the fibres. Tounsi et al (2009) published another solution where a different effect of adherend shear deformation was considered. In this paper the shear deformation was assumed parabolic through the thickness of both the beam and the plate.

Yang and Wu (2007) presented another solution based on the shear deformations of both the beam and the plate as an improvement of Smith and Teng's (2001) solution. The superposition principle and Galerkin's method were used for the addition to the original solution. The authors found the formulae proposed by Smith and Teng (2001) to yield results with sufficient accuracy although they could overestimate the shear stresses. The solutions of the shear deformations was recommended for RC beams strengthened by plates when a thin adhesive layer was used, the adhesive had high Young's modulus and when the length-to-depth ratio was low.

Yang and Ye (2010) proposed an improved closed-form solution to interfacial stresses in plated beams using a two-stage approach. A closed-form solution of interfacial stresses was developed which could accurately predict the transverse normal stresses in the 2 interfaces (adhesive-beam and plate-adhesive). Sub-layers were introduced which could allow the analysis of beams with different cross-sections and multilayer materials. Uniform shear stress was assumed over the thickness of the adhesive, which would mean that the layer does not

carry any longitudinal normal stresses. The adhesive was assumed to be in plane stress state. Numerical examples were also discussed and it was found that the reinforcement is important in the model as it could reduce the peak value of the interfacial stresses.

2.3.2.2 Intermediate crack debonding solutions

Yuan et al (2004) published the analytical solutions of the entire debonding propagation process of FRP-to- concrete bonded joints. The model was based on the assumptions that the two adherends were subjected to axial deformations and the adhesive layer subjected to shear deformations. The adhesive together with a thin layer of concrete were assumed to be the interfacial element between the two adherends.

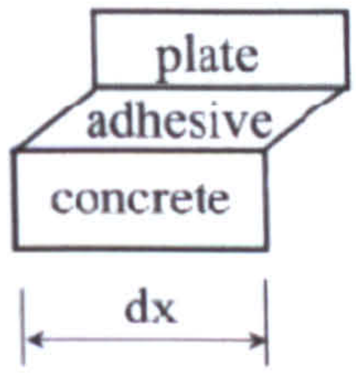

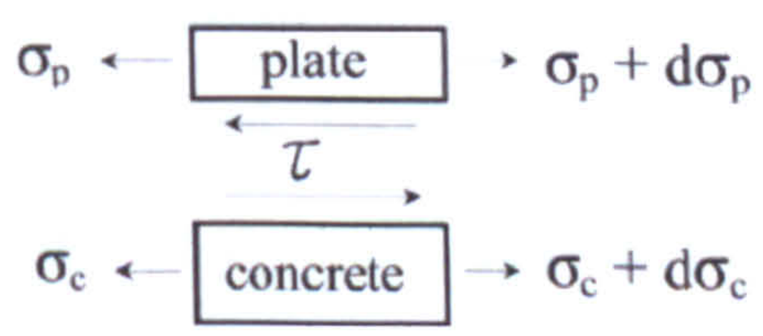

Figure II-6 Deformation and equilibrium of a bonded joint, Yuan et al (2004)

The governing differential equation was expressed as follows:

$$\frac{\mathrm{d}^2\delta}{\mathrm{d}x^2} - \frac{2G_f}{\tau_f^2}\lambda^2 f(\delta) = 0$$

Equation II-5 Governing differential equation for shear stresses, Yuan et al (2004)

and

$$\sigma_p = \frac{\tau_f^2}{2G_f t_p \lambda^2}\frac{\mathrm{d}\delta}{\mathrm{d}x}$$

Equation II-6 Governing differential equation for normal stresses, Yuan et al (2004)

where

$$\lambda^2 = \frac{\tau_f^2}{2G_f}\left(\frac{1}{E_p t_p} + \frac{b_p}{b_c E_c t_c}\right)$$

Equation II-7

where δ is the relative displacement between the two adherends, τ_f is the local bond strength, G_f is the interfacial fracture energy, σ_p is the axial stress in the concrete, E is Young's modulus of the plate or the concrete, t is the thickness of the plate or the concrete, b is the width of the concrete.

The governing equation could therefore be solved if the local interfacial shear stress to the local shear slip referred to as the bond-slip relationship was known. The authors introduced interfacial fracture energy which would be equal to the area under the bond-slip curve in the equation as it would not depend on the shape of the bond-slip curve.

Yuan et al (2004) adopted a bilinear bond-slip model as experimental results suggested would yield good approximation of the real behaviour. The bilinear model would consist of 2 linear branches: the ascending one would indicate the linear increase of the slip until a maximum value τ_f of interfacial stress was reached. Then the descending branch would represent the interfacial softening associated with the formation of micro-cracks. When a given value δ_f of the slip was reached micro cracks would be developed which would indicate shear fracture between the two adherends.

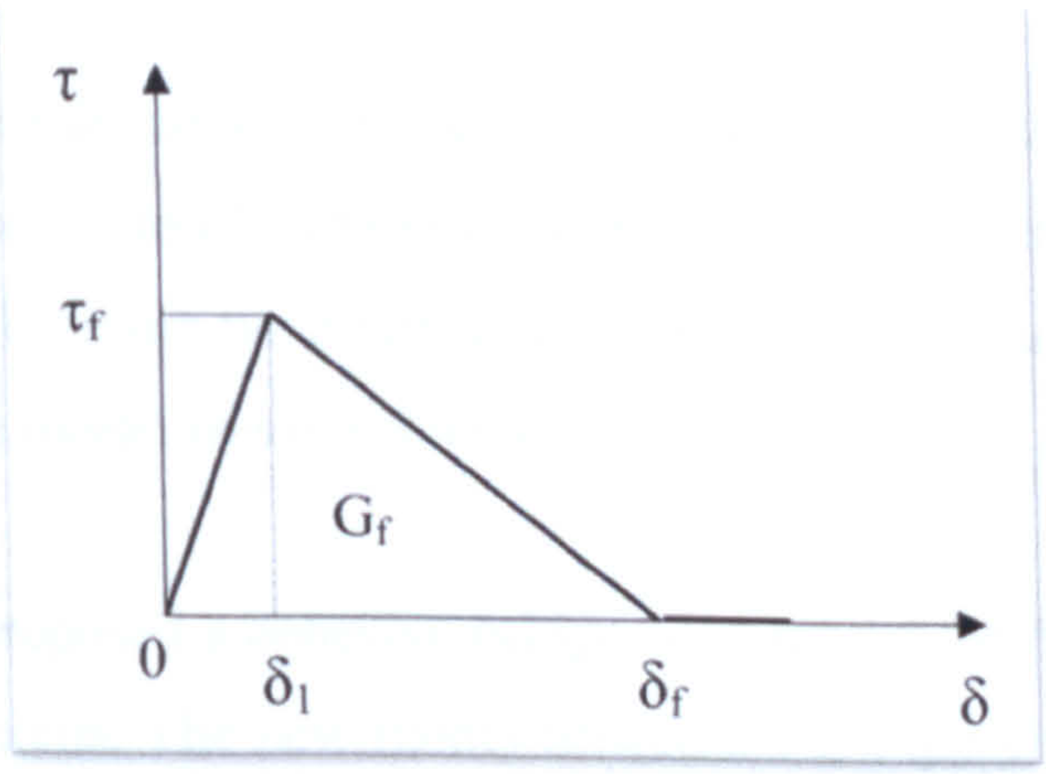

Figure II-7 Local bond-slip model (Yuan et al, 2004)

Four stages were then identified in the propagation of the fracture between the concrete and the plate:

- Elastic stage where the interface would be in an elastic stress state;
- Elastic- softening stage where part of the of the interface would be in the softening state, part in elastic state;
- Elastic-softening- debonding stage where debonding would begin and the peak shear value would move towards the unloaded end of the plate, therefore observing 3 existing stages of the stress state: debonding, softening and elastic;
- Softening- debonding stage where the unloaded end would reach the peak shear value and then would be followed by reduction of the stresses with the load.

Wang (2006) published a study adopting the model proposed by Yuan et al (2004). A FRP strengthened RC beam was analysed as 2 beam elements bonded through the adhesive layer modelled as a fracture processing zone. The debonding process was described in 5 steps and closed- form solutions of interfacial shear and normal stresses were developed: from flexural cracking to complete debonding expressed as:

- Elastic- elastic;
- Elastic- softening- elastic;
- Elastic- softening- softening- elastic;
- Elastic- softening- debonding- softening- elastic;
- Softening- debonding- softening- elastic.

Three bond-slip laws were discussed: bi-linear, triangular and linear-damaging laws, the last two of which were considered a simplification of the bi-linear model. A non-linear relationship such as the bi-linear bond-slip relationship would be a material property of the interface if cohesive zone model was considered.

In 2007 Wang (2007a) proposed a cohesive-bridge zone model for the interface debonding of FRP strengthened RC beams. The new model reflected the experimental observations of the two different failure stage of the debonding- crack processing and particle bridging stage

followed by the complete separation of the surfaces. The author proposed closed-form solutions of the interfacial stress for each stage and verified experimentally.

Ferracuti et al (2007) proposed a new a non-linear shear stress-slip constitutive law for FRP-concrete interface based on Popovics's like formulae; the law included the contribution of the adhesive and concrete cover which was taken as 25- 30mm from the surface. The authors analysed the maximum transmissible load which strongly depended on the softening branch of the law which could then be used to calculate the fracture energy of the interface law. A procedure was proposed to obtain the maximum shear stress, slip and parameter n based on the experimental results.

Qiao and Chen (2008) proposed a bi-material beam theory for beams strengthened with plates. The model included the contribution of interface stresses on the deformation of the adherends and the different rotation of the adherends. Both normal and shear interface stresses were calculated using a closed form solution. The proposed model was applicable for different load cases.

Lu et al (2005) investigated bond–slip models for FRP sheets/plates bonded to concrete. A model of an interface element was developed based on the adhesive and a thin layer of concrete. Two methods were used to describe the bond-slip law: with closely spaced strain gauges on the laminate or load-displacement curves. The authors reviewed the existing bond-slip models and presented three new models. The latter were based on results from FE model which excluded the measurement of the strain of the FRP laminate. From the reviewed models six factors were found to have influence on the bond-slip behaviour: the concrete strength, the bond length, the plate stiffness, the width of the laminate compared to the width of the concrete specimen, the adhesive stiffness and its strength. To find the interfacial fracture energy the ultimate load had to be obtained and a simple model with link and spring elements connected to a rigid base was developed to represent the bond-slip behaviour. The elastic modulus, tensile strength and compressive strength of the concrete where expressed by the cube compressive strength. As a conclusion it was suggested that to accurately model the bond-slip behaviour the ascending and descending branches should be curved but as an approximation a bilinear model could also be adopted.

Teng et al (2006) investigated the behaviour of the FRP-to- concrete interface between two adjacent cracks analytically. Bi-linear local bond-slip model was used. The five possible processes were solved: elastic stage, elastic-softening stage, elastic-softening-debonding stage, softening-debonding stage and softening stage. The bond length and a load parameter were found to be key factors for the failure processes.

Recently, Chen and Qiao (2009) studied the debonding analysis of FRP–concrete interface between two balanced adjacent flexural cracks in plated beams. The intermediate multi crack-induced debonding was described as a second type of IC debonding. In the study the cracks were modelled by rotational springs. Nonlinear bond-slip law was adopted for the interface whilst the concrete and FRP were modelled as linear elastic beams. The normal stresses were neglected and the IC debonding was analysed as a mode II fracture. The authors also discussed the effect of the thickness of the adhesive on the relative longitudinal displacement between the concrete and FRP. Three different failure stages were obtained: linear elastic range, elastic-softening stage and elastic-softening-debonding stage. The interface shear stress and debonding growth were analysed and the propagation of the debonding with increase of the load was discussed in detail.

2.3.2.3 Fracture mechanics approach to failure of RC strengthened beams

The debonding of FRP strengthened systems is by nature an interface fracture problem (Au & Buyukozturk, 2003) and many researchers have adopted the fracture mechanics approaches to study the mechanisms in which the system fails. In order for fracture to occur, the released energy should be greater than the total amount of energy dissipated during debonding which includes the work of separation and the other dissipation mechanisms over the debonding area. For the interface fracture to occur at steady state the amount of energy dissipated should be equal to the change in elastic strain energy of the system due to cracking. Au & Buyukozturk (2003) analysed a FRP strengthened beam as a tri-layer system in which the thickness of the adhesive was considered as an important factor and included in the model. The work defined five possible fracture scenarios:

- FRP-adhesive interface separation;
- Adhesive- concrete interface separation;
- FRP delamination;
- Adhesive decohesion;
- Concrete delamination.

For each case a general solution was derived to compute the total interface fracture energy release rate (ERR) for the corresponding debonding mode. To verify the solutions the authors conducted a numerical study to find the ERR by calculating the stress intensities for the open and shear modes of fracture. A parametric study of the effect of the adhesive thickness and elastic mismatch of the different materials was also conducted. It suggested that a thin layer would be beneficial for the case of high elastic mismatch but to minimise the debonding driving force a thicker layer would be appropriate.

Neto et al (2004) analysed shear tests of a single joint and evaluated the influence of mode II on CFRP strengthened concrete. The material properties which characterized the interface- the shear stiffness, the cohesion and mode II fracture energy of concrete were studied. It was found that the shear stiffness of the interface was only important in the elastic domain, the cohesion had a significant effect on the strain diagram and that for a constant value of the cohesion the ultimate load depended on the fracture energy of the concrete.

The existing stress-based failure criterion were found to be less effective for crack initiation and propagation where brittle failure modes were observed and therefore researchers focused on fracture mechanics based approaches. Rabinovitch (2004) proposed a new failure criterion based on ERR for interfacial delamination. The evaluation of the ERR was achieved by the application of the virtual crack extension method. To evaluate the potential energy of the system, the internal strain energy and external tractions were determined, which did not require the stress state near the crack front to be exactly predicted. This allowed for simplified models for the stress analysis of the system to be used. The models included high-order model, elastic foundation models with 1 and 2 parameters, equivalent beam model and FE analysis. The proposed approach of evaluation of ERR was found to produce good results without the requirement for accurate values of the stress concentration at the crack tip whilst the FE

analysis revealed mesh sensitivity of the total potential energy of the system and a comparison with an analytical method was recommended.

Two main fracture mechanics approaches have become popular when debonding of FRP strengthened systems is investigated: cohesive zone modelling (CZM) and linear elastic fracture mechanics (LEFM). The CZM approach introduces an interface surface where the debonding will occur adopting a traction-separation law allowing perfect bonding to complete separation of the interface (Rabinovitch, 2008). Both normal and tangential stresses and displacements can be simulated. As the separation increases the stresses increase, reach a maximum and then decrease to zero. On the other hand, the LEFM approach uses both stress analysis and fracture analysis to predict the crack propagation. The model assumes a given crack length and then estimates the elastic ERR. Then the ERR is compared to the fracture energy of the interface or material to evaluate the growth of the crack. The LEFM allows different the stress and fracture analyses to be adopted.

Rabinovitch (2008) compared the two approaches for interfacial failure. The advantages of the CZM were the automatic initiation and propagation of the crack, whilst the LEFM would require less computational effort and small number of parameters. The main disadvantage of the CZM was found to be the computational effort to solve the nonlinear model and the calibration of the traction-separation law depended on several parameters. The application of the LEFM depended on the correct description of the debonding physical pattern.

The CZM approach was adopted by Wang (2006) in a study of an IC induced debonding of FRP strengthened RC beams adopting bi-linear bond-slip law, which shape was found little effect on the ultimate load of the FRP plated beam. The following year (Wang, 2007) an improved cohesive-bridging zone model of FRP- concrete debonding was developed and a method to calculate the bond-slip law based on the pulling force and axial displacement of the FRP plate was proposed. In another study Wang (2007b) proposed CZM for debonding under mixed mode loading which would be the case of combined pulling/peeling effect.

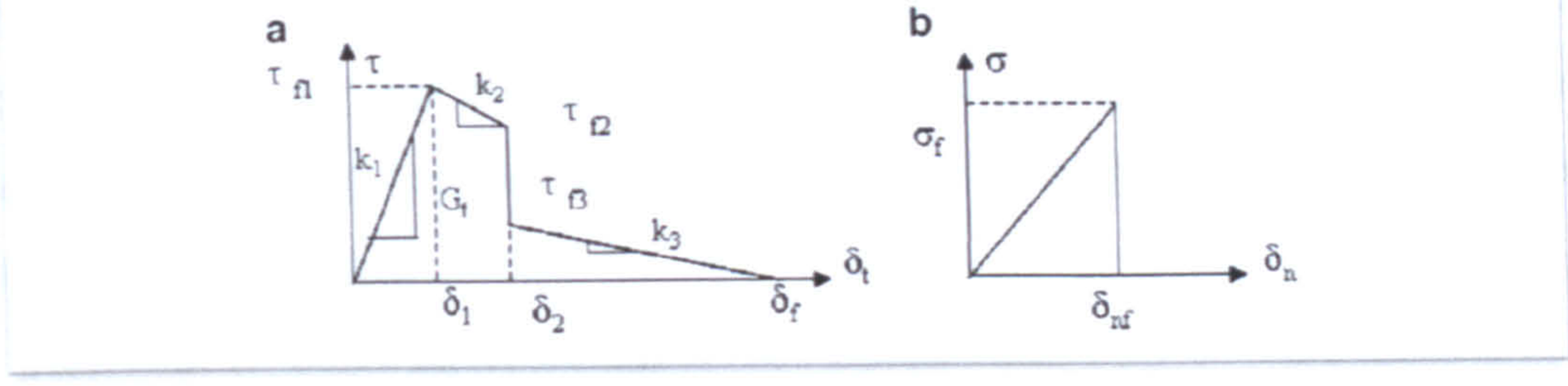

Figure II-8 Traction-separation models (Wang 2007b): a) shear and b) normal traction-separation laws

Wang and Zhang (2008) studied flexural-shear crack induced debonding adopting nonlinear fracture mechanics approach. The numerical study showed that the peeling effect of the debonding reduced with the debonding progression and the mixed mode would turn into mode II.

A global fracture model was proposed by Gunes et al. (2009). They considered the geometry of the beam, the strengthening configuration and the effect of the additional anchorage. The energy dissipation of the system was expressed as plastic energy dissipation due to reinforcement yielding and FRP debonding.

De Lorenzis and Zavarise (2009) proposed a simple analytical solution for the interfacial stresses between a beam working in bending and a thin plate adopting CZM. Only the interfacial shear stresses were taken into consideration to simplify the analysis as the bending stiffness of the beam was greater than the plate and therefore the bending moment and normal stresses could be neglected. The shear cohesive law was taken as bilinear as it could present the fracture energy, the cohesive strength and linear elastic properties with elastic, softening and debonding branches.

Qiao and Chen (2008) conducted experiments with beams under three- point bending to investigate mode I of FRP- concrete bonded interfaces. Two analytical damage models were used: interface cohesive process and concrete tensile plastic damage model. A transition in the failure modes between the interface debonding to concrete cohesive cracking was found by numerical modelling which depended on several interface parameters the interface cohesive strength, concrete tensile strength and the fracture energy of the interface and the concrete.

Carpinteri et al (2009) investigated the edge debonding failure of FRP strip strengthened beams. An equivalent beam model and the shear lag model were reviewed. In the shear lag model the adhesive layer was considered to act as a shear lag. LEFM failure criterion was applied as the relationship between the SERR and the stress field was proven and expressed analytically for the first time.

Greco et al (2007) investigated debonding problems in beams strengthened using composite plates based on a multilayer plate theory where Langrangian multipliers were used for the compatibility of plate elements. The debonding process was analysed adopting the fracture mechanics approach by evaluation of the energy release rate. The beam was presented as one mathematical layer and the adhesive and the plate were represented as another, each of which was described using the first-order shear deformation laminate theory.

FRP reinforced concrete beams were analysed to predict their loading capacity and fracture resistance (Wu and Ye, 2003). Fracture process zone has been adopted for the Mode I fictitious crack propagation. Numerical results of the model were also obtained.

2.4 Effect of elevated temperatures

2.4.1 Effect of elevated temperature on concrete

The effect of elevated temperatures and fire on the mechanical properties of concrete is influenced mainly by the type of cement and aggregate, water content, rate of heating and loading conditions. In this study Portland cement concrete is tested and analysed and a brief overview of the temperature effects is presented.

When concrete is exposed to elevated temperatures the free water evaporates (Bazant and Kaplan, 1996) and at further increase of the heating chemically bound water is released. The pore structure in the concrete changes and the aggregate also loses the evaporable water. At 600°C siliceous aggregates containing quartz experience crystalline transformation. Above 1000°C melting of the concrete begins.

The mechanical properties of the concrete are affected by temperatures. The design compressive strength is reduced above 350°C while the modulus of elasticity is reduced above 150°C (Buchanan, 2001). Values for the stress-strain relationships for different temperatures are given in BS EN 1992-1-2:2004. A mathematical model for stress-strain relationships of concrete under compression at different temperatures is also given. For siliceous aggregate concrete Buchanan (2001) gives approximate thermal elongation which includes shrinkage effects as:

$$\Delta L / L = 18 \times 10^{-6} Tc$$

Equation II-8 Thermal elongation for siliceous aggregate concrete (Buchanan, 2001)

where *Tc* is the temperature of the concrete.

2.4.2 Effect of elevated temperature on polymers

Cadei et al (2004) reported on the application of externally bonded FRPs to steel structures. They reviewed the existing techniques and FRP materials and the effect of heating. It was found that up to a certain temperature a positive effect for post-cure of composite and adhesive could be expected. Due to their polymeric nature the adhesives used for strengthening exhibited properties typical for polymers (Mays and Hutchinson, 1992). The thermal properties of polymers were mainly defined by two temperatures:

- glass transition temperature (T_g) - where the composite begins to soften and exhibits rubber-like behaviour;
- decomposition temperature (T_d).

Three different systems were tested: carbon/epoxy, glass/epoxy, carbon/epoxy (second supplier) by Foster et al (2005) in five different series of tests. The aim was to investigate the residual properties of FRP coupons, single-lap bond (FRP-FRP), pull apart of FRP-concrete bond and perform thermogravimetric analysis (TGA) on FRP and differential scanning calorimetry (DSC) to determine T_g. The samples were heated to temperatures between 100°C and 400°C with 3h maintained constant temperature. The results from TGA showed that since fibres appeared to be relatively insensitive to temperatures up to 600°C the unidirectional

coupons should experience only minor reduction in strength above 350°C. Change of colour for the specimen started at 200°C which was caused by the thermal decomposion of the epoxy. At 400°C the epoxy was burned off leaving a brittle black char. Stress-strain curves were proposed that presented both glass and carbon FRP reduction in strength and modulus above 400°C.

Karadeniz et al (2007) investigated different equations for determining of the coefficient of thermal expansion of fibre reinforced polymers α in longitudinal and transverse direction. The best agreement with experimental results were obtained from the values calculated from the equations of Schapery and Van Fo Fy, expressed by the elastic moduli, the Poisson's ratios and volume fractions of the fibres and the matrix. Typical value from manufacturer for carbon/epoxy polymers of the longitudinal expansion was given as $0\times10^{-6}/°C$.

Fire tests of GRP plates were carried out by Gardiner et al (2004) above kerosene fuel fire for various times up to 10 min. The temp range did not exceed 350°C measured on the surface of the plate. Ignition occurred 30s after the exposure. The damage consisted of charring of the polyester matrix and delamination cracks. The latter developed in the burnt section near the char layer and were probably formed by built-up pressure from volatile gases or by thermally induced strains due to the thermal gradient through the plate. Post-fire response was then tested and it was concluded that there was a significant reduction to the flexural and compressive strength and flexural rigidity. The mechanical properties of the post-fire material could be accurately calculated by using the rule-of-mixtures formulation as the burnt cross-section was presented as bi-layered.

Temperatures of 525, 650, 750 and 850°C were reached in the tests of Mouritz et al (2004). Composite panel 120x240mm was placed horizontally to the electric radiant heat source in a cone calorimeter and exposed to heat flux. The fire exposure lowered the properties of the composite. The composites with a polyester, vinyl ester or epoxy were almost completely degraded to volatiles. The phenolic matrix composites yielded higher amount of char due to the high aromatic content of the resin. The char layer was found constant through the material. Its strength was negligible to the composite strength and stiffness. The results showed good agreement with the proposed post-fire method based on the rule of mixtures analysis.

Another investigation of samples exposed to fire conditions was conducted by Keller et al (2005). Two types of experiments were carried out: for charring and for liquid cooling. The specimens cut from pultruded bridge deck panel were placed over a furnace and thermally loaded to an ISO 834 temperature curve. The charring experiments were burnt and then removed after 15, 30, 45 and 60min of exposure. The liquid cooling specimens were subjected to burning after a desirable water flow rate was circulating through the cell for 90 and then 120min.

The results from the first type of tests initially showed change of the colour from brownish to black char after 5min of exposure, then 1min later flames appeared. Two minutes later smoke and flames were observed on the hot face of the sample (the resin started decomposing). The fuel created by the decomposition lasted for 2min, after which it continued to deeper level. The fibre near the surface became white and visible. After 58min of heating the first mat was broken.

The results from the second experiments showed hot faces of the specimens in a far more damaged state. The reinforcing fibres were foam-like chars and large amounts of the fibre remains were found on the furnace bottom. The effects of the liquid cooling system and flow rates were discussed and it was concluded that the model provides better fire resistance.

Wong et al (2004) investigated the compression strength of glass reinforced plastics in C-shaped channel at different elevated temperatures. Two series of tests were conducted: first group of 30mm long specimens to obtain data on the longitudinal compressive strength of the material and the second consisted of 400mm long columns to study column behaviour.

The results from the first and second test were conducted at different ambient elevated temperature: 20, 60, 90, 120, 150, 200 and 250°C. The modes of failure depended on the temperature- up to 90°C the specimens crushed near the mid-length and at higher temperature the crushing was due to softening of the resin. The colour of the specimen changed from grey to brownish grey at 250°C. The brown substrate was identified as carbon which indicated that decomposition was about to start.

The failure mode at lower elevated temperatures was a result from large local buckling deformation causing large tension stresses at the junctions between web and flanges. Higher

temperatures resulted in a failure mode which was a combination of local crushing, local buckling and bending.

A numerical modeling was conducted using ABAQUS, the specimens were assumed to have the properties of an orthotropic material. Two steps of investigation were taken- eigenvalue analysis and load-deflection analysis. The model was moderately accurate to 200°C after which it overestimated the experimental values.

The effect of fire on FRP reinforced concrete members was described by Saafi (2002). Internal reinforcement with FRP rebars was investigated and as a result a cubic equation was suggested for the temperature distribution in a rectangular beam, the nominal flexural capacity at elevated temperatures and an equation for the nominal shear capacity. Based on the test results the temperature profile at the level of the reinforcement were presented when samples were exposed to fire from which it was concluded that the minimum concrete cover for FRP rebars should be 64mm (for steel it is 30mm).

To illustrate the effect of thermal residual stresses on the strength and time to failure of composite materials under fire representative loading conditions, a simple case study was performed for various loading conditions (Key and Lua, 2006). The used model was a simply supported square plate with applied mechanical and combined thermal-mechanical loading conditions. The mechanical loading condition was a linearly increasing pressure over a small region in the center of the plate, while the temperature gradient for the thermal- mechanical loading condition was applied from the bottom surface of the plate.

The fire distribution was simulated by time-dependent temp distribution through the thickness of the composite plate. The temperature distribution was determined from a 1-D heat diffusion equation. The final finite element model of the quarter plate consisted of 8-noded brick elements. The plate was modelled with 8 elements through the thickness in order to accurately capture the specified temp distribution and also provide the necessary one element per lamina discretization.

Although the model did not take into account any temperature-dependent material properties or strengths, a noticeable amount of structural softening was still observed. The softening was therefore entirely to an increased level of matrix failure in the structure. The increase in matrix failure was a consequence of the large thermal residual stresses that were present in the matrix

constituent. These constituent level stresses would be masked in a typical composite material analysis where only homogenized composite material properties were used.

Keller et al (2006 a, b) and Bai et al (2008) summarized the work of an investigation which aimed to model the thermal and mechanical behaviour of the liquid- cooled and non-cooled GFRP slabs during the 120 min exposure to an ISO 834 fire from the underside of cellular slabs. An approach was developed which aimed at determination of the residual mechanical properties of fire damaged glass-reinforced polyester, vinylester and phenolic composites. The approach included the discretization of the material into two layers; a fully degraded region that was simplified as having little or no residual mechanical properties, and an unaffected region that was simplified as having the same properties as before the fire exposure.
An empirical correlation was expressed between the depth of the fully degraded char layer, the duration of exposure and the time at that charring first occurred. The depth was later measured by pulse-echo instrument and a percentage remaining resin content criterion. It stipulated that the regions with less than 80% of the resin content were considered within the degraded region. Empirical data showed that the stiffness of the char region was 8% of the pre-fire level in tension and 0% in compression. Large-scale experiments however were not carried out.

The experiments for the study showed linear load-deflection curves up to the maximum load. The post-fire experiments showed 40% reduction in bending stiffness. To predict the remaining slab bending stiffness the lost thickness of the lower fire-exposed face sheets was calculated using two different models-a two-layer and three-layer model.

The hot face of the specimen was represented by convective and radiation heat transfer boundary conditions. Radiation was approximated as emitting from a black- body ambient cloud rather than from the interior surfaces of the oven. Though the air was essentially transparent to radiation, many combustion products including carbon monoxide/dioxide and soot had high emissivity.

Other effects and combinations were subject to various experimental works. It was reported that the combination of moisture and sustained load at elevated temperatures caused a significant decrease in the ultimate tensile strength of E-glass/ vinyl-ester composite materials. Water that diffused into the composite could end up either in the matrix or at the interphase region. In the matrix water would act as a plasticizer, increasing free volume, lowering T_g and

relieving the internal stress that was built up during processing of the composite. In turn the modulus may become lower as the matrix became pliable due to the presence of the plasticizer (Abdel-Magid, 2005). Almusallam (2006) described the long-term durability performance of GFRP strengthened beams for both hot-dry and wet-dry climates (salt water, alkaline water, normal water and indirect exposure to sunlight). It was observed that the U shape of the wrapping worked effectively in preventing the debonding of GFRP sheets (50 mm on the sides).

Wang and Kodur (2005) used GFRP and CFRP reinforcing bars as internal reinforcement to test the tensile strength as a function of elevated temperatures and critical temperature for GFRP was found to be 325°C and 205°C for CFRP. Information of the variation of the tensile strength and E modulus of FRP bars with temperature was collected. It was concluded that the critical temperature of the reinforcement had significant effect on the fire resistance of the RC members and that fire resistance of 25-35% from the alternative steel bar reinforcement could be expected.

Abbasi and Hogg (2005a) developed a model to predict the lifetime of beams internally reinforced with GFR plastic rebar. It was based on the calculations for flexural capacity and shear capacity of beams where time and temperature-dependent values for rebar modulus and strength and concrete strength replace the static design values. The results were successful for conventional steel reinforced beams but for composite ones it was not efficient.

A general method of predicting the properties of the constituents in a FRP reinforced beam during fire exposure was described (Abbasi and Hogg, 2005b). Two approaches were used – semi-empirical and finite element method and the results were compared. It was found that the semi-empirical was more accurate than the FE.

Abbasi and Hogg (2006) then carried out tests with GFRP bars reinforced concrete beams. The beams were placed inside a furnace with three sides of them exposed to thermal loading and the upper side under load of 440kN. A standard curve of temperature loading was used. At the beginning of the experiment small deflection was observed which settled after 30min, cracking in the concrete became visible at 75-80 min and flaming occurred at the places as the cracks. Then sudden increase of the deflection was observed and a failure was identified at 94 and 128min. The failure mode was via flexural-shear cracks and spalling of the concrete. The

reinforcement was emitting residual flames as it had reached average temperature resp. 377 and 462° C.

Galati et al (2006) tested 36 specimens reinforced with GFRP, at 70° C, duration of 200h and humidity of 80%. The purpose of the investigation was to determine the effect of elevated temperatures on the bond of FRP rebars and concrete through pull-out tests. Two rebars were placed eccentric and one of in the centre of each sample. The end slip of the bar was measured while load was applied. 16 % reduction was found due to the thermal influence.

2.4.3 Effect of elevated temperature on FRP strengthened structures

Kodur et al (2005) presented the results of full scale fire resistance experiments of 2 square RC columns, one unstrengthened and one FRP-wrapped and insulated. The columns were tested under sustained concentric axial compressive load while heated. The unprotected column failed at 800°C measured in the core and the steel temperature was more than 700°C.The protected column reached 300°C in the core for the full fire exposure. During the testing it could not be concluded, however, how effective the FRP remained during testing and it was recommended that material tests on the endurance of FRPs should be done. The general conclusion was that the behaviour of FRP strengthened and protected column under fire conditions was reliable as it did not fail for at least 4 hours.

Han et al (2006) presented a parametric study on the fire resistance of columns. For the temperature analysis a nonlinear finite element method was used, where due to its small thickness the performance of the FRP jacket was ignored and further investigation was carried out for the behaviour of column and steel. The parameters taken in consideration were: section size, steel reinforcement ratio, slenderness ratio, load eccentricity, strength of the steel bars and concrete and depth-to-width ratio.

Green et al (2006) described a study of the behaviour of FRP wrapped columns in three main extreme conditions: cold regions, corroded RC columns and fire exposure. The effect of wrapping showed good results for the first two simulations. In general the wrapping did not show loss of strength and behaved as a protection in the corrosion tests. The third type of tests

was performed with CFRP and GFRP wrapping. Temperature levels were recorded at the interface between FRP and concrete, which exceeded T_g of the FRP. It was concluded that the insulation did not protect the FRP but reduced the internal temperature of the column so that the load capacity was intact.

Carbon/epoxy FRP system and glass/epoxy FRP system were used in another study of Kodur et al (2006) on the loss of strength and stiffness of the FRP and the bond between FRP and concrete. The tests were carried out in a full-scale column furnace. Fire protection was developed. All five columns were tested under axial compressive load which was maintained at a constant value until failure or up to 5h of fire exposure. The temperature at the level of the FRP maintained 100°C (4h of exposure) due to the work of the insulating system. The temperature of the concrete and steel was less than 200°C. The overall performance of the column was not reduced by the exposure. However, there wasn't sufficient information about the effectiveness of the FRP wrapping after the T_g was reached.

FRP wrapped columns were tested by Zhang et al (2003) to assess their durability in field exposure. The exposure was 6,12 and 18 months with 4 rings cut from the central portion of each blank for burst testing and a 5^{th} ring for short beam-shear test and assessment of T_g. In the systems it was observed that standard deviation of results occurred substantially in the 2^{nd} period of exposure, which can be correlated to non-uniform through-thickness moisture absorption levels and gradients. In the 3^{rd} period a more uniform level of moisture through the thickness was attained. For the prefabricated shells the main mode of failure the adhesive was observed to tend to allow debonding and separation. The wet lay-up failed through separation of the outer ply and local tearing (1^{st} period), through a combination of inter-layer splitting and fracture of bundles (2^{nd} period) and then in the 3^{rd}- again with local splitting/tearing in the hoop direction.

Another study on the durability of FRP wrapped RC columns under severe conditions was conducted by Debaiky (2006). An aggressive environment of high temperatures and salt water was used to corrode the RC specimens and in the post-wrapping phase to investigate the efficiency of the CFRP wraps in decreasing and stopping the corrosion. The experiment included 12 large-scale circular columns, 10 of which were cast with 3% chlorides in the outer 75mm thick ring and corroded in aggressive environment, then 4 of the columns were treated

with electrochemical chloride extraction and all 10 columns were wrapped with CFRP. The second stage of the experiments comprised of 52 small-scale reinforced cylinders corroded and wrapped at several stages.

2.5 Concluding remarks

This chapter presented a literature review on the main techniques of strengthening of RC beam, failure modes and analytical solutions. The effect of elevated temperatures on the mechanical properties of the different materials was discussed and examples of experimental studies on the behaviour of FRP strengthened systems were included last. The following conclusions were drawn from the presented review of the literature:

- The failure modes of FRP-to-concrete joints depend on the bond length, type of support, laminate-to-concrete width ratios. Most of the recent experimental work has been carried out to investigate the interfacial bond-slip model to which analytical solutions have been developed.
- Failure in the concrete has been observed in bonded joints with similar width of the laminate and the concrete sample.
- Two main groups of failure modes of FRP laminates strengthened RC beams are identified as plate end debonding and intermediate crack induced interfacial debonding. The most common failure mode is reported to develop at the plate end of the laminate.
- The plate-end failure is governed by concentration of shear and normal stresses at the end of the laminate.
- The intermediate crack induced interfacial debonding occurs due to concentration of stresses induced by a crack in the RC beam.
- Polymers soften when heated to their glass transition temperature T_g. Adhesives used in civil engineering have a T_g below 100°C. FRP laminates reach their T_g at 100°C.
- Fire tests of FRP strengthened RC columns have shown that at an early stage of the heating the T_g of the FRP material is exceeded and the strengthening effect is lost. During the heating however, the process of loss of composite action has not been determined.

Chapter 2

The behaviour of CFRP strengthened RC beams has been found to be a complex experimental and analytical problem. However, little information is available on the performance of CFRP strengthened beams after heating and cooling and more studies are necessary to evaluate the effect of elevated temperatures. The reduction of strength and stiffness of the strengthened systems and materials need to be investigated to assess and predict the structural performance of strengthened RC beams.

Chapter 3
Effect of elevated temperature on the bond strength of CFRP-to-concrete joints

Experimental results of the effect of elevated temperatures on the bond strength of CFRP bonded joints are presented in this chapter. The heating regimes, testing procedure and results are discussed for each group of samples. The temperature range considered in the study is from room temperature (taken as 20°C) to 300°C.

3.1. Casting of samples, surface preparation and materials

For the purpose of this study, two series of samples were tested. A total of 63 prisms and 24 cubes were cast, heated, cooled and tested. The first series of 21 prisms were carried out as a pilot study to determine the failure modes, maximum failure load and to modify the testing device. In this chapter the results of the second series were presented and analysed. The samples were divided in seven groups of 3 prisms and 3 cubes. Each group of samples except the ones tested for bond strength at room temperature were heated together and then left to cool to room temperature prior to the testing. The FRP-to-concrete width ratio was chosen as 0.8 to investigate the temperature effect on samples strengthened with wide plates and bond length was chosen based on the anchorage zone of externally strengthened beams.

The samples were cast in one day. The mix design was developed for concrete C30/37 with maximum aggregate size of 20mm. The water/cement ratio of the mix was 0.56.

The used prism moulds had a standard size of 100x100x500mm and the samples were reinforced with a ϕ 6 bar in order to model the contributing effect of the reinforcement in a real beam, which was centred and fixed by two steel wire triangles to secure the rebar during the casting process (Figure III-1). As the samples were to be heated to elevated temperatures no plastic spacers could be used as their expansion would cause internal stresses and cracks in the concrete.

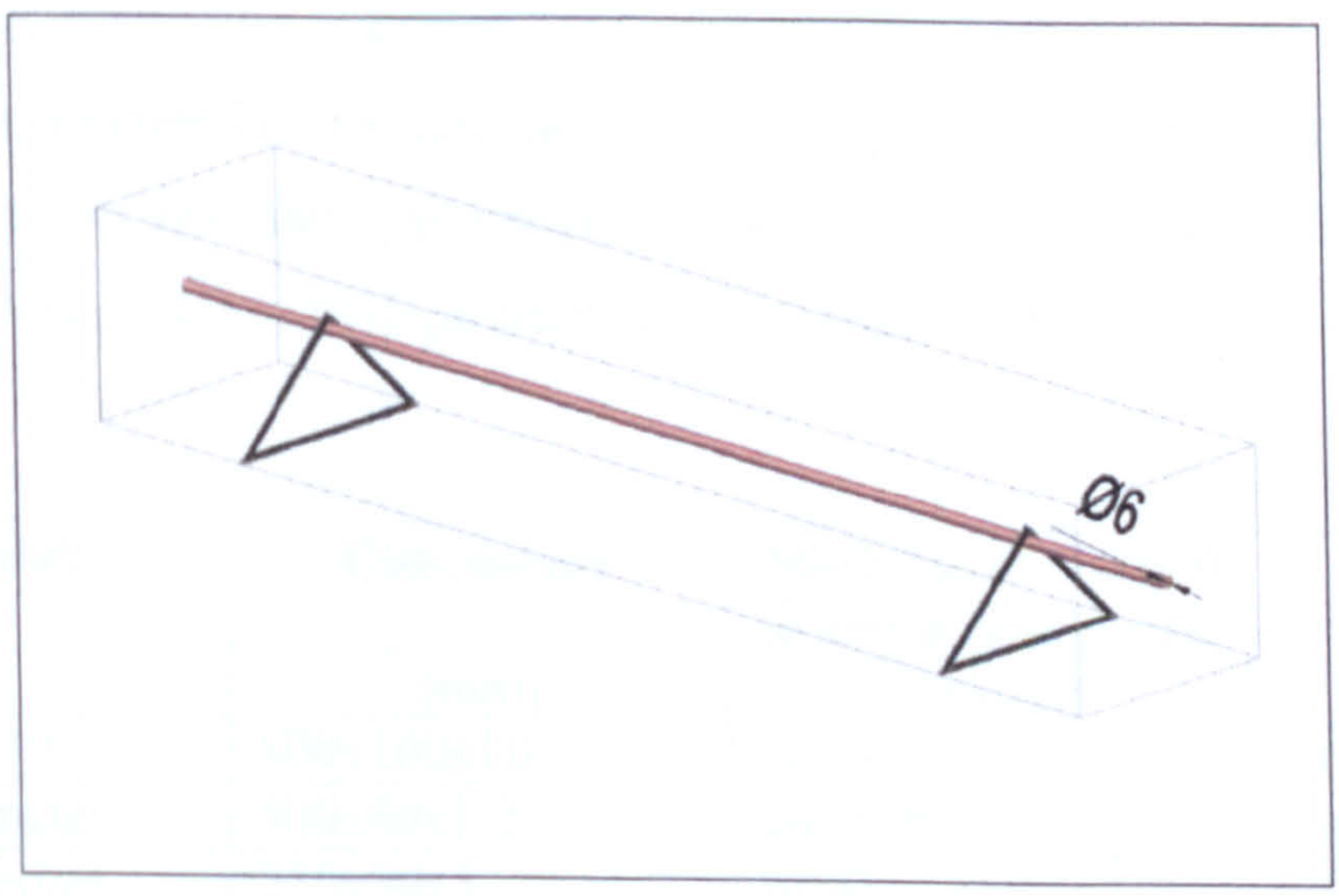

Figure III-1 Reinforcement of the prism

The cubes were cast in 150x150x150mm moulds and three of them were tested on the 28th day to determine the compressive strength of the batch according to BS EN 12390-3:2002.After 28 days of curing at 21°C and 95% humidity, the samples were left to dry for 24h and prepared for strengthening. As the laminates would be bonded to the concrete surface by adhesive the surface of the concrete was treated. A thin layer of the concrete was removed using steel brush and then the surface was cleaned using a vacuum cleaner to ensure a dust free surface. The laminate was also cleaned before the adhesive was applied.

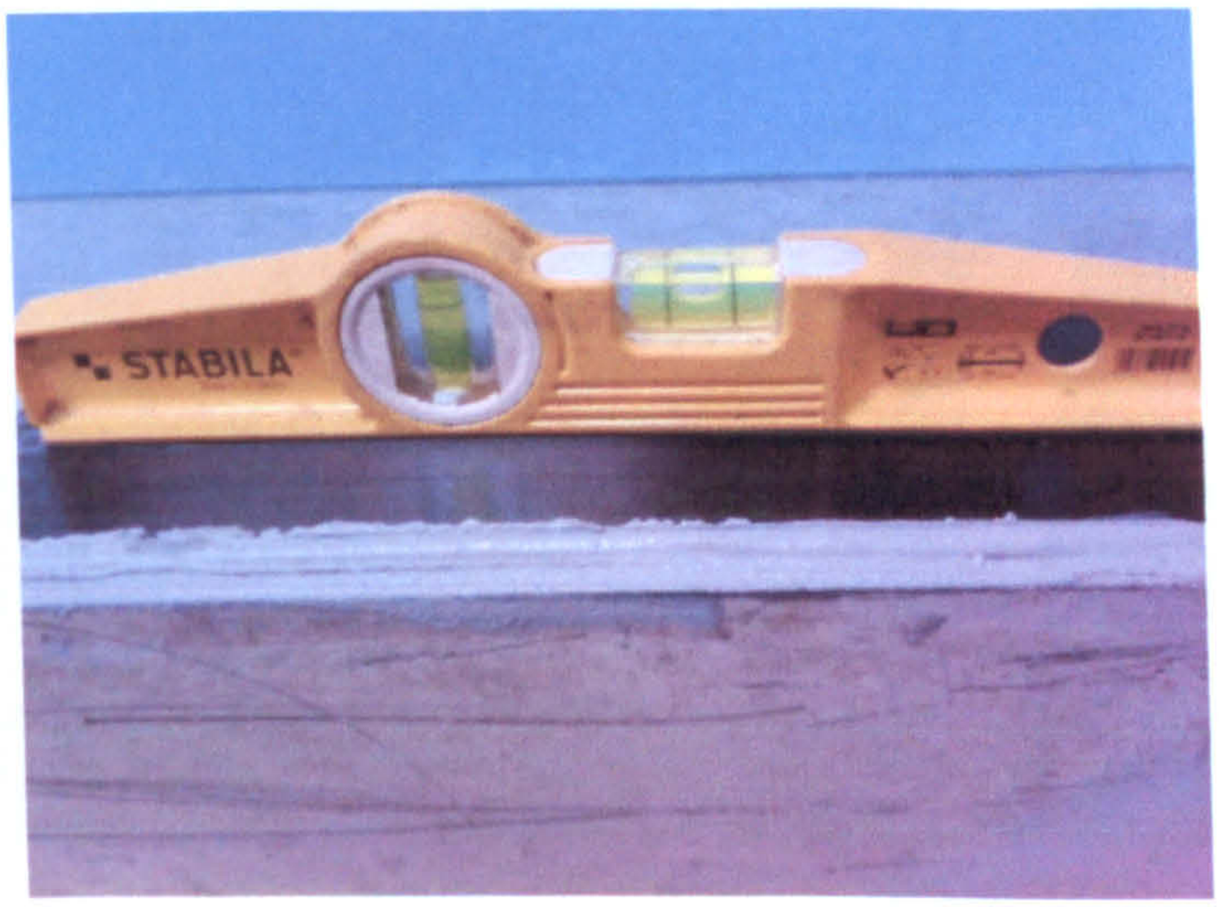

Figure III-2 Level of external reinforcement

The adhesive used was a 2-part epoxy structural adhesive "WEBER epoxy plus". The mix was prepared using 1:2.4 hardener to resin part by mass. Once an even grey colour was achieved an adhesive layer was spread onto the laminate and then attached to the concrete surface (Figure III-2). The excess was squeezed out to remove any air bubbles and ensure full length bond between the concrete and the laminate. To minimise the effect of eccentric loading, the horizontal level of the laminate was checked. The samples were then left to cure at room temperature for 7 days. Table III-1 presents the dimension and typical properties of the used materials.

Material	**Dimensions**	**Modulus of elasticity at room temperature**	**Strength**
	[mm]	[MPa]	[MPa]
Concrete C30	500x100x10	30000	Cube : 37000
CFRP laminate	500x80x1.2	165 000	Tensile :2000
Epoxy adhesive	250x90x3	9800	Lap shear :18
Steel	6mm diameter	210 000	Tensile 275

Table III-1 Dimensions and properties of materials used

3.2 Heating procedure and readings

3.2.1 Position of samples in the oven and thermocouples

Two months after the laminate was attached to the concrete samples, the six groups were heated in a Carbolite oven to the required temperature.

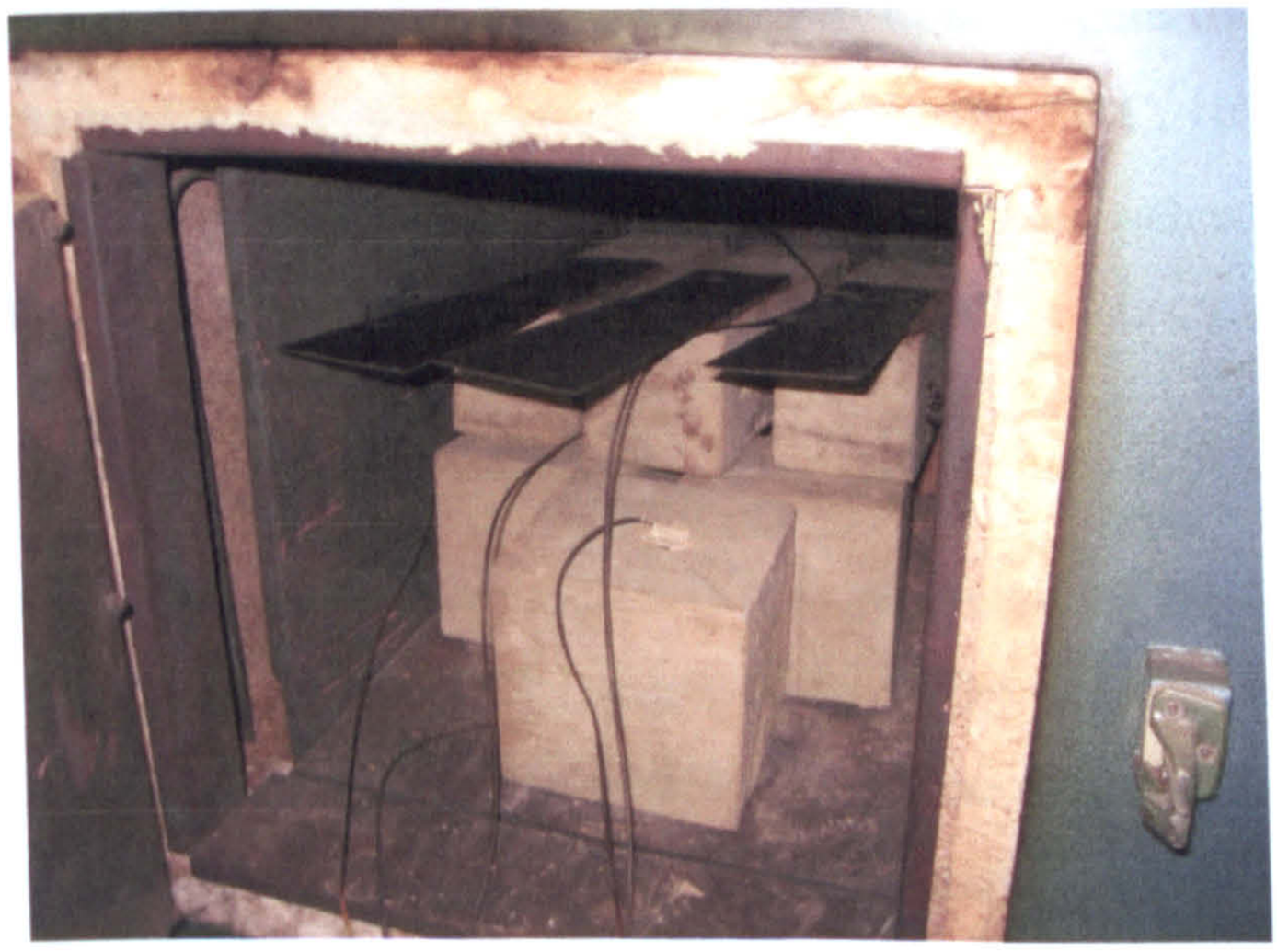

Figure III-3 Position of the samples in the oven

The samples were placed in the oven allowing the hot air to circulate around the six samples to allow uniform exposure to the heat. The temperature was measured with three thermocouples, two measured the temperature at the centre of one of the cubes and one prism, and the third one measured the temperature of the air in the oven. A 5mm diameter hole was drilled to the centre of one cube and one prism from each group where later a thermocouple was inserted. When the cube was later tested to determine the compressive strength the weak surface was placed vertically to minimise the effect on the failure load. The position of the hole drilled in the prism was chosen at the unloaded end of the sample, 50mm away from each surface.

3.2.2 Thermocouples

The thermocouples used were type K (Ni Cr/Ni Al). Prior to testing readings of temperature of boiling water and melting ice were taken to test the accuracy of the thermocouples. The readings were found to be accurate to 0.6°C to the respective temperature. During the

following heating regimes, the uniform distribution of temperature in the samples was taken to ±5 °C. Temperature error of 5 degrees was assumed as a temperature tolerance during the heating as it would not lead to significant thermal stresses in the material.

3.2.3 Uniform heating field

The temperature range in this study was from 50°C to 300°C, see Figure III-4. Each group was heated to a given temperature and was referred to as group 20°C, 50°C, 100°C, 150°C, 200°C, 250°C or 300°C. The chosen range of the temperature allowed samples heated below T_g of the polymers (between 60°C and 100°C), between T_g (100°C) and T_d (200°C) and above the T_d of the polymers to be tested.

To allow the gradual increase of the temperature in the specimens, the heating started after the samples had been placed in the oven. The temperature of the air would reach the required temperature early while the heating of the samples would be a slower process due to their lower conductivity. Exposing samples directly to high temperatures would otherwise cause the so called thermal shock which could produce thermal stresses between the exposed heated surface and the cooler inner core.

The samples of group 50°C were heated for 160 min when uniform temperature field was established and the oven was turned off. Both the temperature in the centre of the cube and the beam were taken into account to determine the heating time and temperature field. Thus the greater dimensions of the cube and the limited area of exposure the middle beam were considered.

Group 100°C were heated for 130min when the readings from the three thermocouples reached the same temperature and the samples were heated for 60 more minutes. Group 150°C, 200°C, 250°C and 300°C were heated for 300 min when the uniform temperature field was established. In another experiment the FRP laminate was found to deform significantly when heated to 300°C thus to prevent the deformation the position of the beams and cubes was swapped and the beams were turned upside-down.

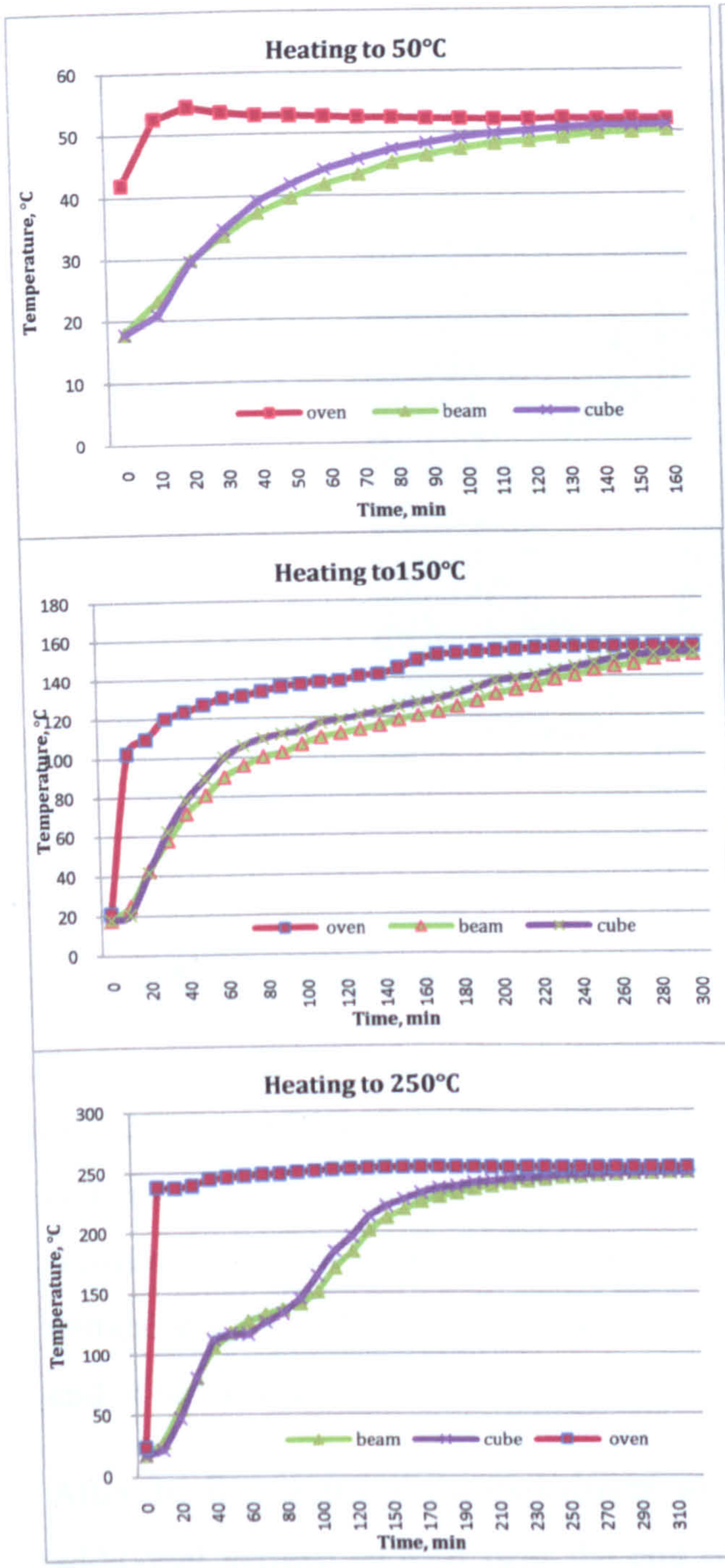

Figure III-4 Heating regimes of samples to 50°C, 100°C, 150°C, 200°C, 250°C and 300°C

To study the effect of cooling on the CFRP strengthened samples thermal images were taken during the last phase of cooling. Group 300°C from series 1 was heated and left to cool for 8 hours. On the following day the concrete samples had uniformly cooled to 50°C whilst on the surface of the CFRP laminate different temperatures were established due to the different rate of cooling of the materials. Highest temperatures were observed at the middle section of the bond length between the laminate and the concrete prism whilst towards the two ends of the

CFRP plate lower temperatures were found. Thermal cracks were later observed between the CFRP plate and the concrete where lower temperature was established, see Figure III-5.

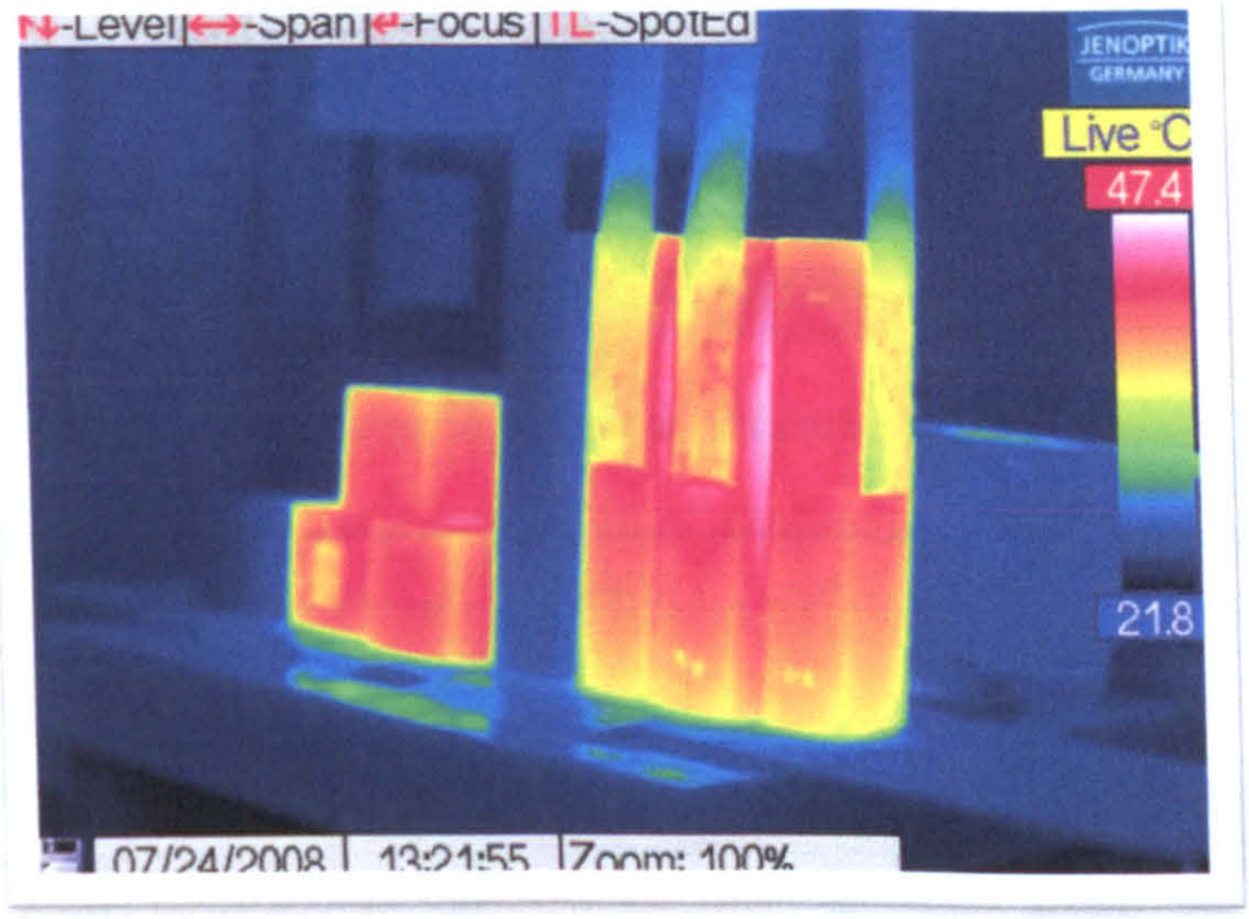

Figure III-5 Cooling of CFRP-to-concrete bonded joints

3.3 Experimental set-up

In order to evaluate the effect of temperature on the bond strength of CFRP strengthened systems, a testing device was designed corresponding to "near end supported single shear test" according to Chen et al (2001) classification. The device was initially designed with one vertical support at the unloaded end and a full height (100mm) horizontal support at the loaded end of the concrete prism.

After the first series of the experiment were tested few adjustments were made including an additional vertical support near the end of the laminate and reduction of the height of the horizontal support at the loaded end to 90mm, see Figure III-6. The changes were necessary to restrict the bending of the specimen which would generate additional tensile stresses in the concrete at the end of the laminate.

To apply the pulling force, the laminate was clamped between two thick steel plates connected to a steel rod. The force was applied as the rod was pulled by a hydraulic ram and the applied load was measured by a load cell at the end of the hydraulic ram. To prevent any possible slip between the laminate and the steel plates silicon carbide paper was glued to the steel plates and the number of bolts clamping the two steel plates together was increased to 9. Three

rollers were placed between a wooden prism and the clamping plates to ensure free horizontal movement, thus allowing the direction of the applied force to be maintained throughout the experiment, see Figure III-7.

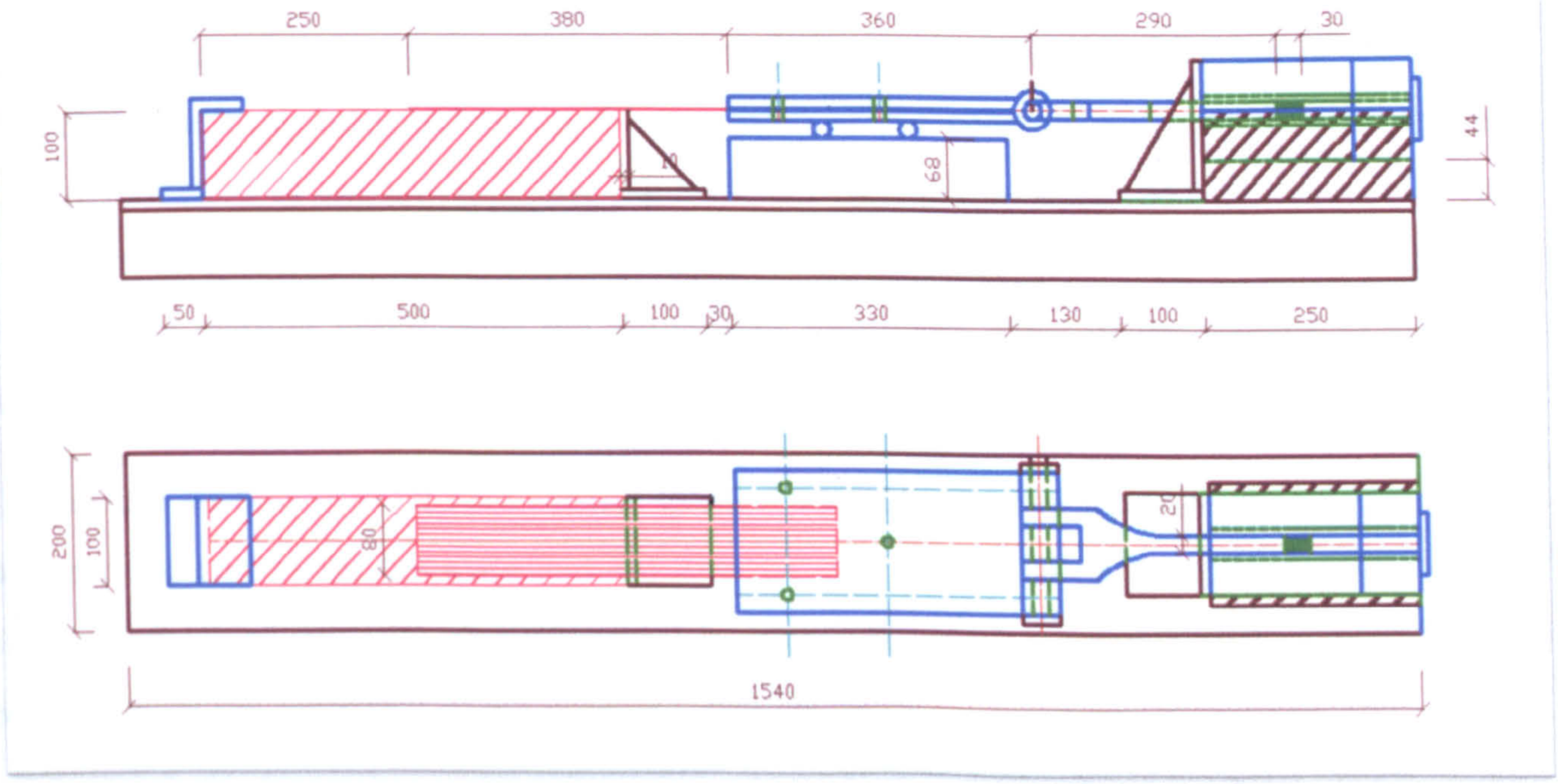

Figure III-6 Experimental set-up

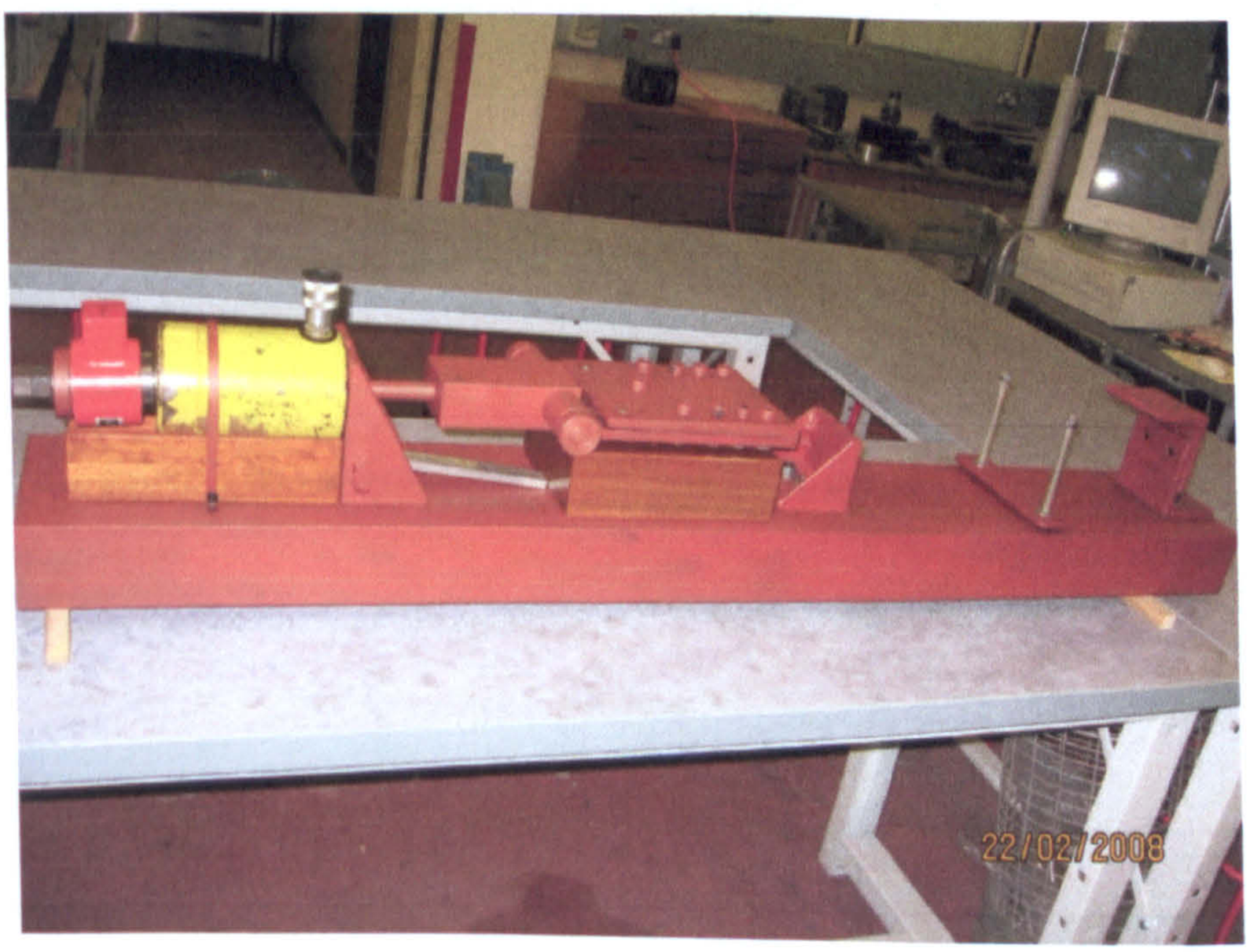

Figure III-7 Final design of the testing device

3.4 Testing- preparation and testing procedure failure modes

3.4.1 Preparation

From the first series of the experiments it was established that samples with the same geometry would fail due to formation of a crack in the concrete near the end of the plate. Therefore the local deformations on the two sides of the concrete were measured, together with deformation of the laminate and the zone between the laminate and the concrete. Five demountable mechanical (DEMEC) strain gauges were attached on the upper half on each side of the prism starting 10mm from the top surface where the effect of the transfer of stresses would be more pronounced, see Figure III-8.

On the top surface two DEMEC strain gauges were attached to measure the displacement between the end of the laminate and the concrete and two more on the laminate itself. The strain of the laminate was also measured by three electrical resistance (ER) strain gauges positioned on the centreline of the laminate, 100mm apart.

Prior to testing the used equipment – 50mm and 150mm DEMEC reader- was zeroed. The readings were later transferred to real deformations applying the corresponding coefficients for each device and ER strain gauges.

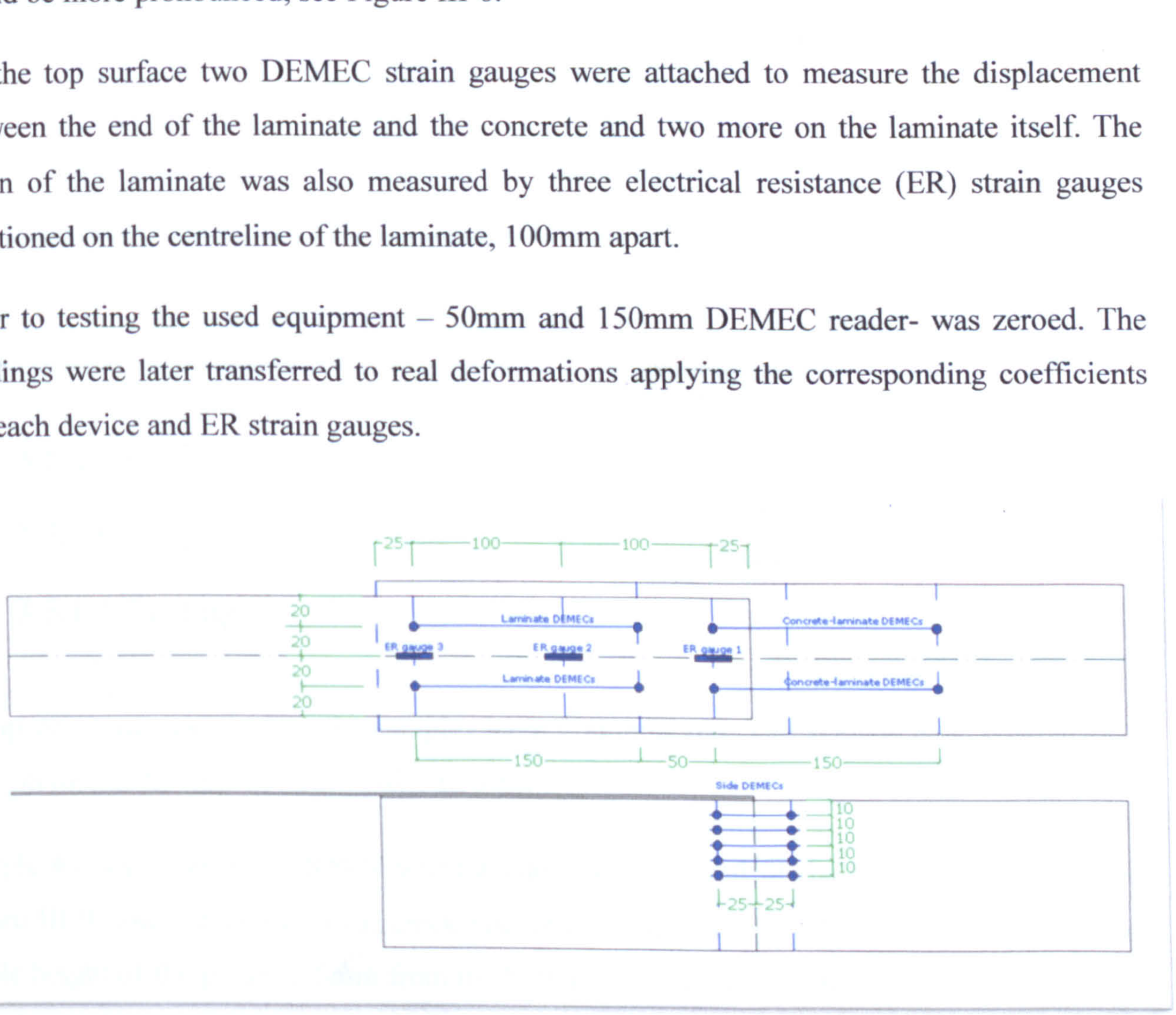

Figure III-8 Position of strain gauges and DEMEC points on a sample

3.4.2 Testing procedure

The flowchart given below shows the experimental procedure for the samples in this study.

Once a sample was placed on the testing device and zero readings were taken, the load was applied 1kN every 10min and two rounds of readings were taken for each load step. The samples were loaded to the complete failure of the sample.

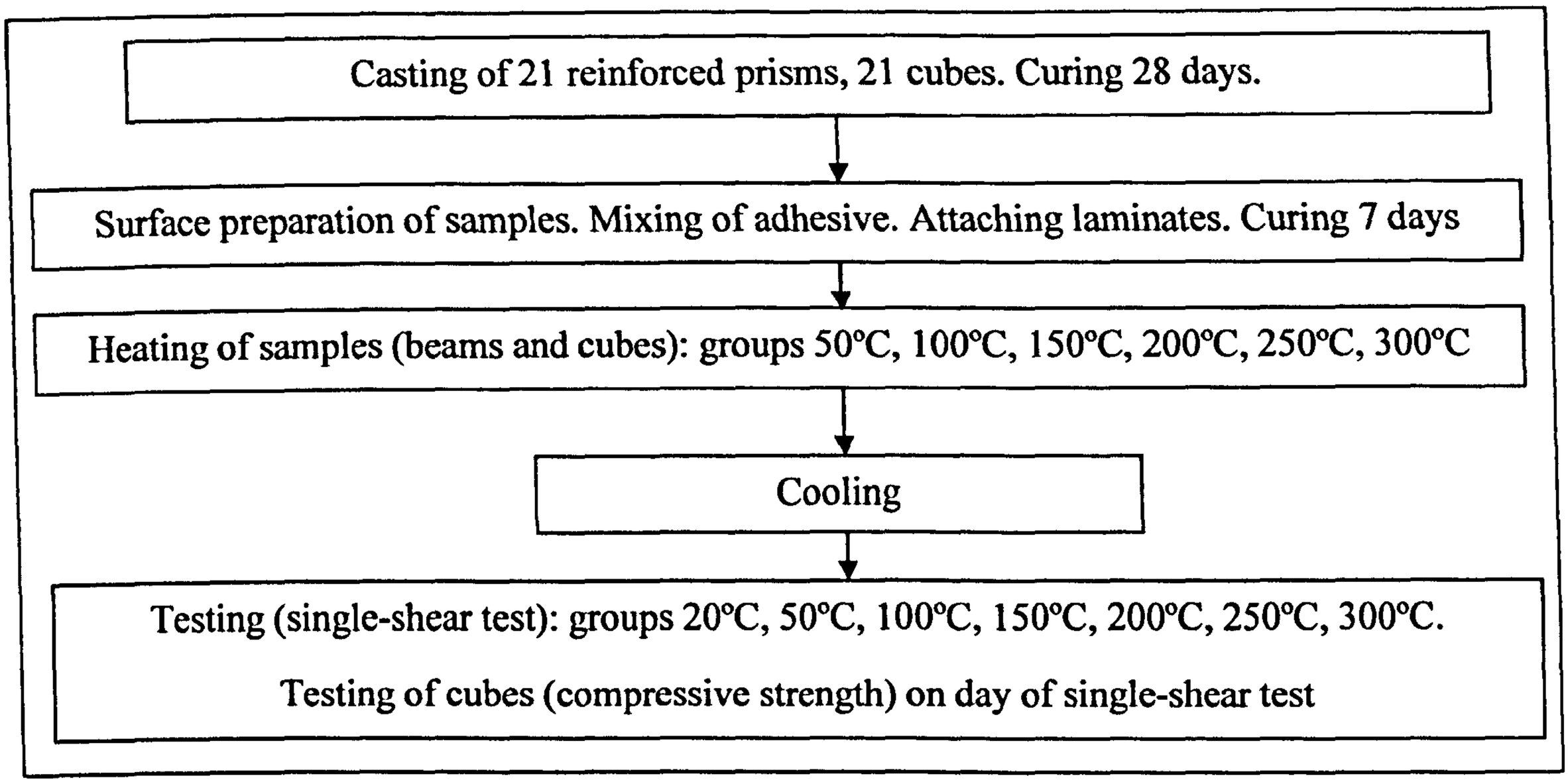

3.5 Results

3.5.1 Group 20°C

3.5.1.1 Testing

Group 20°C was tested when the samples were 4 months old. The average cube compressive strength on the 28th day of casting was 40.2 MPa.

Sample #1 was loaded to 18.8kN when a crack near the end of the laminate occurred, see Figure III-9. The formation of the crack was brittle and it was developed almost through the whole height of the prism to 5mm from the bottom. Due to the deformation of the system the load dropped to 10.8kN. As the sample was subsequently reloaded to 20kN the inclined crack propagated horizontally until the front part was no longer connected to the back half of the prism. The second phase of loading led to the further horizontal expansion of the crack near

the end of the plate and to the vertical relative displacement between the two parts of the prism. A crack was formed due to the concentration of stresses at the contact zone between the front support and the concrete which propagated to the top surface of the concrete and through the adhesive. To minimise the effect of stress concentration in subsequent experiments a thin plate was placed between the front of the prism and the edge of support to distribute the occurring stresses.

Sample #2 failed in a similar manner. The initial crack was observed at 25kN and it consisted of an inclined and horizontal branch. At this point the system was holding 17.4kN or 70% of the failure load. The following increase of the load caused further propagation of the crack. At 23 kN the rotation of the front half of the prism led to the separation of the laminate from the adhesive which reduced the load to 19.2kN. The delamination crack finally propagated to the end of the laminate at 23kN.

The formation of the crack at the end of the laminate of sample #3 was observed at 21kN at which stage the system was holding 14.3kN or 68% of the failure load. The crack was fully formed when reloaded to 21kN and the complete separation of the two parts allowed the rotation of the front half. The load was reduced to 17kN followed by delamination crack between the laminate and the adhesive. Although the system was still holding 12.9kN slight increase of the load caused the quick propagation of the crack and brittle complete failure of the system.

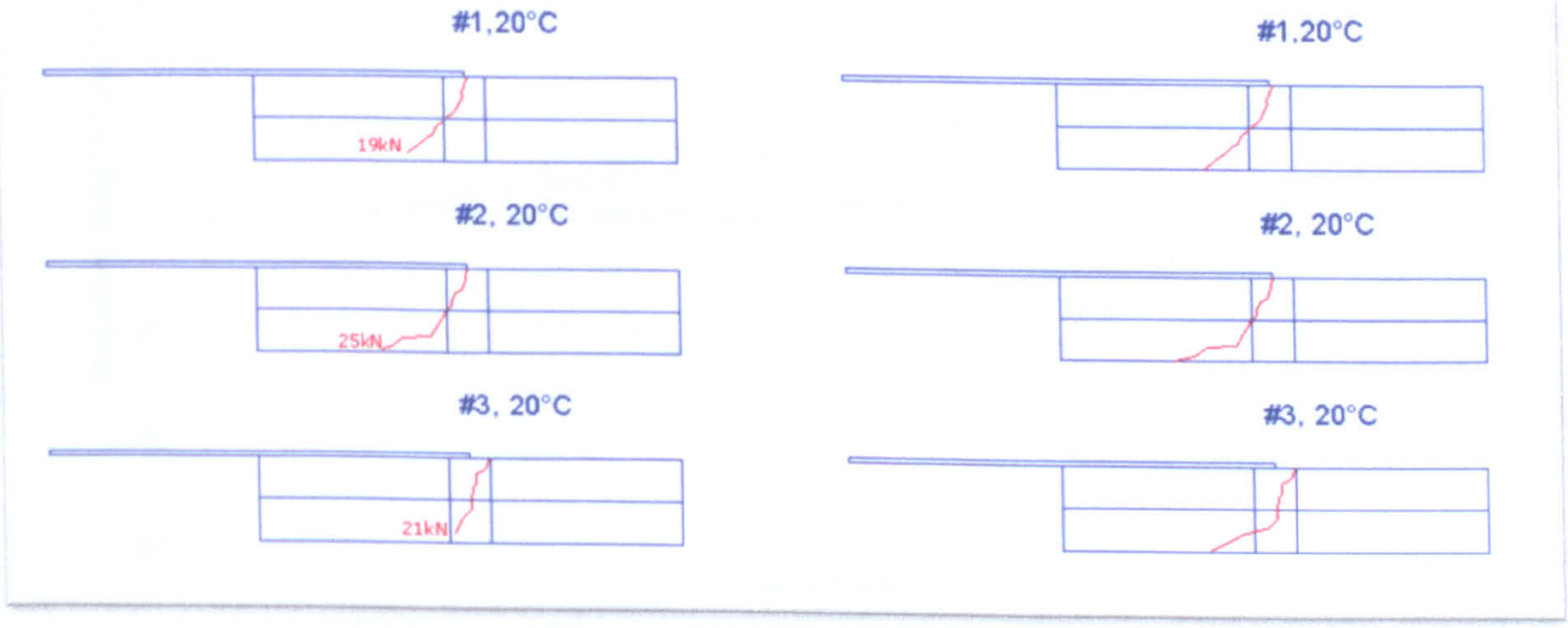

Figure III-9 Crack formation in samples, group 20°C, left- initial crack, right- final crack

3.5.1.2 Side DEMEC strain gauges

The local deformations on the sides of the samples near the end of the laminate were measured by DEMEC strain gauges until a crack was formed (Figure III-10). The deformations were taken as positive if the distance between two points would increase and negative if the distance would decrease.

For all 3 samples of the group the local deformations at level 10mm and 20mm were found to have positive values up the failure load as an indication of tensile stresses transferred to the concrete layer from the laminate. Level 30mm remained neutral to 10kN whilst level 40 and 50mm gave neutral or negative values. The increase of the load led to higher tensile strain closer to the top surface: 10, 20 and 30mm from the top whilst negative strain was measured at level 40 and 50mm. The maximum compressive strain measured for level 50mm was 35 microstrain at 15kN. Prior to the crack formation the local deformations at level 40 and 50mm changed to positive as an indication of higher concentration of the tensile stresses at the end of the laminate and conditions for crack formation in the upper half of the prism.

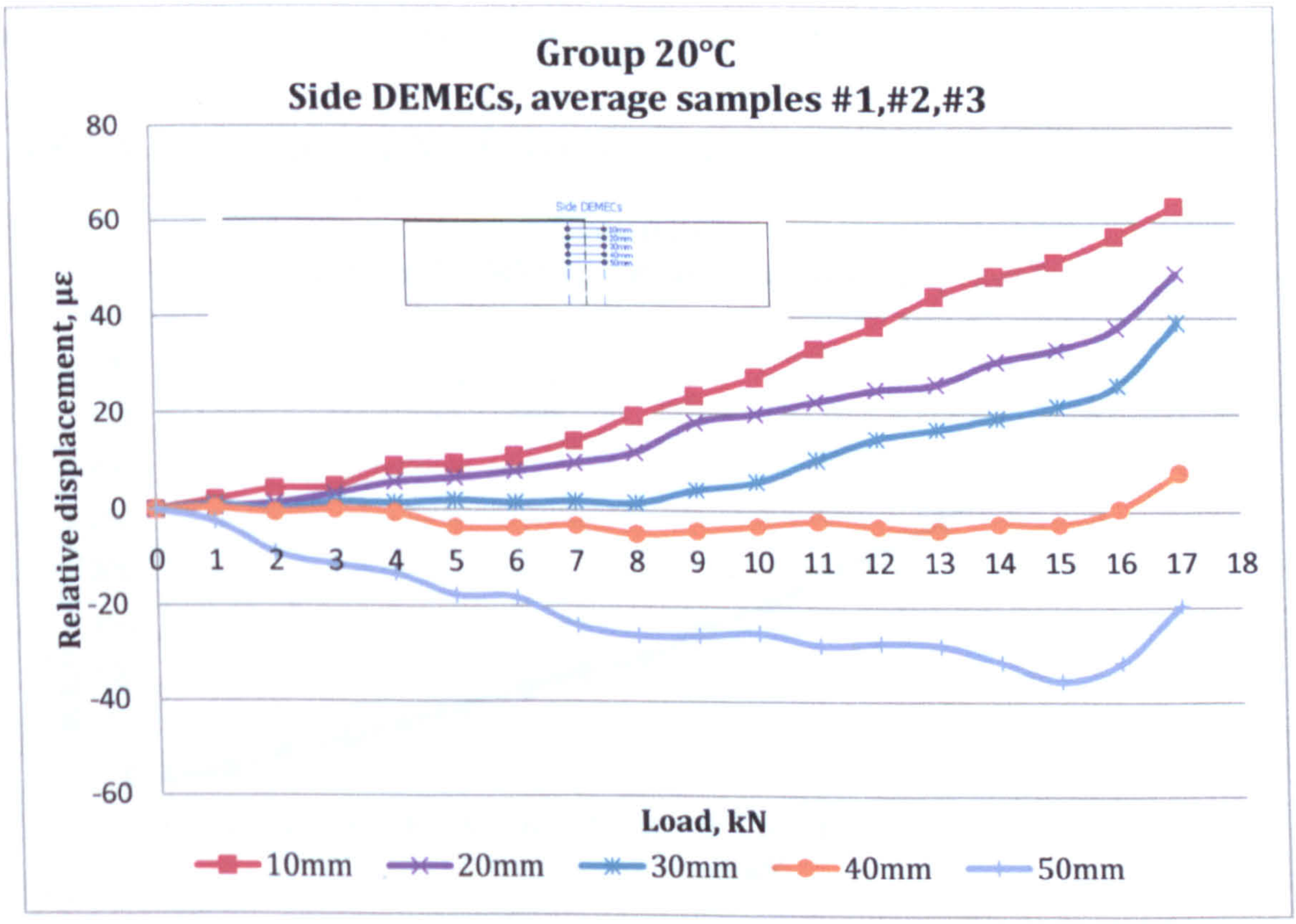

Figure III-10 Average local deformation before failure, side DEMEC strain gauges, group 20°C

3.5.1.3 Concrete- laminate DEMEC strain gauges

The measured relative displacement between the end of the laminate and the concrete (see Figure III-11) indicated a gradual increase of the strain up to 10kN above which the rate of deformations would become steeper especially prior to the formation of the cracks. The average displacement at 17kN was 100 microstrain.

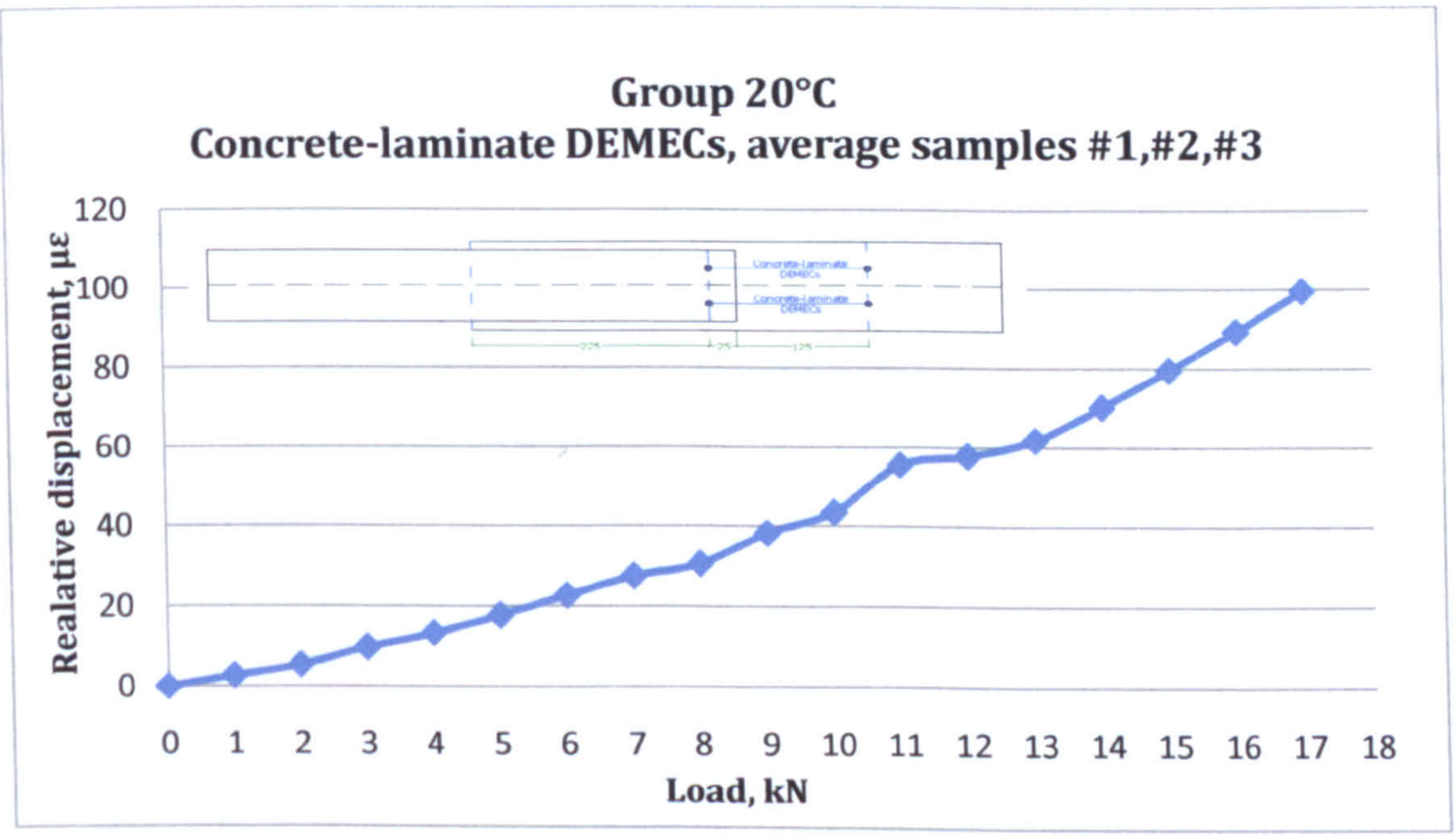

Figure III-11 Average local deformations before crack formation, concrete-laminate DEMEC strain gauges, group 20°C

3.5.1.4 Laminate DEMEC strain gauges

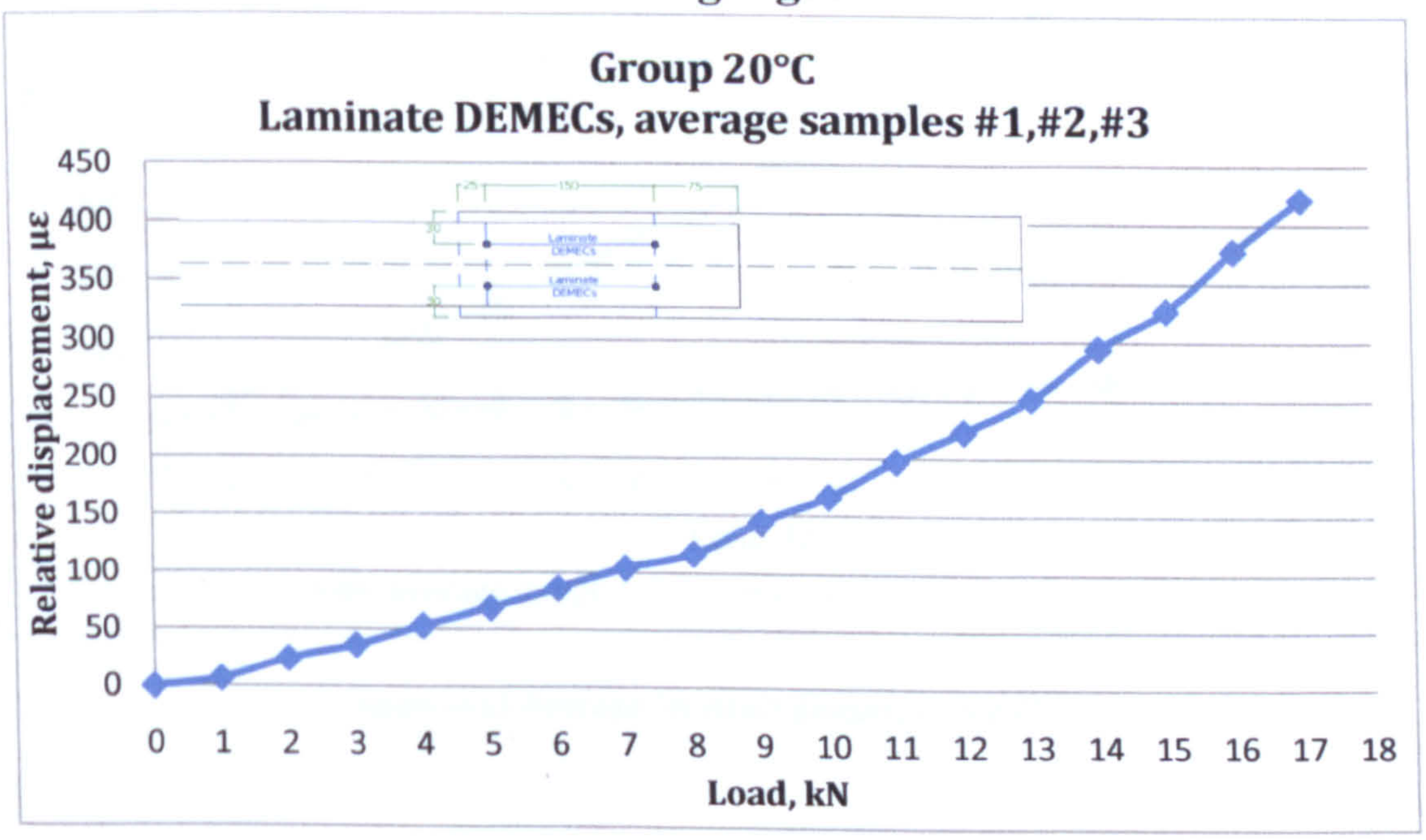

Figure III-12 Average local deformation, laminate DEMEC strain gauges, group 20°C

The strains of the laminate were measured by DEMEC strain gauges. The behaviour of the three samples was very similar with gradual nonlinear increase of the deformation with the load. At 17kN the average value was found to be 421microstrain, see Figure III-12.

3.5.1.5 ER gauges

The results obtained from the ER strain gauges from the three samples were plotted against the load. The increase of the deformations was gradual for strain gauge 1 and 3 (Figure III-13). The strain gauge closest to the applied load deformed most with average value of 787 microstrain and the one closest to the end of the laminate exhibited the least deformations reaching strain of 76 microstrain at 17kN. ER strain gauge 2 exhibited a more pronounced nonlinear behaviour which could be attributed to the redistribution of stresses towards the end of the laminate with increase of the load. The average strain for ER strain gauge 2 was 297microstrain at 17kN.

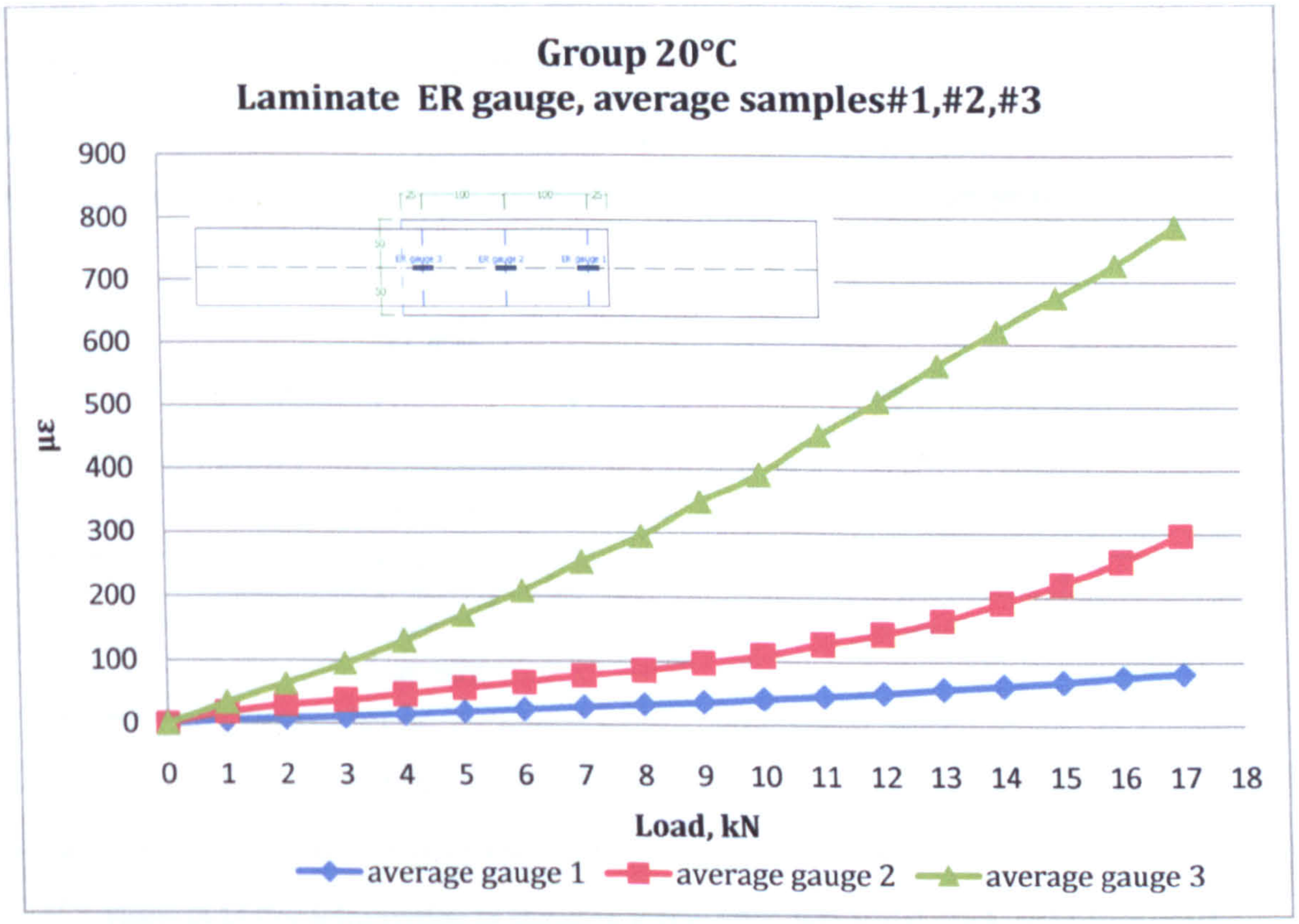

Figure III-13 Average ER strain gauges, group 20°C

3.5.2 Group 50°C

3.5.2.1 Testing procedure

The samples of group 50°C where tested 2 months after the heating of the samples. The average compressive strength of the cubes at the time of testing was 47.15MPa.A parabolic crack was formed through the full height of the concrete near the end of the laminate of sample #4 at 27kN, see Figure III-14. The deformation of the system caused 25% drop of the load to 21.3kN. The load was then gradually increased to 23kN which led to the horizontal and vertical relative displacements of the two parts of the concrete and free rotation of the front half, which reduced the load to 20kN. The final delamination occurred at 22.5kN in a brittle manner.

The other two samples in this group failed at the same load- 24kN. Sample #5 and #6 retained 76% and 77% respectively of the failure load after the formation of the crack. The complete propagation of the crack for the former sample was achieved at reloading to 22kN, followed by drop by 3kN. The rotation of the front half continued to 21kN until delamination between the laminate and the adhesive was initiated and the load dropped to 10kN load. At this point the crack had developed quickly and the next step of the loading caused full delamination.

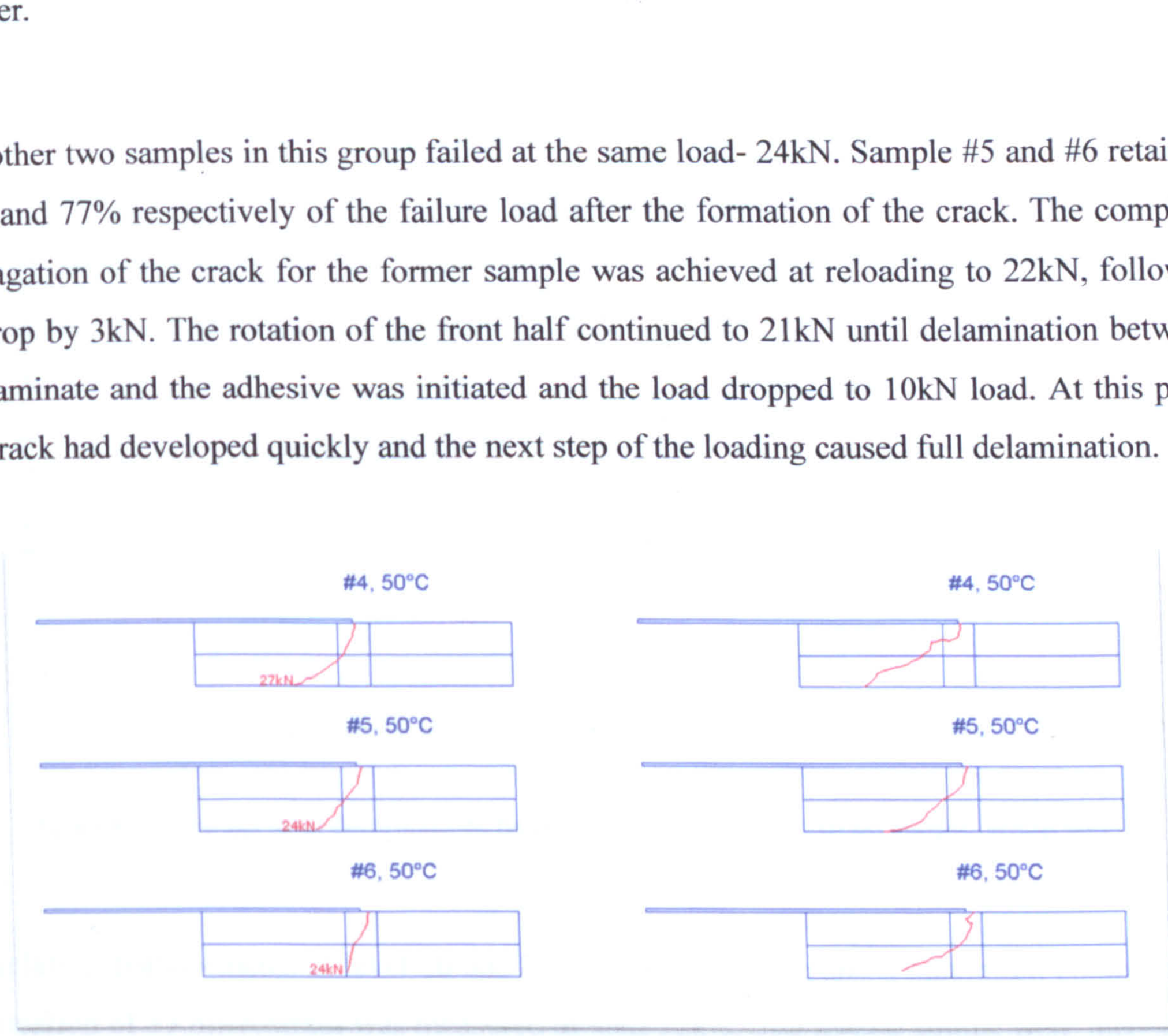

Figure III-14 Crack formation in samples, group 50°C, left-initial crack, right-final crack

After the initial crack of sample #6, the following increase to 20kN resulted in a horizontal propagation of the crack causing relaxation of the load to 15kN. Delamination was initiated at the next reloading stage when complete separation of the two halves was achieved at 19kN

and the subsequent free rotation and drop of the load to 12.4kN. The full delamination was observed at 16kN.

3.5.2.2 Side DEMEC strain gauges

The average local deformations at the end of the laminate for the three samples of group 50°C were plotted for a range of 0kN to a load of 22kN (Figure III-15). The tensile strains were found to develop for level 10 and 20mm to level 30mm where the deformations were zero.

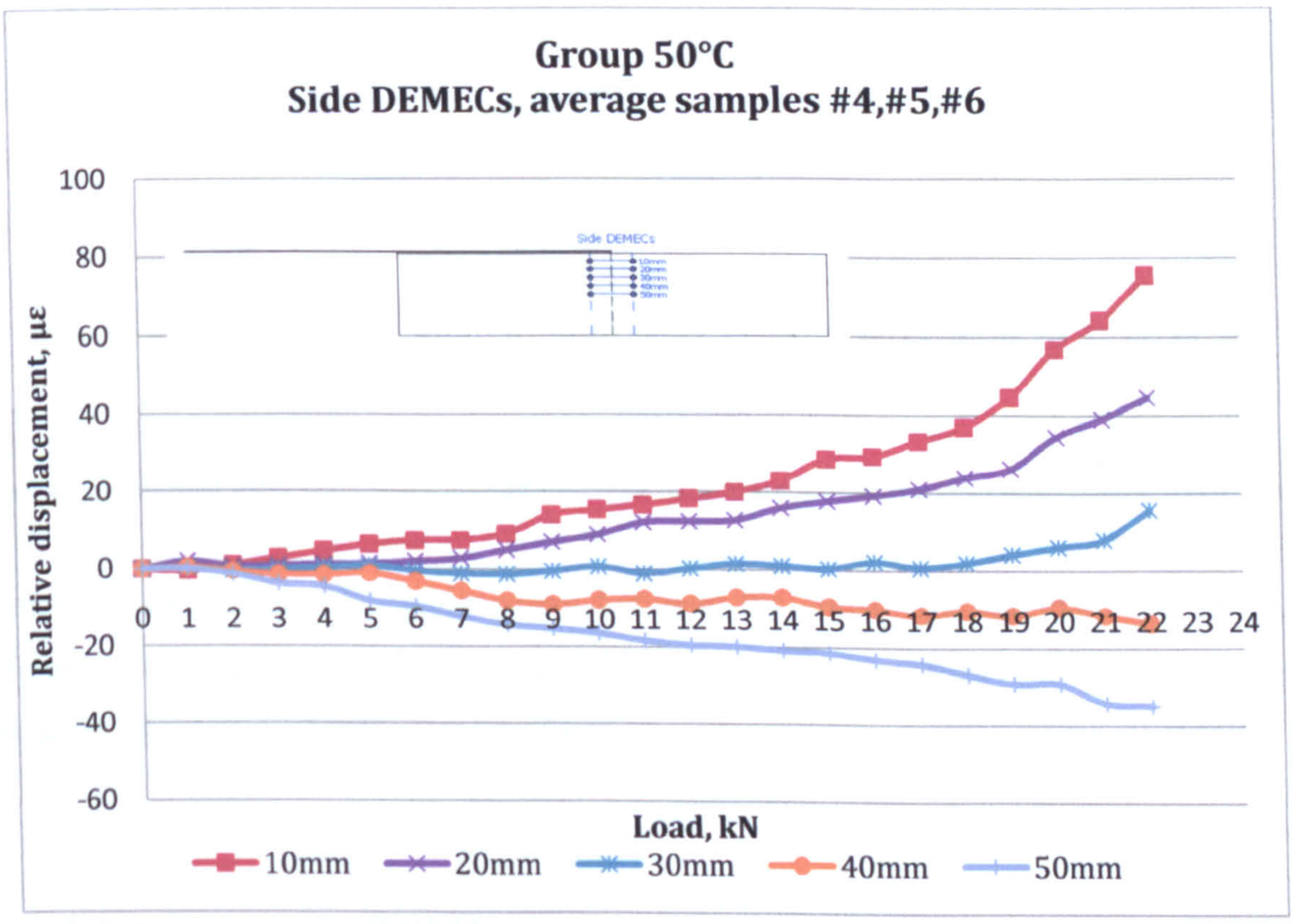

Figure III-15 Average local deformations before failure, side DEMEC strain gauges, group 50°C

The relative displacements at level 40 and 50mm were negative and a maximum compressive deformation of 35 microstrain was measured at load 22kN. The tensile strains were increasing gradually up to 19kN. Further increase of the load caused higher tensile strains with a maximum average value of 75 microstrain at 22kN and eventually formation of a crack in the concrete at the end of the laminate.

3.5.2.3 Concrete- laminate DEMEC strain gauges

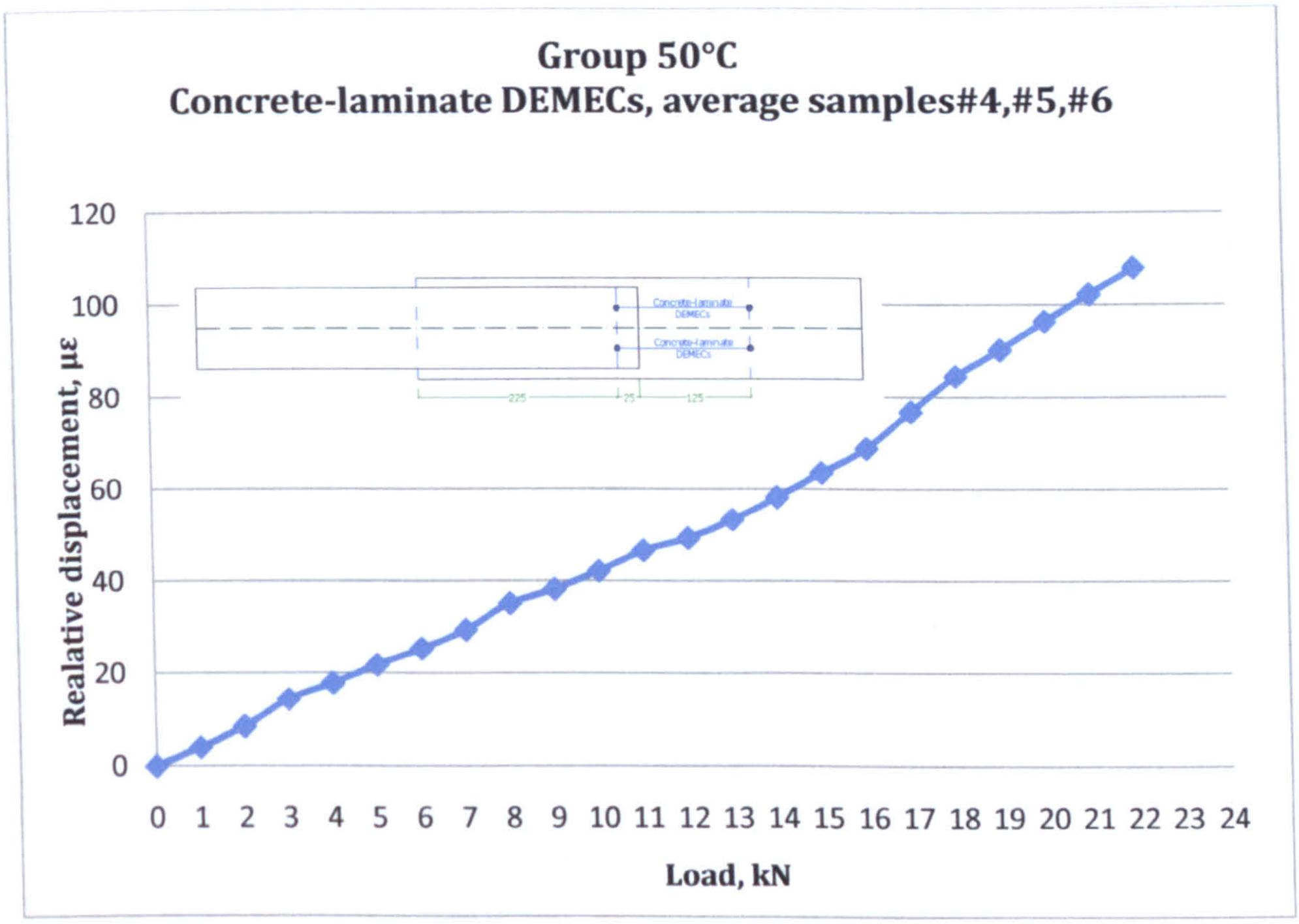

Figure III-16 Average local deformations before crack formation, concrete-laminate DEMEC strain gauges, group 50°C

The increase of the relative displacement between the end of the laminate and the concrete was found to be gradual up to 16kN when a slight change was observed. The average value at 22kN was 108 microstrain (Figure III-16).

3.5.2.4 Laminate DEMEC strain gauges

The relative displacement of the DEMEC points attached to the laminate was described by a gradual nonlinear increase up to the failure of the system (Figure III-17). The average strain at 22kN reached 763microstrain.

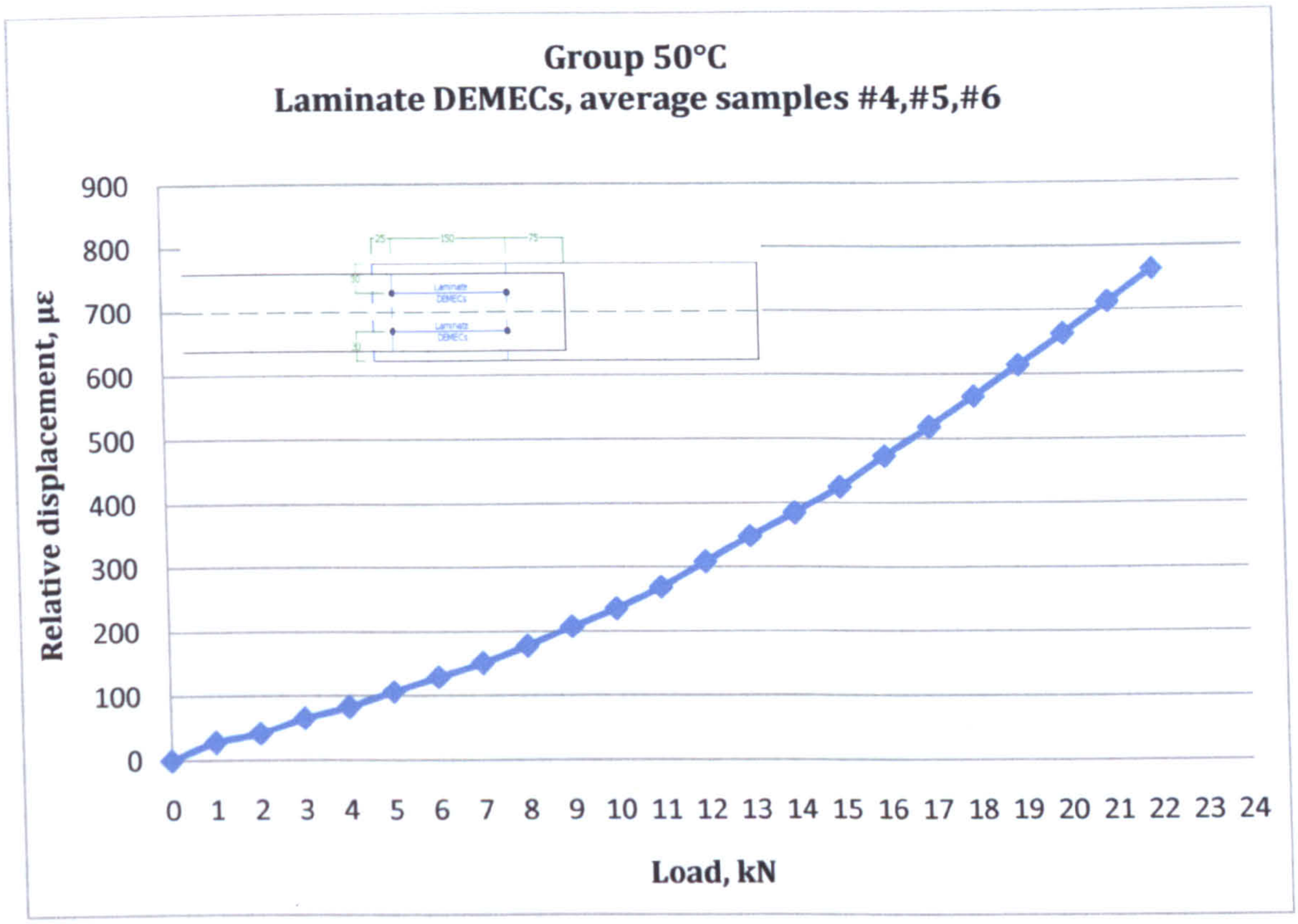

Figure III-17 Average local deformation, laminate DEMEC strain gauges, group 50°C

3.5.2.5 ER gauges

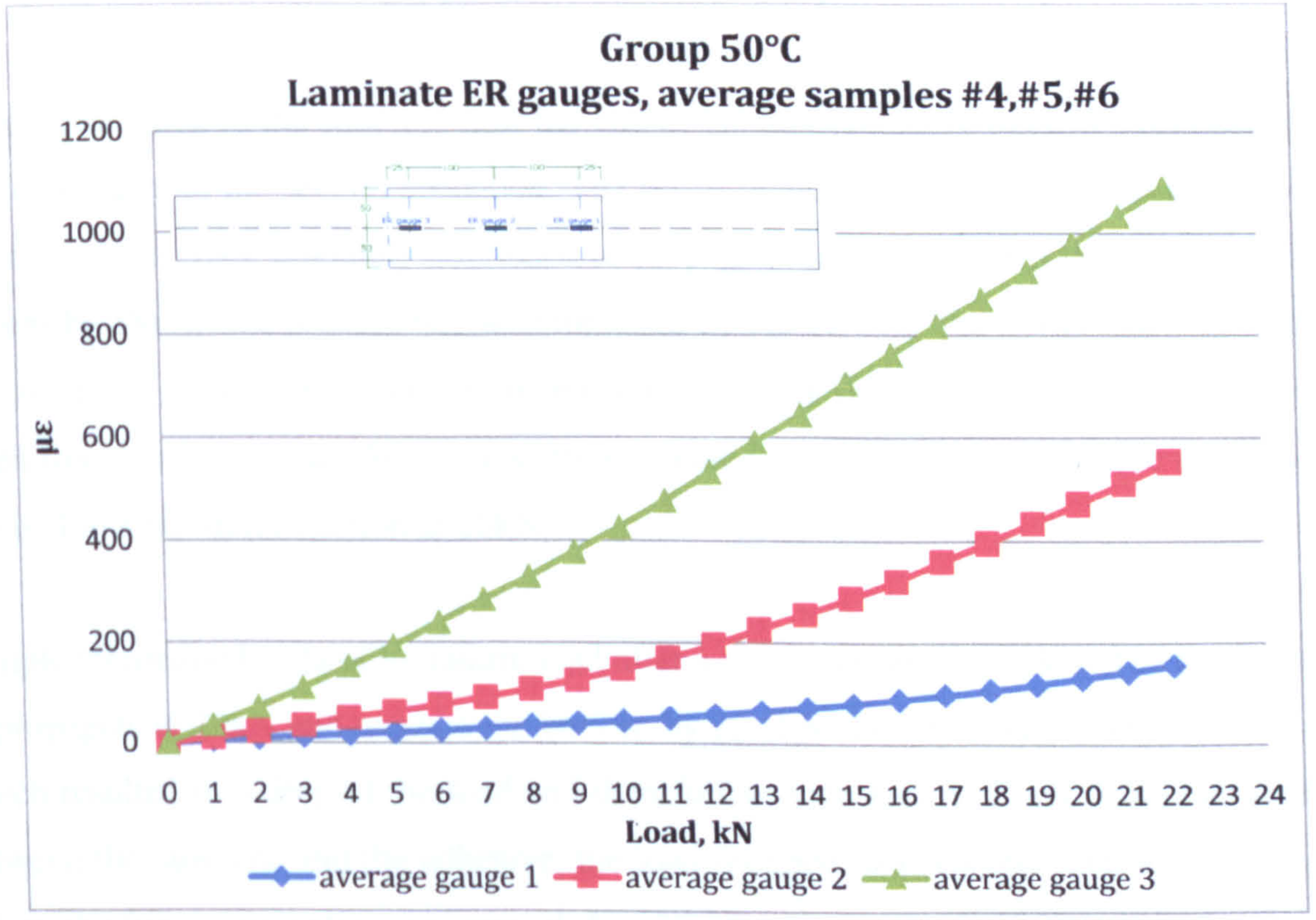

Figure III-18 Average ER strain gauges, group 50°C

ER gauge 3 for group 50°C registered the least deformations from all three gauges-155microstrain at 22kN whilst the average strain of ER gauge 1 was found to be 1089 microstrain at the same load (Figure III-18). The increase of the pulling force resulted in gradual increase of the deformations of ER gauge 2 in a nonlinear manner. At 22kN the value for ER strain gauge 2 was 554microstrain.

3.5.3 Group 100°C

3.5.3.1 Testing

The samples of group 100°C were tested 5 months after the heating. At the time of the testing the achieved average cube compressive strength was 43.5MPa.

Sample #7 was loaded to 27kN when a sudden drop of the load was registered (Figure III-19). The subsequent increase of the load resulted in the development of a crack between the laminate and the adhesive near the front support. The premature failure was attributed to a small eccentricity of the applied load. The results of the testing of the sample were taken to 75% of its maximum load when the data of the three samples were compared later.

An inclined crack in the concrete near the end of the laminate developed at 21kN almost to the bottom surface of the second specimen. The prism retained 11.1kN and at the further increase of the load the crack gradually continued to propagate horizontally at 14kN and it reached the bottom by 18kN. The process was accompanied by the vertical and horizontal displacement of the two parts of the prism. The complete separation of the two parts was observed at 22kN when free rotation began. At 24kN a crack initiated at the concrete- adhesive interface which resulted in a full delamination at 26kN.

Sample #9 retained 77% of its failure load after a crack occurred at 23kN. The crack continued to propagate at 20kN and reached the bottom by 22.5kN. The front half started its free rotation which resulted in a drop of the load and then further increase. At 22kN delamination initiated between the laminate and the adhesive, the load dropped to 17kN and then the maximum load before the full delamination was recorded as 19kN.

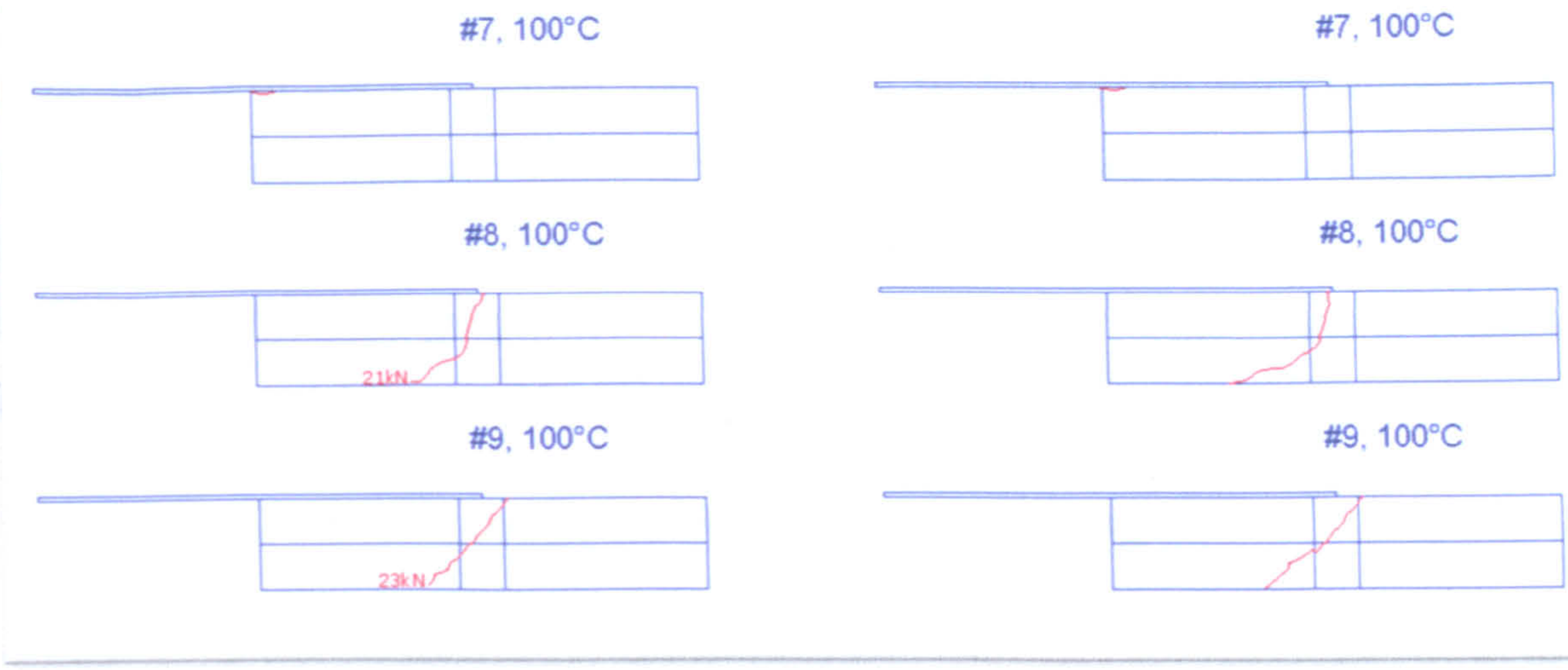

Figure III-19 Crack formation in samples, group 100°C, left-initial crack, right-final crack

3.5.3.2 Side DEMEC strain gauges

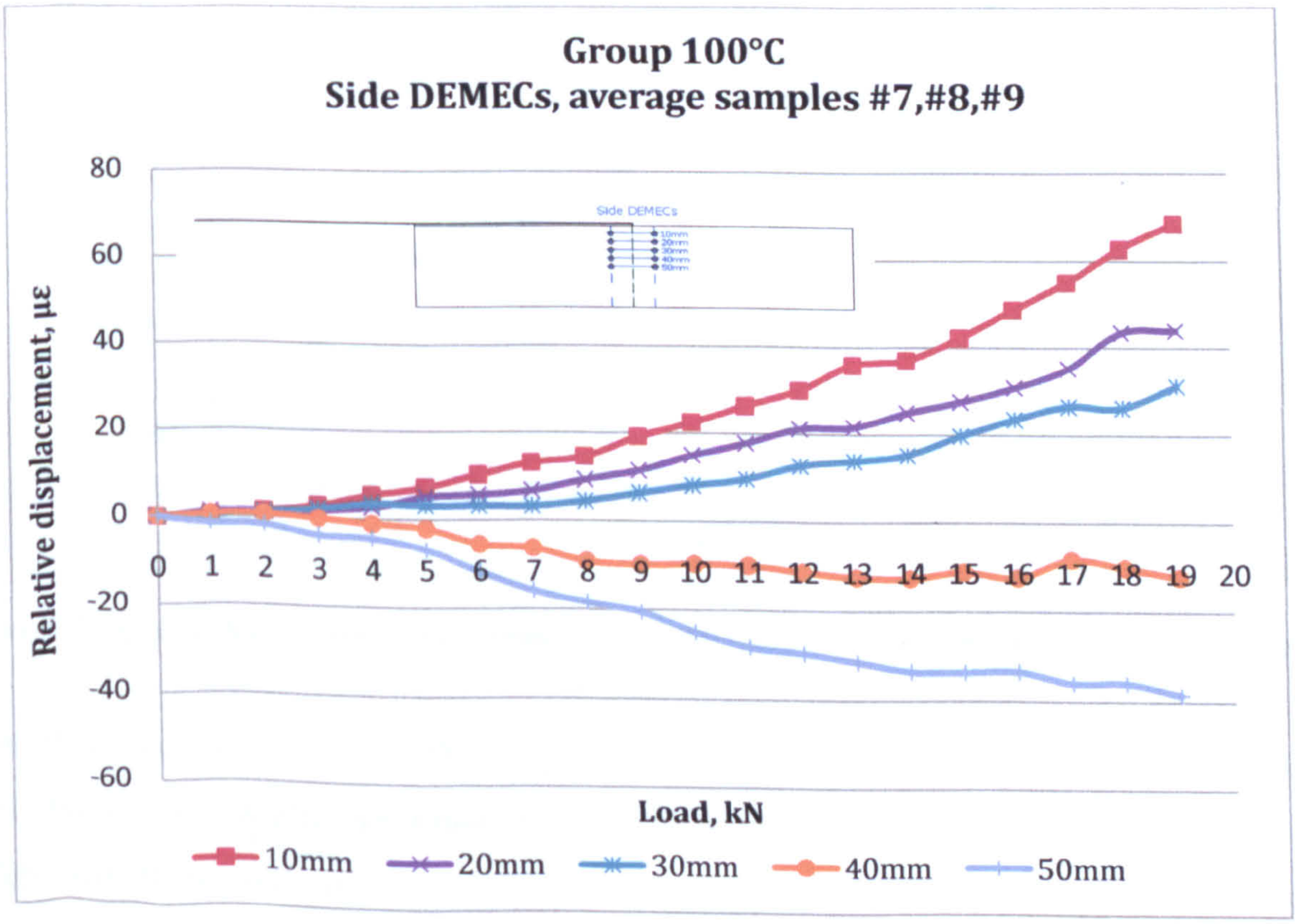

Figure III-20 Average local deformations before failure, side DEMEC strain gauges, group 100°C

The average deformation of the concrete at the end of the laminate was plotted for a range of loading from 0 to 19kN for group 100°C (Figure III-20). For all three samples increasing tensile deformations were established for level 10mm, 20mm and 30mm whilst at level 40mm and 50mm the predominant relative displacements were negative. Thus the neutral axis was found between the strain gauges at level 30 and 40mm. The average values at 19kN were 68 microstrain for level 10mm and 39microstrain for 50mm.

3.5.3.3 Concrete- laminate DEMEC strain gauges

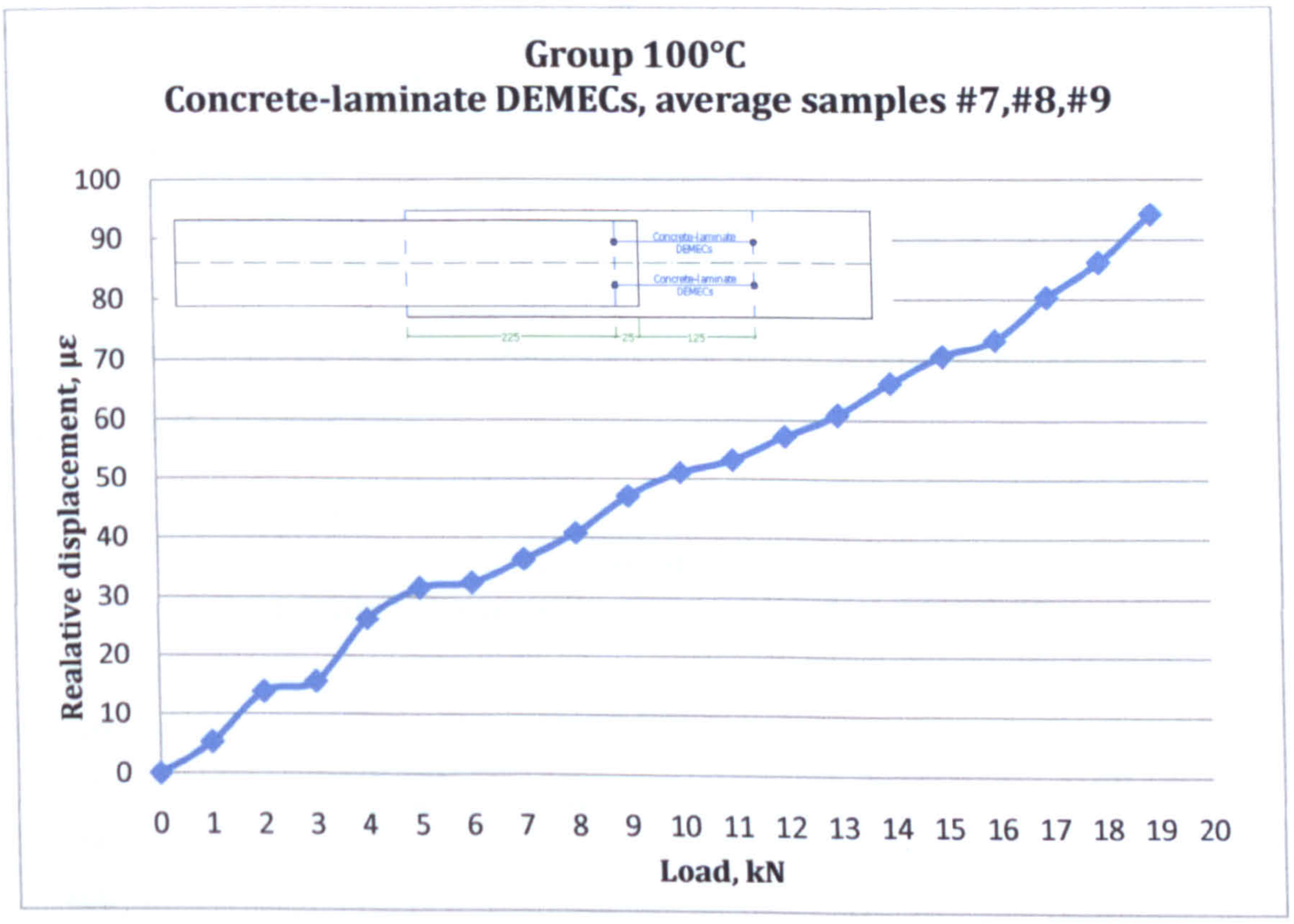

Figure III-21 Average local deformations before crack formation, concrete-laminate DEMEC strain gauges, group 100°C

For the three samples of group 100°C a gradual increase of the deformation was established to 16 kN above which higher deformations were measured, see Figure III-21. The average strain at 19kN was 94 microstrain.

3.5.3.4 Laminate DEMEC strain gauges

Gradual increase of the local deformations was established for the three samples of group 100°C to 19kN and the average deformation at 19kN was 668microstrain, see Figure III-22.

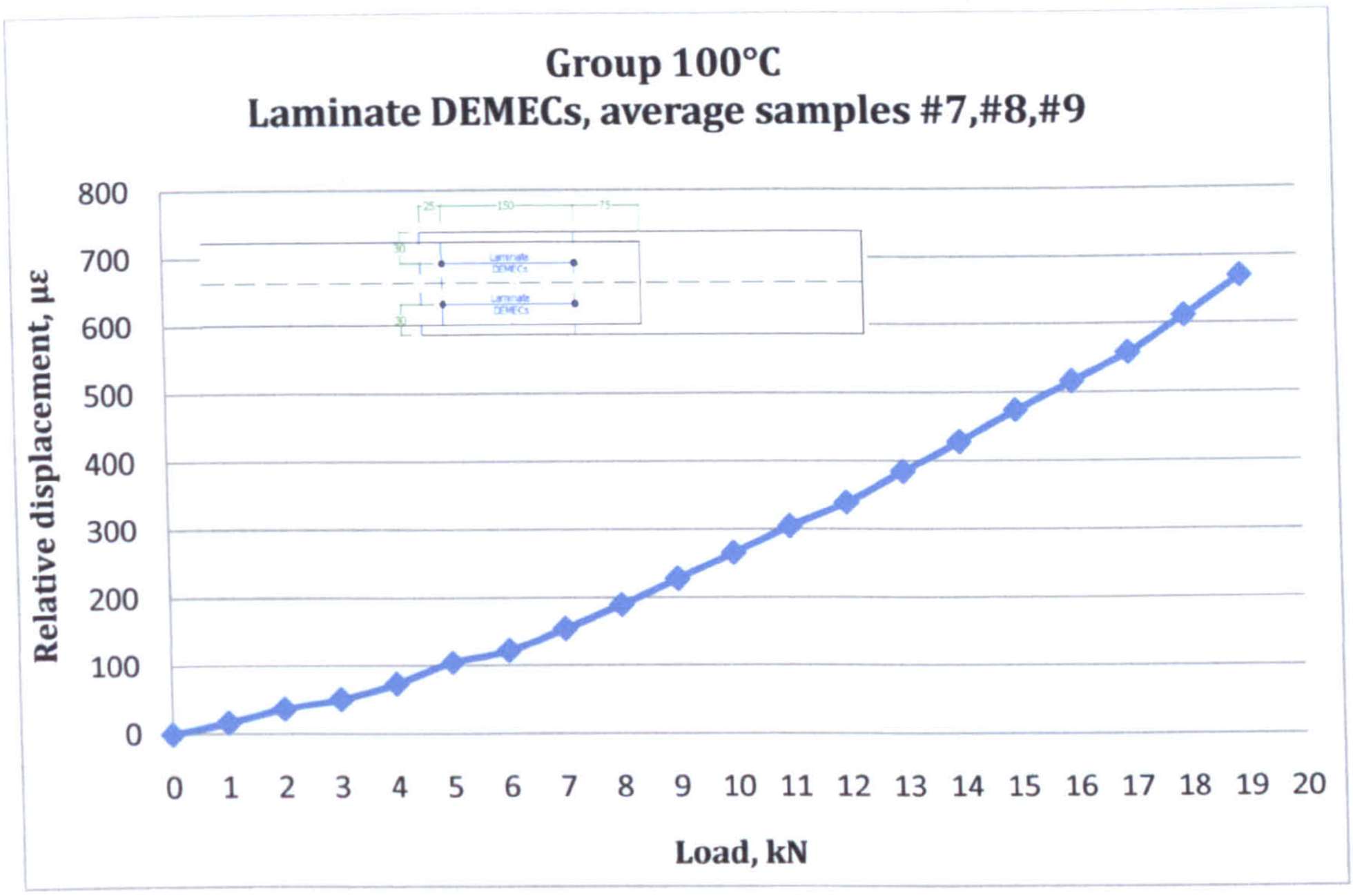

Figure III-22 Average local deformation, laminate DEMEC strain gauges, group 100°C

3.5.3.5 ER gauges

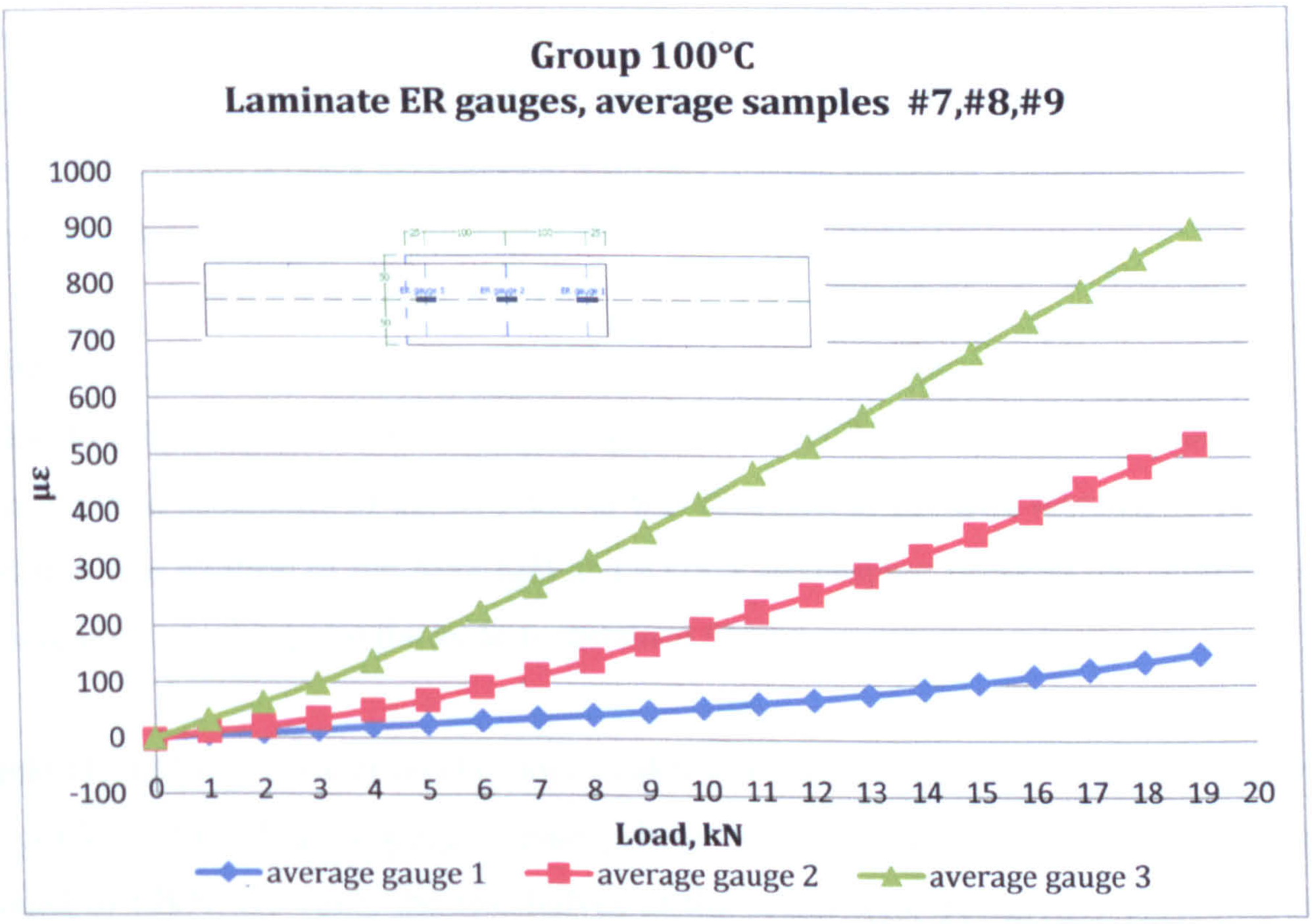

Figure III-23 Average ER strain gauges, group 100°C

The local deformations from the ER strain gauges attached to the laminate were plotted for loading up to 19kN, see Figure III-23. The average strain for ER gauge 1 was 154microstrain at 19kN and 900microstrain was measured for ER strain gauge 3. At 19kN the strain of ER gauge 2 was 521microstrain and the distribution of the strain was linear along the length of the laminate. Up to 12kN ER strain gauge 2 exhibited nonlinear behaviour with higher increase of the deformation above 12kN.

3.5.4 Group 150°C

3.5.4.1 Testing

The testing of the samples of group 150°C was conducted 9 months after their heating. At the time of the experiments the average cube compressive strength was 42.5MPa.

Samples #10 and #11 failed due to a crack in the concrete at the end of the laminate at the same level of load: 19kN (Figure III-24). Sample #10 retained 10kN or 53% of its failure load and was subsequently reloaded to 19kN when the crack reached the bottom of the prism. The increase of the load also resulted in the gradual vertical and horizontal displacement of the two halves. The load dropped to 16kN and was increased to 19kN which allowed the free rotation of the front half until a crack between the laminate and the adhesive were observed. The crack reduced the load to 11.6kN.

Sample #11 retained 65% of its failure load after the brittle failure of the system. The further increase to 18kN resulted in the full propagation of the crack and its vertical and horizontal expansion. Full separation of the two halves was achieved at the third increase to 18kN which resulted in free rotation of the front half and a crack developing between the laminate and the adhesive layer. At this point the system sustained 9kN.

Sample #12 failed at a lower level of load -16kN but was able to retain 36% of its failure load. The crack continued to propagate mainly in a horizontal direction when the system was reloaded to 12kN. By 16kN the two halves of the prism were completely separated and free

rotation was observed. A crack initiated between the laminate and the adhesive, which resulted in a drop of the load to 11.9kN.

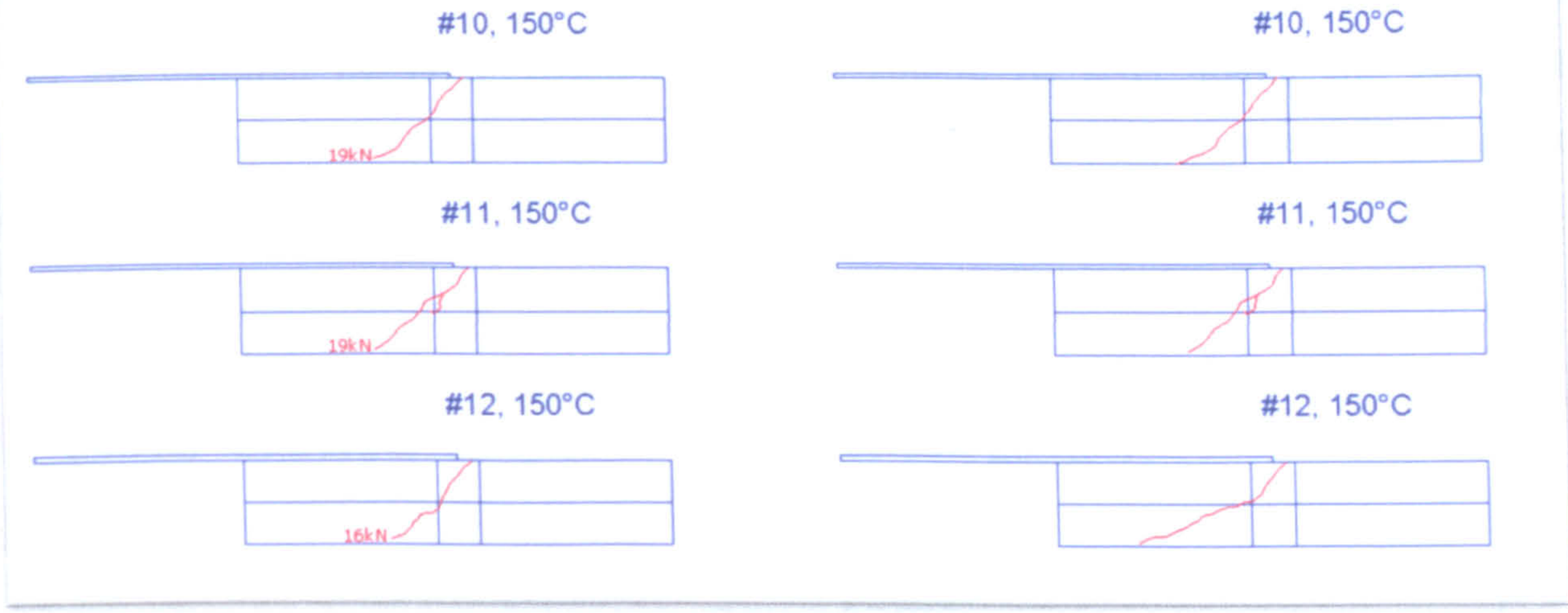

Figure III-24 Crack formation in samples, group 150°C, left-initial crack, right-final crack

3.5.4.2 Side DEMEC strain gauges

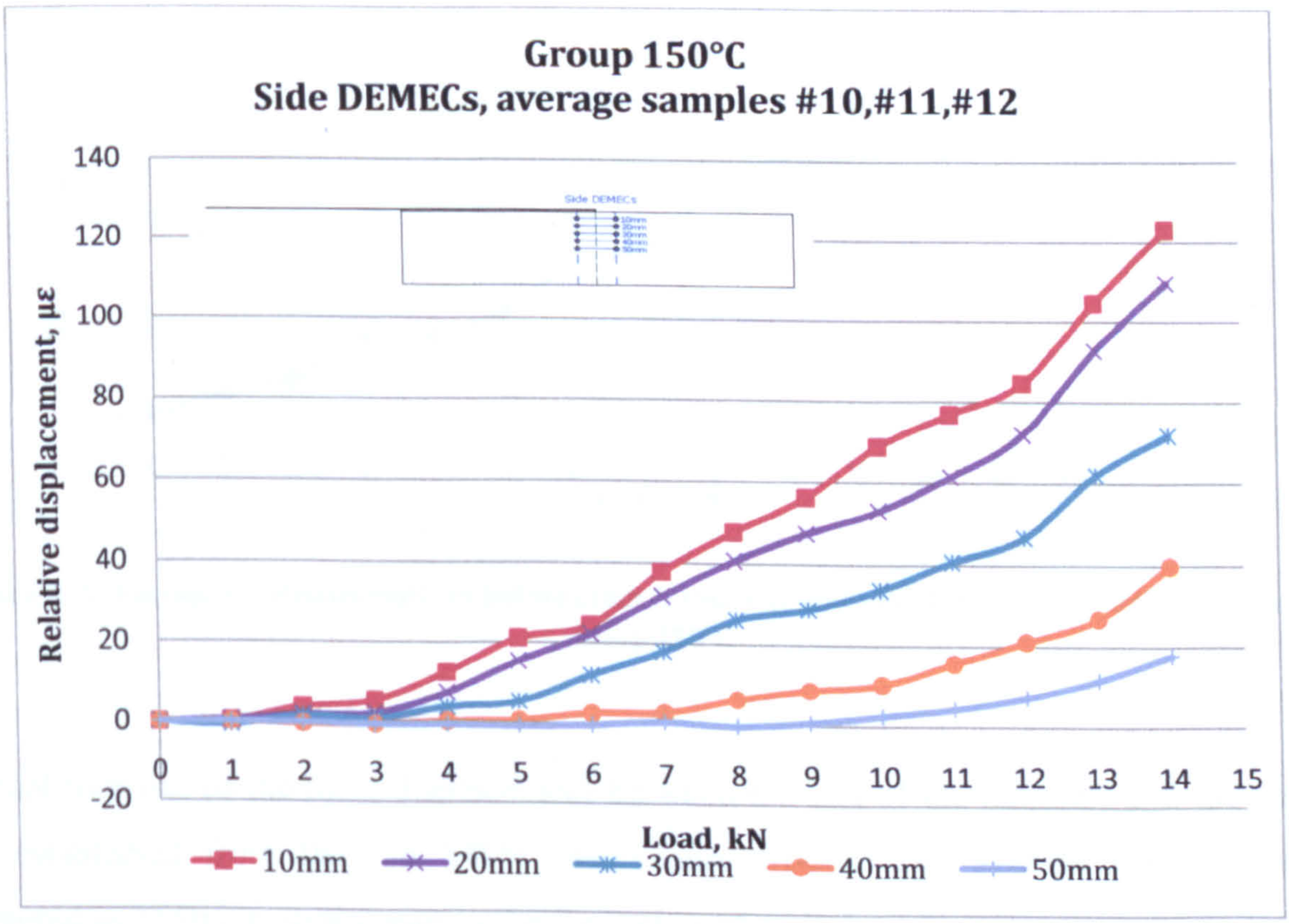

Figure III-25 Average local deformations before failure, side DEMEC strain gauges, group 150°C

The side local deformations in the concrete at the end of the laminate were plotted for a range of 0 to 14kN (Figure III-25). For all three samples of the group the deformations in the upper half of the beam were positive or neutral. Level 10mm reached tensile strain of 123microstrain at 14 kN followed by 110microstrain for level 20mm. At level 40mm and 50mm the deformations were detected at 7kN reaching average values of 40microstrain for 40mm and 18microstrain for 50mm.

3.5.4.3 Concrete- laminate DEMEC strain gauges

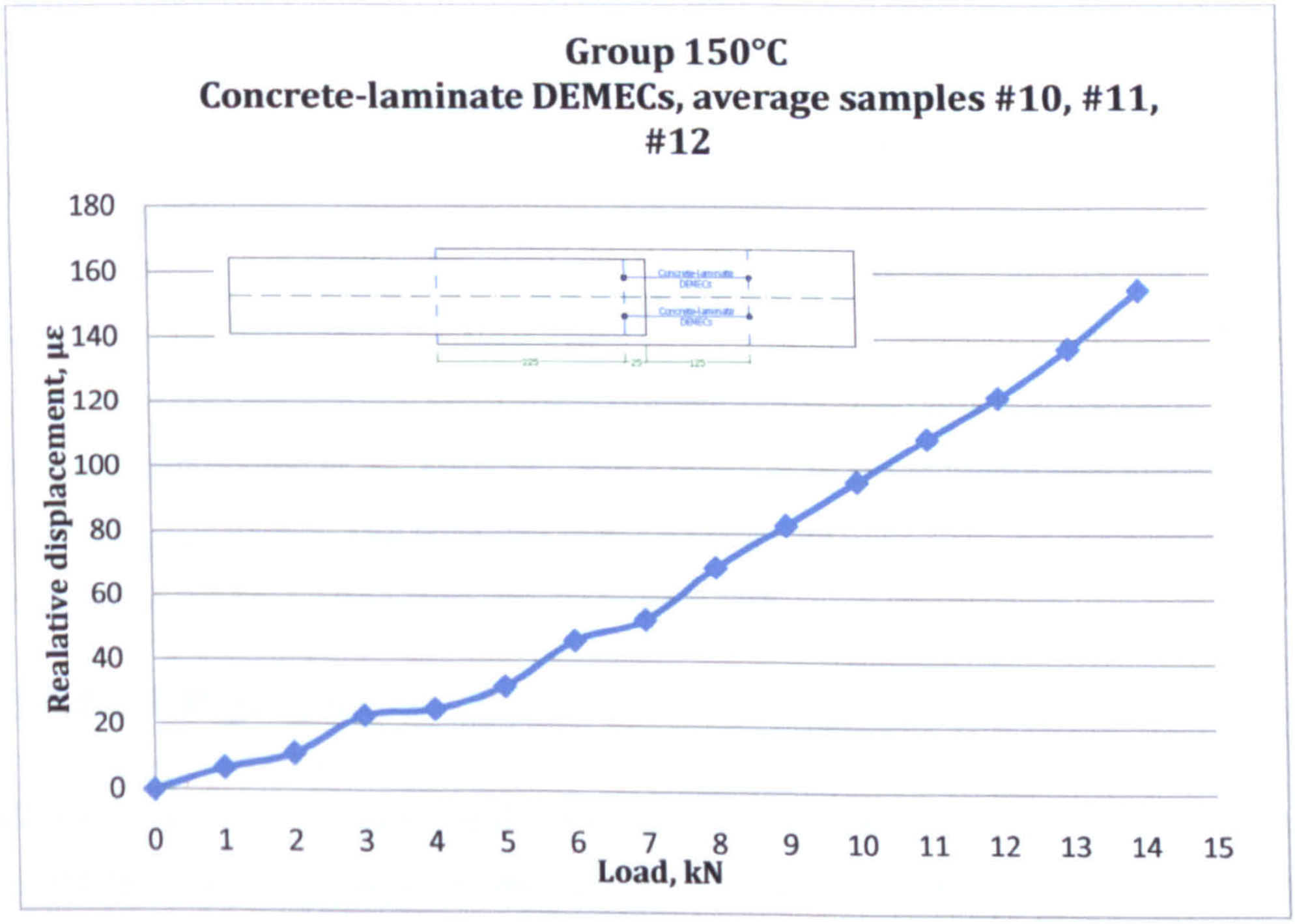

Figure III-26 Average local deformations before crack formation, concrete-laminate DEMEC strain gauges, group 150°C

Gradual increase of the local displacement between the end of the laminate and the concrete was established from 0kN to 14kN (see Figure III-26). The average deformation was registered as 155microstrain prior to the formation of a crack.

3.5.4.4 Laminate DEMEC strain gauges

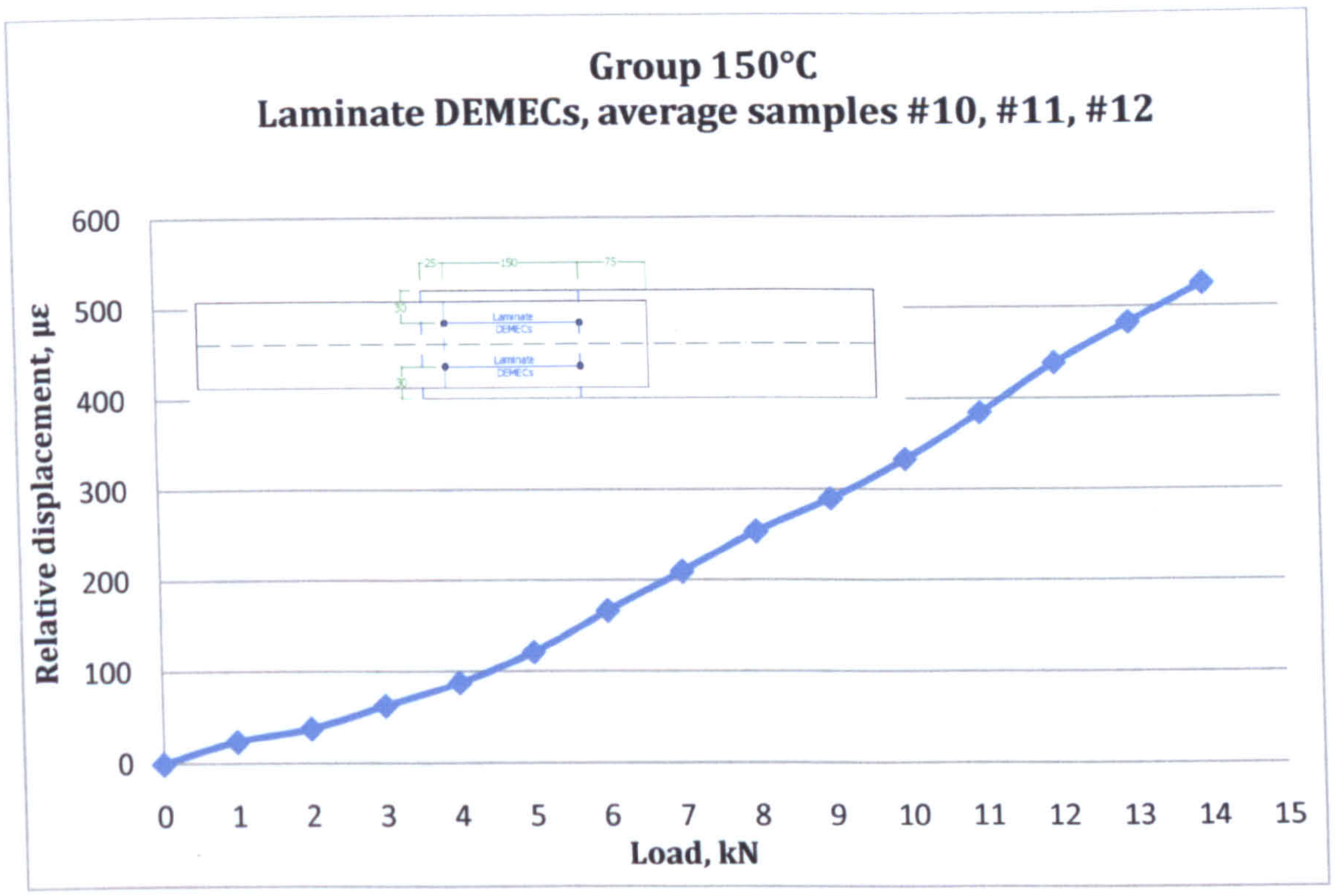

Figure III-27 Average local deformation, laminate DEMEC strain gauges, group 150°C

The relative displacement of the DEMEC points attached to the laminate was plotted for loads up to 14kN (Figure III-27). The behavior of the system was nonlinear and the average value of the tensile strain for the highest load was 524microstrain.

3.5.4.5 ER gauges

For all three ER strain gauges the deformation was increasing gradually up to 14kN, see Figure III-28. For ER gauge 1 the value at 14kN was 683microstrain, for ER 2-336microstrain and from the ER gauge closest to the end of the laminate average strain was found to be 76microstrain.

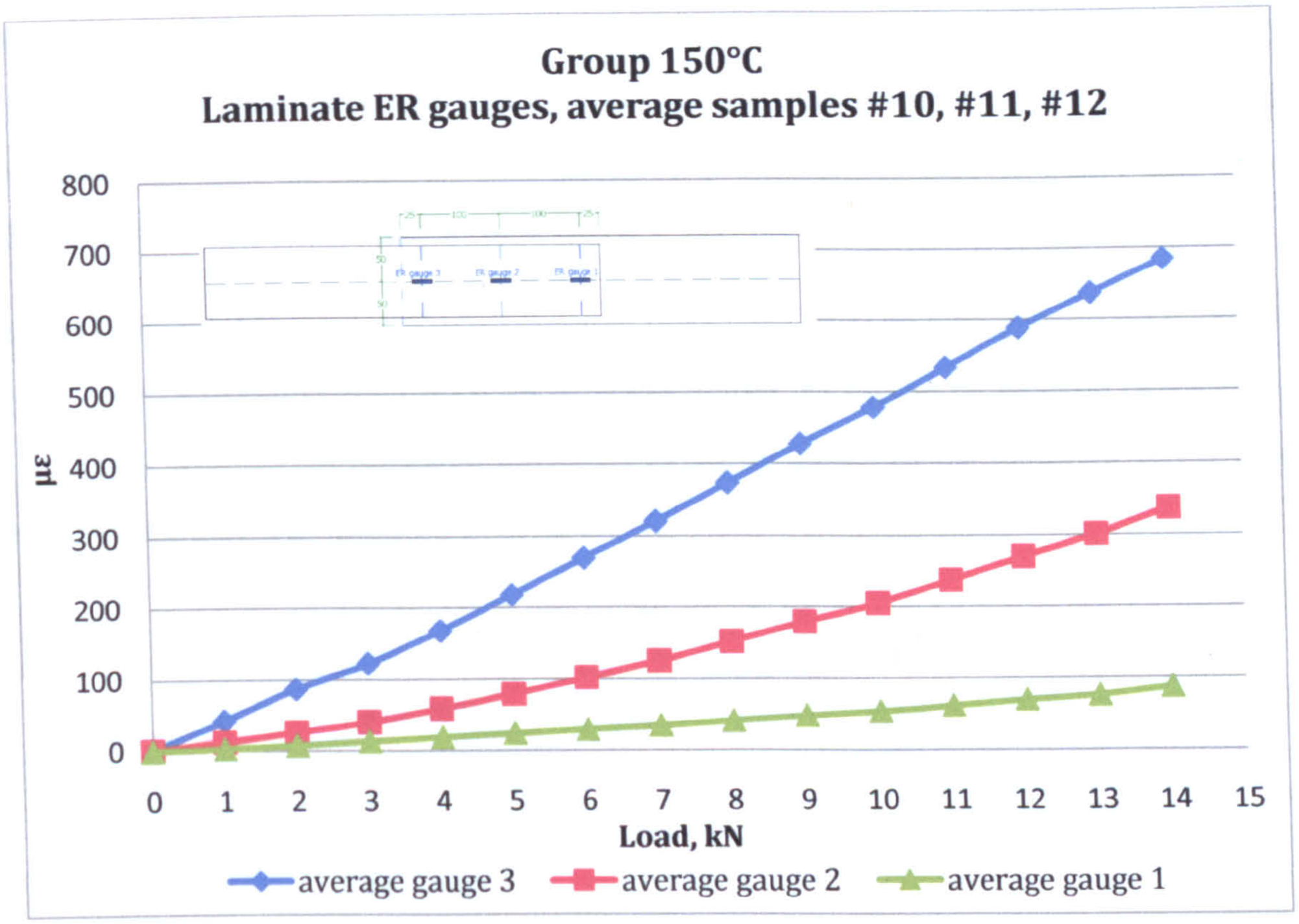

Figure III-28 Average ER strain gauges, group 150°C

3.5.5 Group 200°C

3.5.5.1 Testing

The samples of group 200°C were tested 9 months after their heating. At the time of the experiments the average cube compressive strength was 39.18 MPa.

The samples of the group 200°C failed at the same level of load-10kN due to a crack in the concrete near the end of the laminate (Figure III-29). The crack propagated through the upper half of the prism of sample #13 after which the system retained 8.9kN. The crack continued to propagate downwards up to 11kN after which its direction changed to horizontal until at 16kN the bottom was reached. Rotation followed with reduction of the load to 14kN. The maximum load which triggered delamination between the adhesive and the concrete was achieved at 18kN, after which the system carried 10.3kN before complete delamination occurred.

Sample #14 carried 79% after the initial crack had propagated through ¾ of the height of the prism. With increase of the load the crack continued to develop at 45°angle until at 14.7kN it

had propagated through the whole height of the prism. The two halves were then separated and free rotation of the front half was observed before the load dropped to 8.6 kN. Delamination was initiated between the laminate and adhesive at further increase to 10kN and the system held 7.4kN before full delamination took place.

Sample #15 behaved in a very similar manner to sample #14. The load dropped to 7.8kN after the initial crack had propagated through ¾ of the height, followed by gradual increase to 15kN when the crack had fully propagated through the whole height of the concrete and free rotation began. Delamination was initiated at 6.7kN.

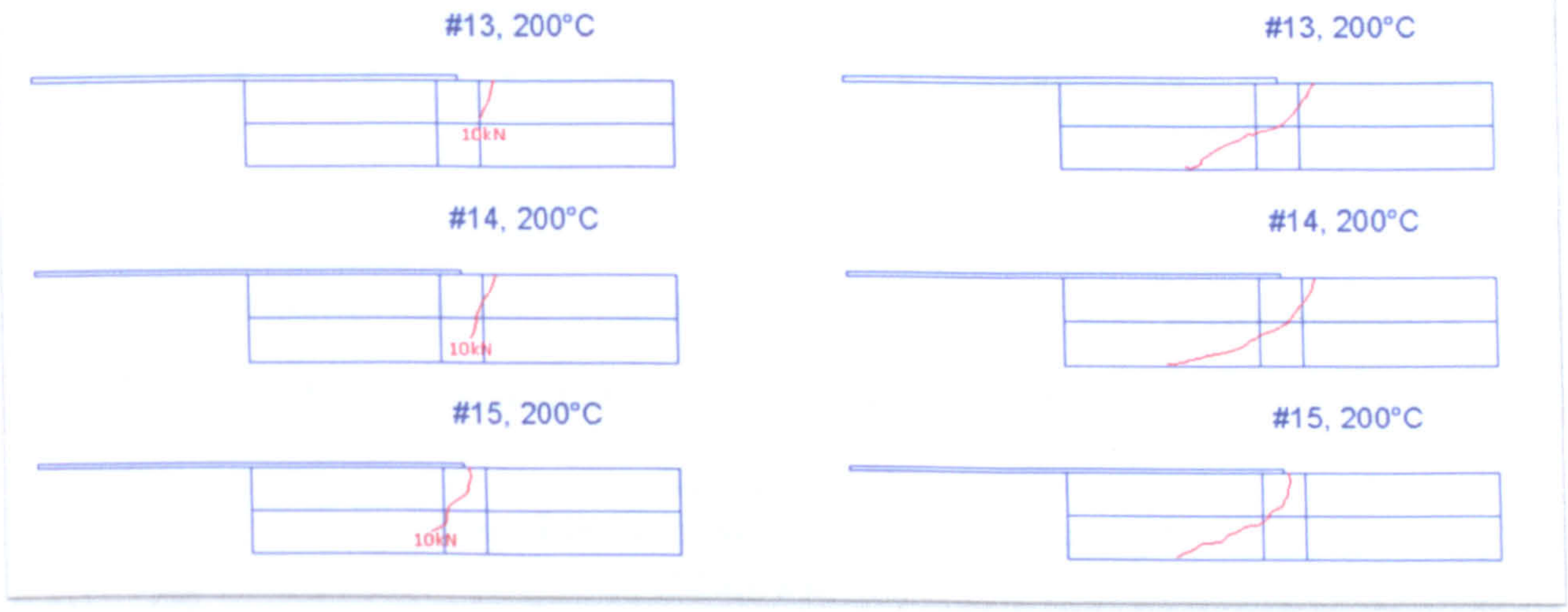

Figure III-29 Crack formation in samples, group 200°C, left-initial crack, right- final crack

3.5.5.2 Side DEMEC strain gauges

The side local deformations of the concrete at the end of the laminate were plotted from 0kN to 8kN, see Figure III-30. Tensile strains were measured to level 30mm with increase of the load. At level 40mm and 50mm the displacements started to increase from 5kN. The average strain at level 8kN for level 10mm was 164microstrain and at level 50mm the displacement was 20microstrain.

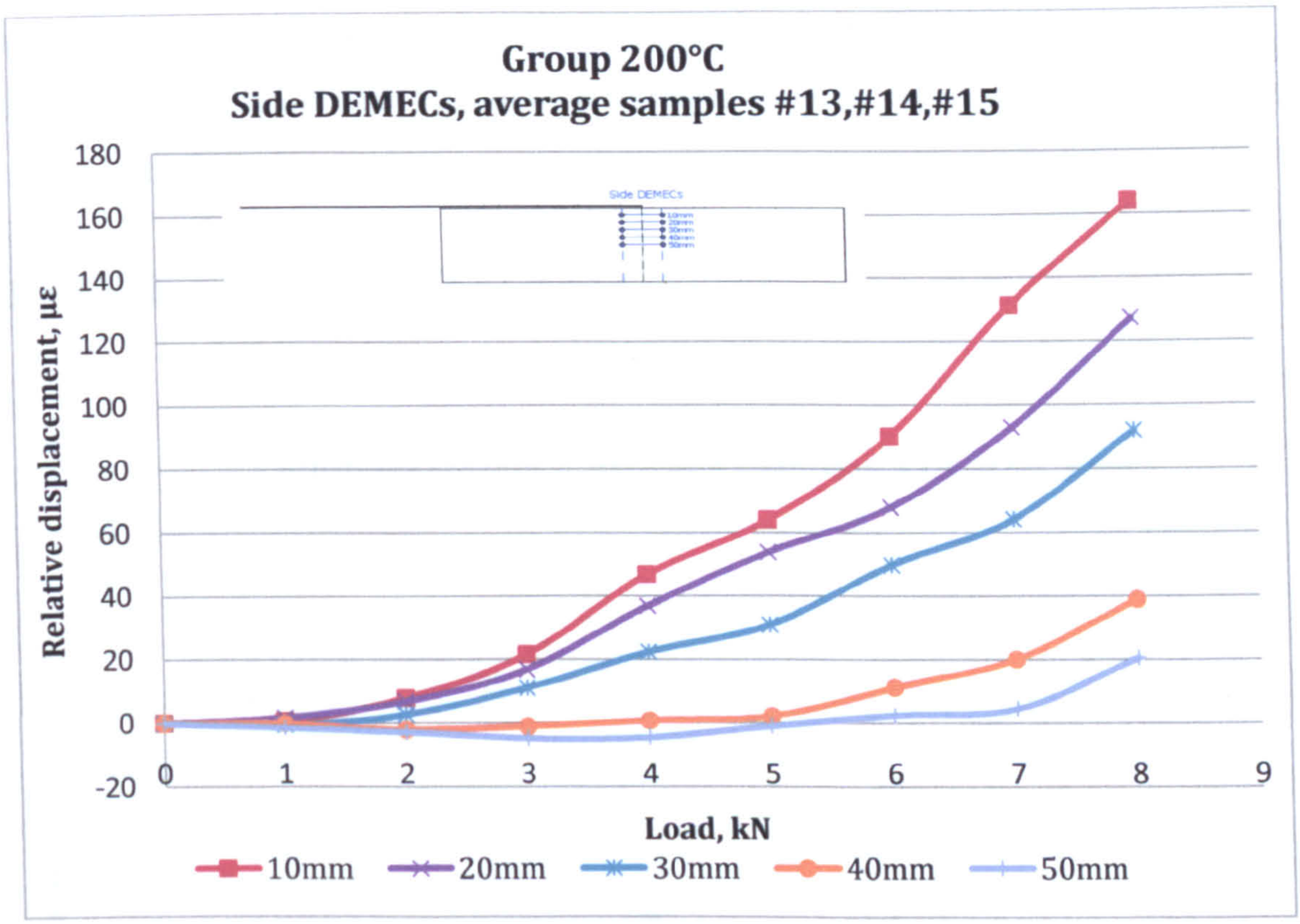

Figure III-30 Average local deformations before failure, side DEMEC strain gauges, group 200°C

3.5.5.3 Concrete- laminate DEMEC strain gauges

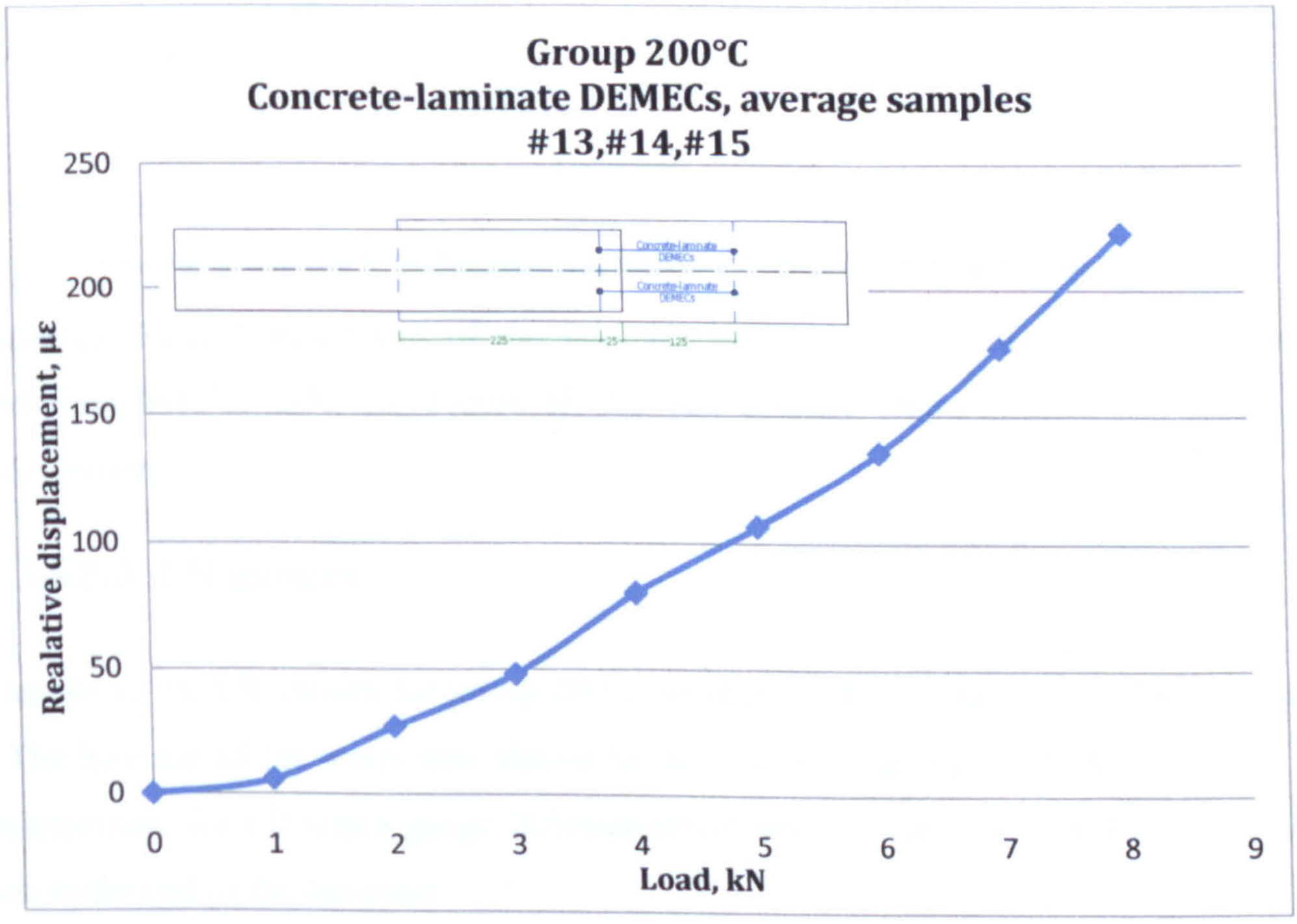

Figure III-31 Average local deformations before crack formation, concrete-laminate DEMEC strain gauges, group 200°C

For the three samples of the group gradual increase of the deformations between the end of the laminate and the concrete were observed from 0kN to 8kN, see Figure III-31. The average strain at 8kN was 223microstrain.

3.5.5.4 Laminate DEMEC strain gauges

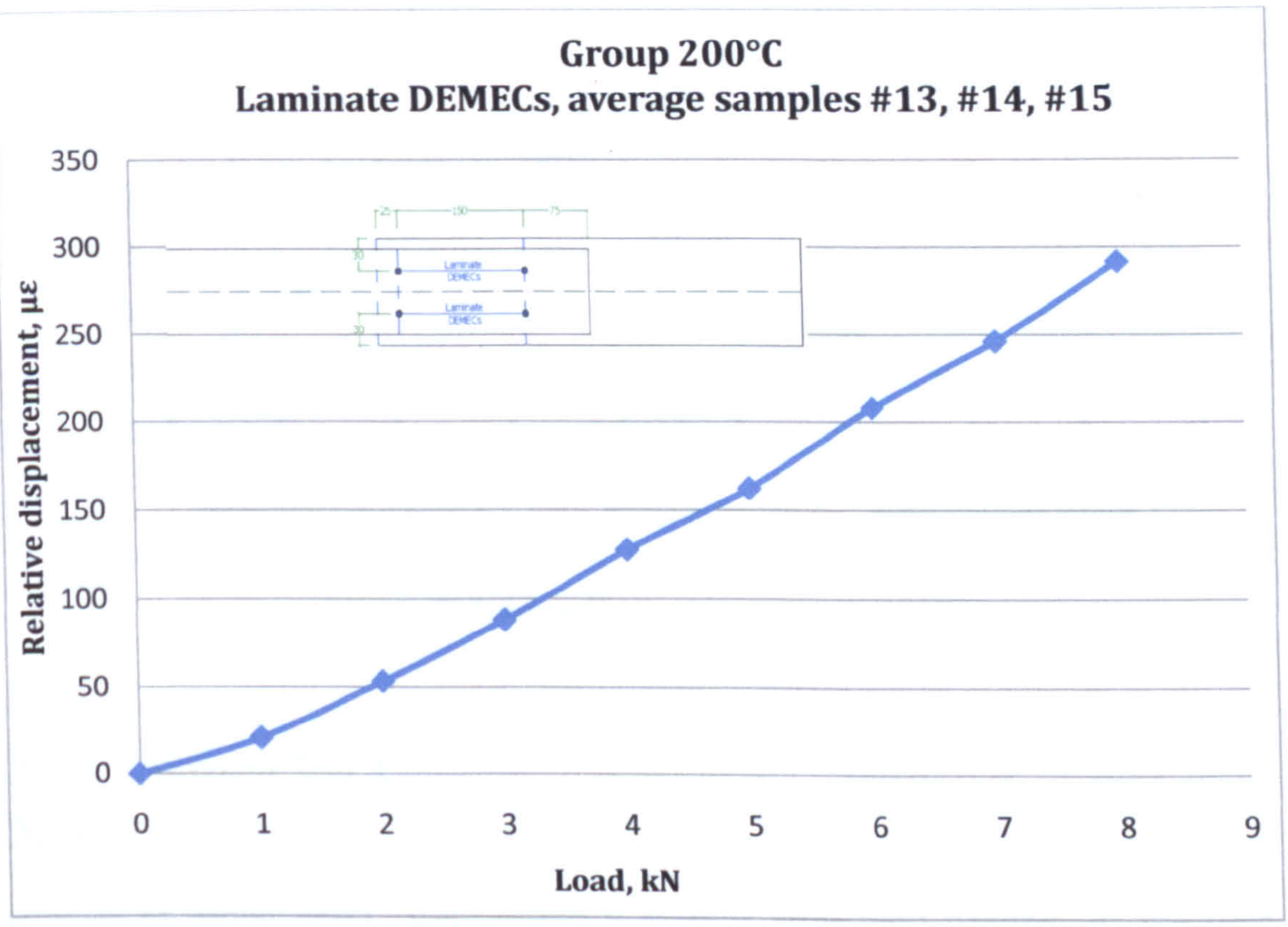

Figure III-32 Average local deformation, laminate DEMEC strain gauges, group 200°C

The average local displacement of the laminate measured by DEMEC strain gauges was plotted from 0kN to 8kN, see Figure III-32. The average strain at 8kN was found to be 291microstrain.

3.5.5.5 ER gauges

The results of the ER gauges for group 200°C were plotted for loads 0kN to 8kN (Figure III-33). The increase of the strain was almost linear. The average value of the ER gauge 1 was 418microstrain, for ER strain gauge 206microstrain and 51microstrain for ER strain gauge 1 closest to the end of the laminate.

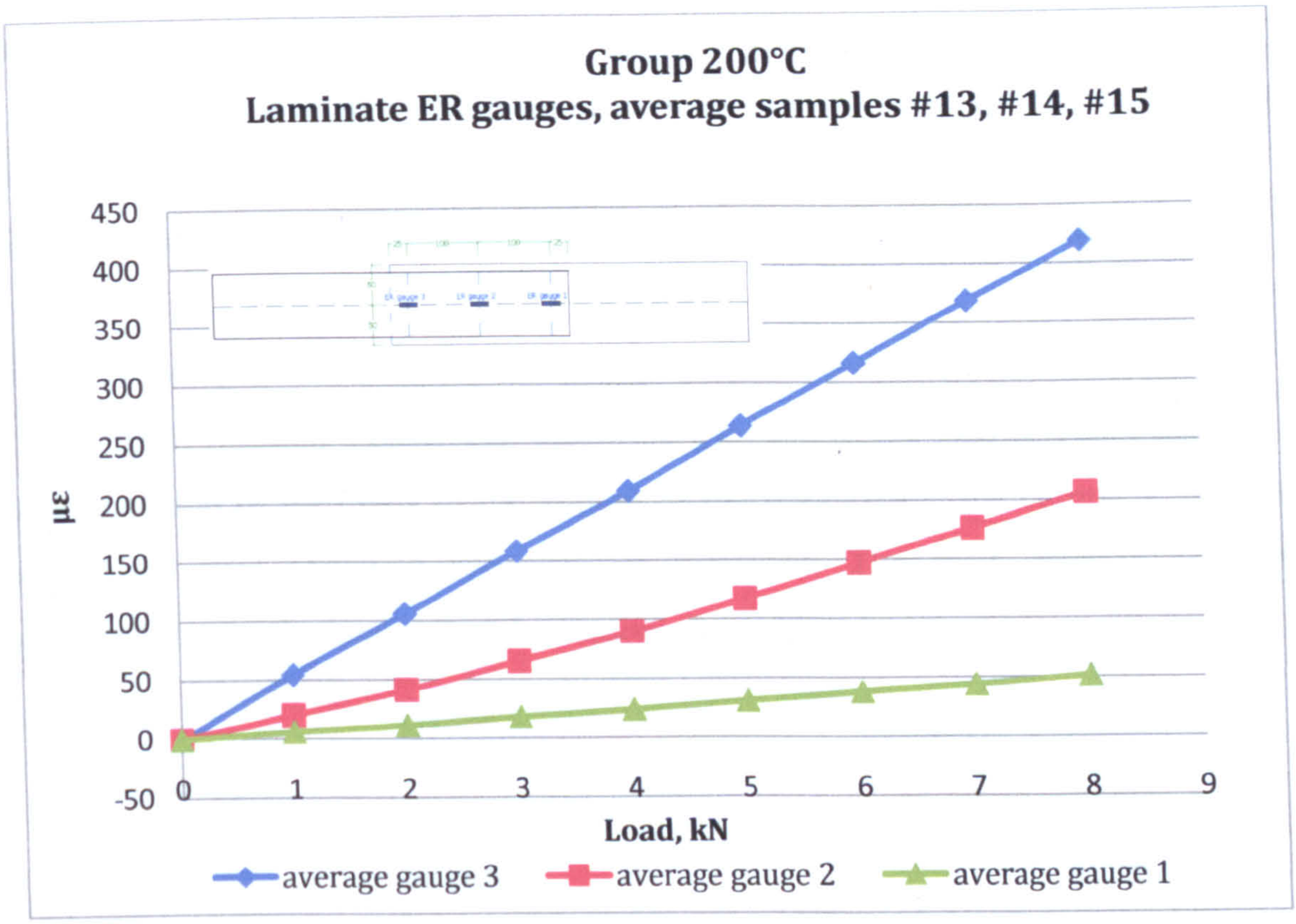

Figure III-33 Average ER strain gauges, group 200°C

3.5.6 Group 250°C

3.5.6.1 Testing

The samples of group 250°C were tested 9 months after their heating. At the time of the experiments the average cube compressive strength was 34.3 MPa.

Sample #16 failed at 7kN by a 45° angle through the upper half of the prism after which the system held 5.5kN, see Figure III-34. The reloading of the system to 6.5kN resulted in further propagation in combination of 45° angle and horizontal crack. At 9.6kN the crack had propagated to the front of the prism causing free rotation of the front half followed by drop of the load to 3.3kN. The delamination between the laminate and the adhesive was initiated at 4kN and the further increase resulted in a more significant rotation of the concrete compared to the more slow propagation of the crack until the full delamination was completed.

A vertical crack propagated through 2/5 of the height of sample #17 at 7kN. After the crack occurred the load dropped by only 0.2kN and at further increase to 8kN it continued to

develop vertically. At higher loads another crack started to develop from the tip of the first crack as a parabolic crack until it reached the front side of the prism and free rotation was observed. The load dropped to 6.3kN after which the further increase of the load led to significant rotation before the initiation of the crack between the laminate and adhesive.

The failure of sample #18 occurred at loading to 9kN due to the formation of a 45° angle crack, although it retained 6.8kN. The following increase of the load to 12kN resulted in the further propagation of the crack to the bottom of the prism when the complete separation of the two halves was observed and rotation followed. The load dropped to 6kN and delamination between the laminate and adhesive was initiated.

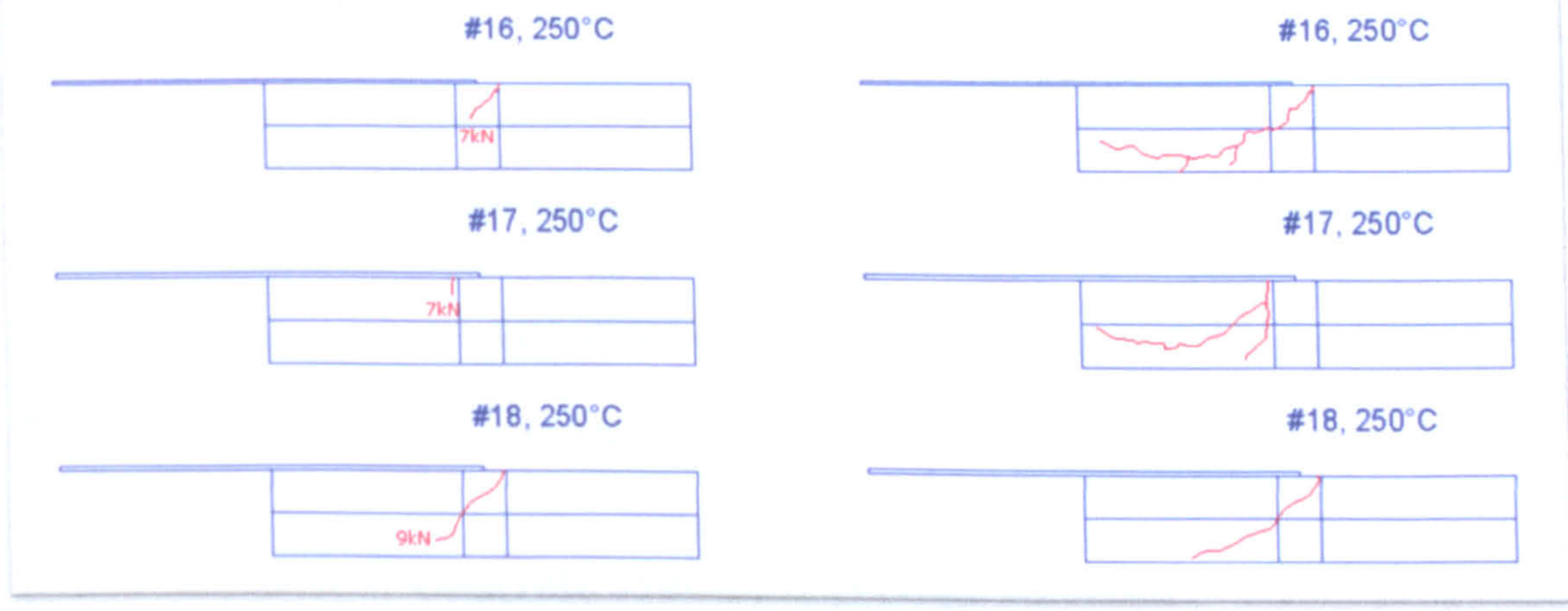

Figure III-34 Crack formation in samples, group 250°C, left-initial crack, right-final crack

3.5.6.2 Side DEMEC strain gauges

The average local deformations at the end of the laminate for the three samples of group 200°C were plotted for a range of 0kN to a load of 6kN, see Figure III-35. The tensile strains were found to develop from the top to level 50mm where the deformations were zero. Increase of the load to 6kN resulted in tensile strains with a maximum average value of 108microstrain prior to the formation of a crack in the concrete at the end of the laminate.

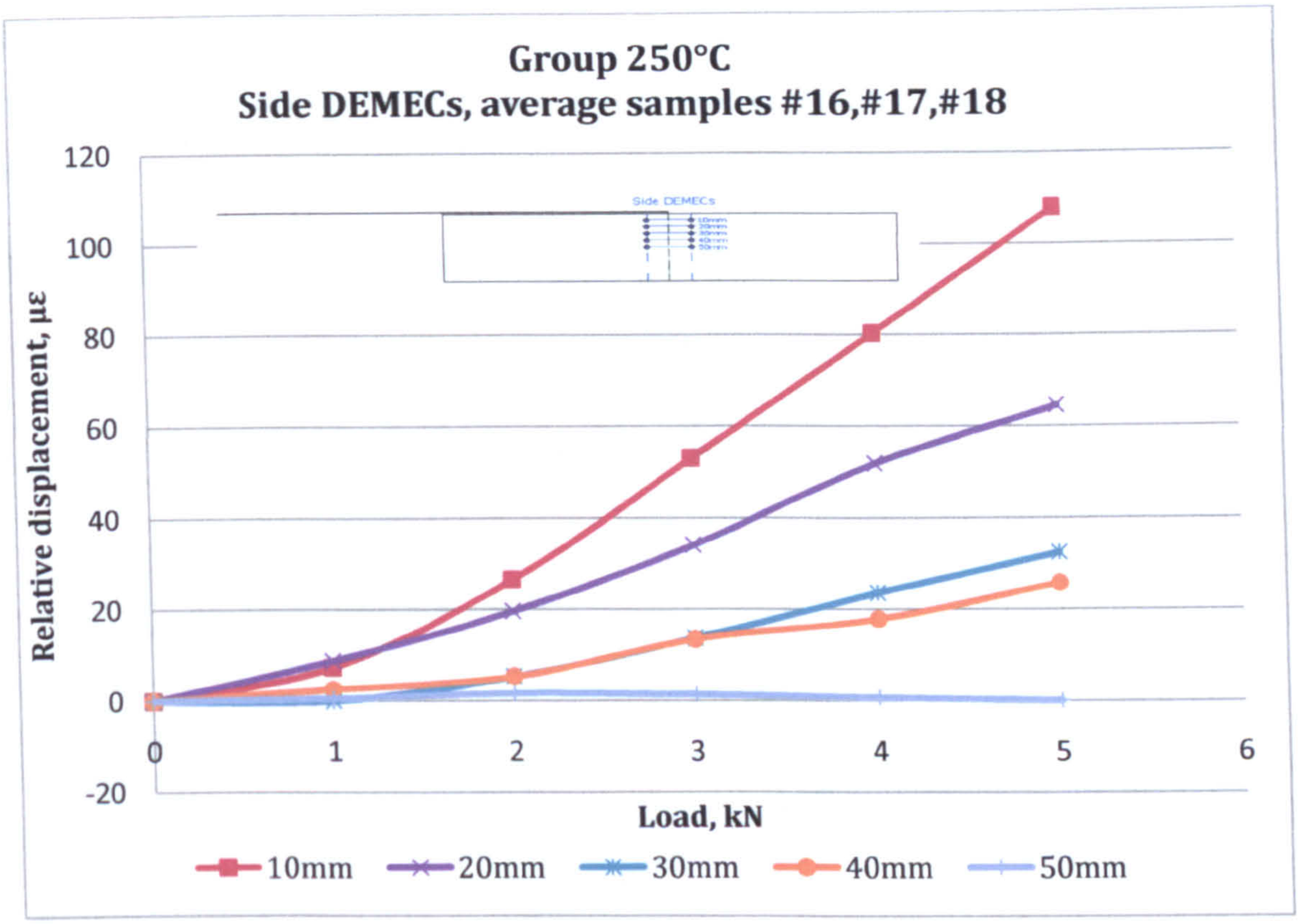

Figure III-35 Average local deformations before failure, side DEMEC strain gauges, group 250°C

3.5.6.3 Concrete- laminate DEMEC strain gauges

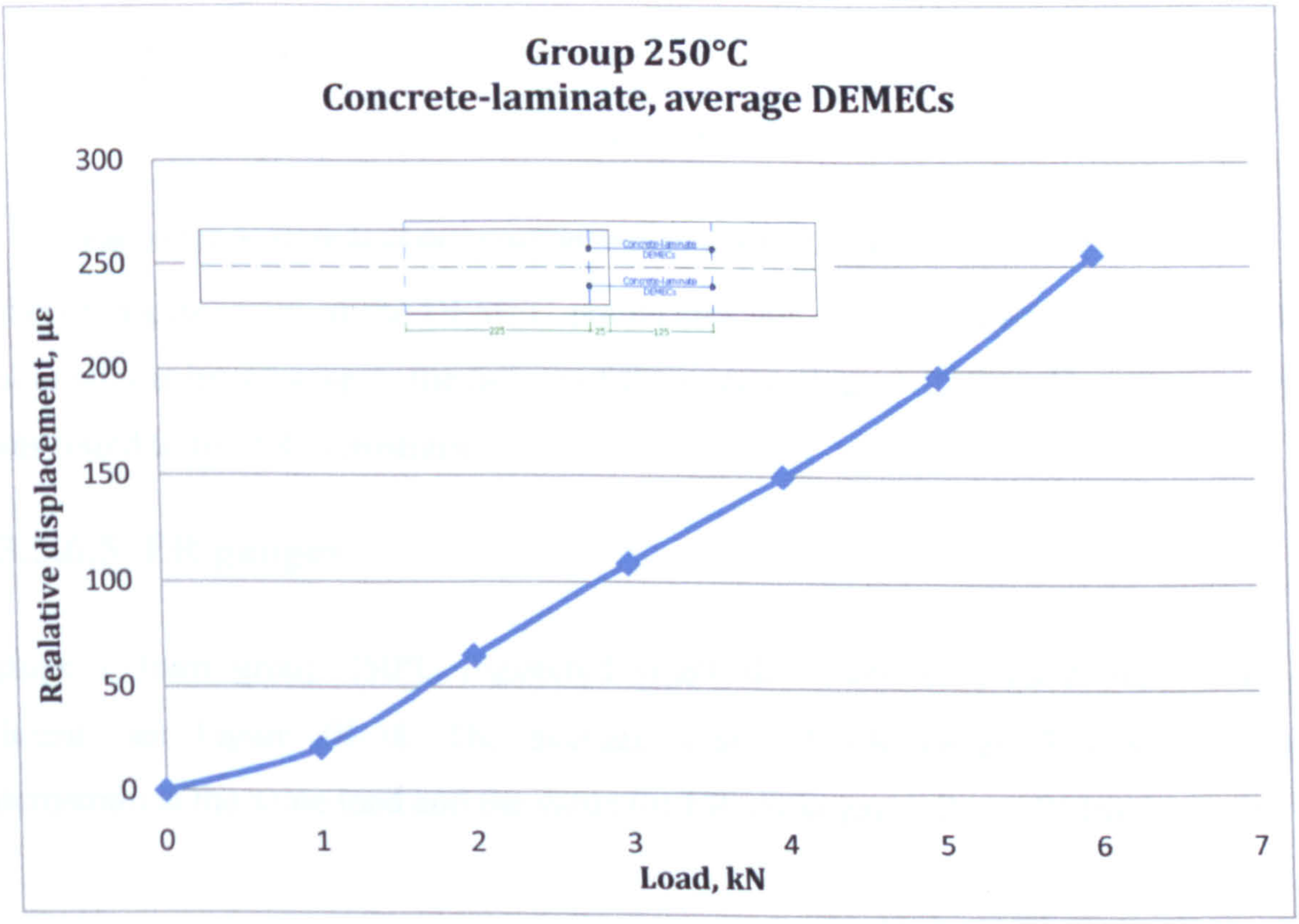

Figure III-36 Average local deformations before crack formation, concrete-laminate DEMEC strain gauges, group 250°C

The increase of the relative displacement between the end of the laminate and the concrete was found to be gradual up to 6kN, see Figure III-36. The average value was found to be 255microstrain.

3.5.6.4 Laminate DEMEC strain gauges

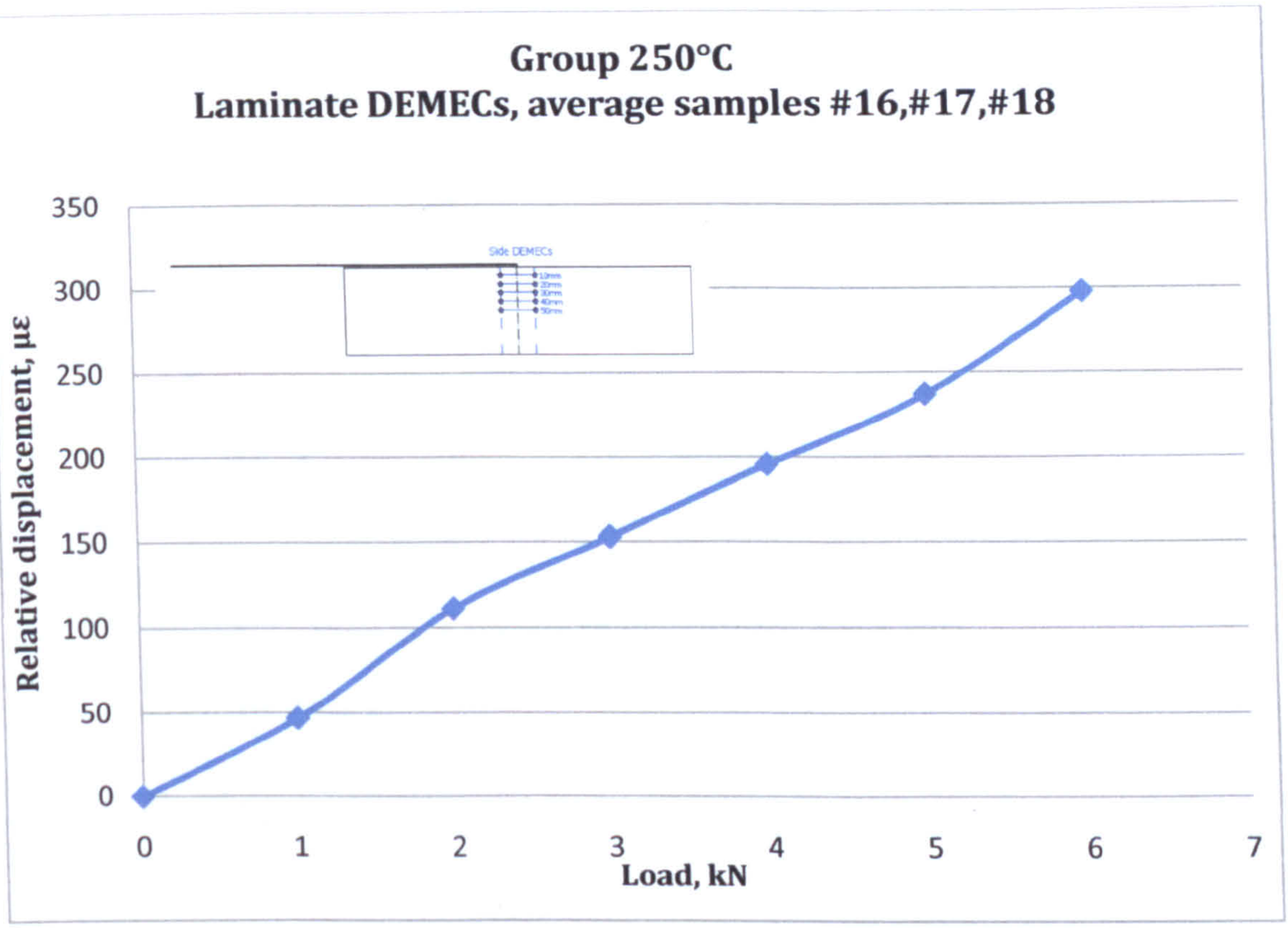

Figure III-37 Average local deformation, laminate DEMEC strain gauges, group 250°C

The relative displacement of the DEMEC points attached to the laminate was described by a gradual nonlinear increase up to the failure of the system (Figure III-37). The average strain at 6kN was found to be 298microstrain.

3.5.6.5 ER gauges

ER gauge 1 from group 250°C registered small deformations 10microstrain during the experiment, see Figure III-38. The average strain of ER gauge 3 was found to be 372microstrain at the same load and the value for ER strain gauge 2 was 261microstrain.

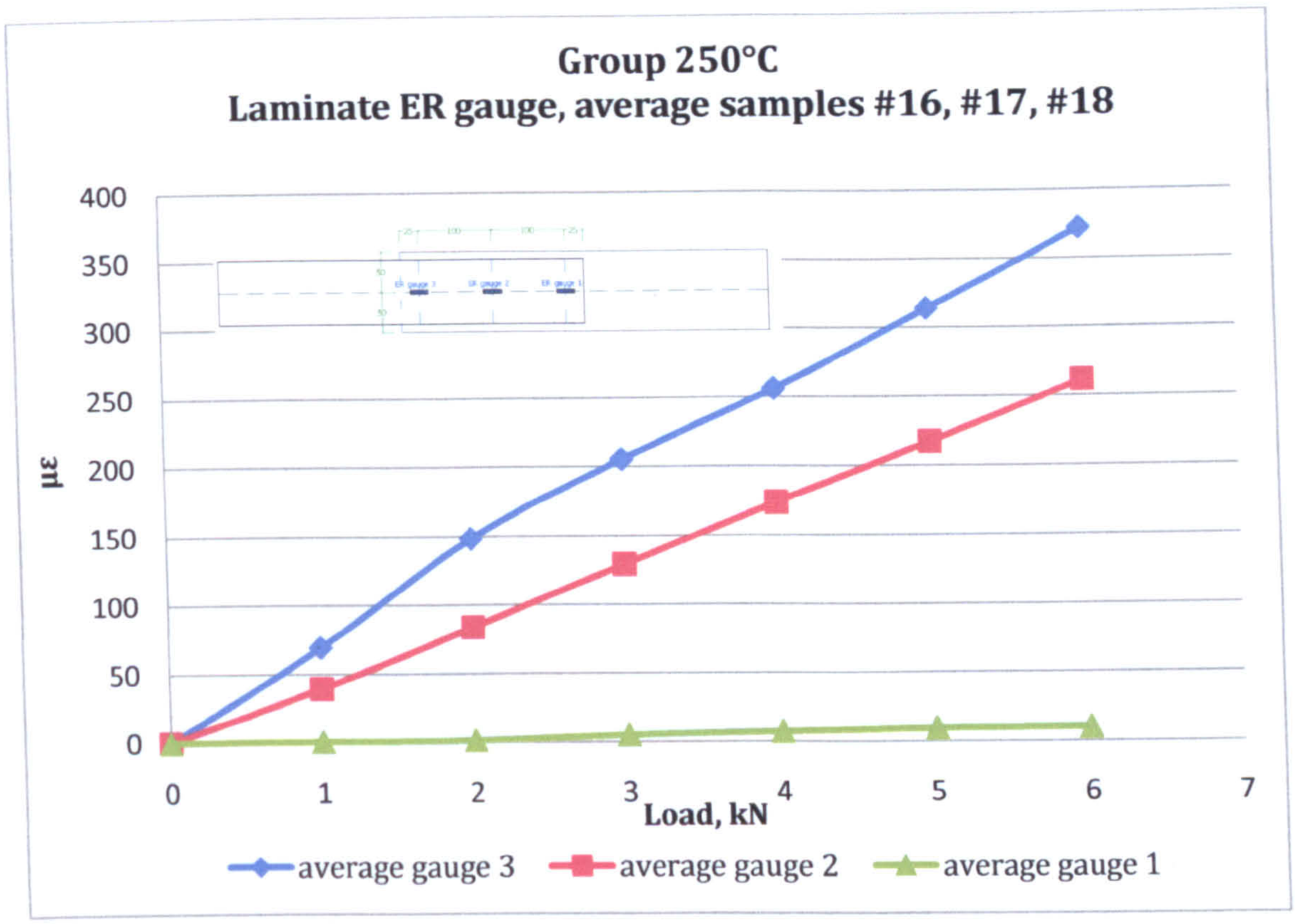

Figure III-38 Average ER strain gauges, group 250°C

3.5.7 Group 300°C

3.5.7.1 Testing

The samples of group 300°C were tested last, about 10 months after their heating. The average cube strength tested about the time of the testing was 31.01MPa.

Crack developed through ¾ of the height of sample #19 when the load reached 8kN, which then was reduced to 6kN or by 25% from the failure load, see Figure III-39. At the further increase of the load another crack propagated at 45° angle which resulted in a rotation of the front half until at 7.2kN sudden delamination between the laminate and the adhesive occurred.

Sample #20 failed at 8kN due to a crack through the upper half of the prism. The sample then held 70% of the failure load. Further increase of the load to 8kN led to further propagation of the crack at 45° angle and reduction of the load. Delamination was observed when the system was reloaded to 8kN followed by reduction to 1.3kN before the full delamination.

Sample #21 exhibited some cracking in the concrete at level 6kN without reduction of the load. Cracks developed through ¾ of the height of the prism at 9kN which caused drop of the load to 5.2kN. Further increase of the load led to the propagation of the crack through the full length of the interface.

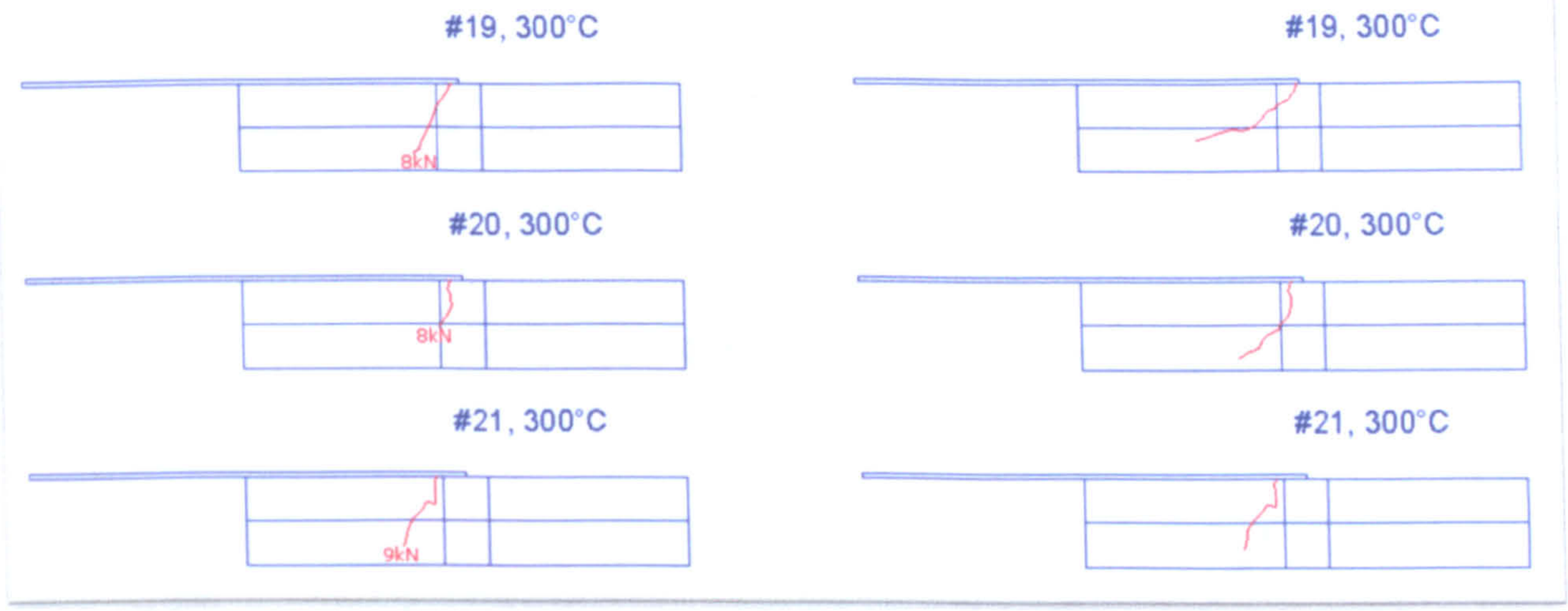

Figure III-39 Crack formation in samples, group 300°C, left-initial crack, right-final crack

3.5.7.2 Side DEMEC strain gauges

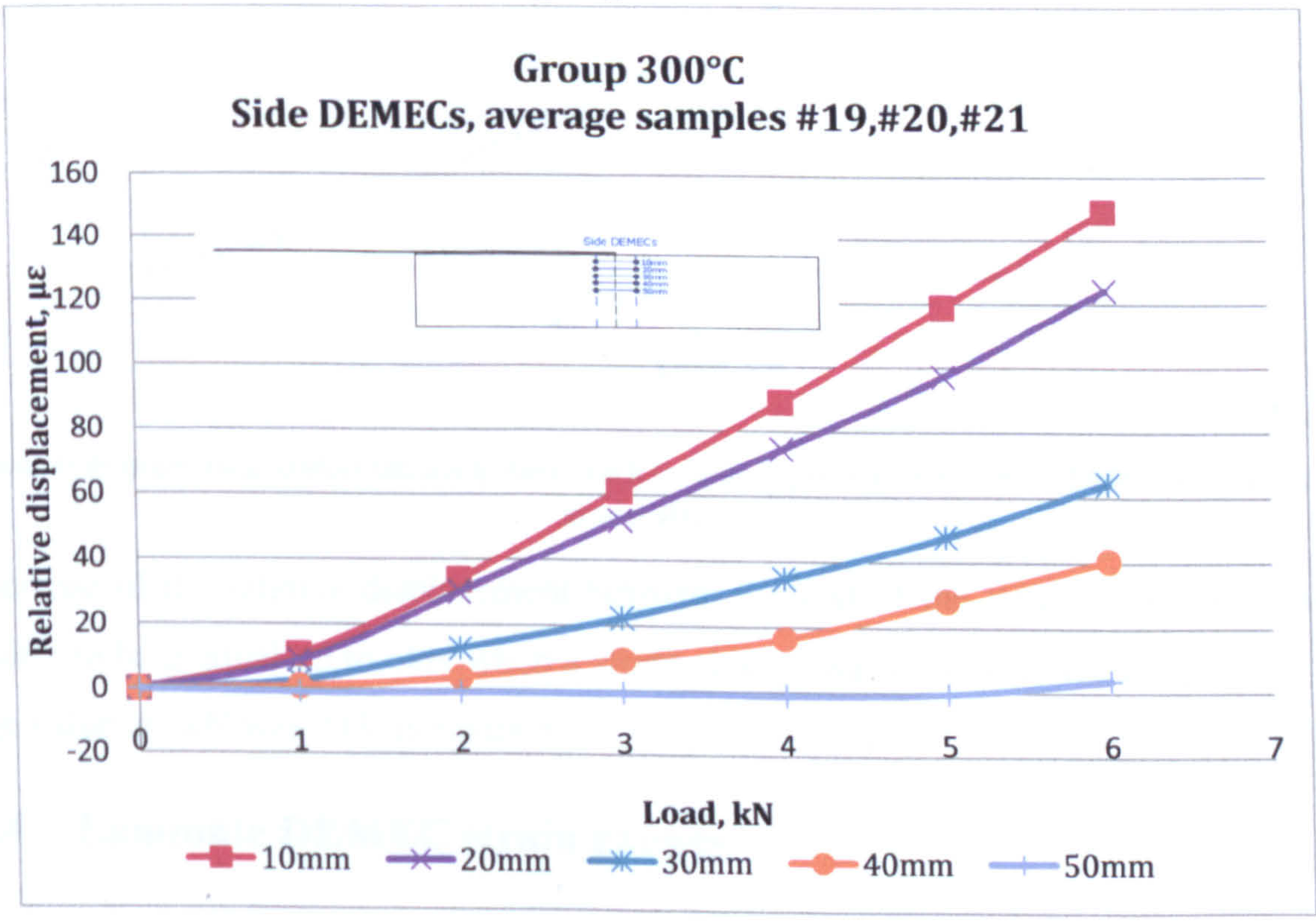

Figure III-40 Average local deformations before failure, side DEMEC strain gauges, group 300°C

For all 3 samples of the group #19,#20 and #21 the local deformations to level 40mm were found to be positive and at level 50 neutral relative displacements were measured (Figure III-40). Level 10mm and 20mm reached 149 and 124 microstrain at 6kN and at level 30 and 40mm the local deformation increased to 64 and 40 microstrain before the formation of the crack.

3.5.7.3 Concrete- laminate DEMEC strain gauges

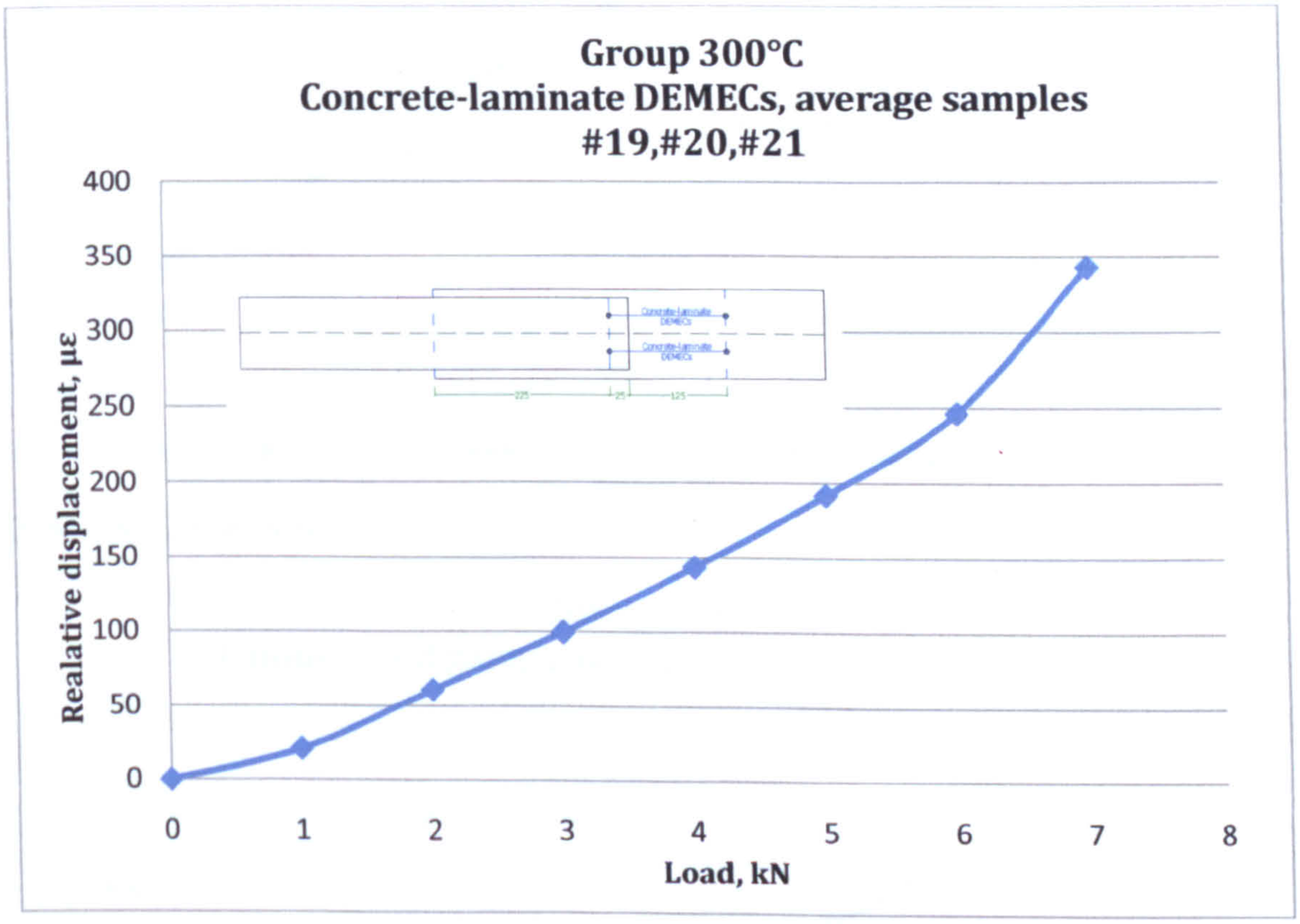

Figure III-41 Average local deformations before crack formation, concrete-laminate DEMEC strain gauges, group 300°C

The increase of the relative displacement between the end of the laminate and the concrete was found to be gradual up to 6kN when a slight change was observed, see Figure III-41. The average value at 7kN was 343microstrain.

3.5.7.4 Laminate DEMEC strain gauges

The relative displacement of the DEMEC points attached to the laminate was described by a gradual increase up to the crack formation in the concrete. The average strain at 7kN was found to be 366 microstrain, see Figure III-42.

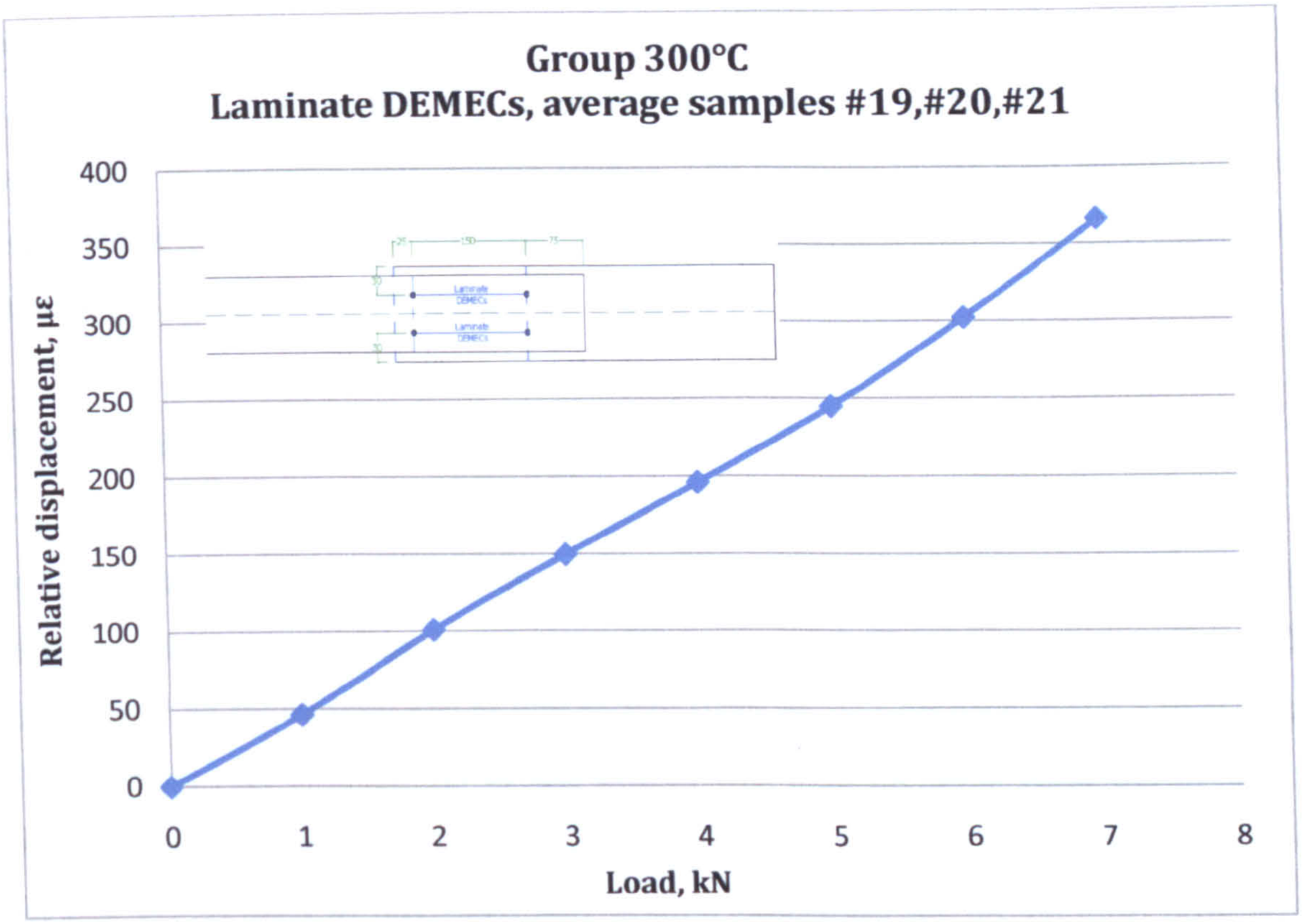

Figure III-42 Average local deformation, laminate DEMEC strain gauges, group 300°C

3.5.7.5 ER gauges

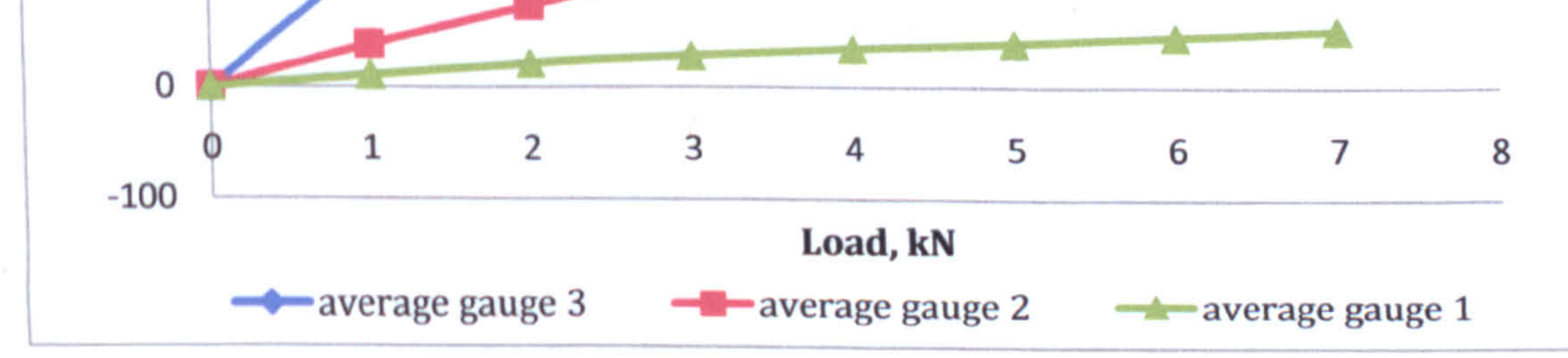

Figure III-43 Average ER strain gauges, group 300°C

ER gauge 1 for group 50°C registered the least deformations from all three gauges-155microstrain at 22kN whilst the average strain of ER gauge 1 was found to be 1089microstrain at the same load (Figure III-43). The increase of the load resulted in gradual increase of the deformations of ER gauge 2 in a more nonlinear manner. At 22kN the value for ER strain gauge 2 was 554microstrain.

3.6 Concluding remarks

The experimental results from a study on the residual bond strength of CFRP-to-concrete bonded joints were presented in this chapter. The average deformations measured at different critical positions on the sample and failure modes were plotted for each group. Descriptions of the failure modes and propagation of the cracks was also included from the initial cracks occurring in the samples to the full failure of the strengthened systems. Finally, the experimental set-up used in this study and heating procedure for the uniform heating of the samples were presented and discussed.

Chapter 4

Heating of small-scale CFRP strengthened RC beams

The process of heating of small-scale CFRP strengthened RC beams is investigated in this chapter. The experimental set-up is discussed first and the results obtained for each minibeam are presented.

4.1 Preparation of samples

The samples of experiment II were designed as small-scale RC beams which are referred to as minibeams in the text. The aim of experiment IIA was to investigate the effect of heating to 300°C of loaded samples and determine the deformability and residual strength of CFRP strengthened RC beams.

Twenty one minibeams with standard size of 100x100x500mm were cast. Each beam was reinforced with a cage of $4\phi6$ mild steel rebars and $7\phi3$ stirrups, see Figure IV-1. Due to its relatively short shear span special consideration was taken to increase the shear capacity of the beams. Seven stirrups per beam were made ensuring the distance between two stirrups would be less than the maximum allowable spacing according to EC2:

$$s_{\max} = 0.75d(1+\cot\alpha) = 0.75\times 85 = 63.75mm > 60mm$$

Equation IV-1 Spacing between stirrups

The concrete cover was taken as 10mm from each side.

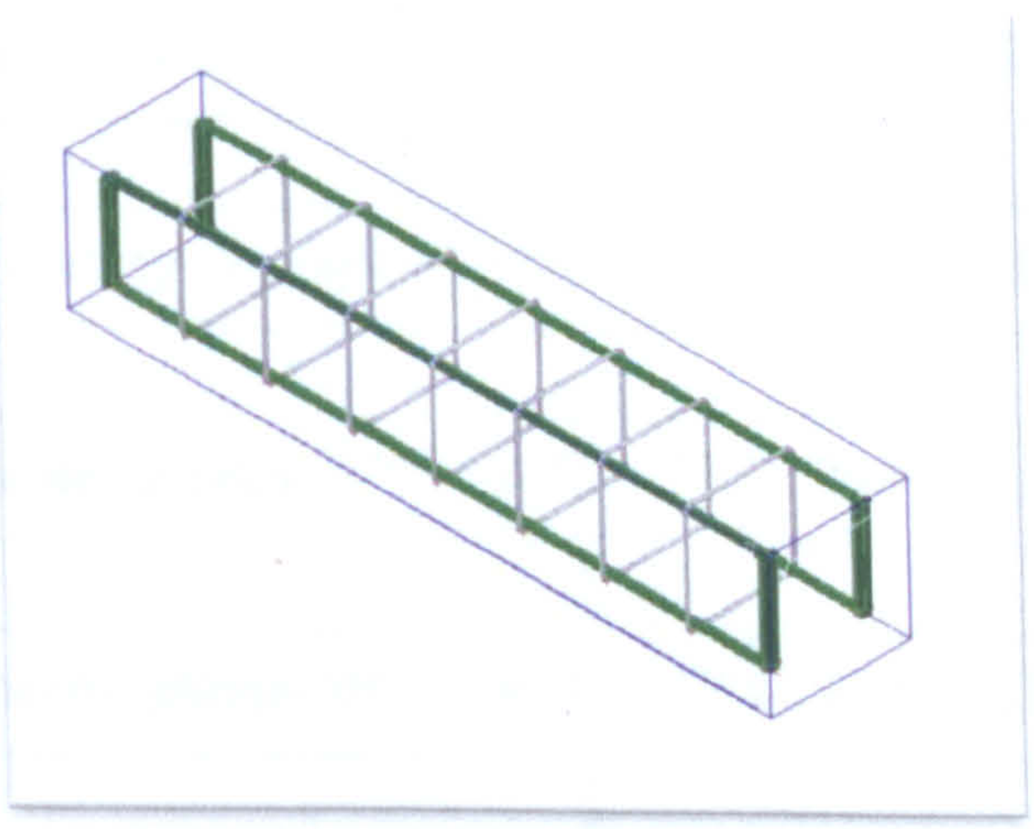

Figure IV- 1 Reinforcement of the minibeams

The samples were designed as small-scale RC beams and the concrete mix design was based on 10mm maximum aggregate size. A concrete mix for C25/30 was developed with water/cement ratio of 0.56. Three cubes were cast, cured and tested in compression to determine the compressive strength of the batch on the 28^{th} day.

The minibeams were cast and cured at 21°C and 95% humidity. Once the curing time of 28 days was completed the samples were removed and left to cure at room temperature. The age of the samples about the time they were strengthened and heated was 20 months old. Thus the effects of heating on fresh concrete would be avoided.

The minibeams were strengthened with 20mm wide CFRP laminate. To ensure good bonding between the beam and the laminate the side of the concrete where the strengthening would be attached was treated. A thin layer of the surface of the minibeam was removed using steel brushes, the roughened concrete was vacuumed and then the adhesive was applied. The two parts of the epoxy were mixed together and then applied to the laminate and the concrete prism. The plates were cut to 400mm length and 20mm width, cleaned and then attached to the concrete surface. The excess adhesive was removed and the samples were left to cure for at least 7 days. Each minibeam was then loaded in 3 point bending and heated (see flowchart below).

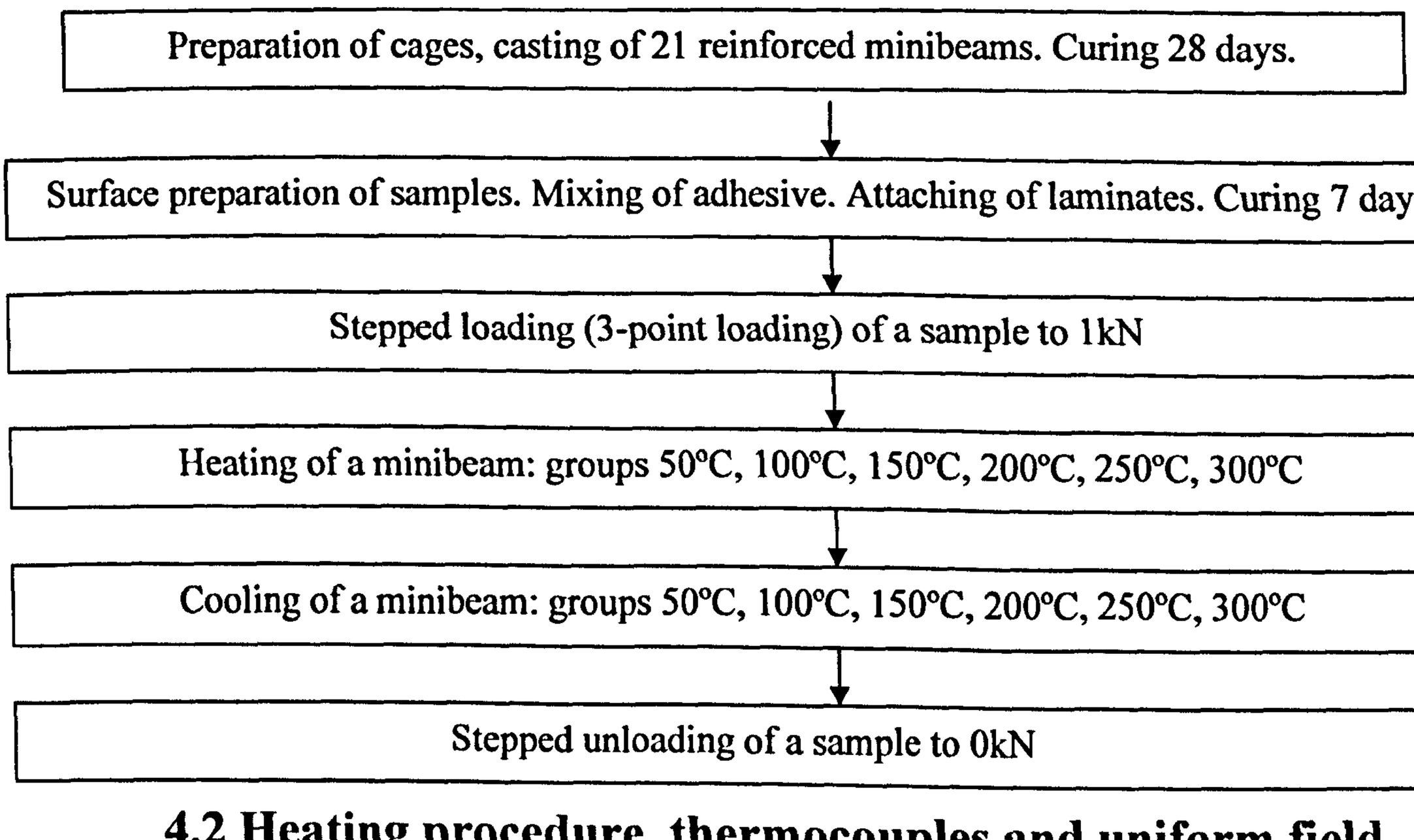

4.2 Heating procedure, thermocouples and uniform field

The samples were heated individually to a specified temperature. Three samples were exposed to a temperature of 50°C, 100°C, 150°C, 200°C, 250°C or 300°C for the same time period.

Prior to heating, a static load of 1kN (to represent serviceability load) was applied at the centre of the beam in 5 load steps and deflection readings were taken for each 0.2kN.

To measure the temperature distribution inside the oven three thermocouples type K were used at three different levels of the beam: near the top, at the middle and near the bottom of the oven. The thermocouples were also placed in three different positions in relation to the beam. One was fixed near the front face of the beam, one between the steel supports and one behind the basket. Two additional readings were also taken from thermocouples in a cube and a concrete prism. The criterion for heating was then taken as the temperature attained inside the concrete prism. Once the specified temperature was reached, the samples were heated for additional 60 min to ensure uniform distribution of the temperature around and inside the sample and then the oven was turned off.

Figure IV-2 Position of the thermocouples and applied load

During the cooling process deflection readings were taken every minute until a slow change of the temperature in the oven was established. The sample was then left to cool to room temperature for at least 12h. The load was then removed in a 0.2kN step and readings were taken for each load step, see Figure IV-2.

4.3 Experimental set-up

The second type of experiments was designed to investigate the effect of heating of CFRP strengthened RC beams during the thermal loading. The strengthened minibeams were exposed to elevated temperature in an oven and the mechanical properties of the materials of the strengthened system changed. To track the effect of the heating a new system was developed where the deflection of the minibeams was measured together with the increase of temperature in the oven.

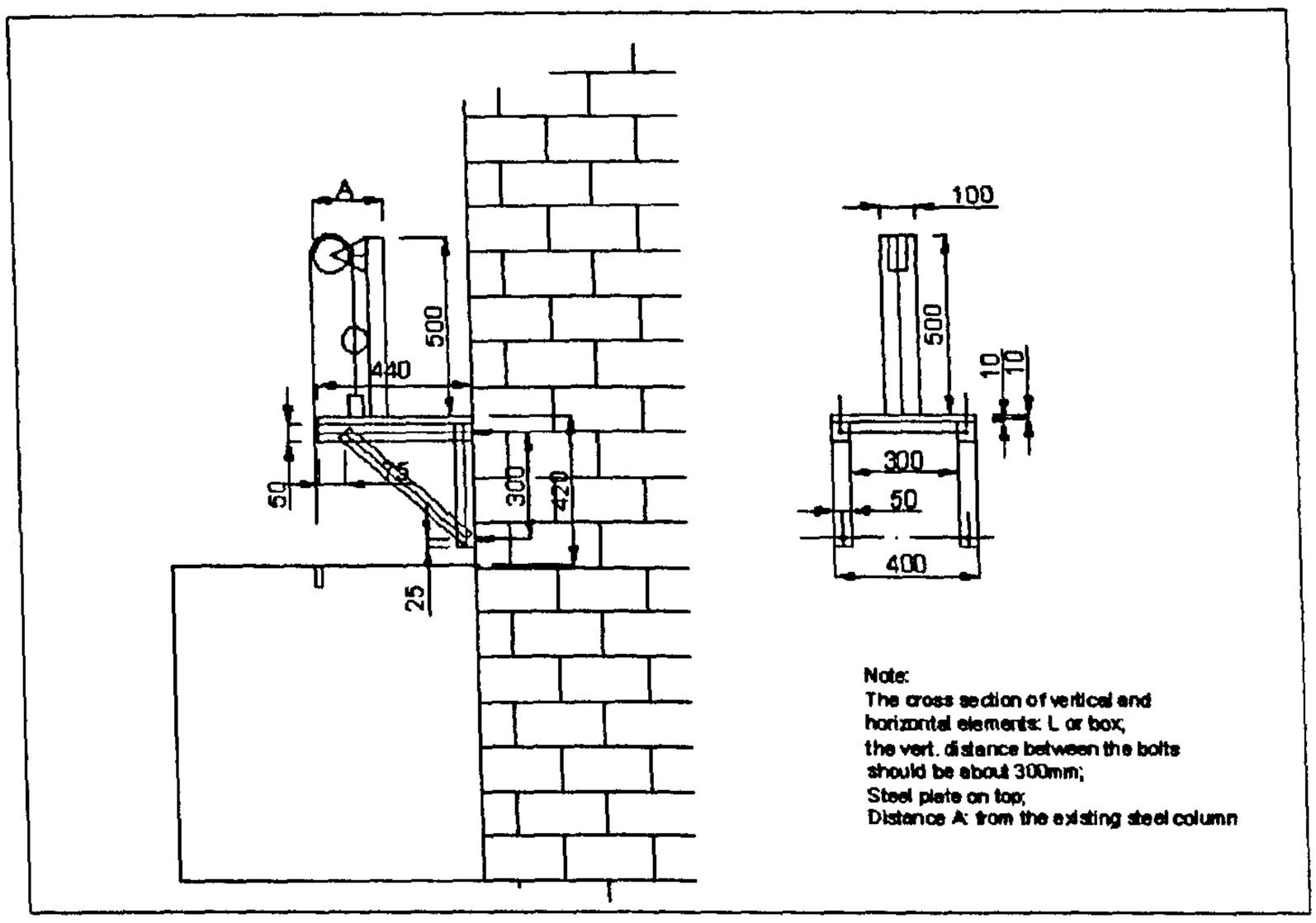

Figure IV-3 Position of dial gauge above the oven

During the heating each sample was loaded with a 1kN static load. A load of 1kN was chosen as it would represent the average service load which a real beam would experience in its lifetime.To support the beam a steel frame was made, it consisted of 2 hollow steel sections welded to a thick steel plate to prevent deformations of the frame during heating. The minibeam was then placed on the two vertical supports and the load was applied on the beam by a steel basket. The load was applied gradually 0.2kN every 5min until 1kN load was reached.

To measure the deformation of the beam an invar wire was hooked to the steel basket and then connected to a dial gauge above the oven which was fixed on a steel shelf, see Figure IV-3. To minimise any effect of thermal exposure a distance of 300mm was left between the shelf and

the oven. Thus the dial gauge was not directly exposed to elevated temperatures. Any additional thermal effects on the dial gauge were considered negligible compared to the expansion of the steel frame and invar wire.

The invar wire was chosen for its lower CTE of $1.2x10^{-6}$/°C compared to concrete and steel. The expansion of the invar wire was10 times less than the expansion of the concrete and the steel inside the oven. Due to the significant length and direct exposure to heating the contribution of the wire was taken into account. Linear decrease of the temperature was assumed between the oven and the roller over a length of 80mm and the length of the exposed to direct heating wire was found to be 50mm.

Figure IV-4 Frame and loading basket

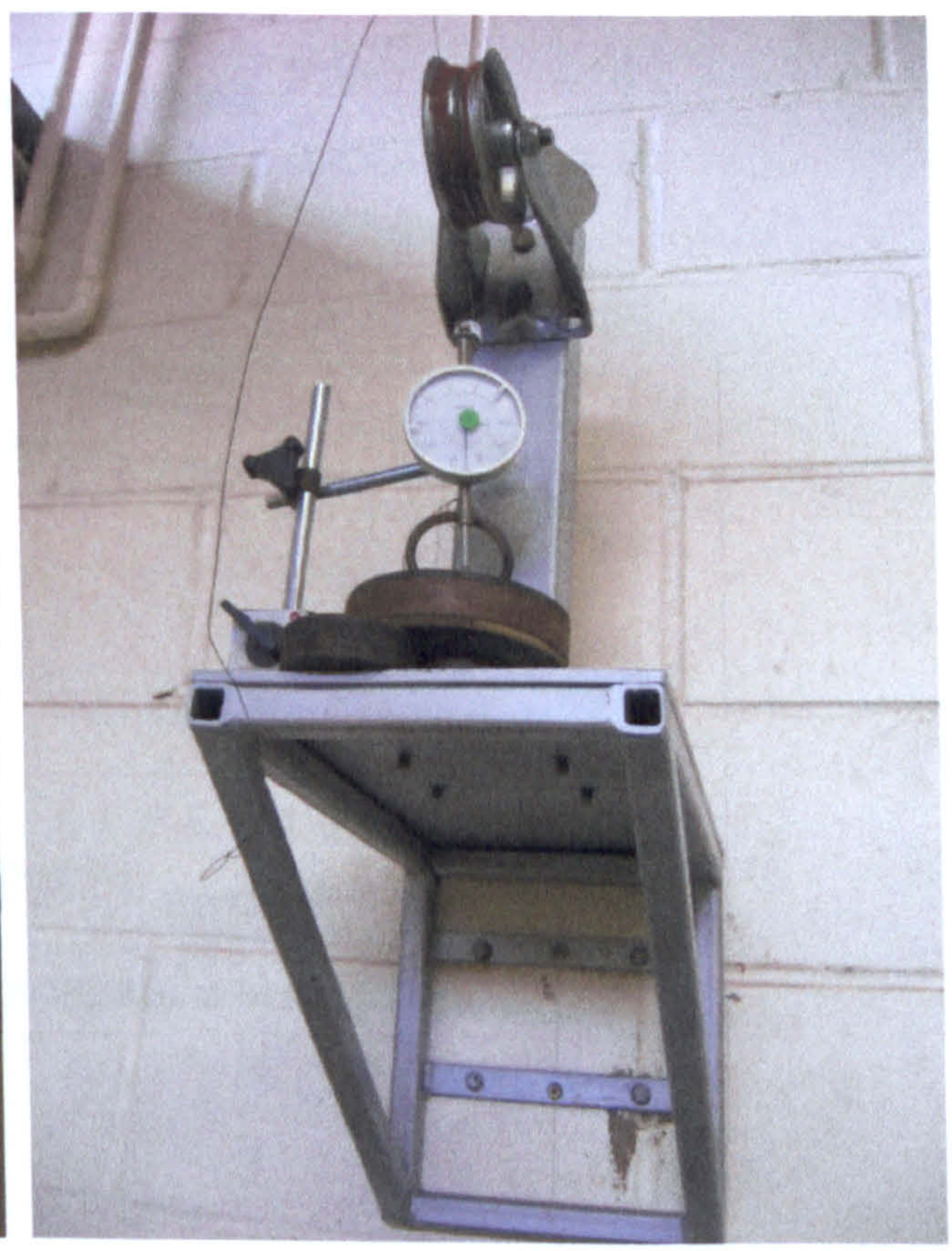

Figure IV-5 Invar wire and dial gauge

4.4 Heating regimes

4.4.1 Group 50°C

The different groups were heated to temperatures from 50°C to 300°C. The beams of group 50°C were exposed to temperature for 150 min, see Figure IV-6. Higher temperatures were measured by the top and middle thermocouples and within the first 15min the temperature of the air in the oven reached 50°C. The centre of the beam reached 50°C after 90min of heating and was left for additional 60min to ensure uniform temperature distribution through the cross section of the beam. The oven was then turned off and readings of the deflection and the temperature in the oven were taken for 200 minutes until the ambient temperature reached 30°C. The last reading was taken the following day which was taken as 600min after the beginning of the experiment.

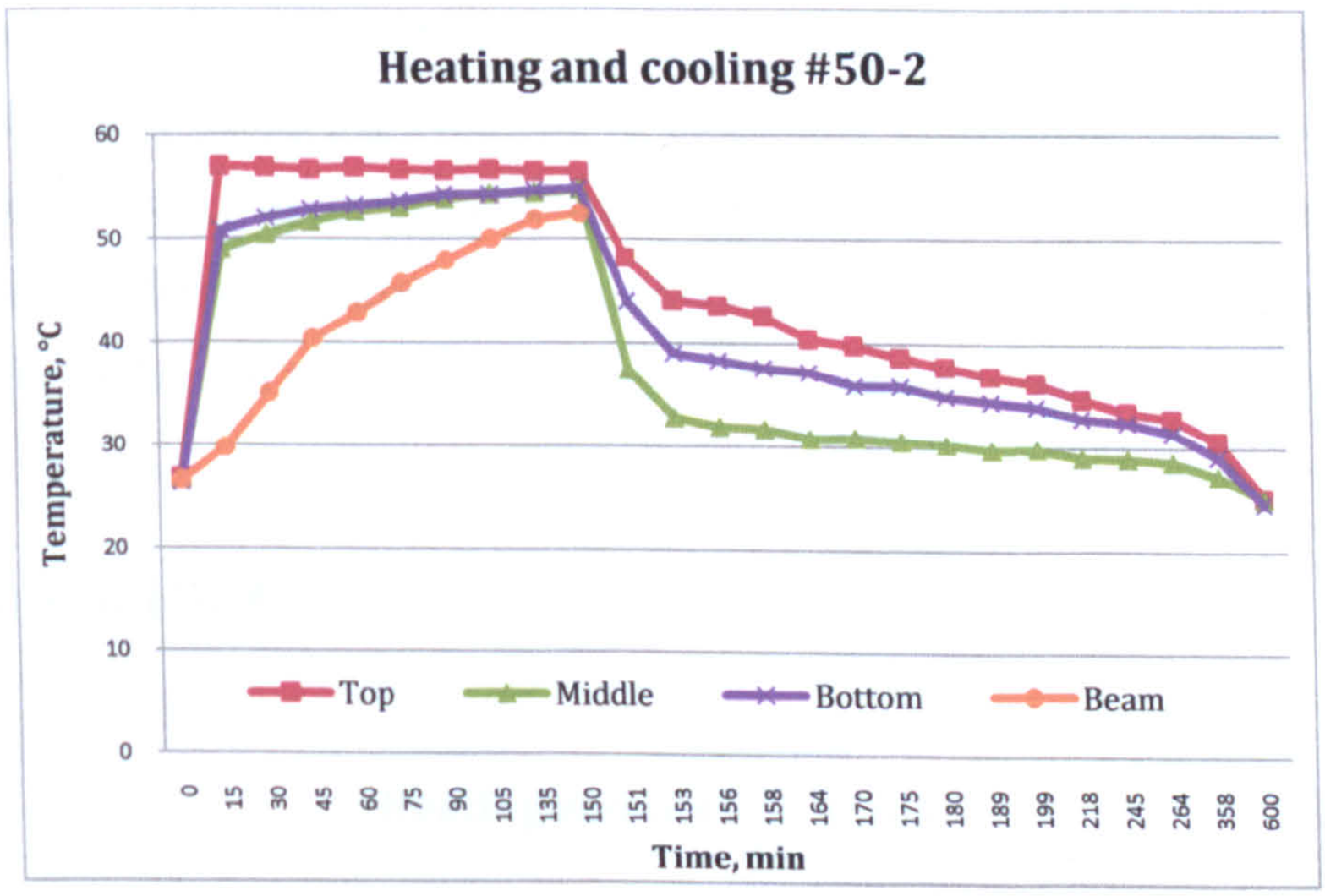

Figure IV-6 Heating and cooling time of beam, 50°C

4.4.2 Group 100°C

The beams of group 100°C were heated for 180min (Figure IV-7) when the temperature was assumed to be uniform and the oven was turned off. Within the first 15min the temperature of the air measured at the top of the oven increased to 100°C and 60 min later was followed by the thermocouples at the middle and bottom levels in the oven.

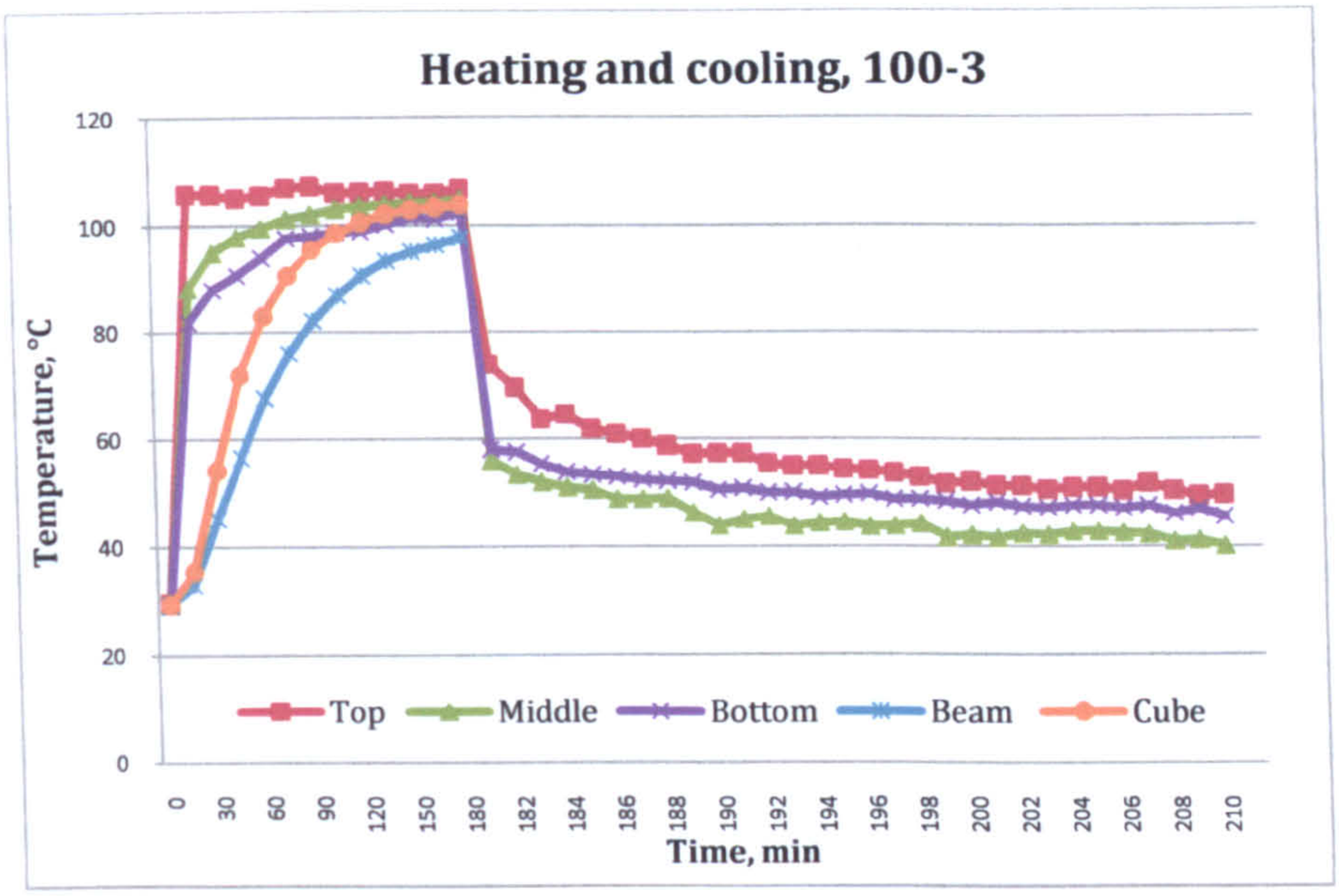

Figure IV-7 Heating and cooling time of beam, 100°C

The temperature was also measured at the centre of a cube and a minibeam with higher temperatures registered inside the cube due to its smaller dimensions. The beam was heated for 120min when the required temperature was attained and then allowed to heat for additional 60 min to ensure uniform temperature throughout the cross section of the beam. Deflection readings were then taken for the first 30 min of cooling until the temperature of the air reached 45°C.

4.4.3 Group 150°C

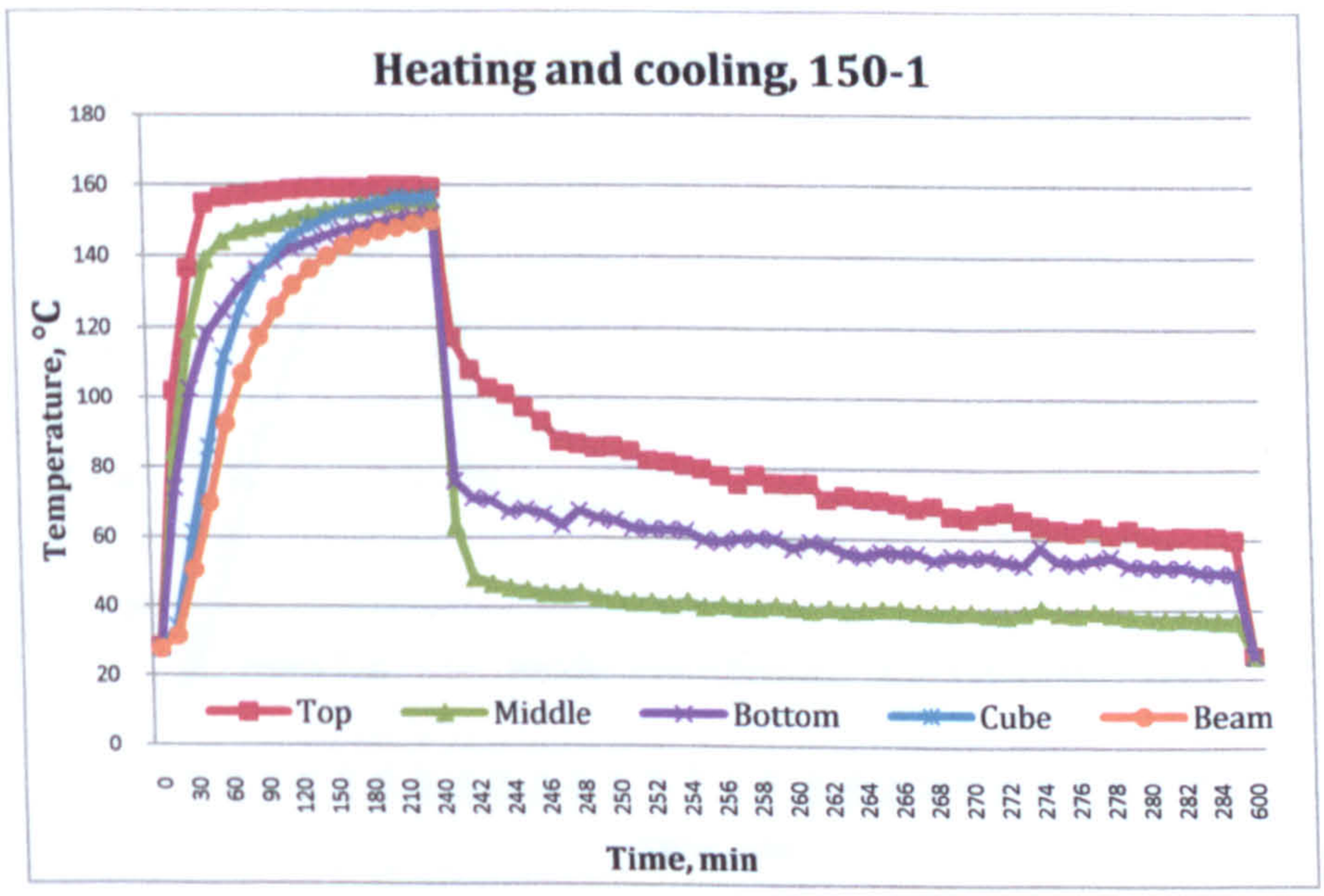

Figure IV-8 Heating and cooling time of beam, 150°C

The beams of group 150°C were heated for at least 240 minutes and then the oven was turned off. After the first 45 minutes the required temperature was registered at the level of the top thermocouple in the oven, see Figure IV-8. The temperature at midlevel rose quickly in the first 45 minutes followed by slow increase to 150°C. Similar development was found at the lower level when at the 120th minute slow increase of the temperature was established. As in the previous heating procedures the cube was the first to reach the required temperature at the 150th minute followed 30 min later by the thermocouple at the centre of the beam. After 240 min of heating the oven was turned off and readings were taken until the average temperature in the oven dropped to 60°C. The beams were then left to cool until the following day which was denoted as 600min.

4.4.4 Group 200°C

The heating procedure of Group 200°C continued 330 min when the required uniform temperature distribution was attained, see Figure IV-9. Both the top and midlevel thermocouples registered quick increase of the temperature in the first 90 min. At bottom level gradual increase began after 120min of heating. At the 270th min the temperature at the centre of the cube and the beam reached the required temperature. The minibeams were then heated for 60 more minutes to ensure uniform distribution of the temperature inside and outside the samples. Readings of the deflection were then taken for the first 60 min of the cooling phase.

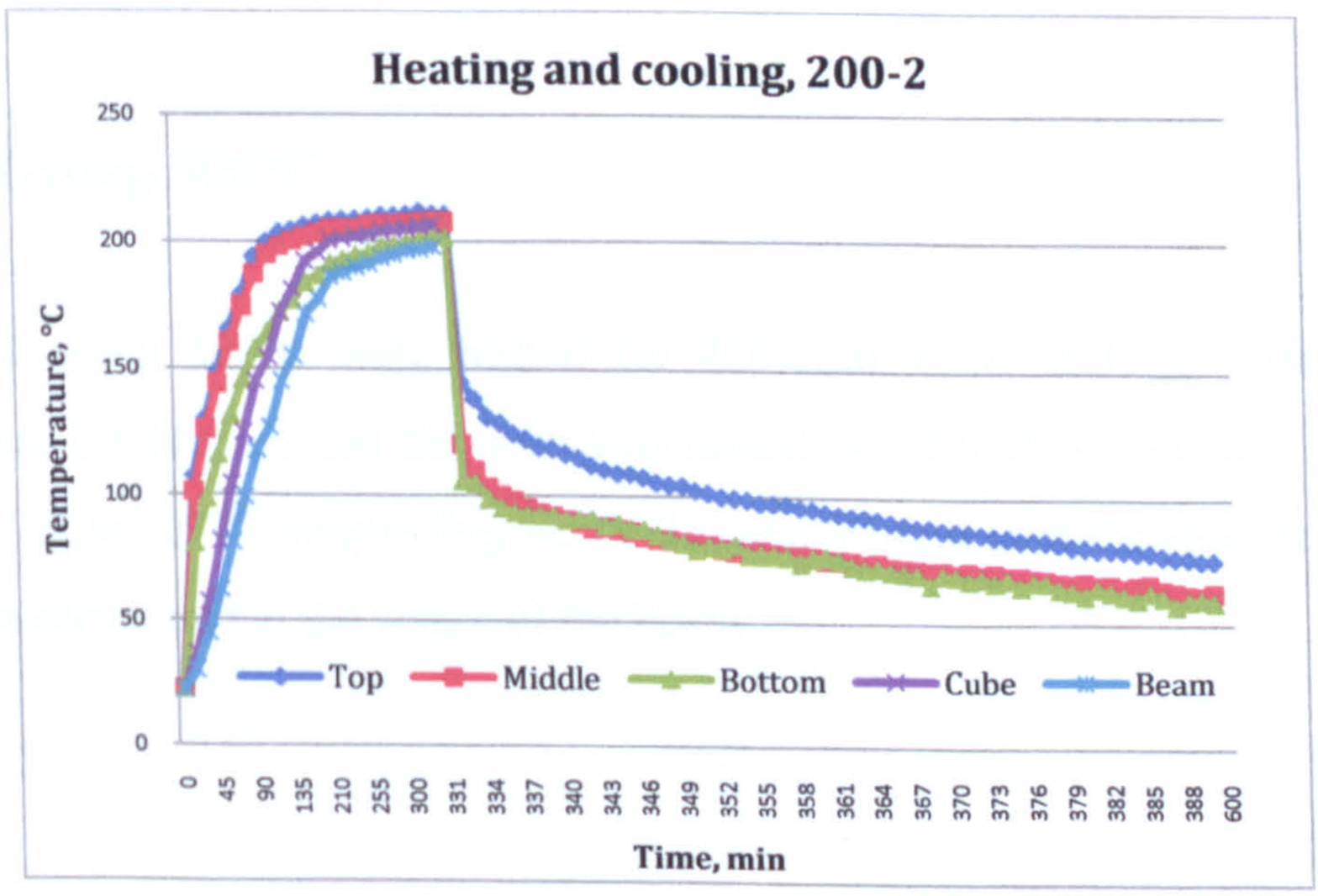

Figure IV-9 Heating and cooling time of beam, 200°C

4.4.5 Group 250°C

Group 250°C was heated for 360 min (Figure IV-10) when the established temperature field in the oven was uniform. The temperature at top level was attained after 180 min of heating. The thermocouple at midlevel reached 250°C at the 270th min. At the centre of the cube and beam the thermocouple registered the same temperature at the 300th min. The samples were then exposed to heating for additional 60 min and then left to cool. Deflection readings were taken for 60min until the average temperature in the oven dropped to 50°C.

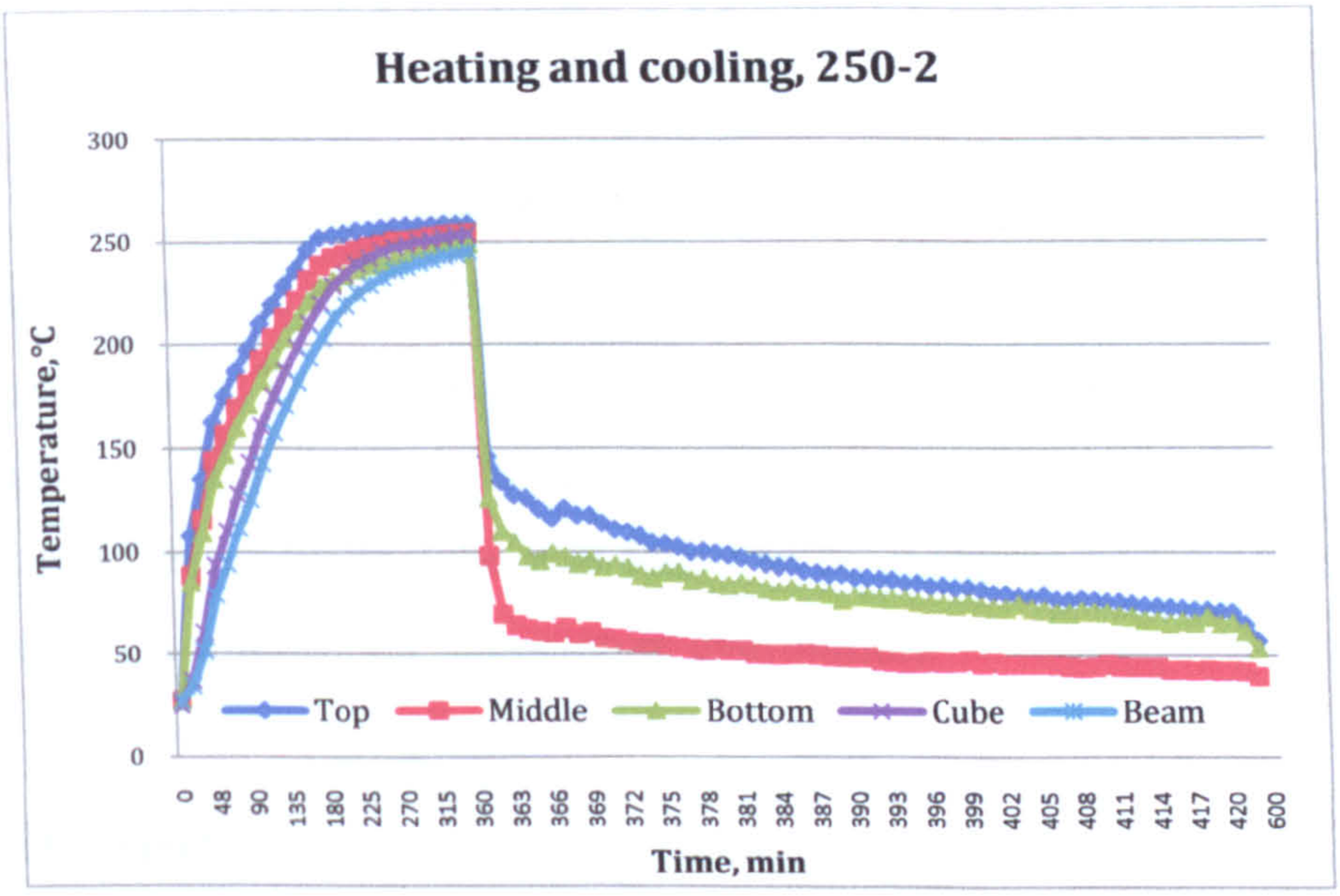

Figure IV-10 Heating and cooling time of beam, 250°C

4.4.6 Group 300°C

The beams of group 300°C were heated for 420 min when uniform distribution of the temperature was established and the oven was turned off. The thermocouple at the top level reached 300°C at the 270th minute (Figure IV-11) and 90 min later the same temperature was registered at midlevel and at the centre of the beam.

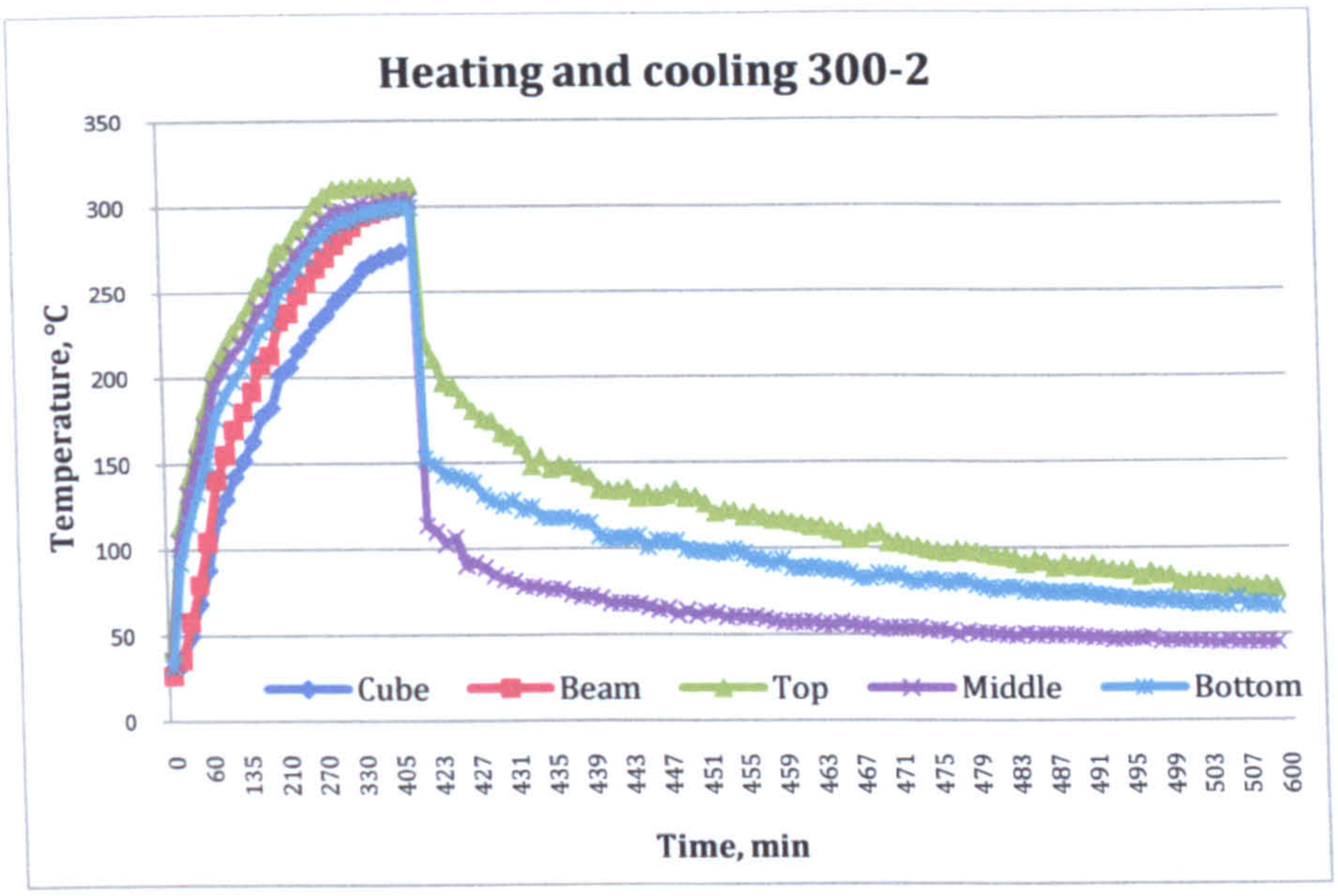

Figure IV-11 Heating and cooling time of beam, 300°C

The sample was then heated for additional 60min and left to cool. Deflection readings were taken for the first 180min. The sample was then removed from the oven on the following day when the temperature had dropped to room temperature. During the heating process the thermocouple inside the concrete cube was found to be defective and the readings were not taken into account as a criterion for temperature distribution.

4.5 Deflection

Deflection readings were taken for each beam from the moment of applying the first load step to the phase when the beam was cooled and unloaded. For simplification all readings were plotted against time with 0 min considered the beginning of the heating phase. Each load step was separated by 15 min intervals. When the beam was heated and cooled, the unloading steps were also plotted in 15 min intervals.

Due to the significant thermal expansion of the steel frame and the length of the invar wire exposed to elevated temperatures, the deflection readings were later corrected. With increase of the temperature the steel frame would expand resulting in lower readings and then gradually contract during the cooling phase. After the oven was turned off the dial gauge detected higher deformations during the first few minutes of the cooling phase when the temperature difference between the oven air and steel frame were higher. Later in the cooling phase the

deflection readings changed gradually until the temperature of whole system decreased to room temperature and a final reading for the phase was taken.

A simple procedure was applied to take into account the expansion of the steel frame and invar wire:

$$\text{Steel frame height}*\alpha T*\Delta T + \text{directly exposed invar wire length } *\alpha T*\Delta T$$

$$+\text{length of invar wire } *\alpha T*\Delta T = 665*0.000014*(\Delta T) +50*0.0000012*(\Delta T)$$
$$+800*0.0000012*((\Delta T)/2)$$

Equation IV-2 Expansion of steel frame and invar wire

In the correction equation ΔT was taken as the difference between the room temperature and the average temperature readings from the top, middle and bottom levels of the oven. To evaluate the effect of the temperature correction two graphs were plotted for each beam with corrected readings and actual readings. The experimental results for one beam from each group were presented and the values of the main points of the loading, heating, cooling and unloading phases were given.

4.5.1 Group 50°C

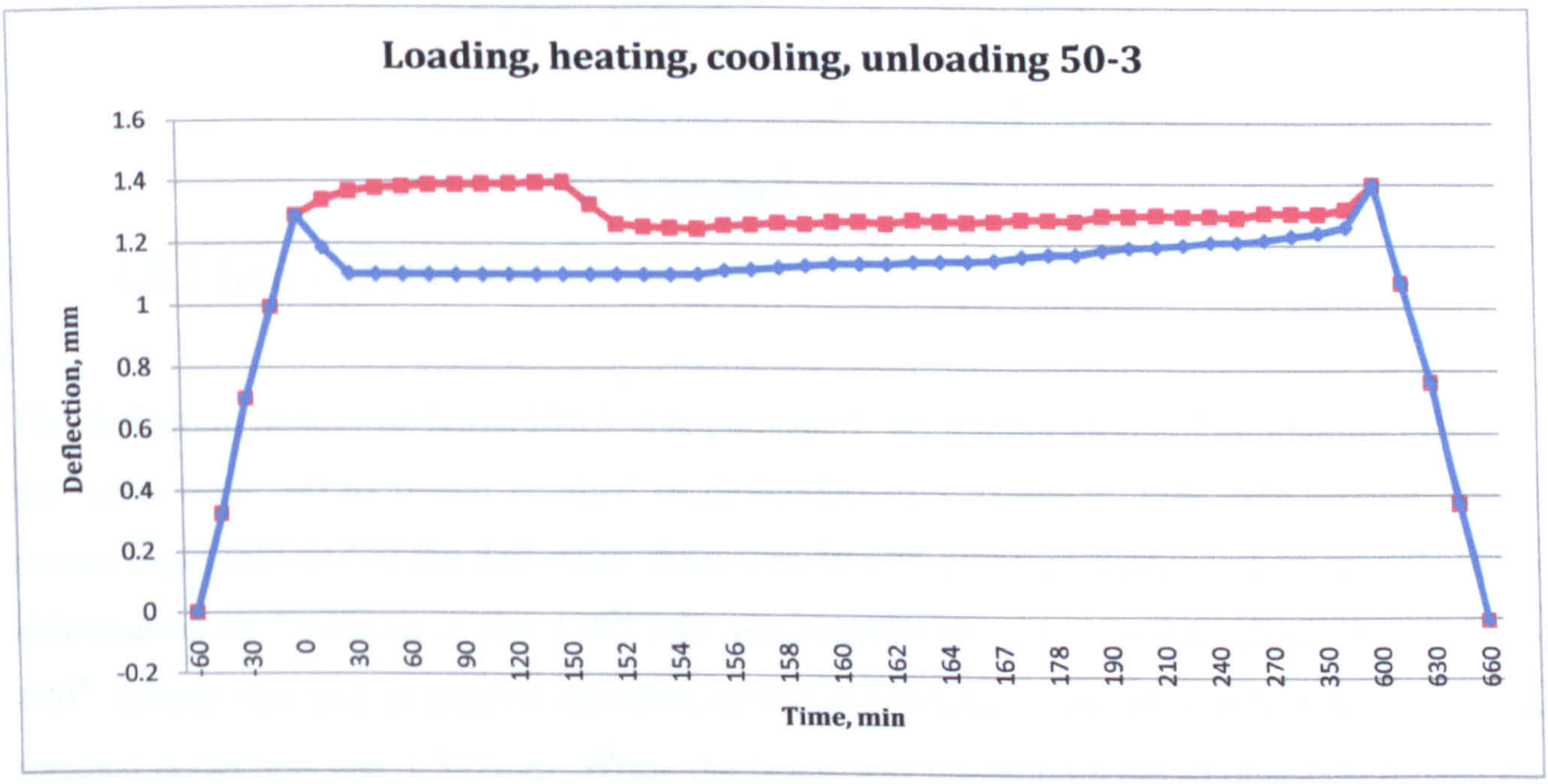

Figure IV-12 Loading, heating, cooling and unloading deflection history of a beam, 50°C

The deflection of beam 50-3 was plotted for time from -60 to 660 min, see Figure IV-12. The first branch of the graph from -60min to 0min presented the stepped loading from 0.2kN at -60min to 1kN at time 0 min. The deflection of the beam at the end of loading phase at 0 min reached 1.3mm. The heating process was then started at 0min and ended at 150th minute causing gradual increase of the deflection to 1.397mm. Deflection readings were then taken during the cooling process from minute 150 to 350 where the two graphs began to converge. The readings from minutes 600 to 660 presented the unloading stage with initial deflection of 1.398mm. When the beam was unloaded the residual deformation was 0.008mm which indicated that the deformations due to static and thermal load for CFRP strengthened RC beams to 50°C were recoverable.

Samples 50-1 and 50-2 exhibited similar deformations (Table IV-1) with highest value for the end of the heating phase of 1.496mm which was 7% higher than beam 50-3. The readings at the end of the cooling phase deviated by maximum 6% for beam 50-1 and at the unloading stage a value of 0.006mm. Beam 50-2 registered residual deflection of 0.104mm.

Deflection, mm			
Beams	**Heating**	**Cooling**	**Unloading**
50-1	1.496	1.32	0.006
50-2	1.398	1.36	0.104
50-3	1.397	1.398	0.008

Table IV-1 Deflection group 50°C

4.5.2 Group 100°C

The deflection history of beam 100-1 was presented, see Figure IV-13. The loading phase of the beam from -60 to 0 min resulted in deflection of 1.33mm at 1kN. The heating phase caused rapid increase of the deflection from 0 to 30 min and then more gradual growth of the deformation to 1.642mm at the 150th min was established. The cooling phase from 150 to 180th minute resulted in gradual decrease of the deformations and on the following day the residual deflection was 1.372mm. When the beam was unloaded from minute 600 to 660 the final reading was 0.169mm.

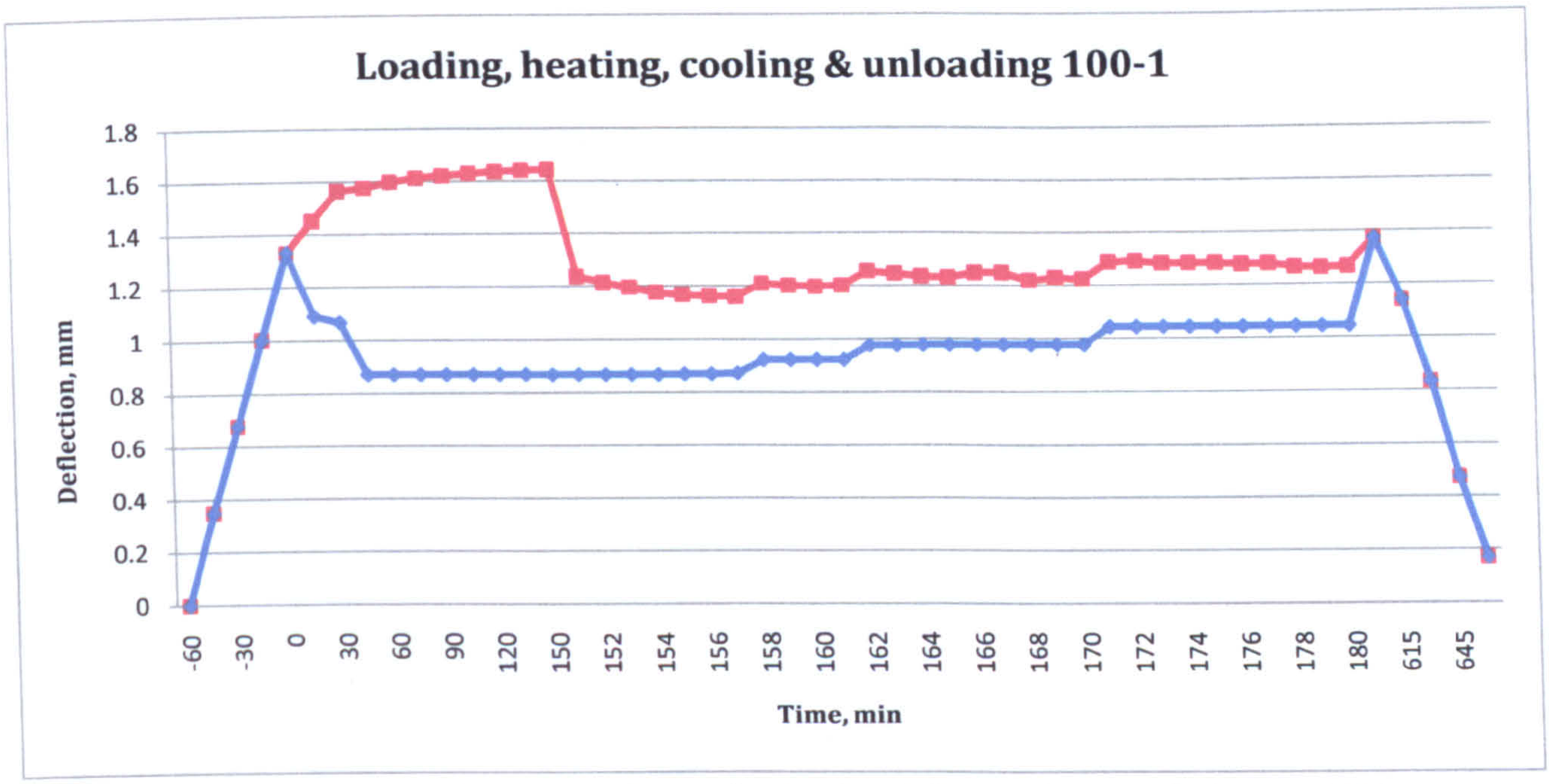

Figure IV-13 Loading, heating, cooling and unloading deflection history of a beam, 100°C

Beam 100-2 and 100-3 deflected at the end of the heating phase (Table IV-2) to 1.524 and 1.660 which was less than 7% from the deflection of beam 100-1 (Figure IV-13). At the end of the cooling phase the residual deformations deviated more significantly from beam 100-1 showing increase to 10%. The final deflection readings registered higher deviation of the deformations from 0 to 0.24mm.

Deflection, mm			
Beams	**Heating**	**Cooling**	**Unloading**
100-1	1.642	1.372	0.169
100-2	1.524	1.472	0.24
100-3	1.660	1.5	0

Table IV-2 Deflection group 100°C

4.5.3 Group 150°C

The vertical displacement of beam 150-2 was plotted from -60 to 660 min, see Figure IV-14. At the end of the loading phase the deflection increased to 1.278mm. The beam was then heated for 270min until uniform temperature field was established. During the first 45min the

temperature in the oven rose from room temperature to 150°C which resulted in increase of the deformations to 1.776mm and then the vertical displacement continued to grow gradually. At the end of the heating phase the deflection reached a value of 1.889mm. The cooling phase continued from 270th min to 390 during which decrease of the deformations was registered. At the end of the cooling phase at minute 600 the deflection was recovered to 1.399mm and then the beam was unloaded resulting in 0.253mm residual deflection.

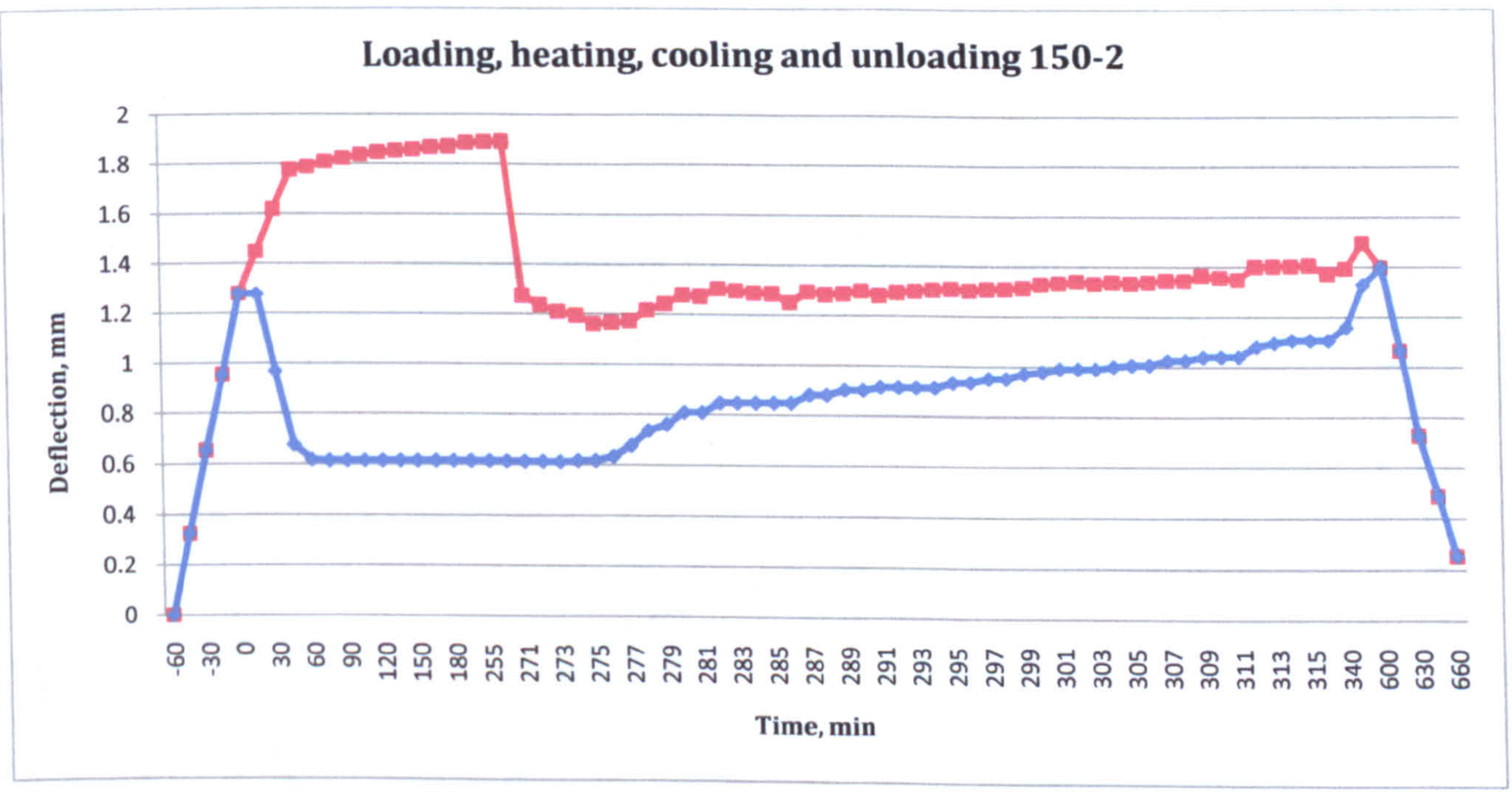

Figure IV-14 Loading, heating, cooling and unloading deflection history of a beam, 150°C

Lower deformations were registered by beam 150-1 at the end of the heating and unloading phases compared to beam 150-2 (Table IV-3). Beam 150-3 exhibited similar deformations to beam 150-2 at the end of the heating and cooling process with a lower residual deflection when the load was removed.

Deflection, mm			
Beams	**Heating**	**Cooling**	**Unloading**
150-1	1.342	1.414	0.034
150-2	1.889	1.399	0.253
150-3	2.019	1.572	0.132

Table IV-3 Deflection group 150°C

4.5.4 Group 200°C

The loading, heating, cooling and unloading phases of beam 200-2 were plotted from -60 to 660 min (Figure IV-15). When the full load was applied the deflection of the beam reached 1.535mm and the samples were heated to 200°C for 330min. Rapid increase of the deflection was observed in the first 120min to 1.458mm and at the end of the heating phase it reached 1.69mm. Readings of the deflection were taken for 60 min after the oven was turned off. On the following day the deformation at the end of the cooling phase was 1.876mm and at the end of the unloading phase the residual deflection reached 0.472mm.

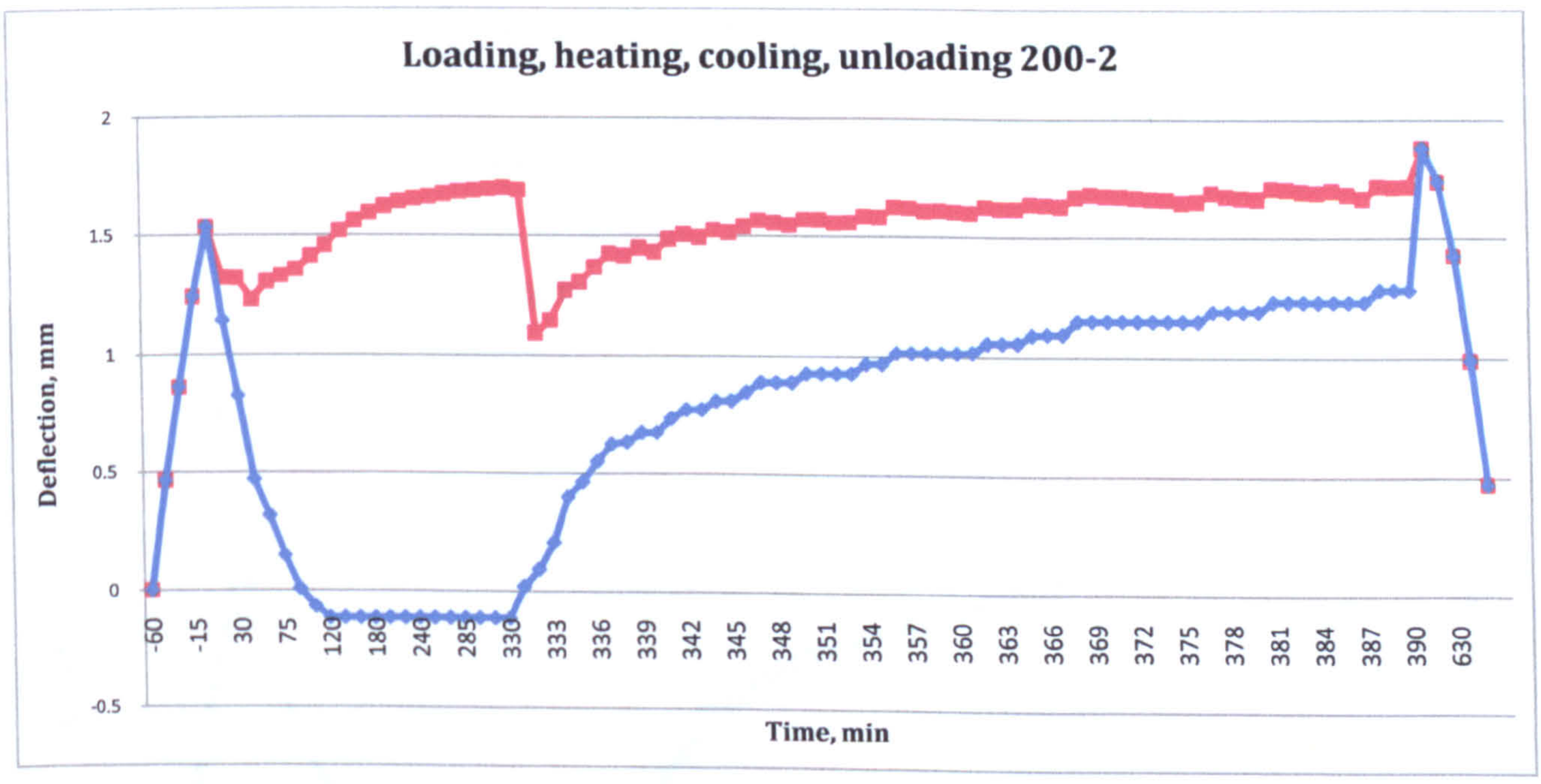

Figure IV-15 Loading, heating, cooling and unloading deflection history of a beam, 200°C

Deflection, mm			
Beams	**Heating**	**Cooling**	**Unloading**
200-1	1.326	1.787	0.554
200-2	1.699	1.876	0.472
200-3	1.640	1.855	0.559

Table IV-4 Deflection group 200°C

The deflection readings at the end of the heating and cooling phases for beam 200-2 and 200-3 were found to be consistent, see Table IV-4. Beam 200-1 registered lower deflection at the first phase but then the deformations at the end of the cooling and unloading phases were consistent with the rest of the group.

4.5.5 Group 250°C

The deflection of beam 250-2 was plotted for time from -60 to 960 min, see Figure IV-16. The deflection of the beam at the end of loading phase at 0 min reached 1.342mm. The heating process was then started at 0min and ended at 420th minute causing gradual increase of the deflection to 2.001mm. Deflection readings were then taken during the cooling process to the 495th min and the last reading was taken on the following day of 1.950mm. When the beam was unloaded the residual deformation was 0.874 mm.

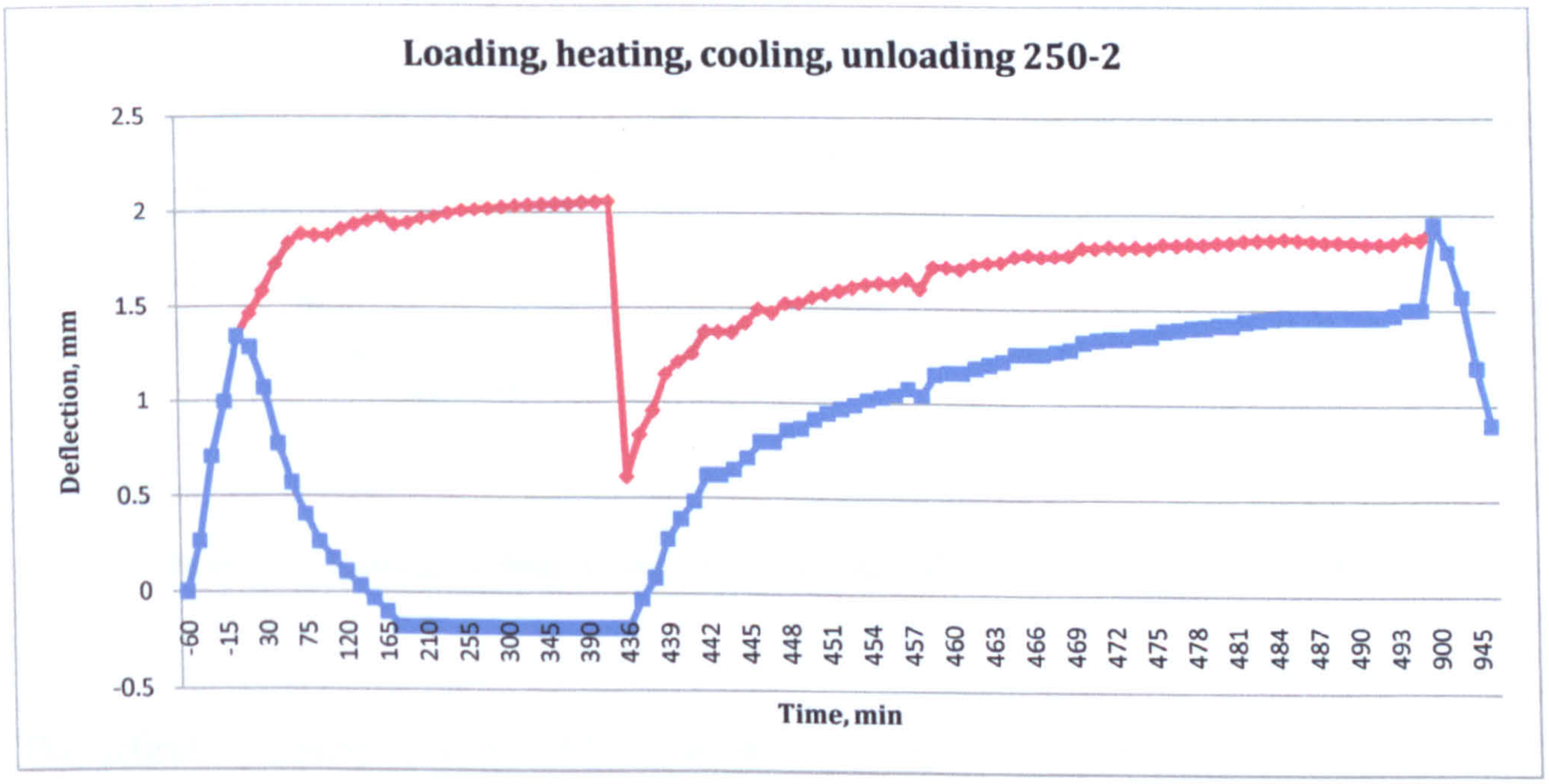

Figure IV-16 Loading, heating, cooling and unloading deflection history of a beam, 250°C

Beams 250-1 and 250-3 exhibited similar deformations with the lowest value at the end of the heating phase of 1.728mm (Table IV-5). The readings at the end of the cooling phase deviated by maximum of 16% for beam 250-3. Both beams 250-1 and 250-3 registered residual deflection of 1mm when the load was removed.

Deflection, mm			
Beams	**Heating**	**Cooling**	**Unloading**
250-1	1.980	2.004	1.082
250-2	2.001	1.950	0.874
250-3	1.728	1.638	1.013

Table IV-5 Deflection group 250°C

4.5.6 Group 300°C

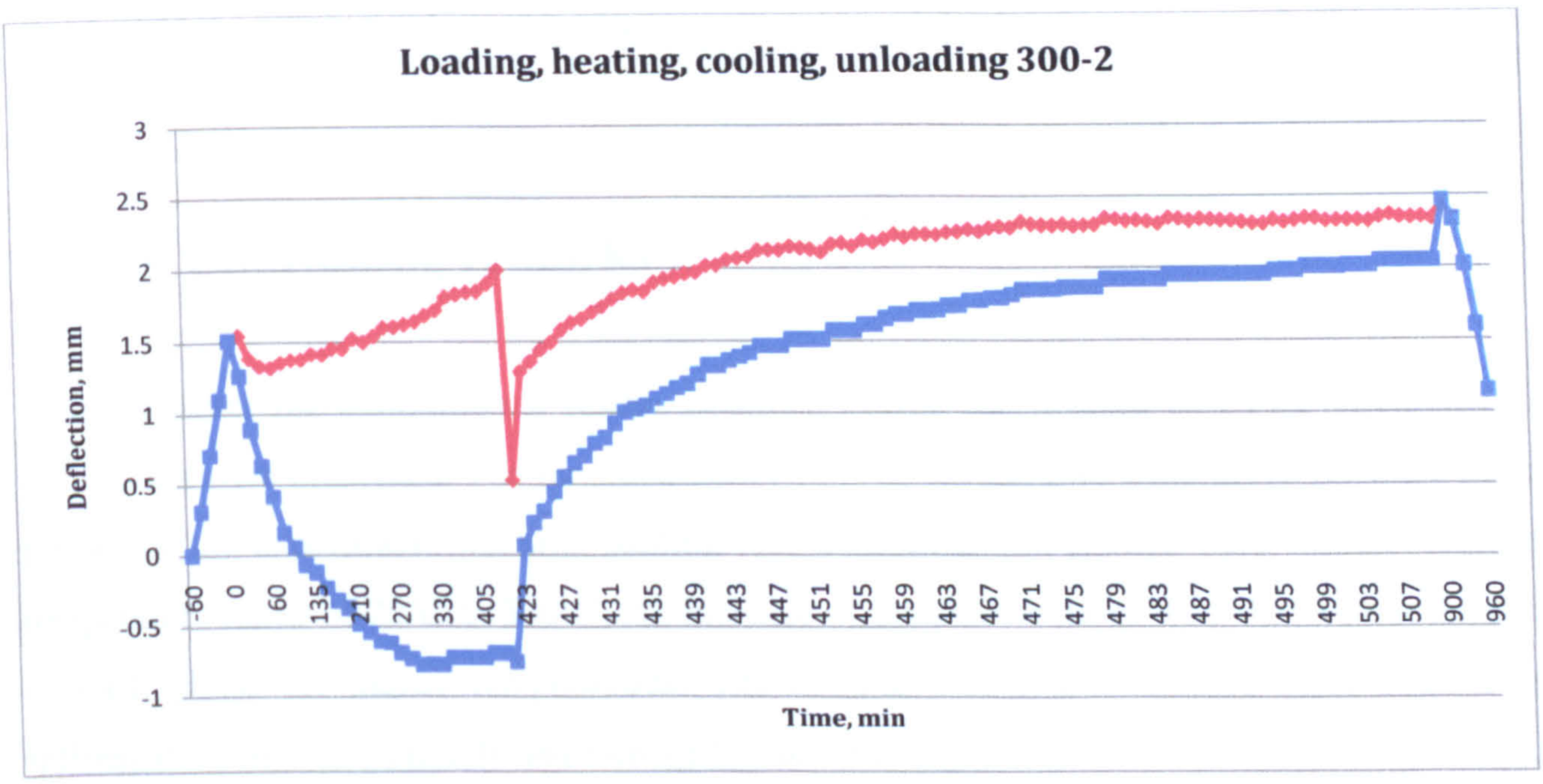

Figure IV-17 Loading, heating, cooling and unloading deflection history of a beam, 300°C

The deflection history of beam 300-3 was presented from -60 to 960min, see Figure IV-17. The loading phase of the beam from -60 to 0 min resulted in deflection of 1.514 mm at 1kN. The heating phase continued to minute 420 and significant increase of the deflection was observed to the 285th min with a final increase to 1.9mm deflection at the end of the phase. During the cooling phase the deformations continued to increase to 2.457mm. When the beam was unloaded from minute 900 to 960 the final reading was 1.143mm.

Deflection, mm			
Beams	**Heating**	**Cooling**	**Unloading**
300-1	1.606	1.560	0.304
300-2	1.900	2.457	1.143
300-3	2.129	2.676	1.147

Table IV-6 Deflection group 300°C

Beam 300-1 exhibited low deformability at the end of the heating, cooling and unloading phases. The deflection readings from 300-3 (Table IV-6) were found to be consistent with sample 300-3 with deflection of 2.129mm at the end of the heating process, 2.676mm when the sample was cooled and 1.147mm after the load was removed.

4.6 Concluding remarks

In this chapter the experimental results obtained during the heating of CFRP strengthened minibeams were presented. The recorded deflections of the samples were given for the 3 main phases of the experiment: heating, cooling and unloading. Six groups were heated within a temperature range of 20°C to 300°C. An increase of the deformations was observed at the end of each phase for higher temperatures. The heating was found to have most significant influence on the residual deformations of the samples after they had been heated, cooled and unloaded.

Chapter 5
Residual strength of CFRP strengthened beams after heating

The residual flexural strength of small-scale CFRP strengthened RC beams is investigated in this chapter. The effect of heating was discussed in chapter 4. The minibeams are loaded in four-point bending and tested to complete failure of the samples. The results from the different temperature groups are presented.

5.1Experimental set-up

The minibeams were tested under four point bending. The load was applied through a hydraulic ram welded to a steel loading frame and a loading cell. In order to prevent local concentration of stresses in the concrete due to the applied load or the support, steel plates were placed between the minibeam and the respective load point. The distance between the supports was 450mm. The dimensions of the small-scale samples including the width of the laminate were chosen based on 1:4 scale of the dimensions of a 2m beam strengthened with 80mm wide laminate. The span/ depth ratio was checked and found to be more than 2.

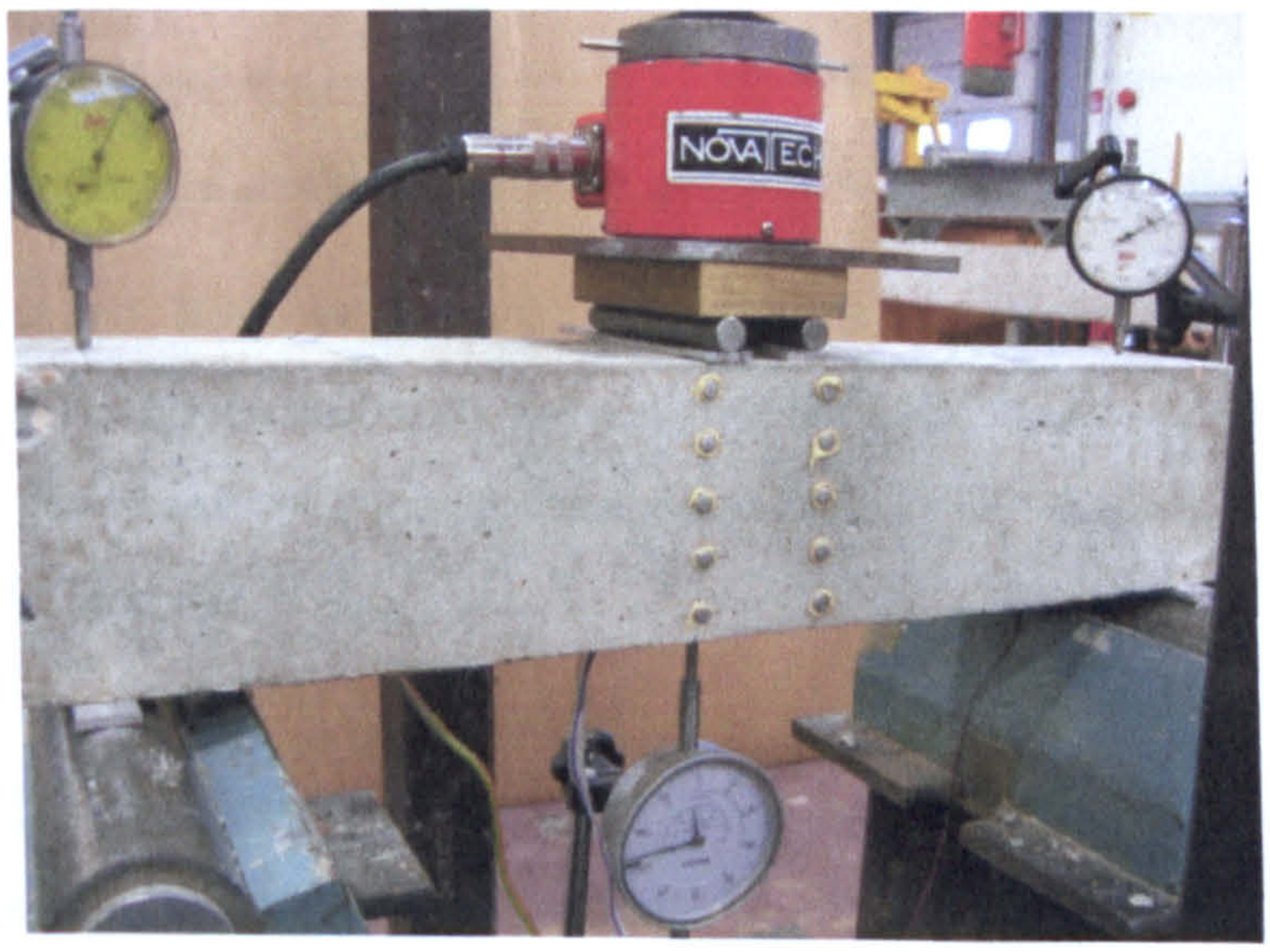

Figure V-1 Loading scheme

In order to track the flexural behaviour of the minibeams 3 systems of measurements were used. Five couples of DEMEC points with base length of 50mm were attached on one side of the beam. The deflection was measured with three dial gauges – one at midspan of the beam and two above the supports, see Figure V-1. Three ER strain gauges were also attached on laminate which was bonded to the bottom side of the beam. Before each experiment the visible cracks which occurred during the heating process were measured and the measuring devices were zeroed and readings were taken for load 0kN.

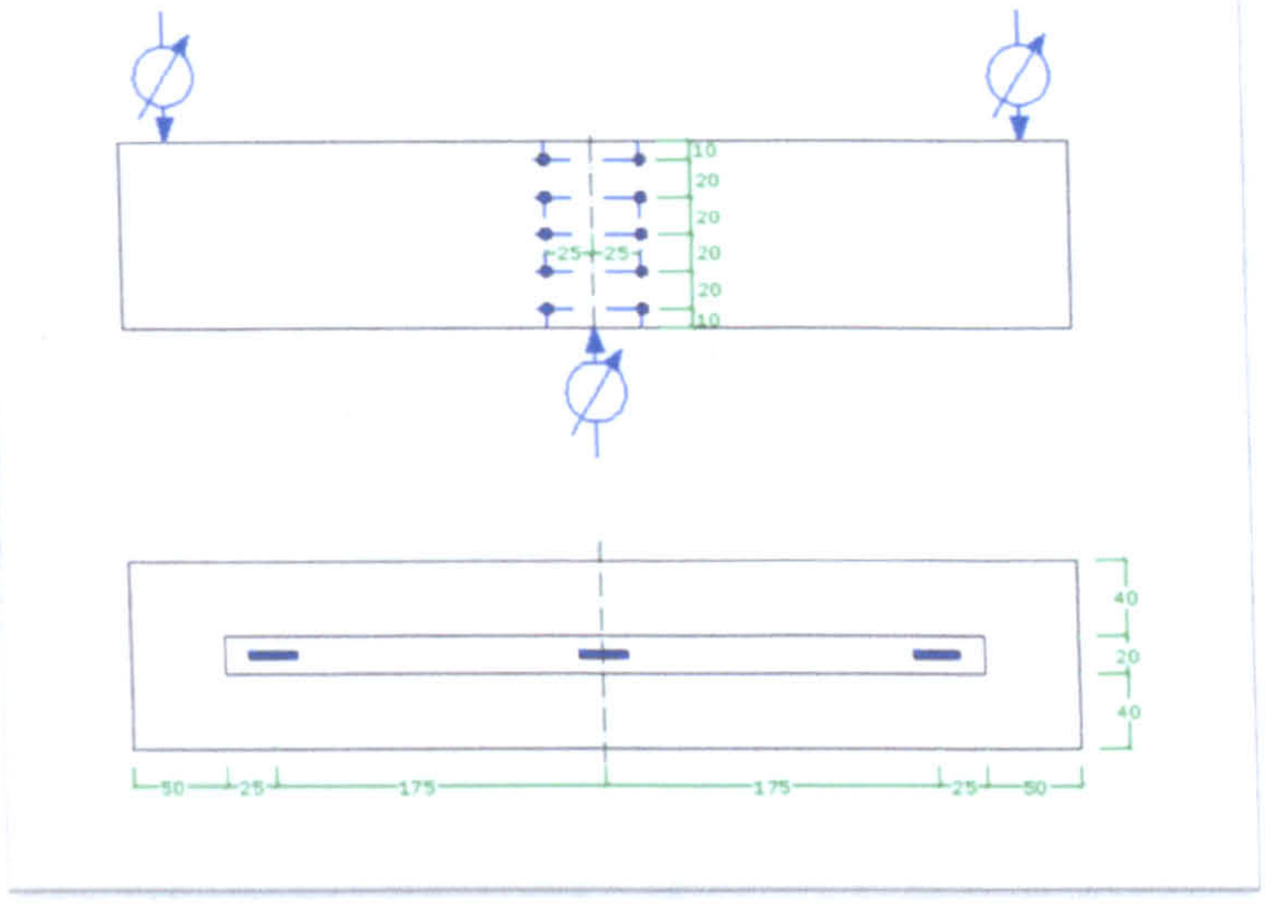

Figure V-2 Position of DEMEC strain gauges, dial gauge indicators and ER strain gauges

The load was applied 1kN every 10min until the failure of the minibeams. After the debonding of the laminate, the load was applied until the beam could not sustain any further increase. The results show only the applied load as the deadweight of samples was not included in the analysis.

5.2 Group 20°C

5.2.1 Testing, cracking and failure load

Sample #20-1 was loaded to 19kN when a brittle shear crack developed in the right half of the beam, see Figure V-1. The crack propagated through the lower face of the beam reaching the concrete- adhesive interface and the crack propagated to the end of the laminate. The crack led to a relaxation of the system to 16.6kN. With increase of the load another type of failure started to develop in the left half leading to a flexural- shear crack at 23kN and subsequent drop of the load to 18.4kN. On the lower face the beam the crack propagated to the concrete-adhesive interface and then to the left end of the laminate. To find the maximum load of the system the beam was reloaded until at 24kN no further increase was possible.

Beam #20-2 failed in a more gradual manner. Flexural cracks were observed at 13kN which continued to propagate upwards. Cracks started to propagate at 17kN towards the adhesive on the strengthened face on the left side of the beam but at later stage did not lead

to delamination. Failure occurred in the right half of the beam at 23kN when the crack propagated to 10mm from the top of the beam and complete delamination was achieved between the adhesive and concrete interface.

The last beam of the group #20-3 exhibited similar behaviour to sample #20-2. Flexural cracks developed at 16kN and they continued to propagate to 18kN when a flexural-shear crack was formed on the left side of the beam which quickly propagated almost to the top surface. Delamination occurred at 20kN followed by drop of the load to 15kN. The maximum load the beam could then sustain was 24.5kN.

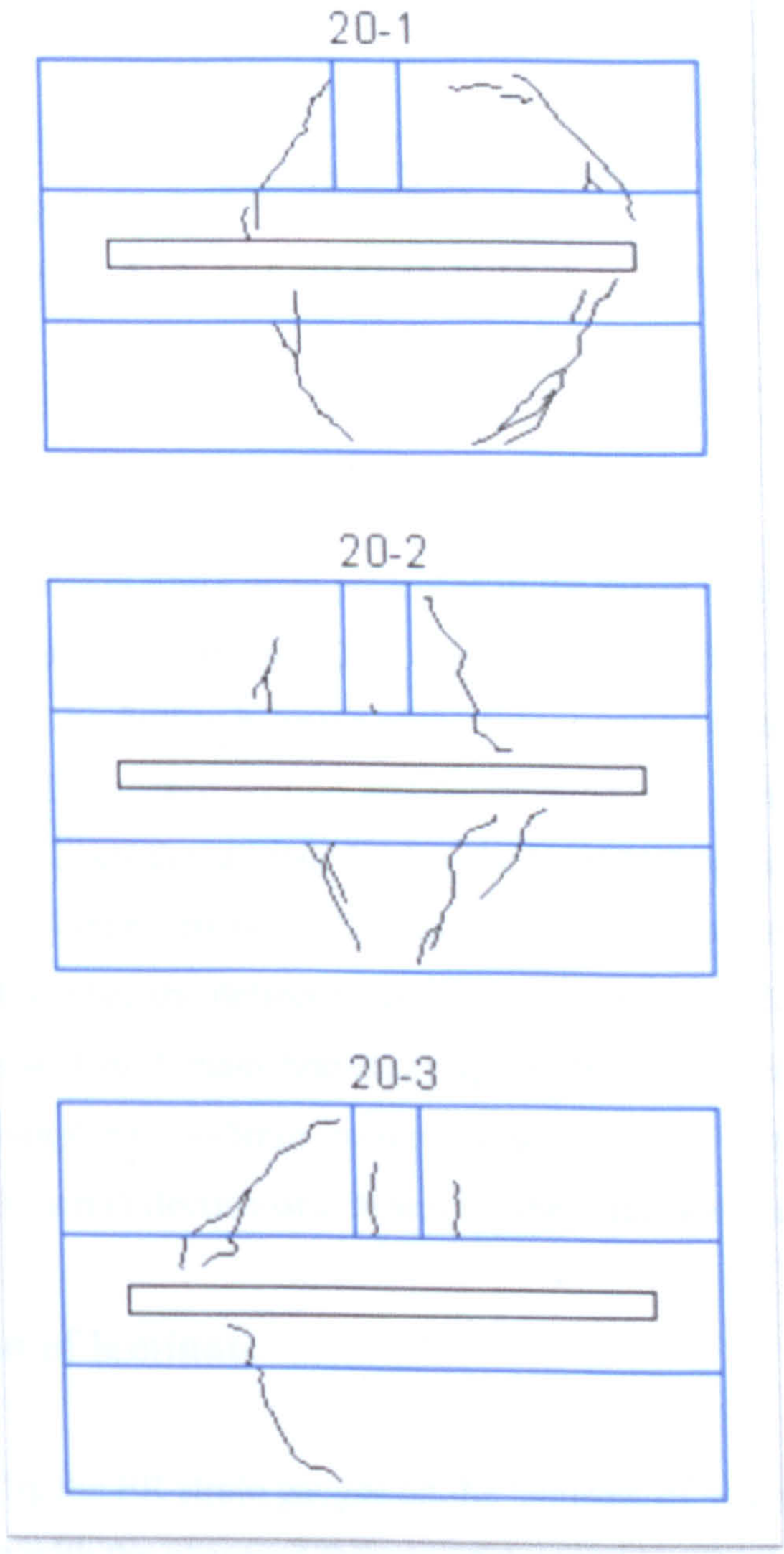

Figure V-3 Crack formation and failure of beams, group 20°C

5.2.2 Deflection

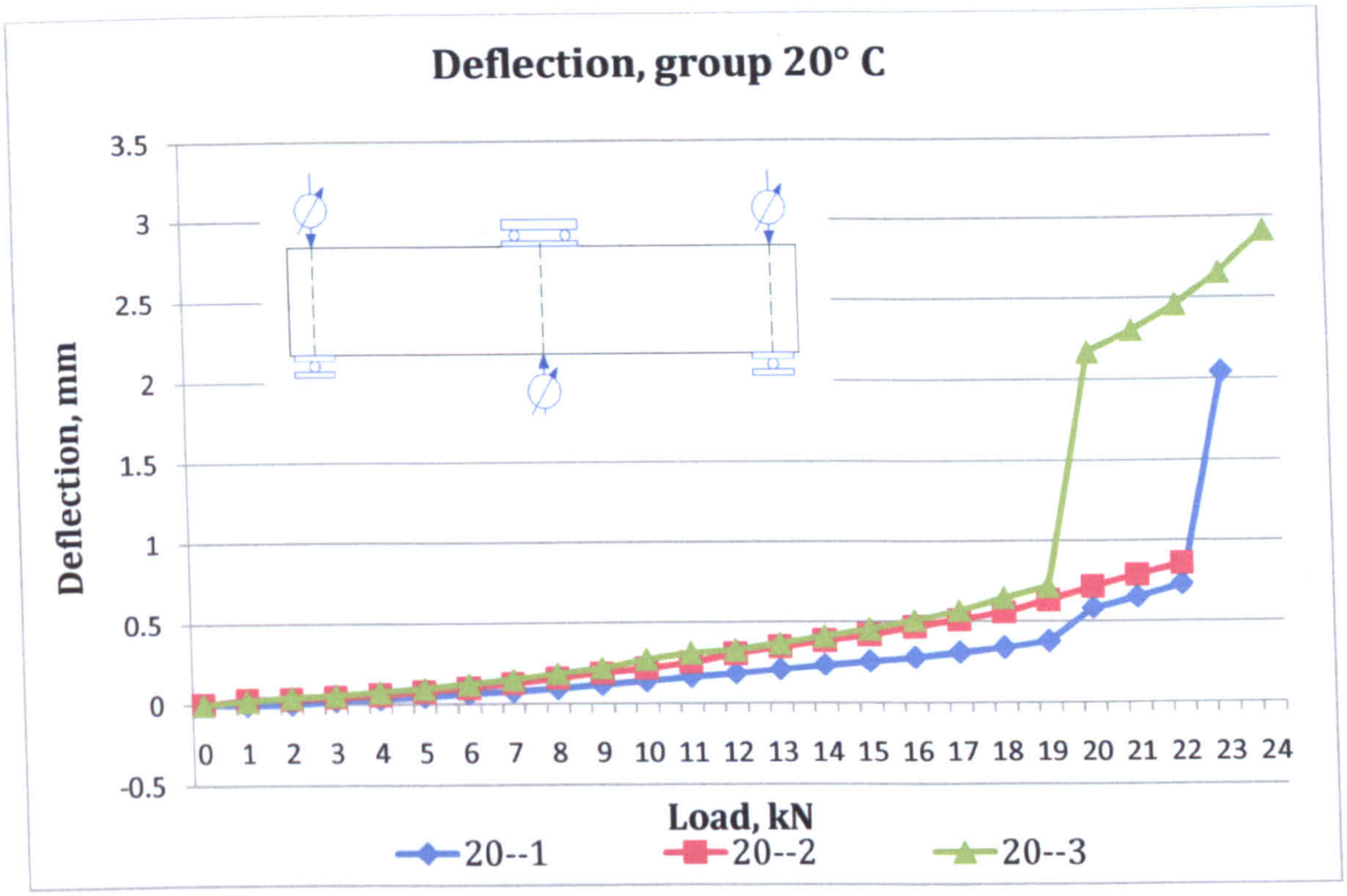

Figure V-4 Deflection, group 20°C

The deflections of the three samples were presented in the range of 0kN to maximum load for the beams, see Figure V-4. Beam #20-1 deflected to 0.379mm at 19kN before it reached its failure load. The further increase of the force resulted in significant increase of the deformation due to the cracked section and the development of new failure in the left half of the beam until at 23kN the ultimate load of the beam was reached. The deflection at the last stage was 2.041mm. Beam #20-2 exhibited a gradual deflection up to the maximum load of 22kN when the deflection reached 0.859mm. The load- deflection curve for beam #20-3 consisted of 2 main branches: up to 19kN the increase was gradual to 0.715mm, when a "jump" to 2.165mm occurred caused by the formation of a flexural-shear crack. The maximum deflection of 2.91mm for the beam was measured at 24kN.

5.2.3 Strain of laminate

The strains recorded by the ER strain gauges on the laminate of beam #20-1 were found to be in good agreement with the observed failures of the sample (Figure V-5). From 16kN to 19kN a sudden increase of the strain to 401microstrain was observed for gauge 3 at the

right end of the laminate before a shear crack was formed. The delamination which occurred at 19kN only led to debonding of 20-30mm from the end of the laminate and at further increase of the load the gauge would register negative values. Thus, ER gauge 2 would continue to register increase of the strain above 19kN up to 22kN when maximum strain of 1745microstrain was recorded. The left strain gauge did not detect high deformations at the end of the laminate although a value of 89microstrain was recorded at 22kN prior to the formation of the flexural-shear crack and subsequent delamination.

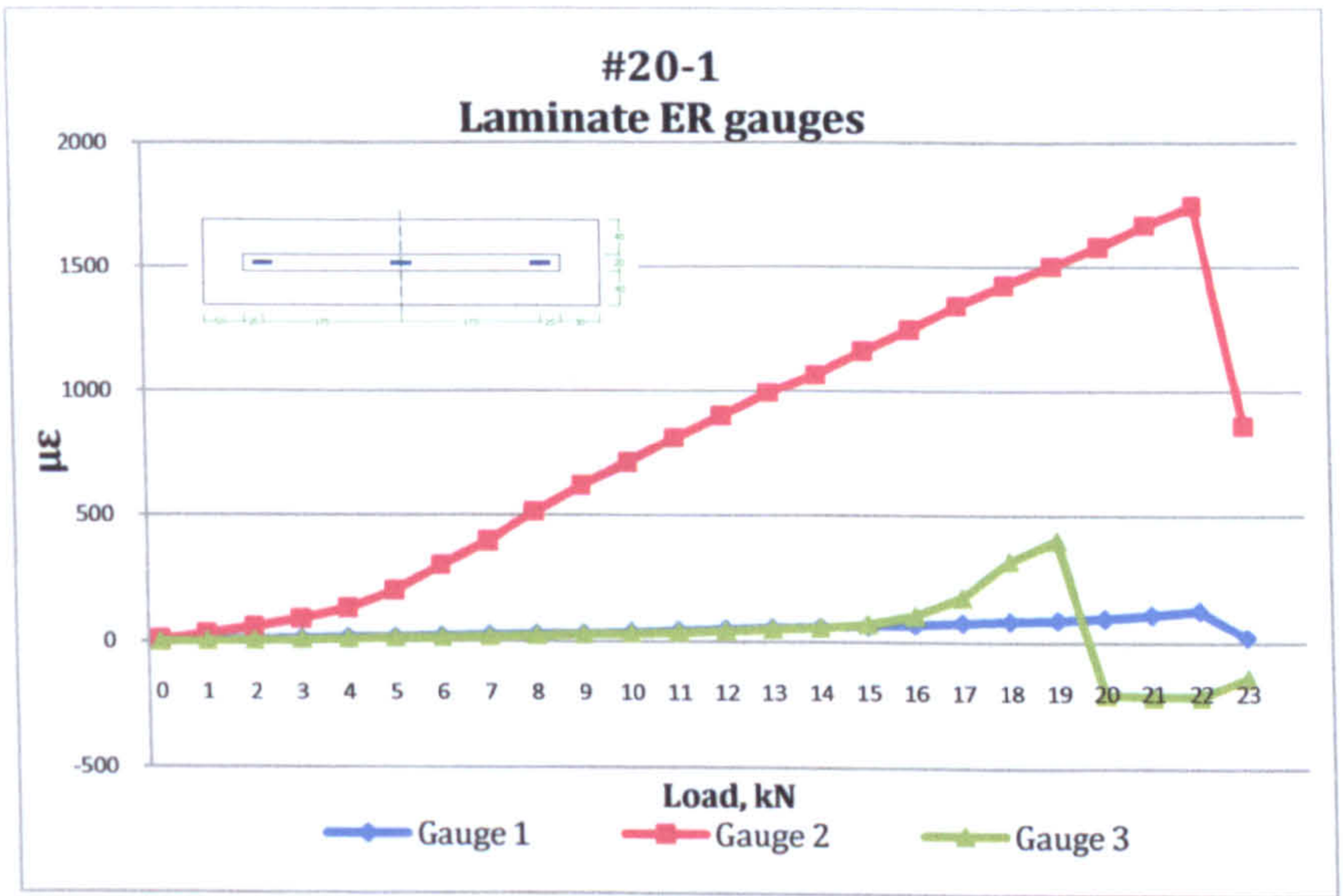

Figure V- 5 Laminate ER gauges, sample #20-1

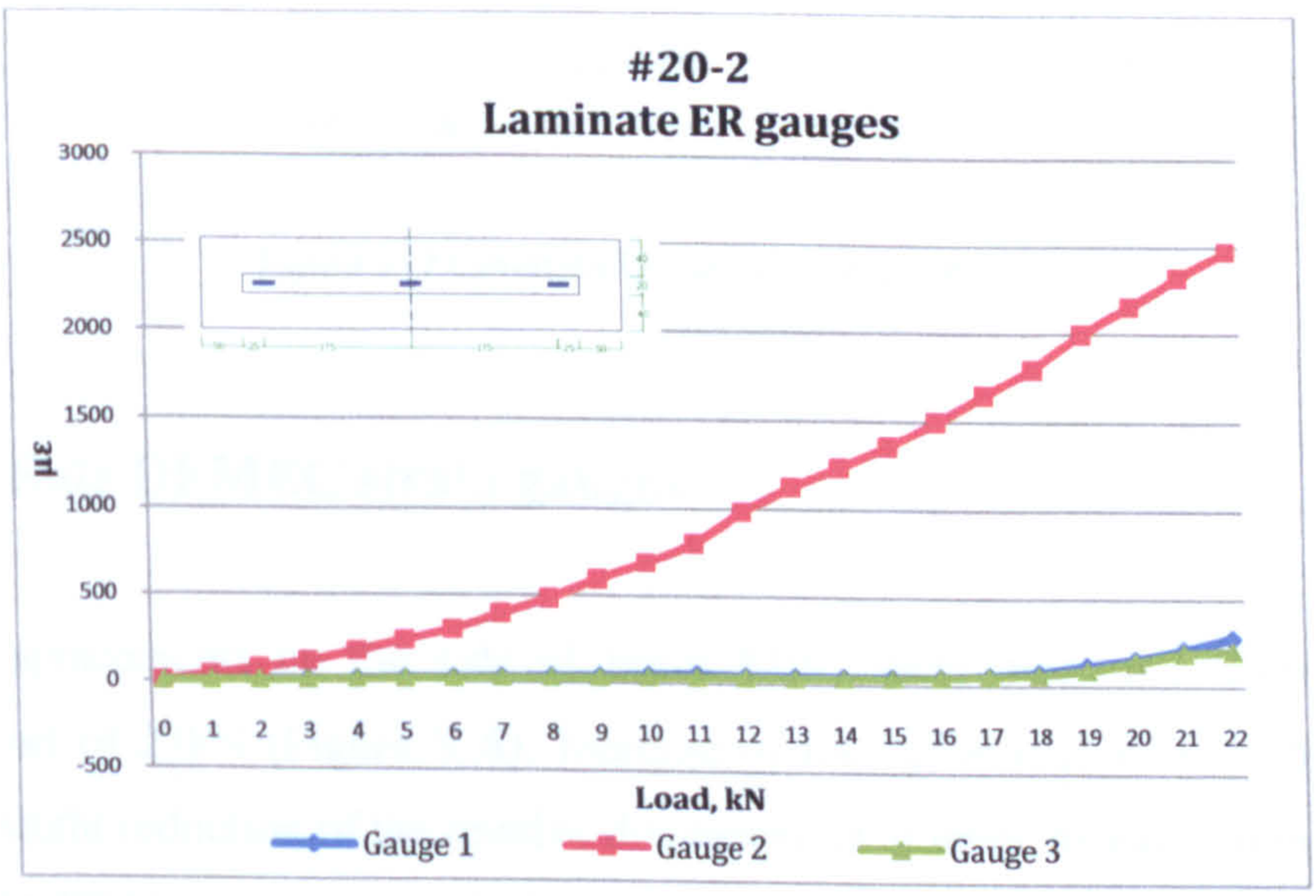

Figure V- 6 Laminate ER gauges, sample #20-2

The strain of the laminate of sample #20-2 was plotted for load 0kN to 23kN, see Figure V-6. ER gauge 2 revealed gradual increase up to the maximum load when strain of

2472microstrain was reached. The strain gauges at the ends of the laminate exhibited slight increase of the deformations above 17kN when significant crack development was observed. Maximum strains for ER gauge 1 and ER 3 prior to failure were 285microstrain and 207microstrain respectively.

The strain of the laminate of sample #20-3 was plotted for load 0kN to 24kN (Figure V-7). At 19kN prior to the delamination at the left side ER gauge 2 reached a maximum value of 2451microstrain. Increase of the strain was observed for ER gauge 1 from 16kN when flexural cracks occurred to 19kN with maximum value of 405microstrain prior to the delamination. Maximum value for ER gauge 3 was also measured at 19kN with a value of 197microstrain.

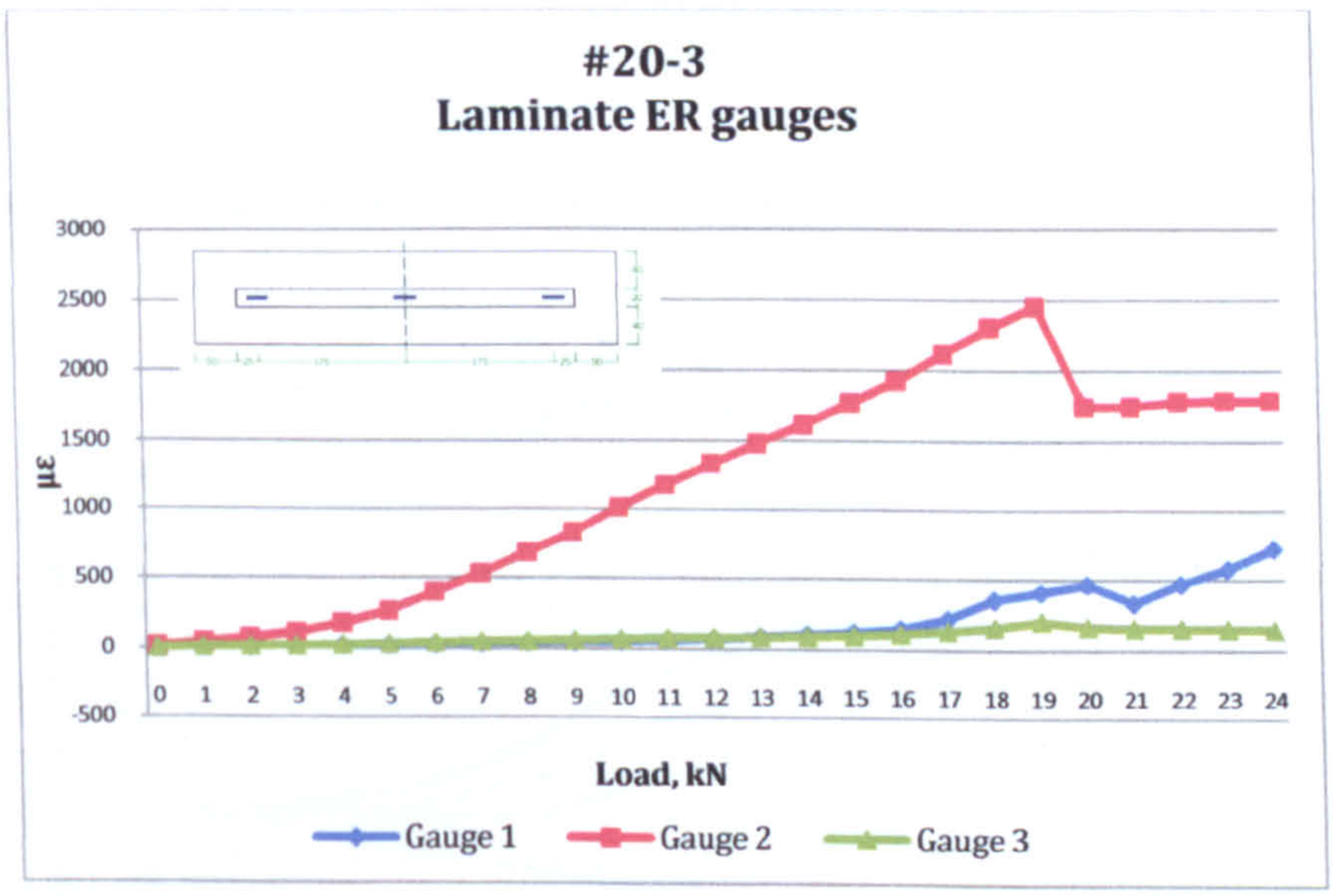

Figure V- 7 Laminate ER gauges, sample #20-3

5.2.4 Side DEMEC strain gauges

The local displacements on the side of beam #20-1 were measured from 0kN to the maximum load of 23kN (Figure V-8). Increase of the deformations was observed up to 19kN when slight reduction of the relative displacement at level 90 and 70mm from the top was found. At 22kN maximum level of 1892microstrain was measured for level 90mm and minimum negative value of 777microstrain for level 10mm followed by delamination and subsequent reduction of the deformations. Although the average maximum tensile strain of

150microstrain was exceeded at an early load, no visible flexural cracks were visible until the first crack at 19kN was formed.

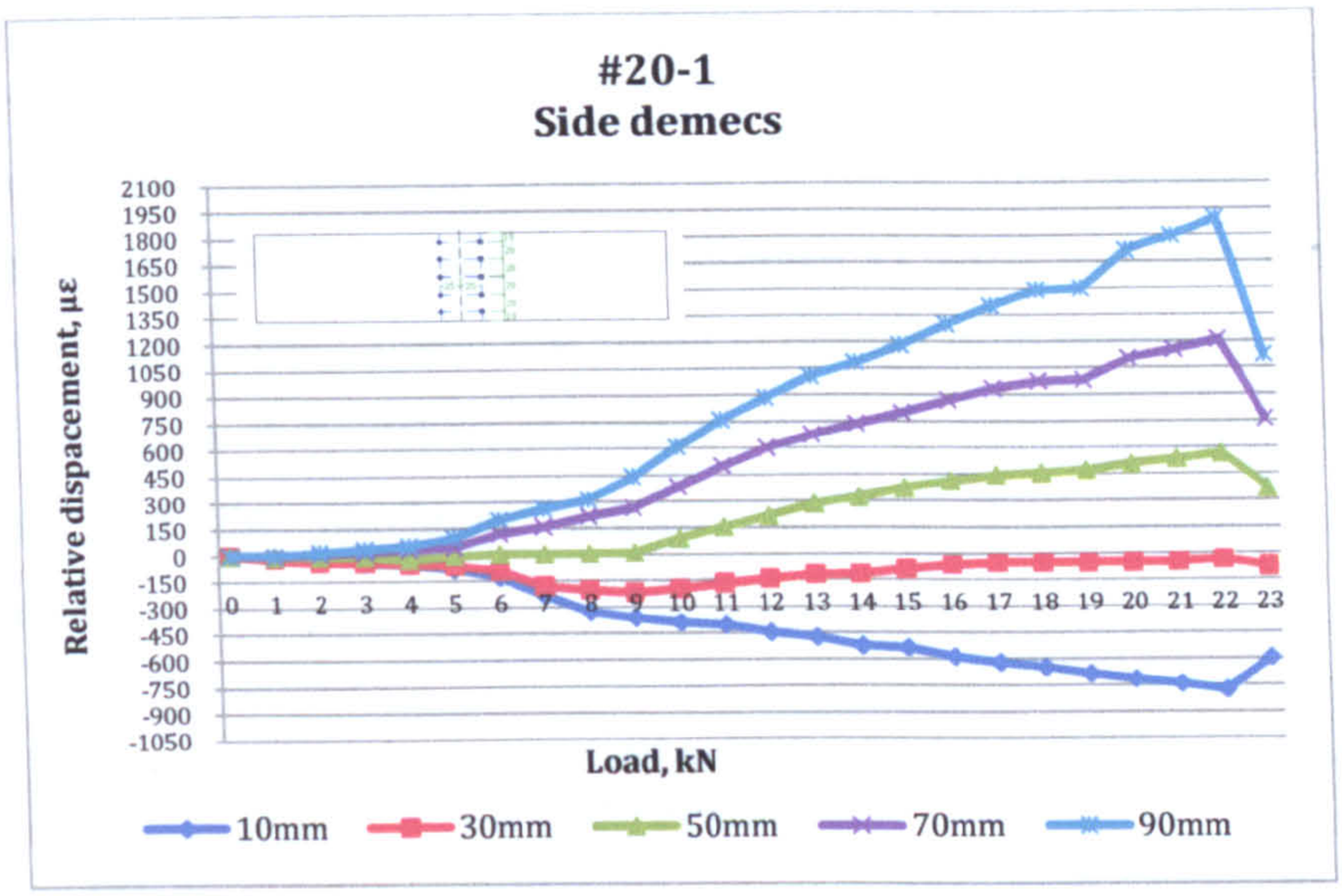

Figure V- 8 Local deformations, Side DEMEC strain gauges #20-1

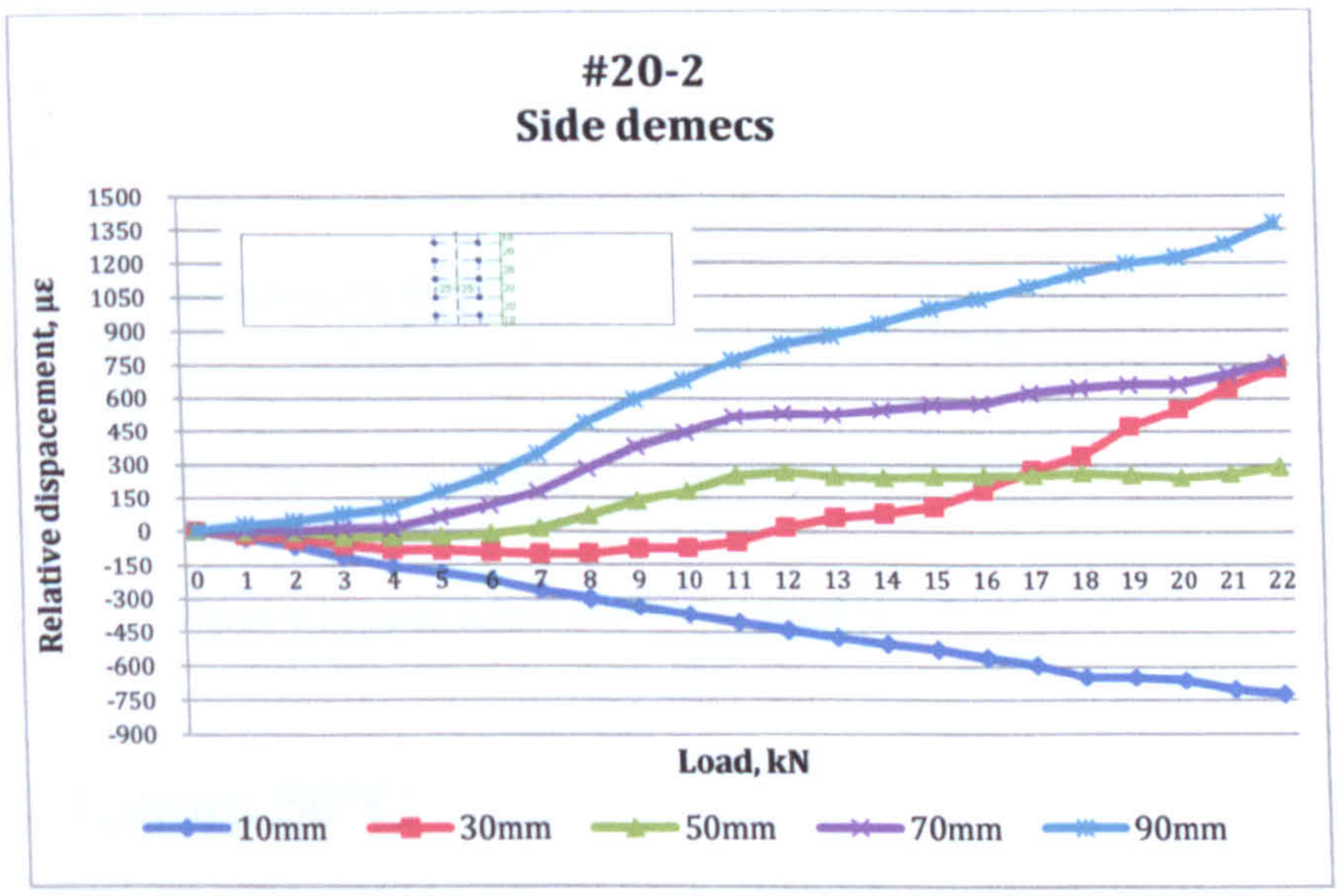

Figure V- 9 Local deformations, Side DEMEC strain gauges #20-2

Sample #20-2 exhibited different behaviour, see Figure V-9. The first observed cracks were formed at load 12kN outside the strain gauge distance and one within the strain gauge length. With increase of the load the cracks propagated to level 30 to 50mm at 17kN. The measured deformations for gauge 30mm revealed a significant change of the strain for loads above 11kN. In the first steps of loading the deformations at level 30mm were negative, above 11kN the relative displacement would start to increase and at 22kN a maximum value of 756microstrain was measured. Level 10mm exhibited strictly

compressive deformations and at the maximum load the deformation reached a value of -725microstrain.

Local deformations were measured for sample #20-3 from 0kN to the failure load of 19kN, see Figure V-10. First flexural cracks were observed at 16kN outside and within the strain gauge length and those propagated upwards up to 18kN. With increase of the load the tensile deformations at level 90 to 50mm continued to grow with the same rate while DEMEC strain gauge at level 30mm was found to change from negative to positive above 10kN. The maximum deformation measured at level 30mm at load of 19kN was 555microstrain and the maximum negative relative displacement at 19kN was 553microstrain.

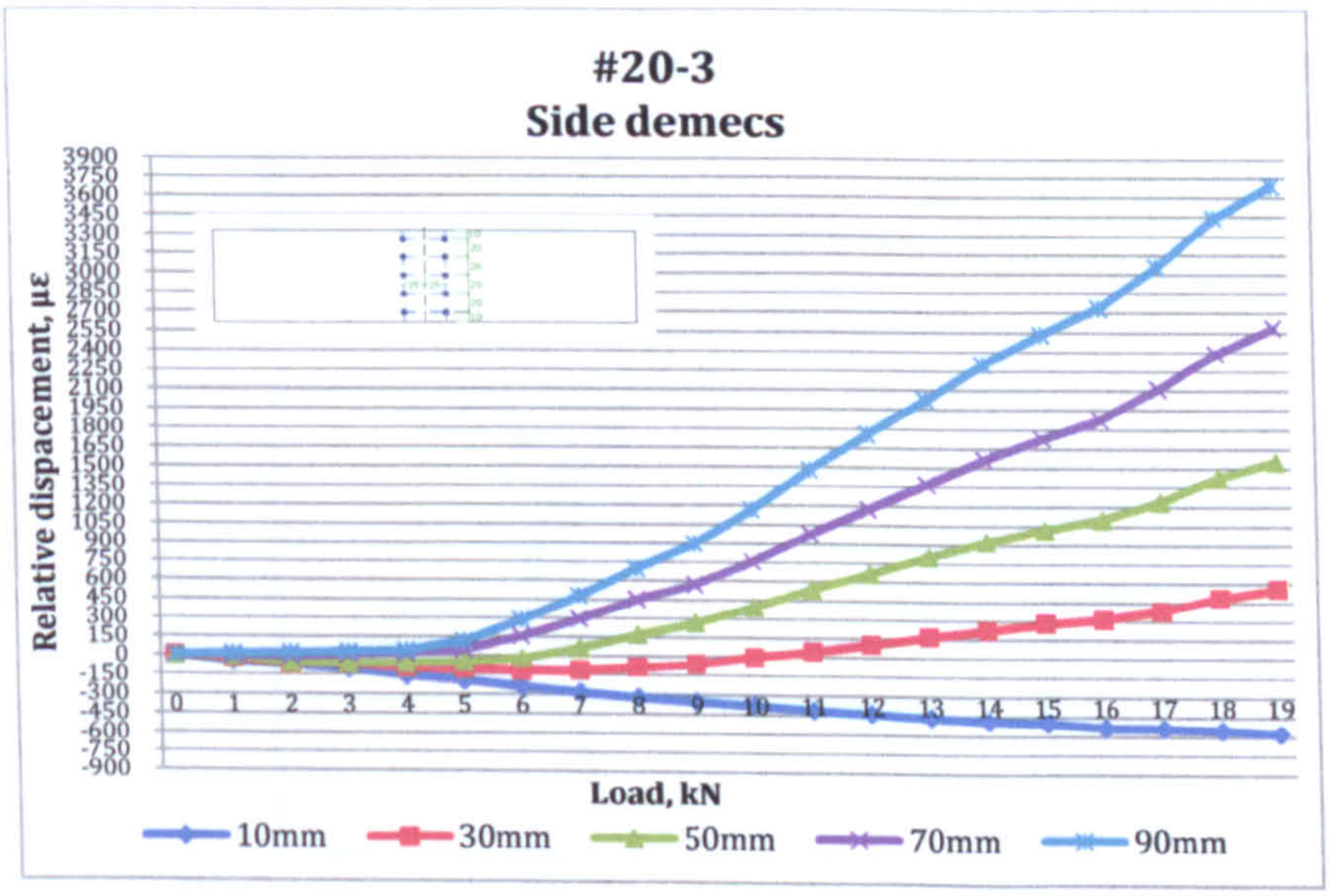

Figure V-10 Local deformations, Side DEMEC strain gauges #20-3

5.3 Group 50°C

5.3.1 Testing, cracking and failure load

Sample #50-1 developed flexural cracks at 15kN of which one continued to propagate upwards with increase of the loading (Figure V-11). The crack had propagated at 18kN almost to the top when delamination between the adhesive and the concrete occurred. The system then held a load of 11.5kN and was further increased to 22.2kN when the maximum load was reached.

Sample #50-2 exhibited similar behaviour to sample #50-1. Flexural cracks were formed at 15kN and half of those did not propagate further. With increase of the load to 18kN a major crack had developed on the left side of the beam. The crack had propagated through the tension face of the beam to the interface between the adhesive and the concrete. Delamination followed and the load was reduced to 12.9kN. The beam was then reloaded and at 23.7kN the maximum load was reached.

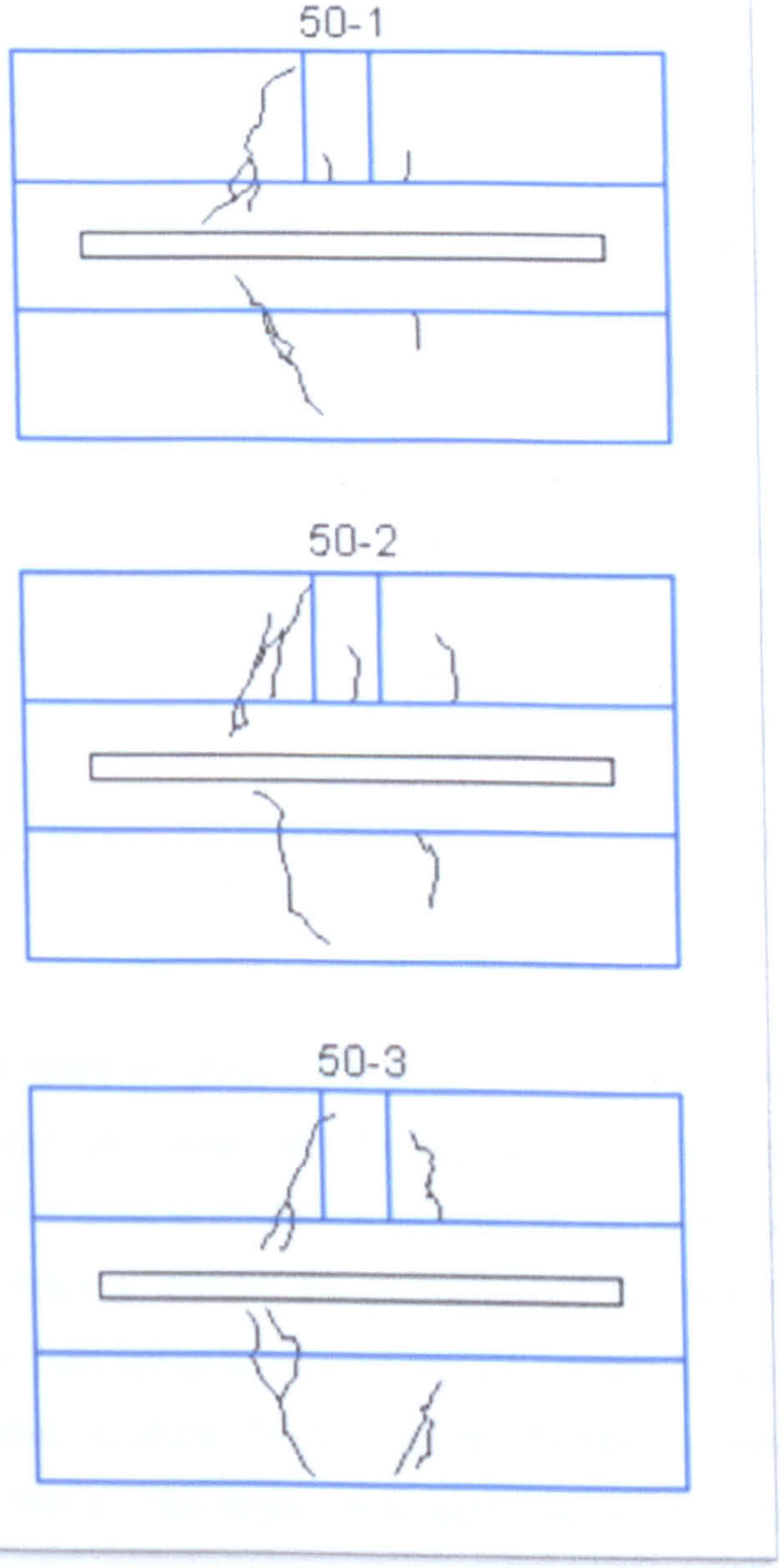

Figure V- 11 Crack formation and failure of beams, group 50°C

Flexural cracks were formed in sample #50-3 when the load reached 14kN. The cracks were developed almost symmetrically about the centre line of the beam and at further increase all of them propagated vertically. At 20kN delamination at the left side of the

beam was observed followed by reduction of the load to 12.9kN. The system was then able to sustain maximum load of 22.6kN.

5.3.2 Deflection

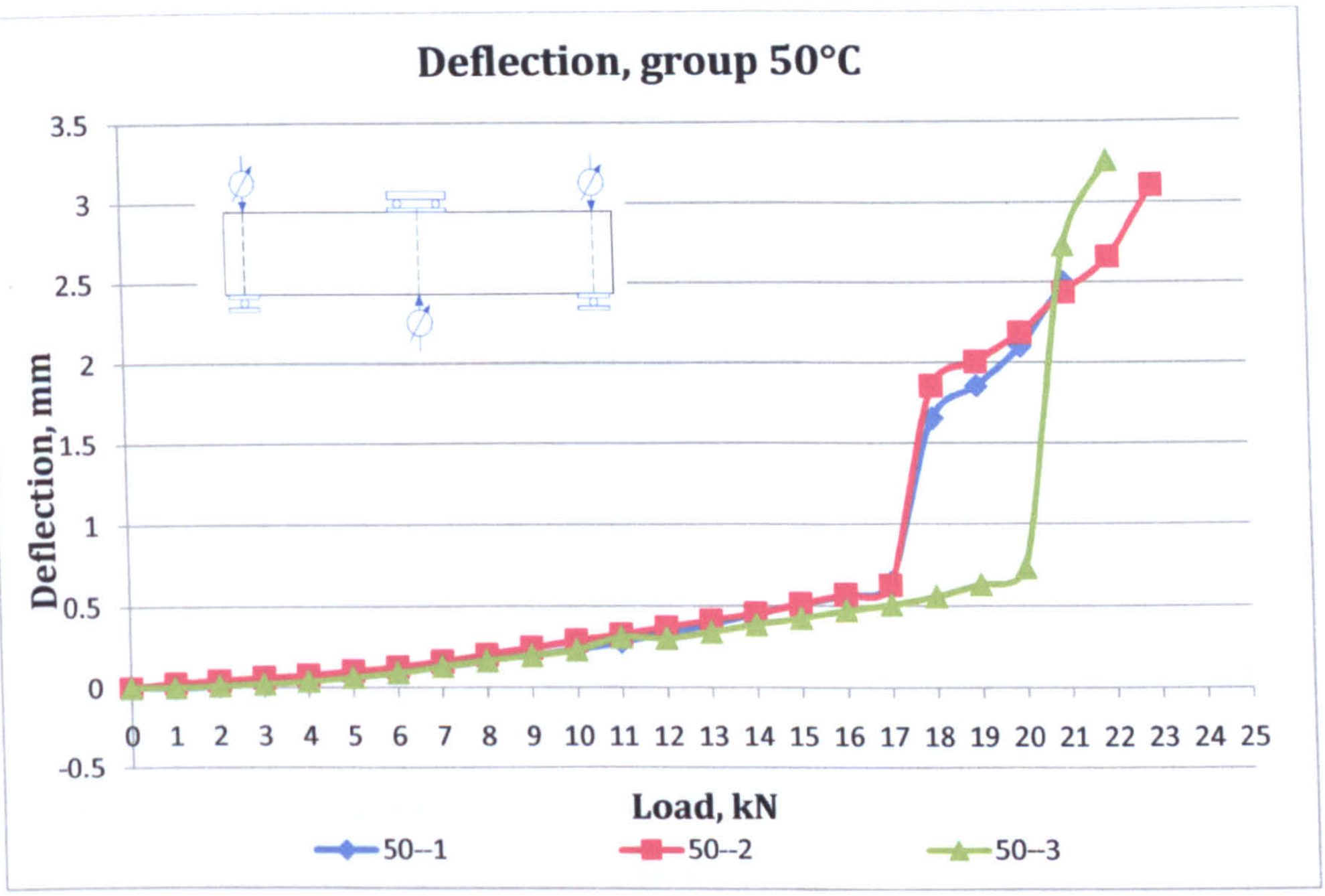

Figure V-12 Deflection, group 50°C

The deflection of the samples of group 50°C were presented for loads from 0kN to the maximum load the beams could sustain after the separation of the plate from the RC prism (Figure V-12). Beam #50-1 exhibited gradual increase of the deflection up to 18kN when delamination occurred. Prior to failure the deflection of the beam was 0.643mm. The following increase of the load led to significant increase of the deformation of the beam to 2.495mm when the load reached 21kN. Similar behaviour was observed for the deformation of beam #50-2. The beam had deflected to 0.627mm at 17kN before delamination occurred. The subsequent loading of the system resulted in deflection of 3.1mm when the maximum load was reached at 23kN. Beam #50-3 was loaded to 20kN with deflection of 0.73mm before delamination was observed. The maximum deflection which was recorded at 22kN was 3.256mm.

5.3.3 Strain of laminate

The deformations recorded by strain gauges attached to the laminate of beam #50-1 reached highest values at 17kN (Figure V-13). Strain of 2065microstrain was recorded by strain gauge at the midspan of the beam before the failure load was reached. The strain gauge at the left end of the laminate registered slight increase of the deformations at 15kN to 192microstrain at 17kN until delamination occurred. The strain gauge at the right end of the laminate was gradually increasing during the loading process and it reached 115.5microstrain prior to delamination. Further increase of the load did not cause any increase the strain in the laminate.

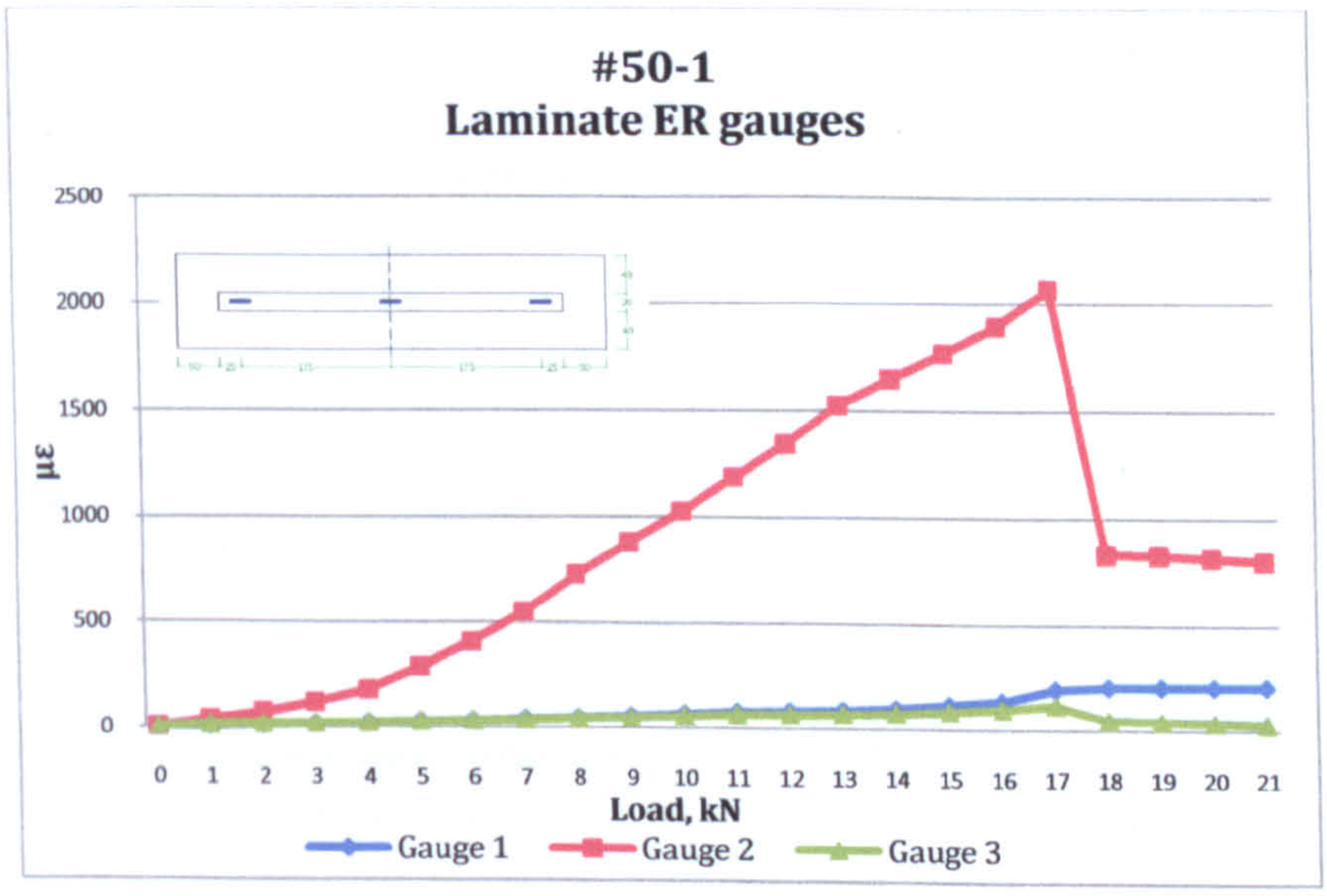

Figure V- 13 Laminate ER gauges, sample #50-1

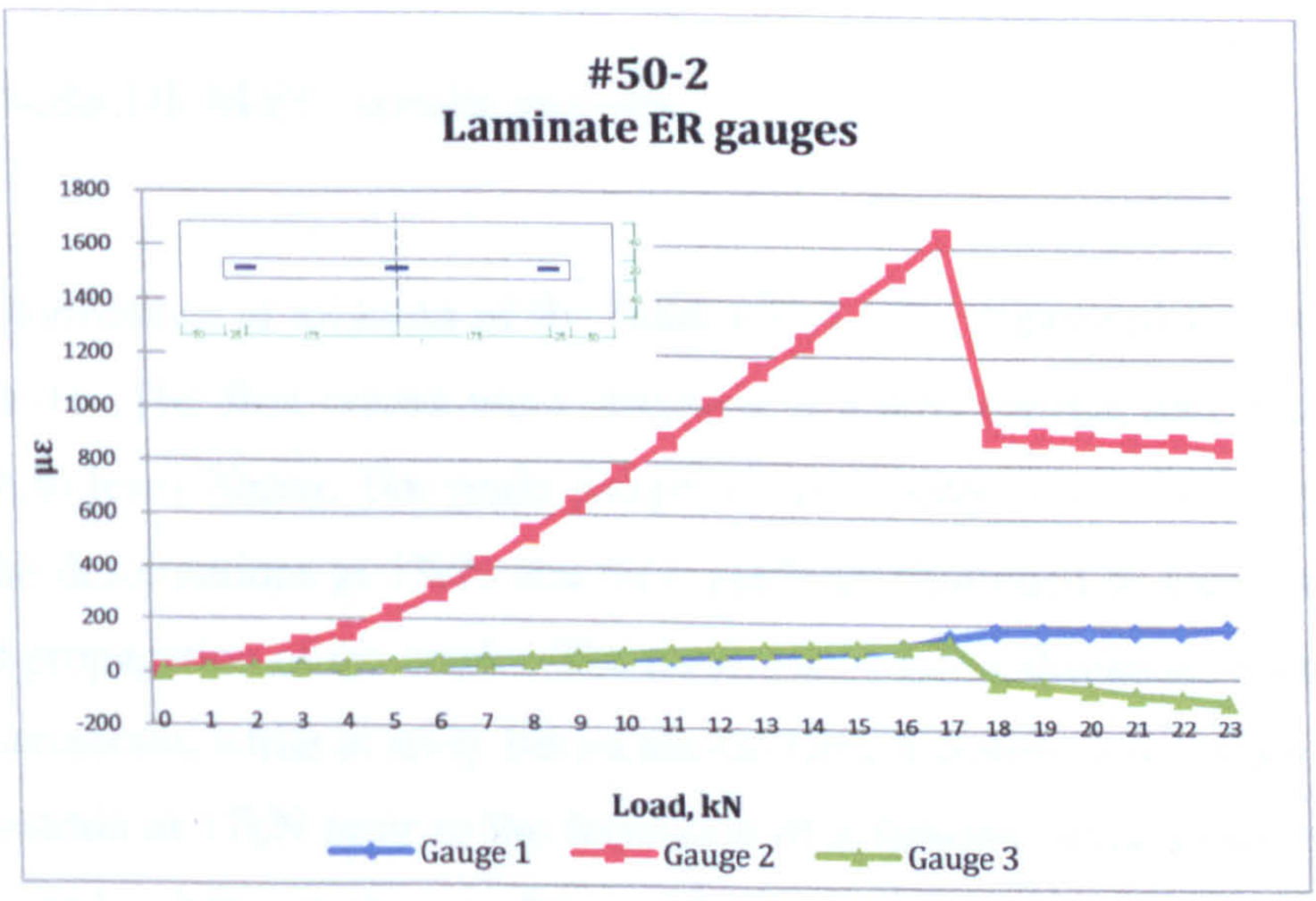

Figure V-14 Laminate ER gauges, sample #50-2

The strain of ER gauge 2 at 17kN was 1640.5microstrain for beam #50-2 (Figure V-14). The measured strains at the left and right end of the laminate were similar and only at 17kN a slight increase to 149.5microstrain was observed at the left side. The right strain gauge reached a maximum value of 125.5microstrain before the failure.

Beam #50-3 was loaded to 20kN when maximum values for the three strains were measured, see Figure V-14. At midspan the strain reached a value of 2346.5microstrain prior to failure. The left and right strain gauges registered similar deformations up to 14kN when slight increase of the strain at the left end of the laminate was observed with increase of the load. At 20kN ER gauge 3 reached strain of 402microstrain which was higher than the strain registered at the left end of the laminate: 357microstrain.

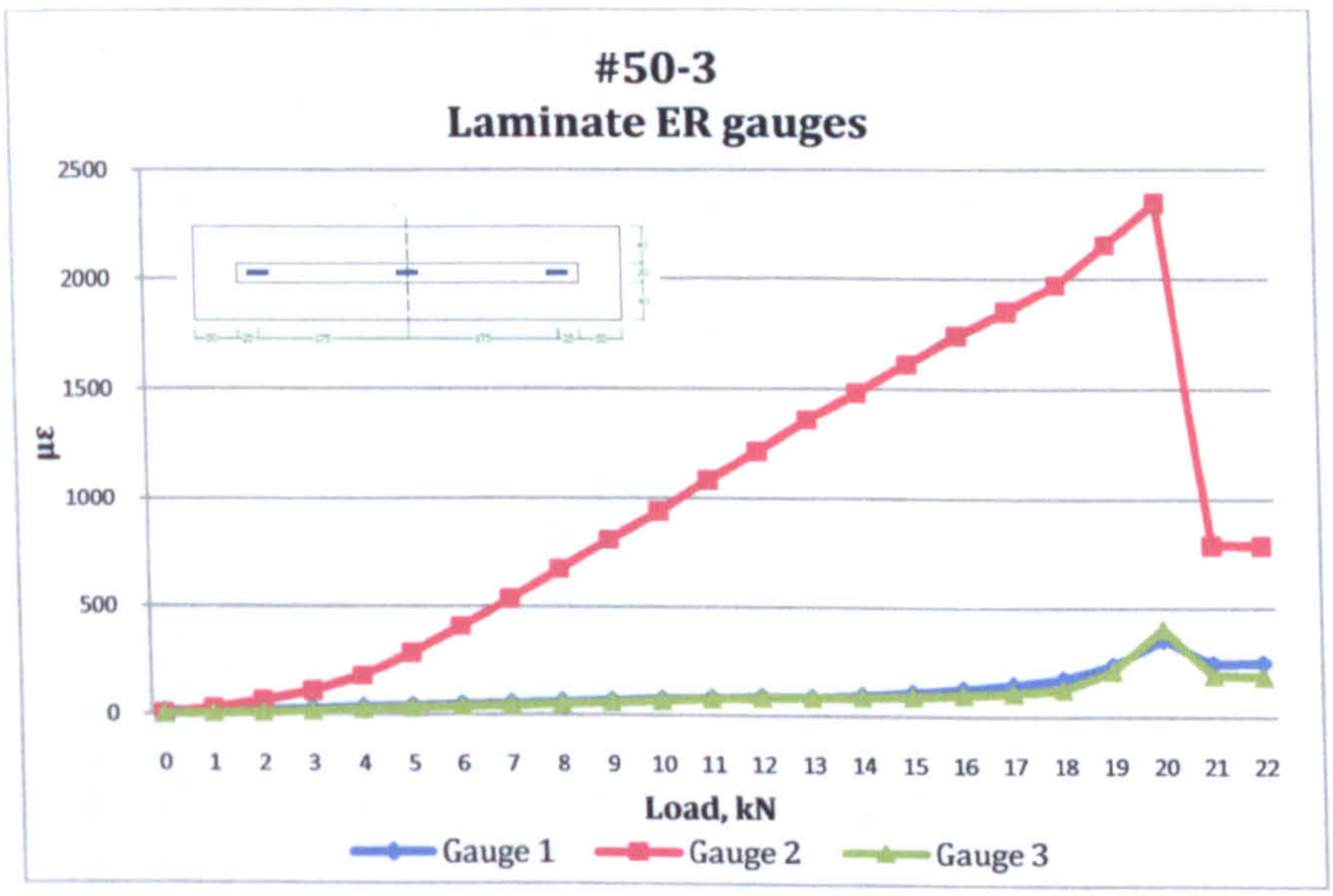

Figure V- 15 Laminate ER gauges, sample #50-3

5.3.4 Side DEMEC strain gauges

The local deformations at midspan of the beam #50-1 were measured from 0kN to 21kN, see Figure V-16. The first cracks were observed at 15kN, outside and within the strain gauge length to level 70mm. The strain gauges at level 90mm and 70mm registered slight change of the deformations at 13kN and their readings continued to increase with further opening and propagation of the cracks. The maximum relative displacement at level 90mm was 2437microstrain, while at level 10mm the maximum compressive strain was found to be 485microstrain at 17kN prior to the formation of a flexural- shear crack in the left half of the beam. At level 30mm change of the strain was registered between 8kN and 9kN with increase of the strain at 17kN to 318microstrain. After the failure load of the beam was

reached the deformations measured at midspan did not indicate any further contribution of the cracked sections.

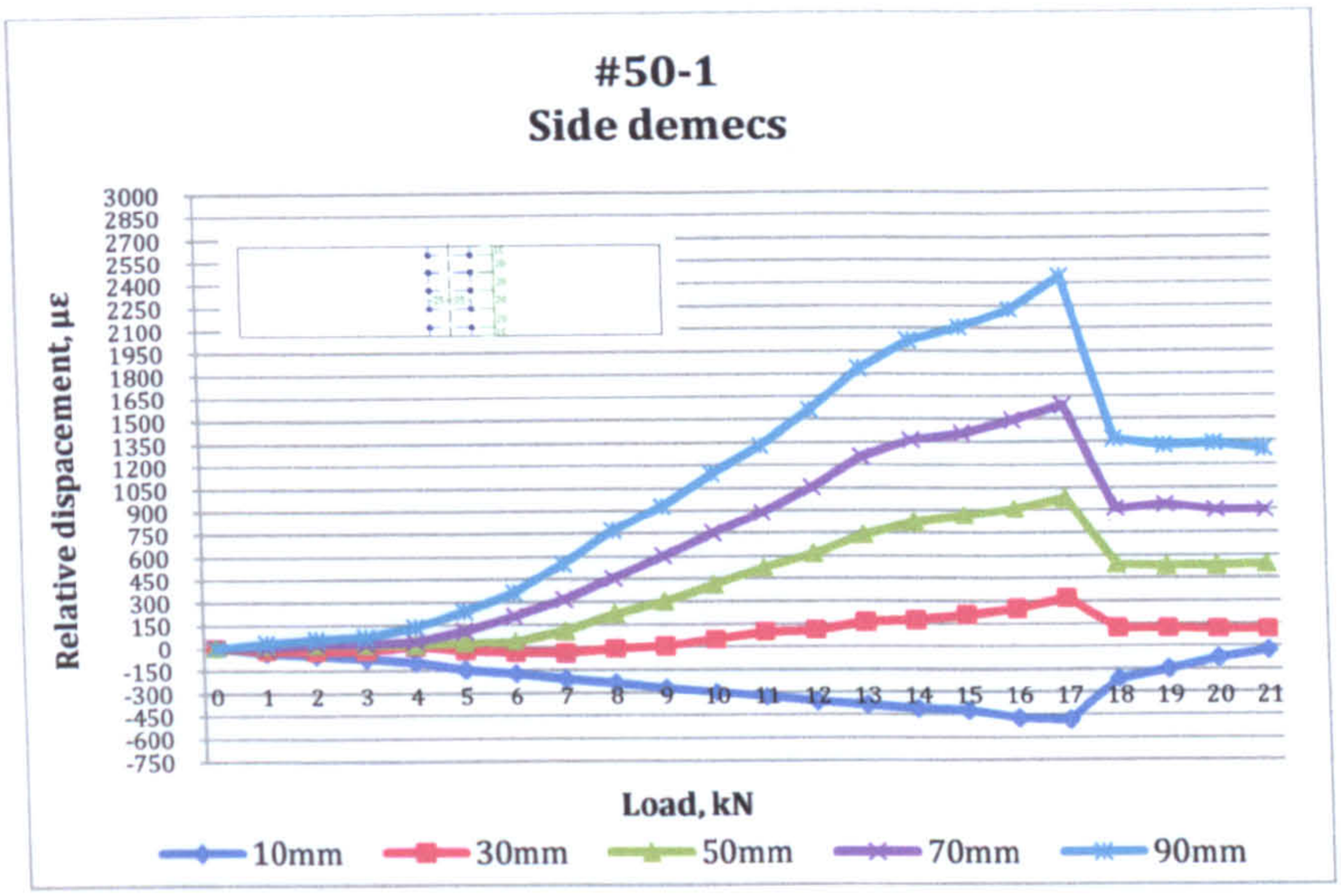

Figure V- 16 Local deformations, Side DEMEC strain gauges #50-1

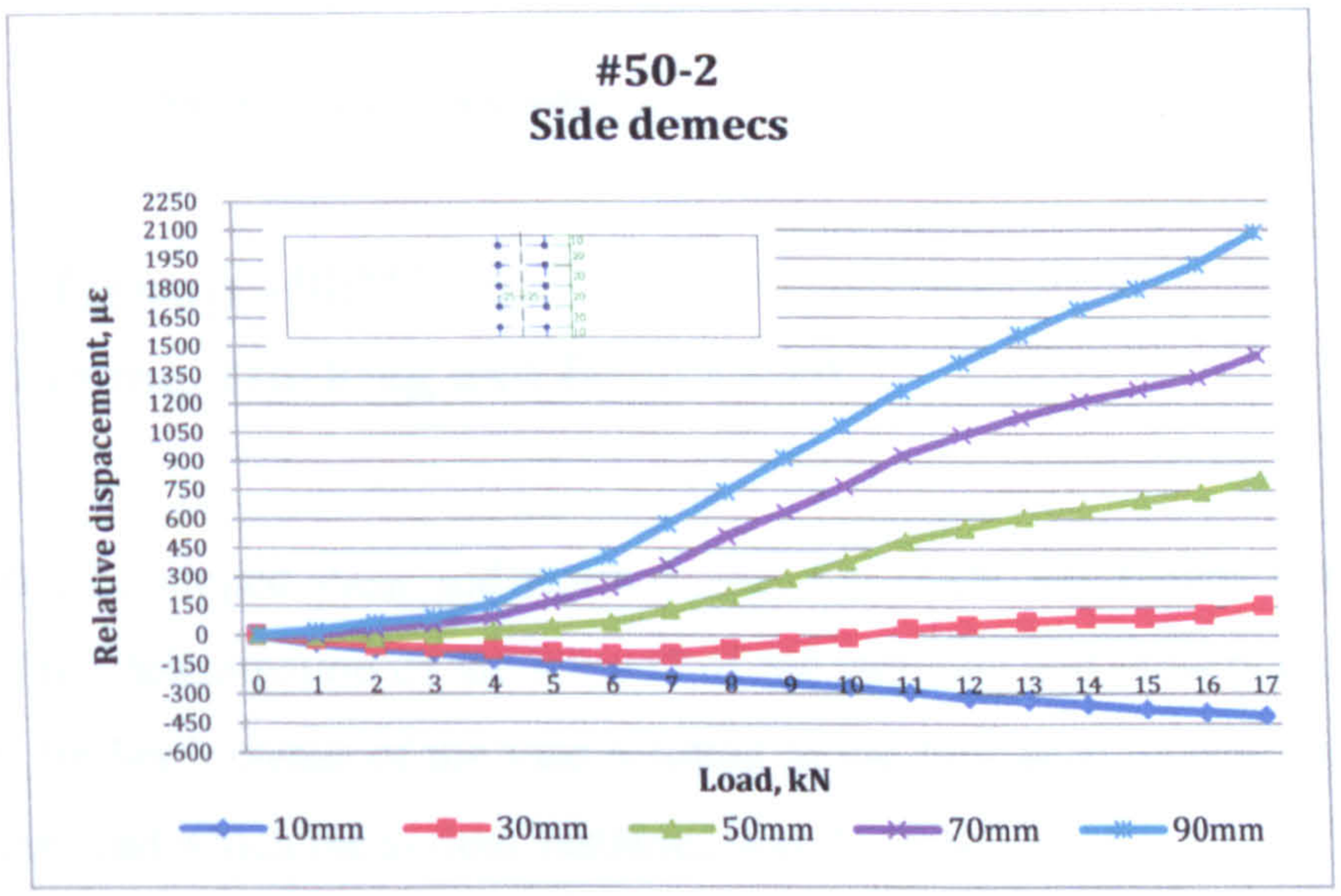

Figure V- 17 Local deformations, Side DEMEC strain gauges #50-2

The relative displacement measured at midspan of beam #50-2 was plotted from 0kN to 17kN, see Figure V-17. The first cracks were formed at 15kN outside the strain gauge base length. Maximum tensile deformation of 2083microstrain was measured at level 90mm at 17kN and maximum compression strain of 410microstrain was recorded for level 10mm. The deformations at level 30mm were found to change sign from negative to positive between 10 and 11kN reaching value of 157microstrain prior to failure.

The local deformations measured at midspan for beam #50-3 were plotted for load 0kN to 22kN, (Figure V-18). The maximum values for level 90mm were 1756microstrain at 20kN when delamination occurred. At level 10mm the compressive strain reached a value of 293microstrain at the failure load. The deformation at level 30mm changed from compressive to tensile at 10kN and at the failure load the deformation was 221microstrain.

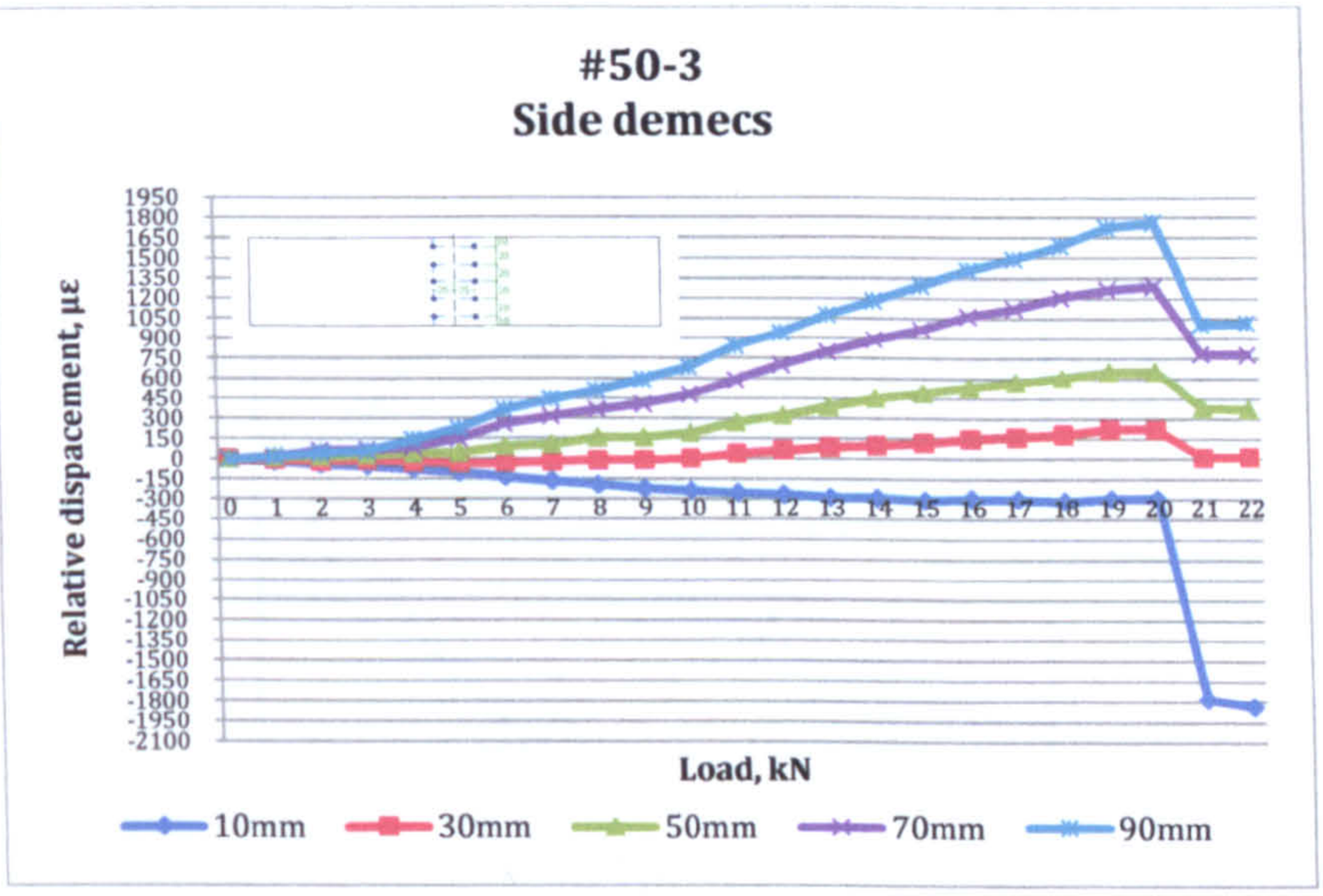

Figure V- 18 Local deformations, Side DEMEC strain gauges #50-3

5.4 Group 100°C

5.4.1 Testing, cracking and failure load

Sample #100-1 developed shear and flexural cracks at 16kN, see Figure V-19. The shear crack caused the delamination of the left end of the laminate and reduction of the load to 13.4kN. The further increase of the load resulted in the formation of new flexural cracks. The maximum load which the system sustained was 21.9kN.

The second beam of group 100°C formed flexural cracks at 15kN which continued to propagate vertically up to 18kN. At 21kN a new flexural-shear crack was formed which resulted in the delamination at the left side of the beam. The load dropped to 15.9kN and was then gradually increased to 22.7kN when the ultimate capacity of the system was reached.

Sample #100-3 formed one flexural crack in the midspan of the beam which continued to propagate vertically to 12kN. When the load was increased to 13kN a new inclined crack was formed in the right half of the beam which led to a brittle diagonal crack before second readings for the same load were taken. The right side of the laminate and adhesive layer had then separated from the concrete and the load dropped to 1.2kN. The beam was then reloaded to 2.3kN when the maximum capacity of the beam was reached.

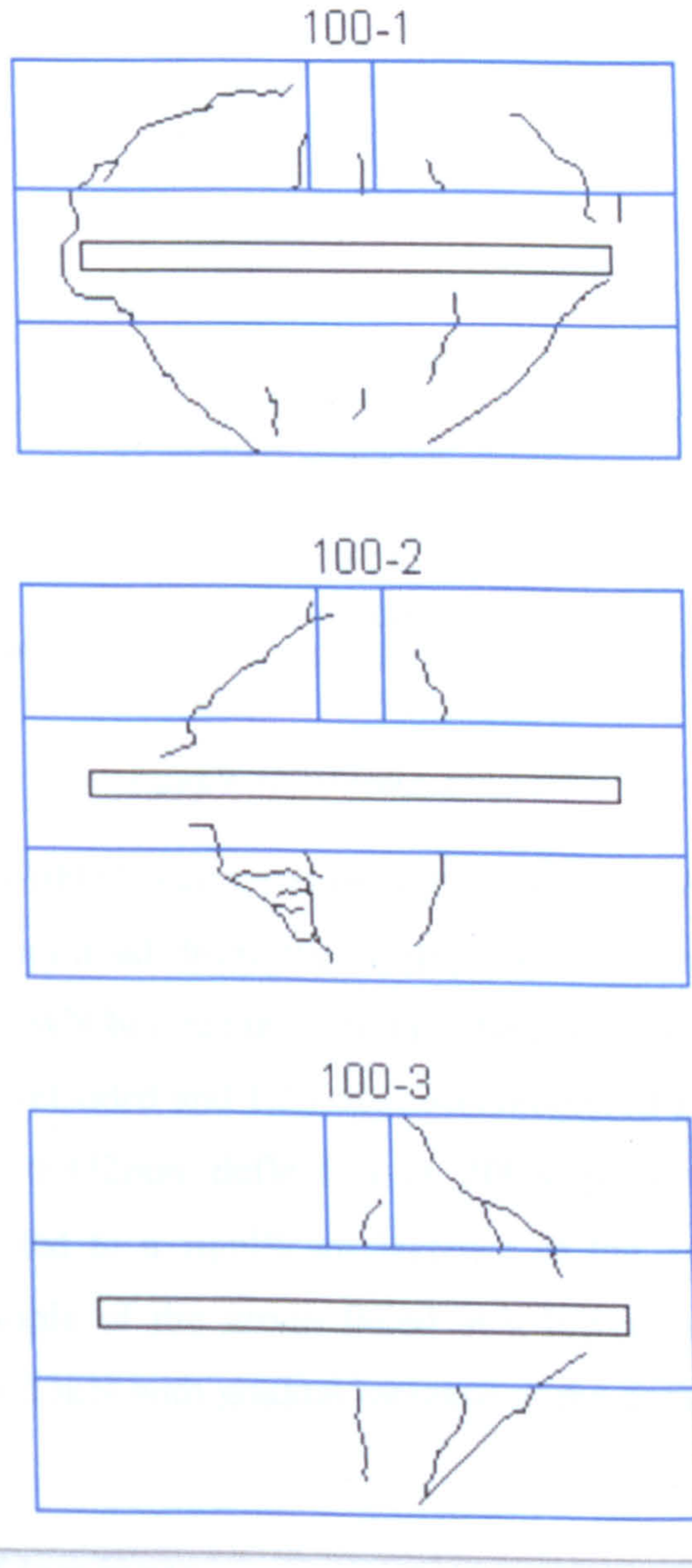

Figure V- 19 Crack formation and failure of beams, group 100°C

5.4.2 Deflection

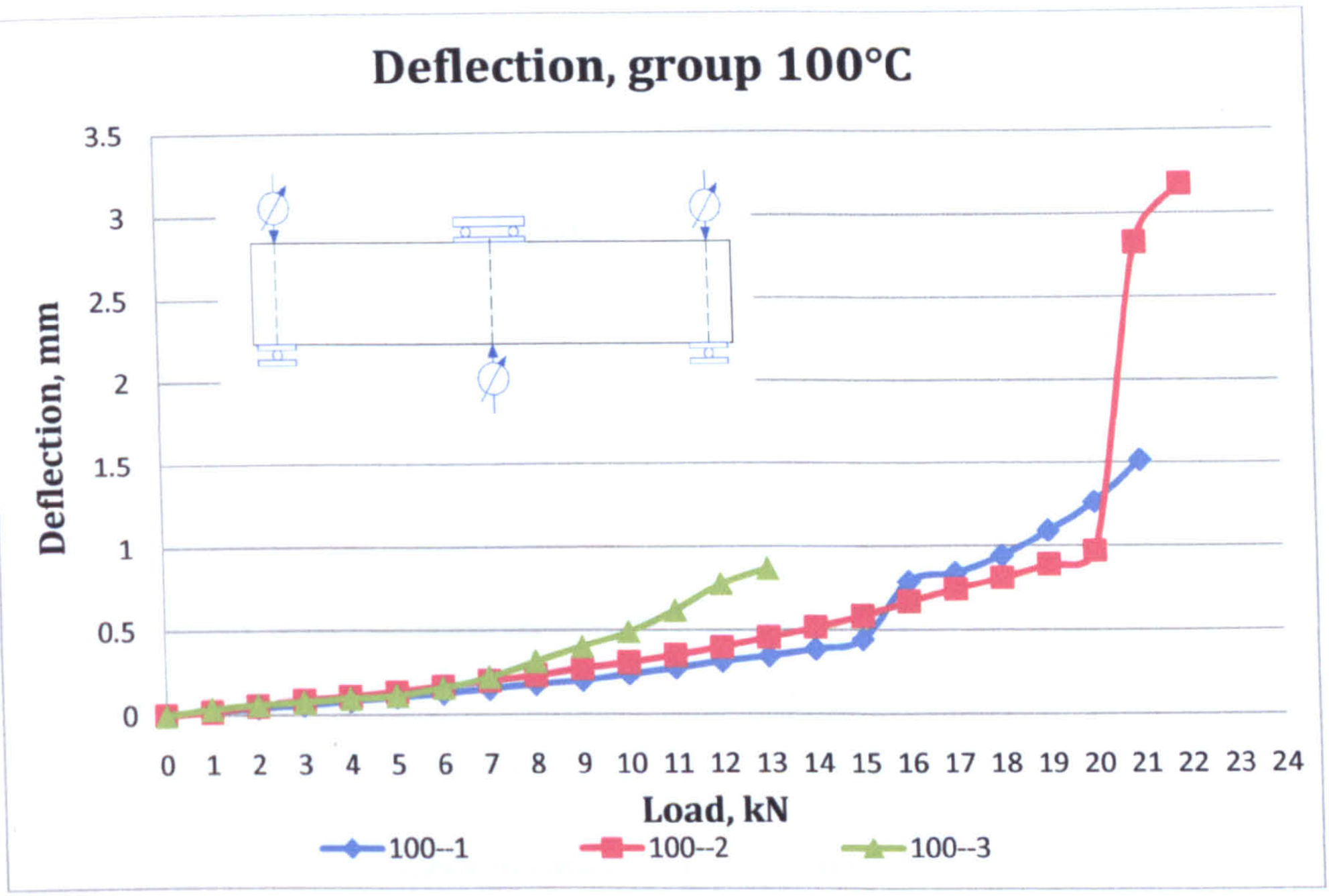

Figure V- 20 Deflection, group 100°C

The deflection of group 100°C was presented for loads from 0kN to 23kN (Figure V-20) which was the maximum load from the testing of the three samples. Beam #100-1 deflected to 0.44mm at 15kN before the beam failed due to formation of a shear crack. The beam was subsequently reloaded and 1.263mm was measured as the maximum deflection. Beam #100-2 reached 0.972mm deflection at 20kN prior to failure. The following reloading of the beam led to a significant increase of the deflection was measured to 3.171mm. The last sample of the group failed at a lower load compared to the other samples of the group at 13kN with gradual increase of the deflection to 0.864mm prior to failure.

5.4.3 Strain of laminate

The strain measured by ER strain gauge 2 of beam #100-1 was gradually increasing to 15kN reaching the value of 1362 microstrain before failure occurred at the left side of the sample (Figure V-21). Relative increase of the deformation was registered by ER gauge 1

at 9kN compared to the strain measured at the right end of the laminate and a maximum value of the strain was achieved at 15kN equal to 358microstrain. The further increase of the load caused the strain at midspan to continue to grow and the maximum value registered reached 1933microstrain. The strain of ER gauge 3 indicated gradual increase of the deformation to maximum 323microstrain.

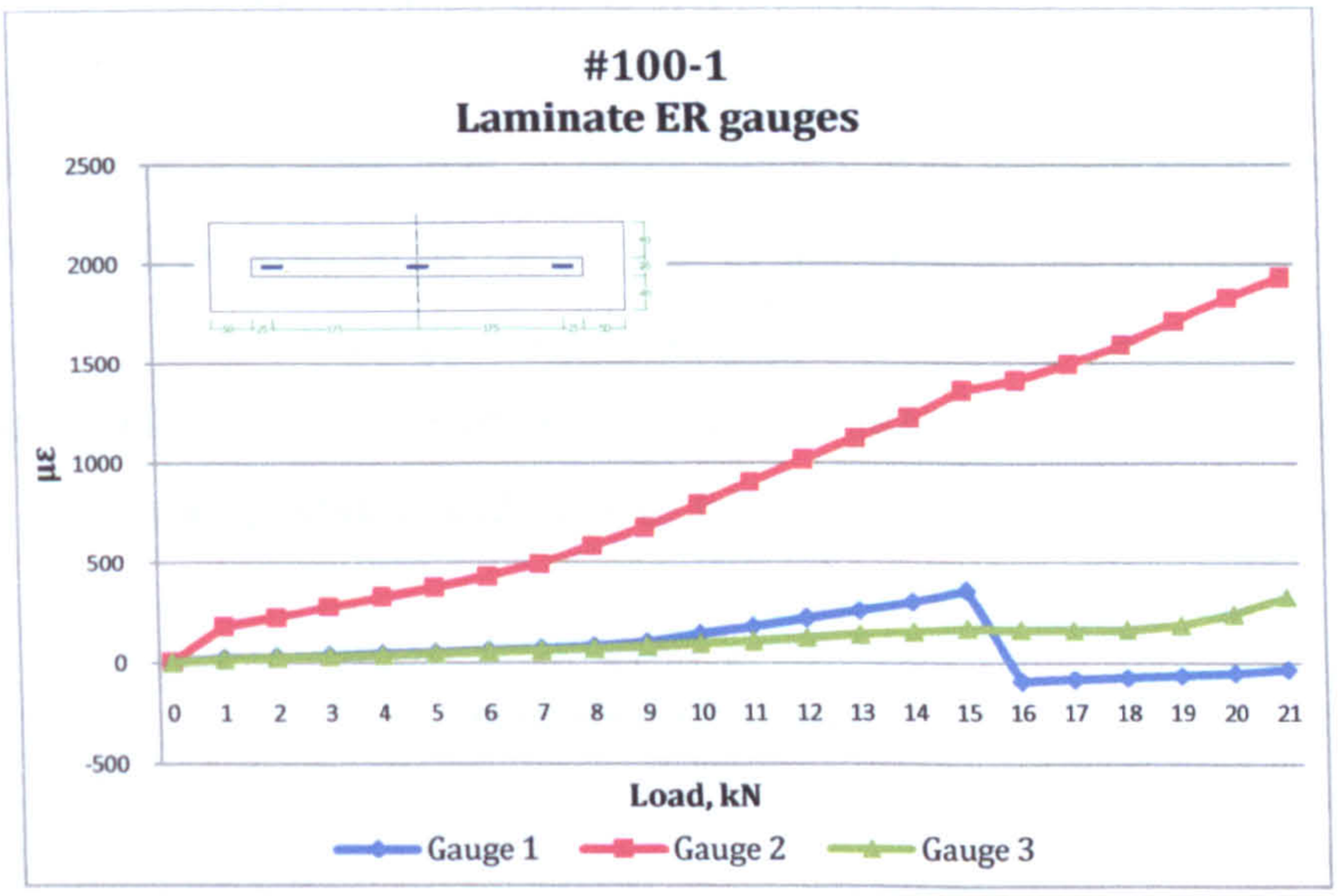

Figure V- 21 Laminate ER gauges, sample #100-1

Flexural cracks were observed on beam #100-2 at 15kN when the strain of the laminate at midspan reached a value of 1553.5 microstrain, see Figure V-22.

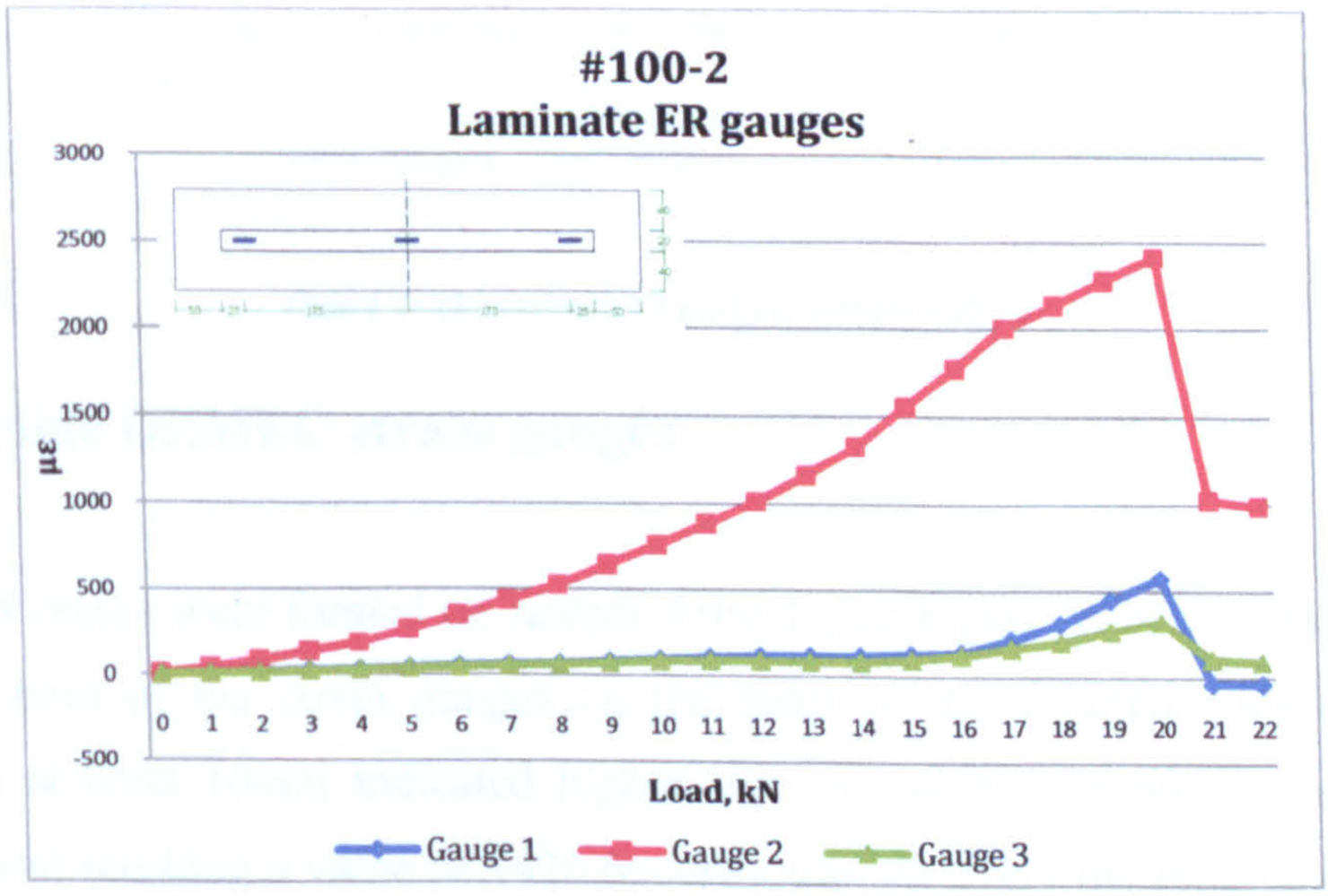

Figure V- 22 Laminate ER gauges, sample #100-2

The further increase of the load resulted in a steeper growth of the strain and the deformation reached a value of 2411microstrain at 20kN before the beam failed. The left and right strain gauges both registered increase of the deformations above 16kN. ER gauge 1 reached 570 microstrain prior to delamination at 21kN whilst ER gauge 3 registered lower deformation of 320.5 microstrain.

Beam #100-3 registered significantly higher rate of deformation with increase of the load above 6kN at midspan, (Figure V-23). The strain at 6kN was 283microstrain whilst at 13kN the deformation was more than 10 times higher- 2454 microstrain mainly due to the flexural crack which occurred at an early stage of the loading and continued to propagate with increase of the load. ER gauge 3 registered higher deformations at the right end of the laminate which reached a value of 445microstrain at 13kN. The strain at the left end of the laminate was increasing gradually and prior to failure the value was 133microstrain.

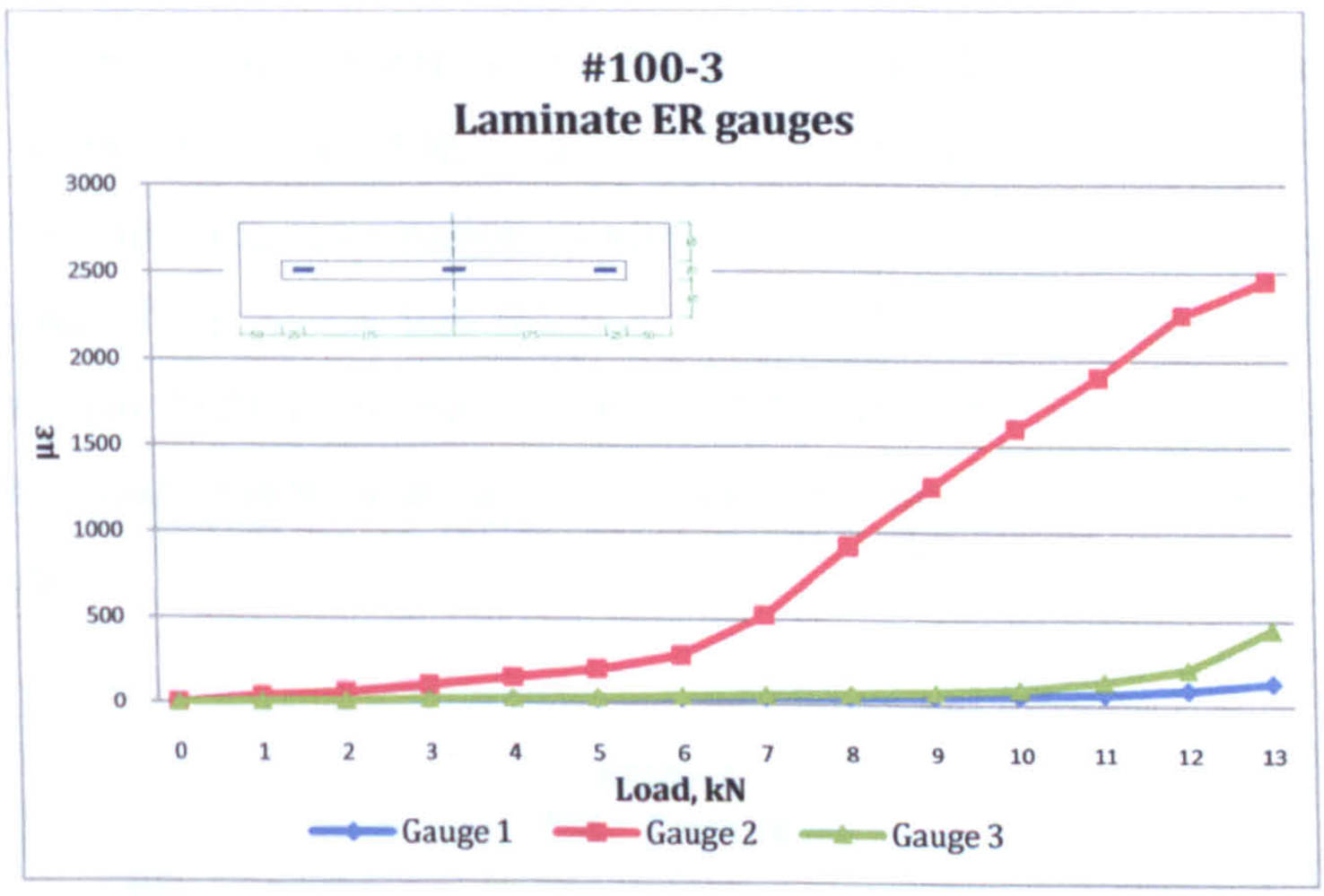

Figure V- 23 Laminate ER gauges, sample #100-3

5.4.4 Side DEMEC strain gauges

First flexural cracks were formed on sample #100-1 (see Figure V-24) at 16kN inside and outside the base of the strain gauges on the sides of the concrete. Above 16kN the deformation at level 10mm indicated higher increase of the compressive strains up to maximum load reaching a value of 1420.6microstrain. At 21kN the relative displacement at level 90mm was 2155.5microstrain. The deformation at level 30mm remained negative during the experiment although a slight decrease of the deformations was observed as the maximum load was reached.

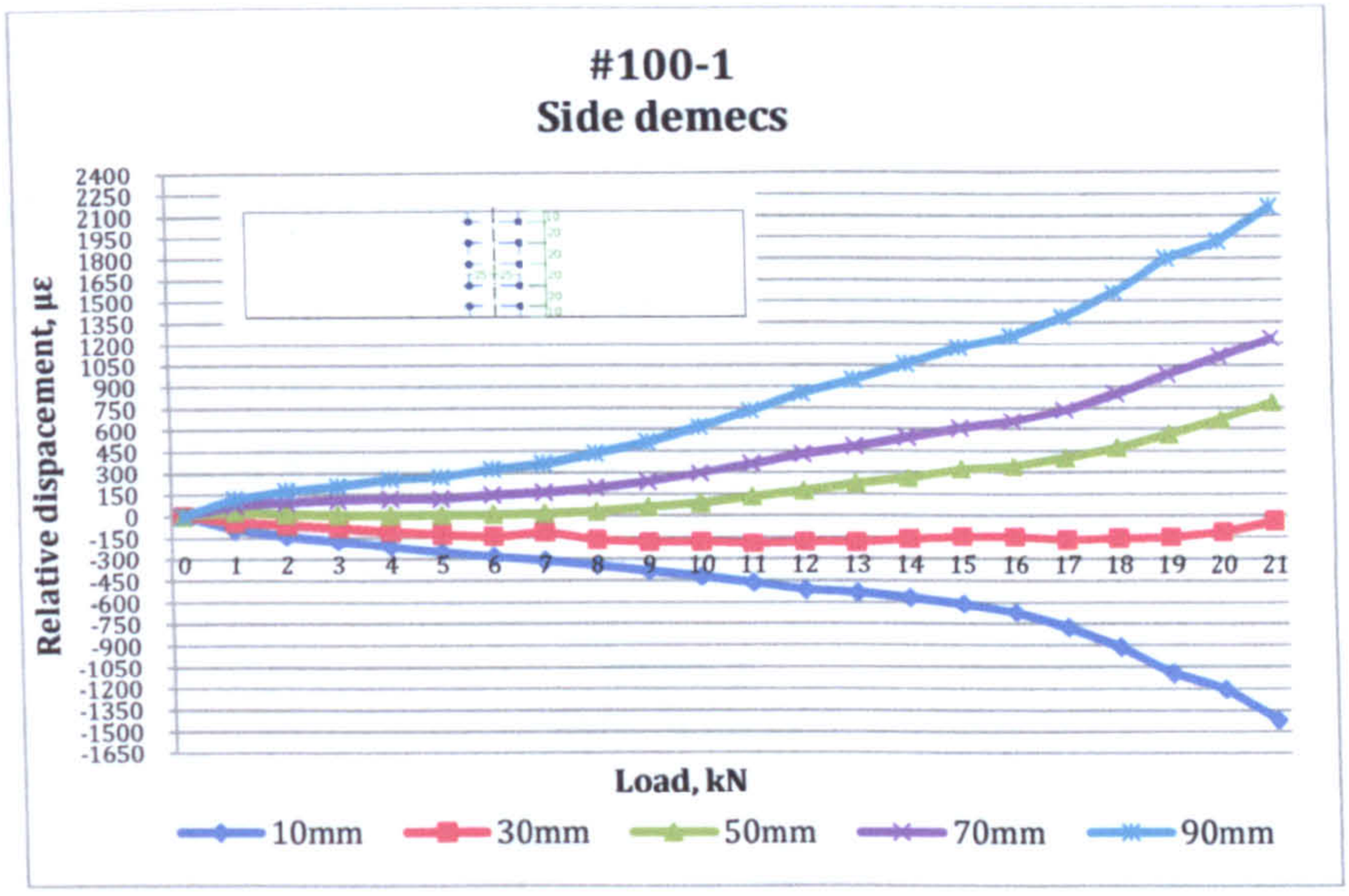

Figure V- 24 Local deformations, Side DEMEC strain gauges #100-1

Sample #100-2 developed flexural cracks outside the base length of the strain gauges at 15kN and at further increase of the load to 17kN a crack was formed within the base length. At level 10mm the deformations reached maximum value of 687microstrain before the ultimate load of the system was reached. At level 90mm the relative displacement at maximum load was 2720 microstrain. Change of the strain for level 30mm was observed between 13kN and 14kN and at 21kN the maximum relative deformation was 373microstrain.

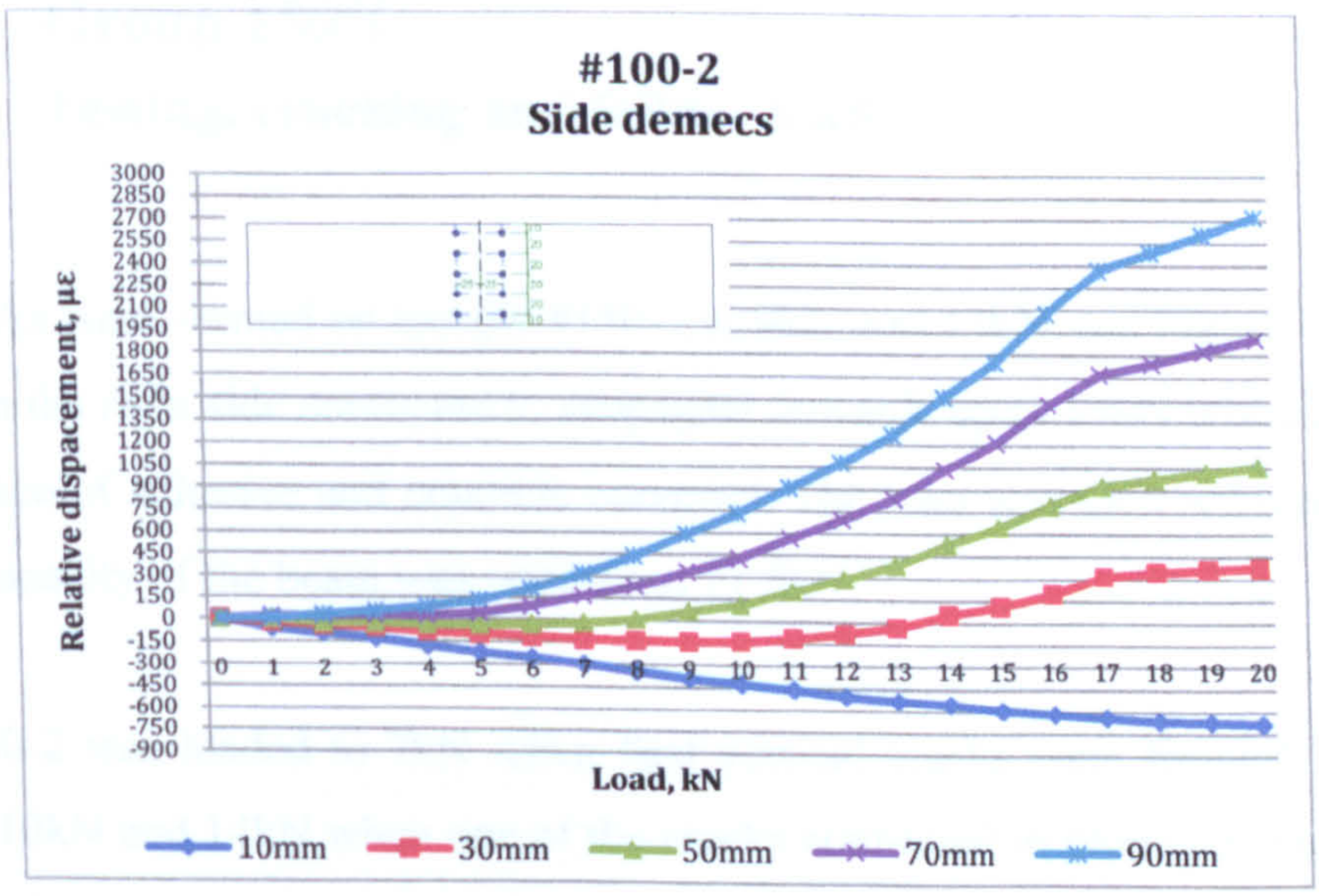

Figure V- 25 Local deformations, Side DEMEC strain gauges #100-2

Sample #100-3 was loaded to 8kN when a flexural crack was formed within the strain gauge base length at level 90mm and at further increase of the load significant growth of the relative displacement was measured, see Figure V-26. The maximum deformation at failure load of 13kN reached a value of 3222 microstrain at level 90mm and at level 10mm the compressive relative displacement increased to a value of 373 microstrain. The strain at level 30mm changed from compressive to tensile between 9kN and 10kN reaching maximum deformation of 574microstrain at 13kN.

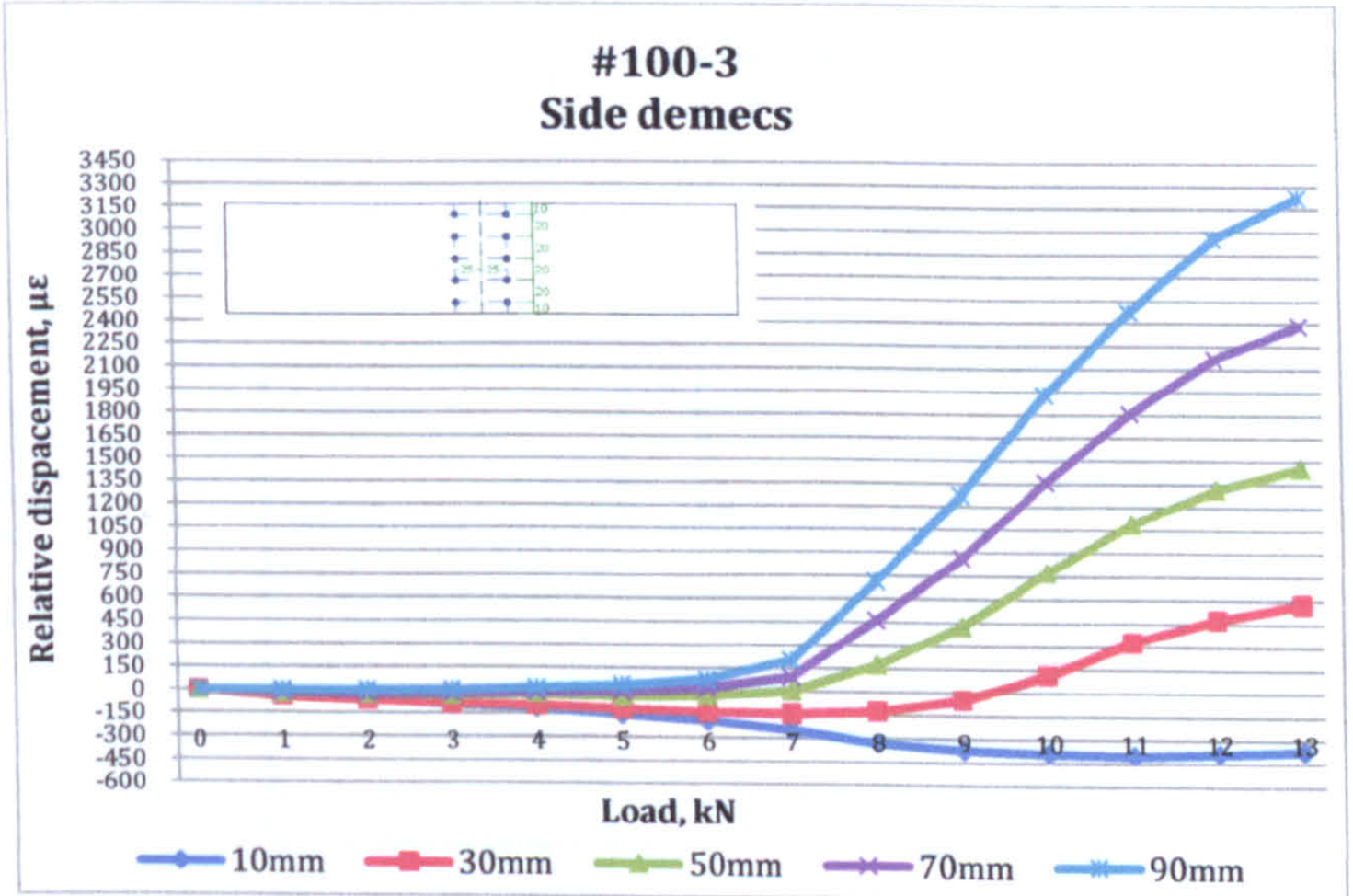

Figure V- 26 Local deformations, Side DEMEC strain gauges #100-3

5.5 Group 150°C

5.5.1 Testing, cracking and failure load

Vertical cracks were formed on sample #150-1 at 9kN and 13kN, see Figure V-27. One of the cracks on the right side continued to propagate upwards up to 15kN when delamination at the interface of adhesive and concrete occurred. The load was then reduced to 11.5kN. Maximum capacity of the beam was reached at 21.5kN.

Sample #150-2 was loaded to 7kN when first vertical cracks were formed. More cracks occurred at 10kN and 14kN when one of the cracks continued to propagate vertically up to 18kN. After the delamination the load dropped to 13.2kN and was further increased to the maximum load of 22.9kN.

Sample #150-3 failed at a lower load of 11kN. Vertical cracks were observed at 10kN and an increase by 1kN led to a formation of brittle flexural crack and the load was reduced to 0.8kN. The maximum capacity of the system was then reached at 2.2kN.

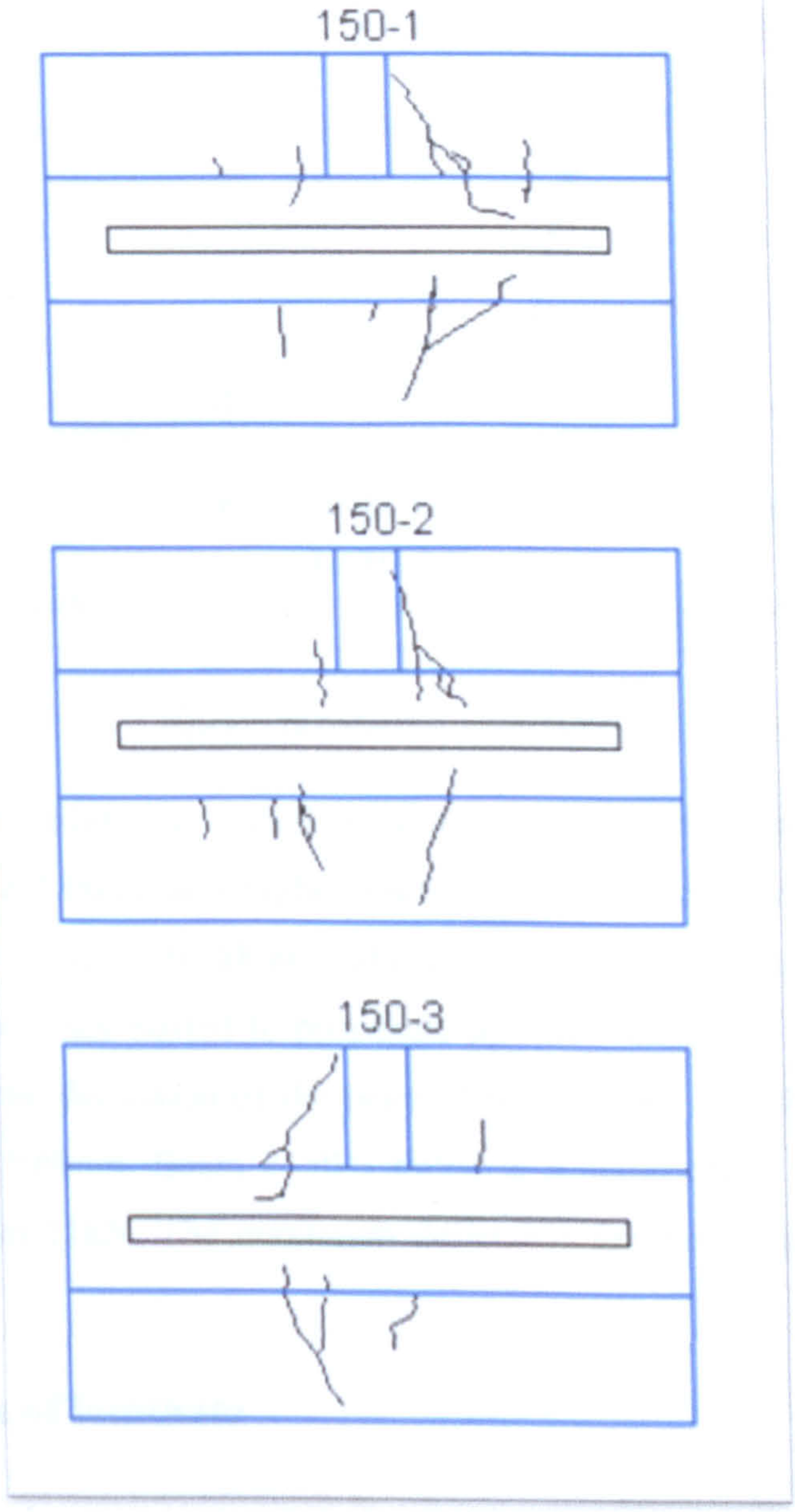

Figure V- 27 Crack formation and failure of beams, group 150°C

5.5.2 Deflection

The deflection of the three samples of group 150°C was plotted for loads from 0kN to 22kN which was the highest maximum load of the group, see Figure V-28. The deflection of beam #150-1 was increasing gradually up to 14kN when due to a flexural-shear crack a "jump" of the deflection was observed.

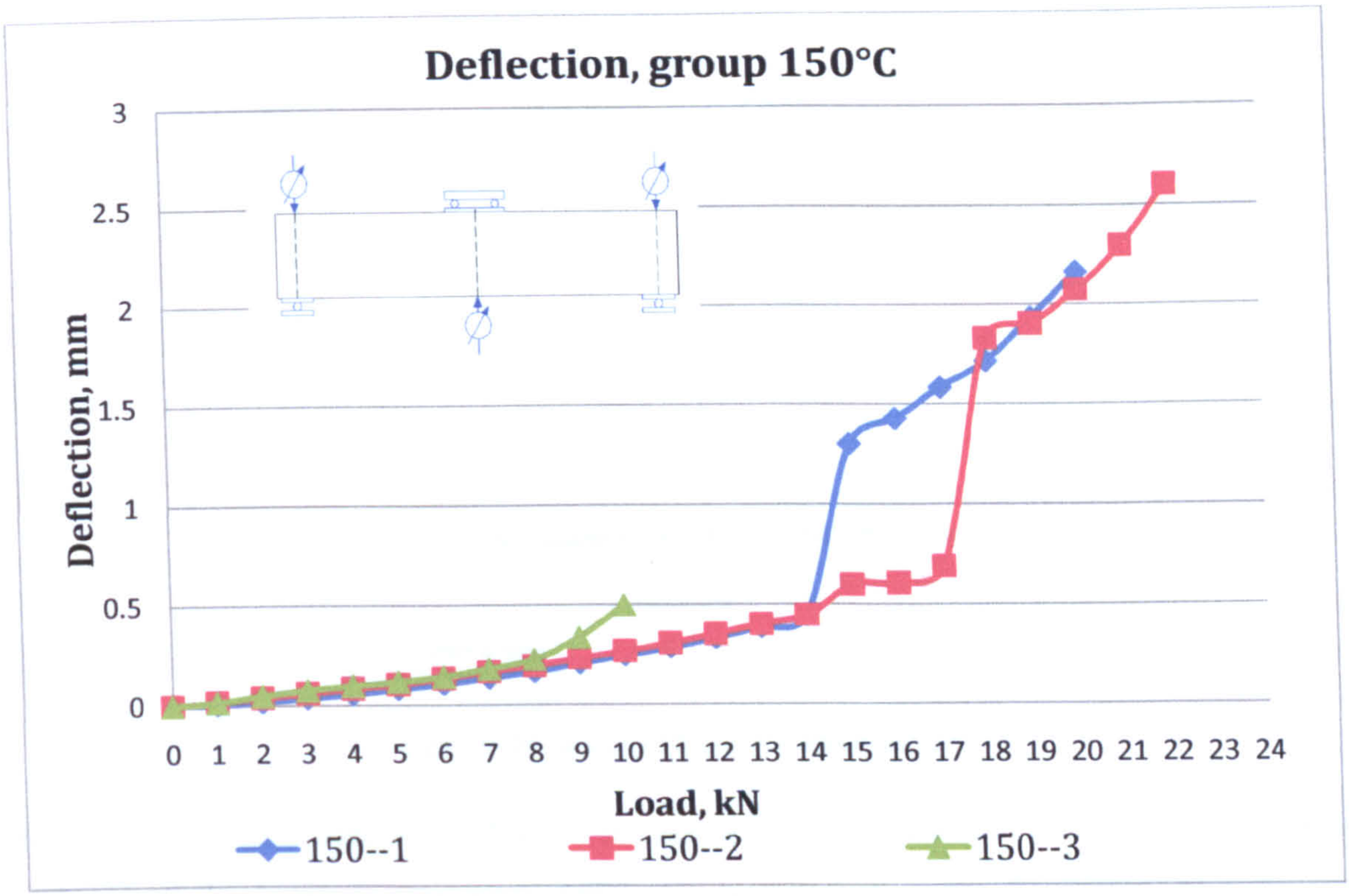

Figure V- 28 Deflection, group 150°C

The deflection prior to failure load was 0.443mm and at maximum load of 20kN it reached 2.164mm. Beam #150-2 failed at a higher load of 17kN due to a flexural crack when the deflection reached a value of 0.688mm. The deflection was increasing gradually up to 14kN when a flexural crack started to propagate upwards leading to failure at 17 kN and subsequent jump of the deflection of the beam. Ultimate load was then reached at 22kN with deflection of 2.599mm. Beam #150-3 failed at a significantly lower load due to a flexural-shear crack at 11kN. The maximum deflection for the sample prior to failure at 10kN was 0.497mm.

5.5.3 Strain of laminate

Strain gauge 2 of beam #150-1 registered gradual increase of the deformation at midspan of the beam up to 14kN when the reading reached 1374 microstrain (Figure V-29). Further increase of the load led to delamination and no increase of the strain was observed. The strain gauge at the right side of the beam registered gradual increase of the deformations up to 14kN when a value of 46.5 microstrain was reached. The strain measured at the left side of the laminate was lower- 22 microstrain at 14kn, due to the cracking of the adhesive after the heating and cooling of the samples.

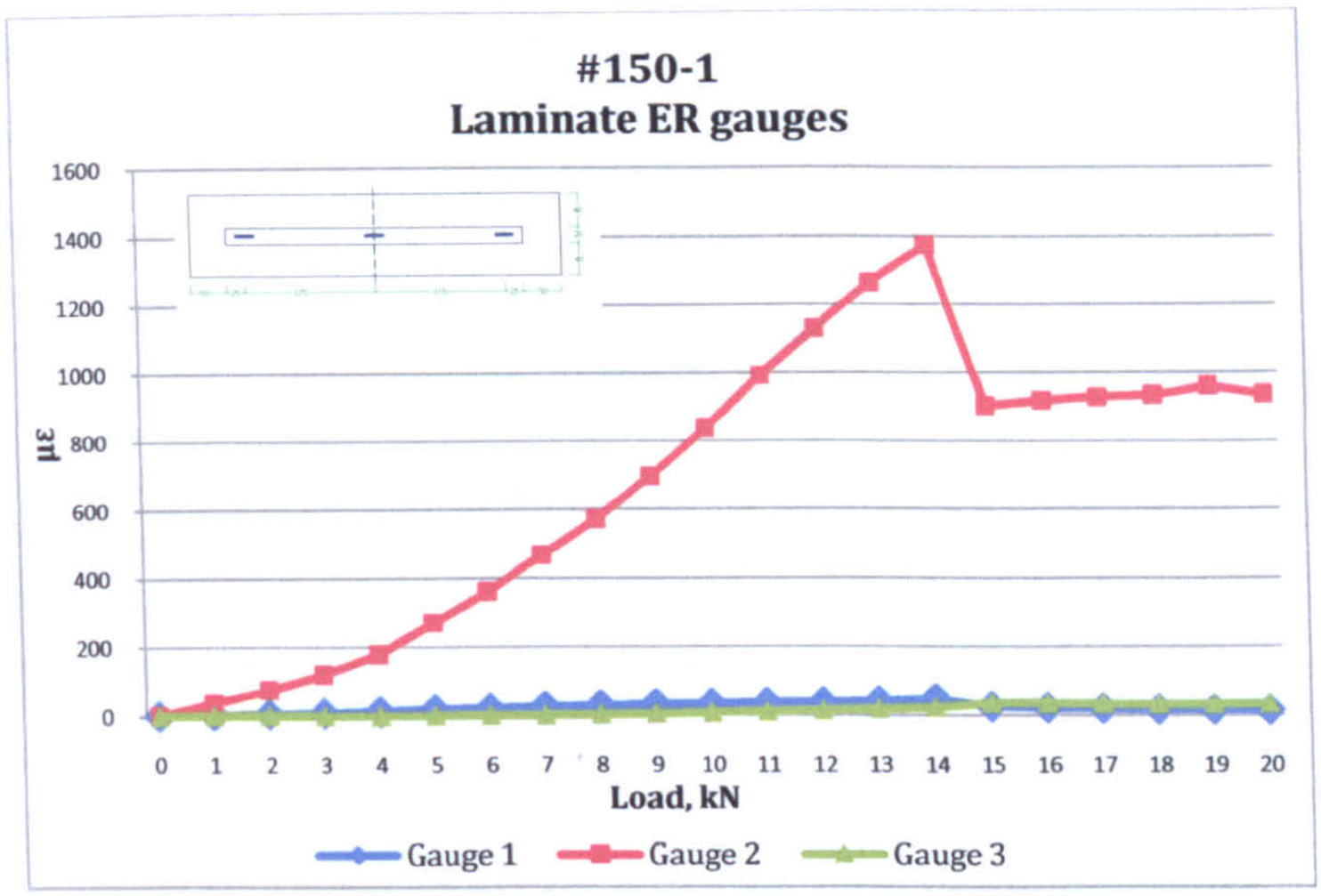

Figure V- 29 Laminate ER gauges, sample #150-1

Beam #150-2 was loaded to 17kN prior to failure load was reached. The strain measured at midspan of the beam increased to 1499 microstrain before the formation of a flexural crack. The strain measured at the right side of the laminate gradually increase up to 14kN and with further increase the rate of growth was higher resulting in 503 microstrain prior to failure. The strain at the left side increased to 2kN before the failure load was reached with a maximum strain of 111.5 microstrain.

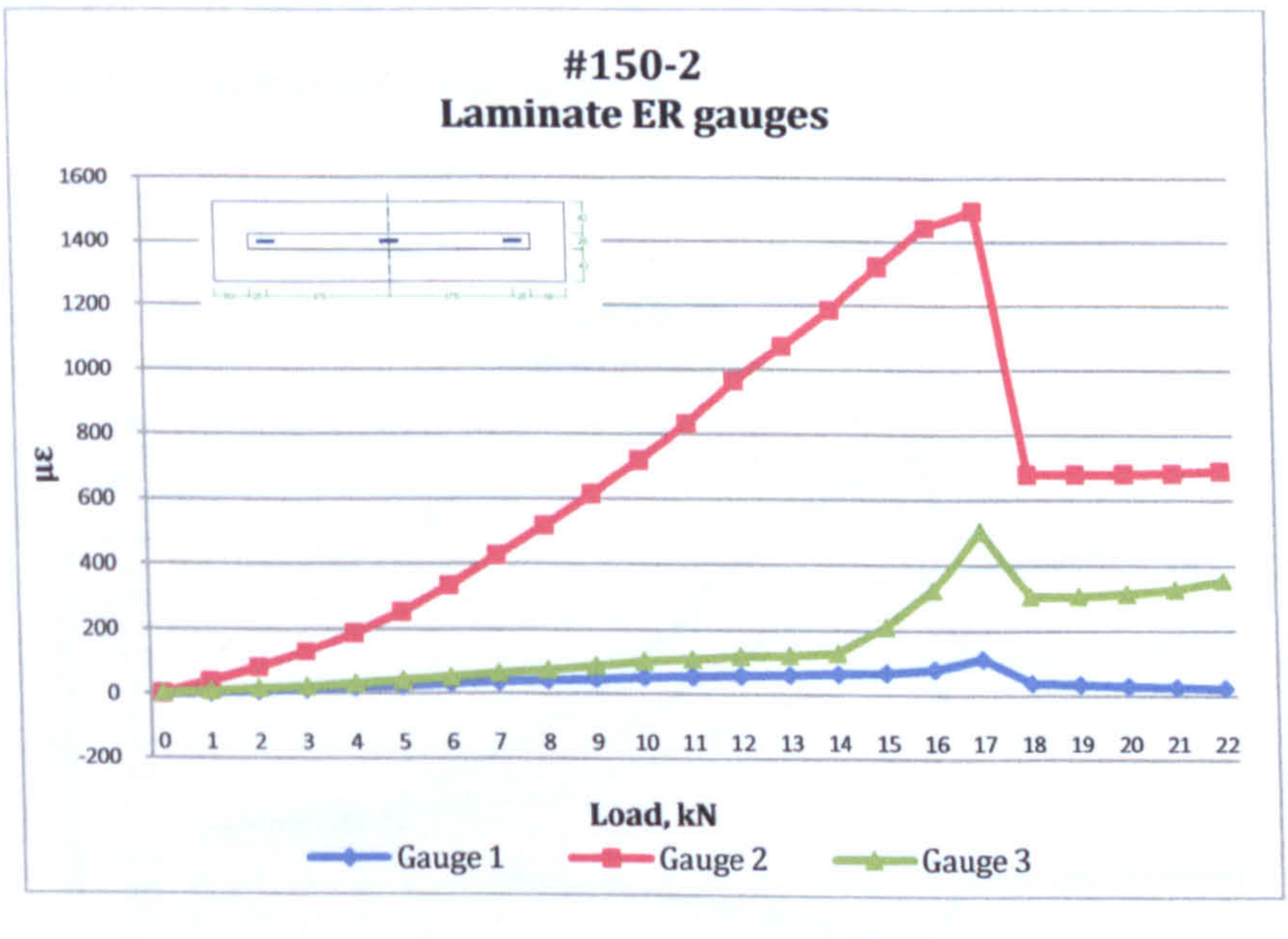

Figure V- 30 Laminate ER gauges, sample #150-2

Change of the deformation at the midspan of beam #150-3 was observed at 7kN and the maximum of the strain was measured prior to failure of the beam. At 10kN the deformation reached 1614 microstrain before a flexural- shear crack was formed. The strain measured

at the left and right end of the laminate reached values of 50 and 67 microstrain respectively at 10kN.

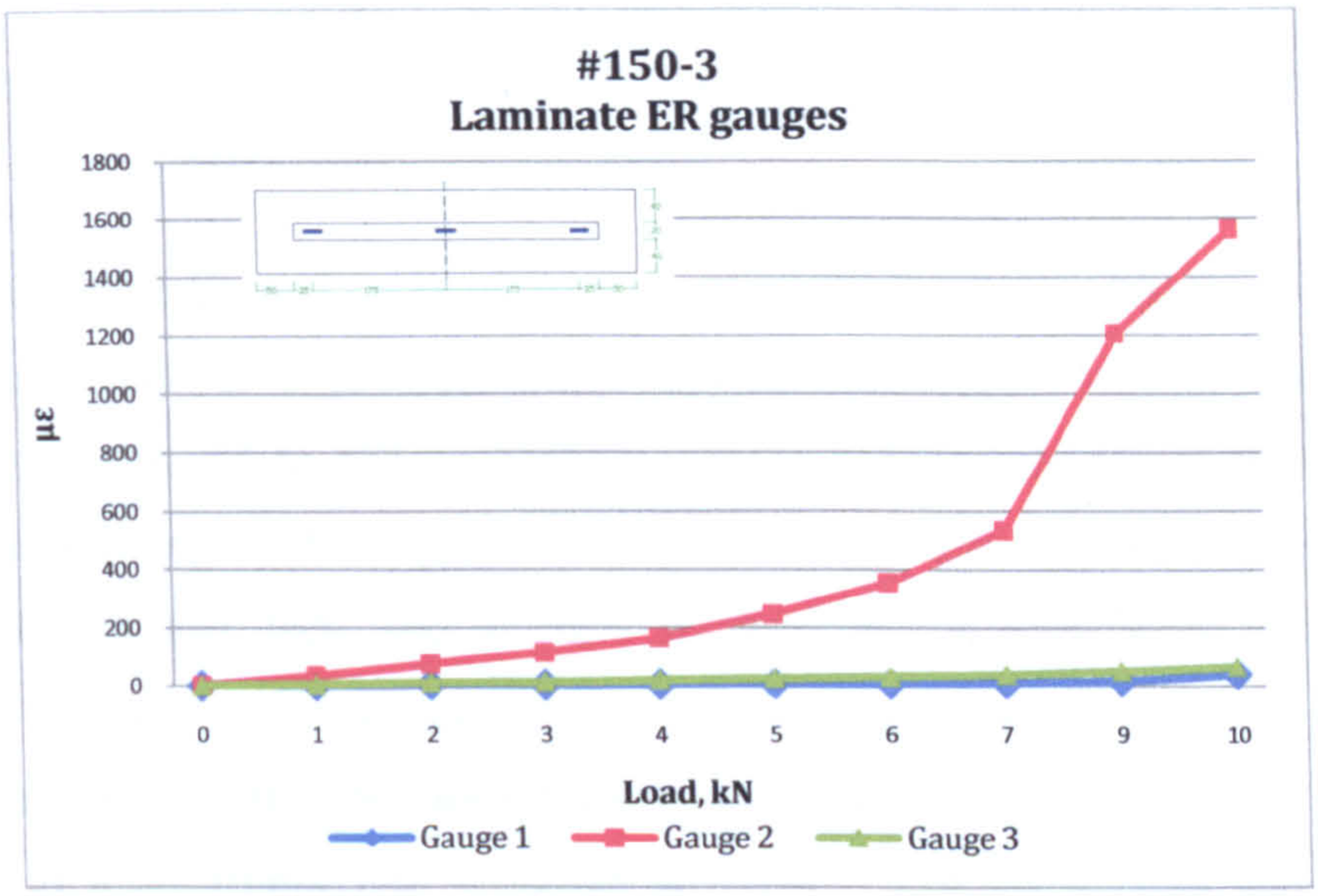

Figure V- 31 Laminate ER gauges, sample #150-3

5.5.4 Side DEMEC strain gauges

First cracks appeared on sample #150-1 at 9kN outside the base of the strain gauge and a slight increase of the deformations was observed from level 90mm to 50mm, see Figure V-32.

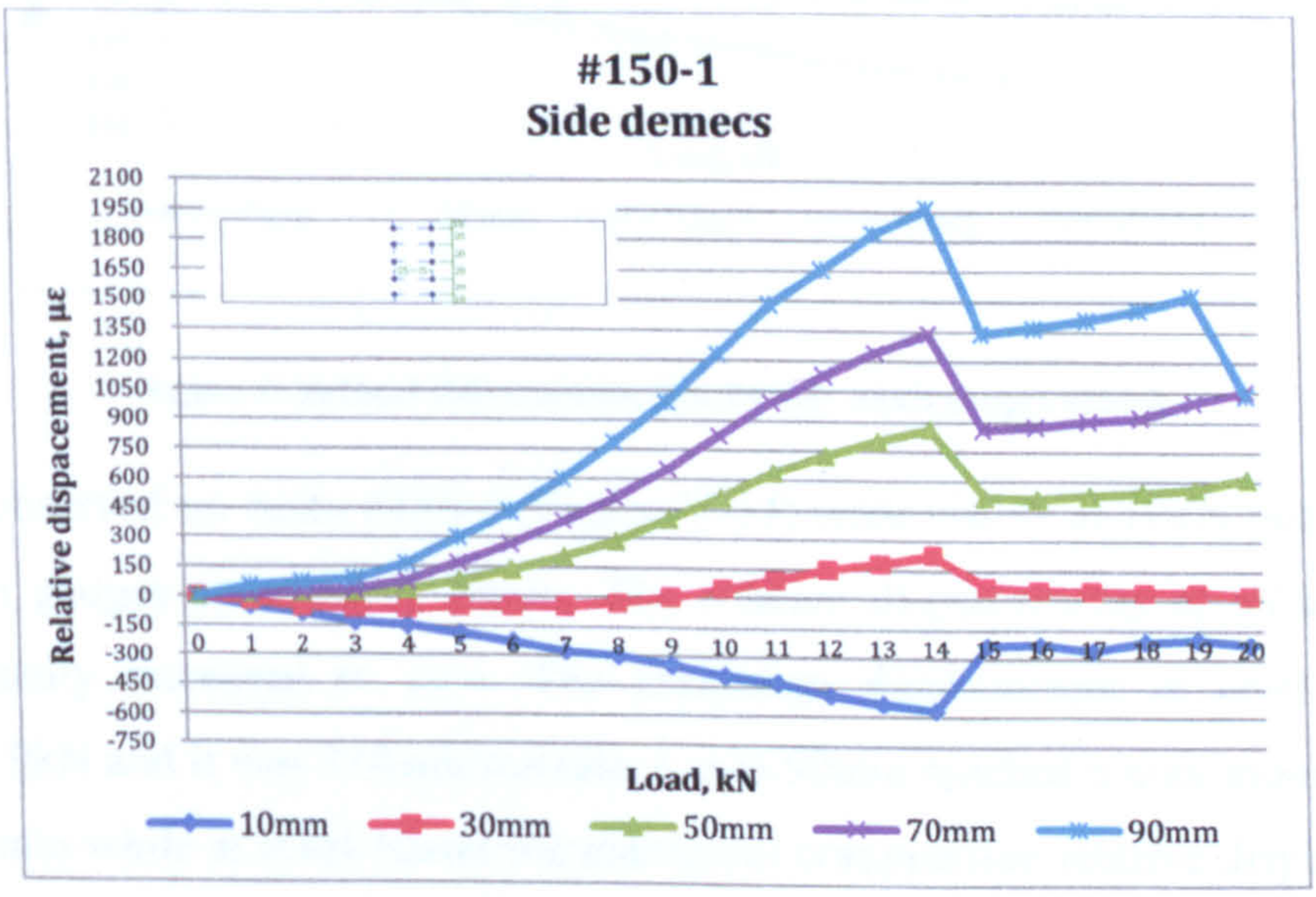

Figure V- 32 Local deformations, Side DEMEC strain gauges #150-1

Prior to loading to failure the relative displacement at level 90mm reached a value of 1963 microstrain. At level 10mm compressive deformations were registered up to failure and at 14kN the relative displacement was 567 microstrain. The deformation at level 30mm changed from tensile to compressive at 9kN and increased to 226 microstrain prior to formation of flexural-shear crack.

Flexural cracks were formed on beam #150-2 when the beam was loaded to 7kN and the relative displacements at level 90 to 70mm reached their highest values. The deformation at level 90mm increased to 182 microstrain and no further increase of the displacement was registered. Changes of the relative displacements were observed for levels 50 and 30mm between 8 and 9kN and at 9kN respectively. A significant increase of the deformation was registered at level 30mm due to the propagation of a crack which progressed under the attached demec point up to 18kN. The maximum compressive deformation at level 10mm was achieved at 17kN – 419 microstrain above which the flexural crack propagated upwards and the measured deformations were tensile.

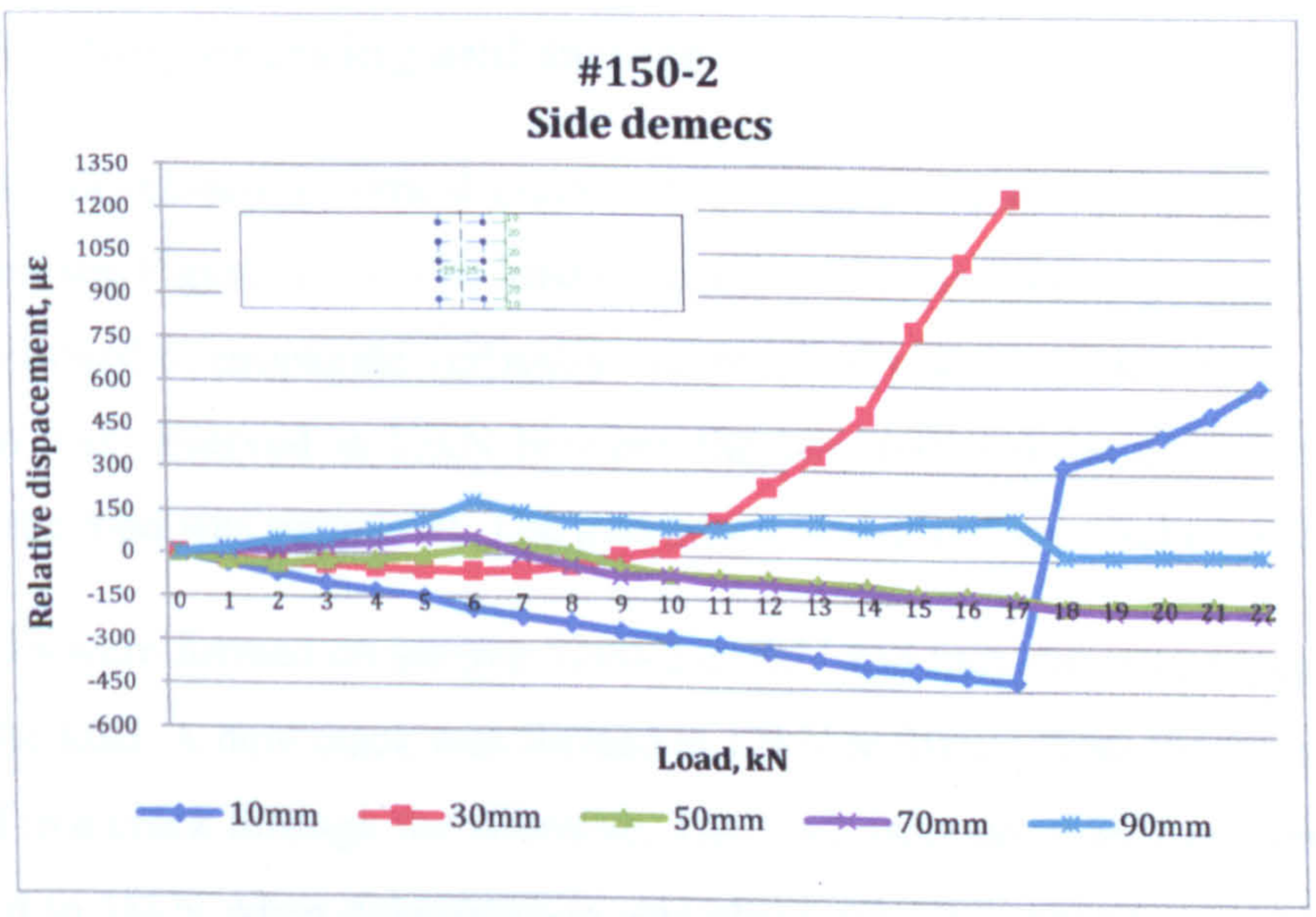

Figure V- 33 Local deformations, Side DEMEC strain gauges #150-2

The cracks observed on beam #150-3 (Figure V-34) were visible at 10kN outside the base of the strain gauges up to level 50mm. The relative displacements at all levels except 90mm gradually increased to 7kN. The maximum displacement at level 90mm was measured at 9kN and it was 318 microstrain. Level 50mm reached a maximum at 7kN with 206 microstrain while at level 10mm the maximum compressive relative displacement was reached at 10kN and it was 336 microstrain.

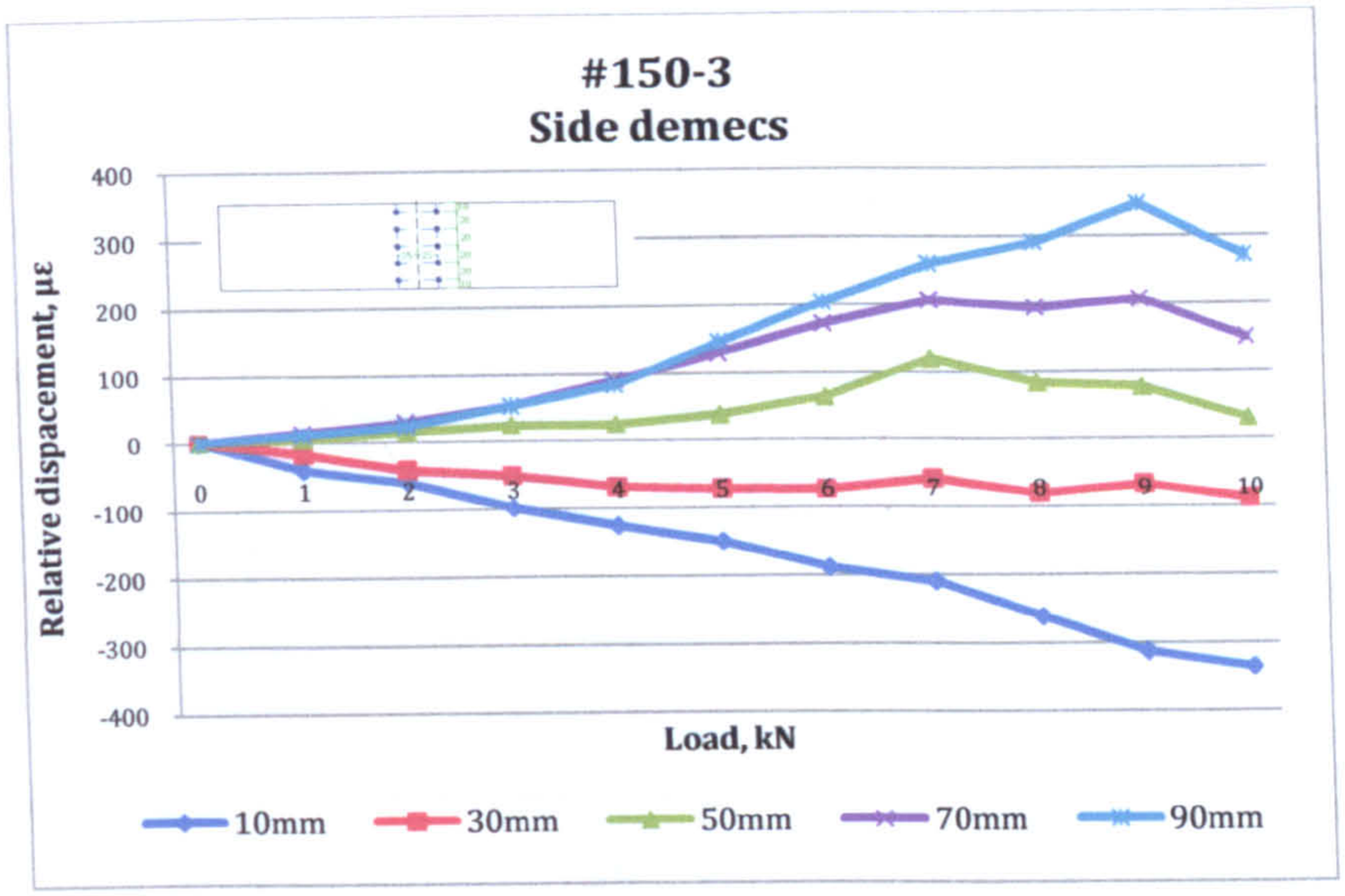

Figure V- 34 Local deformations, Side DEMEC strain gauges #150-3

5.6 Group 200°C

5.6.1 Testing, cracking and failure load

Sample #200-1 developed a vertical crack at 9kN which had also propagated through the adhesive layer, see Figure V-35. The load dropped to 7kN and was then increased. At 9kN the crack continued to propagate vertically and resulted also in the widening of the crack. Delamination was observed at 17kN between the laminate and the adhesive although no reduction of the load was registered. The maximum load was then reached at 22.6kN.

Vertical cracks were formed on sample #200-2 at 9kN and they did not propagate at further increase of the load. A new crack was formed at 12kN to 30mm from the top surface which also resulted in a crack through the adhesive. The load dropped to 8kN and the sample was then reloaded to 18kN when delamination was observed. The separation occurred between the adhesive and the laminate which did not lead to reduction of the load. The system was then further loaded to 21.3kN above which the beam could not sustain more loading.

The last sample of the group formed few vertical cracks at 10kN one of which developed to the level of DEMEC 30mm at 11kN. The development of the crack led to delamination between the adhesive and the concrete mostly due to an existing crack due to the heating of the system. The load dropped to 9kN and was then further increased until the maximum load of 23.1kN was reached.

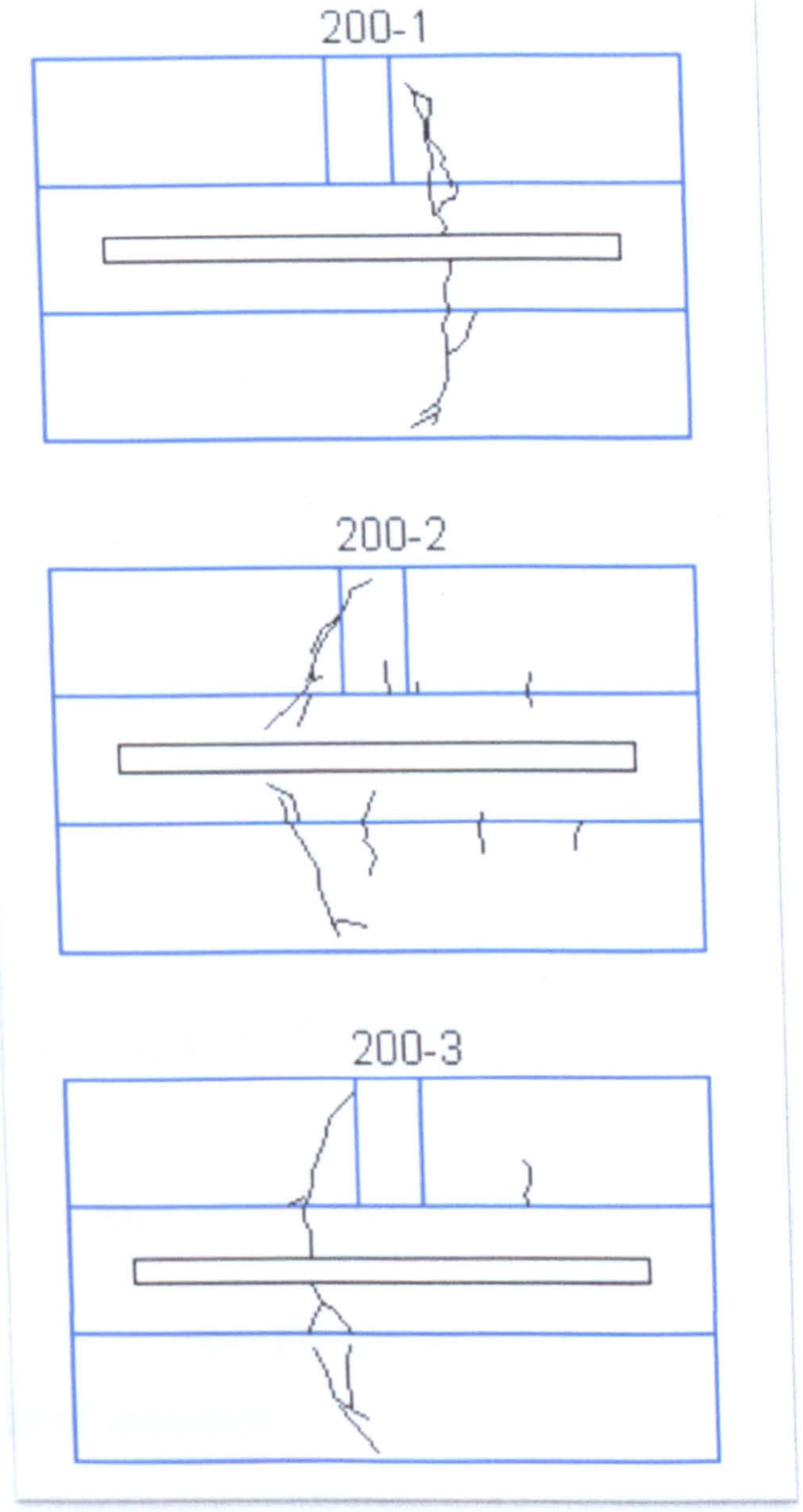

Figure V-35 Crack formation and failure of beams, group 200°C

5.6.2 Deflection

The deflection of the samples of group 200°C was plotted for loads from 0kN to 22kN which was the highest maximum load for the group (Figure V-36). The deflection of beam #200-1 increased gradually up to 8kN before a flexural crack developed at the right side of the beam. The deflection reached a value of 0.238mm before a "jump" of the curve occurred with further increase of the load. Maximum load was applied at 22kN and the deflection reached 3.349 mm. Beam #200-2 was loaded to 12kN when a flexural crack was formed, prior to failure 0.4mm deflection was measured. The ultimate capacity of the

system was then achieved at 18kN when the deformation reached 2.415mm. The last sample of group 200°C failed at 11kN with gradual increase of the deflection to 0.327mm prior to the formation of a flexural crack. The ultimate load was then achieved at 22kN when the deflection reached a value of 2.743mm.

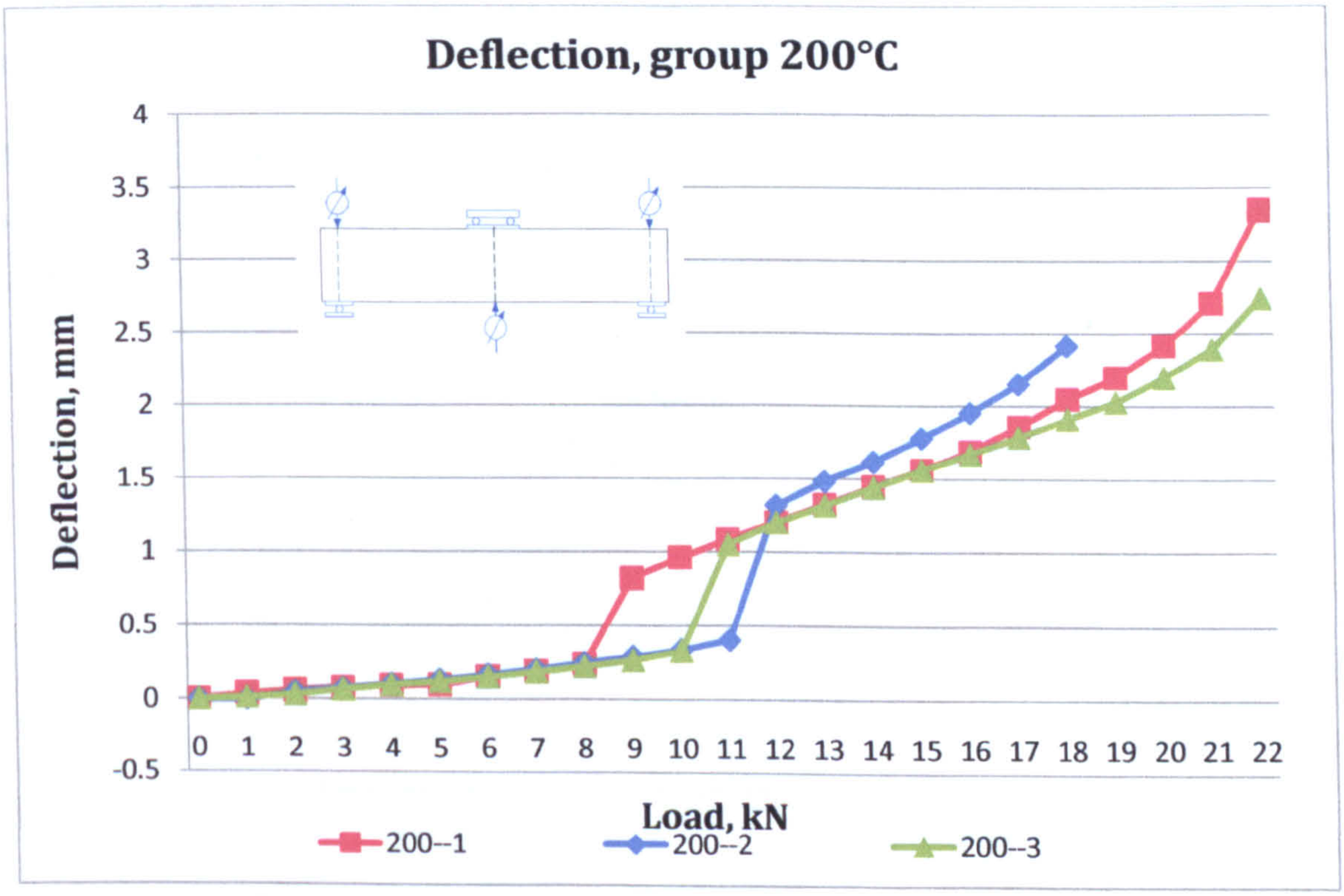

Figure V-36 Deflection, group 200°C

5.6.3 Strain of laminate

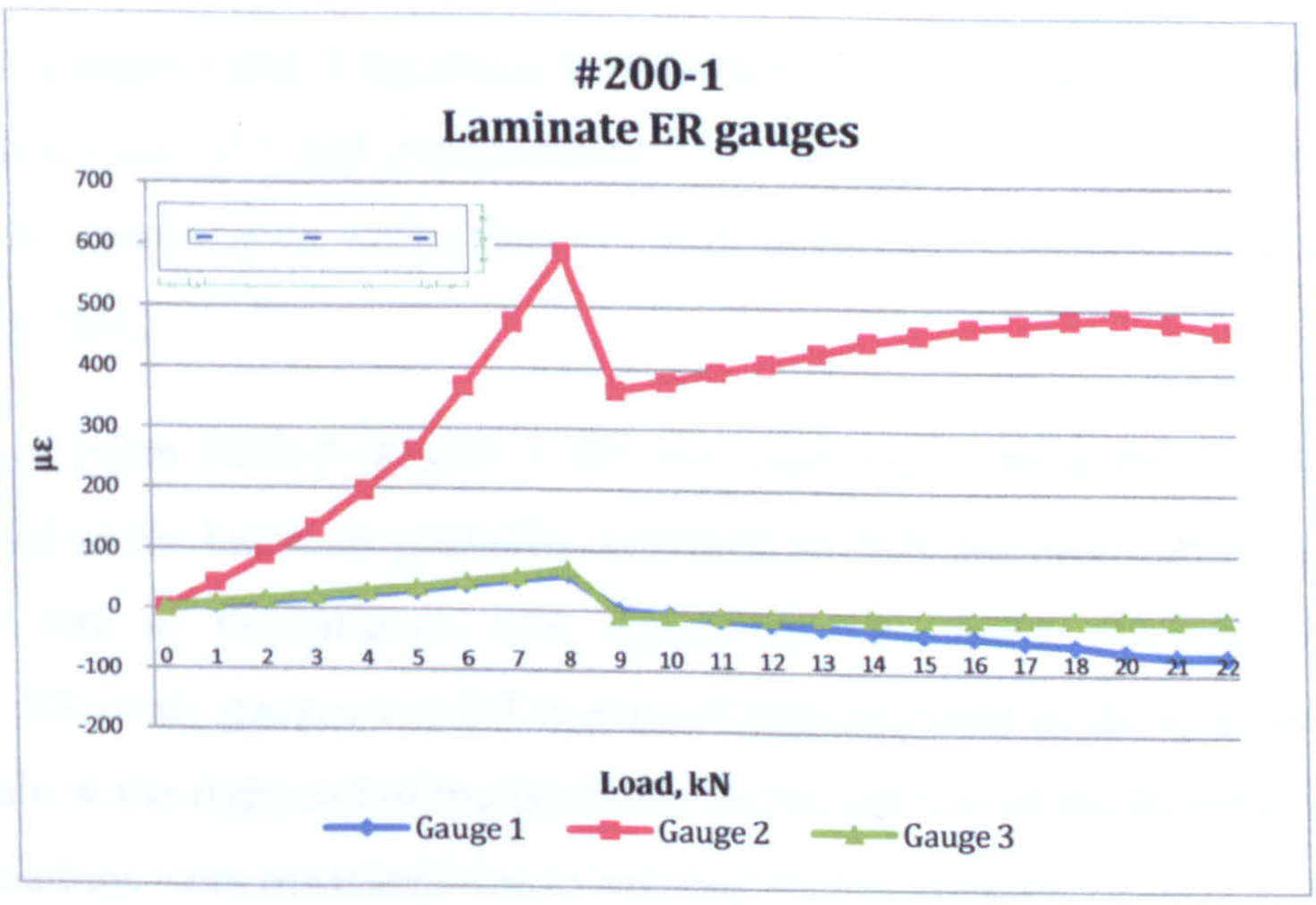

Figure V- 37 Laminate ER gauges, sample #200-1

The strain measured at midspan of beam #200-1, see Figure V-37, increased gradually up to 5kN when higher rate of growth of the strain was measured reaching 588 microstrain prior to the cracking of the beam at 9kN. The strain dropped and a slight increase was registered up to 20kN which was attributed to residual local deformation above the failure load of the system. Both the left and right ER strain gauges registered increase of the deformation up to 8kN when 60 microstrain and 70 microstrain were measured respectively by ER strain gauge 1 and ER strain gauge 3.

Beam #200-2 exhibited similar behaviour to sample #200-1. The deformation measured prior to the formation of a flexural crack at 12kN at midspan was 952 microstrain followed by drop of the strain.

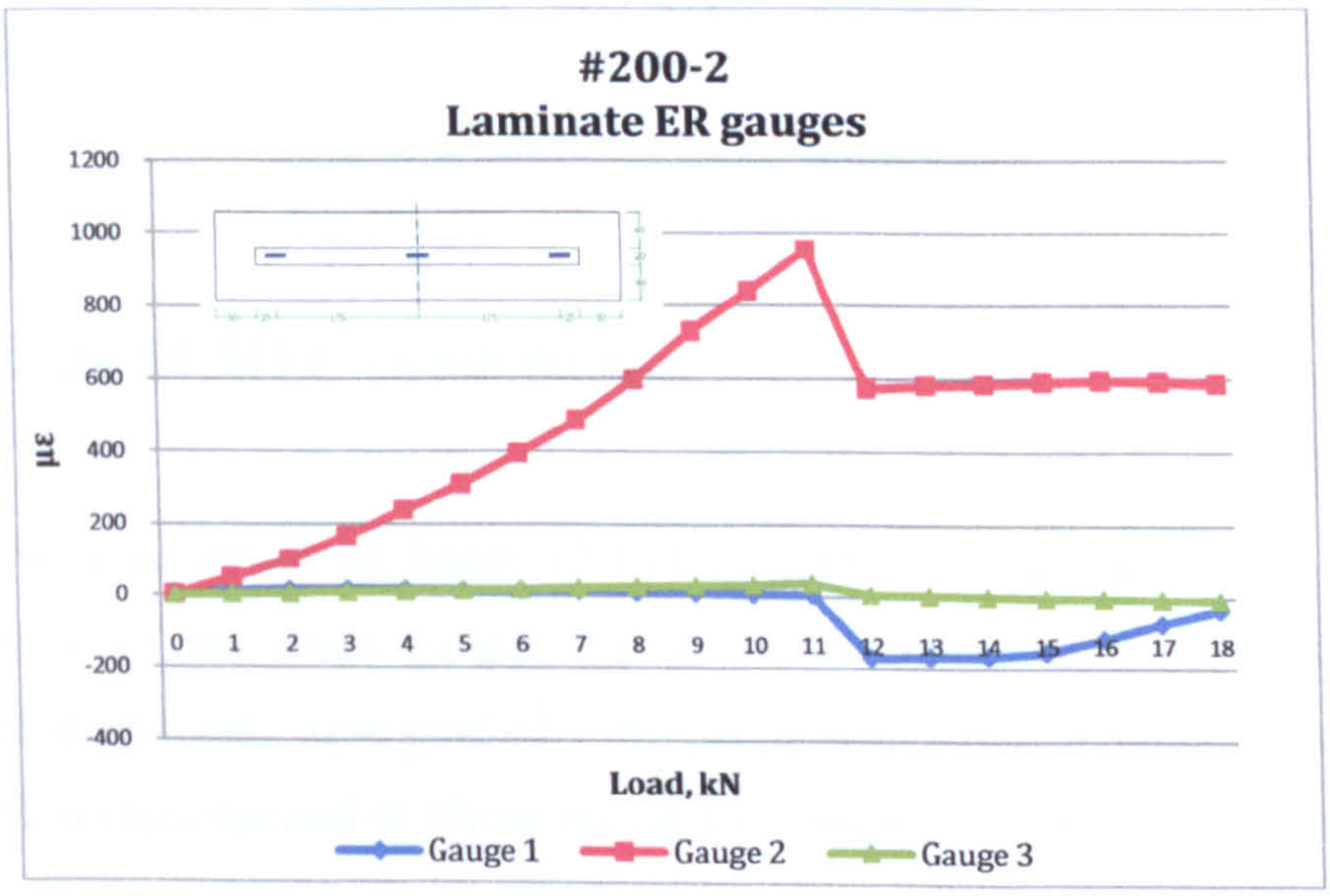

Figure V- 38 Laminate ER gauges, sample #200-2

The ER strain gauges 1 and 3 registered little increase of the deformation at the ends of the laminate with a value of 7 and 37microstrain respectively at 11kN. ER strain gauge 1 then registered only compressive strains due to the delamination which occurred with increase of the load by 1kN.

At midspan of beam #200-3 (Figure V-39) the local deformation measured by the strain gauge attached to the laminate gradually increased to 5kN and with further increase of the load higher rate of deformation was registered. The strain reached 1137 at 10kN microstrain. ER strain gauges 1 and 3 registered little increase of the local deformations to 24 microstrain at the right end of the laminate. At the left end of the laminate no significant local deformations were measured due to existing thermal cracks.

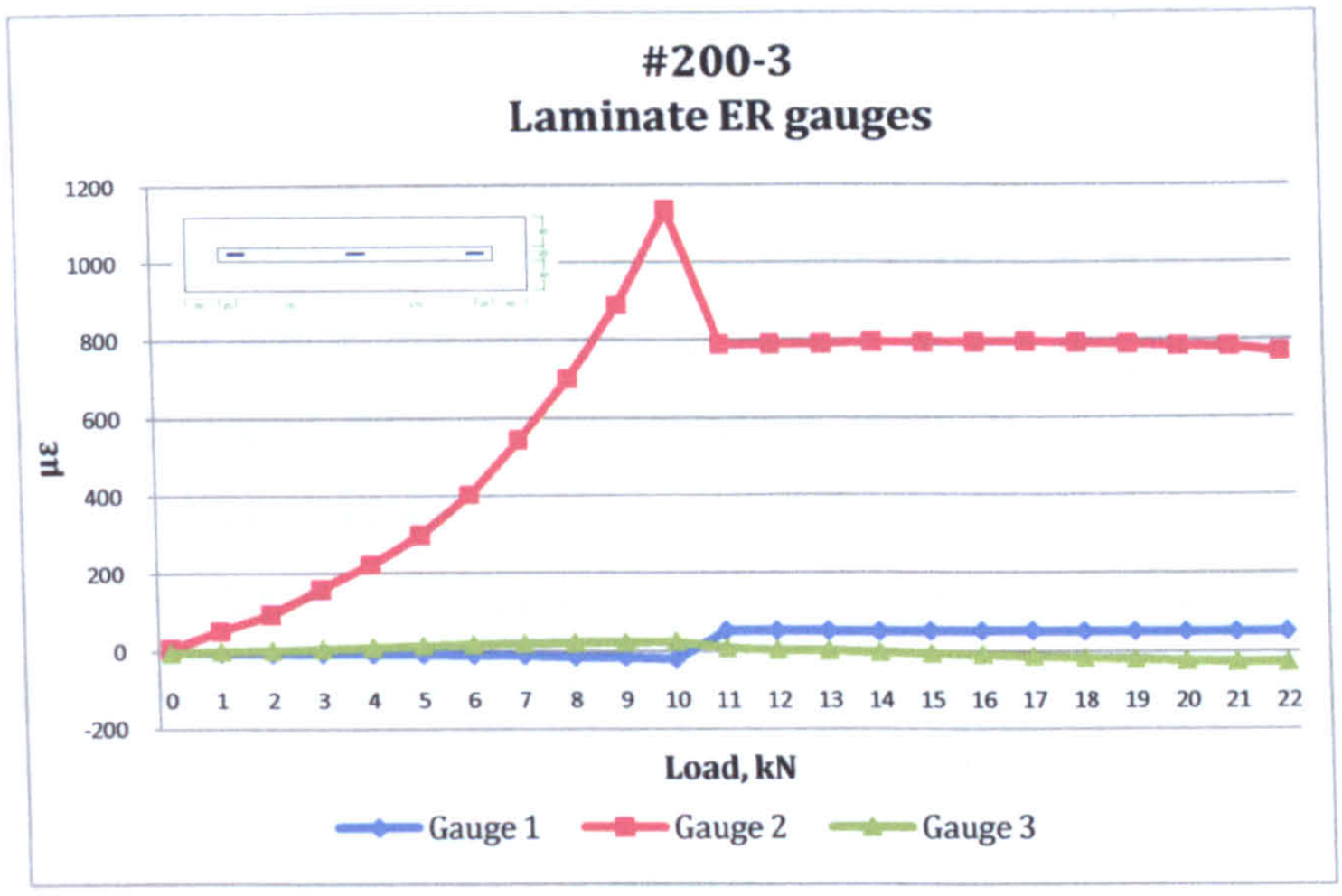

Figure V- 39 Laminate ER gauges, sample #200-3

5.6.4 Side DEMEC strain gauges

First cracks were observed on beam #200-1 (Figure V-40) at 9kN up to level 30mm outside the base of the strain gauges. Up to the formation of the cracks the relative displacements at all levels were gradually increasing with a maximum deformation at level 90 mm of 508 microstrain and at 10mm maximum compressive strain of 439 microstrain.

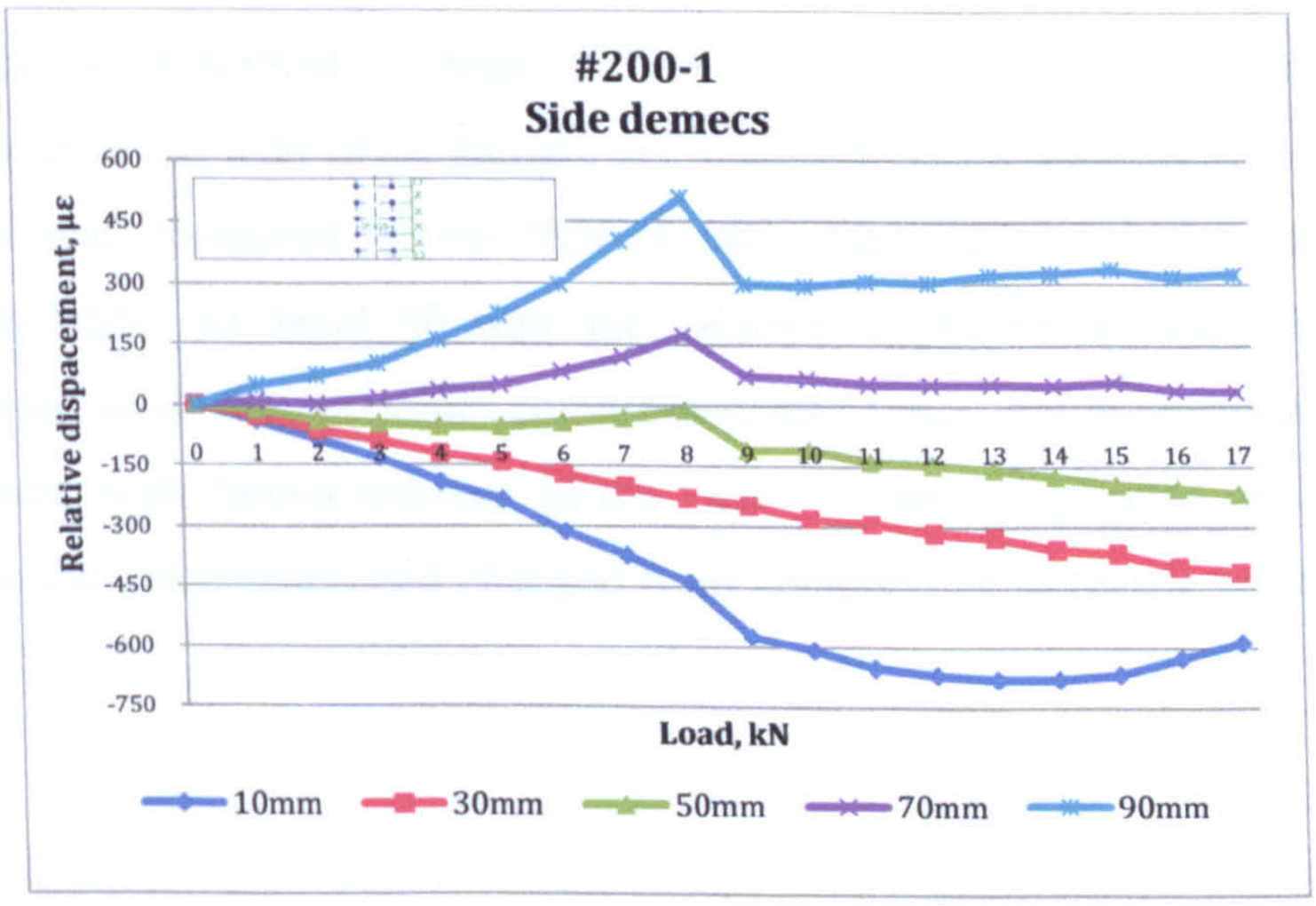

Figure V-40 Local deformations, Side DEMEC strain gauges #200-1

Above the failure load the strain at level 30 and 10mm continued to grow. The maximum value at level 10mm of 679 microstrain was registered at 14kN followed by propagation of the flexural crack to 10mm from the top surface.

First cracks up to level 90mm were observed on beam #200-2 at 9kN outside the base of the side strain gauges which did not lead to change of the deformations at midspan. Maximum values for level 90 mm were obtained at 10kN reaching a value of 1259 microstrain while highest compressive strains of 532 microstrain were measured at level 10mm at 13kN. The deformations at level 30mm changed from compressive to tensile between 10 and 11kN with further increase of the load however, the crack propagated to the same level.

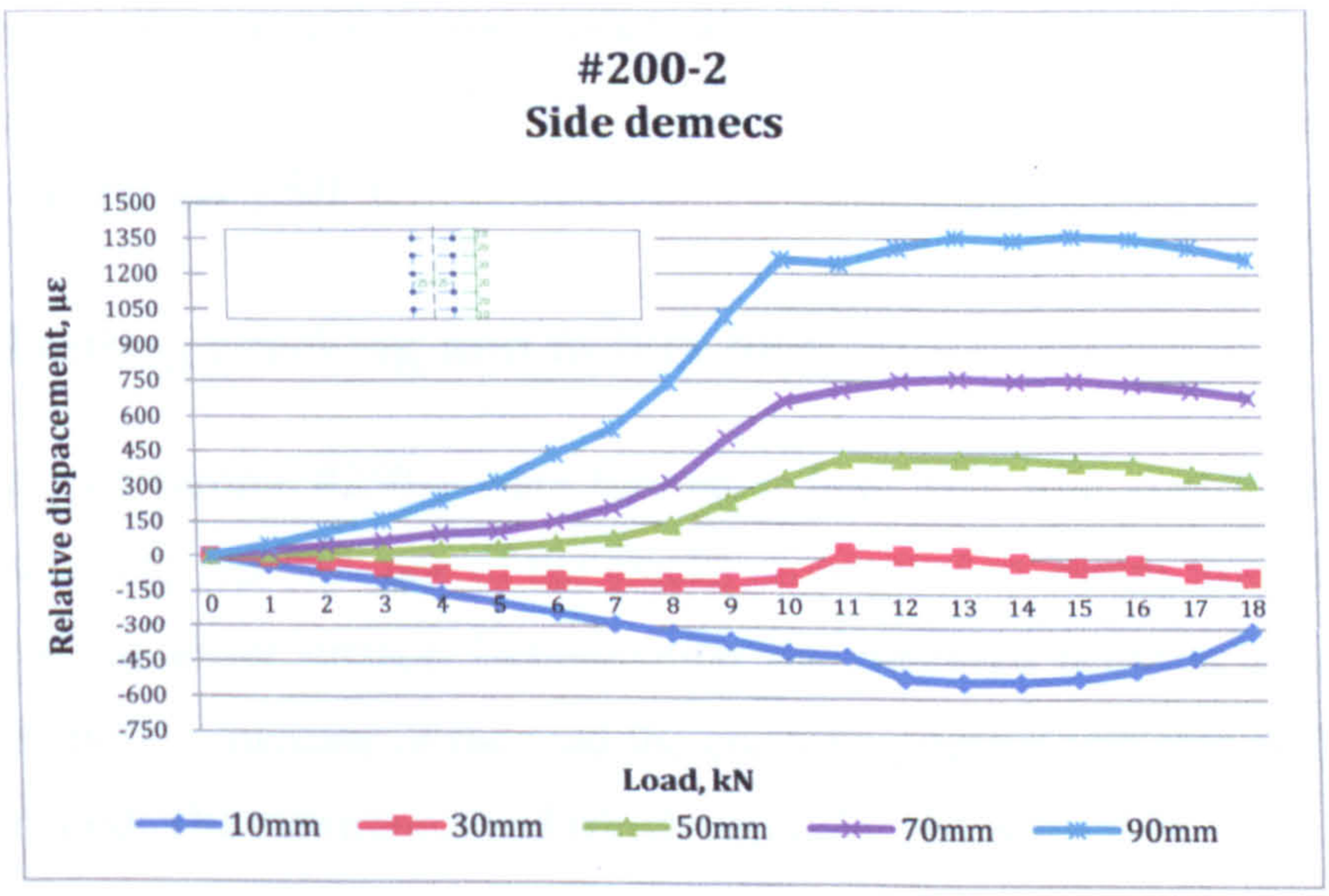

Figure V-41 Local deformations, Side DEMEC strain gauges #200-2

Flexural cracks were formed on beam #200-3 at 10 kN up to level 70mm inside and outside the base of the side strain gauges, see Figure V-42. A significant increase of the deformations was measured above 5kN d and maximum local deformations were registered at 10kN. At level 90 mm the relative displacement reached a value of 1665microstrain while the maximum compressive strain was 299 microstrain 10mm from the top surface. With further increase of the load the crack propagated upwards to level 30mm where the deformation had changed from compressive to tensile between 7kN and 8kN.

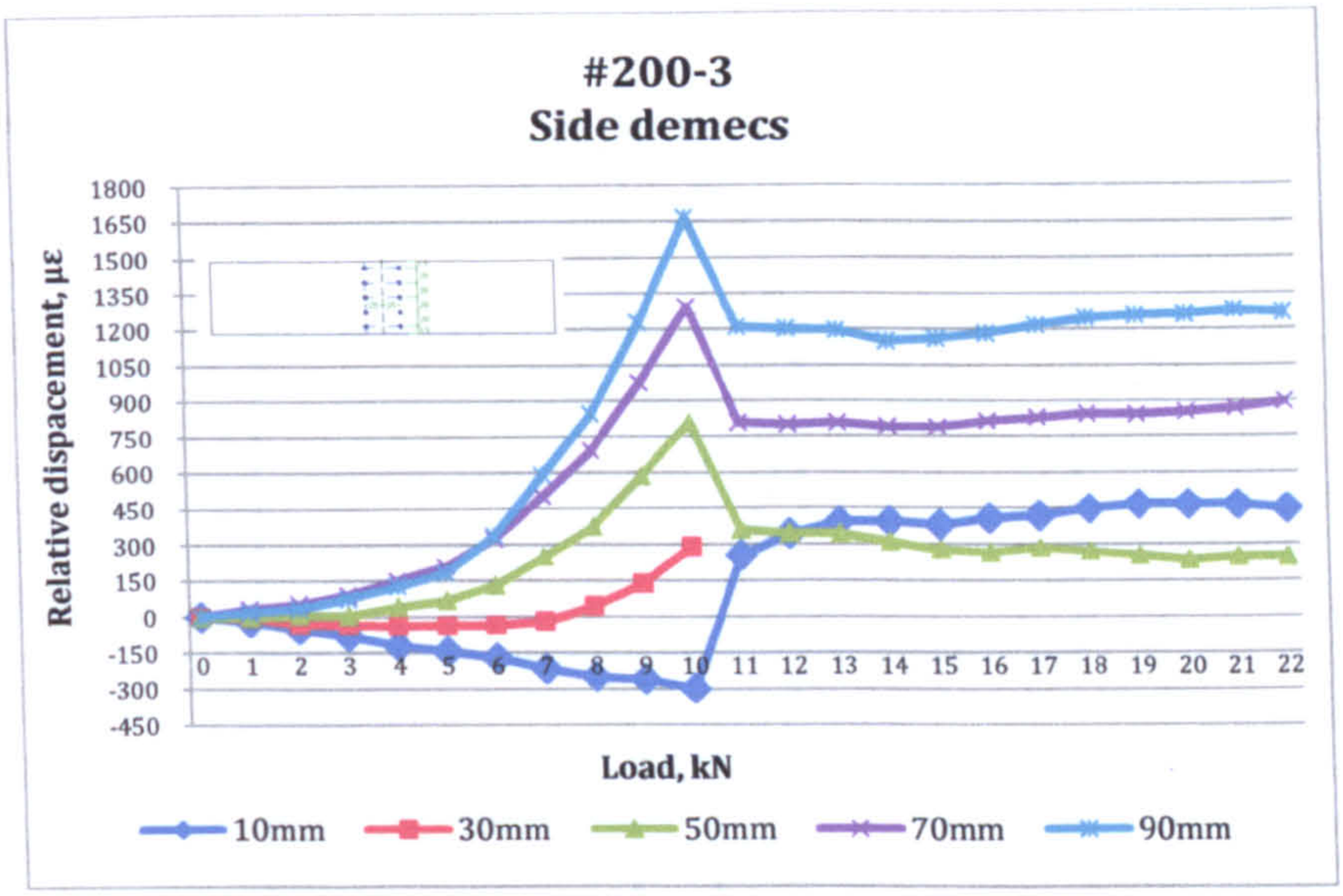

Figure V- 42 Local deformations, Side DEMEC strain gauges #200-3

5.7 Group 250°C

5.7.1 Testing, cracking and failure load

The first cracks on sample #250-1 were formed at load 6kN with approximate length of 20mm (Figure V-43). At 9kN one of the cracks propagated to 20mm from the top and to the adhesive on the lower surface. Delamination was observed between the adhesive and concrete. With further increase of the load the crack propagated upwards and the width of the crack increased. The maximum load which was achieved was 19kN.

Sample #250-2 developed one crack at 5kN which propagated to 20mm from the top at 6kN. Delamination between the laminate and the adhesive occurred. The load was then increased which resulted in opening of the crack including trough the adhesive layer. The maximum load which could be applied was recorded at 17kN.

The last sample of the group #250-3 developed a crack at 5kN which later propagated at 8kN and delamination between laminate and adhesive followed. The load was reduced to 7.1kN and then the beam was reloaded to 20.2kN when the capacity of the beam was reached.

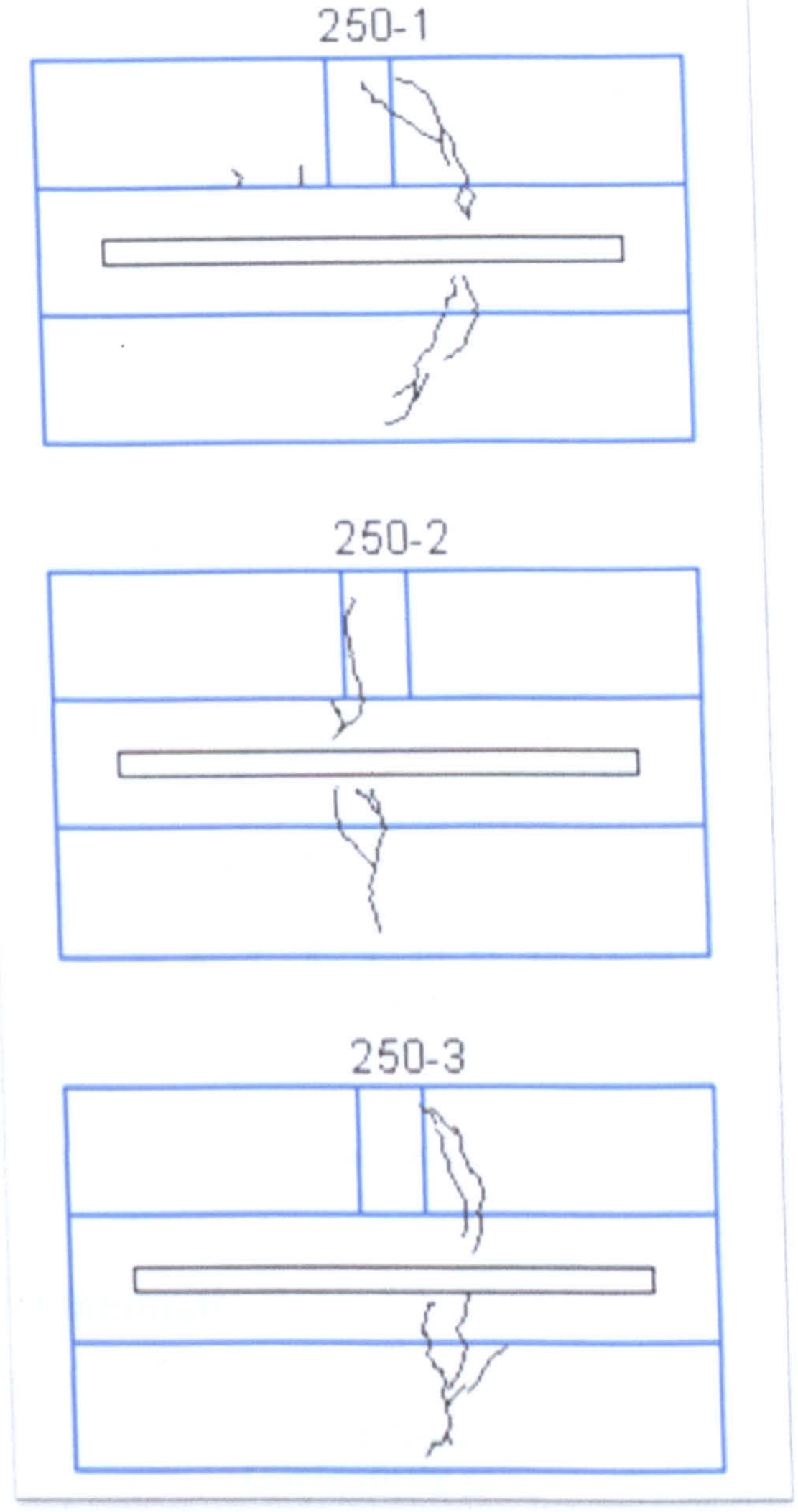

Figure V- 43 Crack formation and failure of beams, group 250°C

5.7.2 Deflection

The deflection of the samples of group 250°C were plotted for load from 0kN to 20kN, Figure V-44. Beam #250-1 was loaded to 9kN when delamination occurred and the deflection increased from 0.309mm at 8kN to 0.685mm at 9kN. Maximum load was reached at 19kN when the deflection was increased to 2.892mm. Beam #250-2 failed at 7kN due to a flexural crack and delamination. At 6kN the deflection increased to 0.183mm and at maximum load of 17kN the deflection reached 3.453mm. The last sample of the

group reached deflection of 0.27mm before the beam failed at 8kN due to formation of a crack and delamination. At 20kN the deflection reached 0.277mm.

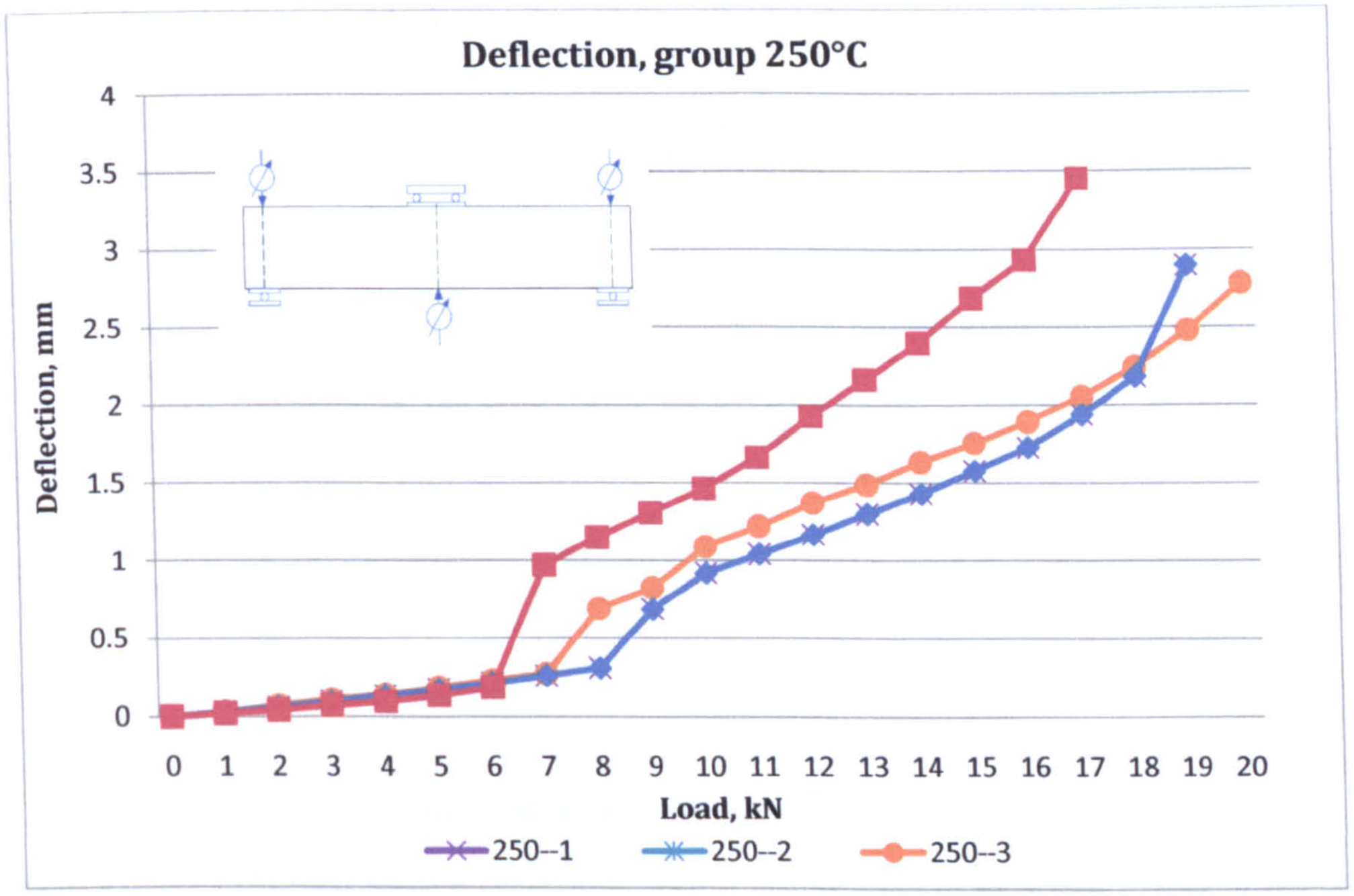

Figure V- 44 Deflection, group 250°C

5.7.3 Strain of laminate

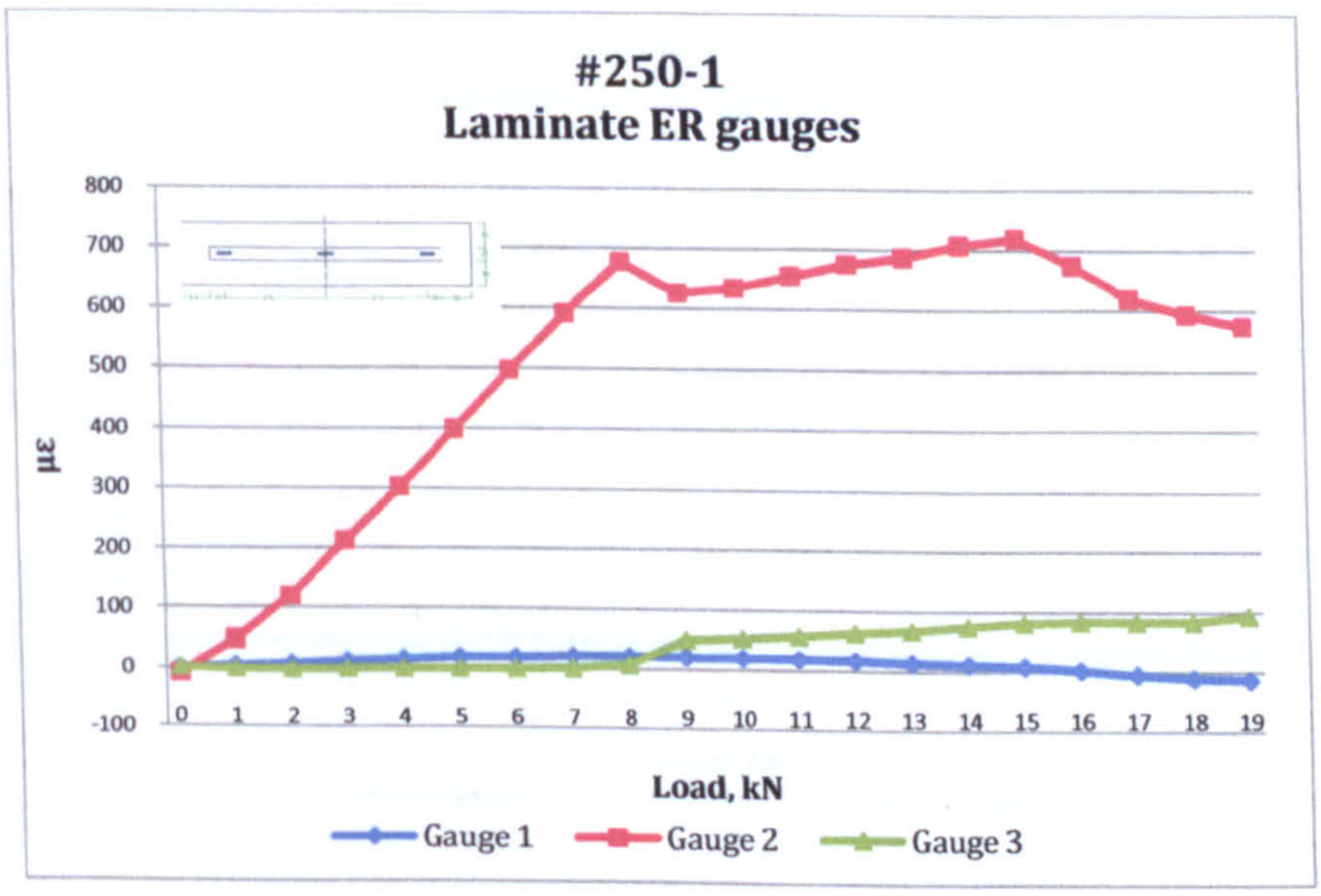

Figure V- 45 Laminate ER gauges, sample #250-1

The strain measured at midspan of beam #250-1 gradually increased to 8kN when a value of 677 microstrain was measured. With increase of the load by 1kN delamination occurred. The local deformations measured at the ends of the laminate registered little increase due to thermal cracks between the concrete and the adhesive layer.

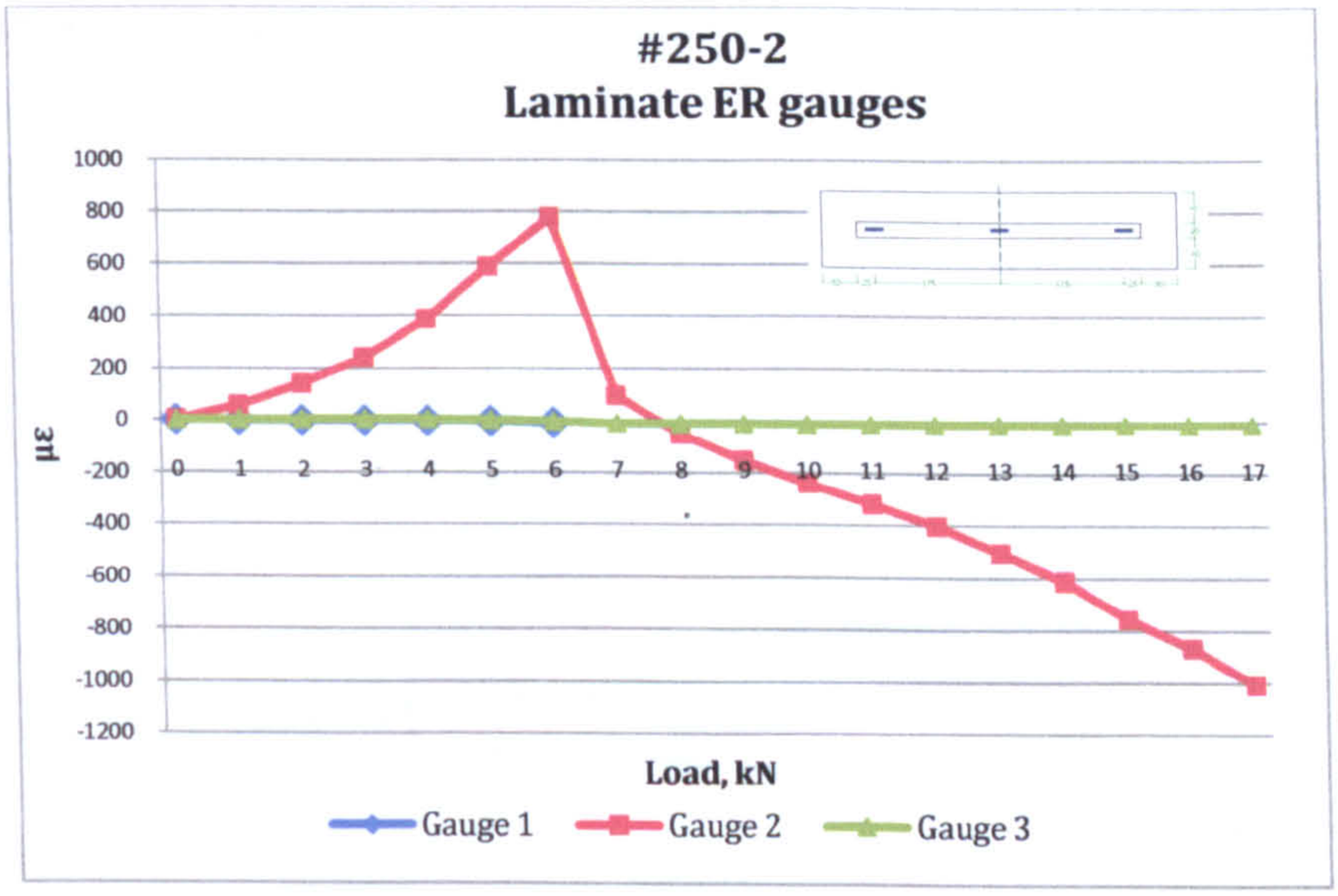

Figure V- 46 Laminate ER gauges, sample #250-2

Beam #250-2 exhibited similar behaviour with a failure load at 6kN, see Figure V-46. At midspan the local deformation reached a value of 777 microstrain before failure due to a flexural crack occurred. At the left and right end of the laminate no significant increase of the strain was registered due to existing thermal cracks.

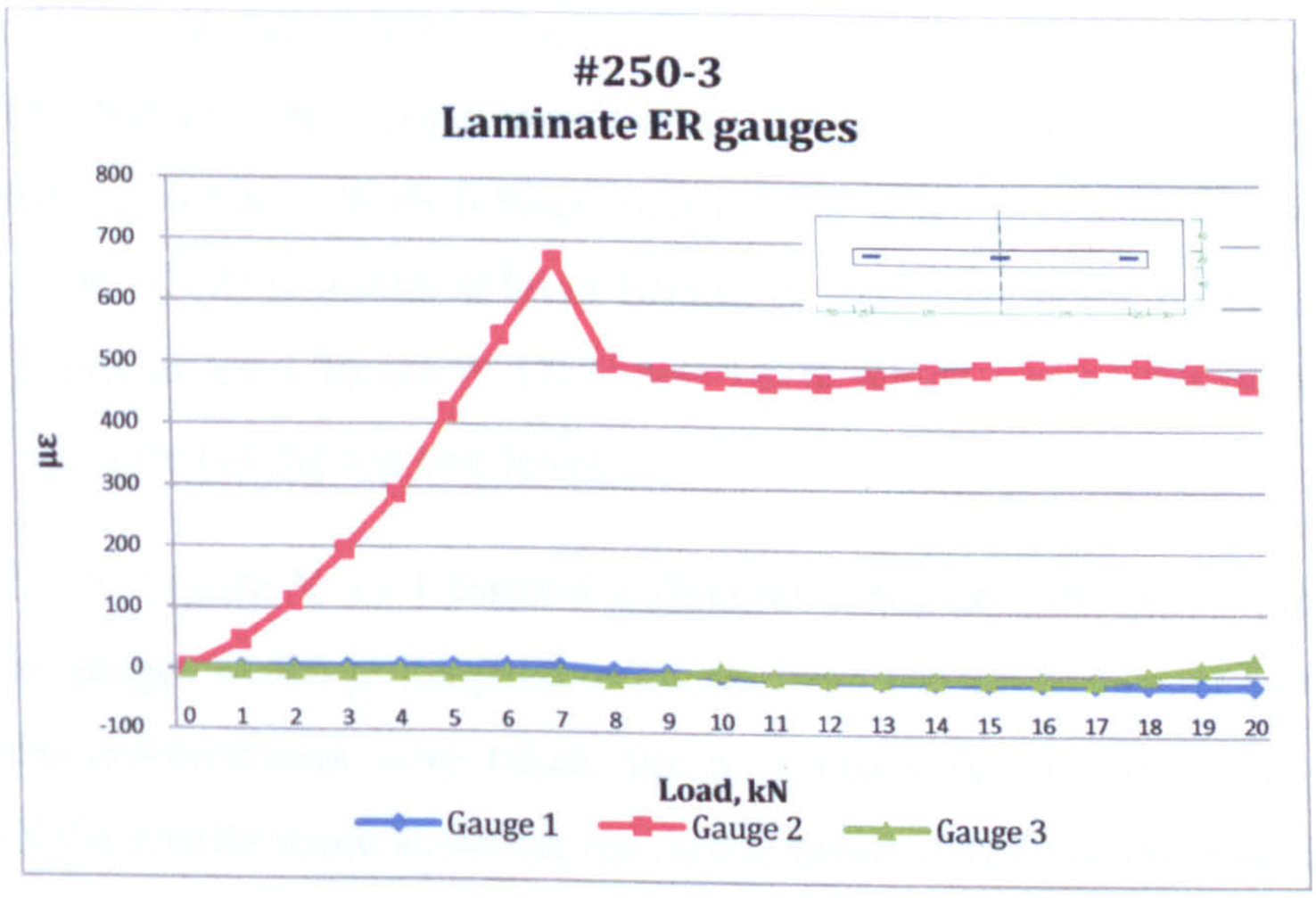

Figure V- 47 Laminate ER gauges, sample #250-3

At 7kN the strain at midspan reached a value of 668 microstrain before a crack was formed on the right side of the beam #250-3 followed by delamination. The local deformations measured at the ends of the laminate registered no increase due to thermal cracks between the laminate and the adhesive layer.

5.7.4 Side DEMEC strain gauges

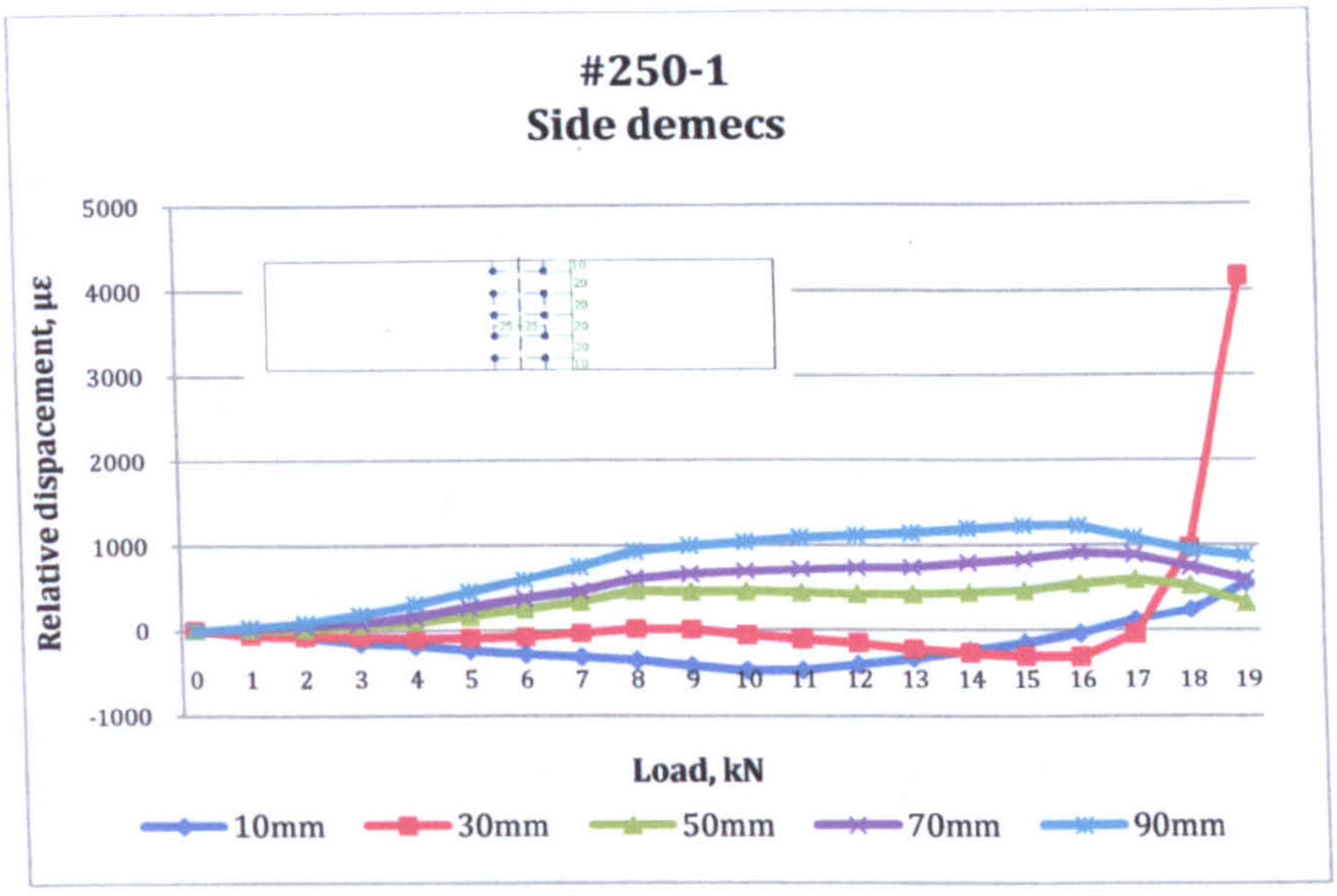

Figure V-48 Local deformations, Side DEMEC strain gauges #250-1

The first flexural cracks appeared on the side of beam #250-1 at 6kN. The relative displacements gradually increased to 8kN when at level 90mm the local deformation reached 936 microstrain and at level 10 mm the compressive strain reached a value of 353 microstrain. The flexural-shear crack was formed outside the base of the strain gauge to 20mm from the top surface. With further increase the crack propagated upwards until it reached one of the DEMEC points at level 10mm. A secondary crack propagated between the DEMEC points at level 30mm at 17kN and 18kN which caused the rapid increase of deformations measured at the top two levels.

Beam #250-2 (see Figure V-49) formed a flexural crack at 5kN inside the base of the DEMEC strain gauges which propagated to 20mm from the top surface at 6kN. No further readings of the deformations were taken due to a crack developed under the DEMEC points. At 6kN the tensile strain at 90mm reached a value of 1677 microstrain and at 10mm compressive deformation of 310microstrain. At 10mm the compressive relative displacement increased to 840 microstrain when the maximum load of the beam was applied.

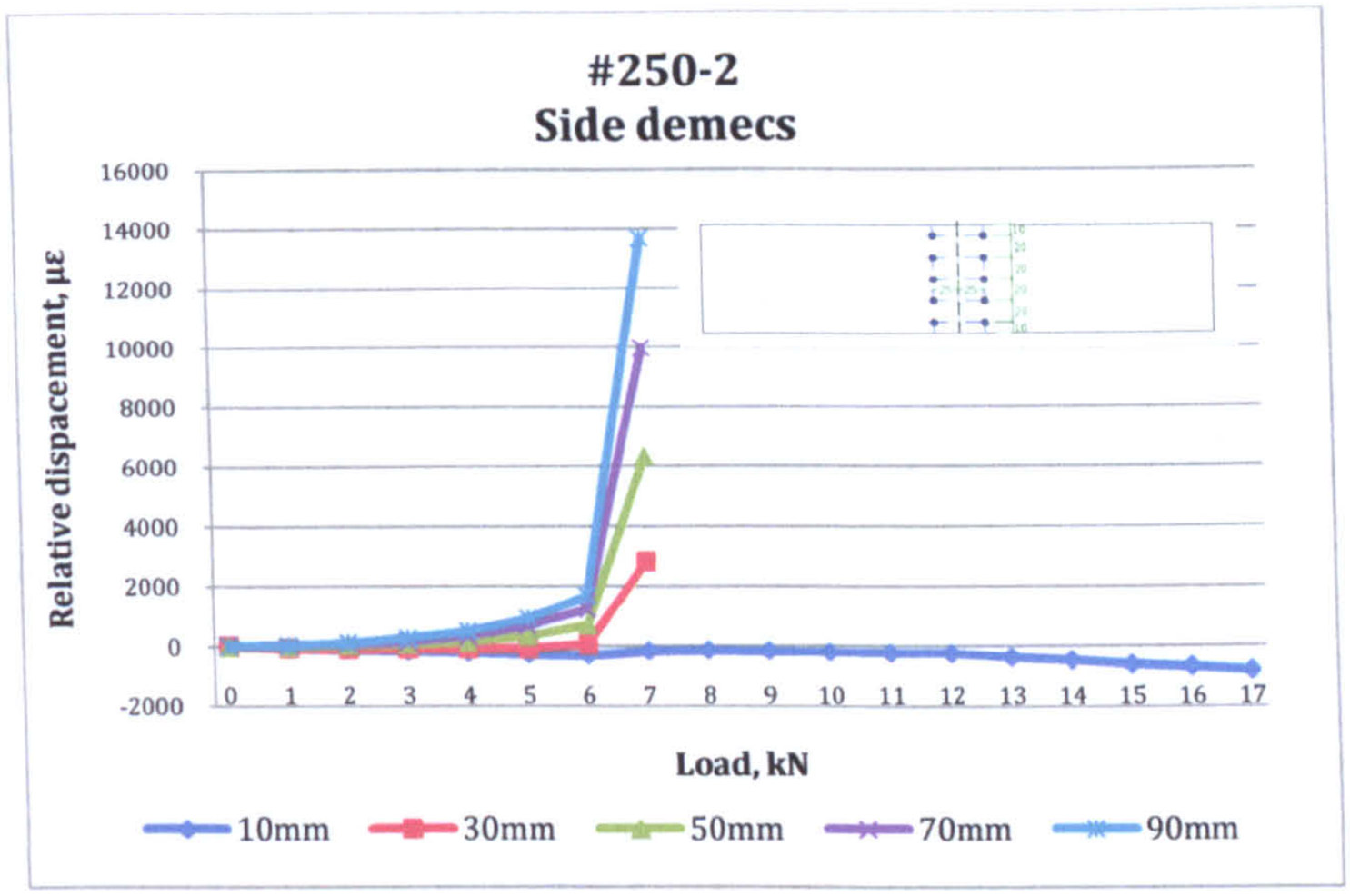

Figure V- 49 Local deformations, Side DEMEC strain gauges #250-2

The highest deformation of beam #250-3 was measured at 90mm when the load reached 7kN. The relative displacement increased to 862 microstrain and the compressive strain reached 241 microstrain prior to failure. With further increase of the load the crack propagated to level 30mm and at 9kN reached 10mm.

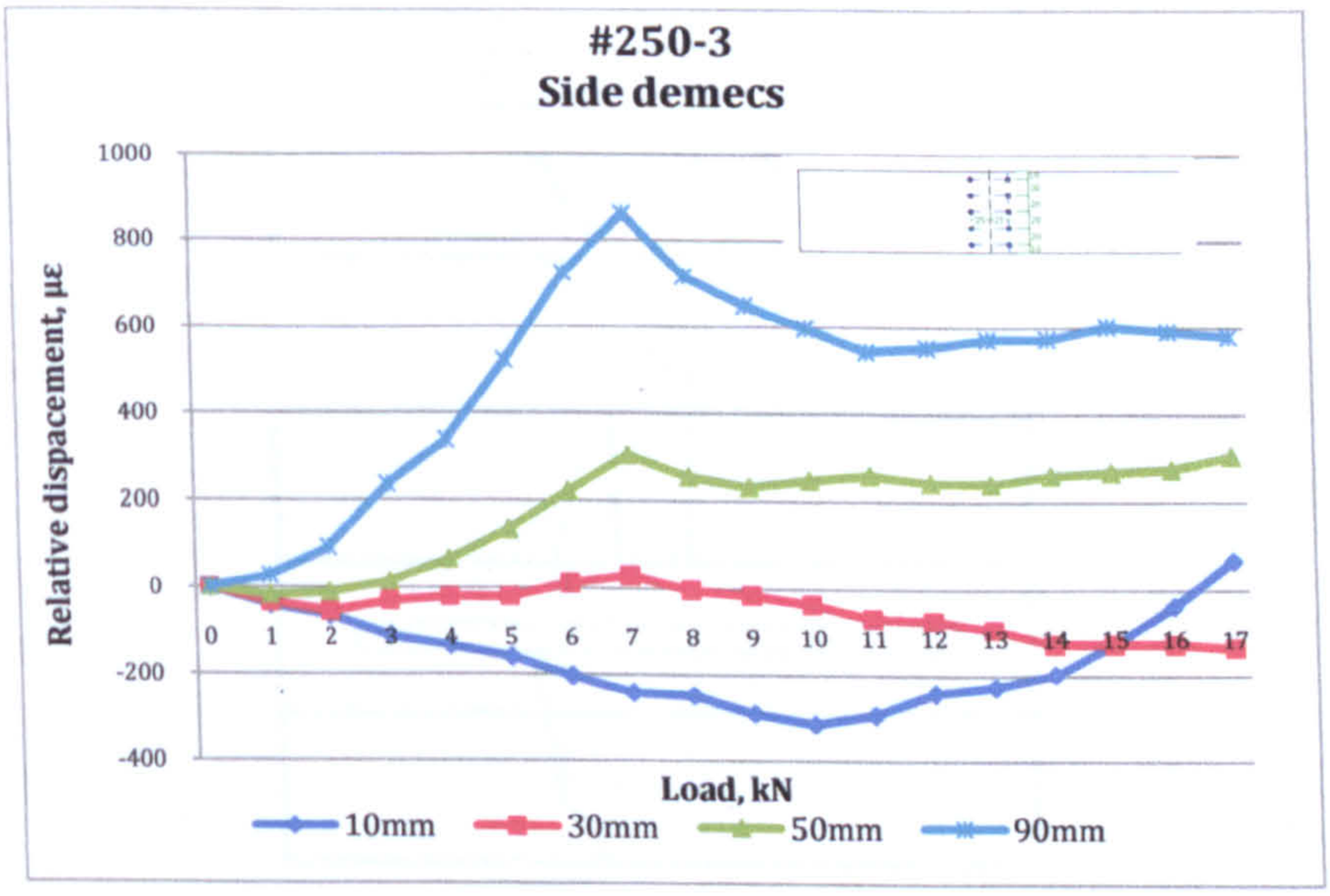

Figure V- 50 Local deformations, Side DEMEC strain gauges #250-3

5.8 Group 300°C

5.8.1 Testing, cracking and failure load

Sample #300-1 failed at a low level of loading, see Figure V-51. At 4kN a flexural crack occurred almost though the full height of the beam followed by mixed laminate-adhesive-concrete delamination. The load was reduced to 1.2kN and then at 1.5kN the maximum load was reached.

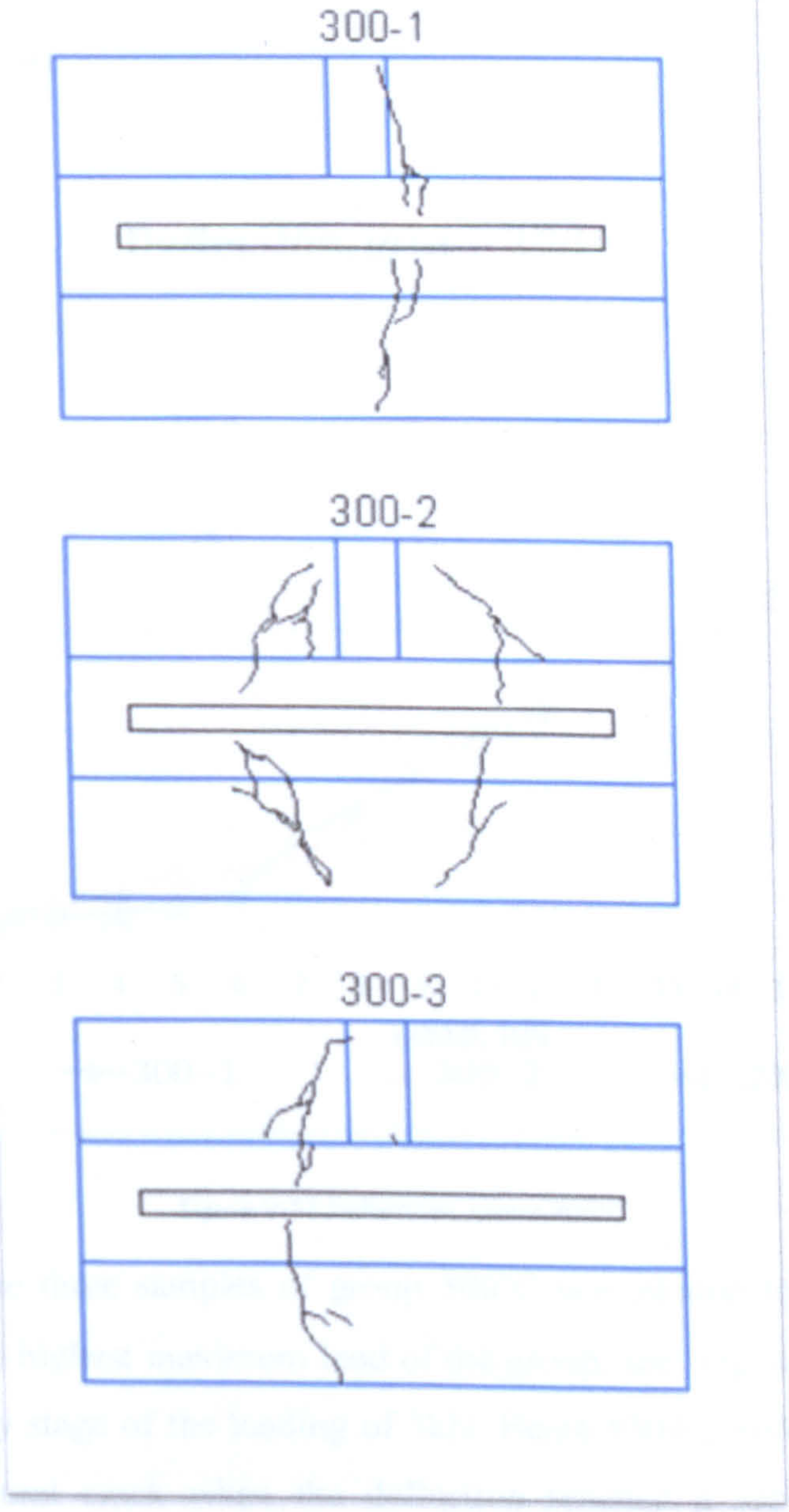

Figure V- 51 Crack formation and failure of beams, group 300°C

First cracks appeared on sample #300-2 at 5kN which propagated upwards at 8kN and 9kN symmetrically about the central axis of the beam. Delamination was observed at 9kN on the left side of the beam. The further increase of the load led to the further propagation of the cracks until at 19.8kN the maximum load was reached.

The last sample of group 300 developed short flexural cracks at 6kN.At 7kN another crack had developed which resulted in a reduction of the load to 6.3kN and complete delamination. The crack then propagated upwards up to 11kN. Maximum load was reached at 21.2kN.

5.8.2 Deflection

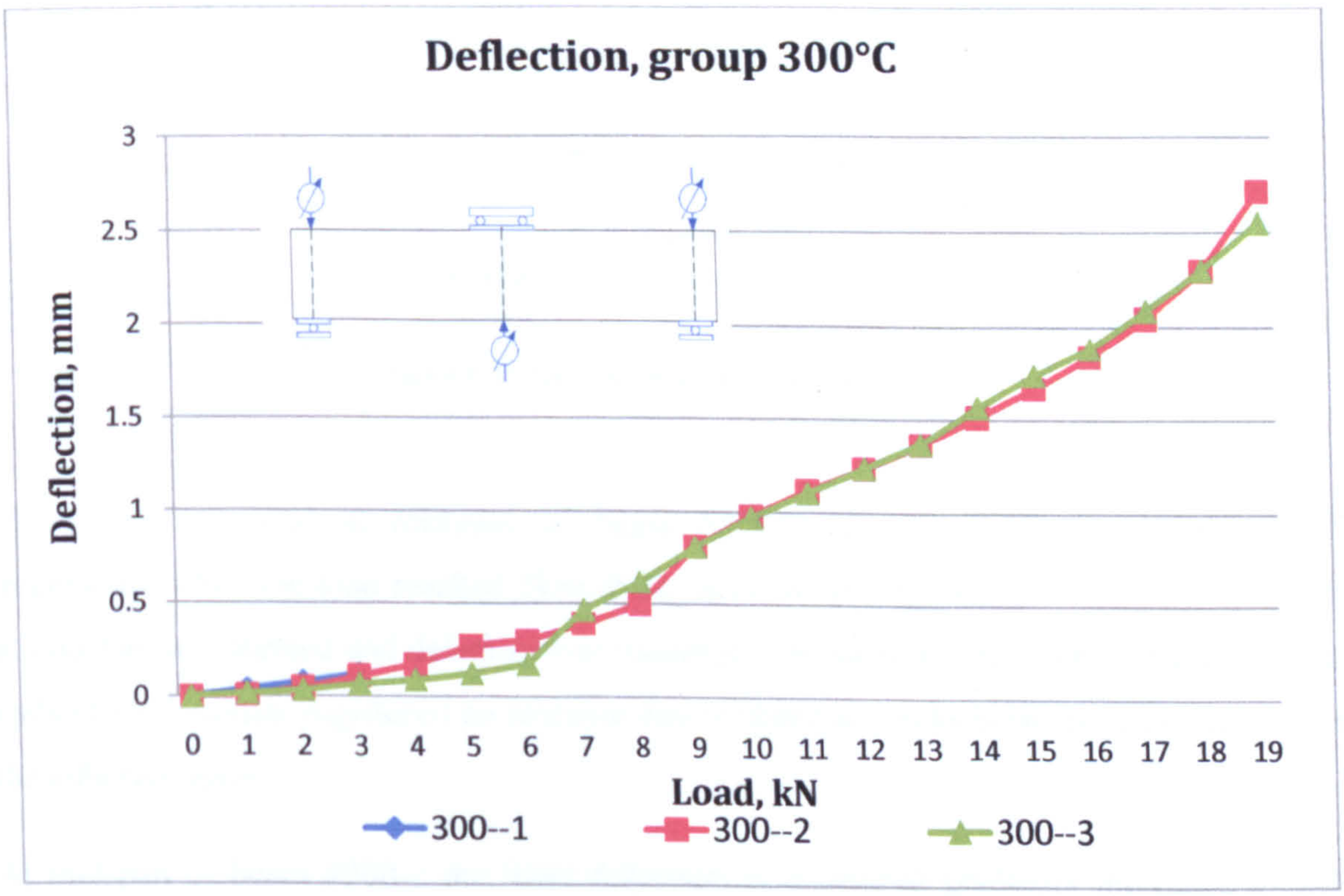

Figure V-52 Deflection, group 300°C

The deflection of the three samples of group 300°C was plotted for loads from 0kN to 19kN which was the highest maximum load of the group, see Figure V-52. Beam #300-1 failed at a very early stage of the loading of 3kN. Beam #300-2 failed at a higher load of 8kN due to a flexural crack when the deflection reached a value of 0.498mm. The deflection was increasing gradually up to 5kN when the first flexural cracks were observed and the maximum load was then reached at 19kN after with maximum deflection of

2.711mm. Beam #300-3 failed when the beam was loaded to 7kN with a deflection reading of 0.171mm before delamination occurred. The load was then increased and reached 2.545mm at 19kN.

5.8.3 Strain of laminate

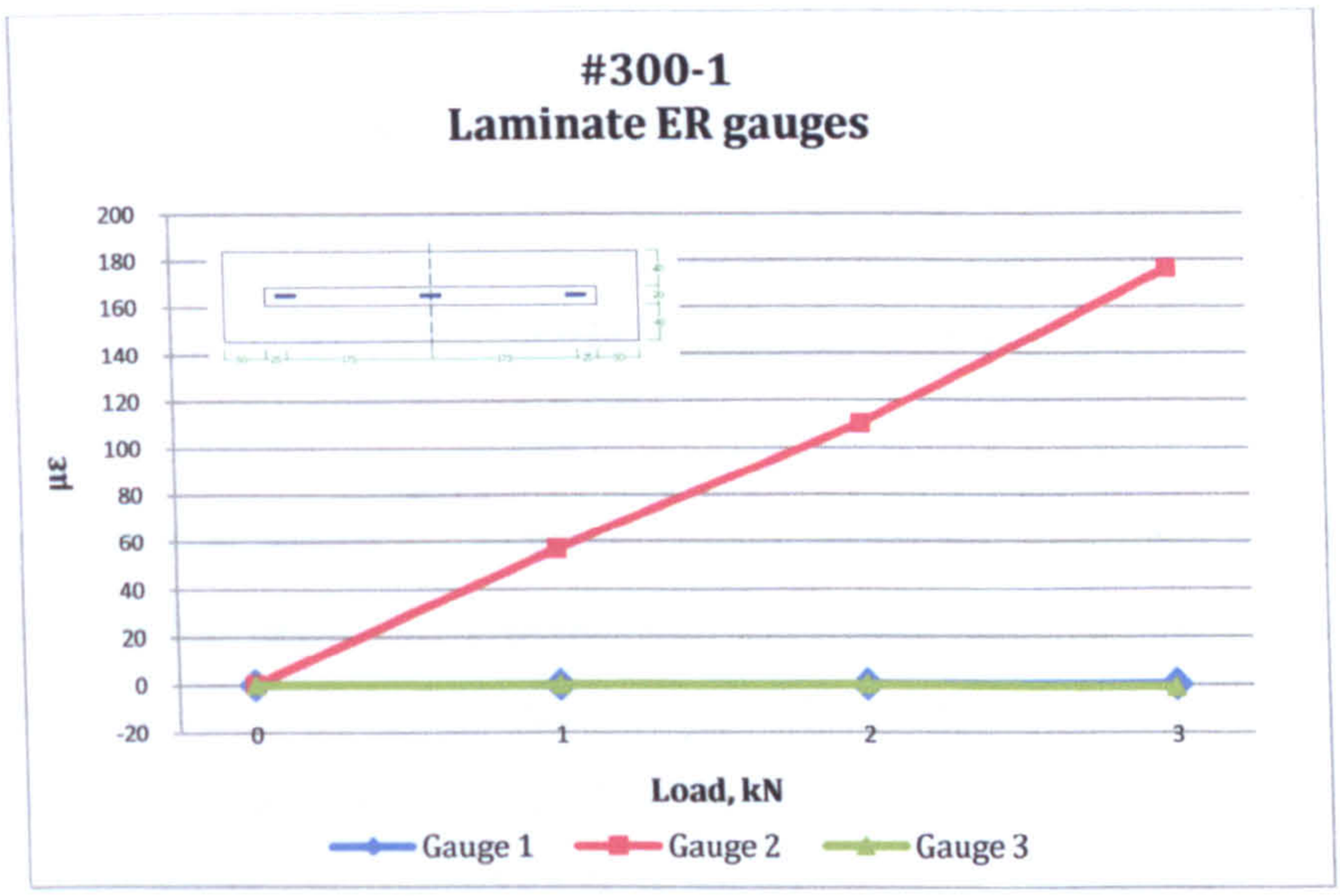

Figure V- 53 Laminate ER gauges, sample #300-1

The strain measured at midspan of beam #300-1 (Figure V-53) increased to 176 microstrain when the load reached 3kN. With increase of the load by 1kN a vertical crack at midspan was formed and delamination occurred. The local deformations measured at the ends of the laminate registered no increase due to thermal cracks between the concrete and the adhesive layer.

At midspan of beam #300-2 the local deformation measured gradually increased to 5kN until the first cracks were formed and with further increase of the load to 8kN maximum strain of 694microstrain was registered. ER strain gauges 1 registered no increase of the local deformations and ER gauge 3 detected compressive strains from 5kN to 9kN. The concentration of the stresses at the right end of the laminate was caused by the cracks developed during the heating process and the following peeling action at the ends.

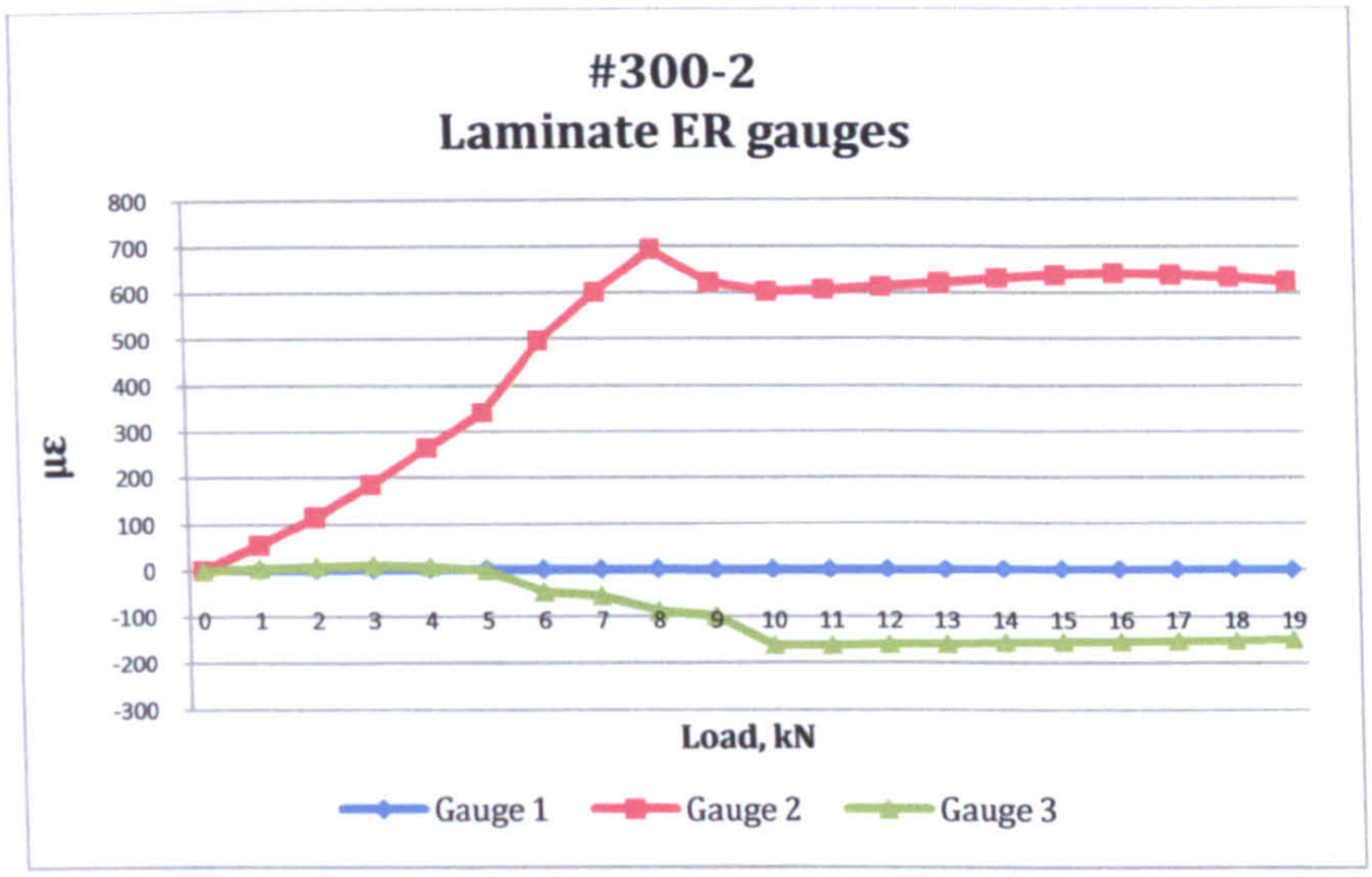

Figure V- 54 Laminate ER gauges, sample #300-2

The strain measured at midspan of beam #300-3 increased gradually up to 6kN when before the beam failed due to a flexural crack and delamination, see Figure V-55. The strain continued to increase when the system was reloaded up to 16kN which was attributed to residual local deformation above the failure load of the system. Both the left and right ER strain gauges registered no increase of the local deformation.

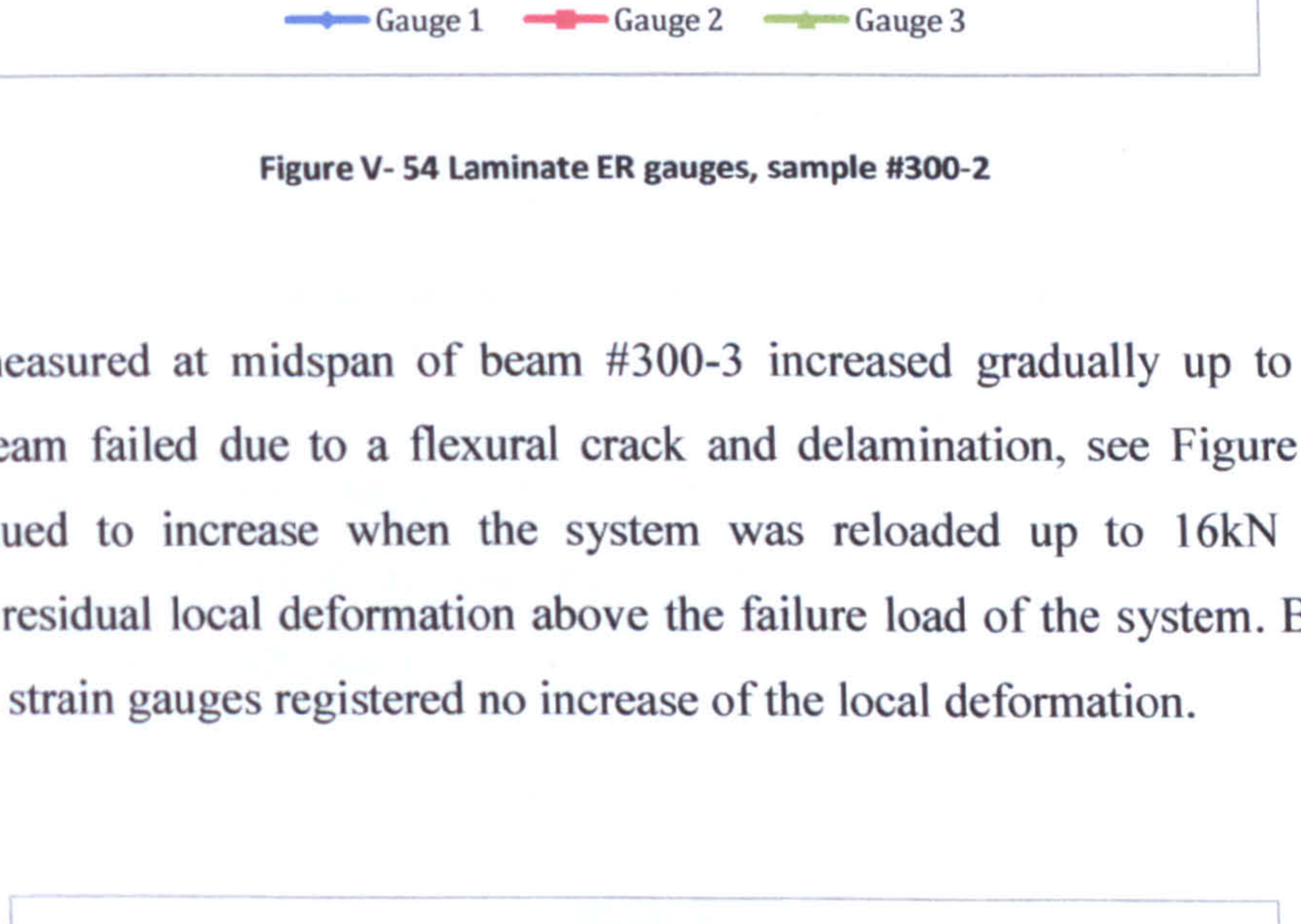

Figure V- 55 Laminate ER gauges, sample #300-3

5.8.4 Side DEMEC strain gauges

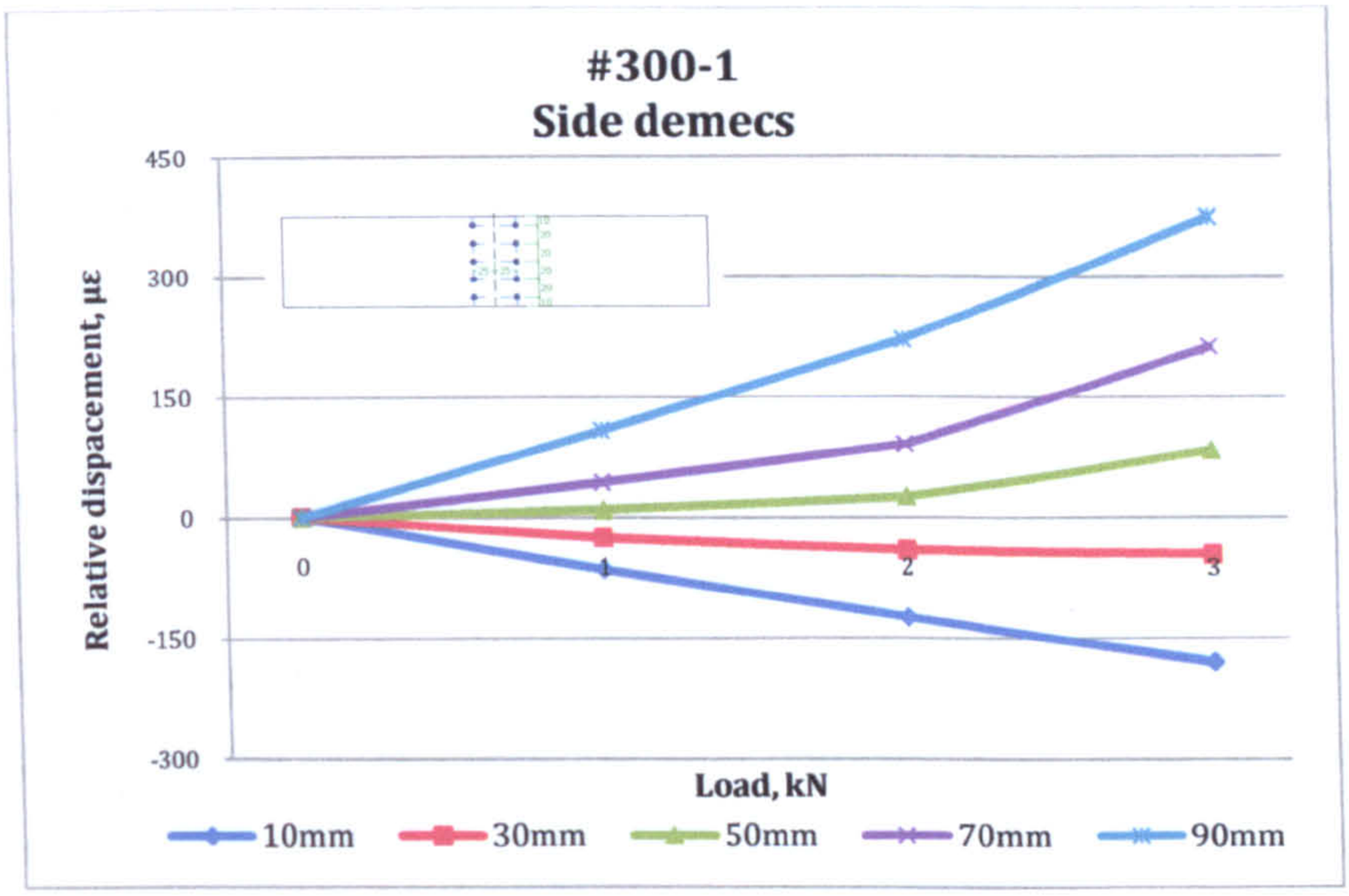

Figure V- 56 Local deformations, Side DEMEC strain gauges #300-1

The relative displacement of beam #300-1 at 3kN reached 179microstrain at level 10mm and 374 microstrain at level 90mm. The readings at the different levels increased gradually up to the failure load of 4kN, see Figure V-56.

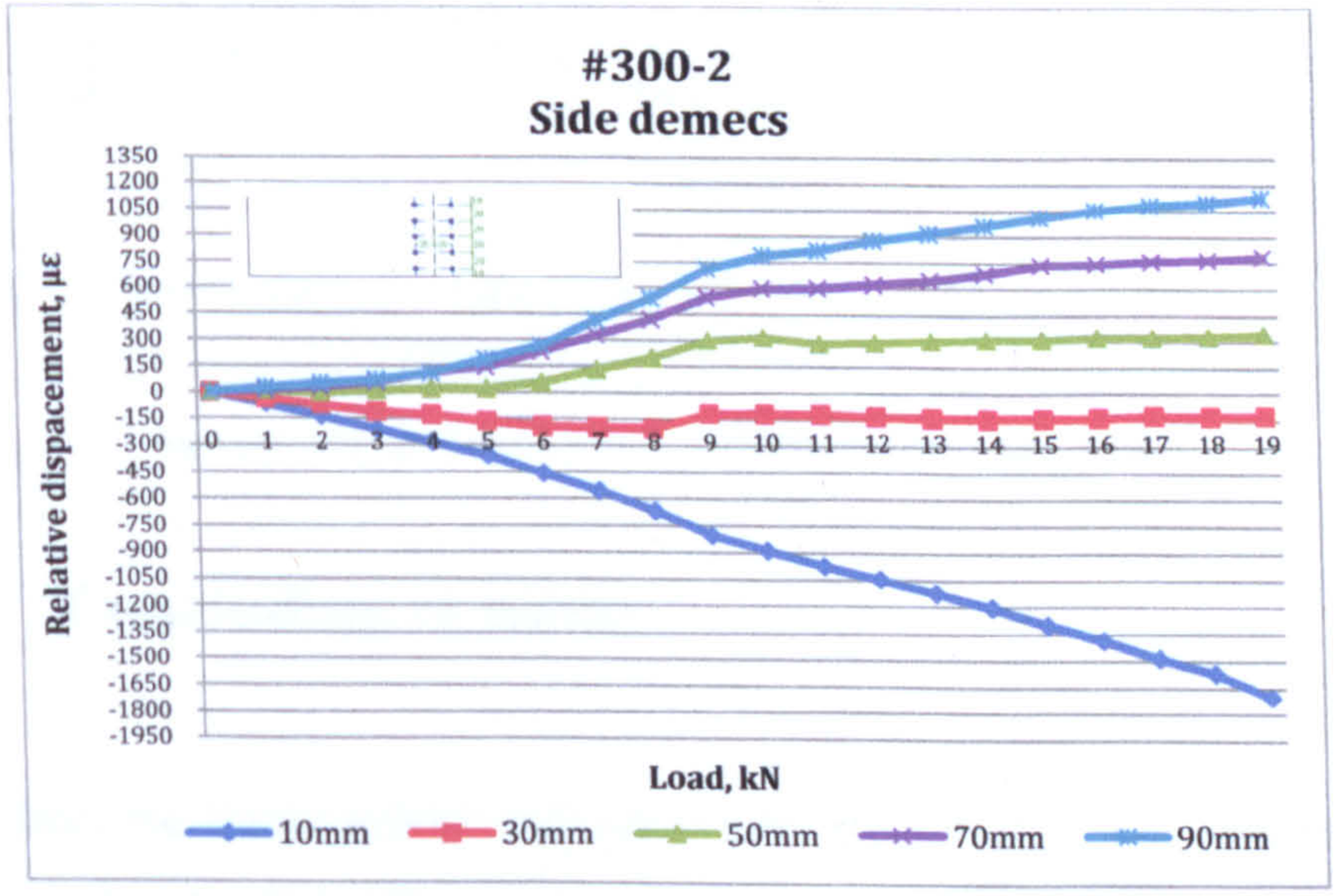

Figure V- 57 Local deformations, Side DEMEC strain gauges #300-2

Flexural cracks were formed outside the base of the DEMEC strain gauges at 5kN and they continued to propagate to the top surface at 13kN. The relative displacements gradually increased up to 8kN when a crack was formed inside the base of the strain gauges. The deformation at level 90mm increased to 1125 microstrain at maximum load. At level 10mm the compressive strain continued to grow to 19kN and reached a value of 1705microstrain.

Gradual increase of the local deformations was observed at all levels of beam #300-3 (Figure V-58) to 6kN when flexural cracks were formed outside the base length of the strain gauges and delamination on the left side followed. With subsequent increase of the load the cracks continued to propagate upwards reaching level 10mm at 13kN. The local deformation at level 10mm then changed to positive and at 19 kN the tensile deformation reached 278 microstrain.

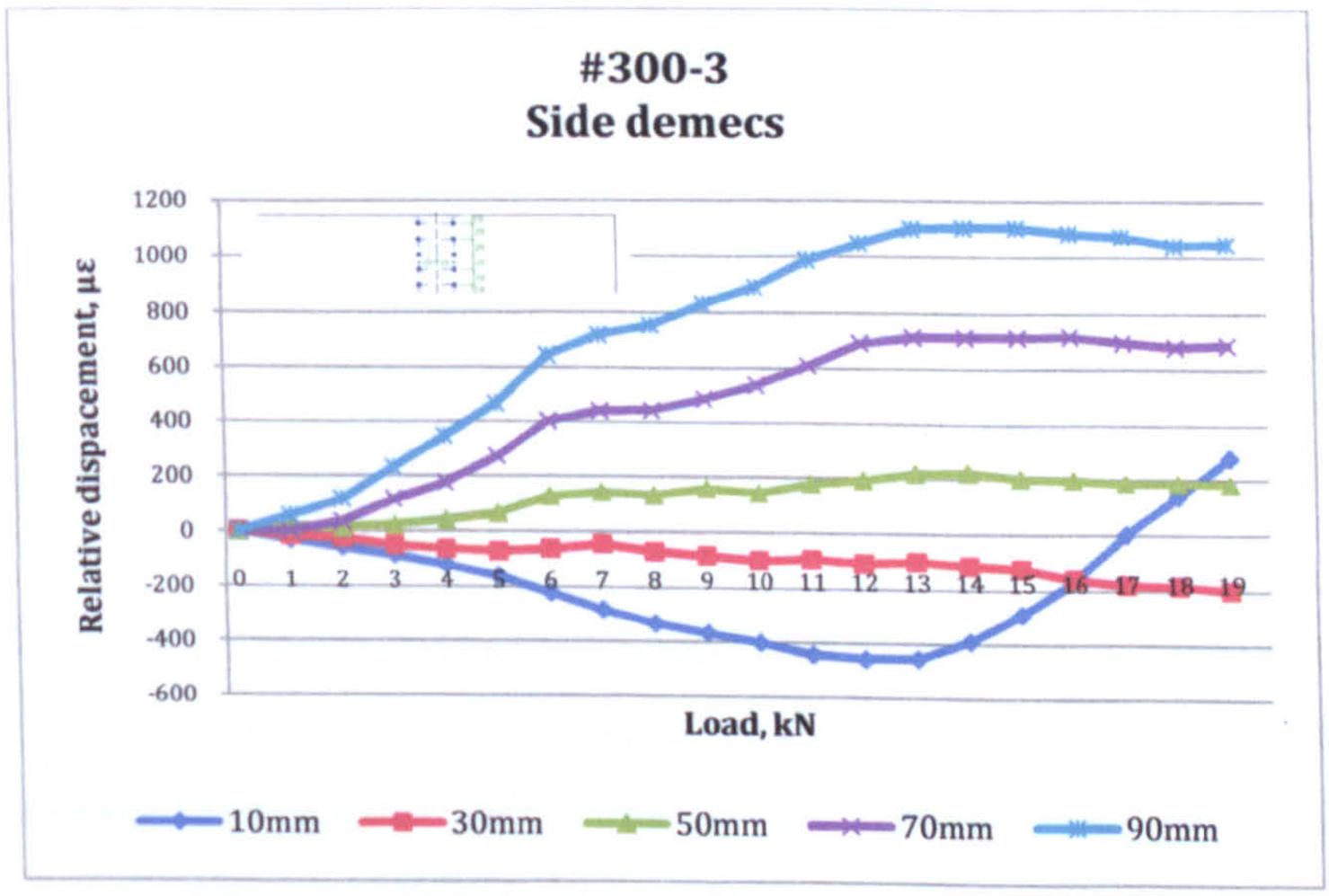

Figure V- 58 Local deformations, Side DEMEC strain gauges #300-3

5.9 Concluding remarks

The results from the third experimental study were presented in this chapter. The heated and cooled minibeams from the second study were tested in a four point bending until failure. The propagation of cracks was presented for each minibeam together with the results of the local deformations in the concrete beam and CFRP laminate. An intermediate debonding was observed as the most common mode of failure.

Chapter 6
Analysis of the results

The results from the 3 experiments are compared and analysed in this chapter. The trends for the increase of the deformability and decrease of strength are presented and discussed. The effect of elevated temperatures and width of the laminates are compared for the first experiment. Finally, physical changes of the adhesive and laminate at different temperatures are also described.

6.1 Bond strength of CFRP-to-concrete joints

6.1.1 Comparison and analysis of the results

To analyse the results of the first experimental study the measured deformations were compared at different levels of loading. The initial load step of 6kN was chosen and was based on the lowest failure load from the 7 tested groups. To investigate the development and increase of the deformations the results were compared at half the load step. Then the load step was doubled and at 12kN the groups from 20°C to 150°C were compared. The same approach was applied for all 4 different deformations measured on the side of the concrete prism, between the end of the laminate and the concrete and the elongation of the laminate measured by DEMEC and ER strain gauges.

6.1.2 Effect of elevated temperatures on the deformations in the concrete (Side DEMEC strain gauges)

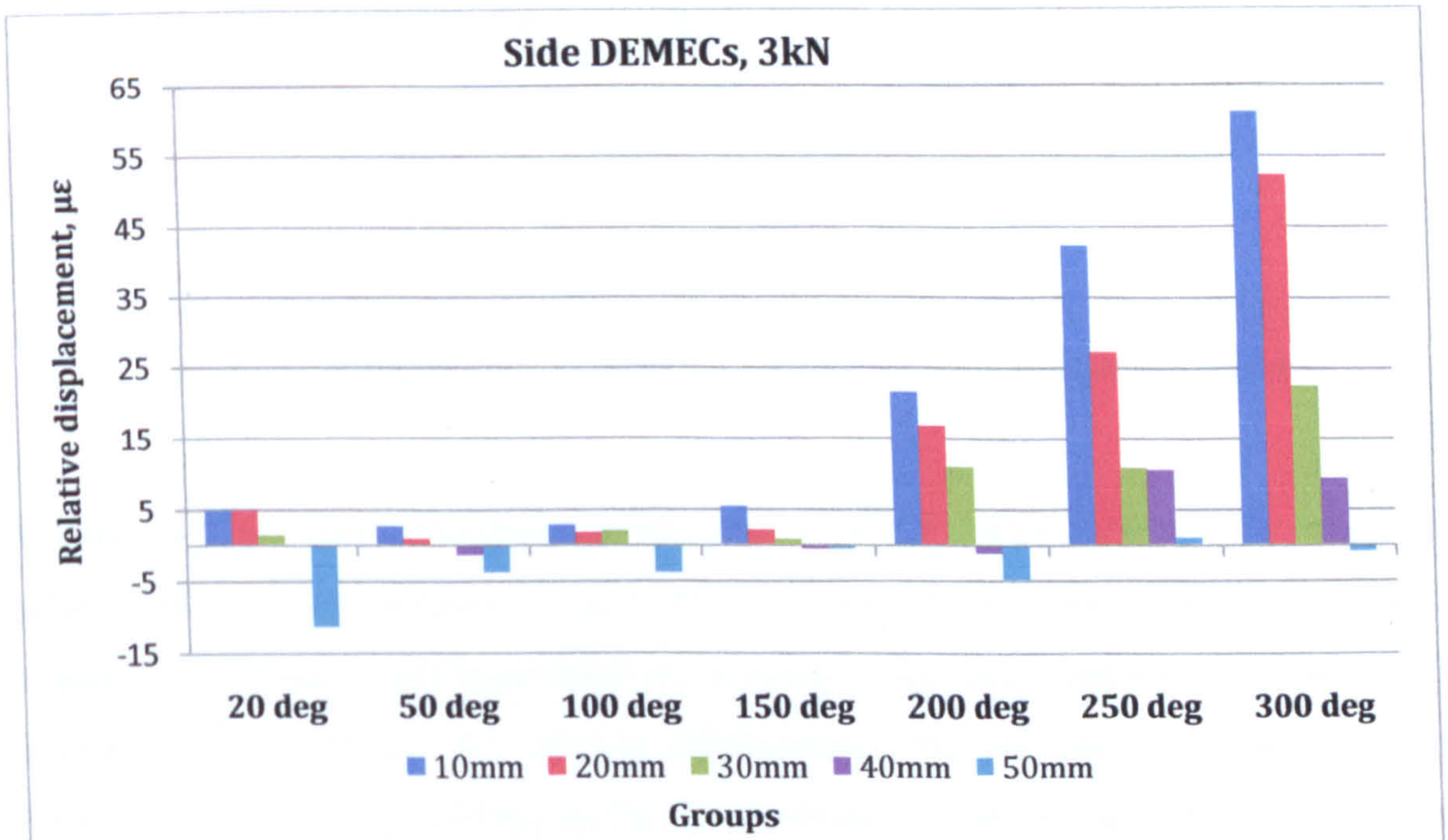

Figure VI- 1 Effect of elevated temperatures on the side deformations of the concrete at 3kN

Groups 20°C to 150°C exhibited lower deformations at 3kN in the upper half of the concrete prism than the rest of the groups, see Figure VI-1. The average relative displacement varied between 5 and -5 microstrain with the exception of group 20°C for which higher

compressive strain was detected. The higher value at level 50mm was attributed to limited number of samples. Groups 200°C to 300°C registered 4 to 12 times higher deformations which were predominantly tensile. A parabolic increase of the relative displacements was observed at levels 10 and 20mm whilst levels 30 to 50mm registered more linear increase as an indication that the distribution of stresses through the height of the concrete prism was nonlinear. An increase of the temperature resulted in a decreased modulus of elasticity after the cooling phase which caused higher deformations at lower loads.

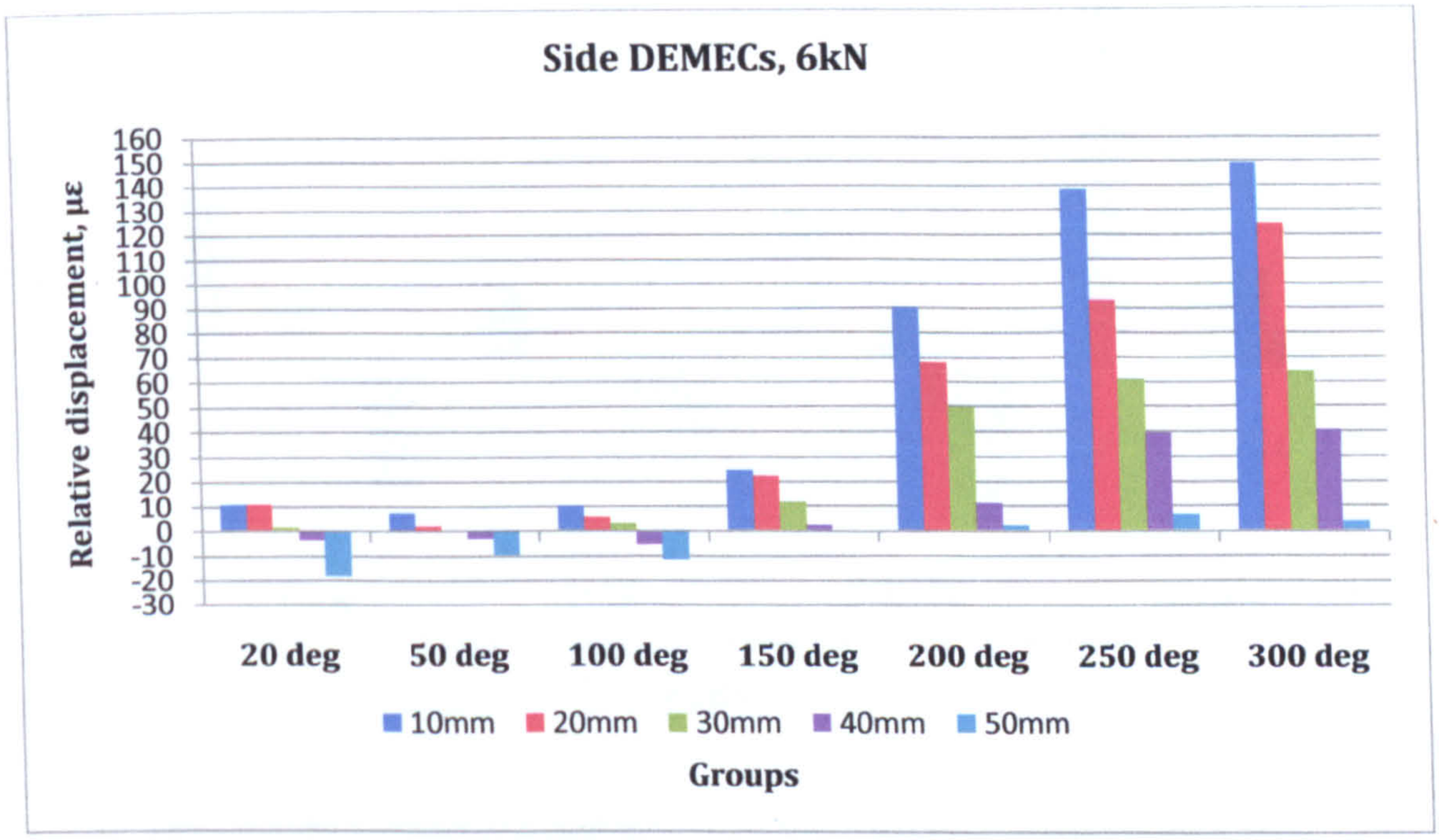

Figure VI-2 Effect of elevated temperatures on the side deformations of the concrete at 6kN

Groups 20°C to 100°C exhibited similar trend at 6kN the deformations with values of the relative displacement between 10 and -10 microstrain for the upper half of the prism, see Figure VI-2. Group 150°C registered an increase of the deformations with change of the neutral level to 50mm. The relative displacements for the higher temperature groups continued to increase reaching tensile deformations 15 times higher than those at room temperature. The distribution of the deformations through the height of the prism was observed to be close to linear with neutral axis below the 50mm level. The deformability at higher temperatures- 250°C and 300°C was influenced by two main factors: the reduction of the modulus of elasticity of concrete and the thermal effects on the mechanical properties of the adhesive and the CFRP laminate. The difference in the coefficients of thermal expansion

and the exposure to temperatures above the decomposition of the polymers resulted in residual cracks in the adhesive both between the laminate and the adhesive and between the adhesive and the concrete. Those were visible to the naked eye for all prisms from groups 250°C and 300°C. The disrupted connection at the end of the laminate resulted in a shift of the transferred stresses and local deformations and the failure crack towards the loaded end.

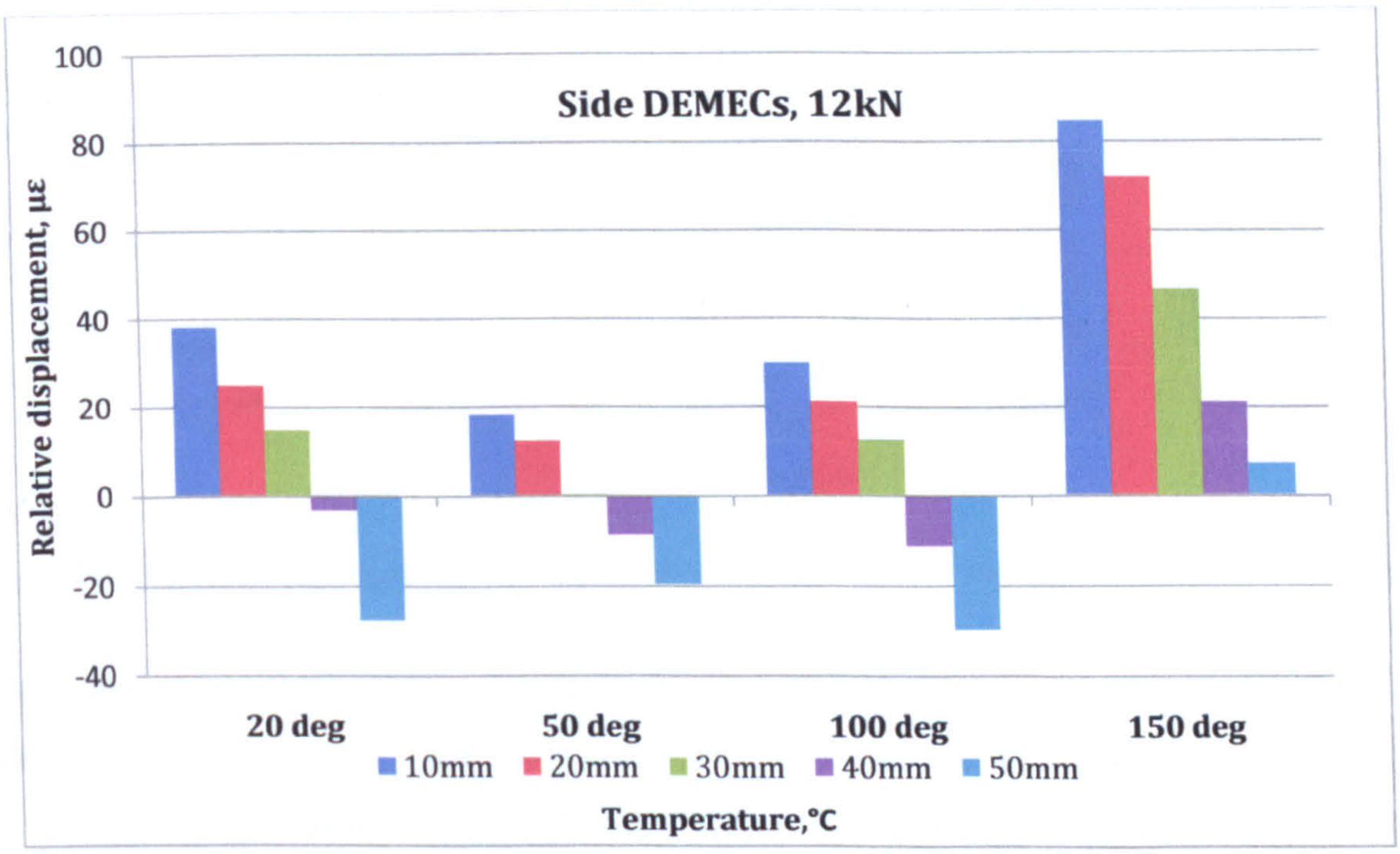

Figure VI-3 Effect of elevated temperatures on the side deformations of the concrete at 12kN

The change of deformations between 100°C and 150°C in the upper half of the prism was evident at 12kN, see Figure VI-3. Group 20°C exhibited tensile relative displacements to level 30mm with maximum value of 38 microstrain at level 10mm and -27 microstrain at level 50mm. Group 50°C then exhibited less deformability due to the curing of the adhesive layer and the concrete, achieving relative displacement between -20 and 20 microstrain in the upper half of the prism. The deformations of group 100°C increased to the values close to those registered for group 20°C with tensile strains above level 30mm. Thus parabolic decrease was observed from 20°C to 50°C and parabolic increase from 50°C to 150°C. Furthermore, at 150°C the tensile relative displacements were increased by more than 200% compared to 20°C and the distribution of tensile strains and stresses was entirely in the upper half of the prism.

6.1.3 Effect of elevated temperatures on the relative displacements between the concrete and the laminate

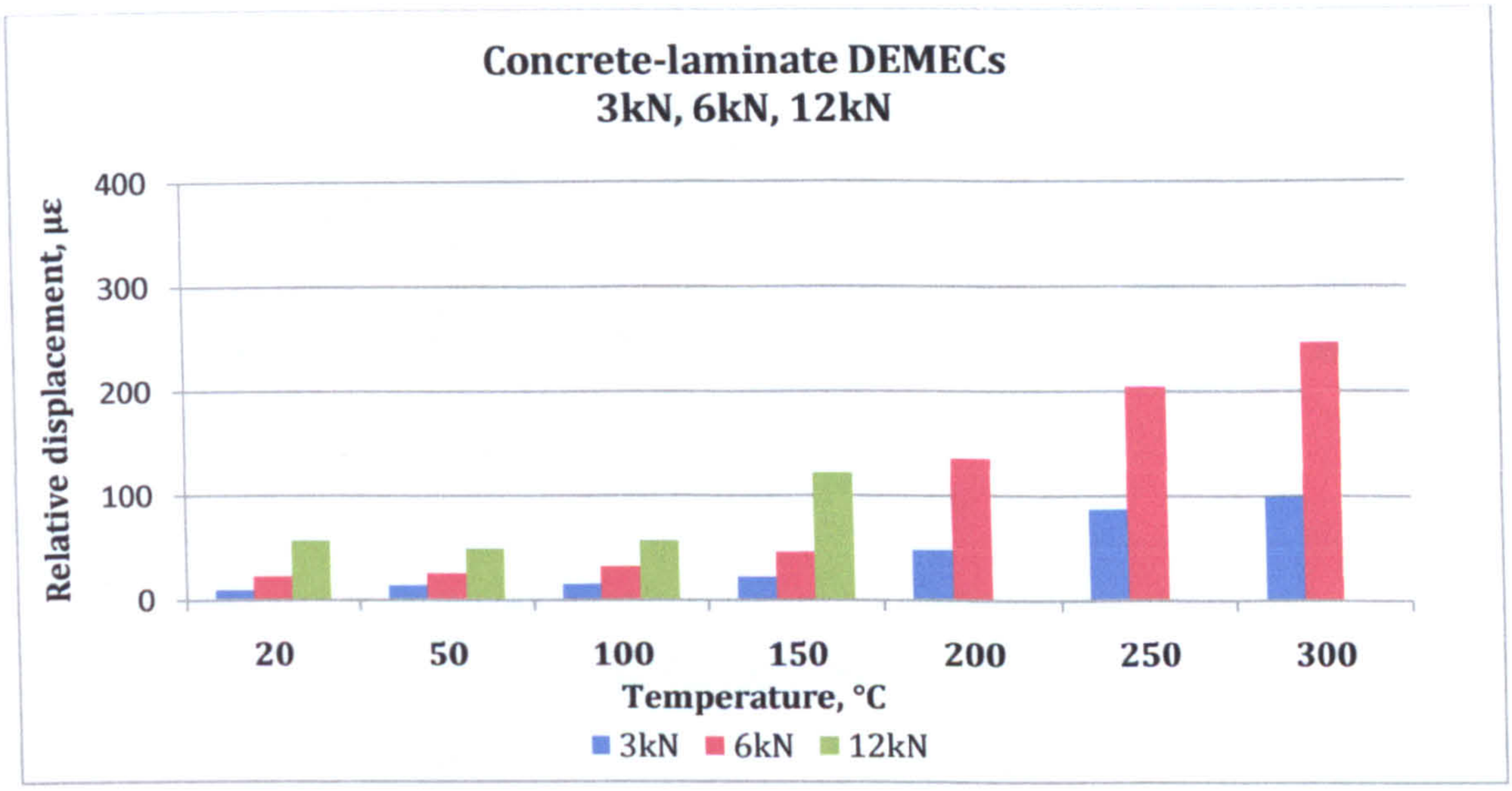

Figure VI-4 Effect of elevated temperatures on the local deformations between the concrete and the laminate at 3kN, 6kN, 12kN

The deformation measured at 3kN between the laminate and the concrete maintained low levels up to group 150°C. From 200°C to 300°C the relative displacements reached values 2 to 5 times higher than those at 150°C with rapid increase between 150°C and 250°C. The same tendency was observed at 6kN as the deformations increased 3 to 6 times more than the deformation of group 150°C. With increase of the load to 12kN the deformability of group 150°C increased reached values 2 times higher than the group 100°C. Thus, gradual increase of the deformability was observed with increase of the load from 3 to 12kN leading to a more pronounced parabolic law for the higher temperature groups.

6.1.4 Effect of elevated temperatures on the local deformations on the laminate (DEMEC strain gauges)

Over a distance of 150mm the relative displacement was measured between the loaded and far end of the laminate. For 3kN and 6kN the deformability of the laminate was found to decrease at 100°C by 20% and 6% respectively compared to the group 50°C.

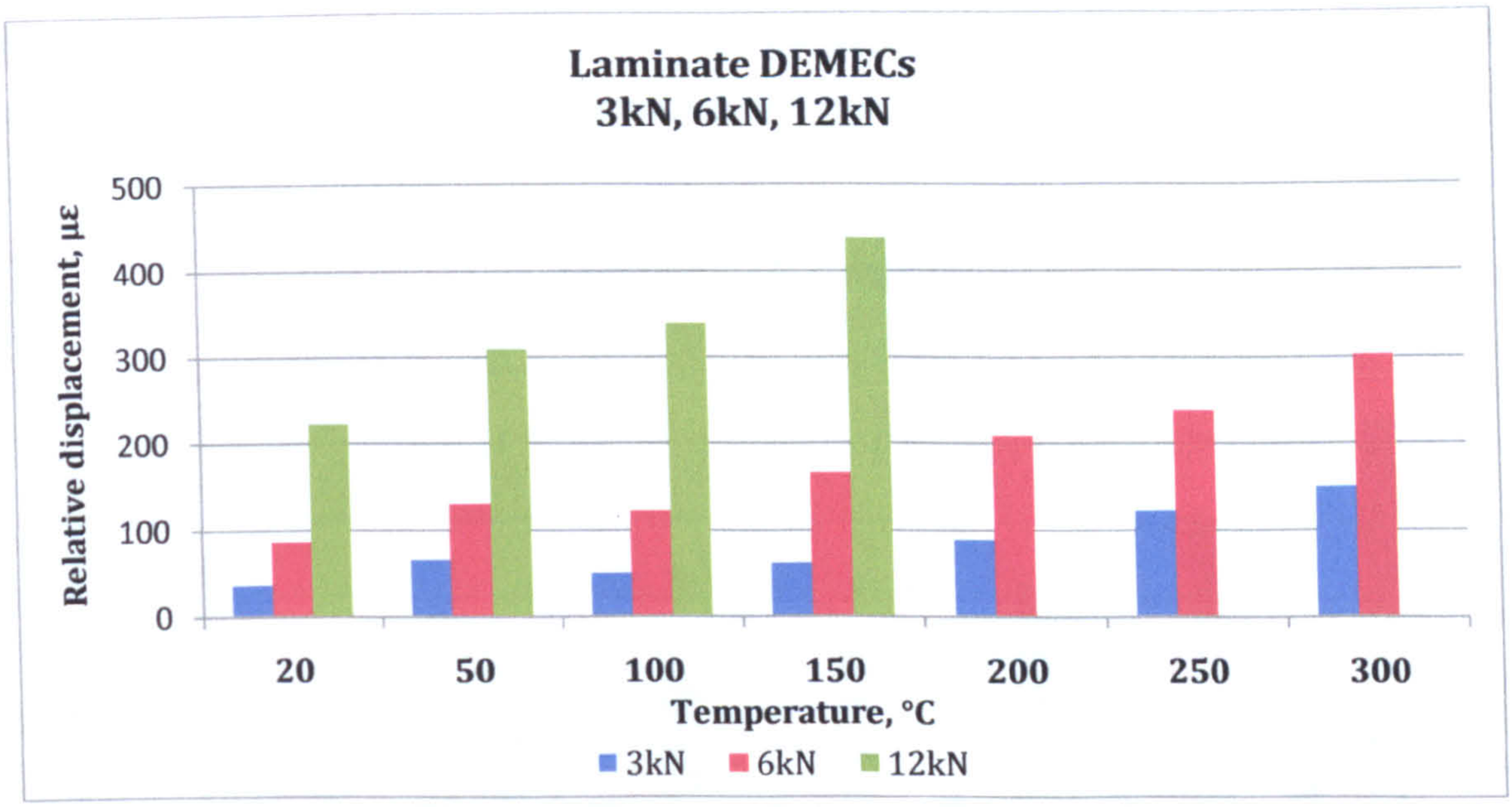

Figure VI-5 Effect of elevated temperatures on the local deformations on the laminate (DEMEC strain gauges) at 3kN, 6kN, 12kN

The local deformations registered a 10% increase at load 12kN compared to group 50°C. Above 150°C gradual increase of the relative displacements was observed. Overall, the local deformations between the loaded and far end of the laminate showed close to linear increase for groups 100°C to 300°C which included temperatures above T_{GM} of the laminate.

6.1.5 Effect of elevated temperatures on the local deformations on the laminate (ER strain gauges)

ER gauge 1 registered little increase of the deformations at 3kN up to 150°C and slight reduction for group 250°C. ER gauge 2 registered higher values for groups 200°C and 250°C with decrease of the deformations at 300°C. Finally the strain gauge closest to the loaded end of the laminate registered gradual increase of the local deformations from 100°C to 300°C. Two interesting effects were observed in this graph: group 100°C exhibited low deformations similar to those at room temperature and group 250°C which registered significant increase of the deformations by ER gauge 2 compared to the groups 200°C and 300°C. The higher deformability of the group could be attributed to an increase in the thermal cracking at the ends of the laminate and the transfer of higher stresses to the middle section of the bonded length. With increase of the temperatures above T_g of the adhesive significant reduction of the strength and stiffness could be expected. On the other hand, group 300°C experienced volume change of the laminate due to thermal changes of the

epoxy resin matrix and the composite action of the laminate was affected which resulted in a more gradual distribution of the deformations in the laminate.

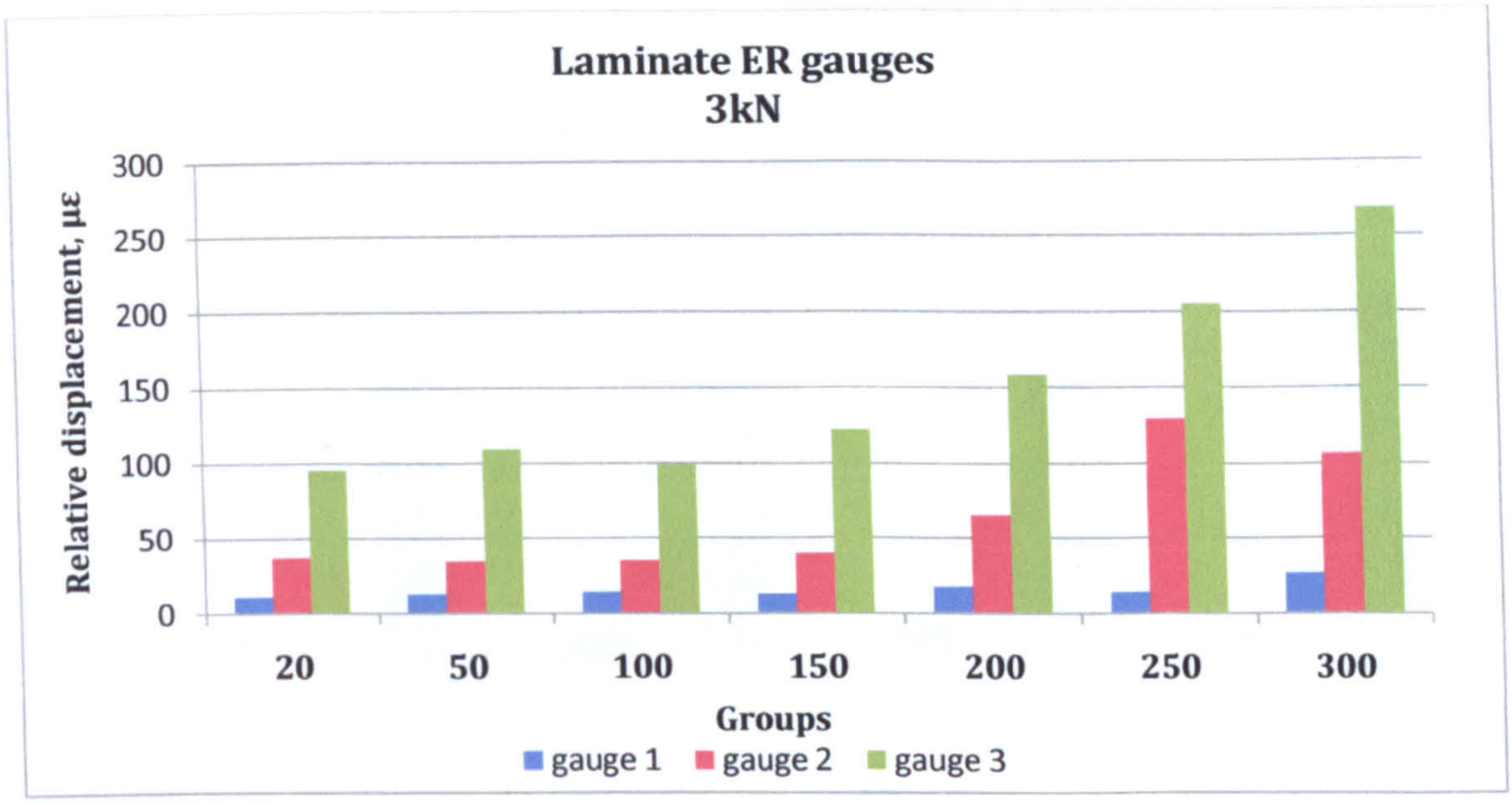

Figure VI-6 Effect of elevated temperatures on the local deformations on the laminate (ER strain gauges) at 3kN

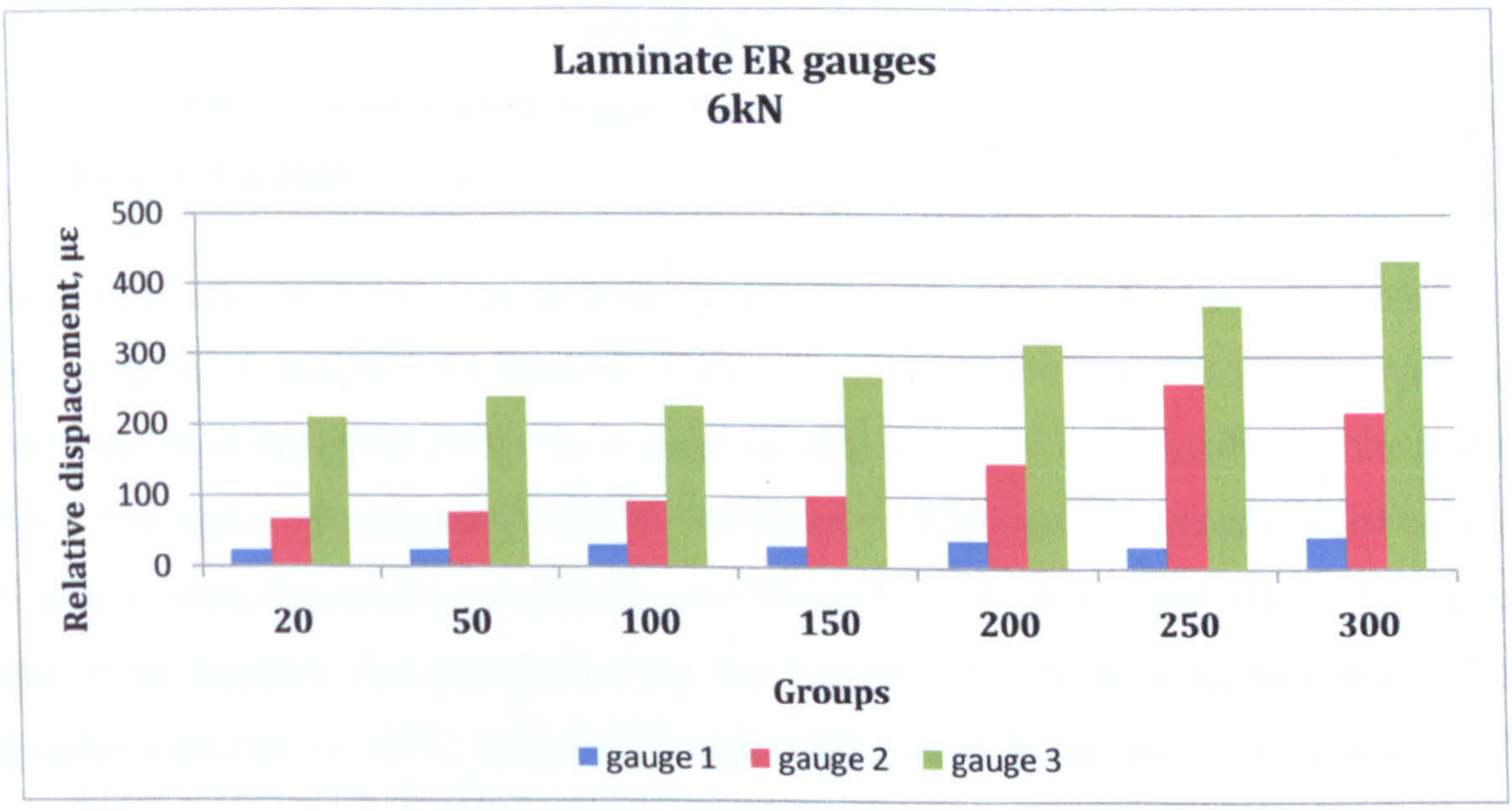

Figure VI-7 Effect of elevated temperatures on the local deformations on the laminate (ER strain gauges) at 6kN

Similar effects were observed at 6kN. Increase of the deformations was observed above 150°C but the rate of increase of the deformations decreased for groups 200°C to 300°C compared to the results at 3kN. For example, at strain gauge 3 group 20°C registered increase from 95 to 209 microstrain when the load was doubled and group 300°C registered

increase from 268 to 435 microstrain from 3kN to 6kN. The same tendency was observed at higher load of 12kN when the increase of the deformations could be approximated by a linear relationship.

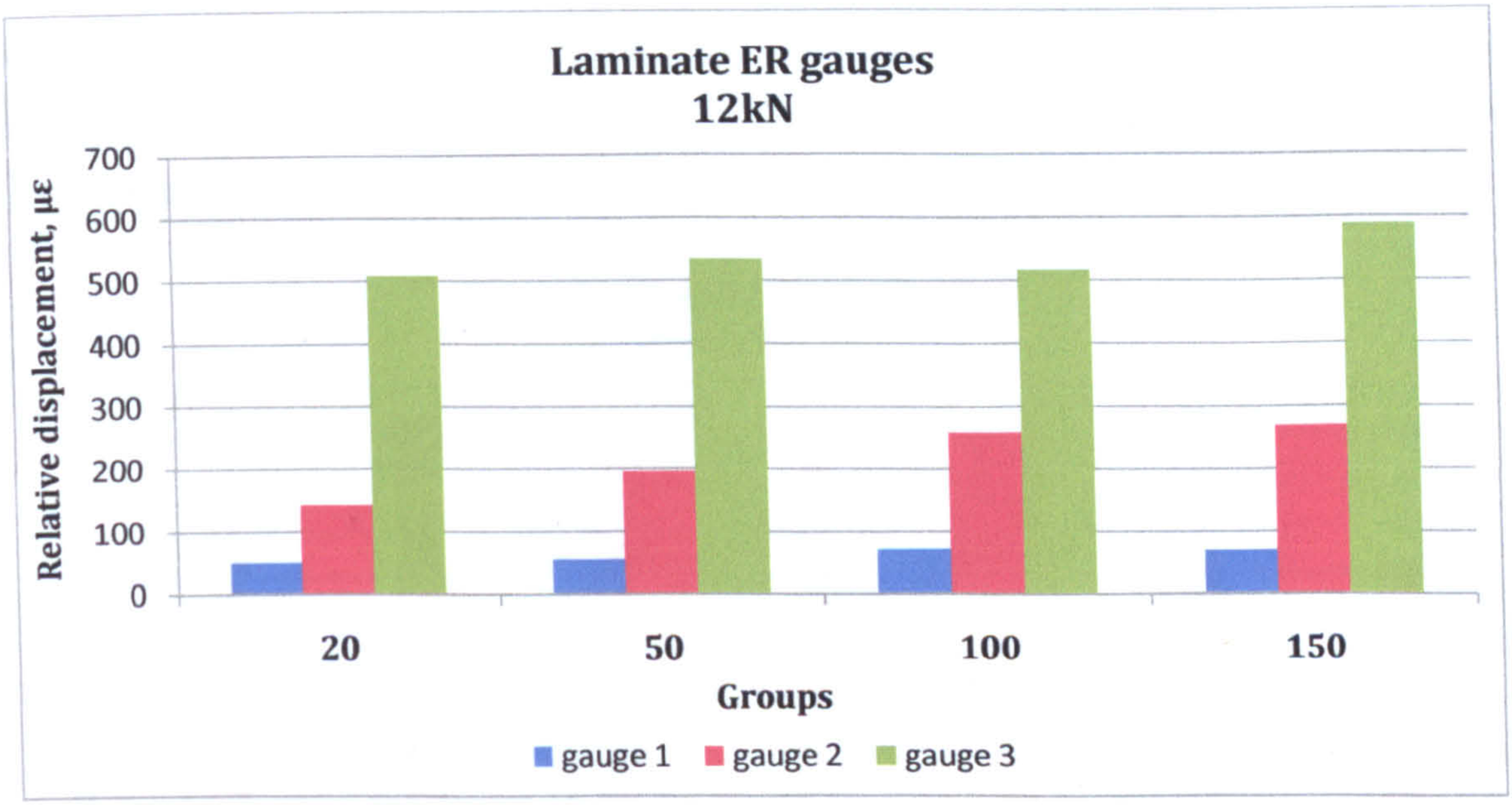

Figure VI-8 Effect of elevated temperatures on the local deformations on the laminate (ER strain gauges) at 12kN

6.1.6 Effect of elevated temperatures on bond strength of CFRP bonded joints

The compressive strength of the different groups was obtained at the time of the testing of the strengthened samples. An increase in the strength by 17% from the room temperature was established for group 50°C which could be attributed to the curing effect of the heating phase. For higher temperatures to 200°C the achieved compressive strength varied between 43 and 42 MPa followed by a reduction by 18% and 26 % for 250 and 300°C. The failure load of the samples was also plotted for the 7 groups. A similar trend was observed for samples heated up to 100°C, followed by rapid decrease of the failure loads between 150°C and 200°C by more than 50%. Groups 250°C and 300°C exhibited similar behaviour as group 200°C and registered slightly lower failure loads. Thus, it could be said that CFRP strengthened concrete samples exposed to temperatures between 200°C and 300°C would fail at about 70% lower loads compared to room temperature samples, but above 200°C no significant reduction of the failure load was established.

The tensile strength of the concrete is the main failure factor for the occurrence of cracks in concrete; in particular for plate end failure modes of FRP plated RC beams. Due to the large scatter of results of tensile strength for heated and cooled concrete a straightforward relationship was difficult to be proposed. However, for samples heated to 150°C the reduction of the strength of the system was found to be less than 20% compared to room temperature samples. The failure load was found to drop to 1/3 of the room temperature load above 200°C.

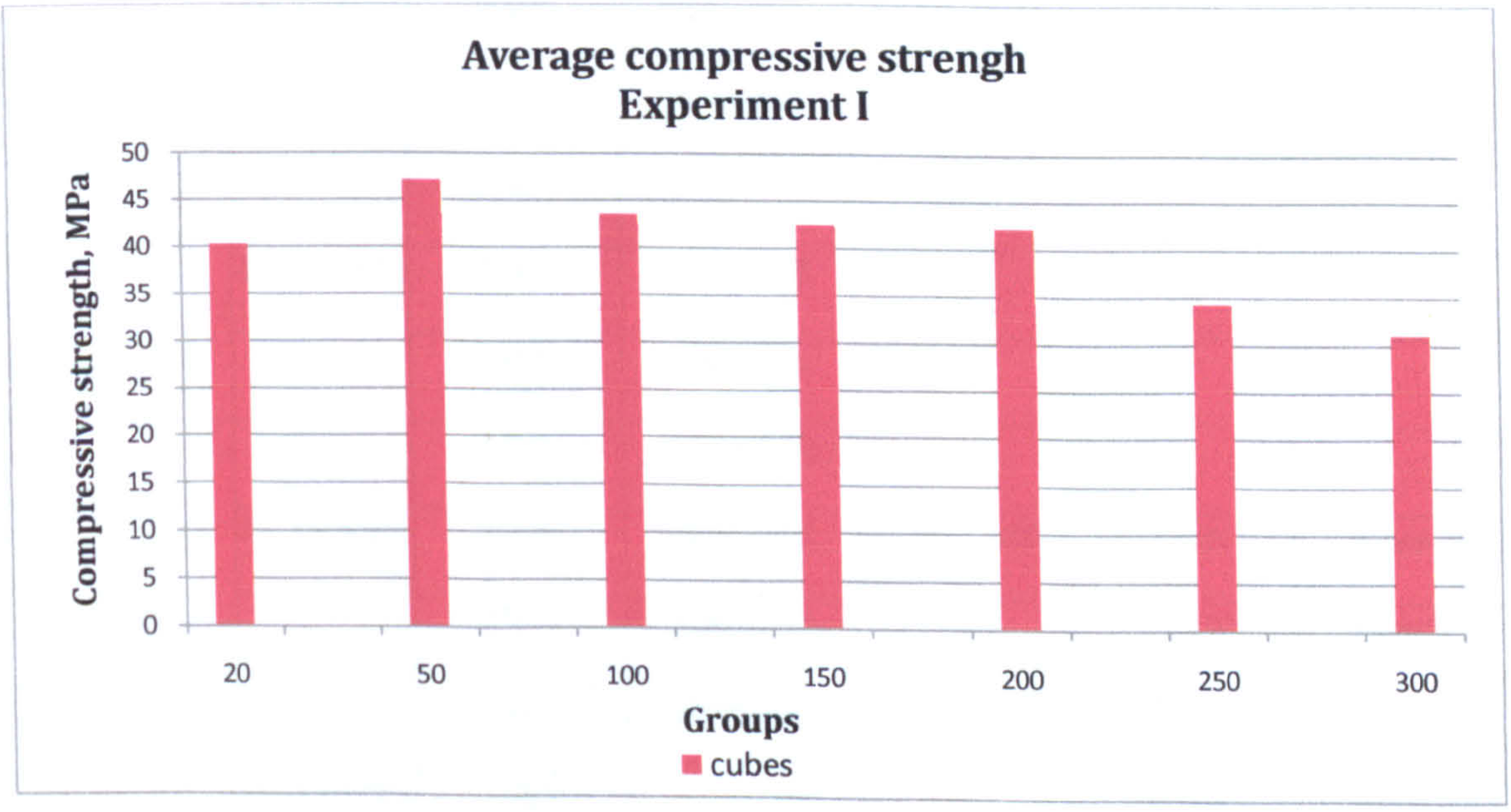

Figure VI-9 Average failure load, cubes

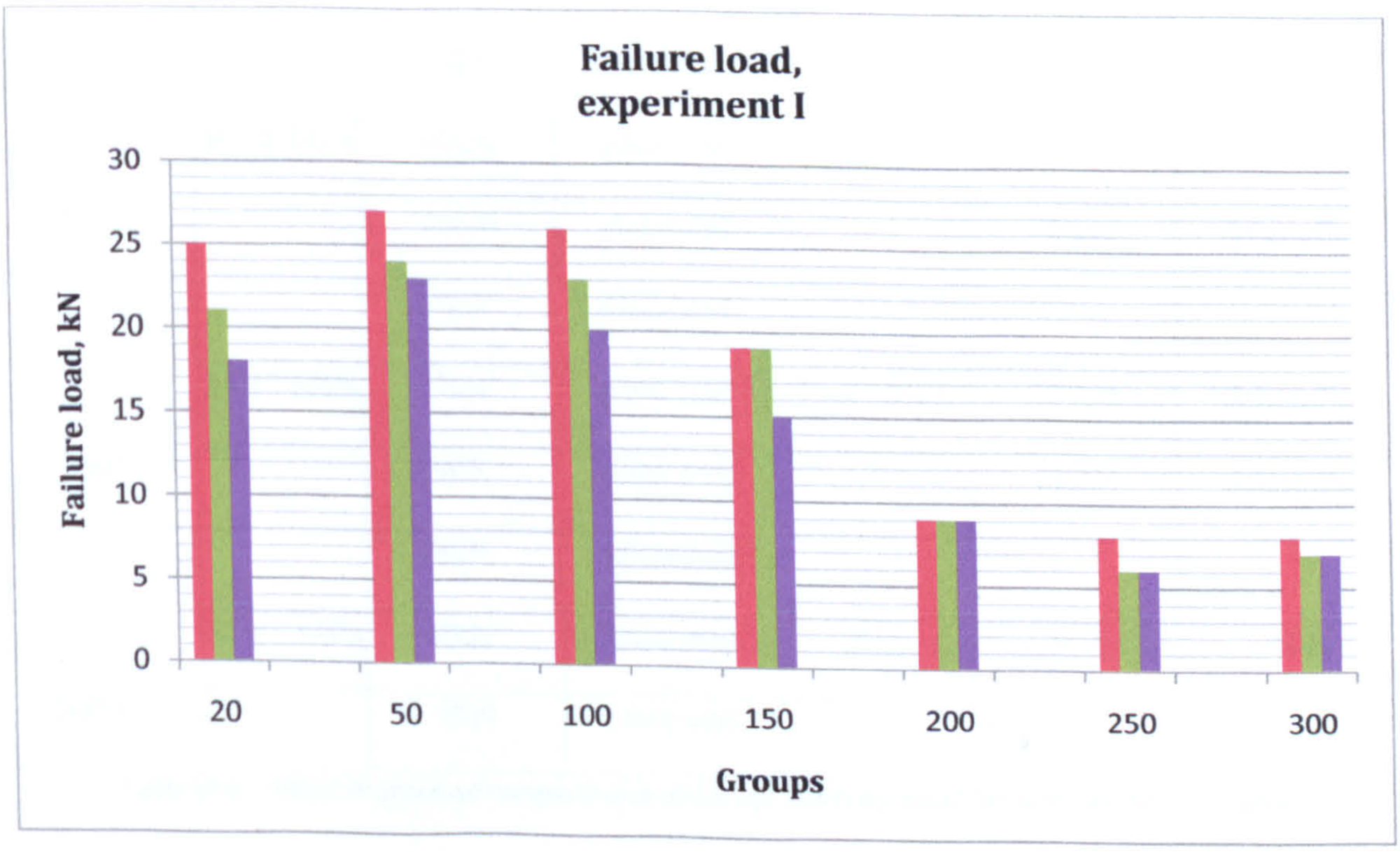

Figure VI- 10 Failure load of CFRP-to-concrete bonded joints

6.1.7 Effect of elevated temperatures and plate width on bond strength and failure modes

	80mm			50mm		
Temperature	**Cubes**	**Failure load**	**Failure mode**	**Cubes**	**Failure load**	**Failure mode**
20°C		19kN	plate-end		24 kN	plate-end
	40.2 MPa	25kN	plate-end	44.63 MPa	20 kN	plate-end
		21kN	plate-end			
50°		27kN	plate-end			
	47.15 MPa	24kN	plate-end	N/A	N/A	N/A
		24kN	plate-end			
100°		27kN	debonding			
	43.15 MPa	21kN	plate-end	44.453 MPa	25 kN	plate-end
		23kN	plate-end		28 kN	plate-end
150°		19kN	plate-end			
	42.15 MPa	19kN	plate-end	N/A	21 kN	plate-end
		16kN	plate-end		20 kN	plate-end
200°		10kN	plate-end			
	39.18 MPa	10kN	plate-end	44.26 MPa	15 kN	debonding
		10kN	plate-end		15 kN	debonding
250°		7kN	plate-end			
	34.13 MPa	7kN	plate-end	33.62 MPa	11 kN	debonding
		9kN	plate-end		11 kN	debonding
300°C		8kN	plate-end			
	31.01 MPa	8kN	plate-end	N/A	N/A	N/A
		9kN	plate-end			

Table VI-1 Effect of elevated temperatures and plate width on bond strength and failure modes

The effect of two plate widths (80mm and 50mm) with the same width of the concrete prism was studied. After the samples had been heated to elevated temperatures and cooled the failure modes and loads were compared. The experimental results obtained for this study and the work conducted by Ali (2010) at Kingston University were used.

The width of the plate and the exposure to elevated temperatures were found to have a significant influence on the failure load and mode. All but one samples strengthened with a 80mm width plate failed, due to a crack in the concrete at the end of the laminate. Samples strengthened by 50mm width plate failed in two different ways: up to 150°C the failure was in the concrete and for higher temperatures debonding between the concrete and the laminate was observed. Thus it could be expected that the bond strength at elevated temperatures could depend on the strength of the materials and the ratio of the strengthening to the width of the beam.

6.1.8 Physical changes of heated and cooled CFRP-to-concrete joints with temperature

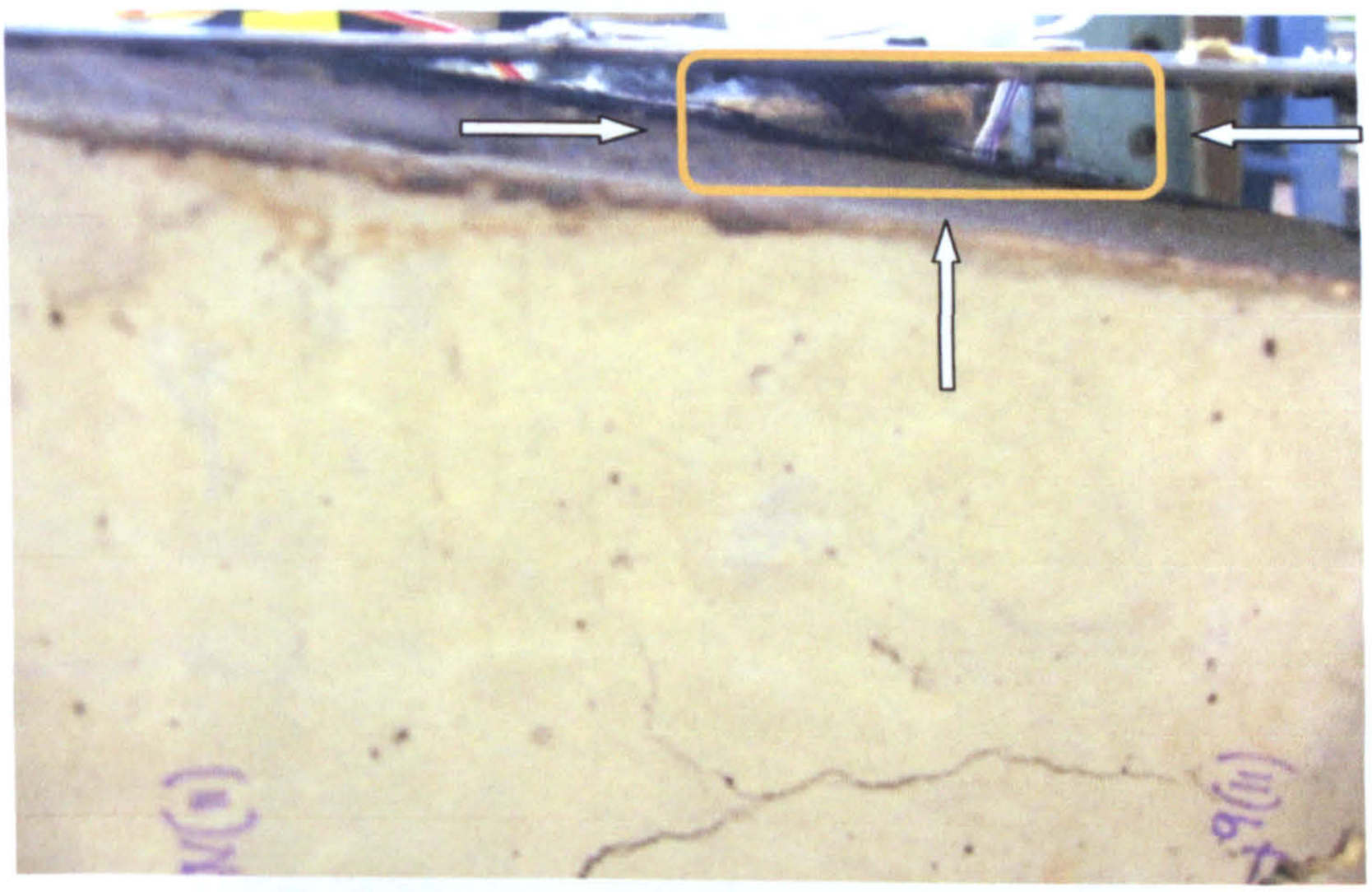

Figure VI- 11 Separation of fibres from laminate, group 250°C

During the testing of the samples several physical changes of the adhesive layer and laminate were observed. For group 250°C and 300°C separation of the external layer of fibres was observed and fibres attached to the adhesive were found after the samples had been tested. Colour change of the adhesive was found to be the main indicator for the maximum temperature as visible change was observed above 150°C. The adhesive was

brown at 200°C and at 250°C it changed to dark brown or black. At 300°C the adhesive was found to turn black but unlike the lower temperatures the laminate was found to change its volume.

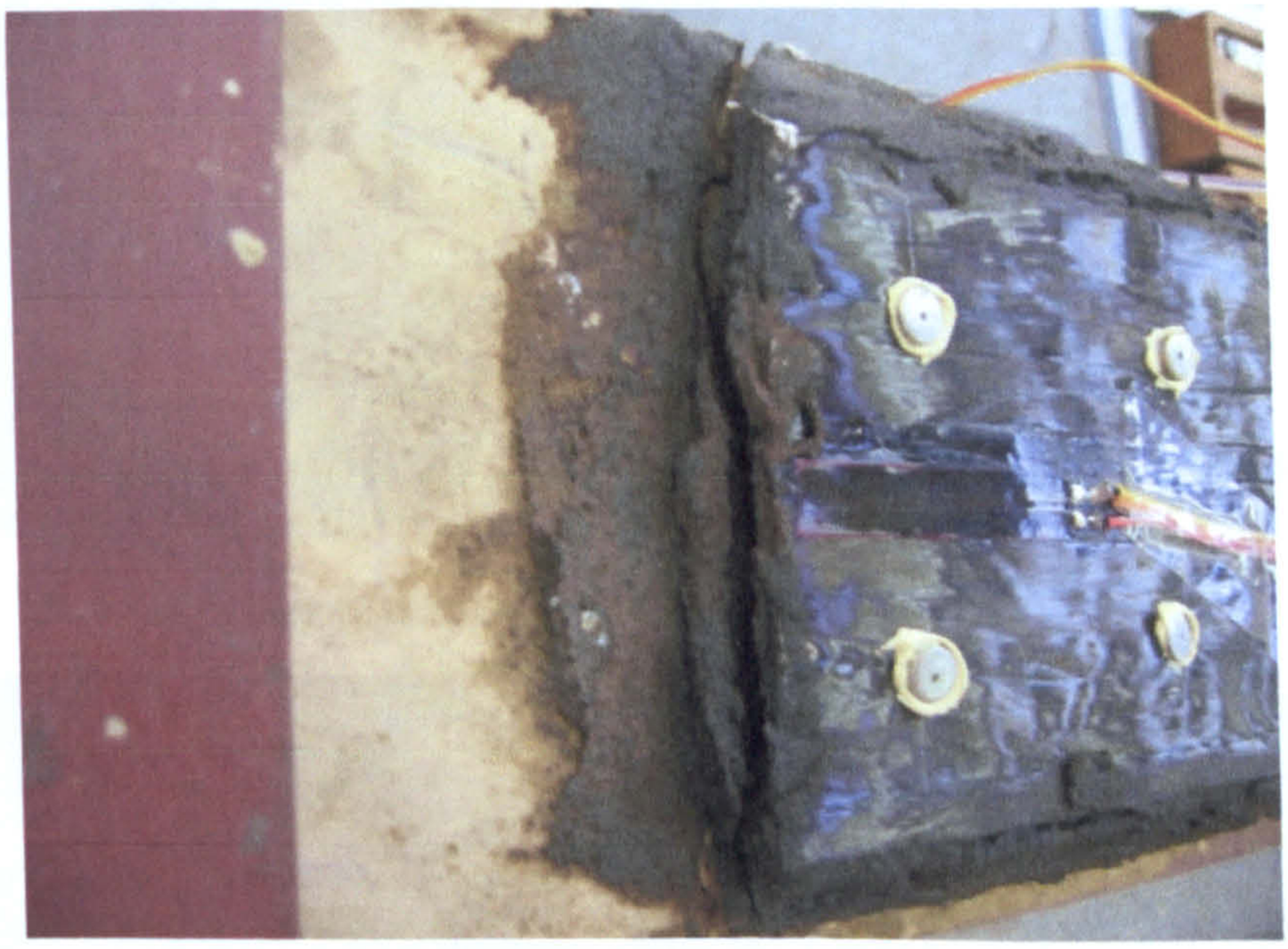

Figure VI- 12 Laminates exposed to 300°C

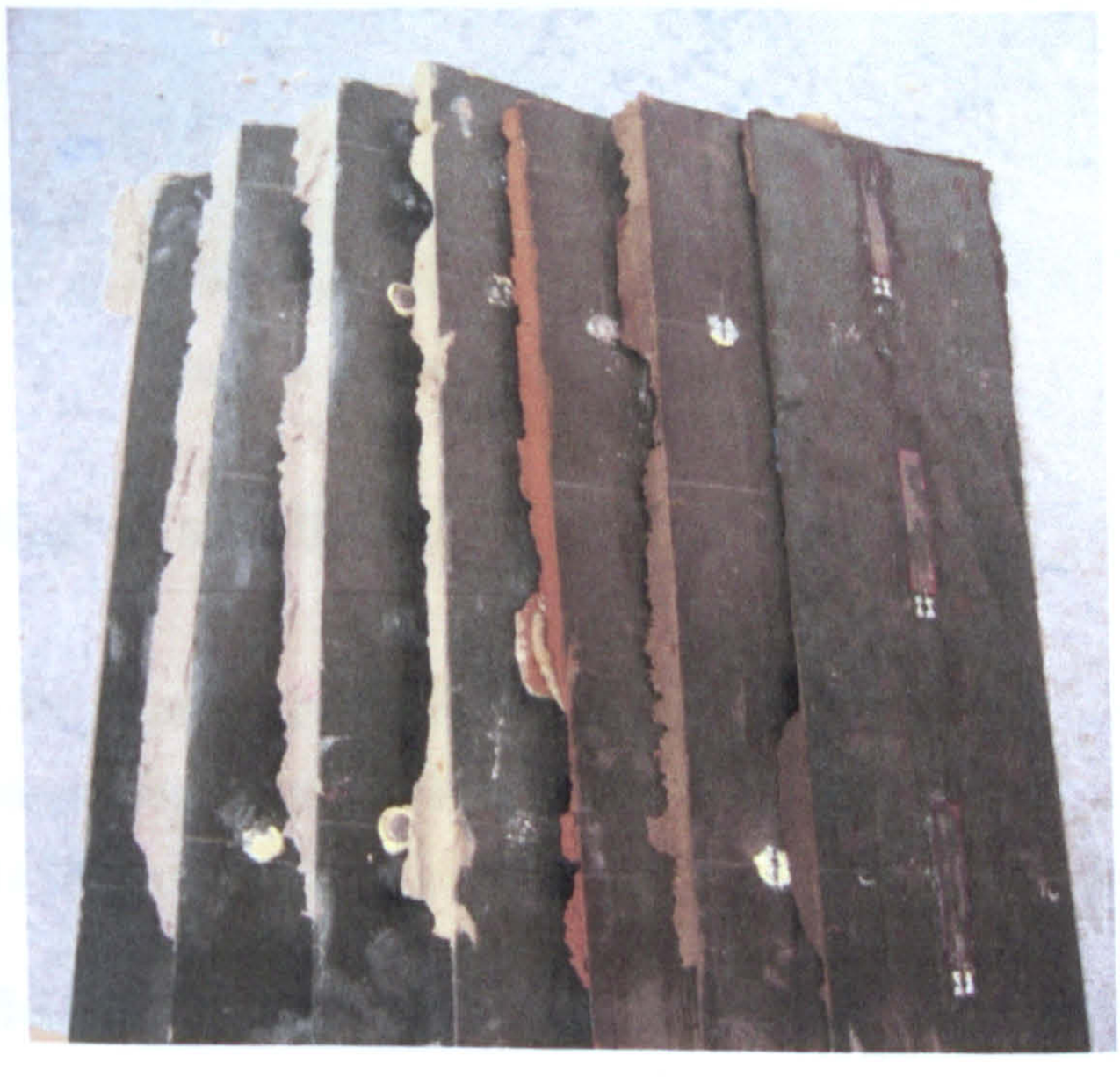

Figure VI- 13 Colour change of the adhesive for groups 20°C to 300°C

Another change in the behaviour of heated samples was observed above 200°C. The separation between the laminate and the adhesive was brittle and did not require significant increase in the load but at 250°C it was found that the propagation of the crack was gradual and it was dependant on the applied load.

Figure VI-14 Deformability of a sample, group 250°C

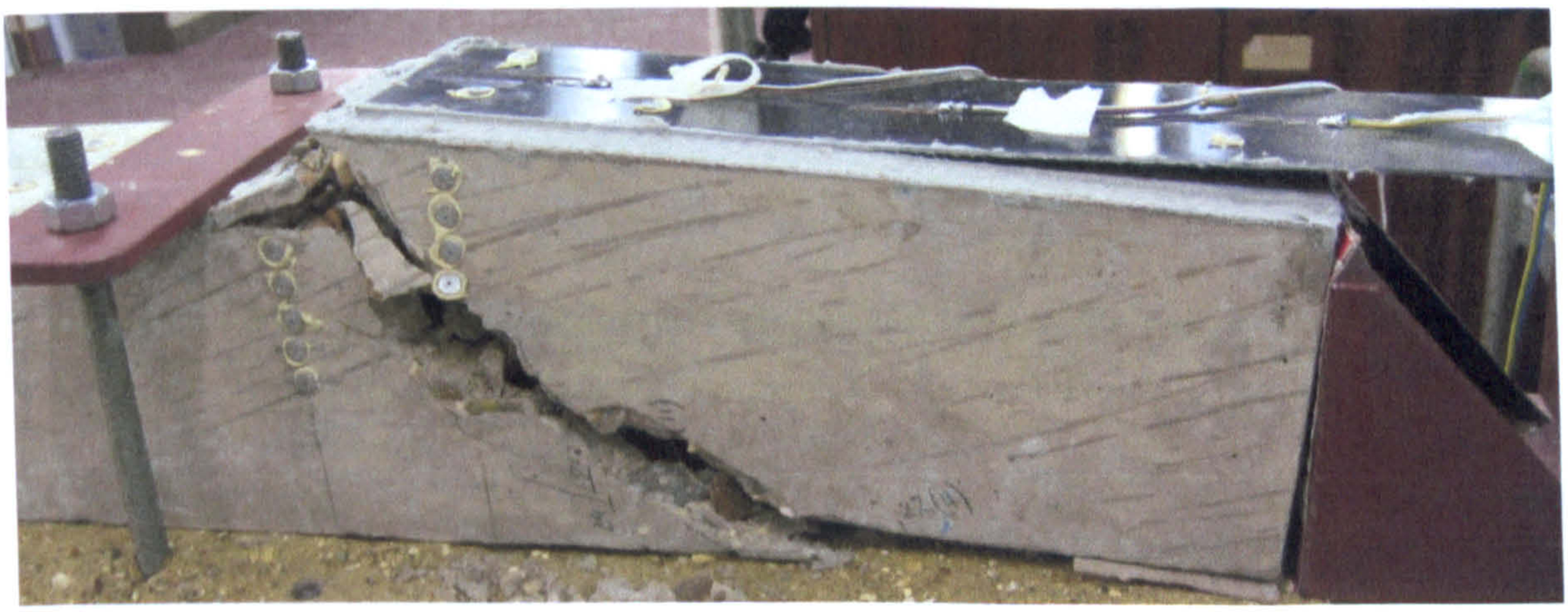

Figure VI- 15 Deformability of a sample, group 50°C

6.2 Heating of small-scale CFRP strengthened RC beams

The results from the second experimental study was analysed in this section. The effect of elevated temperatures was compared for the different temperatures at the end of the heating phase, at the end of the cooling phase and when the minibeams were unloaded.

6.2.1 Deflection of loaded and heated beams 50°C to 300°C

The obtained deformations at the end of the heating process were plotted for each sample and average per group. It should be mentioned that above 50°C T_g of the adhesive was exceeded which for heated samples resulted in reduction of the strength and higher deformability. Increase in deflection from 1.43mm to 2.01mm was found for temperatures

from 50°C to 300°C. Gradual increase of the deflection was observed in the experimental data.

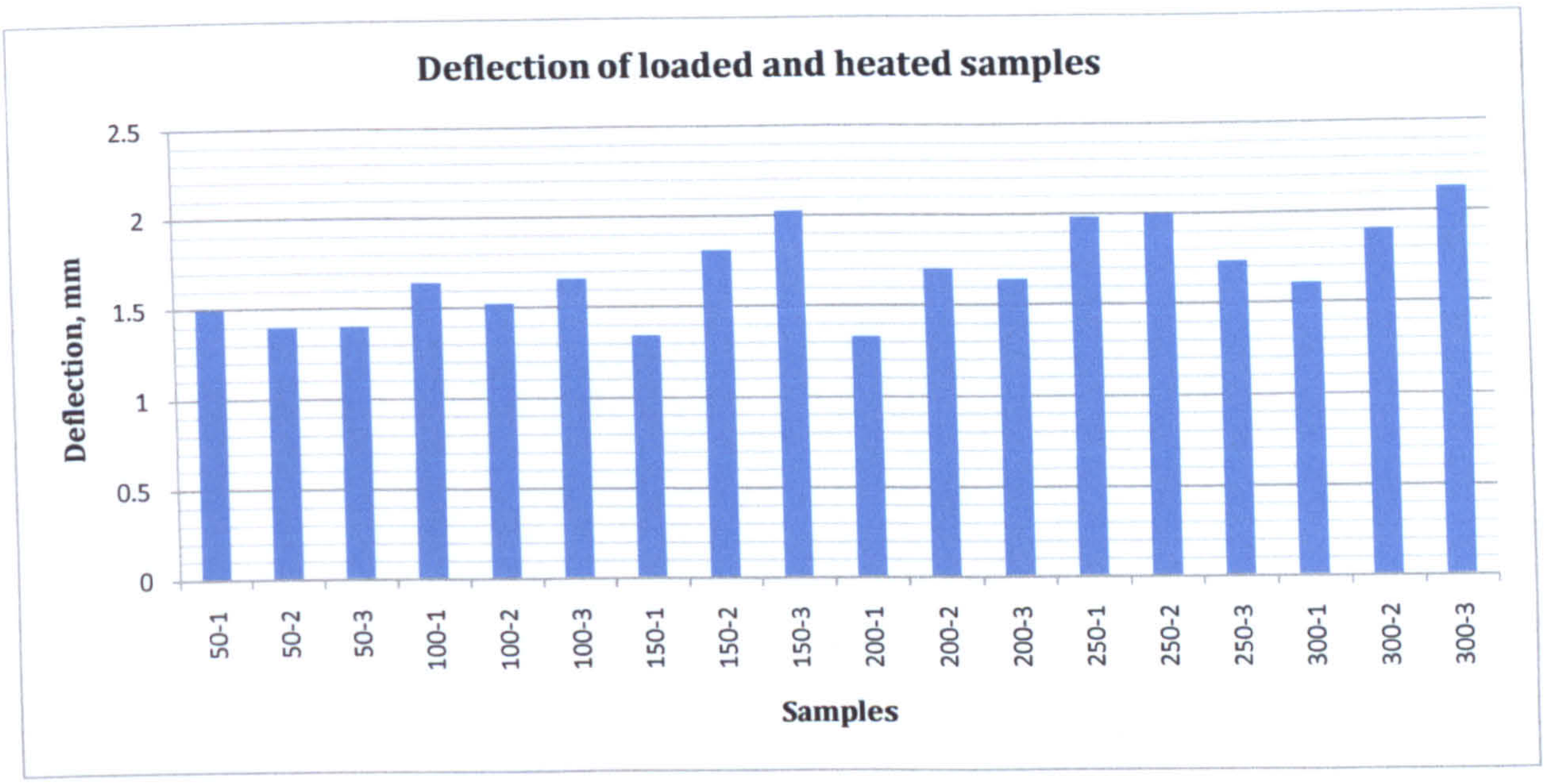

Figure VI- 16 Deflection of loaded and heated samples, 50°C to 300°C

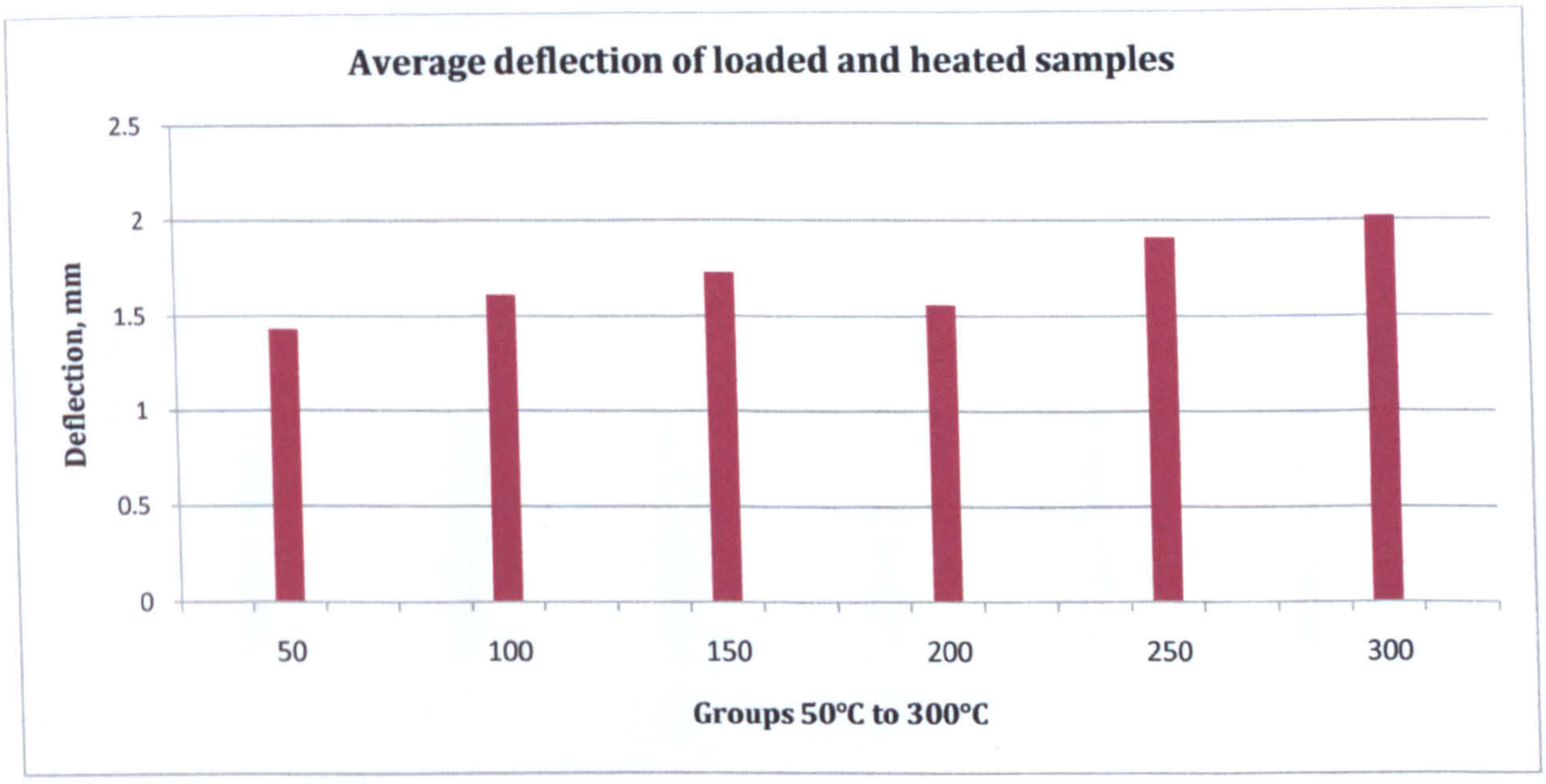

Figure VI-17 Average deflection of loaded and heated samples, 50°C to 300°C

6.2.2 Deflection of loaded and cooled beams 50°C to 300°C

Gradual increase of the deflection readings was also observed obtained at the end of the cooling process before the unloading of the system. From 50°C to 300°C the deflection increased from 1.36mm to 2.57mm. For low levels of heating the deformation at the end of

the cooling process would be recovered but for higher temperatures above 200°C residual deflection was recorded as an indication for irreversible thermal effects.

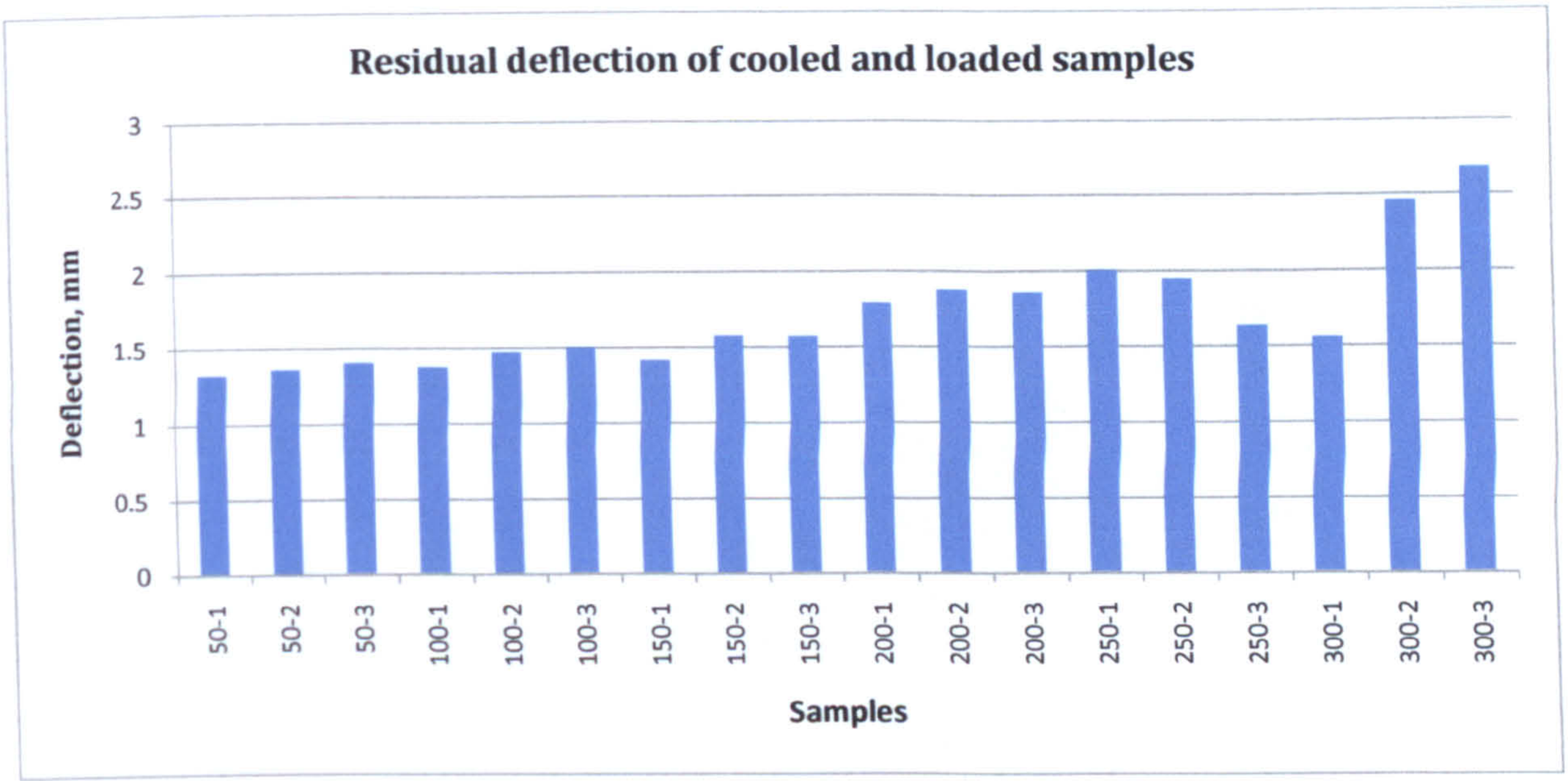

Figure VI-18 Residual deflection of loaded and cooled samples, 50°C to 300°C

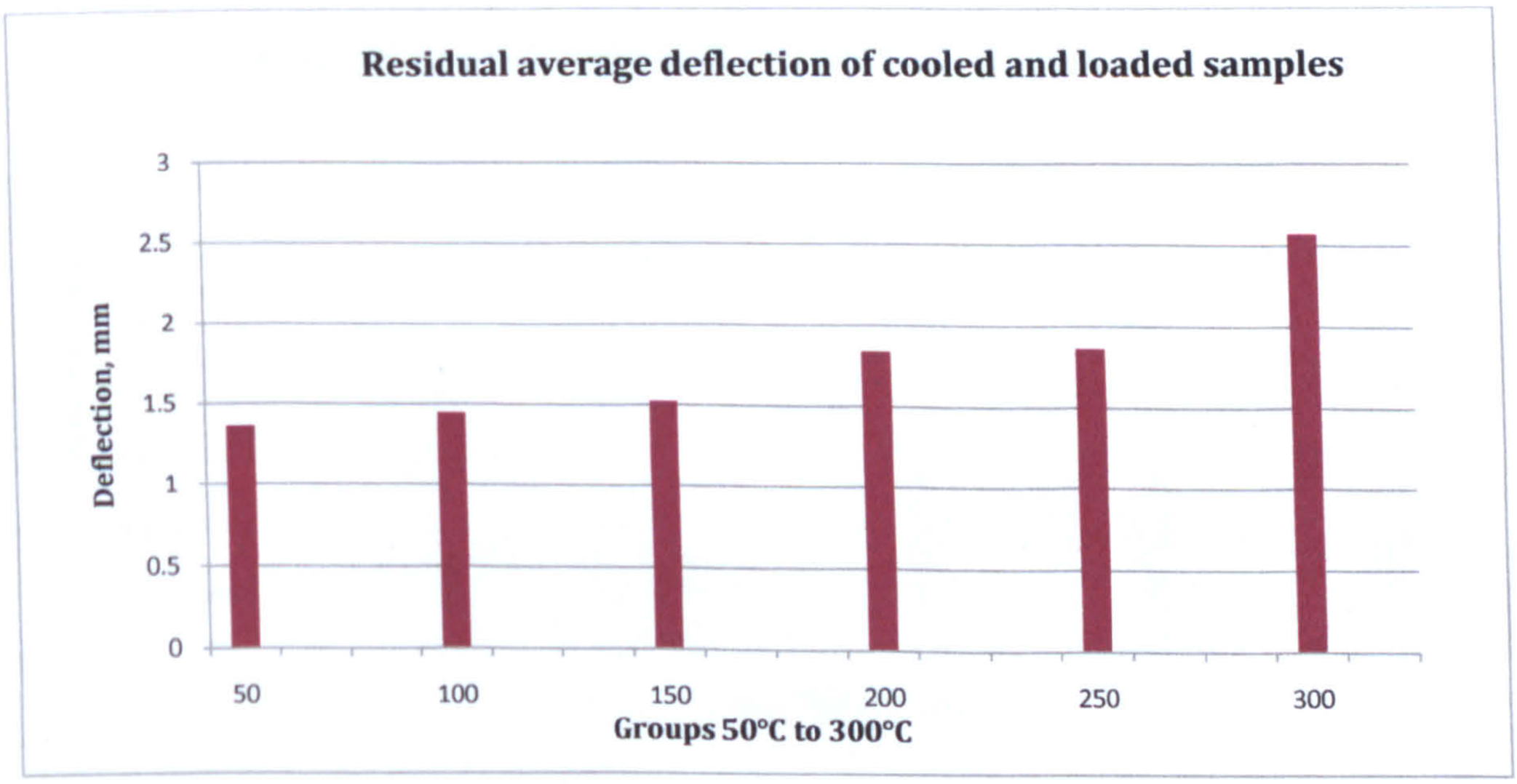

Figure VI-19 Residual average deflection of loaded and cooled samples, 50°C to 300°C

6.2.3 Residual deflection of cooled and unloaded beams 50°C to 300°C

The minibeams were unloaded and the measured deflections were compared. For temperatures up to 150°C the results varied between 0 and 0.2mm and above 150°C distinct increase of the residual deformation was observed reaching a maximum at 300°C of

1.15mm. Thus the residual strength of loaded and heated CFRP strengthened systems would be most affected when heated to 200°C and above.

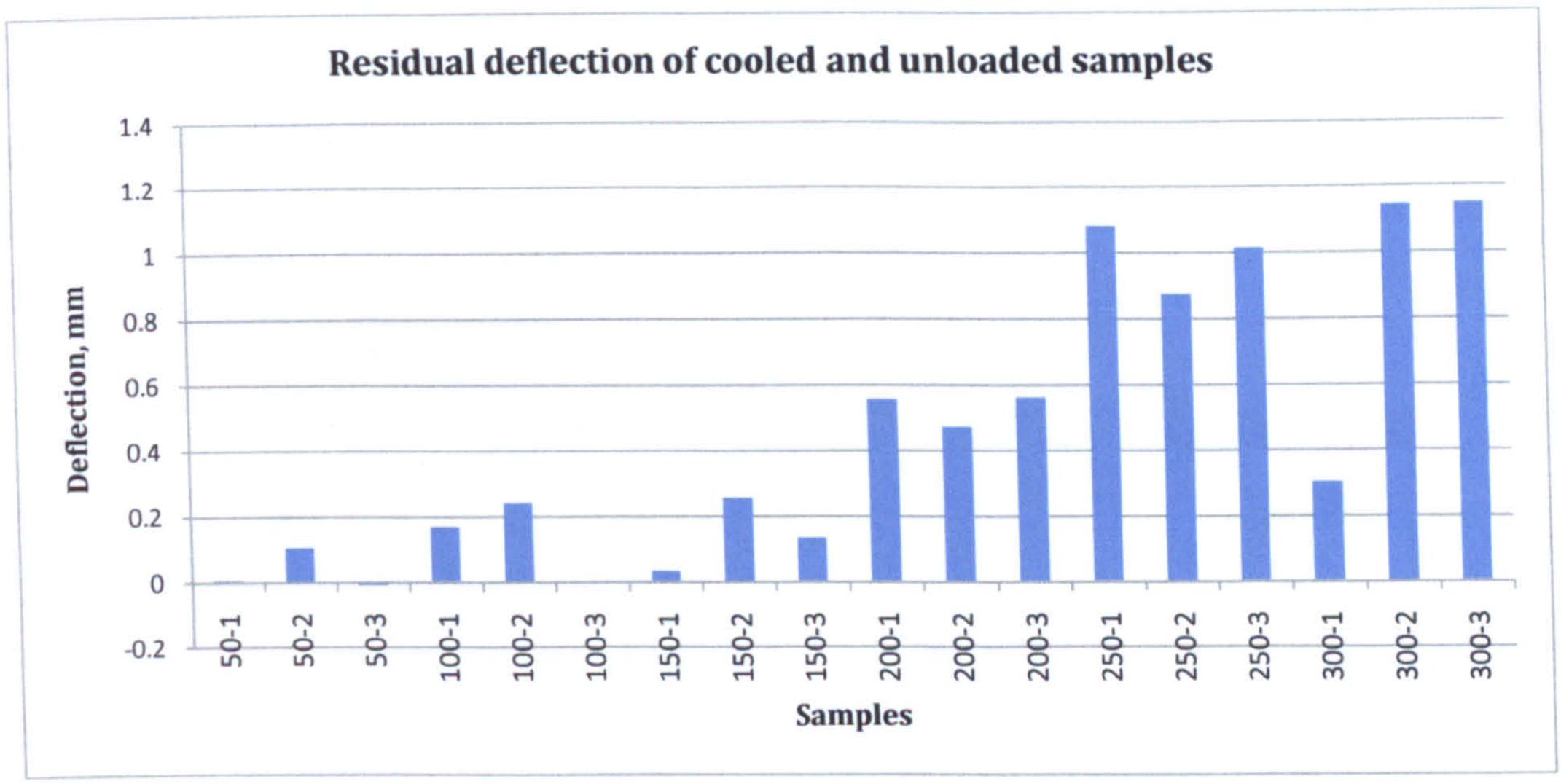

Figure VI-20 Residual deflection of cooled and unloaded samples, 50°C to 300°C

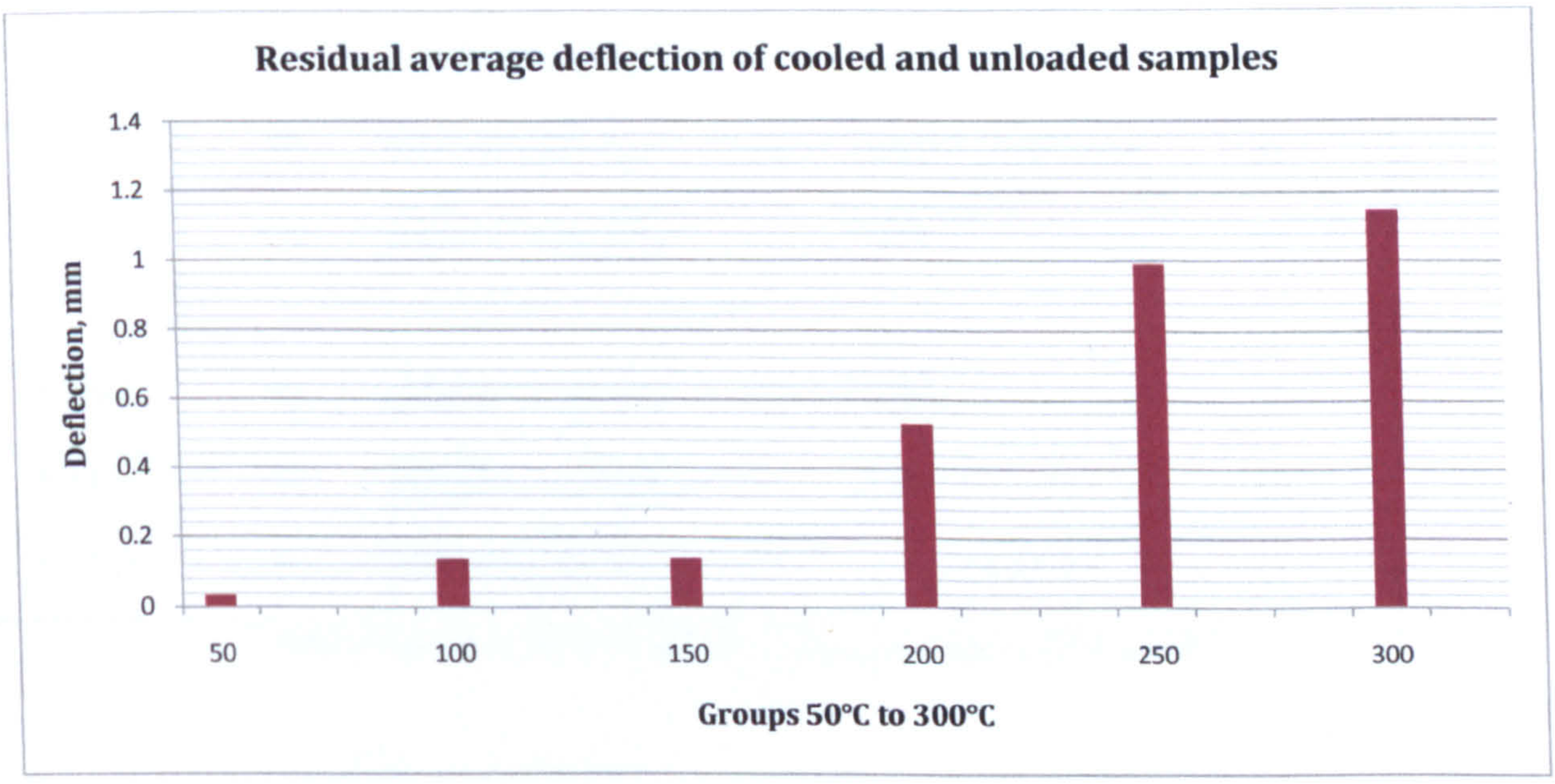

Figure VI-21 Residual average deflection of cooled and unloaded samples, 50°C to 300°C

6.2.4 Residual length of bond after heating and cooling 150°C to 300°C

The heating and cooling processes for loaded minibeams resulted in thermal cracks visible by the naked eye. Two samples from group 150°C and 200°C were found to be affected by

the different rates of expansion of the adhesive, concrete and laminate. This trend was observed for all samples in group 250°C and 300°C where the length of the cracks was found to increase with the increase of the temperature. Therefore the residual strength of the strengthened systems would be reduced not only due to change of the material properties but also the reduced length of the bond.

	Right end		Left end		
Sample	**Crack length**	**Between**	**Crack length**	**Between**	**Residual length**
	mm		**mm**		**mm**
#150-1	13	adhesive-laminate			187
#200-3			50	adhesive-concrete	150
#250-1	90	adhesive-concrete	30	adhesive-concrete	80
#250-2	30	adhesive-laminate	130	adhesive-laminate	40
#250-3	112	adhesive-concrete	17	adhesive-laminate	71
#300-1	60	adhesive-concrete	85	adhesive-laminate	55
#300-2	62	adhesive-concrete	92	adhesive-concrete	46
#300-3	52	adhesive-concrete	125	adhesive	23

Table VI-2 Residual length of bond after heating and cooling 150°C to 300°C

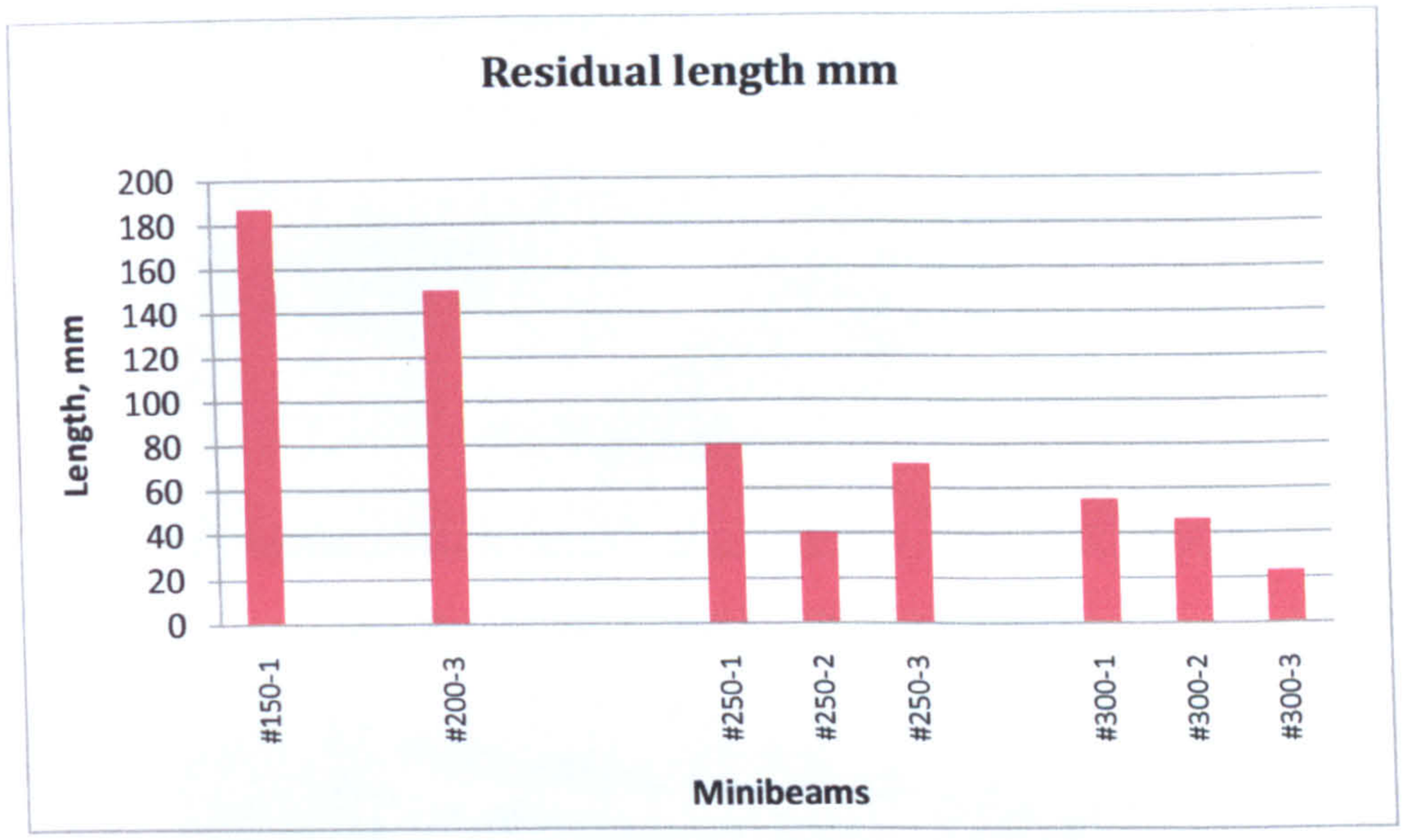

Figure VI-22 Residual length of bond after heating and cooling 150°C to 300°C

6.2.5 Physical changes of heated and cooled CFRP strengthened minibeams

Change in the colour of the adhesive at 200°C was also observed in this experimental study. The colour was black at 250°C as an indication for the exceeded decomposion temperature and the significant reduction of strength of the material. As previously observed volume changes of the laminate were observed at 300°C.

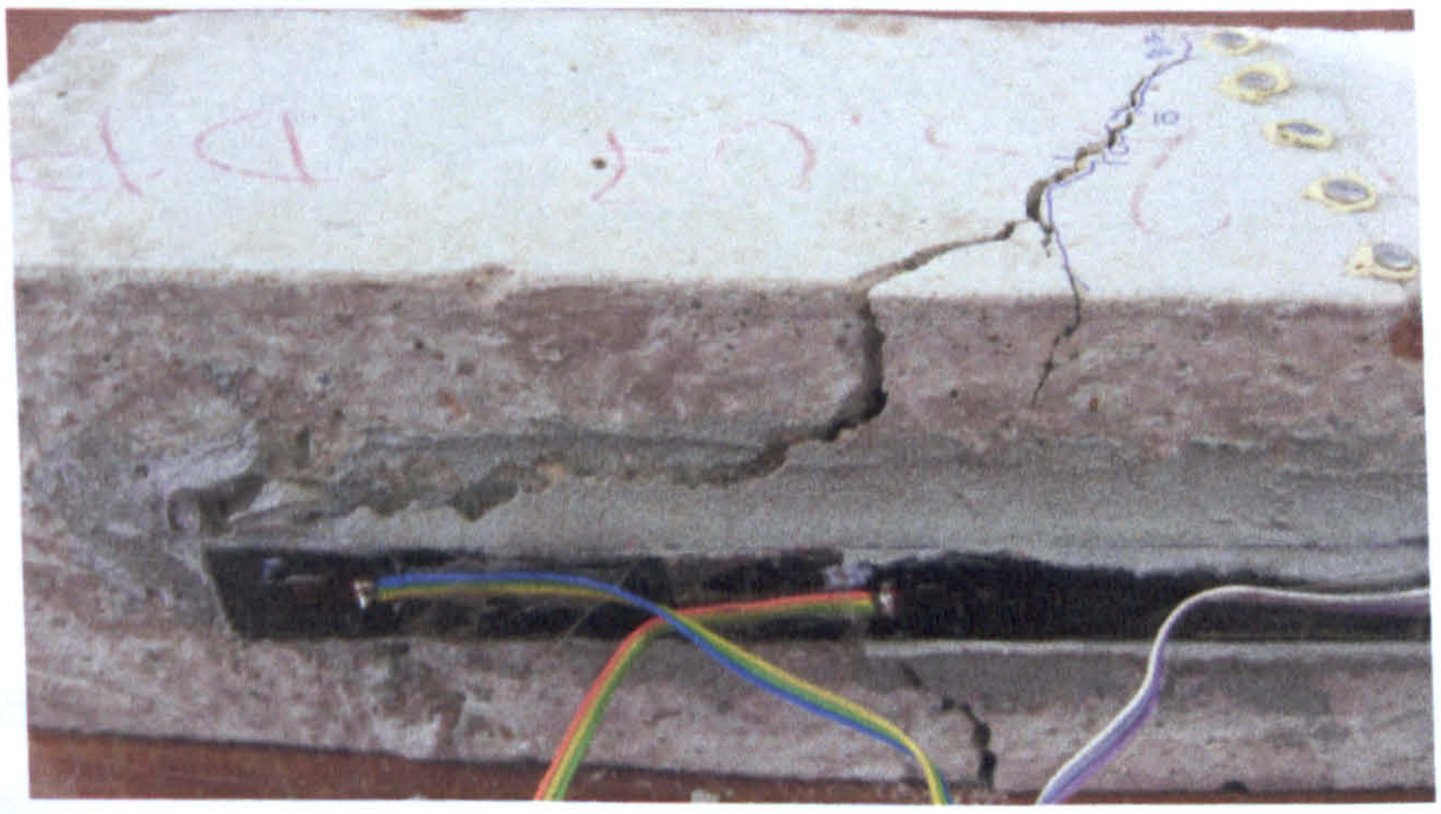

Figure VI- 23 Tested minibeam heated to 150°C

Figure VI-24 Minibeam heated to 200°C before testing

Figure VI- 25 Minibeam heated to 250°C before testing

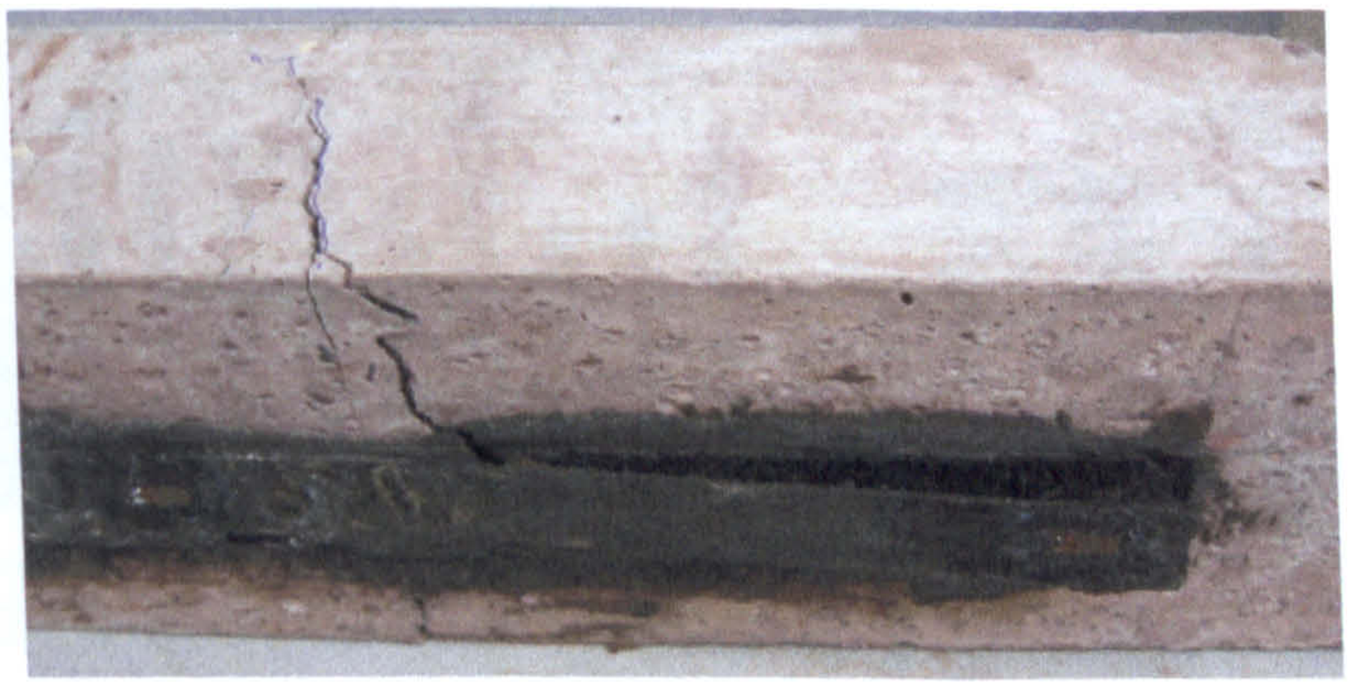

Figure VI- 26 Tested minibeam heated to 300°C

6.3 Residual strength of CFRP strengthened beams after heating

The third experiment determined the residual strength of CFRP strengthened minibeams after they had been heated to elevated temperatures and cooled to room temperature. Four types of graphs were presented describing the failure load of the minibeams and the

deformations of the systems. Reduction in the ultimate flexural capacity of the beams was observed. The minibeams were tested in a four point bending and failure was observed when loss of composite action the strengthened systems had occurred. The predominant failure mode for this study was intermediate flexural or flexural-shear induced debonding.

6.3.1 Effect of elevated temperatures on the failure load of CFRP strengthened RC beams

The delamination load was found to decrease gradually for samples from group 20°C to group 300°C. The average load for group 20°C was found as 20kN and for group 300°C the average load was 7kN excluding sample #300-1 for its weak performance. Thus a reduction of 65% was found for the temperature range of 20°C to 300°C which is consistent with the findings in the first experiment. The reduction of the delamination load was approximated by a linear function as it was found to be a close fit to the experimental results.

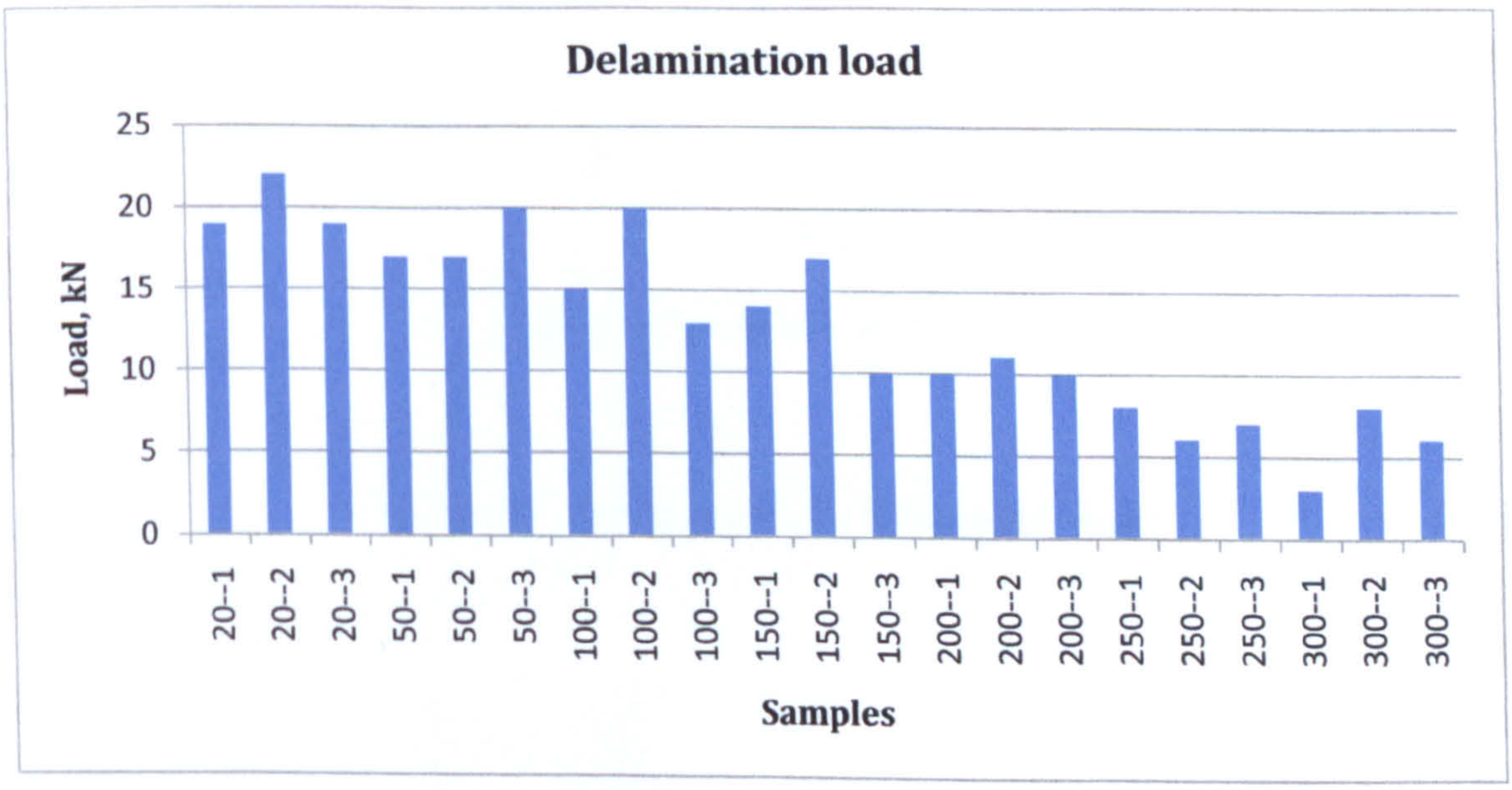

Figure VI- 27 Delamination load for heated and cooled minibeams

6.3.2 Effect of elevated temperatures on the deflection of CFRP strengthened RC beams

The deflection of the systems for the different temperature groups is presented in this section. The reduction of the deformations with increase of the temperature was found to be gradual with the exception of two of the samples of group 100°C. The higher results obtained for group 100°C was due to a higher failure load for beam #100-2 and the higher deformability of sample #100-3. Sample #150-2 was also found to exhibit higher deflection at failure load which was increased due to the propagation of flexural crack at an earlier stage. Beam #300-2 also showed higher deflection value due to occurrence of cracks at an early stage of the loading.

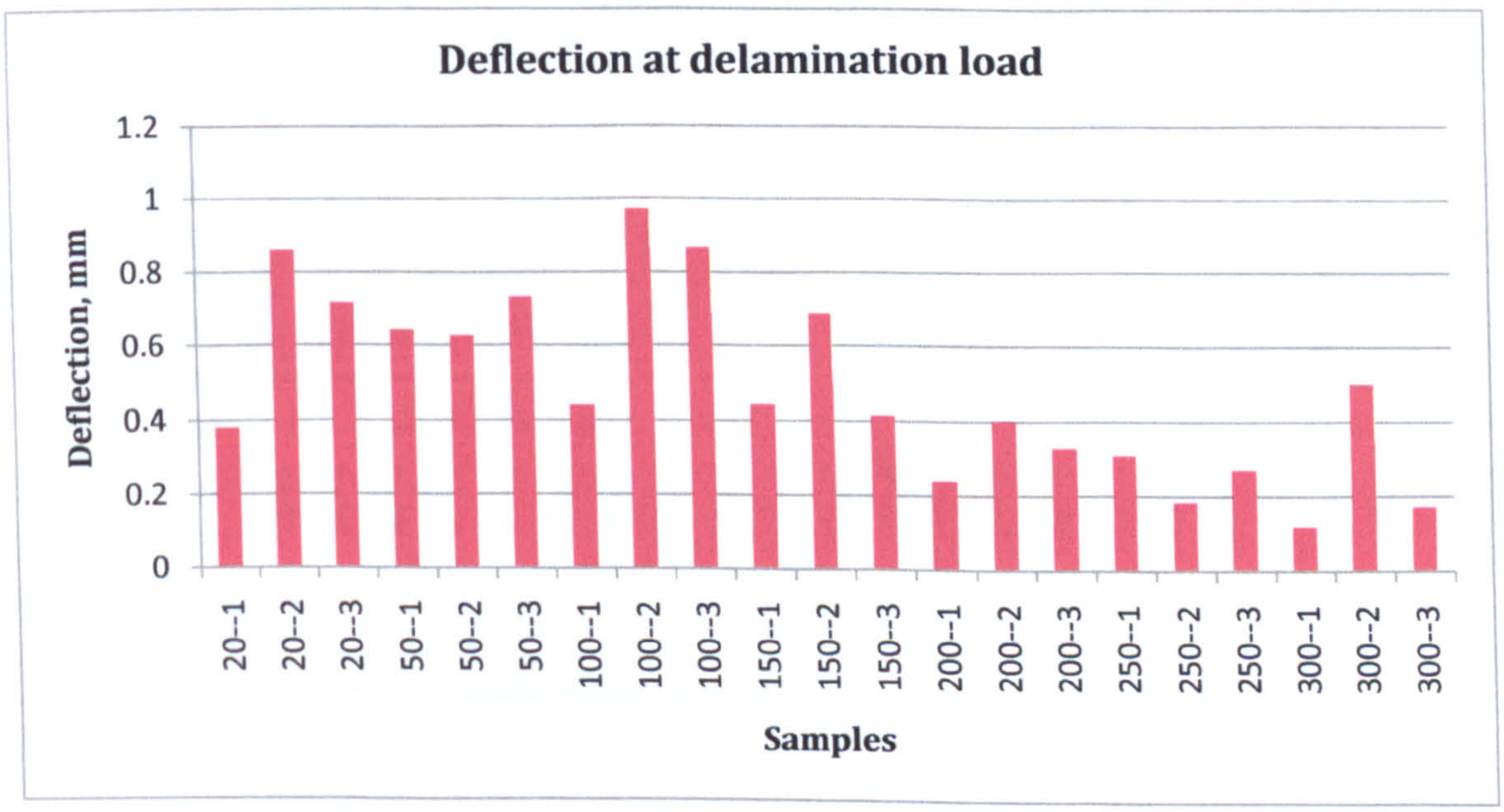

Figure VI- 30 Deflection at delamination load

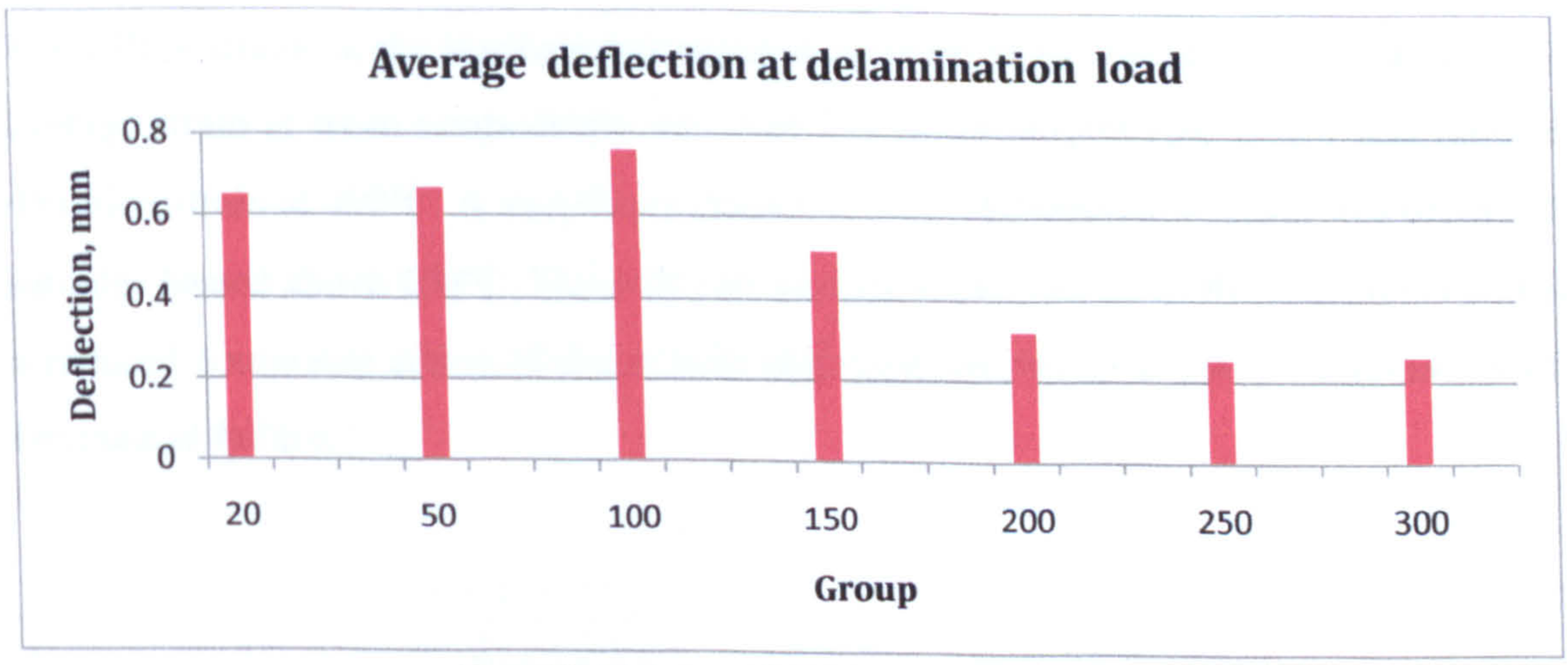

Figure VI- 31 Average deflection at delamination load

6.3.3 Effect of elevated temperatures on the local deformations of CFRP strengthened RC beams

The compressive relative displacements prior to delamination were plotted for each beam. The results revealed a gradual decrease from average 660microstrain at room temperature to an average of 200microstrain at 300°C at level 10mm from the top.

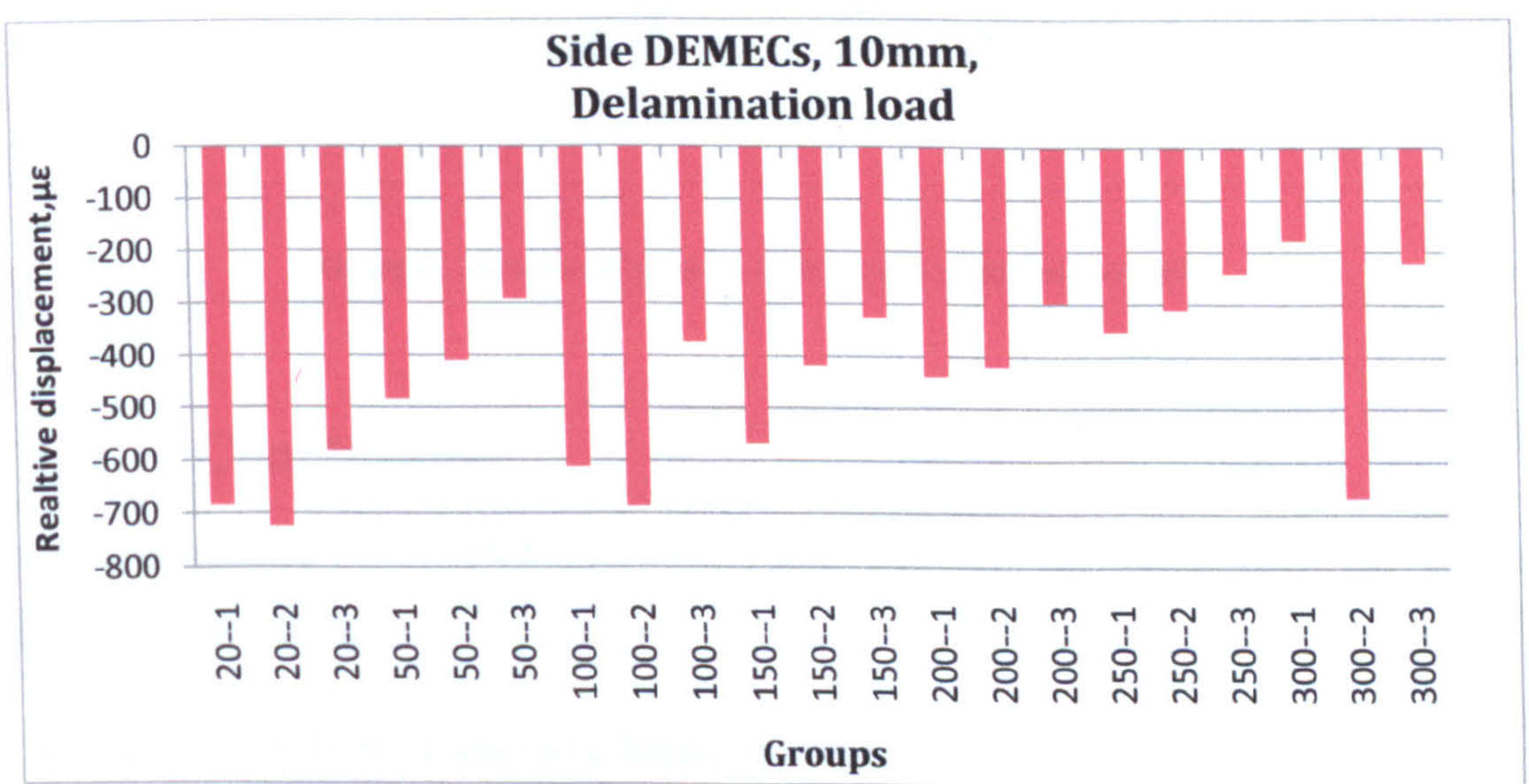

Figure VI-28 Relative displacement at delamination, level 10mm from the top

6.3.4 Effect of elevated temperatures on strain of laminate at midspan

The failure strains in the laminate measured at midspan were also plotted for all beams. The average strain at room temperature was found to be 246microstrain which was reduced to 491microstrain at 300°C. A significant decrease of the delamination strain was observed for samples heated above 150°C. The effect of heating above the T_g of the polymers resulted in a reduced composite action of the system and therefore lower levels of deformation of the laminate at failure.

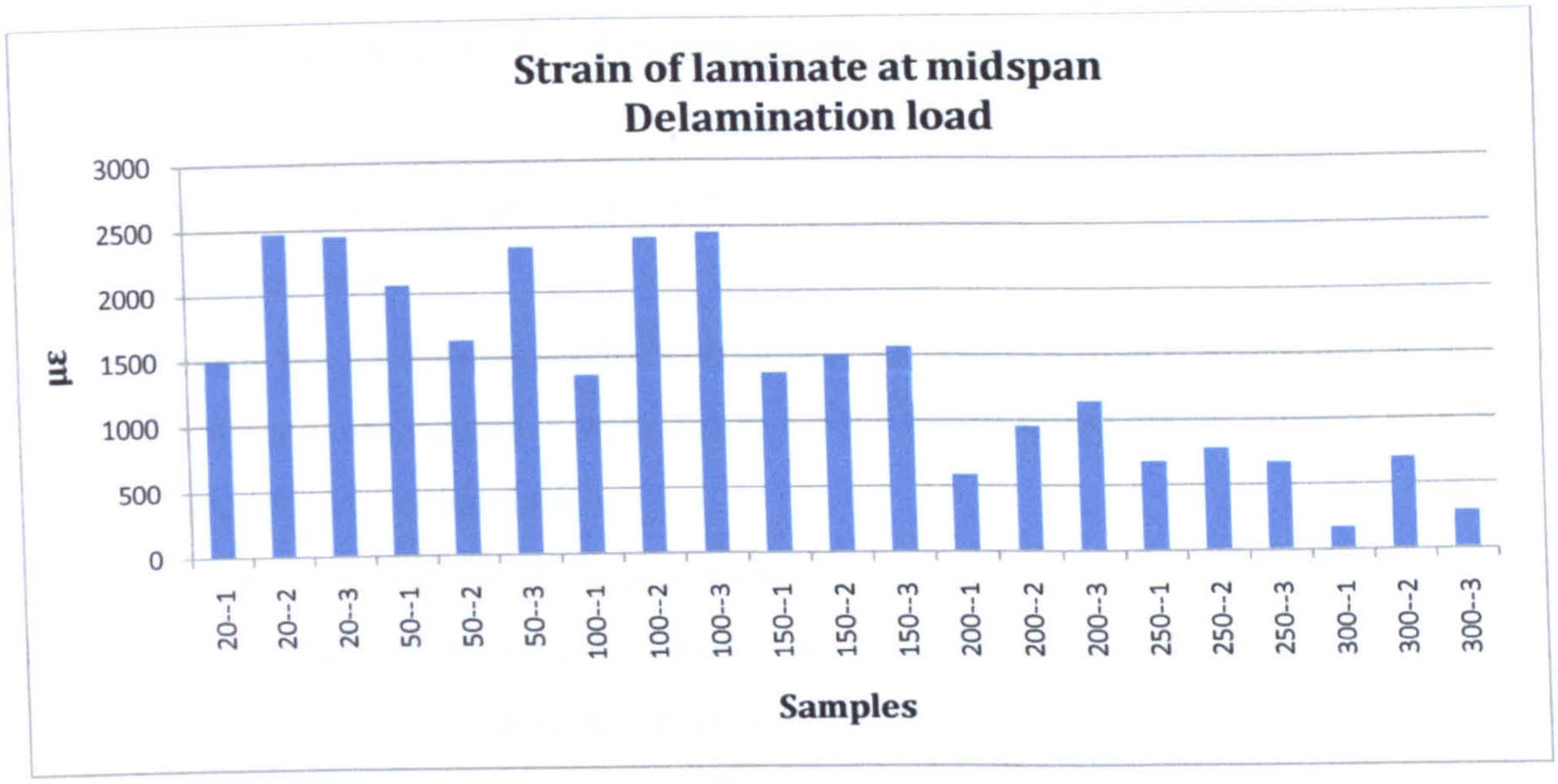

Figure VI- 29 Strain of laminate at midspan, delamination load

6.4 Conclusions

From the conducted experimental studies and analysis of the results the following conclusions were drawn:

6.4.1 CFRP-to-concrete bonded joints

- A reduction of 1/3 of the bond strength was observed for samples heated to 300°C compared to room temperature
- The development of tensile strains in the concrete close to the attached laminate is relatively small (up to 150°C) of heating and increases significantly at 200°C and above.
- Above 200°C the deformability is lower and is governed by the stabilizing effect of the FRPs
- At 50°C and 100°C the relative displacement between the end of the laminate and the concrete is smaller than at 20°C due to the curing of the concrete and adhesive.
- The range of deformations and transfer of stresses increase with increase of the temperature.
- Heated RC samples strengthened with wide FRP laminates could fail in one mode.

6.4.2 Small-scale CFRP strengthened minibeams

- During the heating and cooling process the deformation is gradual with increase of the temperature
- Residual deformations could be expected for samples heated above 200°C
- Minibeams strengthened with 20mm CFRP plates failed due to flexural and flexural-shear induced debonding
- The deformability of the heated samples increases with increase of the temperature
- The decrease of delamination load is proportional to the increase of temperature
- The effect of the heating has a more pronounced influence on the delamination load than the maximum deflection at the ultimate load
- The effect of heating causes reduction of the delamination by 65% at 300°C.

Chapter 7
FE modelling

In this chapter results from a finite element (FE) modelling of FRP strengthened system are presented. Two cases are investigated and analysed. A FE model of a bond strength test is presented first and the effect of different coefficients of thermal expansion are given in the second part of the chapter.

7.1 Finite element analysis

The finite element (FE) method is a numerical method for approximate solutions of engineering problems. It has become a popular technique of analysis of structures with complex geometry, specific material properties and loading conditions. In civil engineering FE programmes are used to solve static and dynamic problems, to analyse the behaviour of elements with material nonlinearities, stability problems, fluid flow and others.

The FE method involves several steps, most important of which are discretization of the geometrical model, development of the element matrix, assembly of the matrices, application of boundary conditions and solution of the equations. In general form the global system of equations is given by:

$$Ku=F$$

Equation VII-1 Global stiffness equation

where K is the stiffness matrix of the system, u is the vector of the unknowns (i.e. stress, displacement, etc) and F is the force vector (Madenci & Guven, 2006).

The FE models presented in this chapter are based on three dimensional analysis of CFRP-to-concrete bonded joints. A hexahedral element is chosen as the main finite element in the numerical analysis with stiffness matrix formulated by:

$$[k]=\int_{-1}^{1}\int_{-1}^{1}\int_{-1}^{1}[\mathrm{B}]^{T}[\mathrm{D}][\mathrm{B}][J]\,ds\,dt\,dz'$$

Equation VII-2 Isoparametric formulation of the stiffness matrix

according to Logan (1992), where $[k]$ is the stiffness matrix, [B] is a matrix which relates the strain to nodal displacement, [D] is a matrix which relates stress to strain, $[J]$ is a Jacobian matrix and s,t,z' are isoparametric coordinates of the nodes.

7.2First FE model of CFRP-to-concrete bonded joint

This chapter presents a numerical model of a CFRP-to- concrete bonded joint which was developed to simulate the conditions of a single shear test and reflect the change of mechanical properties of the materials with increase of the temperature. The aim of FE model was to apply a stress based criterion to predict conditions for crack formation in the concrete and verify the obtained experimental failure loads with numerical results.

7.2.1 Assumptions and failure criterion

Two models were developed for this study. The first FE simulation investigated the conditions of formation of a crack near the end of the laminate in the concrete block. The model was based on an experimental study carried out by Donchev et al (2007) at Kingston University London. The governing factor for the failure of the samples was found to be the tensile strength of the concrete and it was considered the main failure criterion for the formation and development of a crack in the concrete. Based on experimental observations, the position of the crack and length was assumed to be known and the FE model was divided to three steps to reflect the observed propagation of the crack.

The thermal loading consisted of heating of the samples for at least 2h at different constant temperatures from room temperature (20°C) to 250°C to ensure evenly distributed temperature in the cross sections of the samples. The laminate was loaded in tension after the cooling of the specimens simulating longitudinal shear loading at this zone. The behaviour of the strengthened system did not exhibit substantial difference with specimens loaded up to 100°C. The decrease of strength of the system in the range 100-250°C was approximately linear which was mainly governed by the reduction of the strength of the concrete. At 250°C the ultimate strength of the strengthened system was reduced to 65% of the strength at room temperature.

7.2.2 Materials and heating

Four materials are considered in the numerical model: steel bar, concrete, adhesive and CFRP laminate. The behaviour of concrete and steel at elevated temperatures and fire are well

investigated and information of their properties was available in the literature, i.e. Buchanan (2001). Up to 300°C concrete experiences changes in its mechanical properties including reduction of its compressive and tensile strength and Young's modulus. It was also observed that the magnitude of reduction is similar to both compressive strength and elastic modulus. However, the available information about the residual properties of polymers: both adhesives and FRP, is scarce and limited to mainly to internal reinforcement and exposure to fire. The properties of the materials at room temperature used in this study are given in Table VII-1.

Material	Modulus of elasticity at room temperature	Coefficient of thermal expansion
Concrete C20	30000 MPa	$10x10^{-6}$/°C
CFRP laminate	165 000 MPa	$0x10^{-6}$/°C
Epoxy adhesive	9800 MPa	$33x10^{-6}$/°C
Steel	210 000 MPa	$12x10^{-6}$°C

Table VII- 1 Typical values of materials in a strengthened system

Bisby et al (2005) suggested a semiempirical analytical expression of the reduction of the material properties of the carbon/epoxy FRP, this was adopted in this study. Although the information on the materials used was not available at the time of the numerical simulations a reduction rate of the material properties of similar materials, i.e GFRP bars, was adopted.

7.2.3 Numerical model

The numerical modeling was performed with a finite element programme: ANSYS 10 Multiphysics. Solid 45 (Figure VII-1) was used for the numerical simulation.

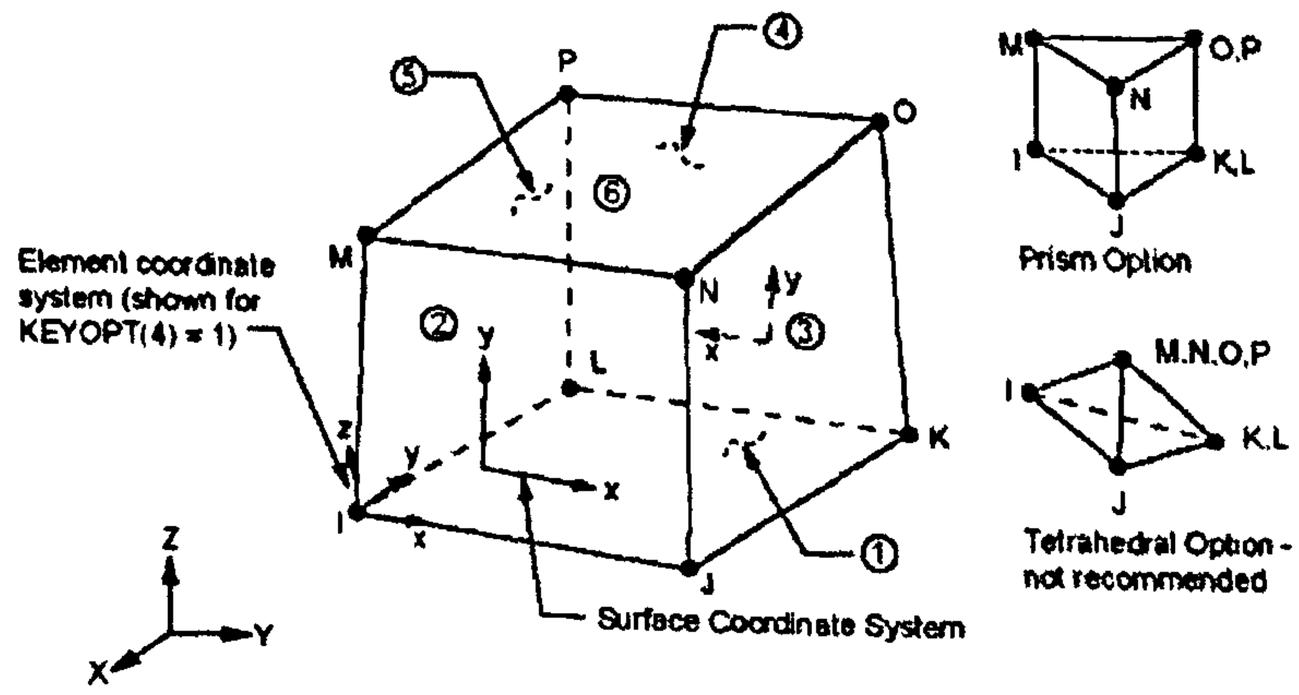

Figure VII-1 Solid 45 geometry, Ansys 11 Manual

The element was defined by eight nodes with three degrees of freedom at each node: translations in the nodal x, y, and z directions (Ansys 10 Manual). A solid element was chosen for a 3D analysis to allow path operations along the axis of the bonded joint.

Material	Height	Width	Length
	[mm]	[mm]	[mm]
Concrete block	75	75	300
CFRP Laminate	6	35	250
Steel rod	Φ8		300
Adhesive	2	35	100

Table VII-2 Geometrical model of the bonded joint

Three dimensional model (see table VII-2, Figure VII-2) was based on the materials dimensions used in the experimental study. The concrete block with dimensions of 300x75x75 mm was modelled with a solid element 45 as well as the FRP plate. The laminate had dimensions 250x35x6 mm with bond length to the concrete prism of 100mm. A R8 steel rod which was used as the reinforcement of the concrete sample was modelled at the centre of the prism. Finally, a 2mm adhesive element was modelled between the concrete and laminate.

The analysis was divided in two steps, the first step simulated the behaviour of the CFRP strengthened concrete prism at normal temperatures as pulling force was applied to the laminate and maximum tensile stresses were evaluated. When at normal temperature the tensile strength of the concrete was exceeded the prism was assumed to have failed due to a crack.

The second step simulated the bonded joint with temperature dependent material properties of its constituents: concrete, CFRP, adhesive and steel at temperatures from room temperature to 250°C. The specimen was also loaded in tension simulating testing of the residual strength of the sample after the heating and cooling phase.

The mesh size and shape of the FE model were chosen based on the capabilities of the programme. In total more than 19000 elements were created with refined mesh near the bond areas to allow the accurate detection of stress concentration.

The boundary conditions applied on the concrete prism were the same as the experimental conditions. Horizontal restriction was applied on the near side of the prism where the pulling force was applied and a vertical constraint was applied on the top surface in order to prevent rotation.

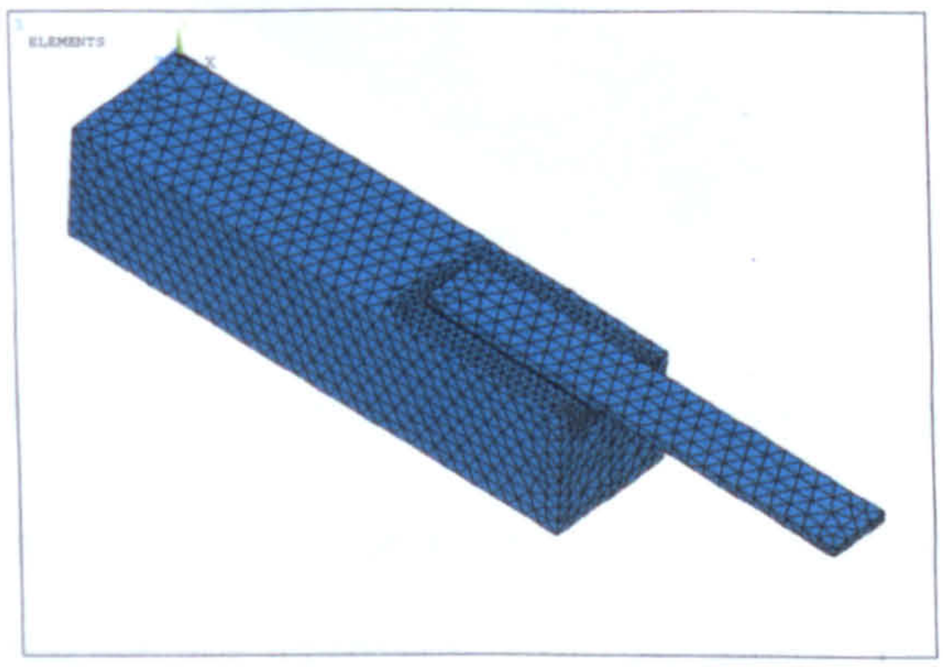

Figure VII- 2 Finite element model

7.2.3 Results

7.2.3.1 Step One

The load was applied to the sample and the maximum tensile stresses were evaluated for each step. When the load reached 4kN the maximum normal stress in the adhesive was found to be approximately 2.5 MPa, this was less than the tensile strength of the adhesive of 17MPa. The concentration of stress at the end of the laminate in concrete was close to 2MPa. The tension capacity for concrete C20 was calculated as 2.78MPa based on a formula given by Clark (1983):

$$f_t = 0.556\sqrt{f_{cu}}$$

Equation VII-3 Tensile strength of concrete, Clark (1983)

Thus, when the load was increased to 4.7kN (see Figure VII-3) the tensile strength of the concrete was reached and failure of the system was assumed. The high tensile stresses at the

end of laminate were an indication for initiation of a crack due to low tensile strength of the concrete. However, other possible failure modes were not considered in this study as the conditions for failure in the concrete were developed at an early stage of the loading and the experimental data confirmed the formation of a crack in the concrete for normal temperature.

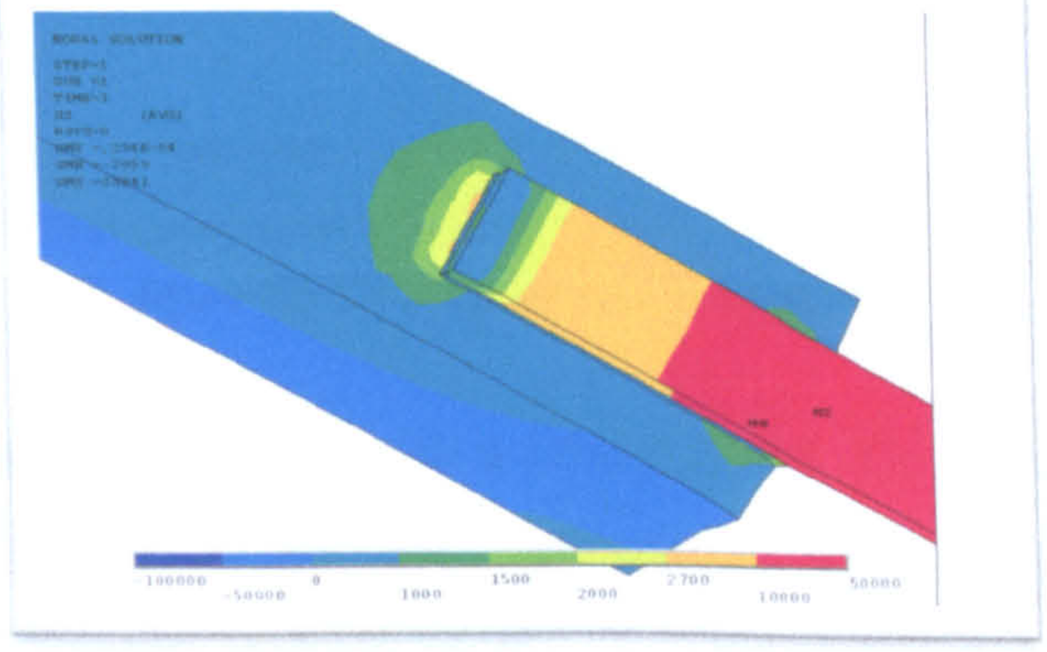

Figure VII- 3 Normal stresses in the longitudinal cross section at 4.7 kN

In order to simulate the conditions for crack development through the prism a 10mm vertical crack in concrete at the end of the laminate was modelled. At higher levels of loading the stress concentration at the crack tip was estimated in order to predict the further propagation of the crack. The direction of the propagation of the crack was vertical as observed during the testing of the samples.

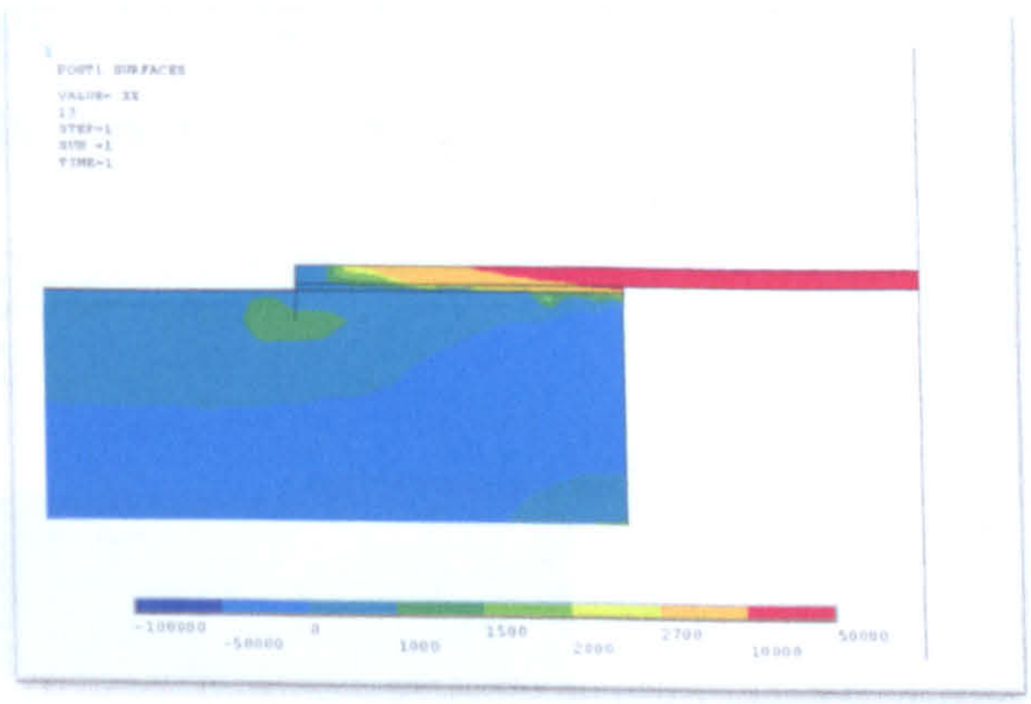

Figure VII- 4 Normal stresses at load 7kN

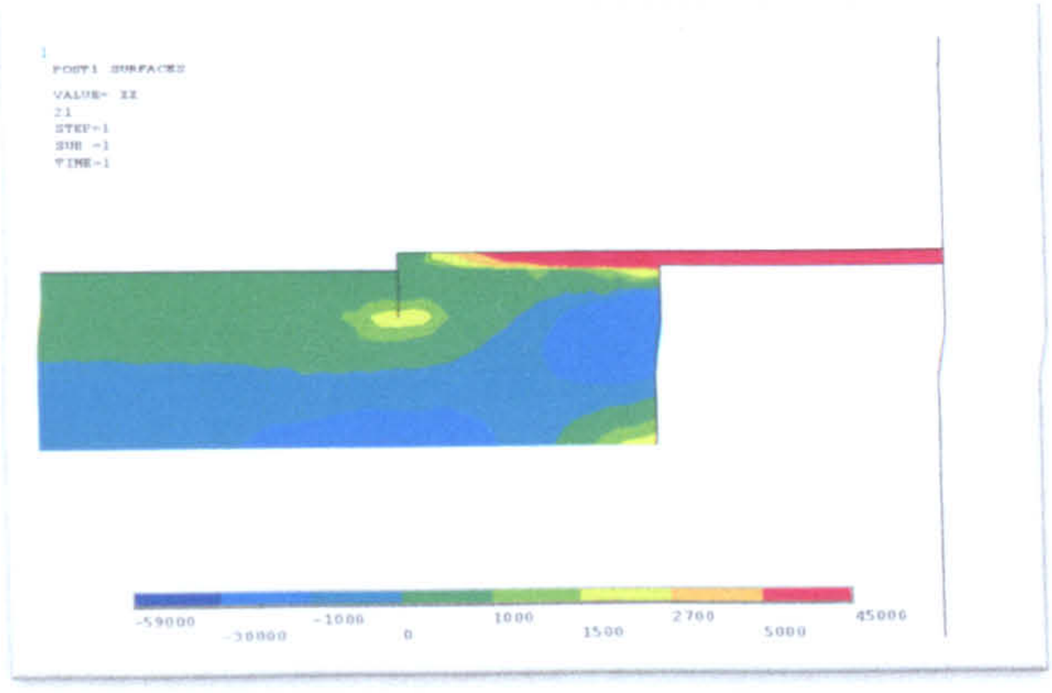

Figure VII- 5 Normal stresses at load 8.5kN

The geometry of the sample was updated with a 10mm at the end of the laminate and then the pulling load was applied to the model. The increase of the applied force resulted in an additional concentration of normal stresses in the concrete at the zone around the tip of the crack. When the ultimate tensile strength of the concrete was reached, it was assumed that the conditions for the further propagation of the crack in vertical direction were satisfied and a new geometry of the prism was used.

As the third step of the study the distribution of stresses around 20mm deep crack due to increased loading was analysed. Figure VII-6 shows concentration of stresses at the tip of the crack at 8.5kN. It was found that the distribution of normal and principal stresses was predominantly in horizontal direction, therefore the propagation of the crack would continue in horizontally governed by the direction of the principal stresses in the concrete.

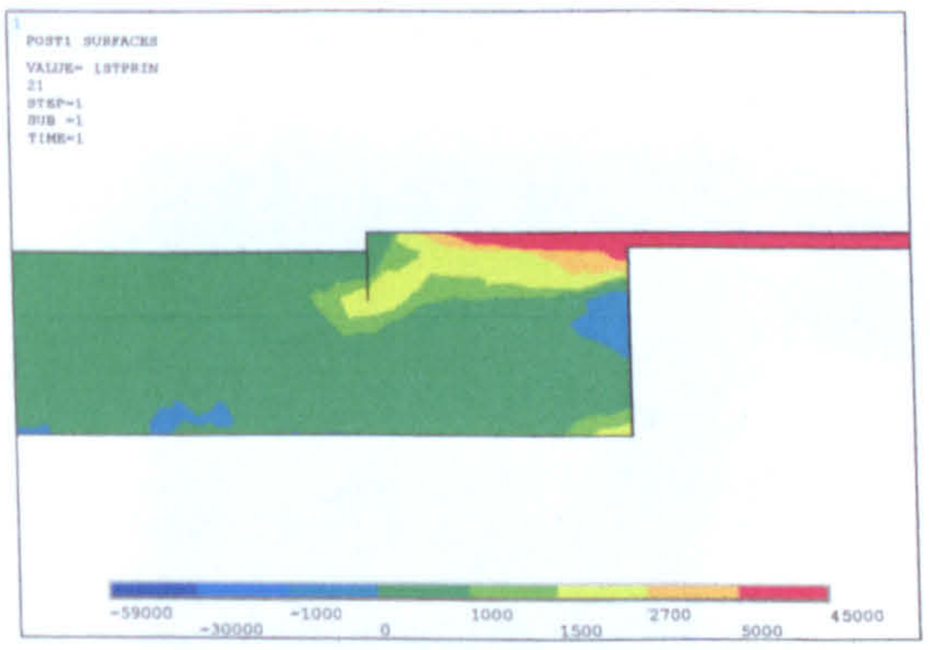

Figure VII- 6 Principal stresses at 8.5kN

The experimental results also confirmed possible parabolic curving of the crack and change of its direction after the formation of a vertical crack. The wide area of relatively high tensile

stresses would contribute the fast propagation of a horizontal crack which would result in a brittle failure.

7.2.3.2 Step Two

The second stage of the numerical analysis reflected the effect of elevated temperatures on the mechanical properties of the materials to the simulation of the crack formation the concrete. The thermal effects on the elastic modulus of the concrete and FRP were taken into account and the corresponding reduction of the tensile strength was also considered.

The changes of the mechanical characteristics (see figure VII-8) of the model at elevated temperatures resulted in the development of conditions for the formation of the initial crack and propagation at lower levels of loading which was observed during the experiments. The numerical results also showed gradual increase of the thermal stresses induced in the materials due to their different coefficients of thermal expansion.

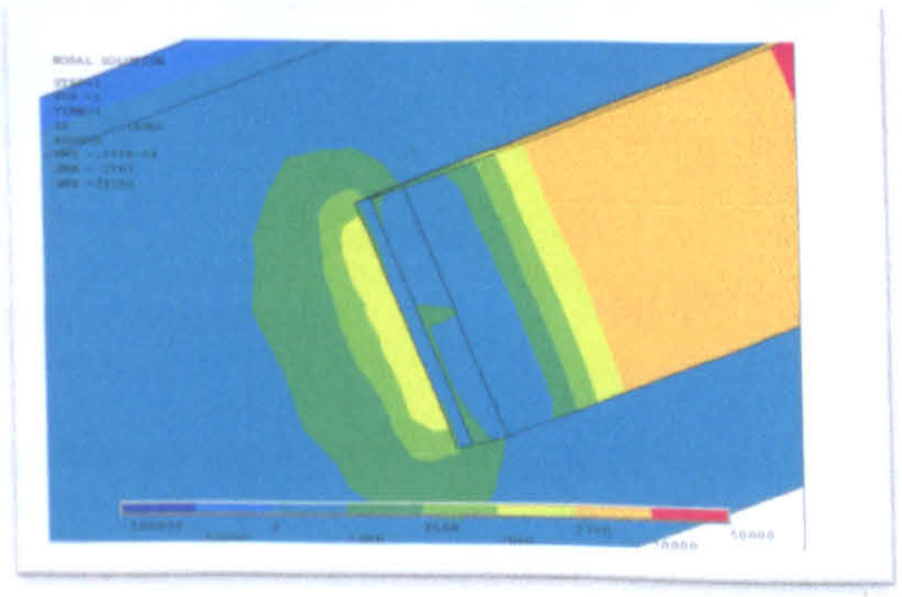

Figure VII- 7 Normal stresses at 4.5kN normal temperatures

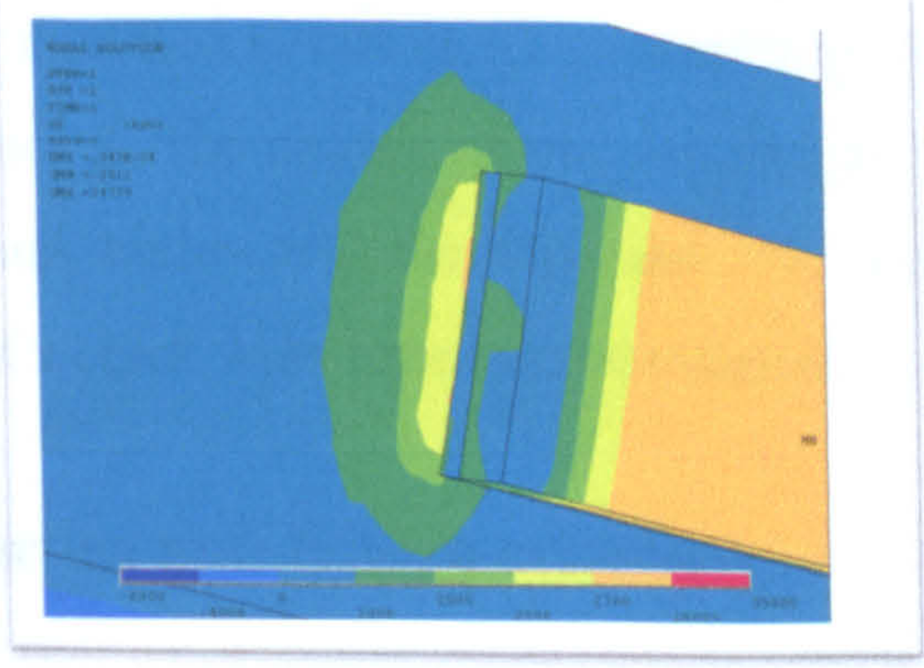

Figure VII- 8 Normal stresses at 4.5kN, 250 degrees

Comparison of the numerical and experimental results was presented in Figure VII-9. The predominant failure mode of the tested bonded joints was a failure in the concrete which initiated with a vertical crack in the concrete at the end of the laminate. High concentration of stresses at the tip of the crack was observed and further development of stress concentration zone horizontally led to the development of conditions for the separation of the concrete cover. Overall, good agreement was found between the experimental and numerical results, except for samples 50°C which failed at significantly lower loads due to lower strength.

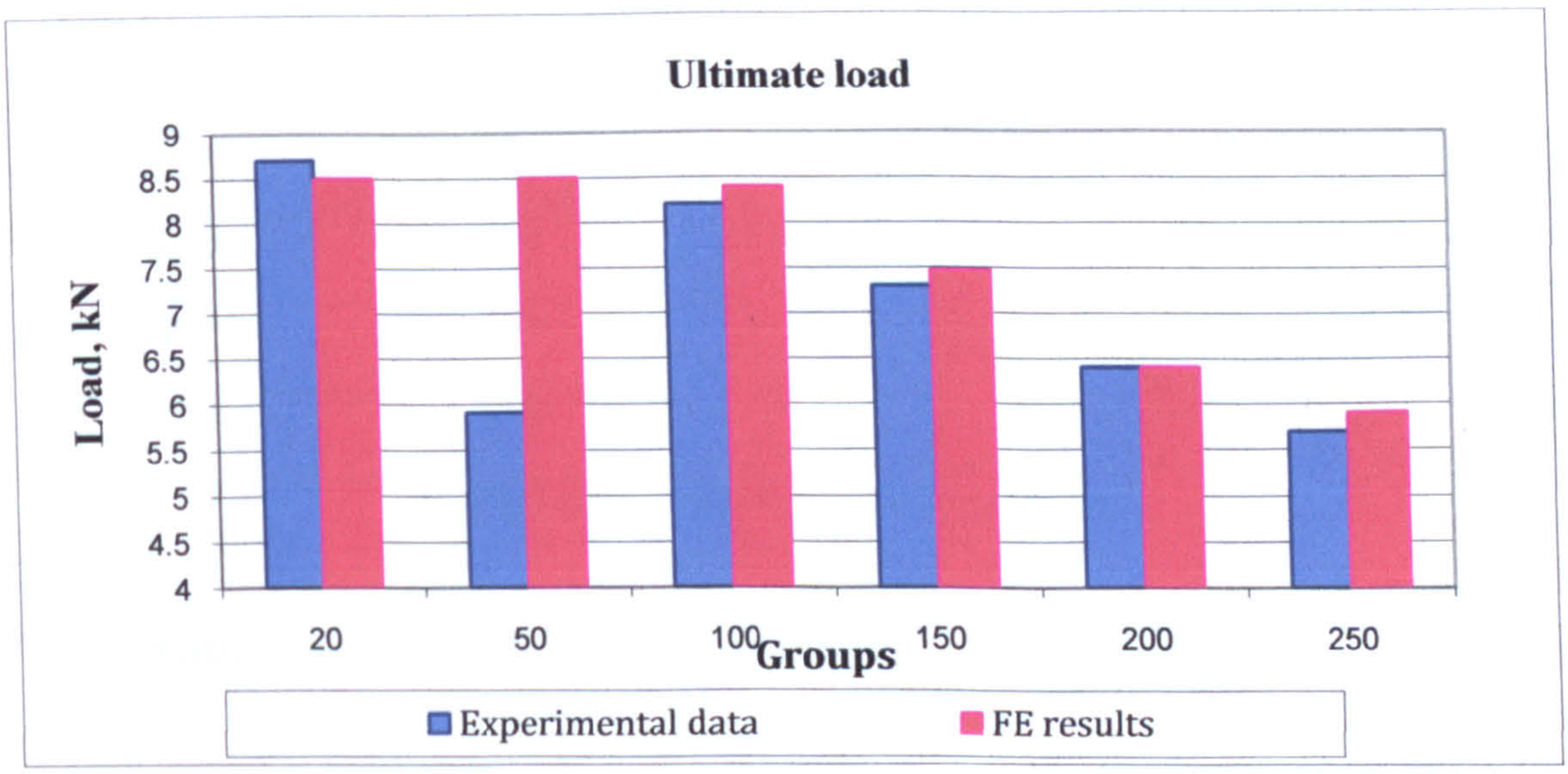

Figure VII-9 Comparison of experimental data and finite element analysis

7.3 Second FE model of CFRP-to-concrete bonded joint

The first FE model was further modified to reflect the geometry and mechanical properties of the samples described in Chapter 3. The change of the mechanical properties was based on data collected from experimental studies and the literature. The samples were loaded until conditions for the occurrence of a crack were found in the concrete at the end of the laminate.

7.3.1 Material properties and failure criterion

Four groups were compared from 20°C to 300°C. The reduction of the modulus of elasticity of the concrete was based on the reduction of the compressive strength obtained from tested cubes for each group. The tensile strength was then obtained from the formula proposed by

Clarke (1983). To take the thermal effects into account the tensile strength was further reduced by 80% and 60% respectively for group 200°C and 300°C as proposed in BS EN 1992-1-2:2004. Finally, the reduction of the modulus of elasticity of the laminate was based on the experiments carried out by Halli, (2009) to investigate the residual strength of FRP laminates. Due to lack of sufficient data, the residual properties of the adhesive layer were not taken into account.

Temperature	Modulus of elasticity Laminate	Modulus of elasticity Concrete	Failure criterion
	GPa	MPa	MPa
20°C	180	30	3.52
100°	175	32.25	3.67
200°C	173	31.5	3.60
300°C	140	23.1	3.10

Table VII-3 Material properties and failure criteria

7.3.2 Numerical model, load and boundary conditions

Solid 45 was also used in the second numerical model. New geometry corresponding to the samples tested and presented in Chapter 3 was introduced.

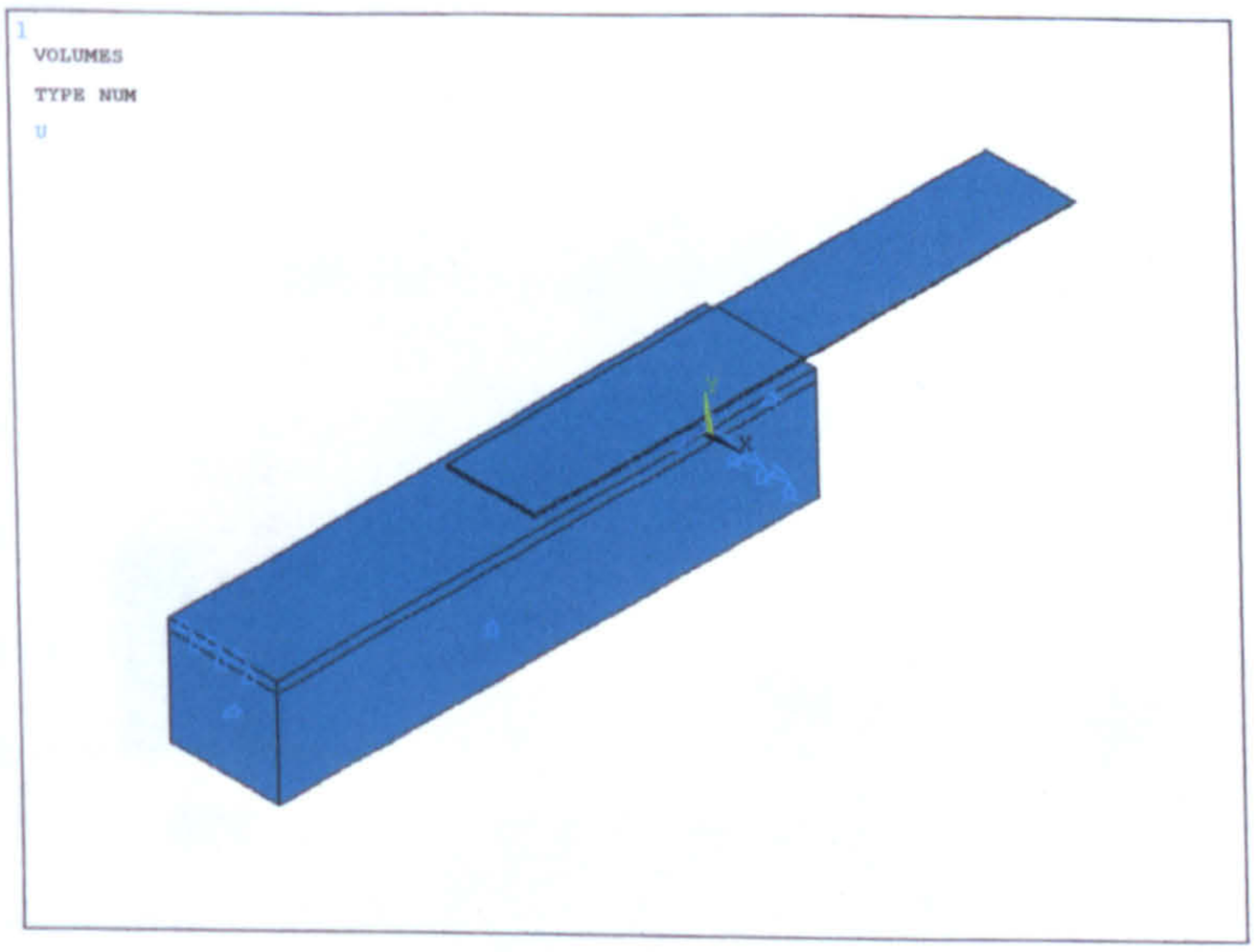

Figure VII-10 Boundary conditions, experiment I

The finite mesh was further improved with regular size elements. In total more than 40000 elements were used. The solid model was constrained in the vertical and horizontal direction and the load was applied at the end of the laminate. Mesh elements with a regular shape and 0.01mm size was applied to every element of the strengthened system.

7.3.3Numerical results

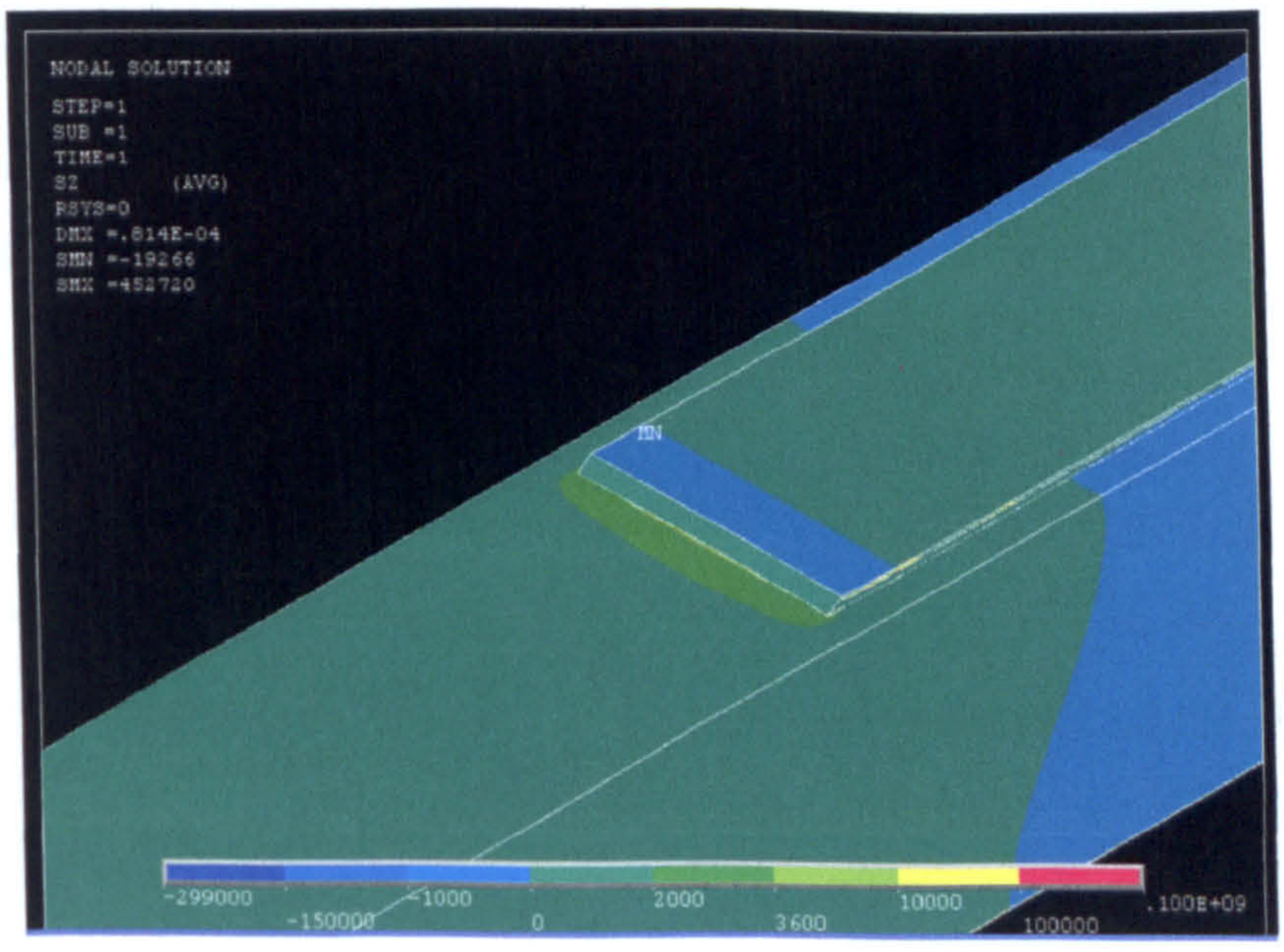

Figure VII- 11 Beam loaded to 30.4kN 100°C normal stresses conditions for crack

Failure load was reached when the tensile stresses at the end of the laminate increased to a critical value. The load was then taken and compared to the average experimental result for the given group. The same deviation from the experimental results was observed for the four groups of samples.

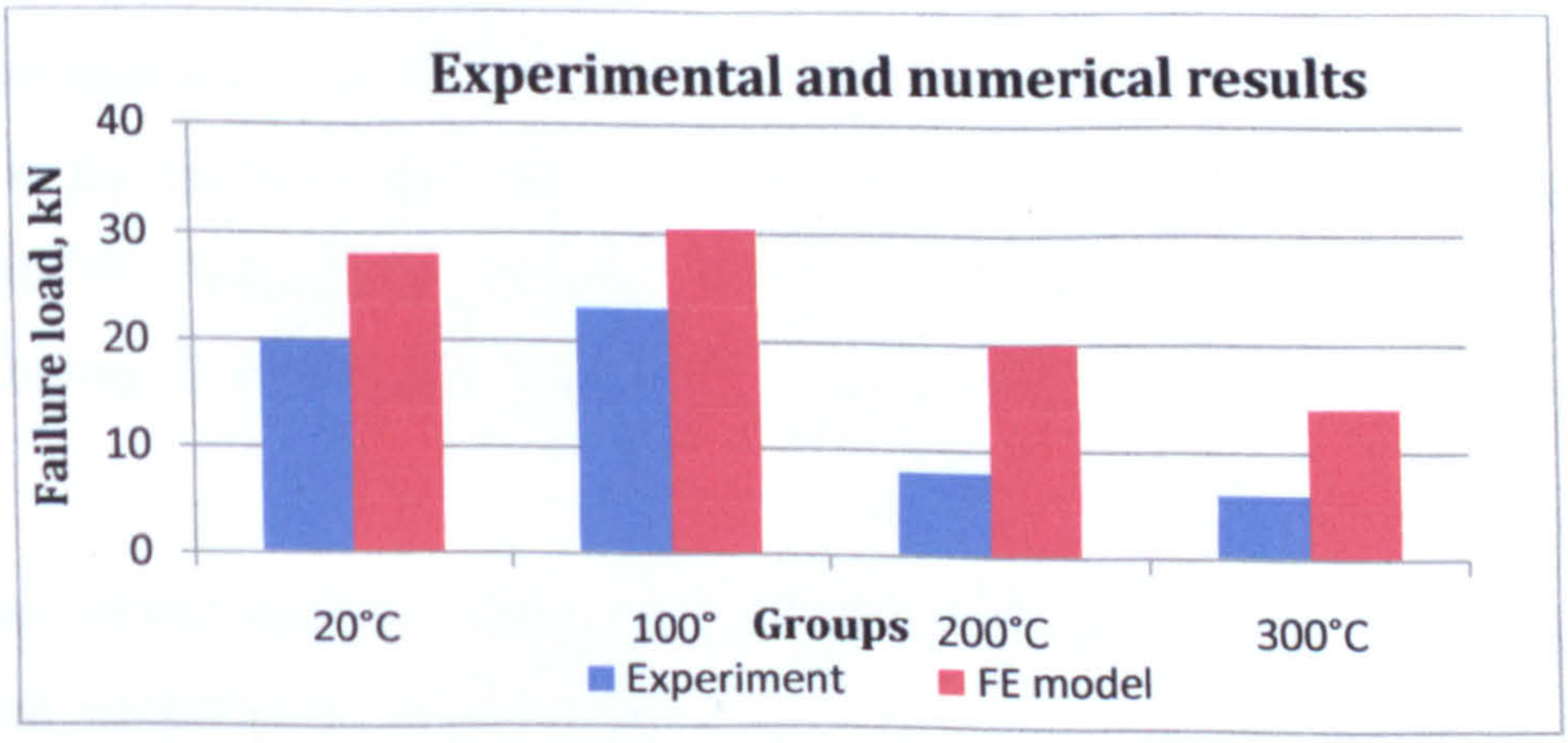

Figure VII-12 Experimental and numerical results

It could be expected that the high variation of the tensile strength of the concrete samples and the residual reduction of the modulus of elasticity after heating and cooling have a significant influence on the obtained numerical results. The model is thus to be calibrated with more precise information about the material properties of the system.

7.4 FE model of the effect of different material CTEs

The third numerical study was based on the first finite element model presented in this chapter. The aim of this FE simulation was to investigate the effect of different CTEs of CFRP strengthened systems when exposed to elevated temperatures. Due to the significantly different CTEs of the CFRP polymers and adhesives at elevated temperatures high concentration of stresses could occur and this could lead to conditions for premature failure of the system. In this study the temperature range is chosen from room temperature (20°C) to 60°C which is T_g of the adhesive- the weakest element in the strengthened system.

The coefficient of thermal expansion of polymers is determined from the properties of the fibres and the resin. In the case of unidirectional laminates, the expansion of the CFRP in the longitudinal direction the CTE of the laminates could be an important factor. However, in most cases it is usually accepted to be zero due to the practically negligible expansion of the fibres. In the transverse direction its influence is ignored due to the limited distance of its application.

Information about the Young's modulus of the CFRP polymers was found in the literature (Cadei et al, 2004) and the corresponding values were included in the analysis (see Table VII-4). It should be mentioned that the CTE of the adhesive used in the experimental studies was not available in the literature and alternative adhesive was used (see Table II-2) assuming a value of 33×10^{-6}/°C. The effect of glass transition was taken into account as in the case of heating and cooling, it could contribute to the redistribution of stresses between the different materials.

For the purpose of this study a 3D finite element model was developed to estimate the effect of the elevated temperature on the strengthened system. The dimensions of the different

elements are given in table VII-2. The temperature loading was realised in two steps, analysing first the effect of heating and then the opposite process of cooling.

7.4.1 Heating of CFRP-to-concrete bonded joints

In reinforced concrete both the constituents - concrete and steel reinforcement - behave similarly in terms of thermal expansion when subjected to environmental conditions. In a strengthened system which includes adhesive and CFRP laminate, the change of temperature may cause significant stress development due to the difference of the CTEs. In the longitudinal direction the laminate has the lowest CTE whilst the adhesive could have 3 to 9 times higher CTE than concrete.

Material	Tg	CTE
Concrete C20	-	$10x10^{-6}$/°C
CFRP laminate	100°C	$0x10^{-6}$/°C
Adhesive	60°C	$33x10^{-6}$/°C*

Table VII- 4 CTE of concrete, adhesive and CFRP laminate

The free expansion of concrete at elevated temperatures would not lead to development of thermal stresses from a structural point of view. The bonded laminate, however, could bring a limitation as the concrete would expand and the limiting effect would be equivalent to a compression load applied along the bonding length. The laminate, respectively, would be loaded in tension due to the contact with the concrete. Hence, the deformed shape of the system during heating would be governed by the compression in the concrete at the bonded area and elongation in the far end of the prism, which was confirmed by the numerical results (see Figure VII-13).

The zone at the end of the laminate is subjected to a local concentration of thermal stresses in the three constituents. From those three, the adhesive is the one with highest CTE, which combined with characteristics of adjacent materials leads to the development of high compression stresses in the adhesive during the heating process. The result from the FE modelling showed that the difference of the expansion rate of the laminate and the concrete

resulted in conditions for the development of tensile stresses in the concrete. The tensile stresses reached a value of 6 MPa (see Figure VII-14) which in reality could lead to a development of a crack in the concrete at the end of the laminate.

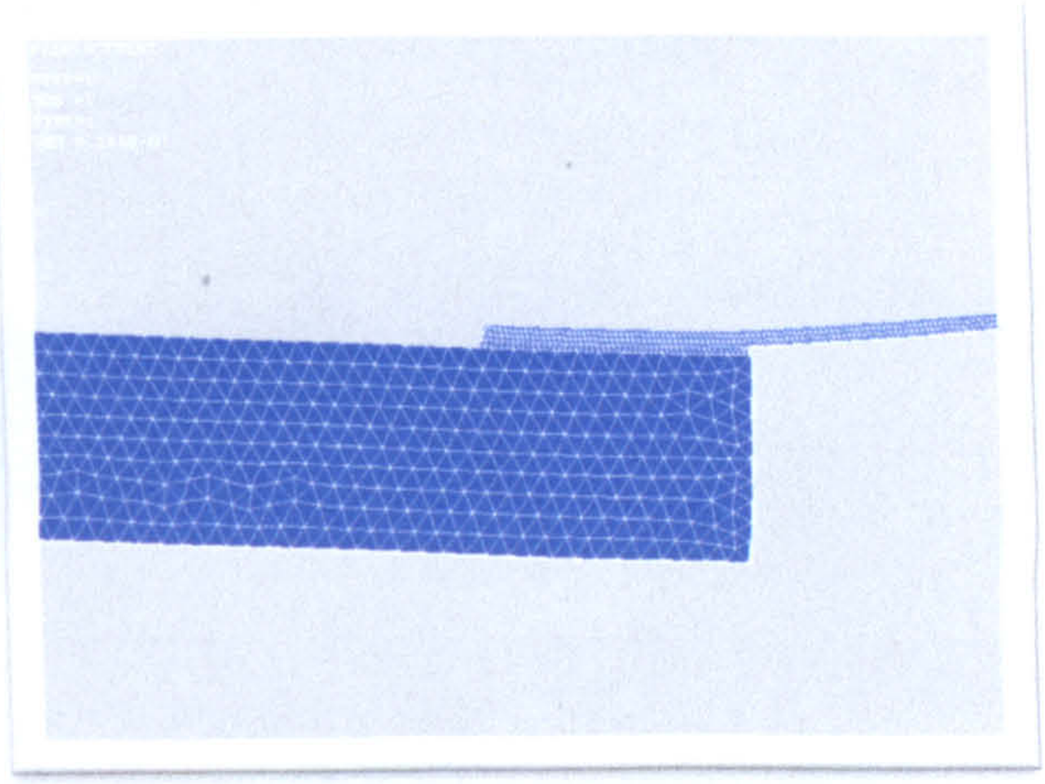

Figure VII- 13 Deformed shape after heating to 60°C

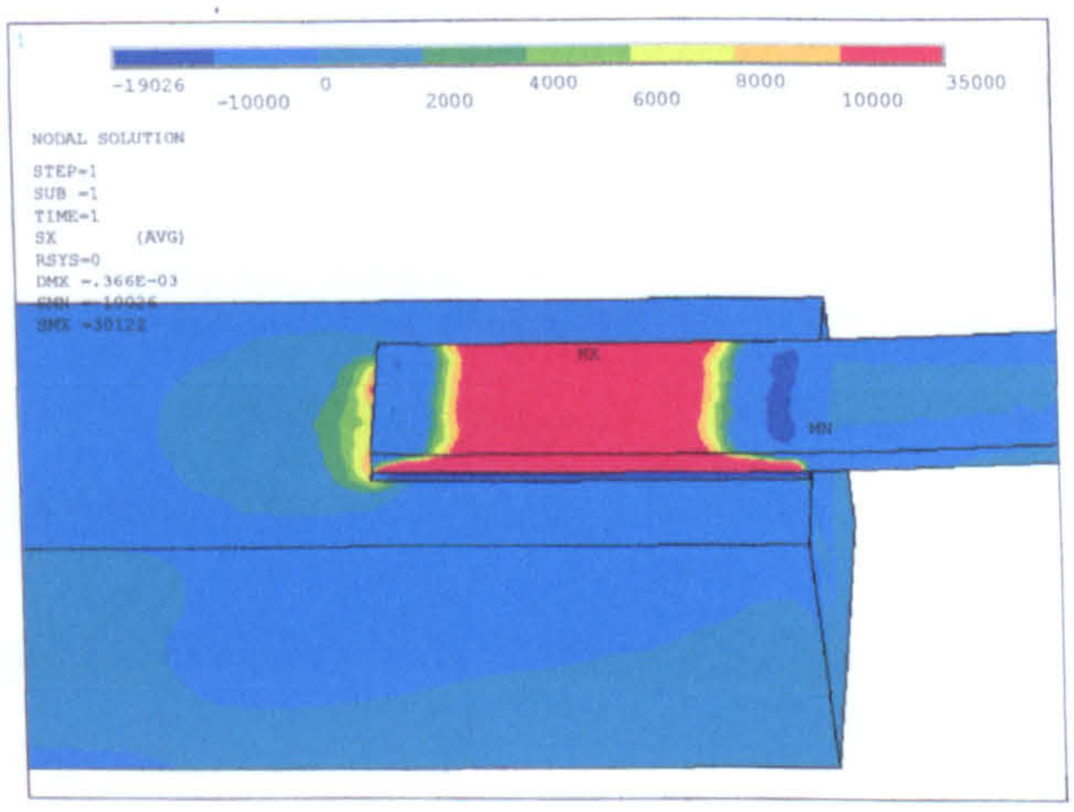

Figure VII- 14 Normal stress distribution during heating up to 60°C

Heating the materials above the T_g of the adhesive could lead to a new process of stress relaxation at the interfaces of the constituents. As the T_g of the adhesive is approached, the material enters a transition from solid to viscous with the corresponding decrease of stiffness. In the case of strengthened systems the expansion of the concrete would no longer be limited by the polymer and therefore the laminate would no longer be subjected to tension. Therefore it could be expected that at temperatures above T_g the elements would reach a stress relaxation stage and their deformation would be free. Based on this assumption the second step of the analysis was carried out next.

7.4.2 Cooling of CFRP-to-concrete bonded joints

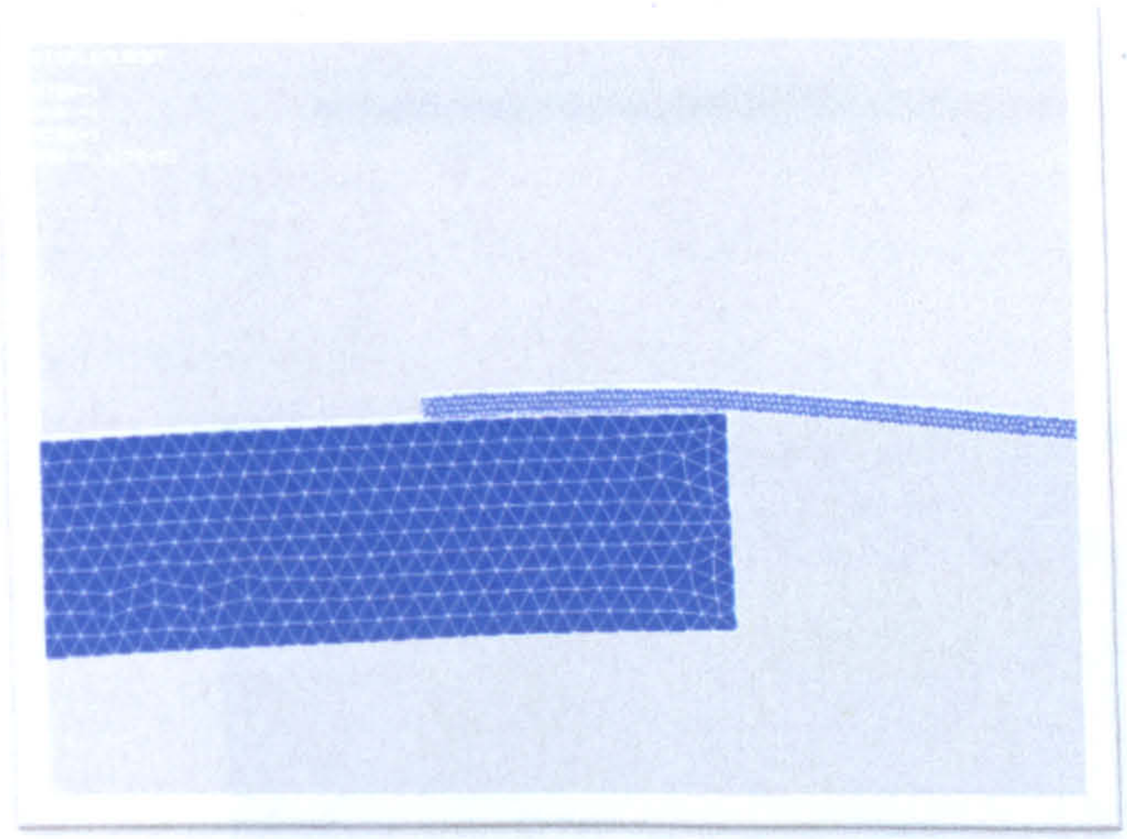

Figure VII- 15 Deformed shape after cooling to room temperature

The next stage of the modelling is the cooling of the sample to room temperature. Once the relaxation of stress due to the softening of the adhesive is realized, the process of cooling is introduced as zero internal forces between the constituent materials. When the thermal condition decreases to temperatures under T_g, the adhesive is assumed to regain its strength and stiffness, causing interaction with the adjacent elements.

The deformed shape of the numerical model is given in Figure VII-15. The cooling phase has an opposite effect on the behaviour of the strengthened system compared to phase heating. At room temperature the laminate is loaded in compression due to its lack of thermal contraction which prevents the concrete to return to its original state. The deformation of the strengthened system is again governed by the different behavior of concrete and laminate. The shape of the specimen reflects the deformation of the contracting concrete due to the decreasing temperature.

The process of cooling leads to stress relaxation in the concrete at the end of the laminate. The concrete is subjected to tension along the bonding area with values reaching 4 MPa (see Figure VII-14). The distribution of the tensile stresses in depth is similar to the formation of the horizontal crack which develops before the concrete cover separation mode of is observed.

The residual tensile stress at the level of the adhesive is significant and could lead to failure due to high concentration of stresses in this element of the strengthened system.

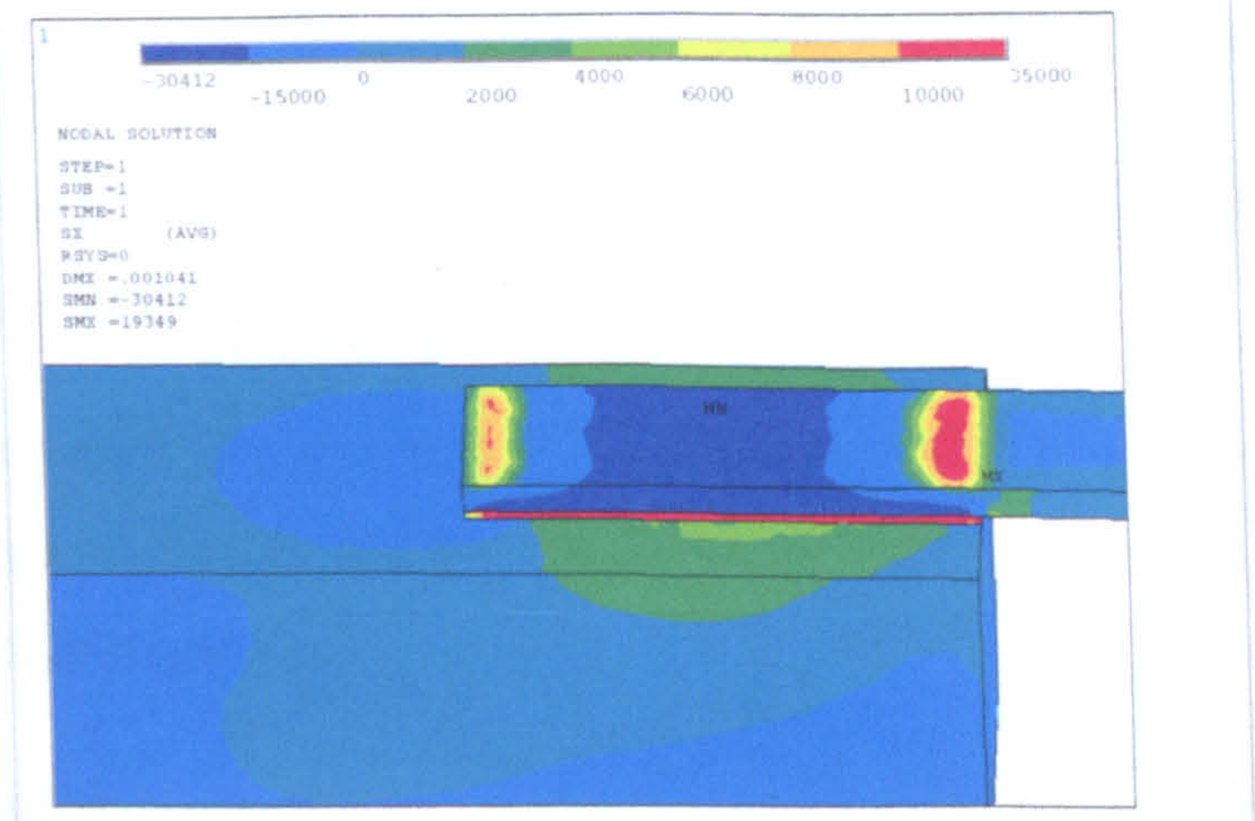

Figure VII- 16 Normal stress distribution after cooling to room temperature

7.4.2 Combination of residual thermal stress and stress due to external forces

When CFRP-to-concrete bonded joints are subjected to heating, cooling and then loaded in tension, the remaining capacity and corresponding failure mode are governed by several important factors. The thermal loading and thermal effects on the materials, the development of microcracks in concrete, the glass transition temperature of the polymers and the condition of the interface between the adhesive and concrete are some of the problems that have to be considered. However, the failure modes observed in the experimental work prove that the behaviour of the CFRP strengthened systems is most affect at temperatures exceeding the decomposition temperature of the polymers.

Residual tensile stresses in the concrete and compressive stresses into the laminate after heating above T_g and cooling were observed in the theoretical model. This distribution of thermally induced stresses would have negative effect on the capacity and deformability of CFRP strengthened systems after exposure to elevated temperatures. The material most susceptible to premature failure of a strengthened system is the concrete as it is weaker in tension than any of the other materials and additional stresses due to thermal loading could lead to early micro cracking at temperatures below 100°C.

7.5 Conclusions

7.5.1 CFRP-to-concrete bonded joint

On basis of the presented research the following main conclusions could be drawn:

- A finite element model of CFRP-to-concrete bonded joint was developed and crack formation in the concrete at the end of the laminate was evaluated;

- Reduction of the strength and stiffness of the materials at elevated temperatures up to 300°C was incorporated in the model. Obtained results were found to be in good agreement with experimental results;

- The obtained results and the model could be used for assessment of the condition of CFRP strengthened RC beams after heating to elevated temperatures.

7.5.2 Effect of different CTEs

As a result of the developed theoretical modelling, the following conclusions could be drawn:

- Temperature induced stresses in the concrete close to the edge of the laminate during heating were significant and could exceed the tensile strength of the concrete;

- During the heating process significant tensile stresses in the laminate and compression stresses in the concrete were generated. Those stresses were below the corresponding strength of the materials.

- When heated above T_g and cooled the system of concrete and CFRP laminate developed temperature induced stresses of compression in the laminate and tension in concrete. Such stresses could cause local cracking in the concrete and additional deformability at the strengthened system.

Chapter 8
Conclusions and recommendations for future work

8.1 Conclusions

8.1.1 Experimental work

The effect of elevated temperatures on the behaviour of CFRP strengthened beams was investigated in this work. Three main experiments were designed to investigate the residual strength of small-scale beams after exposure to elevated temperatures, to measure the temperature effect on the deflection of heated and loaded samples and the study the bond strength of CFRP strengthened systems.

- The existing test methods and experimental work on the bond strength of FRP-to-concrete bonded joints were reviewed. A testing device corresponding to a single shear test was designed and manufactured. The failure modes of the tested experimental samples were found in agreement with results reported in the literature. All samples, including heated to 300°C, failed due to a crack in the concrete.

- The main findings of the first experimental programme were the reduction of the strength with increase of the temperature and the increased deformability of the strengthened systems. The exposure to elevated temperatures was found to have positive influence on the performance of CFRP strengthened systems to a certain temperature. Samples heated to 50°C and 100°C exhibited higher strength and lower deformations due to a combination of factors such as curing of the concrete and adhesive. In the upper half of the prism both tensile and compressive strains were measured for samples heated up to 150°C. Early development of tensile strains and stresses in the concrete at the end of the laminate was more pronounced in samples heated to temperatures above 200°C. Significant change of the deformability was observed at 200°C but for higher temperatures (250°C and 300°C) the behaviour of the systems was governed by the stabilising effect of the FRPs.

- One failure mode of the CFRP-to-concrete bonded joints was observed for all groups in the temperature range of 20°C to 300°C. The failure occurred in the concrete at the end of the laminate due to stress concentration exceeding the tensile strength of the

concrete. The bonded length was reduced at and above 200°C due to cracks between the adhesive and the concrete and the position of the initial crack changed towards the loaded end. The development of the crack was affected by reduction of the stiffness of the concrete with increase in the temperature.

- The deflection of small-scale CFRP strengthened beams was investigated during the process of heating. The beams were statically loaded during the heating process with a point load of 1kN at midspan. Samples heated above 200°C exhibited higher deformability during the heating phase. Group 50°C reached deflection of 1.43mm and group 300°C registered deflection of 2.01mm when uniform temperature was achieved. Higher residual deformations were registered for samples heated above 200°C as well as visible cracks between the adhesive and concrete and adhesive and laminate.

- The typical failure modes of flexurally strengthened RC beams were reviewed and two main types of failure were identified: at the plate's end and crack induced. The observed failure modes were found in good agreement with experiments reported in the literature. The experimental results showed increased deformability of the beams at higher temperatures. The effect of the heating was found to have a more pronounced influence on the delamination load than the maximum deflection at the ultimate load.

- The cracking pattern was presented for each group with lower loads of initial cracks with increase of the temperature. The failure loads for the different groups were affected by the exposure to different temperatures and proportional decrease of the delamination load was found with increase of the temperature. This effect however had a more significant influence on the failure load than the ultimate flexural load of the systems. For the range of 20°C to 300°C the reduction of failure load was found to be by 65%.

8.1.2 Numerical work

The numerical simulations were also included in this work. Two main studies were conducted on the failure of CFRP bonded joints and the effect of different coefficients of thermal expansion. The results were presented and also analysed.

For the failure load of CFRP strengthened joints good agreement was found between the experimental simulations and the obtained results for the first and second study. The numerical model was updated with the geometry and material properties obtained at a later stage of the work.

The advantage of the proposed model was the straightforward approach to obtain the failure loads based on the tensile strength of the concrete. The reduction of the strength and stiffness of the materials was incorporated in the numerical simulation which could allow further modification and investigation of additional aspects of the heated and cooled systems like thermally induced stresses or shrinkage. The obtained results and the model could be used for assessment of the condition of CFRP strengthened RC beams after heating due to fire or other thermal influences.

In the second numerical study the different rates of thermal expansion of the concrete, adhesive and laminate were investigated. It was found that during the heating process for relatively low temperatures thermally induced stresses near the end of the laminate could develop. Due to the low tensile strength of the concrete the induced stresses could reach critical values and approach the tensile strength of the concrete causing cracking. Another aspect of the heated samples would be the generation of significant tensile stresses in the laminate and compressive stresses in the concrete within the bonded length. However, those stresses were found to be below the corresponding strength of the materials and were unlikely to lead to significant residual deformations. The opposite thermal effect was also investigated. The two different temperature phases of heating of samples to T_g of the adhesive and then cooling were found to induce thermal stresses due to compression in the laminate and tension in the concrete. Such stresses could cause local cracking in the concrete and additional deformability at the strengthened system.

8.2 Recommendations for future work

The purpose of this study was to investigate the properties of CFRP strengthened beams during and after exposure to elevated temperatures. The experimental programme and analysis revealed certain expected reduction of the residual properties of the strengthened systems based on the susceptibility of the polymers to rapid loss of strength due to heating but also increase of the strength for temperature range from 20°C to 100°C. Based on the findings from this study recommendations for further experimental and numerical could include:

- To extend the range of thermal loading to higher temperatures and fire;
- To increase the range of fibre reinforced polymer products for studies of the effect of elevated temperatures and fire;
- To investigate the behaviour of FRP strengthened RC beams for the combined effect of elevated temperature and variation of applied load;
- Large and full scale experiments;
- Further development of the numerical simulations to model different failure modes of the strengthened systems including the effect of heating.

References

References

Abbasi, A & Hogg, P, (2005a) "A model for predicting the properties of the constituents of a glass fibre rebar reinforced concrete beam at elevated temperatures simulating a fire test", *Composites*, part B, vol. 36, pp. 384-393

Abbasi, A & Hogg, P J, (2005b) "Prediction of the failure time of glass fiber reinforced plastic reinforced concrete beams under fire conditions", *Journal Composites for Construction*, pp 450-457

Abbasi, A & Hogg, P J, (2006) "Fire testing on concrete beams with fibre reinforced plastic rebar", *Composites*, part A, vol. 37, pp. 1142-1150

Abdel-Magid, B, Zinee, S, Gass, K & Schneider M, (2005) "The combined effects of load, moisture and temperature on the properties of E-glass/ epoxy composites", *Composite Structures*, vol. 71, pp 320-326

Ahmed, O, Van Gemert, D & Vanderwalle, L, (2001) "Improved model for plate-end shear of CFRP strengthened RC beams", *Cement & Concrete Composites*, vol. 23, pp. 3-19

Al-Amery, R & Al-Mahaidi, R, (2006) "Coupled flexural–shear retrofitting of RC beams using CFRP straps", *Composite Structures*, vol.75 pp. 457–464

Ali, R (2010) *Anchorage of CFRP to RC beams at elevated temperatures* Unpublished BEng(Hons) dissertation, Kingston: Kingston Univesity

Almusallam, T H, (2006) "Load-deflection behavior of RC beams strengthened with GFRP sheets subjected to different environmental conditions", *Cement & Concrete Composites*, vol. 28, pp 879-889

Aprile, A & Feo, L, (2007) "Concrete cover rip-off of R/C beams strengthened with FRP composites", *Composites: Part B*, vol. 38, pp. 759–771

Avril, S, Vautrin, A, Hamelin, P & Surrel, Y, (2005) "A multi-scale approach for crack width prediction in reinforced-concrete beams repaired with composites", *Composites Science and Technology*, vol. 65, pp 445-453

Au, C & Buyukozturk, O (2003), "Debonding of FRP plated concrete: A tri-layer fracture treatment", *Engineering Fracture Mechanics,* vol. 73 pp. 348–365

ANSYS, Inc (2009), *ANSYS 11 Documentation, Theory Reference*

Bai, Y, Vallee, T & Keller, T, (2008) "Modelling of thermal responses for FRP composites under elevated and high temperatures", *Composites Science and Technology,* vol. 68, pp. 47-56

Bazant, Z & Kaplan, M (1996) *Concrete at high temperatures,* Longman Group Limited, England

Bisby, L A, Green, M F & Kodur, V K R, (2005) "Modelling the behaviour of fiber reinforced polymer- confined concrete columns exposed to fire", *Journal of Composites for Construction,* vol 9, No 1

Brena, S F & Macri, B M, (2004) "Effect of Carbon-Fiber-Reinforced Polymer Laminate Configuration on the Behavior of Strengthened Reinforced Concrete Beams" *Journal of composites for construction,* May/June, pp.229- 240

Buchanan, A (2001).*Structural design for fire safety,* John Wiley & Sons, Ltd, England

Buyukozturk, O, Gunes, O & Karaca, E, (2002) "Chractersization and modeling of debonding in RC beams strengthened with FRP composites", 15th ASCE Engineering Mechanics Conference ,June 2-5, 2002, Columbia University, New York, NY

Cadei, J M C, Stratford ,T J, Hollaway, L C, Duckett, W G(2004). *Strengthening metallic structures using externally bonded fibre-reinforced polymers.* CIRIA, London

Camata, G, Spacone, E & Zarnic, R, (2007) " Experimental and nonlinear finite element studies of RC beams strengthened with FRP plates". *Composites,* part B, vol.38, pp 277-288

Carpinteri, A, Cornetti P & Pugno, N, (2009) "Edge debonding in FRP strengthened beams: Stress versus energy failure criteria", *Engineering Structures*, vol. 31, pp. 2436-2447

Casas, J R, Pascual, J, (2007) "Debonding of FRP in bending: Simplified model and experimental validation", *Construction and Building Materials,* vol. 21, pp.1940–1949

CEB-FIP Model Code 1990, Thomas Telford

Ceroni, F & Pecce, M, (2007) "Cracking behaviour of RC beams externally strengthened with emerging materials", *Construction and Building Materials*, vol. 21, pp. 736–745

Ceroni, F & Pecce, M, (2009). "Design provisions for crack spacing and width in RC elements externally bonded with FRP", *Composites: Part B*, vol. 40, pp. 17–28

Chen, J F & Teng, J G (2001). "Anchorage strength models for FRP and steel plates bonded to concrete", *Journal of Structural Engineering*, ASCE, vol.127 (7), pp.784–91

Chen, J F, Yang Z J, Holt G D (2001)."FRP or steel plate-to-concrete bonded joints: effect of test methods on experimental bond strength", *Steel Composite Structure*, vol.1(2), pp.231–44

Chen, F & Qiao, P, (2009) "Debonding analysis of *FRP–concrete interface between two* balanced adjacent flexural cracks in plated beams", *International Journal of Solids and Structures*, vol. 46, pp.2618–2628

Cho, K, Cho, J-R, Chin, W-J, Kim, B-S, (2006) "Bond-slip model for coarse sand coated interface between FRP and concrete from optimization technique", *Computers and Structures*, vol.84, pp. 439–449

Clark L A (1983). *Concrete bridge design to BS5400.* Construction press

Debaiky, A S, Green, M F & Hope, B, (2006) "Long-term monitoring of carbon fiber-reinforced polymer-wrapped reinforced concrete columns under severe environment ", *ACI Structural Journals,* vol.103, N 6

De Lorenzis, L & Zavarise, G (2009) "Cohesive zone modeling of interfacial stresses in plated beams", *International Journal of Solids and Structures*, vol. 46, pp. 4181–4191

Donchev,T, Wen, J & Papa, E (2007) "Effect of elevated temperatures on CFRP strengthened structural elements" *11th International conference Fire and materials, San Francisco, USA*

Ferracuti, B, Savoia, M & Mazzotti, C, (2006)"A numerical model for FRP–concrete delamination", *Composites: Part B* , vol.37, pp.356–364

Ferracuti B, Savoia, M &, Mazzotti C, (2007) "Interface law for FRP–concrete delamination", *Composite Structures*, vol. 80, pp. 523–531

Foster, S K & Bisby, L A, (2005) "High temperature residual properties of externally-bonded FRP systems". In: *Proceedings of the 7th international symposium on FRP reinforcement for concrete structures,* vol 2, pp 1235-1252

Galati, N, Nanni, A, Dharani, L R, Focacci, F & Aiello, M A, (2006) "Thermal effects on bond between FRP rebars and concrete", *Composites:* part A , vol 37, pp. 1223-1230

Garden, H N & Hollaway, L C 1998. "An experimental study of the influence of plate end anchorage of carbon fibre composite plates used to strengthen reinforced concrete beams", *Composite Structures,* vol.42, pp 175-188

Gardiner, C P, Mathys, Z & Mouritz, A P, (2004) "Post-fire structural properties of burnt GRP plates", *Marine Structures* ,vol. 17, pp 53-73

Greco, F, Lonetti, P & Nevone B, (2007) "An analytical investigation of debonding problems in beams strengthened using composite plates", *Engineering Fracture Mechanics*, vol. 74 , pp. 346–372

Green, M F, Bisby, L A, Fam, A Z & Kodur, V K R, (2006) "FRP confined concrete columns: Behaviour under extreme conditions", *Cement & Concrete Composites*, vol. 28, pp. 928-937

Gunes, O, Buyukozturk, O & Karaca, E, (2009) "A fracture-based model for FRP debonding in strengthened beams", *Engineering Fracture Mechanics,* vol.76, pp. 1897–1909

Halli, M (2009) *FRP at elevated temperatures* Unpublished BEng(Hons) dissertation, Kingston: Kingston Univesity

Han, L H, Zheng, Y Q & Teng, J G, (2006) "Fire resistance of RC and FRP-confined C columns", *Magazine of Concrete Research,* vol.58, no. 8, pp. 533-546

Hassanen, M & Raoof, M, (2001) "Design against premature peeling failure of RC beams with externally bonded steel or FRP plates", *Magazine of Concrete Research, vol. 53, No 4, pp. 251-262.*

Hollaway, L C and Leeming, M B, eds (2000). *Strengthening of reinforced concrete structures using externally-bonded FRP composites in structural and civil engineering.* Woodhead publishing limited, Cambridge England

Karadeniz, Z H & Kumlutas, D, (2007) "A numerical study on the coefficients of thermal expansion of fiber reinforced composite materials", *Composite Structures,* vol 78, pp 1-10

Keller, T, Tracy, C & Zhou A, (2006a) "Structural response of liquid-cooled GFRP slabs subjected to fire. Part I. Material and post-fire modeling", *Composites*: *part A*, vol. 37, pp 1286-1295

Keller, T, Tracy, C & Zhou A, (2006b) "Structural response of liquid-cooled GFRP slabs subjected to fire. Part II: Thermo-chemical and thermo-mechanical modeling", *Composites,* part A, vol. 37, pp 1296-1308

Keller, T, Zhou, A, Tracy, C, Hugi, E & Schnewlin, P, (2005) " Experimental study on the concept of liquid cooling for improving fire resistance of FRP structures for construction", *Composites Part A,* vol. 36, pp. 1569-1580

Key, C T & Lua, J, (2006) " Constituent based analysis of composite materials subjected to fire conditions", *Composites,* part A, vol.37, pp 1005-1014

Kodur, V K R, Bisby, L A,Green, M F & Chowdhury, E, (2005) "Fire endurance of insulated FRP-strengthened square concrete columns".In: *Proc 7th int symp FRP reinforcement for concrete structures,* vol 2, pp 1253-1268

Kodur, V K R, Bisby, L A & Green, M, (2006) "Experimental evaluation of the fire behaviour of insulated fibre-reinforced-polymer-strengthened reinforced concrete columns", *Fire Safety Journal,* vol.41, pp. 547-557

Logan, D (1992). *A first course in the finite element method, 2nd edition,* PWS publishing company, USA

Leung, C KY, (2006). "FRP debonding from a concrete substrate: Some recent findings against conventional belief", *Cement & Concrete Composites,* vol. 28, pp. 742–748

Li , LJ , Guo, Y C, Liu , F & Bungey J H, (2006) " An experimental and numerical study of the effect of thickness and length of CFRP on performance of repaired reinforced concrete beams", *Construction and Building Materials*, vol.20, pp. 901–909

Lu, X Z, Jiang, J J, Teng, J G & Ye, L P, (2006) "Finite element simulation of debonding in FRP-to-concrete bonded joints", *Construction and Building Materials,* vol. 20, pp 412-424

Lu, X Z, Teng, J G , Ye, L P & Jiang, J J, (2005) "Bond–slip models for FRP sheets/plates bonded to concrete", *Engineering Structures*, vol.27, pp. 920–937

Maalej, M & Bian, Y, (2001) "Interfacial shear stress concentration in FRP-strengthened beams", *Composite Structures,* vol. 54, pp. 417-426

Maalej, M & Leong, K S, (2005). "Effect of beam size and FRP thickness on interfacial shear stress concentration and failure mode of FRP-strengthened beams", *Composites Science and Technology*, vol. 65, pp. 1148–1158

Madenci, E & Guven., I (2006). *The finite element method and applications in engineering using ANSYS* ,Springer Science+Business Media, USA

Matthys, S & Taerwe, L, (2006) "Evaluation of ductility requirements in current design guidelines for FRP strengthening", *Cement & Concrete Composites*, vol. 28, pp. 845–856

Mays, G C & Hutchinson, A R (1992). *Adhesives in civil engineering,* Cambridge University press, UK

Mazzotti, C, Savoia, M & Ferracuti, B, (2008)"An experimental study on delamination of FRP plates bonded to concrete", *Construction and Building Materials*, vol. 22, pp.1409–1421

Mazzotti, C, Savoia, M & Ferracuti, B, (2009) "A new single-shear set-up for stable debonding of FRP–concrete joints", *Construction and Building Materials*, vol. 23, pp.1529–1537

Mouritz, A P, Mathys, Z & Gardiner, C P, (2004)"Thermomechanical modelling the fire properties of fibre-polymer composites", *Composites*, part B, vol.35, pp 467-474

Neto, P, Alfaiate, J, Almeida, J R & Pires, E B, (2004) "The influence of mode II fracture on concrete strengthened with CFRP", *Computers and Structures*, vol.82, pp.1495–1502

Oehlers, D J, (2006) "Ductility of FRP plated flexural members", *Cement & Concrete Composites*, vol. 28, pp. 898–905

Oehlers, D J, (2006) "FRP Plates Adhesively Bonded to Reinforced Concrete Beams: Generic Debonding Mechanisms", *Advances in Structural Engineering,* Vol. 9 No.6, pp. 737-750

Oehlers, D J, Griffith, M C & Mohamed Ali, M S, (2009) "Ductility components and limits of FRP-plated RC structures", *Construction and Building Materials*, vol. 23, pp. 1538–1543

Oehlers, D J, Park, S M & Mohamed Ali, M S, (2003) "A structural engineering approach to adhesive bonding longitudinal plates to RC beams and slabs", *Composites: Part A*, vol. 34, pp 887–897

Pesic´, N & Pilakoutas, K, (2003) "Concrete beams with externally bonded flexural FRP-reinforcement: analytical investigation of debonding failure", *Composites: Part B,* vol. 34 pp. 327–338

Pham, H & Al-Mahaidi, R, (2004) "Assessment of available prediction models for the strength of FRP retrofitted RC beams", *Composite Structures*, vol. 66, pp. 601–610

Pham, H & Al-Mahaidi, R. (2004) "Experimental investigation into flexural retrofitting of reinforced concrete bridge beams using FRP composites", *Composite Structures*, vol. 66, pp. 617–625

Qiao, P & Chen, F, (2008) "An improved adhesively bonded bi-material beam model for plated beams", *Engineering Structures,* vol. 30, pp.1949–1957

Qiao, P & Chen, Y, (2008) "Cohesive fracture simulation and failure modes of FRP–concrete bonded interfaces", *Theoretical and Applied Fracture Mechanics,* vol.49 pp. 213–225

Rabinovitch, O, (2004) "Fracture-mechanics failure criteria for RC beams strengthened with FRP strips—a simplified approach", *Composite Structures,* vol.64, pp. 479–492

Rabinovitch, O, (2008) "Debonding analysis of fiber-reinforced-polymer strengthened beams: Cohesive zone modeling versus a linear elastic fracture mechanics approach", *Engineering Fracture Mechanics*, vol. 75, pp. 2842–2859

Rabinovitch, O & Frostig, Y, (2003) "Experiments and analytical comparison of RC beams strengthened with CFRP composites", *Composites: Part B*, vol. 34, pp. 663–677

Ramana, V P V, Kant, T, Morton, S E, Dutta, P K, Mukherjee, A & Desai,Y M, (2000) "Behavior of CFRPC strengthened reinforced concrete beams with varying degrees of strengthening", *Composites: Part B,* vol. 31, pp. 461-470

Saafi, M, (2002) "Effect of fire on FRP reinforced concrete members", *Composite Structures,* vol. 58, pp. 11-20

Smith, S T & Teng, J G, (2001) "Interfacial stresses in plated beams", *Engineering Structures,* vol. 23, pp. 857–871

Smith, S T & Teng, J G, (2002)"FRP-strengthened RC beams. I: review of debonding strength models", *Engineering Structures*, vol. 24, pp. 385–395

References

Smith, S T & Teng, J G, (2002)"FRP-strengthened RC beams. II: assessment of debonding strength models", *Engineering Structures*, vol. 24, pp. 397–417

Teng, J G, Yuan, H & Chen, J F, (2006) "FRP-to-concrete interfaces between two adjacent cracks: Theoretical model for debonding failure", *International Journal of Solids and Structures*, vol. 43, pp. 5750–5778

Thomsen, H, Spacone, E, Limkatanyu, S & Camata, G, (2004) "Failure Mode Analyses of Reinforced Concrete Beams Strengthened in Flexure with Externally Bonded Fiber-Reinforced Polymers", *Journal of composites for construction*, vol. March/April, pp. 123-131

Tounsi, A, (2006) "Improved theoretical solution for interfacial stresses in concrete beams strengthened with FRP plate", *International Journal of Solids and Structures*, vol. 43, pp. 4154–4174

Tounsi, A & Benyoucef, S, (2007) "Interfacial stresses in externally FRP-plated concrete beams", *International Journal of Adhesion & Adhesives,* vol 27, pp. 207–215

Tounsi , A, Hassaine Daouadji, T, Benyoucef, S, & Addabedia, E A, (2009)." Interfacial stresses in FRP-plated RC beams: Effect of adherend shear deformations", *International Journal of Adhesion & Adhesives,* vol. 29, pp. 343–351

Wang, J, (2006) "Debonding of FRP-plated reinforced concrete beam, a bond-slip analysis. I. Theoretical formulation", *International Journal of Solids and Structures*, vol. 43, pp. 6649–6664

Wang, J,(2006) "Cohesive zone model of intermediate crack-induced debonding of FRP-plated concrete beam", *International Journal of Solids and Structures*, vol. 43 6630–6648

Wang, J, (2007) "Cohesive-bridging zone model of FRP–concrete interface debonding", *Engineering Fracture Mechanics*, vol.74, pp. 2643–2658

Wang, J, (2007) "Cohesive zone model of FRP-concrete interface debonding under mixed-mode loading", *International Journal of Solids and Structures*, vol. 44, pp. 6551–6568

Wang, J & Zhang, C, (2008) "Nonlinear fracture mechanics of flexural–shear crack induced debonding of FRP strengthened concrete beams", *International Journal of Solids and Structures* vol.45, pp. 2916–2936

Wang, Y C & Kodur, V, (2005) "Variation of strength and stiffness of fibre reinforced polymer reinforcing bars with temperature", *Cement & Concrete Composites*

Wenwei, W & Guo, L, (2006) "Experimental study and analysis of RC beams strengthened with CFRP laminates under sustaining load", *International Journal of Solids and Structures*, vol.43 pp. 1372–1387

Wong, P M H, Davies, J M & Wang, Y C, (2004) "An experimental and numerical study of the behaviour of glass fibre reinforced plastics (GRP) short columns at elevated temperatures", *Composite Structures,* vol. 63, pp. 33-43

Wu, Z J & Ye, J Q, (2003) "Strength and fracture resistance of FRP reinforced concrete flexural members", *Cement & Concrete Composites*, vol. 25, pp. 253–261

Wu, Z, Yuan, H, Kojima, Y & Ahmed E, (2005)" Experimental and analytical studies on peeling and spalling resistance of unidirectional FRP sheets bonded to concrete". *Composites Science and Technology,* vol.65, pp 1088-1097

Yang, J & Wu, Y-F, (2007) "Interfacial stresses of FRP strengthened concrete beams: Effect of shear deformation", *Composite Structures*, vol. 80, pp. 343–351

Yang, J & Ye, J, (2010) "An improved closed-form solution to interfacial stresses in plated beams using a two-stage approach" , *International Journal of Mechanical Sciences*, vol. 52, pp. 13–30

Yao, J, Teng, J G & Chen, J F, (2005) "Experimental study on FRP-to-concrete bonded joints", *Composites: Part B*, vol. 36, pp.99–113

References

Yuan, H, Teng, J G, Seracino, R , Wu, Z S & Yao, J, (2004)" Full-range behavior of FRP-to-concrete bonded joints", *Engineering Structures*, vol.26, pp. 553–565

Zhang, J S, Karbhari, V M, Wu, L & Reynaud, D, (2003) "Field exposure based durability assessment of FRP column wrap systems". *Composites,* part B, vol.34, pp 41-50

Appendix

List of publications

Petkova,D, Donchev, T, Wen, J, Etebar, K & Hadaviania (2007) "Effect of elevated temperatures on the bond between FRP and concrete", *Interflam 2007 Proceedings of the eleventh International Conference*, Vol. 1, pp 783-790

Petkova,D, Donchev, T, Wen, J (2008) "FE modelling of the effect of elevated temperatures on the anchoring of CFRP laminates", *Excellence In Concrete Construction Through Innovation: Proceedings Of The International Conference On Concrete Construction.* Kingston University, Kingston upon Thames 9-10 September 2008. London: Taylor & Francis, pp. 351-356.

Petkova,D, Donchev, T (2010) " Behaviour of externally strengthened RC elements at elevated temperatures", *Interflam 2010 Proceedings of the eleventh International Conference*

Effect of Elevated Temperatures on the Bond between FRP and Concrete

Diana Petkova, Ted Donchev, Jennifer Wen, Kamran Etebar and Homayoun Hadavinia
Kingston University, London

INTRODUCTION

In recent years the fibre reinforced polymers (FRP) have become a very popular material for structural maintenance due to their outstanding mechanical properties and easy to install application. As a relatively new material in construction the polymers are still subject to further research about their performance in different environmental conditions. The influence of elevated temperatures on the composite systems could be an important factor. As recent experiments[2,4] have proved one of the weakest points of composite strengthened systems is the anchorage. The problem is complicated due to the local concentration of stresses and the possibilities for several different modes of failure. The influence of thermal load could be one of the reasons for a poorer performance of the materials and it could lead to premature failure due to the undergone physical and chemical changes in them.

The purpose of this paper is to investigate the effect of elevated temperatures on externally strengthened reinforced concrete beams with carbon fibre reinforced polymers (CFRP). The focus of the work is to evaluate the performance of the anchoring zone of the laminates with the consideration of elevated temperature as an additional factor. The possible modes of failure are analyzed on the basis of assessment of crack propagation.

A finite element model is developed in order to determine the behaviour of the strengthened system in respect of temperature-dependent mechanical properties. The investigation is compared with experimental results of concrete prisms with attached CFRP plates tested after heating and cooling.

THEORETICAL BACKGROUND

The experimental work on concrete beams externally strengthened with CFRP laminates has shown basically three modes of failure at the anchoring zone (figure 1) - debonding in the FRP composite-adhesive interface, debonding in the concrete-adhesive interface and so called "concrete cover separation". The investigation of the problem is influenced by different factors due to the wide variety of properties of materials of the composite element - reinforced concrete, adhesive and laminate.

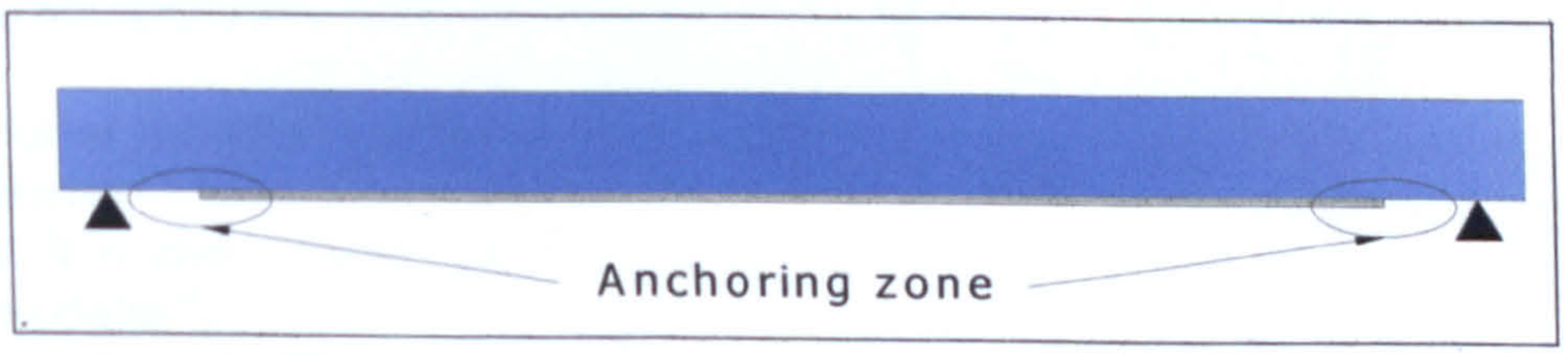

Figure 1. Externally strengthened reinforced concrete beam

At normal temperatures the ultimate behaviour of the strengthened system has been subject of numerous studies. The modes of failure in connection with different factors have been substantially investigated in order to develop measures to prevent premature failure of the strengthened system. In 1998 Garden et al[1] tested externally bonded CFRP laminates to reinforced concrete beams. The failure modes were related to the shear span/depth ratios which lead to partial or full cover separation. High shear span/ depth ratios were connected with failures due to high bending moments away from the end of the laminate. The authors recommended anchorage of the plate end at the support region of the beam which would prevent a premature failure.

In their work Buyle-Bodin et al[3] observed that all the reinforced concrete beams externally strengthened with CFRP plates failed in one manner- by concrete cover separation. As the experiments were not

conducted with initially pre-cracked beams the development of cracks was influenced by the additional plates. The process of delamination was described to start with shear cracks at the end of the laminate at 80 % of the ultimate load, which connected with existing flexural cracks and then a horizontal crack developed in a brittle manner at the level of the internal reinforcement.

Yang et al[4] used a discrete crack approach to model numerically the crack propagation in FRP strengthened beams. The effect of different lengths of the attached plates was investigated. The influence of 2200mm long plate attached to 2500mm beam in comparison with an unstrengthened element was expressed in significant reduction in the crack propagation process. However, a 1600mm long plate attached to the same beam lead to brittle failure of the concrete in cover separation mode as the propagation of shear cracks outside the strengthened zone was not prevented.

Up-to-date there is insufficient information in the literature about the influence of elevated temperatures on the behaviour of composite structures and the corresponding debonding stresses. Due to their nature all the polymers show the same tendency to soften as their glass transition temperature is approached and at high temperatures they decompose[13]. The mechanical properties of the FRP at different temperatures are still subject of investigation. Figure 2 and 3 represent the general reduction of the mechanical properties of glass FRP with temperature as indicated by Davies[8] and Wong[9].

Temperature was included in the experimental work of Klamer et al[5]. Research was carried out in two ranges of elevated temperatures up to 40°C and in 50-75°C and double-lap shear tests were conducted . The specimens at the lower range failed due to concrete cracking leaving 1-3mm of it on the adhesive layer, while at the upper temperature range debonding occurred between the concrete surface and the adhesive. The results were explained as the stiffness of the adhesive was reduced in process of approaching to the glass transition temperature (Tg) of the material.

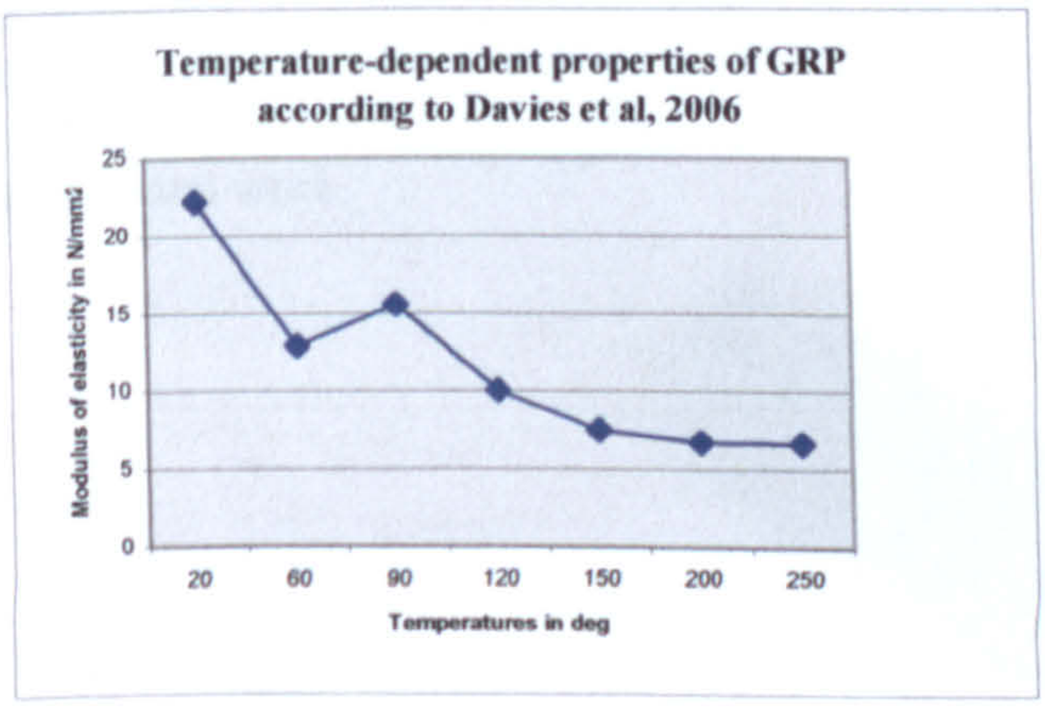

Figure 2.Decrease of modulus of elasticity with temperature

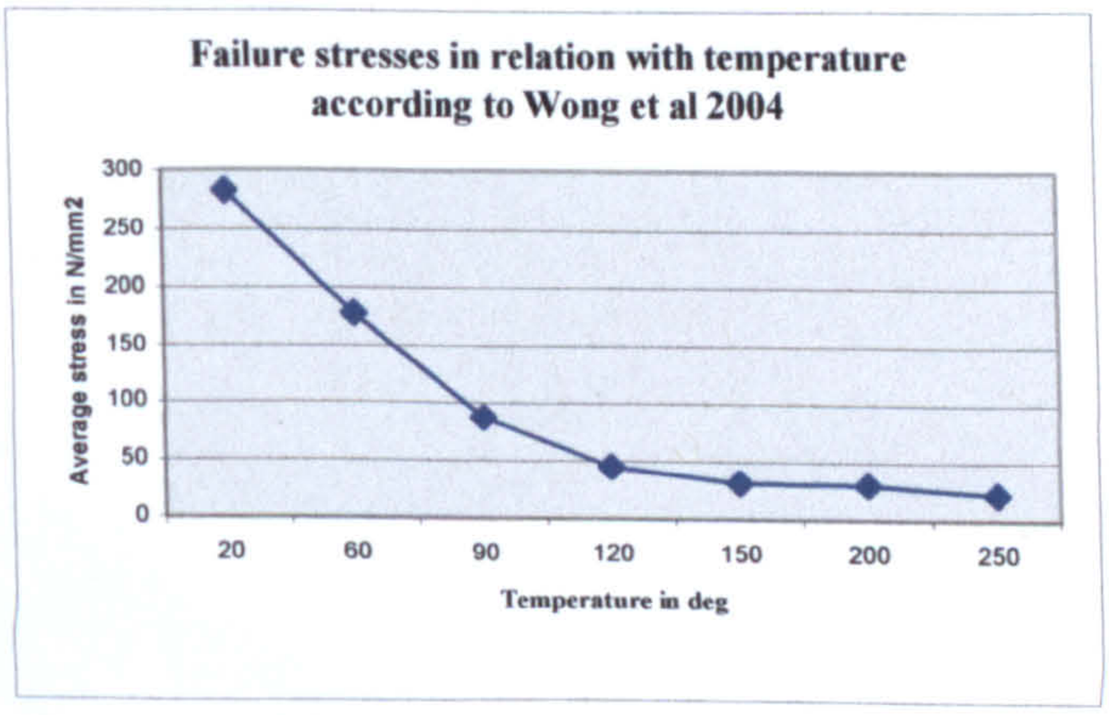

Figure3.Failure stresses from compression tests of glass fibre reinforced plastic channels

NUMERICAL MODELING AND COMPARISON WITH EXPERIMENTAL RESULTS

The behaviour at elevated temperatures of concrete and steel is relatively well known. Up to 300°C concrete experiences changes in its mechanical properties including certain reduction of its strength and Young modulus. It is also observed that the magnitude of reduction is similar to both compressive strength and elastic modulus[14].

The mechanical properties of different fibre reinforced polymers at elevated temperatures are less investigated. At normal temperatures the behaviour of different types of adhesive and polymer is known as is usually provided by manufacturer[13] (table 1).

Material	**Modulus of elasticity at room temperature**	**Coefficient of thermal expansion**
Concrete C20	30000 MPa	$10x10^{-6}$/°C
CFRP laminate	165 000 MPa	$0x10^{-6}$/°C
Epoxy adhesive	9800 MPa	$33x10^{-6}$/°C
Steel	210 000 MPa	$12x10^{-6}$°C

Table1.Typical values of materials in a strengthened system

If the information about temperature-dependent properties is not available then the rule of mixtures can be applied for calculations of the E modulus for an unidirectional composite using the mechanical data of the constituents[13]. The rate of reduction of the strength with the increase of temperature is scarce and the data available is not sufficient to provide relevant guidance for modeling of the thermally degraded polymers. Bisby et al[7] suggested a semiempirical analytical relationship in order to describe the deterioration of the material properties of the carbon/epoxy FRP, which is used for the purpose of the paper.

The numerical modeling is performed using ANSYS. A concrete prism with dimensions of 300x75x75 mm is modeled and a 250x35x6 mm laminate is attached to the prism with 100mm length of anchorage. The prism is reinforced with a R8 steel rod in its centre and as an attaching material a 2mm adhesive element is modeled between concrete and laminate. The analysis is divided in two steps. The first step simulates the behaviour of the anchoring zone at normal temperatures and applied tensile force in order to estimate the stress distribution in the materials. The residual capacity of the constituents in the strengthened system is evaluated in order to predict the mode of failure.

The second step simulates the anchoring zone with temperature dependent material properties of concrete, CFRP, adhesive and steel at temperatures up to 250°C. The specimen is loaded in tension after the corresponding heating and cooling.

The concrete prism, adhesive and laminate are modeled and meshed with solid elements which have the option of assignment of temperature-dependent mechanical properties for each material. Due to the options of the program for refinement of the mesh a tetrahedral element is chosen with a limit of the length of finite elements and the anchorage zone mesh was refined in order to prevent significant error (figure 4). The reinforcing steel was modeled with a link element.

The boundary conditions of the concrete prism are horizontal constraints on the side surface of the solid where the tension force is applied on the laminate and a vertical constraint applied to the opposite surface in order to prevent rotation. The boundary conditions reflect the support conditions from the available experimental work.

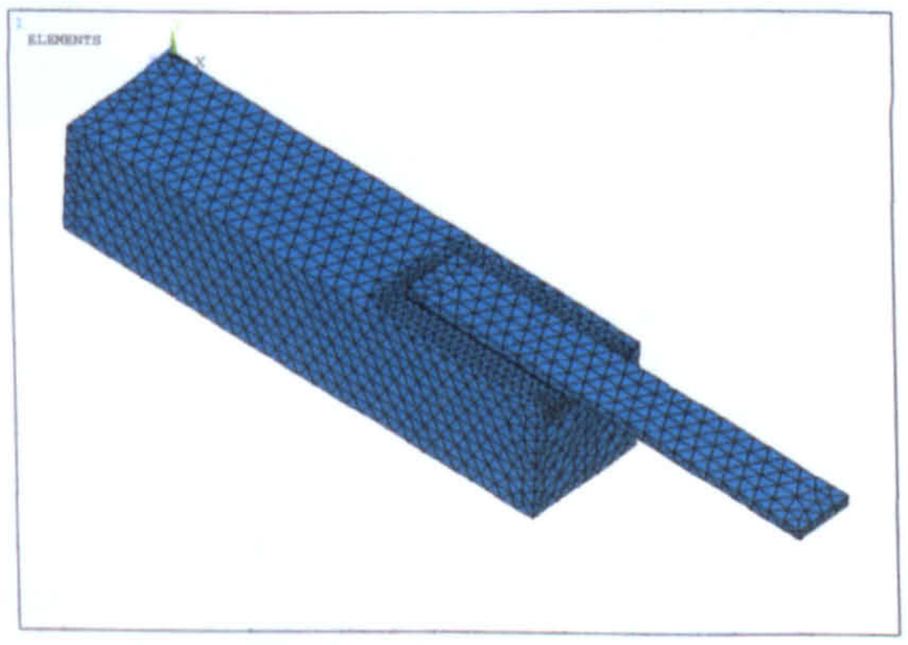

Figure 1. Finite element model

The model simulates the performance of the strengthened system as the stresses from the applied tension force on the laminate are transferred via the adhesive layer to the concrete. At all levels of loading the strength of the CFRP is not exceeded by the corresponding stresses and the failure of the specimen is not expected to occur due to weak performance of the laminate.

Due to applied tension load on the laminate significant concentration of tension stresses in the concrete close to the attached edge of the laminate is observed. The potential failure modes of the system are governed by the stress concentration in the adhesive layer and concrete.

At 4kN external load the maximum normal stress in the adhesive is approximately 2.5 MPa and the concentration of stress at the laminate's end in concrete is close to 2MPa. The capacity of normal stress in the adhesive is 17 N/mm^2 as provided the manufacturer. Assuming concrete C20 for the concrete prism the tension capacity of the concrete is calculated as 2.78MPa on basis of formulae given by Clark[15]:

$$f_t = 0.556\sqrt{f_{cu}} \qquad (1)$$

At 4.7kN at the zone of laminate's end the tension capacity of concrete is exceeded (figure 5) which indicates conditions for initiation of a crack due to tension stresses.

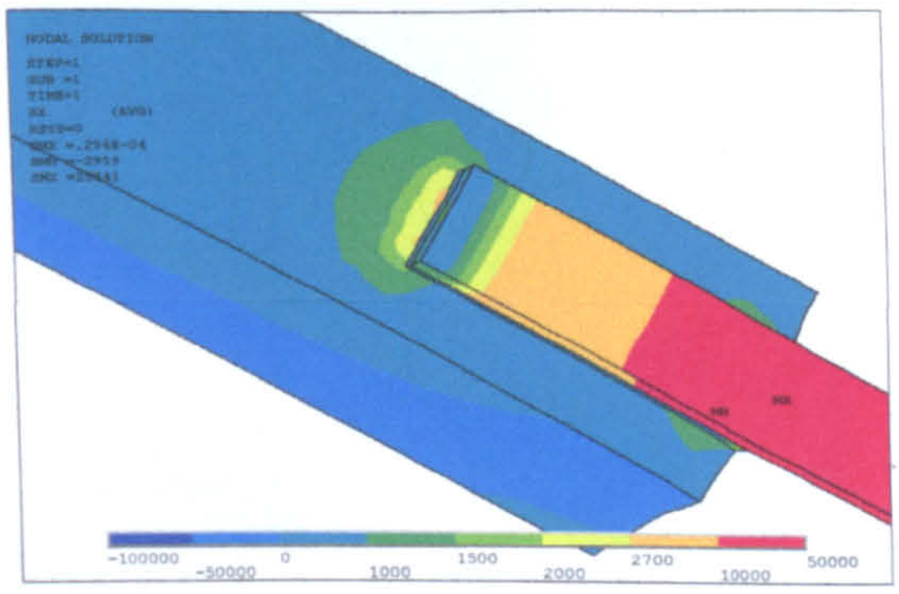

Figure 5 Normal stresses in the longitudinal cross section at 4.7 kN

The occurrence of similar cracks in early stages of loading is reported in literature[4]. The laminate limits the crack propagation inside the strengthened zone thus providing conditions for development of a crack outside the attachment area. The crack is not crucial for the overall performance of the strengthened system due to the action of the steel reinforcement.

In order to model crack development a 10mm vertical opening in concrete at the laminate's end is simulated (figure 6). At higher levels of loading the stress concentration at the crack tip is estimated in order to predict the further propagation of the crack.

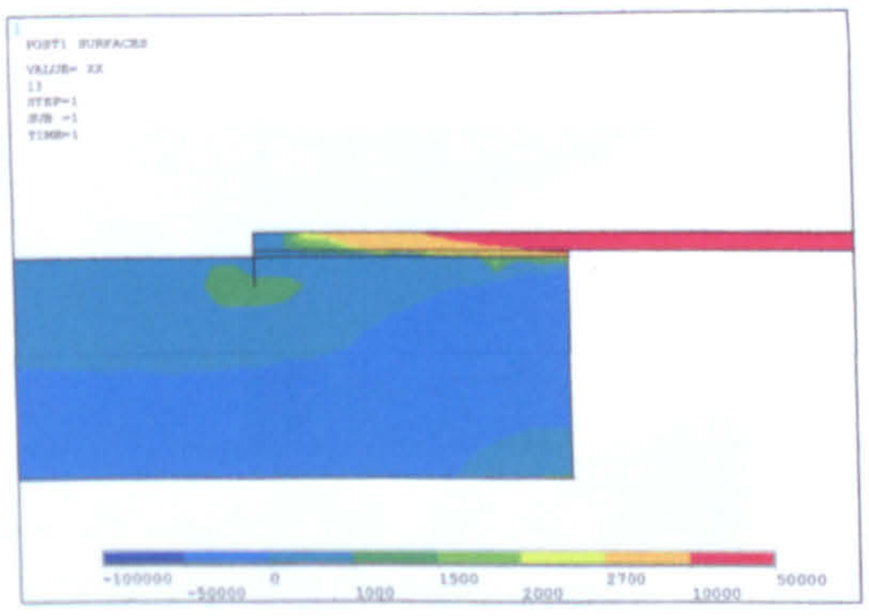

Figure 6 Normal stress at load 7kN

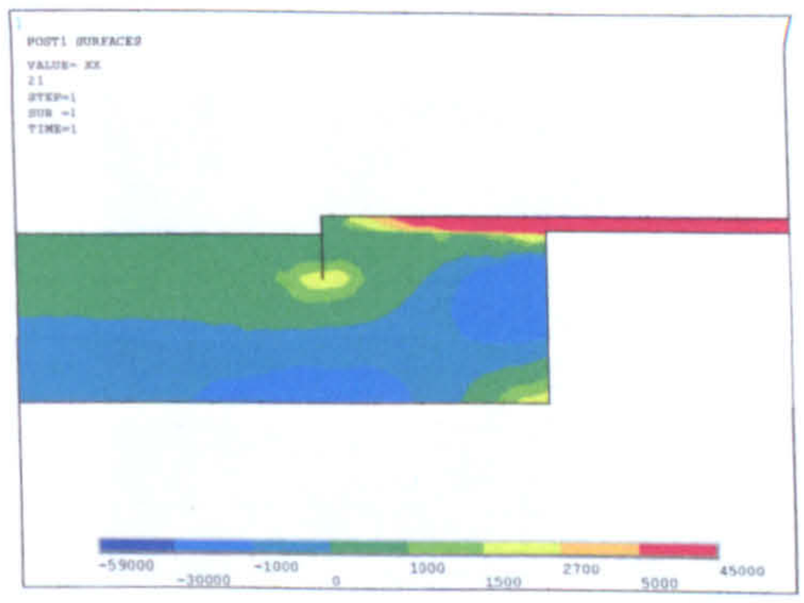

Figure7 Normal stress at load 8.5kN

Due to further increase of external tension force additional increase of normal stresses in the concrete at the zone close to the tip of the crack is observed. When the ultimate tension strength of the concrete is exceeded further propagation of the crack in vertical direction has to be expected in the same manner as indicated in experimental results.

As the third step of development the distribution of stresses around 20mm deep crack due to increased loading is analyzed. At 8.5kN external load the distribution of normal (figure 7) and principal stresses (figure 8) is mainly in horizontal direction, which indicates that the probability of development of the crack in this direction is much higher than in vertical.

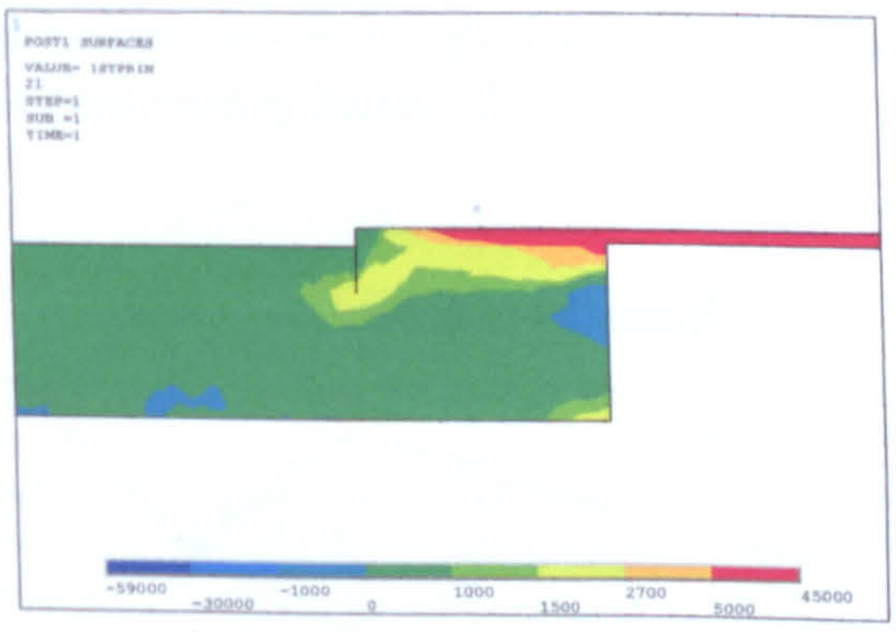

Figure *8 Principal* stress at 8.5kN

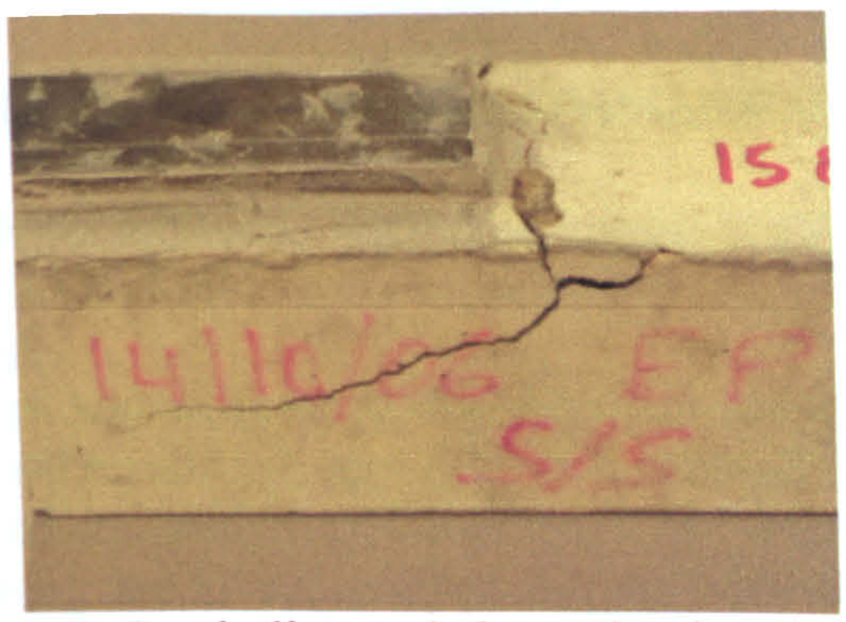

Figure 9. Parabolic crack formation in specimens.

The comparison with experimental results indicates similarly high chance for parabolic curving of the crack and change of its direction (figure 9). The wide area of relatively high stresses leads to opportunity for fast development of horizontal crack accompanied with a brittle failure.

As second stage of development of model reflecting the influence of elevated temperatures on the mechanical characteristics (strength and stiffness) of the materials corresponding changes are introduced. The changes of the mechanical characteristics of the model at elevated temperature lead to conditions of initial crack occurrence and propagation at lower levels of loading as confirmed by experimental data (figure 10 and 11). The numerical results show gradual increase of the thermal stresses induced in the materials due to their different coefficients of thermal expansion. This problem will be subject of future investigation.

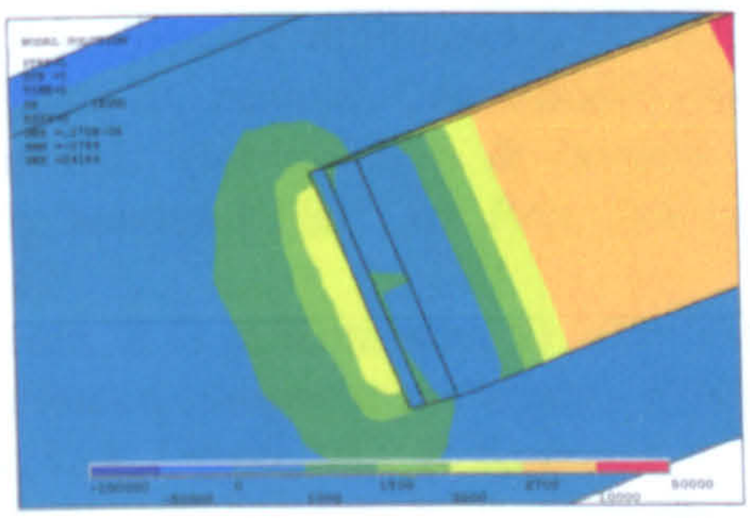

Figure 10 Normal stress at 4.5kN normal temperatures

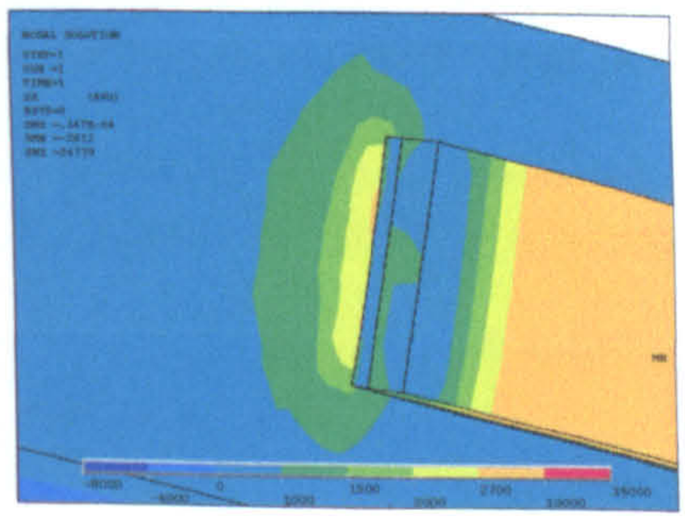

Figure 11 Normal stress at 4.5kN, 250 degrees

VALIDATION OF FINITE ELEMENT MODEL

The FE results are validated via detailed comparison of available data from experimental work on similar concrete prisms with externally attached CFRP laminate. The tests were conducted by Donchev et al[10] with samples heated uniformly up to 250°C and loaded after cooling. The specimens were subjected to one-lap shear testing with the tension applied to the polymer plate and the concrete loaded in compression. The samples were loaded to failure which resulted in a longitudinal crack and corresponding concrete cover separation on the level of the reinforcement. It was observed that the temperature loading lead to visible changes in the colour of the laminates. At 200°C slight change to brownish was reported in the adhesive and up to 250°C delamination occurred in the outer layers of the polymer.

The comparison of the results is presented in figure 12.

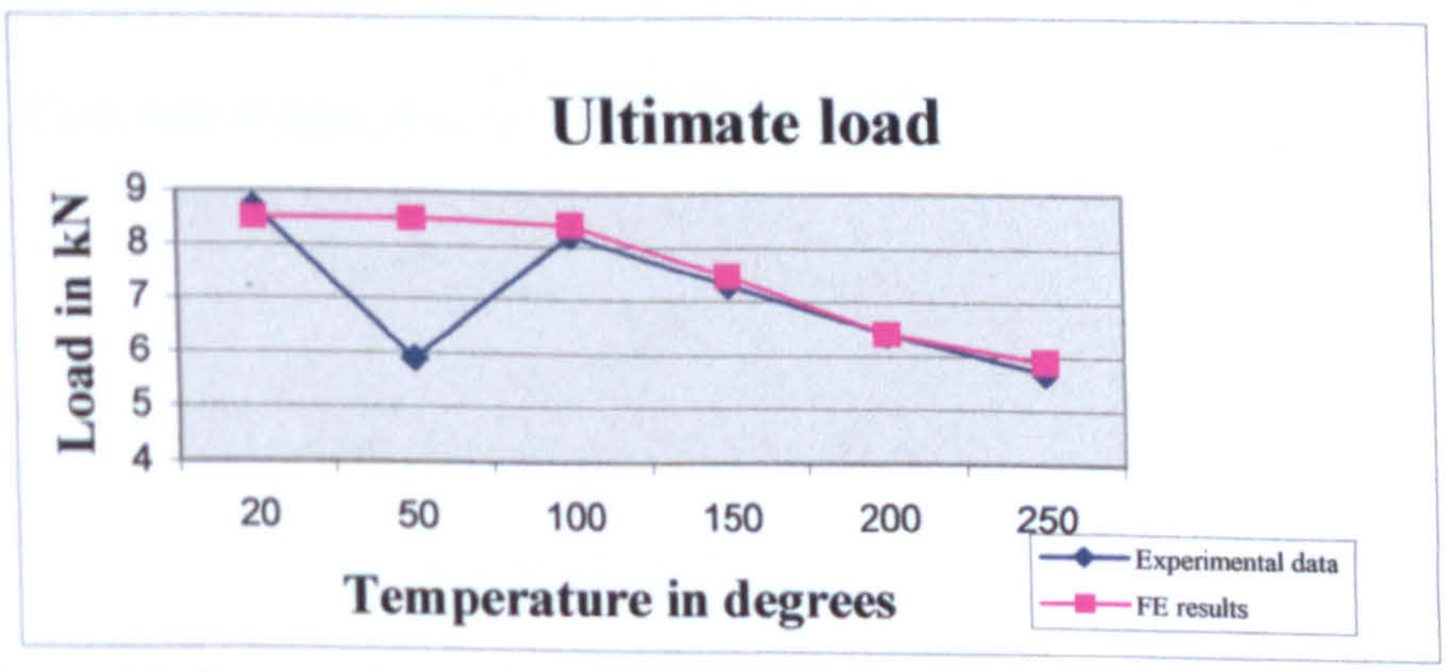

Figure 12. Comparison of experimental data and finite element analysis

CONCLUSIONS AND RECOMMENDATIONS

On basis of the presented research the following main conclusions could be drawn:

- A finite element model of concrete cover separation mode of failure at the anchorage of CFRP laminates to concrete is developed;
- Reduction of the strength and stiffness of the materials at elevated temperatures up to 250°C is incorporated in the model. Obtained results are very similar to relevant experimental results;
- The obtained results and the model could be used for assessment of the condition of CFRP strengthened RC beams after heating due to fire or other thermal influences.

The model is intended to be developed further in order to reflect higher temperatures with corresponding thermal stresses and other possible modes of failure.

REFERENCES

1.Garden, H N & Hollaway, L C 1998. " An experimental study of the influence of plate end anchorage of carbon fibre composite plates used to strengthen reinforced concrete beams". *Composite Structures,* vol.42, pp 175-188

2. Hollaway, L C and Leeming, M B, eds 2000.*Strengthening of reinforced concrete structures using externally-bonded FRP composites in structural and civil engineering.* Woodhead publishing limited, Cambridge England

3.Buyle- Bodin, F, David, E & Ragneau, E 2002. " Finite element modeling of flexural behaviour of externally bonded CFRP reinforced concrete structures". *Engineering Structures,* vol 24, pp. 1423-1429

4.Yang, Z J, Chen, J F & Proverbs, D 2003. " Finite element modeling of concrete cover separation failure in FRP plated RC beams". *Construction and Building Materials,* vol 17, pp. 3-13

5.Klamer, E L, Hordijk, D A & Janssen, H J M 2005."The influence of temperature on debonding of externally bonded CFRP" In: *Proc 7th int symp FRP reinforcement for concrete structures,* vol 2, pp 1551-1567

6.Karadeniz, Z H & Kumlutas, D 2007. "A numerical study on the coefficients of thermal expansion of fiber reinforced composite materials". *Composite Structures,* vol 78, pp 1-10

7. Bisby, L A, Green, M F & Kodur, V K R 2005."Modelling the behaviour of fiber reinforced polymer-confined concrete columns exposed to fire". *Journal of Composites for Construction,* vol 9, No 1

8.Davies, J M, Wang, Y C & Wong, P M H 2006. " Polymer composites in fire", *Composites Part A,* vol 37, pp. 1131-1141

9.Wong, P M H, Davies, J M & Wang, Y C 2004. "An experimental and numerical study of the behaviour of glass fibre reinforced plastics (GRP) short columns at elevated temperatures", *Composite Structures,* vol. 63, pp. 33-43

10.Donchev,T, Wen, J & Papa, E 2007. "Effect of elevated temperatures on CFRP strengthened structural elements" *11th Int conf Fire and materials, San Francisco, USA*

11.BS EN 1992-1-1:2004. *Eurocode 2: Design of concrete structures- Part 1-1: General rules and rules for buildings*

12. BS EN 1992-1-1:2004. *Eurocode 2: Design of concrete structures- Part 1-2: General rules – Structural fire design*

13. Cadei, J M C, Stratford ,T J, Hollaway, L C, Duckett, W G 2004. *Strengthening metallic structures using externally bonded fibre-reinforced polymers.* CIRIA, London

14. Concrete Society 1990.*Assessment and repair of fire-damaged concrete structures.* Technical report No33

15. Clark L A 1983. *Concrete bridge design to BS5400.* Construction press

FE modelling of the Effect of Elevated Temperatures on the Anchoring of CFRP Laminates

D.Petkova, T. Donchev & J.Wen
Kingston University London, UK

ABSTRACT: Carbon fibre reinforced polymers (CFRP) are type of relatively new composite material and its excellent structural performance determines its wide range of applications for various engineering solutions. In the last decades FRPs were found to be appropriate materials for strengthening of existing reinforced concrete structures subjected to different conditions- environmental or as a type of loading. The behaviour of the strengthened system has been the focus of investigation in different aspects of structural problems and challenges. One of these is the effect of elevated and high temperatures due to fire.

A finite element model which represents the work of an anchorage of externally strengthened reinforced concrete beam with CFRP laminates is proposed in order to describe and explain the development of structural and temperature stresses and potential modes of failure during the heating and cooling process. Analysis of obtained results and comparison with similar research will be presented in order to assess the structural behaviour of the strengthened system.

1 INTRODUCTION

The excellent properties of fibre reinforced polymers (FRPs) have made them a popular solution for the increase of loadbearing capacity of timber, steel and concrete structural elements. The various types of polymer products define the wide range of shape and form of application - tendons, rods, fabrics, laminates both as external and internal reinforcement. The low self-weight, high strength and quick installation are some of the advantages of the FRP over the traditional strengthening materials.

Different research has been conducted in the last few decades on the behaviour of FRP strengthened structural elements. The effect and response to elevated temperatures and fire, however, is a relatively new area of investigation for the FRP materials. As the fire resistance of materials is an important requirement for fire safety design of structures, additional research is necessary in order to fully utilise the potential application of the polymers.

For the purpose of this paper, the behaviour of concrete specimens with externally attached CFRP laminates is analysed, reflecting the influence of different factors on the response of elevated temperatures. A finite element model of the anchoring zone of the laminate to the concrete surface is created to investigate the contribution of the different factors such as reduction of strength of the materials, coefficients of thermal expansion and the glass transition temperature of the adhesive to the interfacial stress between the laminate and the specimen.

2 LITERATURE REVIEW

Research on concrete elements strengthened with FRP at elevated temperatures is still in process of development. Green, Benichou, Kodur & Bisby (2007) presented a general overview of the North American and European approaches to the design of structures to address their performance in fire. In the North American method the structural strength is calculated based on the expected temperatures in concrete and reinforcement, FRP is recommended to be ignored in the analysis. The European approaches involve both thermal and structural analysis: the thermal analysis is conducted first and the temperature results are transferred to the structural analysis to calculate the strength of the structural element at a given time during the heat exposure. The authors concluded that more research was required to develop and experimentally validate the method, to better characterise the effects of elevated temperatures on the mechanical behaviour of FRP.

Camata, Pasquini & Spacone (2007) performed tests with different types of adhesives with glass transition temperature (T_g) higher than 85 °C and 2 types

of CFRP: pultruded laminates and unidirectional woven fabrics. It was observed that after the thermal load no cracks were visible, which was explained by the reduction of stiffness and the more uniform distribution of strain along the bond length. Failure occurred in concrete as a layer of the material remained attached to the laminate.

Klamer, Hordijk & De Boer (2007) observed two types of failure in their work.The specimens at the lower range(up to 40 °C) failed due to concrete rupture leaving 1-3mm of it on the adhesive layer, while at the upper temperature (50-75 °C) range the failure occurred between the concrete surface and the adhesive. The results were explained as the stiffness of the adhesive was reduced as approaching to the glass transition temperature (T_g) of the material. From another set of experiments three temperature related effects were found to affect the failure load: the difference in the coefficient of thermal expansion of CFRP and concrete, which caused initial thermal stress distribution in the concrete at the interface with the adesive; the reduction of Young's modulus with increase of temperature and the third effect was the educed bond strength of the concrete-adhesive interace at elevated temperatures.

A study on the bond behaviour at elevated temeratures was conducted by Leone, Aiello & Matthys 2006) up to 80 °C. In the case of bonded FRP laminate for all test temperatures, a mixed failure was obained characterized by cohesion failure, adhesion failure at the epoxy- concrete interface and adhesion failure at the epoxy-FRP interface. Nevertheless, adhesion failures at the epoxy-FRP interface tended to be predominant at higher temperatures. A significant decrease of the maximum bond stress could be observed for elevated temperatures beyond the T_g (55 °C). The bond interface was characterized by a less stiff behaviour.

The bond between the adhesive and concrete at elevated temperatures was investigated by Gamage, Al- Mahaidi & Wong, 2005 and 2006. It was found that exposure to temperatures higher than 80 °C led to substantial decrease in the bond strength between the two materials.

Experiments with heating and loading of concrete prisms with attached CFRP were reported in literature. The temperature range was chosen by the glass transition temperature of the used adhesive (60- 85 °C). All authors discussed above have analysed the behaviour during the heating process. It is unclear, however, what the residual stresses are in the strengthened system after heating and cooling and their contribution to the structural stresses of the loaded samples which is the aim of this work.

3 FACTORS INFLUENCING THERMAL STRESSES BETWEEN LAMINATE AND CONCRETE

Due to their nature the polymers show the tendency to soften as their T_g is approached and at high temperatures they decompose. The coefficient of thermal expansion (CTE) is determined from the properties of the fibres and the resin. In the case of unidirectional laminates, the expansion of the CFRP in the two orthogonal directions is different. In longitudinal direction the CTE of the laminates is accepted to be zero due to the practically negligible expansion of the fibres and in the transverse direction its influence is ignored due to the limited distance of its application.

Information about the Young modulus of the CFRP is provided by the manufacturers and the corresponding values are included in the analysis. During the heating process the adhesive between the laminate and concrete exhibits significant reduction of its stiffness. The lap shear strength of the adhesive drops to 12.7N/mm^2 at 45°C from 18.3 N/mm^2 at room temperature. The failure of specimens loaded at high temperatures has proved to be dependent on the decrease of strength of the adhesive which makes it the most critical element of the whole system. In the case of heating and cooling though the effect of glass transition should be taken into account as it could contribute to the redistribution of stresses in the constituents.

For the purpose of this research a 3D finite element model was used to estimate the effect of the elevated temperature on the strengthened system. Solid elements were used to represent the laminate, concrete prism with 75x75x300mm dimensions and the adhesive. The temperature loading was realised in two steps, analysing first the effect of heating and then the opposite process of cooling. The specific size of the specimens is accepted on the base of previous experimental investigations, see Donchev, Wen, & Papa (2007).

4 PRELIMINARY RESEARCH

In a previous research (Petkova, Donchev, Wen, Etebar & Hadavinia 2007) the behaviour of the anchoring zone of CFRP laminate externally attached to a concrete prism was investigated including considerations for elevated temperature conditions but ignoring the effects due to CTE. Both experimental investigation and theoretical FEA modelling were conducted. The thermal loading consisted of heating of the samples for at least 2h at different constant temperatures up to 250°C to ensure evenly distributed temperature in the cross sections of the samples. The laminate was loaded in tension after the cooling of the specimens simulating longitudinal

shear loading at this zone. The behaviour of the strengthened system did not exhibit substantial difference with specimens loaded up to 100°C. The decrease of strength of the system in the range 100-250°C was approximately linear which was mainly dictated by the reduction of the strength of the concrete. At 250°C the ultimate strength of the strengthened system was reduced to 65% of the strength at room temperature (fig. 1).

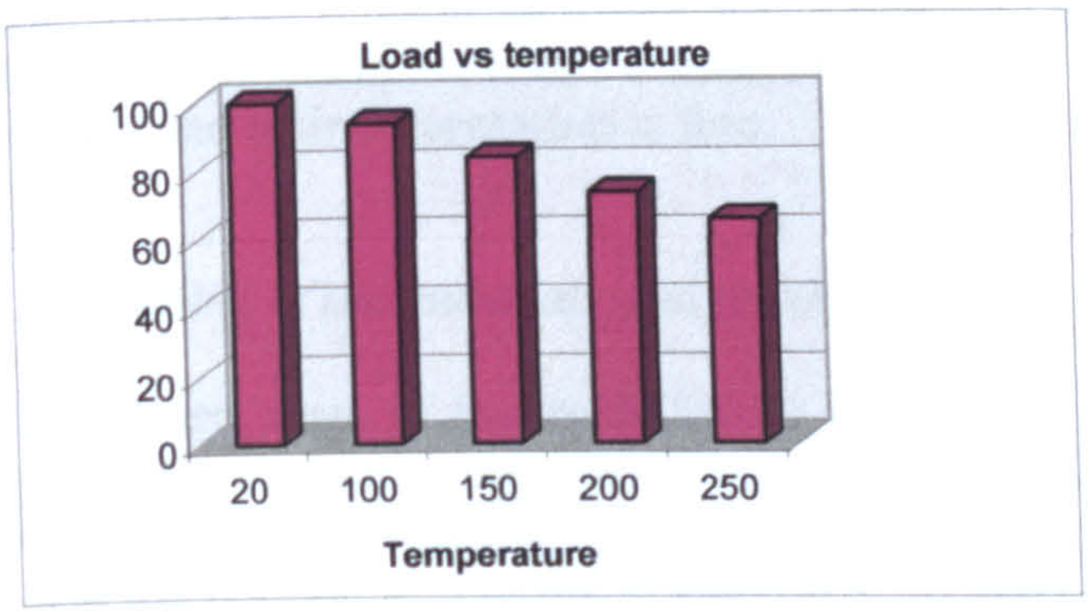

Figure 1. Decrease of strength of the strengthened system

The predominant failure mode was through concrete cover separation which initiated with a vertical crack in the concrete at the laminate's edge. High concentration of stresses at the tip of the crack was observed and further development of stress concentration zone horizontally lead to the development of conditions for the separation of the concrete cover. Good agreement was found between the experimental and numerical results.

5 EFFECT OF THE DIFFERENT COEFFICIENTS OF THERMAL EXPANSION (CTE)

In reinforced concrete both the constituents - concrete and steel reinforcement - behave similarly in terms of thermal expansion when subjected to environmental conditions. In a strengthened system which includes adhesive and CFRP laminate, the change of temperature may cause significant stress development due to the difference of the CTEs (table 1). In the longitudinal direction the laminate has the lowest CTE while the adhesive could have 3 to 9 times higher coefficient compared to concrete.

Material	Glass transition temperature	Coefficient of thermal expansion
Concrete C20	-	$10x10^{-6}$/°C
CFRP laminate	100°C	$0x10^{-6}$/°C
Adhesive	60°C	$33x10^{-6}$/°C

Table 1

5.1 *Heating of the strengthened system*

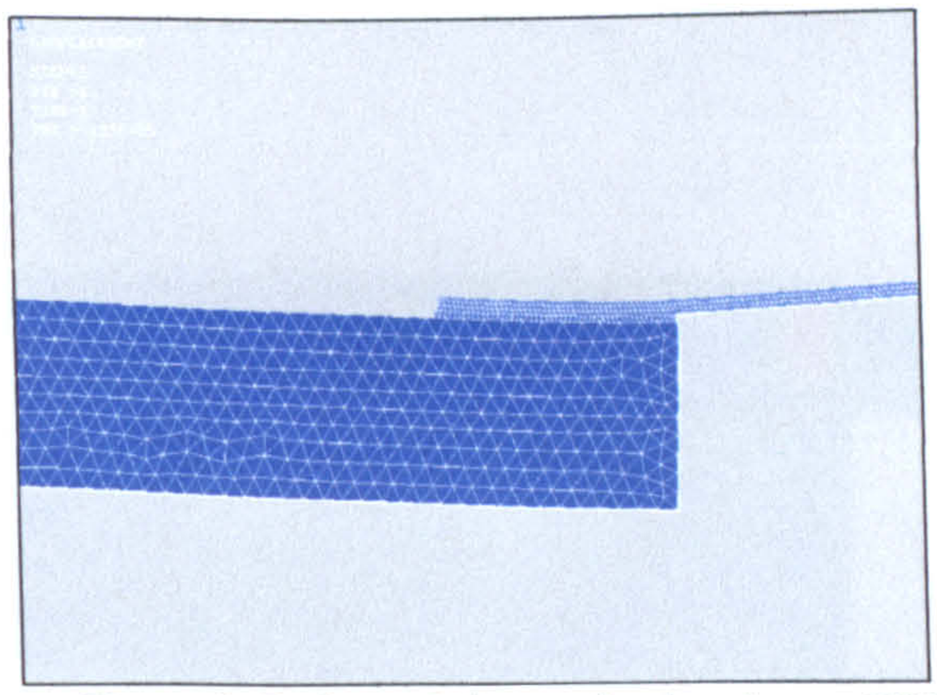

Figure 2. Deformed shape after heating to 60°C

The free expansion of concrete at elevated temperatures does not lead to development of thermal stresses in terms of structural analysis. The attachment of the laminate, however, brings a limitation of the concrete to expand and is equivalent to a loading in compression for it along the bonding length. The laminate correspondingly is loaded in tension at the contacting zone with the concrete. Hence the deformed shape of the system during heating will be defined from compression in concrete close to the laminate and elongation in the far end of the prism (fig2).

From the three constituents, the adhesive is the one with highest CTE, which combined with characteristics of adjacent materials leads to the development of high compression stresses in the adhesive during the heating process (fig.3).

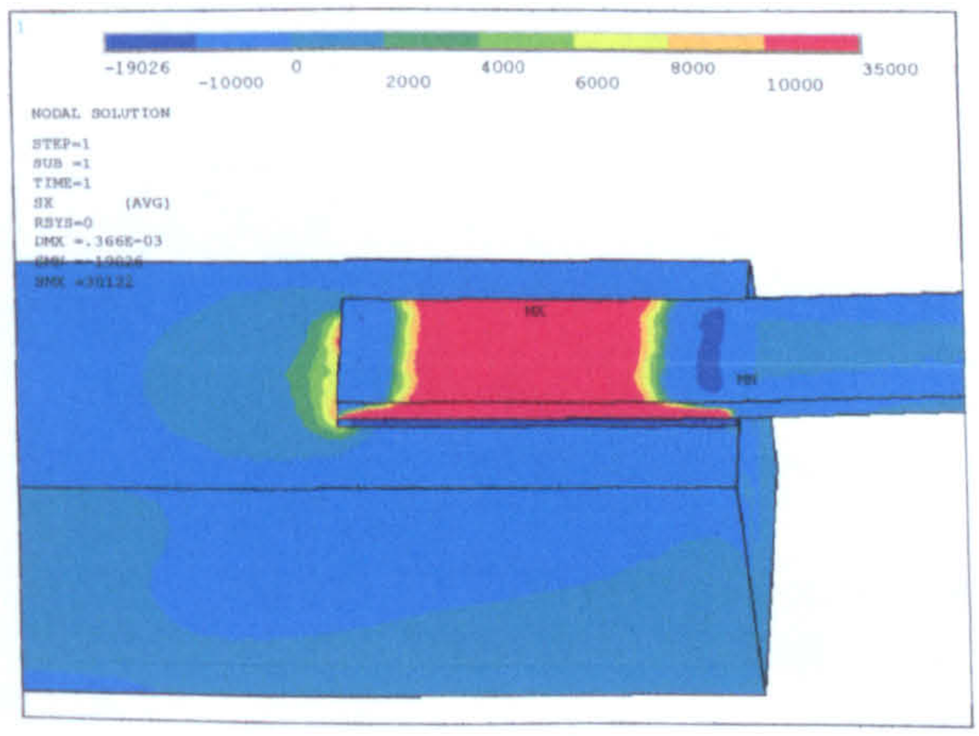

Figure 3. Normal stress distribution during heating up to 60°C

The zone of the laminate's end is subjected to a local concentration of thermal stresses in the three constituents. The difference of the expansion rate of the laminate and the concrete results in conditions for the development of tension stresses in the concrete which reach high values of 6 MPa. The level of tensile stress and potential crack initiation at the zone close to the edge of the laminate of the strengthened system due to the elevated temperature are substantial.

Heating the materials above the T_g of the adhesive leads to a new process of stress relaxation at the interfaces of the constituents. Above 60°C the adhesive can be described as rubbery material with the tendency for free deformation. As the T_g of the adhesive is approached, its state is transformed from solid to viscous with the corresponding decrease of stiffness. The expansion of the concrete is no longer prevented by the limited expansion of the polymer and correspondingly the laminate is no longer subjected to tension. Therefore it could be stated that at temperatures above T_g the elements reach a state of relaxation of stresses and their deformation is free.

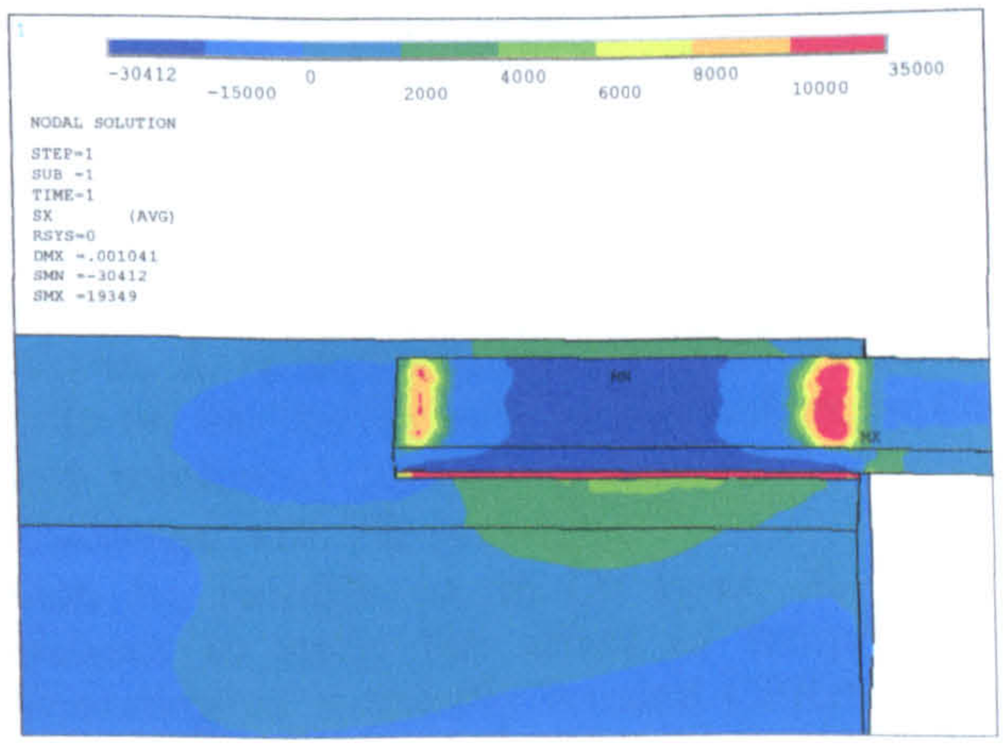

Figure 5. Normal stress distribution after cooling to room temperature

5.2 *Cooling of the materials and residual stress*

The next stage of the modelling is the cooling of the sample to room temperature. Once the relaxation of stress due to the softening of the adhesive is realized, the process of cooling is introduced at zero internal forces between the constituent materials. When the thermal condition decreases to temperatures under T_g, the adhesive is assumed to regain its strength and stiffness, causing interaction with the adjacent elements.

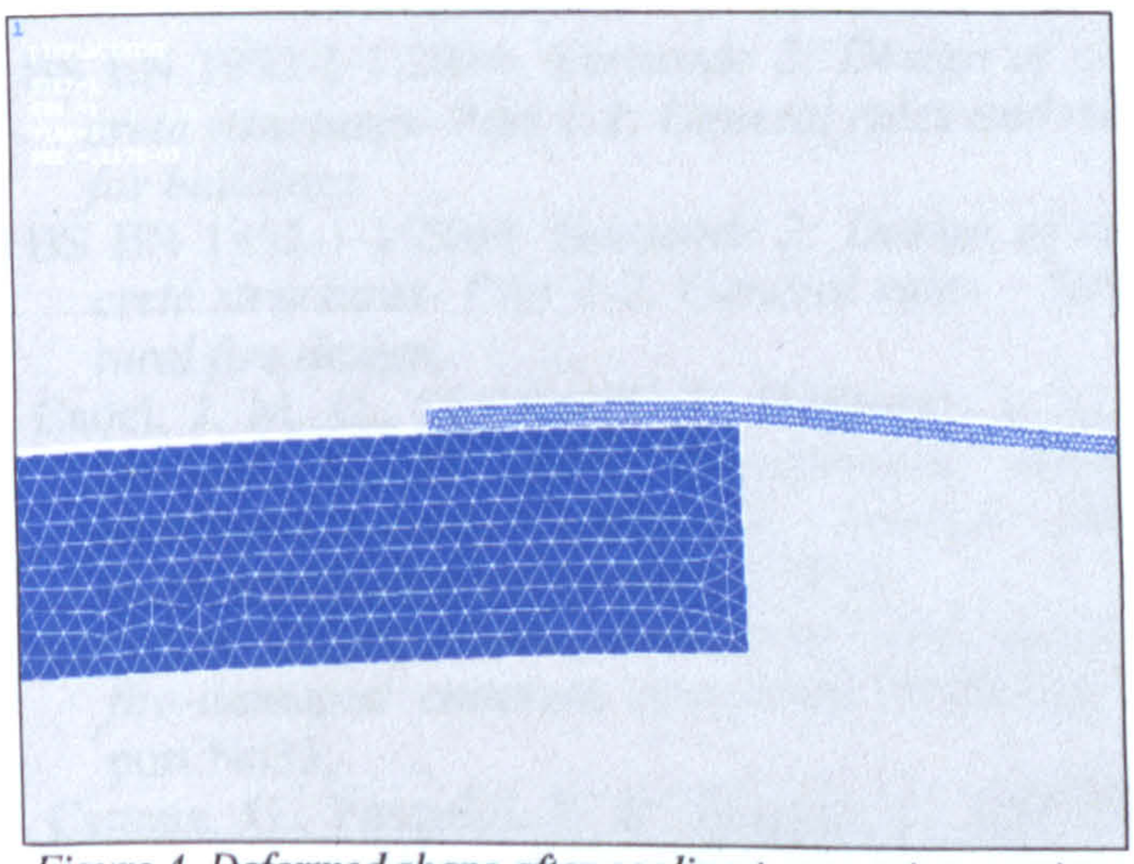

Figure 4. Deformed shape after cooling to room temperature

The performance of the strengthened system at cooling is the opposite of the analysis during heating. At room temperature the laminate is loaded in compression due to its lack of thermal contraction which prevents the concrete to return to its original state. The deformation of the strengthened system is again governed by the different behavior of concrete and laminate during temperature changes due to different CTE. The shape of the specimen is changed in accordance with the tendency for contraction of the concrete when subjected to decrease of the thermal load (fig. 4).

The process of cooling leads to a relaxation of the stress in the concrete at the zone of laminate's end. The concrete is subjected to tension along the bonding area with values up to 4 MPa. The distribution of the tensile stresses in depth is similar to the formation of the horizontal crack which develops before the concrete cover separation mode of failure is observed.

The residual tensile stress at the adhesive on the other hand is significant and could lead to failure due to high concentration of stresses in this element of the strengthened system.

5.3 *Combination of residual thermal stress and stress due to external forces*

When specimens externally strengthened with CFRP laminates are heated, cooled and then subjected to tension, the remaining capacity and corresponding failure mode is dictated by several different factors which make its prediction a complicated task. The thermal loading and its consequent effects on the materials, the development of microcracks in concrete, the phenomenon of glass transition temperature of strengthening materials and the condition of the interface between the adhesive and concrete are some of the problems that have to be considered. However, two main failure modes are observed from the experiments when heated up to 250°C and cooled - the concrete cover separation mode and interfacial failure between concrete and adhesive at the high value of the temperature interval.

The proposed theoretical model indicates residual tension stresses into the concrete and compression stresses into the laminate after heating above T_g and cooling. Such distribution of thermally induced stresses would have negative effect on the capacity and deformability of CFRP strengthened systems after subjected to elevated temperatures. However, it could be stated that the predominant failure of a strengthened system after heating and cooling is governed by the concrete as it is weaker in tension than any of the other materials in the strengthened system, and the development of the concrete cover separation is most likely to occur.

6 CONCLUSION AND RECOMMENDATIONS

As a result of the developed theoretical modelling, the following conclusions could be indicated:

- Temperature induced stresses in the concrete close to the edge of the laminate during heating are significant and close to the tensile strength of the concrete;

- During the heating process significant tensile stresses in the laminate and compression stresses in the concrete are generated. Those stresses are below the corresponding strength of the materials.

- When heated above T_g and cooled the system of concrete and CFRP laminate develops temperature induced stresses of compression in the laminate and tension in concrete. Such stresses could be reason for local cracking in the concrete and additional deformability at the strengthened system.

The obtained theoretical results will be subject of future experimental confirmation.

REFERENCES

BS EN 1992-1-1:2004. *Eurocode 2: Design of concrete structures- Part 1-1: General rules and rules for buildings.*

BS EN 1992-1-1:2004. *Eurocode 2: Design of concrete structures- Part 1-2: General rules – Structural fire design.*

Cadei, J. M. C., Stratford,T. J., Hollaway, L. C. & Duckett, W. G. 2004. *Strengthening metallic structures using externally bonded fibre-reinforced polymers,* London: CIRIA.

Concrete Society, 1990. *Assessment and repair of fire-damaged concrete structures,* Technical report No33.

Camata, G., Pasquini, F. & Spacone, E. 2007.High temperature flexural strengthening with externally bonded FRP reinforcement. *Proceedings of the 8th international symposium on FRP reinforcement for concrete structures,* Patras, Greece.

Donchev, T., Wen, J. & Papa, E. 2007. Effect of elevated temperatures on CFRP strengthened structural elements, *11th International conference on Fire and materials, San Francisco, USA.*

Gamage, J. C. P. H., Al- Mahaidi, R.& Wong, M. B. 2006. Bond characteristics of CFRP plated concrete members under elevated temperatures, *Composite Structures,* Vol. 75, 2006, pp. 199-205.

Gamage, J. C. P. H., Wong, M. B. & Al- Mahaidi, R. 2005. Performance of CFRP strengthened concrete members under elevated temperatures, *Proceedings of the International Symposium on Bond behaviour of FRP in Structures,* pp. 113-118.

Green, M. F., Benichou, N., Kodur, V., Bisby, L. A., 2007. Design guidelines for fire resistance of FRP-strengthened concrete structures, *Proceedings of the 8th international symposium on FRP reinforcement for concrete structures,* Patras, Greece.

Karadeniz, Z. H. & Kumlutas, D. 2007. A numerical study on the coefficients of thermal expansion of fiber reinforced composite materials". *Composite Structures,* Vol. 78, pp 1-10.

Klamer, E., Hordijk, D. & De Boer, A. 2007. FE analyses to study the effect of temperature on debonding of externally bonded CFRP. *Proceedings of the 8th international symposium on FRP reinforcement for concrete structures,* Patras, Greece.

Klamer, E. L., Hordijk, D. A. & Janssen, H. J. M. 2005. The influence of temperature on debonding of externally bonded CFRP, *Proceedings of the 7th international symposium for FRP reinforcement for concrete structures,* Vol. 2, pp 1551-1567.

Leone, M., Aiello, M.-A. & Matthys, S. 2006. The influence of service temperature on bond between FRP reinforcement and concrete, *Proceedings of the 2nd International Congress,* Naples, Italy.

Petkova, D., Donchev, T., Wen, J., Etebar, K. & Hadavinia, H.2007. Effect of Elevated Temperatures on the Bond between FRP and Concrete, *Proceedings if the 11th International conference,* Vol. 1, pp 783-790.

Rabinovitch, O. 2007. On thermal stresses in r.c. beams strengthened with externally bonded FRP strips. *Proceedings of the 8th international symposium on FRP reinforcement for concrete structures,* Patras, Greece.

SBD Weber Product catalogue. Bedford, UK: Dickens Hose.

Behaviour of externally strengthened RC elements at elevated temperatures

Diana Petkova*, Ted Donchev

Kingston University London

ABSTRACT

The paper presents the experimental and analytical work on the behaviour of small-scale reinforced concrete (RC) beams externally strengthened with carbon fibre reinforced polymers (CFRP) laminates. The samples were subjected to elevated temperature and static dead load simultaneously and their deformations throughout the process were measured. The investigation was focused on the overall behaviour of the strengthened system both during and after heating, before and after loading. The presented results are part of a study in which the residual strength and failure modes of the heated minibeams are to be determined.

INTRODUCTION

The purpose of this paper is to present the experimental results of the effect of elevated temperatures on strengthened systems. The samples tested are small scale reinforced minibeams strengthened with CFRP heated to 100°C, 200°C and 300°C. The strengthened minibeams were loaded with a static load of 1000N and then subjected to heating to elevated temperature until uniform distribution of the temperature in the specimen was achieved.

LITERATURE REVIEW

The effect of elevated temperatures on fibre reinforced polymers has been investigated by several researchers although the majority of tests have been conducted with internal reinforcement.

Abbasi and Hogg (2005)[1] presented a model of glass fibre rebar reinforced concrete beam at fire conditions. The authors adopted finite element and semi-empirical approach to simulate the temperature distribution in the beam. The latter was found to be the better fit with the experimental results and was used to determine the effective compressive strength of concrete. The authors also suggested a method to develop equations for the glass FRP rebar used as an internal reinforcement during fire.

Karadeniz and Kumlutas (2005)[2] investigated the different methods to determine the coefficient of thermal expansion of composites. The linear expansion of composites was mostly influenced by the thermal and elastic properties of the constituents and orientation of fibres, at high temperatures though the softening of the resin is the main factor for the dimensional changes of the material. Several analytical methods are compared and it was found that for the longitudinal coefficient of thermal

expansion analytical results were in good agreement with the experiments, while in the transverse direction the results were found to depend on the fibre/matrix ratios.

Wong et al (2004)[3] presented experimental and numerical results of compression tests of GRP channels subjected to elevated temperatures. It was found that up to the heat distortion temperature of the GRP structures the residual strength was quite significant but at higher temperatures the properties were reduced. It was also found that commercial finite element software could predict accurately the behaviour of the GRP columns.

Katz et al (1993)[4] discussed high temperature test of FRP rebars. Tensile tests were conducted with heated samples up to 250°C. It was found that up to 300°C the behaviour of FRP rods was not significantly affected but the bond strength to concrete could change dramatically. The temperature range when reduction of bond strength was found is 80-160°C, above 200°C the strength remained constant.400°C were quoted the maximum temperature as above it no mechanical properties should be expected. The bond modulus was also affected by the temperature.

Little information is available in the literature on the effect of elevated temperatures on CFRP externally strengthened RC beams. As reported by different researchers[9-11] the failure modes for such beams are governed by different factors and several different types of failures are observed. The final stage of this study is aiming to determine the effect of elevated temperatures on the failure modes of CFRP strengthened beams.

EXPERIMENTAL PROGRAMME

Small –scale experiments were conducted to establish the thermal effect on the behavior of CFRP strengthened RC beams.9 reinforced concrete minibeams with dimensions.100x100x500mm were cast and cured. For each beam a 20mm wide CFRP laminate was attached to one surface of the beam and left to cure for 7 days. One specimen at a time was placed in the oven and loaded with static load of 1000N prior to heating.

The beam was then heated to the specified temperature. Deflection and temperature readings were taken every 15 minutes until uniform distribution of temperature was recorded in the cross-section of the beam. The oven was then turned off and the deflection readings were taken for the cooling process. When the system had cooled to room temperature, the beam was unloaded and removed from the oven.

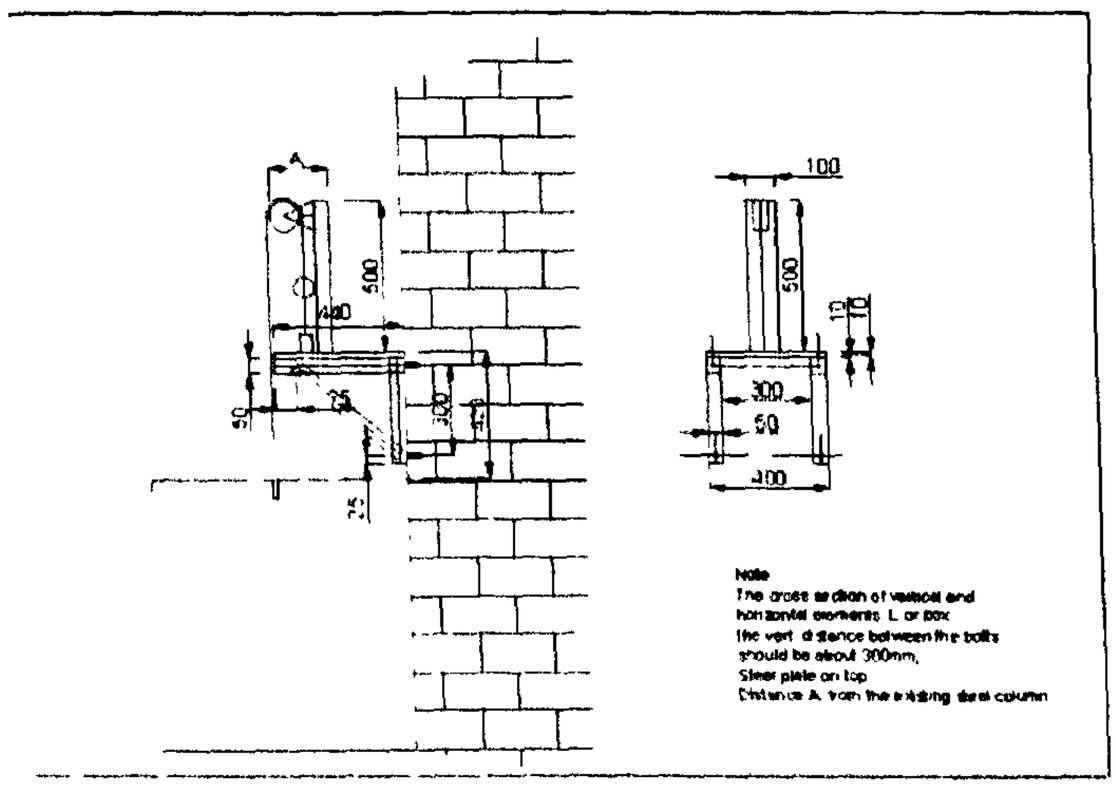

Figure 1 Experimental set-up

To measure the deflection before, during and after heating, a dial gauge was mounted on a shelf above the oven itself as shown on the Figure 1. Invar wire was used to connect the beam to the dial gauge

leaving 300mm between the oven and the shelf to minimize the effect of heating of the recording system itself.

Readings of the temperature were also taken with 5 thermocouples inside the oven, measuring the temperature at the top, middle and bottom of the oven. Temperature was measured inside the beam and a concrete cube as well.

Figure 2 Heated samples to 200 and 300°C

ANALYSIS OF RESULTS

The time for the heating of the specimens was as follows: 150 min for 100°C, 330min for 200°C and 420min for 300°C (figure for samples heated to 300°C). The cooling process of the samples was also recorded and the residual deflection after the cooling was calculated. Since the specimens were statically loaded as well, the deflection after removing the load was also recorded and compared with the initial readings.

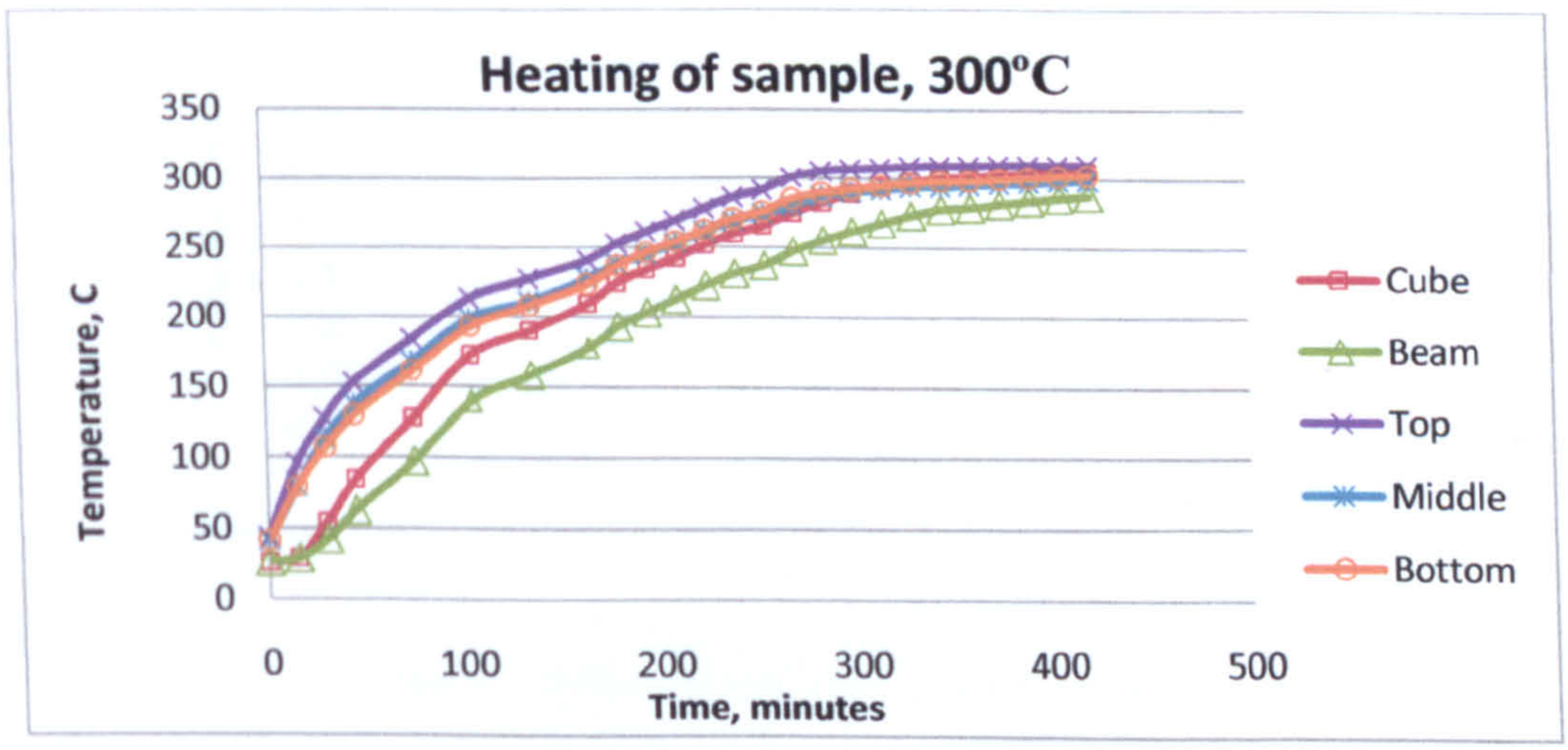

Figure 3 Heating of a sample at 300°C vs. time in minutes

During the heating process, rapid increase of the readings was observed until uniform temperature was established inside the oven. After the oven was turned off, the cooling process lead to decrease of the readings as a function of the time and temperatures inside the oven.

The experimental set-up inside the oven consisted of steel frame which expansion with the change of temperature was also taken into account when calculating the real deflection of the beam. The coefficient of the thermal expansion was taken as constant for the whole range of temperature.

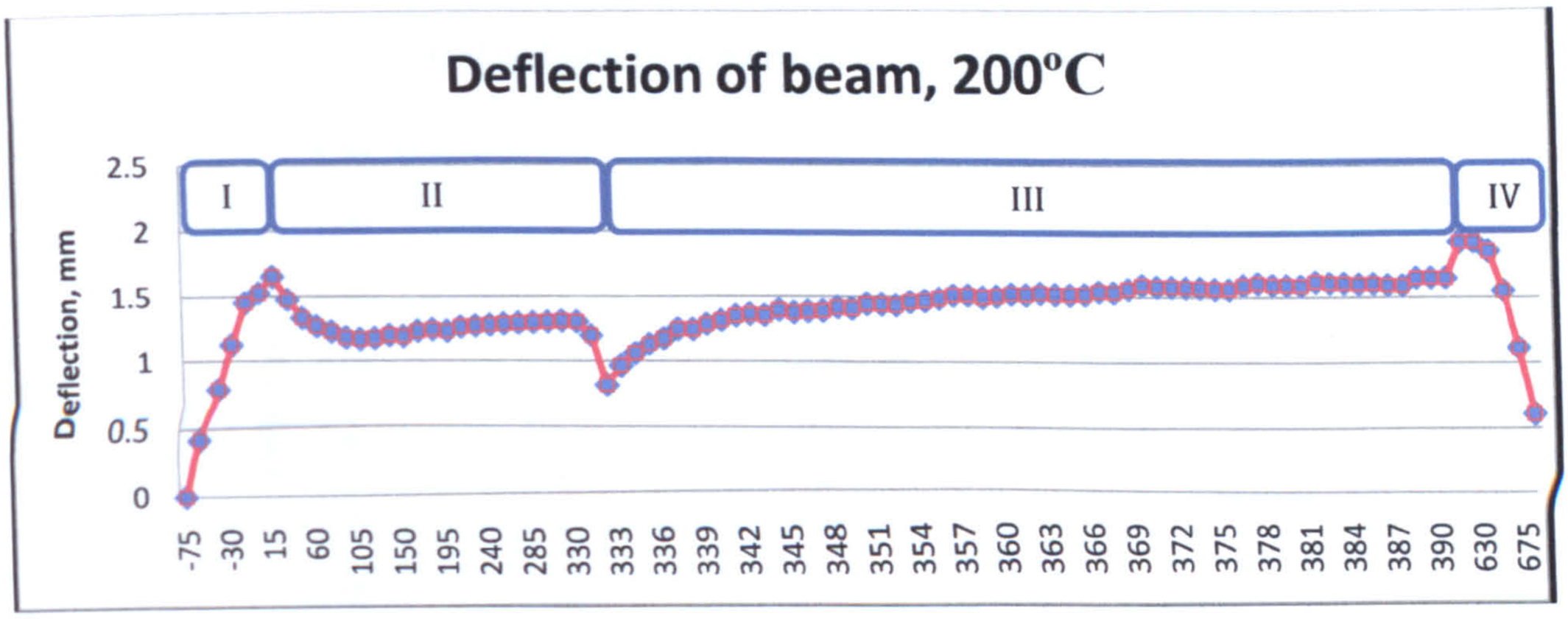

Figure 4 Heating process for a sample (horizontal axis is time, min). The graph presents the loading, heating, cooling and unloading process.

Figure 4 presents the deflection history of a sample heated to 200°C. Stage I of the process presents the linear increase of deflection due to the stepped (200N) application of static load onto the beam (3 point bending) (with final deflection of 1.523mm at 1000N), followed by stage II presented with the gradual decrease of deflection due to the heating of the sample. The cooling process is stage III which has a sudden drop at the beginning due to the quick drop of temperatures inside the oven. The last reading of stage III (1.303mm) is then taken as the residual deflection for the heating and cooling process (0.22 mm). Last stage of the experiment is the unloading –stage IV with a final reading of 0.605mm- the residual deflection after the loading, heating, cooling and unloading process.

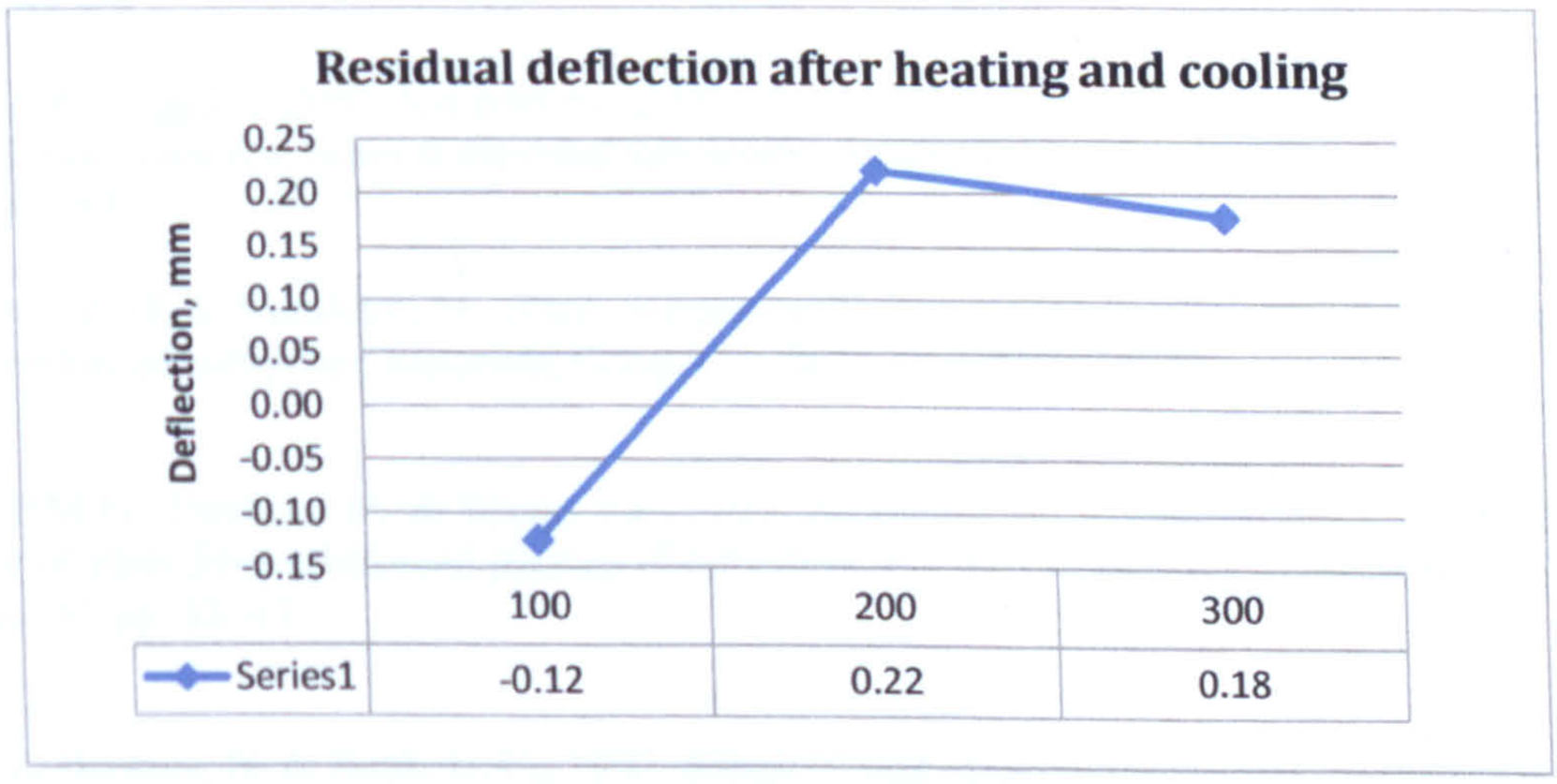

Figure 5 Residual deflection after heating and cooling

Analyzing the heating and cooling process of the different samples reveals a tendency for more substantial deformations at 200 and 300°C. The highest value of deflection for the samples is recorded during the heating to 200°C which is 18% higher than the deflection of samples heated to 300°C (figure 6.). The final deflection of the beams however, follow different tendency- after unloading the beams are most affected after being exposed to 300°C (figure 7).

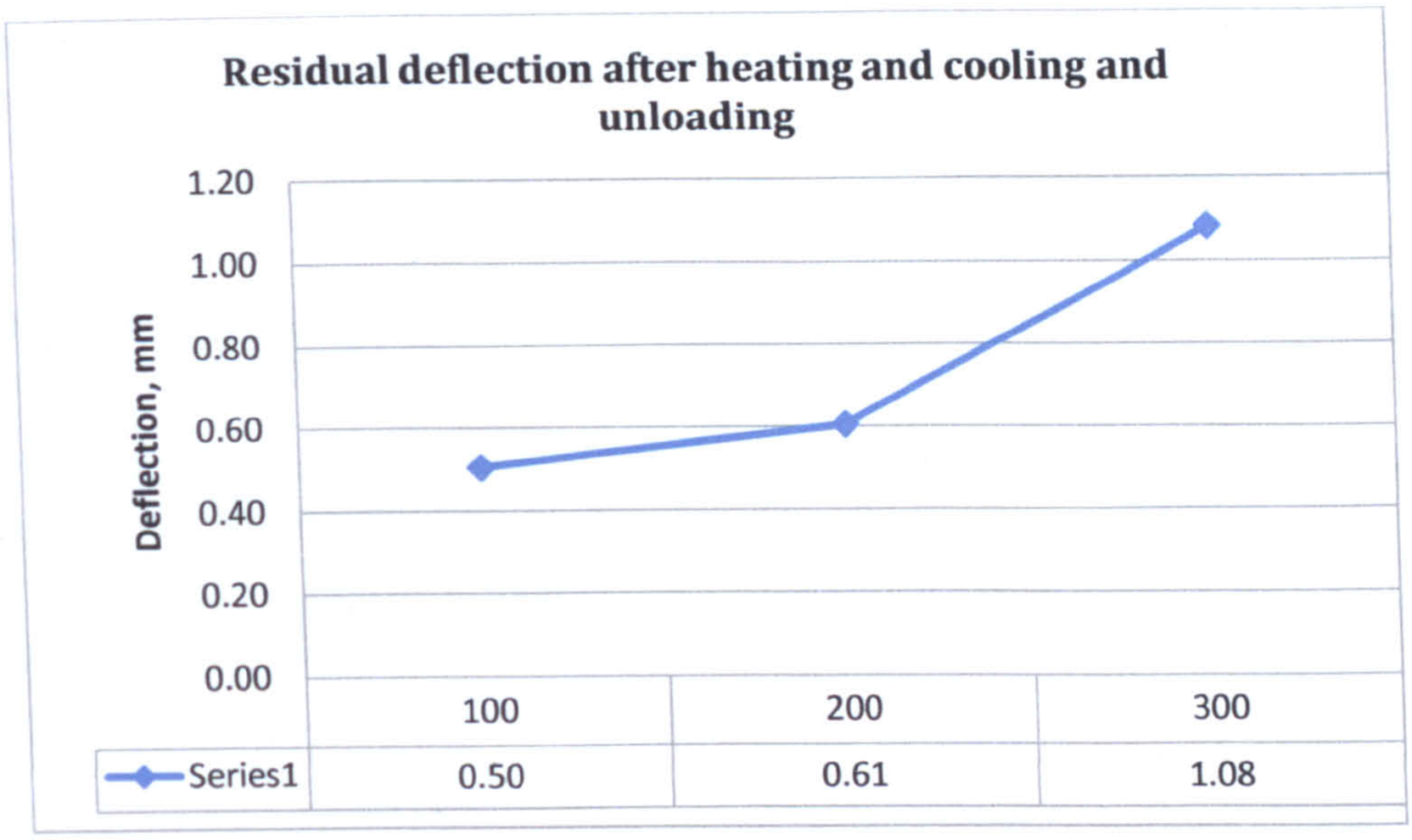

Figure 6 Residual deflection after heating and cooling

CONCLUSION

The effect of elevated temperatures was experimentally investigated and the deflection of the samples was presented. Both deflection caused by heating and cooling processes and after loading and unloading stages are presented revealing a gradual increase of the deformation with increase of temperature.

REFERENCES

1.Abbasi,A.& Hogg,P.J.,2005.A model for predicting the properties of the constituents of a glass fibre rebar reinforced concrete beam at elevated temperatures simulating a fire test. *Composites: Part B* , 36,pp. 384–393

2.Karadeniz, Z. H. & Kumlutas, D., 2007. A numerical study on the coefficients of thermal expansion of fiber reinforced composite materials, *Composite Structures*, 78, pp.1–10

3.Wong, P.M.H., Davies, J.M. & Wang, Y.C. 2004. An experimental and numerical study of the behaviour of glass fibre reinforced plastics (GRP) short columns at elevated temperatures. *Composite Structures*, 63 pp. 33–43

4.Katz, A., Berman, N. & Bank, L. C., 1993. Effect of high temperature on bond strength of FRP rebars, *Journal of composites for construction*, May, pp.73-81

5.Ramroth, W.T., Asaro, R.J., Zhu, B. & Krysl, P., 2006. Finite element modelling of fire degraded FRP composite panels using a rate dependent constitutive model, *Composites: Part A,* 37, pp. 1015–1023

6. Galati, N., Nanni, A., Dharani, L. R., Focacci, F. & Aiello, M. A., 2006. Thermal effects on bond between FRP rebars and concrete, *Composites: Part A*, 37, pp.1223–1230

7.Keller, T., Tracy, C.,& Hugib, E., 2006. Fire endurance of loaded and liquid-cooled GFRP slabs for construction, *Composites: Part A*, 37, pp. 1055–1067

8. Abbasi, A. & Hogg, P.J., 2006. Fire testing of concrete beams with fibre reinforced plastic rebar, *Composites: Part A*, 37, pp. 1142–1150

9. Pham, H. B., & Al-Mahaidi, R., 2007. Modelling of CFRP-concrete shear-lap tests, *Construction and Building Materials*, 21, pp.727–735

10. Wu, Y., Zhou, Z., Yang. Q., & Chen, W., 2010. On shear bond strength of FRP-concrete structures , *Engineering Structures* ,32 pp. 897-905

11.Yao, J. & Teng, J.G., 2007. Plate end debonding in FRP-plated RC beams—I: Experiments, *Engineering Structures* , 29,pp.2457–2471